



University
of Glasgow

Vihermaa, Leena E (2010) *Influence of site factors and climate on timber properties of Sitka spruce (Picea sitchensis (Bong.) Carr.)*. PhD thesis.

<http://theses.gla.ac.uk/2271/>

Copyright and moral rights for this thesis are retained by the author

A copy can be downloaded for personal non-commercial research or study, without prior permission or charge

This thesis cannot be reproduced or quoted extensively from without first obtaining permission in writing from the Author

The content must not be changed in any way or sold commercially in any format or medium without the formal permission of the Author

When referring to this work, full bibliographic details including the author, title, awarding institution and date of the thesis must be given



Influence of site factors and climate on timber
properties of Sitka spruce
(*Picea sitchensis* (Bong.) Carr.)

Leena Vihermaa
MSc.

Submitted in fulfilment of the requirements for the Degree
of
Doctor of Philosophy

Environmental, Agricultural and Analytical Chemistry
Chemistry Department
University of Glasgow

November 2010

Abstract

In plantation grown Sitka spruce, timber density is an important quality concern. Currently Sitka spruce timber meets the requirements for C16 strength grading which is the minimum requirement for construction uses. However, the margin is not exceeded by much and a small reduction in density could lower the log grading. Therefore it is essential to understand how timber density is impacted by site factors and climate in order to predict the potential effects of climate change on timber quality in Sitka spruce in the future. This has important economic implications for UK forestry.

To assess the influence of site factors and climate on growth and resulting timber properties in Sitka spruce, three experiments were established; a large scale wood quality survey (“The Benchmarking experiment”), a detailed inter-site density study (“The Level II experiment”) and a continuous growth monitoring experiment (Dendrometer experiment).

In the ‘Benchmarking’ experiment, increment cores were collected from 68 sites over a geographically wide area in Scotland and Northern England in order to quantify the effect of selected site factors on density. These samples were not suited for climate analysis at annual ring level and therefore disks that allowed reliable dating of the tree rings were collected from three Level II sites. The Level II samples were also used in an acoustic velocity study and an assessment of the within-tree patterns in density. Material from both Benchmarking and Level II sites was used for modelling radial density. In addition to this the Level II data functioned as a test dataset for the different density models that were developed on the Benchmarking data.

Density and other tree ring variables were measured with an ITRAX X-ray densitometer and WinDENDRO software. Some acoustic measurements were also carried out with a purpose built ultrasonic scanner to allow calculation of radial variation in stiffness. A dendrometer experiment was established to monitor short term growth variation in Sitka spruce in real time. The aim was also to use the growth data to date density profiles and hence identify causes for the density differences. Data analysis was carried out in R mainly using linear and non-linear mixed effects models, the dendrochronology software package dplR and methods of time series analysis.

It was found that the largest part of the variation in density was between trees within each site. Both density and stiffness were mostly influenced by the growth rate or by another variable describing the tree vigour. Fast growth decreased density both by increasing earlywood proportion as well as decreasing the density of both earlywood and latewood. Models for the radial behaviour of density and stiffness could be fitted to the data, but random tree effects remained large. This limits the applicability of these models to new sites as reparameterisation would be required, which requires data from time consuming density and acoustic velocity measurements. The possibility of modelling the model coefficients from easily measurable stand and tree variables was investigated but the results were not promising.

The Dendrometer experiment indicated that annual growth in Sitka spruce was initiated in late May and terminated by mid September. Ring widths detected by the dendrometers, micro core measurements and X-ray density based tree ring analysis differed, which caused difficulties in dating the density profile. To decrease these problems in the future the microcore sample storage protocol was revised. The dendrometer data indicated that the growing season was divided into several sections between which the growth rate differed.

Latewood density and maximum density had the strongest correlations with the climatic variables. At one site the correlations included temperature and rainfall in April whereas at the other precipitation throughout the growing season or during the May-August period were important. Temperature was correlated positively with density variables and rainfall negatively.

Table of Contents

1	Introduction	30
1.1	Tree growth	30
1.2	Sitka spruce in UK forestry	36
1.3	Timber quality	38
1.4	Factors influencing the timber quality	40
1.4.1	Climate and growth	41
1.4.2	Site factors and growth	42
1.4.3	Management and growth	44
1.4.4	Density and growth	47
1.4.5	Climate change	48
1.4.6	Climatic signal	49
1.5	Aims of this study	50
2	Density and Tree Ring Analysis	52
2.1	Sample Preparation for the Analysis	52
2.2	Scanning with an ITRAX X-ray Densitometer	53
2.3	Tree Ring Analysis with WinDENDRO	55
3	Magnitude and sources of experimental errors in density analysis	57
3.1	Introduction	57
3.2	Materials and Methods	59
3.2.1	Humidity	59
3.2.2	Sample alignment	60
3.2.3	X-ray density conversion	61
3.3	Results	62
3.3.1	Humidity	62
3.3.1.1	Ring Density	63
3.3.1.2	Ring width	68
3.3.1.3	Variation between the paths	72
3.3.2	Sample alignment	74
3.3.3	Conversion from X-ray density to gravimetric density	78
3.4	Conclusions	82
4	Tree growth dynamics in Sitka spruce	84
4.1	Introduction	84
4.2	Materials and Methods	87
4.2.1	Site and Tree Selection	87
4.2.2	Dendrometers	88
4.2.3	Microcoring	91
4.2.4	Density determination	93
4.2.5	Data analysis	94
4.3	Results	94
4.3.1	Dendrometers	94
4.3.2	Microcores	95
4.3.3	Comparing the core and dendrometer measurements	97
4.3.4	Linking growth to climatic data	99
4.3.5	Density variation within the tree ring	118
4.4	Discussion	124
5	Wood quality survey – “The Benchmarking Experiment”	129
5.1	Introduction	129
5.2	Materials and Methods	132
5.2.1	Sampling	132
5.2.2	Area-weighted density analysis	133
5.2.3	Radial density modelling	135
5.3	Results	136

5.3.1	Density variation	136
5.3.2	Juvenile wood	150
5.3.3	Mature wood	154
5.3.4	Outerwood.....	157
5.3.5	Average density over the entire cross-section.....	160
5.3.5.1	Influence of thinning.....	162
5.3.5.2	Influence of social status.....	165
5.3.5.3	North vs South	171
5.3.6	Radial density profiles.....	174
5.3.6.1	Predicting alphas using additional data from the felled Benchmarking sites	188
5.4	Discussion	193
6	Detailed inter-site density study – “The Level II Experiment”	198
6.1	Introduction	198
6.2	Materials and methods	201
6.3	Results	205
6.3.1	Fitting the radial density model.....	207
6.3.1.1	Deriving coefficients using models from Benchmarking sites	207
6.3.1.2	Deriving coefficients with models from felled Benchmarking sites.....	212
6.3.1.3	Reparameterising the radial density model	213
6.3.2	Testing average density models	219
6.3.2.1	Juvenile wood density	219
6.3.2.2	Mature wood density.....	220
6.3.2.3	Cross-section average density	221
6.3.3	Variation within the tree.....	227
6.3.4	Climate Analysis	233
6.3.4.1	Tree ring and weather relationships at Loch Tummel site.....	240
6.3.4.2	Tree ring and weather relationships at the Coalburn site.....	258
6.3.4.3	Investigating the strongest correlations further.....	273
6.4	Discussion	277
6.4.1	Density modelling	277
6.4.2	Climatic signal	279
7	Radial Stiffness	283
7.1	Introduction	283
7.2	Materials and Methods.....	287
7.3	Results	290
7.3.1	Stiffness.....	299
7.3.2	Average stiffness models	304
7.3.3	Juvenile wood MoE	309
7.3.4	Outerwood MoE.....	312
7.3.5	Models for acoustic velocity	314
7.3.6	Radial stiffness modelling.....	316
7.3.6.1	Predicting a, b and d parameters	321
7.3.7	Comparison to ST300 measurements.....	324
7.4	Discussion	327
8	Discussion	332
8.1	Density in UK grown Sitka spruce.....	333
8.2	Relating ring-based and intra-ring density analysis to weather data.....	339
8.3	Pith to bark density modelling	342
8.4	Stiffness.....	344
8.5	Conclusions	345
8.6	Future work	347

List of Tables

Table 3-1. Relative humidity (%) in the ITRAX chamber during different scans of the selected samples.	59
Table 3-2. R output for the fixed effects in the fitted humidity model for ring density	66
Table 3-3. Variance components in humidity data when humidity fitted as fixed effect. ...	66
Table 3-4. R output for the fixed effects in the fitted humidity model for path average density.	67
Table 3-5. Output for the ring density model fitted to the humidity data in a more realistic operating range (<28%).	67
Table 3-6. R output for the path average density model fitted to density data obtained in relative humidity <28%.	68
Table 3-7. Size of a measurement error caused depending on the density variable and relative humidity range considered.	68
Table 3-8. R output for the ring width model fitted to the humidity experiment data.	71
Table 3-9. R output for the fixed effects in the fitted humidity model for the average path length.	71
Table 3-10. R output for the ring width model fitted to the humidity data in the operating range <28% relative humidity.	71
Table 3-11. R output for the average path length analysis in relative humidity <28%	71
Table 3-12. Size of the measurement error depending on the ring width variable and relative humidity range considered.	72
Table 3-13. Root mean square errors for the individual paths and the samples in average in the X-ray density (kg/m ³) measurements.	72
Table 3-14. RMSE for density measurement at different angles in the realistic working range compared to the 90 degrees to the beam.	77
Table 3-15. P-values for comparing the measurement methods for each sample.	79
Table 3-16. Regression equation for converting ITRAX density to oven dry wood density.	79
Table 3-17. Regression equation for converting ITRAX density to gravimetric density under the scan moisture content.	80
Table 4-1. The selected sample trees at the Griffin site and their DBH and height at the time of plot establishment April 2008.	88
Table 4-2. Paraffin impregnation sequence	92
Table 4-3. Details of the climatic variables obtained from the Edinburgh University monitoring data.	102
Table 4-4. WinDENDRO results for 2008 growth rings from the Griffin dendrometer experiment. Density and ring dimensions reported at 4% moisture content.	118
Table 5-1 Site factors used in the Benchmarking experiment	130
Table 5-2. Stand and tree variables used in the Benchmarking experiment.	134
Table 5-3. Average ring widths and ring densities for different dominance groups in the Benchmarking data. Trees were divided into quartiles according the DBH at each site. ...	138
Table 5-4. Range of density values in the Benchmarking dataset.	139
Table 5-5. Partitioning of variation in density to within the site and between-site components. Density at 4% moisture content was used.	148
Table 5-6. Average density model obtained using the factors from the design as continuous variables.	149
Table 5-7. Growth rate model obtained using the factors from the design as continuous variables.	149
Table 5-8. The Juvenile wood density model. Density values at 4% moisture content were used.	153
Table 5-9. Values of the coefficients in the final mature wood density model	155
Table 5-10. Final outerwood model variables and the diagnostic values associated with them.	158

Table 5-11. Variables in the final average wood density model.....	161
Table 5-12. Selected explanatory variables in the model developed for the thinned and unthinned BM sites at 4% moisture content.	164
Table 5-13. Area-weighted density models for the different dominance classes of trees. Density determined at 4% moisture content.	169
Table 5-14. Cross-section average density model for the Northern and Southern Benchmarking sites separately.....	171
Table 5-15. Concordance correlation coefficient, R^2 -values and variance explained for all the different models attempted for the area-weighted density.	173
Table 5-16. Variance components in the radial profiles of density and ring width in the Benchmarking data.....	174
Table 5-17. Explanatory variables and coefficients in the α_1 models.....	180
Table 5-18. Explanatory variables and coefficients in the α_2 models.....	183
Table 5-19. α_3 models.	186
Table 5-20. The average alpha values for thinned and unthinned Benchmarking sites with standard deviation in parentheses. P-value indicates the difference between thinned and unthinned sites.....	186
Table 5-21. The explanatory variables and coefficients in the model for predicting the alphas at the felled Benchmarking sites. Density at moisture content 4 %.....	191
Table 5-22. Mean values of the coefficients and standard deviations at the felled Benchmarking sites.	193
Table 6-1. Elevation and some average climatic parameters for the sampled Level II sites.	200
Table 6-2. Parameters sampled at the sites for Level II monitoring. Soil classification from the monitoring documents (Author: T. R. Hutchings).	200
Table 6-3. Measurements on the initial site visit and the sample quartiles defined.....	201
Table 6-4. Weather stations used in the Level II climatic effect study.....	204
Table 6-5. Average stand characteristics for each site with standard deviation in the brackets	206
Table 6-6. Summary of average tree ring variables for the studied sites (standard deviation). Density and width reported at 4% MC.	206
Table 6-7. Model prediction the α -values for radial density model derived on the original Benchmarking data.....	208
Table 6-8. The α -values predicted for the Level II sites using the models developed on Benchmarking data and the original Clocaenog and Kershope values. Standard deviation in brackets.	208
Table 6-9. Models to predict α -values derived using data from felled Benchmarking sites.	212
Table 6-10. Values of the radial density model coefficients based on the models built on the data from felled Benchmarking sites for the three Level II sites.	212
Table 6-11. The mean α -values of radial density model reparameterised on the Level II data. The model was fitted to each site individually. The α -values have been adjusted to predict density directly as kg/m^3	214
Table 6-12. Bias in different levels of the selected final radial density model with weights and ARMA autocorrelation structure added. The model was fitted separately to each site.	216
Table 6-13. Distribution of sample disks from Loch Tummel and Coalburn sites to different azimuthal directions and height classes.....	227
Table 6-14. Variance components of the area-weighted density data when the nested structure of the data was allowed for.	232
Table 6-15. Variance components for the ring density data when the mixed effect model was fitted without explanatory variables.....	232
Table 6-16. The effect of height in the different fractions of area-weighted density data from the Loch Tummel and Coalburn sites.....	233

Table 6-17. Weather variables included in the climate influence analysis at the Level II sites.....	234
Table 6-18. Diagnostic values for the different tree ring variable chronologies from Loch Tummel and Coalburn sites	236
Table 6-19. Correlation between mean temperature and the rainfall of the period for Loch Tummel site.....	256
Table 6-20. Correlations between the site average tree ring chronologies of the Loch Tummel site. Level of significance ($\alpha=0.05$) is 0.348.	256
Table 6-21. Correlation between temperature and the rainfall of the period for the Coalburn site. For periods longer than one month the temperature sum (base 5°C) was used. Significant correlations ($\alpha=0.05$) in italics.....	270
Table 6-22. Correlations between the detrended mean site tree ring chronologies for the Coalburn site. Level of significance ($\alpha = 0.05$) is 0.377.....	270
Table 6-23. Significant correlations ($\alpha'=0.05$) between ring indices and weather variables of the current year at the Loch Tummel and Coalburn sites. The sign in front of the ring variable indicates the direction of the correlation. Correlations common to both sites are highlighted in bold.	272
Table 6-24. Significant correlations ($\alpha'=0.05$) between ring indices and weather variables of the previous year at the Loch Tummel and Coalburn sites. The sign in front of the ring variable indicates the direction of the correlation. Correlations common to both sites are highlighted in bold.	273
Table 6-25. Tree ring – climate variable pairs with significant correlations under Bonferroni correction for multiple comparisons ($\alpha' = 0.0009$).	274
Table 7-1. Average MoE values for the studied sites and the p-value for the difference. Standard deviation is reported in the brackets.	299
Table 7-2. Average MoE for different trees social classes. The standard deviations are reported in the brackets and the letters mark differences between classes within site ($\alpha 0.05$).	299
Table 7-3. Juvenile wood MoE for different trees social classes. The standard deviations are reported in the brackets and the letters mark differences between classes within site ($\alpha 0.05$) when tested with analysis of variance.....	299
Table 7-4. Coefficients for the explanatory variables in the average MoE models.....	305
Table 7-5. The final models derived for Juvenile wood MoE at Coalburn and Loch Awe sites.....	309
Table 7-6. The outerwood stiffness models.	312
Table 7-7. Average speed models.	314
Table 7-8. Average model coefficients of the radial stiffness model for Coalburn, Loch Awe and data pooled from both sites. Standard error in the brackets.	318
Table 7-9. Models for the a parameter for Coalburn and Loch Awe. The values of a were derived keeping b fixed at its average value for each site.....	322
Table 7-10. Models for the d parameter for Coalburn and Loch Awe. The values of d were derived keeping b fixed at its average value for each site.....	322
Table 7-11. Models for the d parameter for Coalburn and Loch Awe. The values of d were derived keeping a and b fixed at its average value for each site.	323
Table 7-12. A model for predicting the sum of a and d parameters (a+d). The a and d parameters were derived holding b fixed at its average value at each site.	323
Table 7-13. A model for the b parameter for the Coalburn and Loch Awe site. The values of b were derived holding a and d fixed to their average values at each site.....	324

List of Figures

Figure 1-1. Microscope view of Sitka spruce earlywood tracheids with wide lumina and narrow latewood tracheids. The red scale bar is 50 μm .	32
Figure 1-2. Formation of juvenile wood (brown) and mature wood within a stem.	35
Figure 1-3. Sitka spruce plantations extending into distance on the hill sides near Crianlarich.	37
Figure 1-4. Numbered trees at a Benchmarking plot.	50
Figure 2-1. Sample preparation for the density analysis. Disks drying in the kiln (top). Drawing the radial section cutting patterns on the disks (middle). Some cut radial sections (bottom).	52
Figure 2-2. Left: a milled increment core sample on a purpose made sample holder. Right: Sample strips ready for analysis on the ITRAX X-ray densitometer.	53
Figure 2-3. Wood samples mounted on needles on the ITRAX sample rack. The rack will move forward to bring each needle in turn in front of the x-ray beam. To scan each sample the rack lifts up step by step as defined by the step size.	54
Figure 2-4. ITRAX greyscale image.	54
Figure 2-5. WinDENDRO ring density profile. Earlywood boundary (arrow) is set to 50% of the slope from minimum density at the beginning of the growing season and the maximum latewood density at the end of the ring. The green line marks the end of annual ring.	55
Figure 2-6. A section of analysed WinDENDRO image with two paths on it. The type of path used was a multisegment path that allows the reorientation of the path if the ring direction changes as can be seen in the upper part of the sample.	56
Figure 3-1. Brushes inside ITRAX chamber that separate the samples from outside air conditions.	58
Figure 3-2. Schematic presentation (top view inside the ITRAX chamber) of a sample facing 90 degrees to the X-ray beam (dashed red line). The samples were then turned to the right with respect to the X-ray beam direction to obtain angles 91-105° and for consistency angles 88 and 89° were scanned as well, turning the samples to the left. Throughout, the samples were held straight in the vertical direction.	60
Figure 3-3. The setup of samples (side view to the samples holders) to quantify the potential variation caused by tilting the sample in vertical direction or placing it slightly nearer to the X-ray beam (Front). Normal analysis conditions (Vertical) functioned as the point of comparison.	61
Figure 3-4. Variation in ring density during different scans (A-H)	64
Figure 3-5. Variation in path average density against relative humidity of the run.	65
Figure 3-6. Variation in ring width during ITRAX scans under different relative humidity.	69
Figure 3-7. Variation in total path length with humidity.	70
Figure 3-8. Variation in the ring density due to the differences in the path location. Average across the paths marked with the dashed red line.	73
Figure 3-9. Ring density plotted for the 3 radii analysed in vertical position at the different angles.	74
Figure 3-10. Influence of sample angle on the ring density of the vertically tilted radii.	75
Figure 3-11. Influence of sample positioning on the ring density at 90° angle to the beam.	75
Figure 3-12. Influence of analysis angle on the average density of samples mounted vertically (left) and tilted (right). Dashed lines are the LOWESS curves.	76
Figure 3-13. Comparison between vertical and tilted samples at different analysis angles. Dashed lines are the LOWESS curves.	76
Figure 3-14. Calculated length of the path that x-ray beam travels through the sample strips at different angles (left) and the resulting percent increase in the path length due to the angle (right). The dashes vertical line marks the 95 degree sample angle which is	

considered the upper limit below which the sample angles should lie in normal operating conditions.	77
Figure 3-15. Sample widths determined by the four different measurements. Sample width was measured at one centimetre intervals along the samples strips and each measurement point was numbered. Sample widths were calculated using measurements starting from the end of the sample (Bark), one centimetre from the edge (1 cm) and derived by averaging odd (Odd) or even (Even) numbered measurements. Dashed line represents the mean across the methods.	78
Figure 3-16. ITRAX wood density plotted against the oven dry gravimetric density.	79
Figure 3-17. ITRAX density plotted against gravimetric density at moisture content of a typical scan.	80
Figure 3-18. Moisture contents of the samples in room and ITRAX chamber conditions.	81
Figure 4-1. Road leading to the Griffin experimental site where the dendrometer experiment was established in April 2008.	87
Figure 4-2. Point dendrometer on a tree at the Griffin site, Aberfeldy, Scotland.	88
Figure 4-3. Location of the dendrometer trees and soil moisture probes on the sample plot established at the Griffin site.	89
Figure 4-4. Graphical illustration of the shrinkage (S), recovery (R) and increment (I) phases defined by Downes et al. (1999). Shrinkage will take place from previous day maxima (dashed line) until the afternoon minima. This is followed by a recovery phase which is considered to last until the radius reached the maximum value of the previous day and any increase after that is recorded as radial increment.	90
Figure 4-5. Influence of thermal expansion of wood and thermal expansion of stainless steel on the dendrometer measurements.	90
Figure 4-6. Modified medical needles used to take the microcore samples (left). A microcore and a biocassette used in the paraffin impregnation (right).	91
Figure 4-7. Microcore samples from the Griffin site were cut into thin sections with a rotary microtome (left), lifted out of a water bath (middle) and collected on albumin coated microscope slides that were placed on a hotplate (right).	92
Figure 4-8. Coloured thin sections of Griffin microcores (left). Stained thin section observed under polarised light (right). Earlywood going through the wall thickening stage was characterised by glowing (arrow). Scale bar is 50 μm	93
Figure 4-9. The residuals of LVDT measurements and thermal expansion corrected data for each of the studied trees (left) and the frequency distribution of the residual (right). ...	94
Figure 4-10. Air temperature (black) and relative humidity (blue) for the Griffin site (1st April 2008-13th January 2009) are shown in the top part of the graph. Soil moisture is plotted in the middle graph, where the black line illustrates the mean and the grey area measurements by the individual soil moisture probes. Radial growth detected by the LVDTs is shown at the bottom. LVDTs were fitted as follows; id 1 = tree 48, id 2 = tree 43, id 3 = tree 8, id 4 = tree 15 and id 5 = tree 66.	95
Figure 4-11. Latewood from previous year glowing under polarised light. Shrinkage is visible at the cambial region resulting into a funnel shape. Scale bar 100 μm	96
Figure 4-12. The tree growth measured on microcore samples compared to the growth detected by the LVDT dendrometers at different stages of the growing season.	98
Figure 4-13. Measured ring width for 2008 by ITRAX, microcore and LVDT. The pixel based ITRAX data were modified to remove high density values in the beginning of the ring and decreasing density values at the end of the ring that result from the ring boundary definition. This caused the two ITRAX based readings to differ.	99
Figure 4-14. Comparison of the temperature data measured at the Griffin site with the Met Office Aberfeldy Dull weather station.	100
Figure 4-15. Monthly increments measured by the dendrometers during the 2008.	101
Figure 4-16. Forty day moving correlation between daily mean temperature from the flux tower measurements and daily radial increments in the dendrometer trees.	103

Figure 4-17. Forty day moving correlation between daily mean temperature from the datalogger measurements and daily radial increments in the dendrometer trees.....	103
Figure 4-18. Forty day moving correlation between daily mean air humidity from the datalogger measurements and daily radial increments in the dendrometer trees.....	104
Figure 4-19. Forty day moving correlation between daily rainfall (mm) and daily radial increments in the dendrometer trees.	105
Figure 4-20. Forty day moving correlation between daily volumetric soil moisture (Edinburgh University) and daily radial increments in the dendrometer trees.....	106
Figure 4-21. Forty day moving correlation between daily soil moisture % (datalogger setup) and daily radial increments in the dendrometer trees.....	107
Figure 4-22. Forty day moving correlation between daily mean surface soil (depth 2.5 cm) temperature and daily radial increments in the dendrometer trees.	108
Figure 4-23. Forty day moving correlation between daily mean soil temperature in the lower part of the profile (depth 20-40 cm depending on the sampling location) and daily radial increments in the dendrometer trees.	109
Figure 4-24. Forty day moving correlation between daily mean internal bole temperature at 0.5 m height and daily radial increments in the dendrometer trees.	110
Figure 4-25. Forty day moving correlation between daily mean surface bole temperature at 0.5 m height and daily radial increments in the dendrometer trees.	111
Figure 4-26. Forty day moving correlation between daily mean wind speed (m/s) and daily radial increments in the dendrometer trees.	112
Figure 4-27. Forty day moving correlation between daily mean PPFDd diffuse radiation above canopy ($\mu\text{mol}/\text{m}^2/\text{s}$) and daily radial increments in the dendrometer trees.	112
Figure 4-28. Forty day moving correlation between daily mean global incoming PPFDg above canopy ($\mu\text{mol}/\text{m}^2/\text{s}$) and daily radial increments in the dendrometer trees.	113
Figure 4-29. Forty day moving correlation between daily mean global incoming shortwave radiation RG (W/m^2) and daily radial increments in the dendrometer trees.....	113
Figure 4-30. Monthly precipitation and mean temperature (dashed line) at the Griffin site 2008.....	114
Figure 4-31. Inter correlations between climate variables tested with the forty day moving correlation window. Continued on following pages.	115
Figure 4-32. Inter correlations between climate variables tested with the forty day moving correlation window. Continued above and on following pages.....	116
Figure 4-33. Inter correlations between climate variables tested with the forty day moving correlation window. Continued above and on following pages.....	116
Figure 4-34. Inter correlations between climate variables tested with the forty day moving correlation window. Continued above and the following page.....	117
Figure 4-35. Inter correlations between climate variables tested with the forty day moving correlation window. Continued from above.....	117
Figure 4-36. Density profiles for the 2008 growing season for the monitored trees at the Griffin site. Density values were defined at 4% moisture content.....	119
Figure 4-37. Comparison of the key weather variables during the estimated period of intra annual density band formation in trees 48, 43 and 8 and the surrounding weeks. The curves were smoothed with a three day moving median for easier observation.	121
Figure 4-38. The ITRAX density (black) and day of the year (DOY) in tree 48 plotted against the respective radial increment. The dendrometer measurements were smoothed with a LOWESS curve (blue) and the original measurements showing the diurnal variation are plotted in red. The black arrow indicates the onset of latewood formation.....	122
Figure 4-39. The ITRAX density (black) and day of the year (DOY) in tree 43 plotted against the respective radial increment. The dendrometer measurements were smoothed with a LOWESS curve (blue) and the original measurements showing the diurnal variation are plotted in red. The black arrow indicates the onset of latewood formation.....	122
Figure 4-40. The ITRAX density (black) and day of the year (DOY) in tree 8 plotted against the respective radial increment. The dendrometer measurements were smoothed	

with a LOWESS curve (blue) and the original measurements showing the diurnal variation are plotted in red. The black arrow indicates the onset of latewood formation.	123
Figure 4-41. The ITRAX density (black) and day of the year (DOY) in tree 15 plotted against the respective radial increment. The dendrometer measurements were smoothed with a LOWESS curve (blue) and the original measurements showing the diurnal variation are plotted in red. The black arrow indicates the onset of latewood formation.	123
Figure 4-42. The ITRAX density (black) and day of the year (DOY) in tree 66 plotted against the respective radial increment. The dendrometer measurements were smoothed with a LOWESS curve (blue) and the original measurements showing the diurnal variation are plotted in red. The black arrow indicates the onset of latewood formation.	124
Figure 5-1. Map showing the locations of the Benchmarking experiment sampling sites.	131
Figure 5-2. Ring density (left) and ring width (right) data at 4 % moisture content from all the Benchmarking sites plotted against ring number. LOWESS curve marked with a dashed red line.	137
Figure 5-3. Average ring densities plotted against the average ring widths for different dominance groups in Table 5-3.	138
Figure 5-4. Relationship between ring width and ring density in the mature part of the radius (ring number >10) for all the Benchmarking sites. Red line is the LOWESS curve fitted to the data.	139
Figure 5-5. Cross-section average density, juvenile wood density and mature wood density determined at 4% moisture content at the Benchmarking sites. Dashed grey line marks the mean across the sites.	140
Figure 5-6. Area-weighted density of different dominance classes at thinned (left) and unthinned (right) sites. The mean is marked with a dashed grey line. Density determined at 4% moisture content.	141
Figure 5-7. Shape of ring width curves at thinned (top) and unthinned (bottom) benchmarking sites. Dashed lines mark the LOWESS curves for each dominance quartile.	143
Figure 5-8. Influence of thinning on ring widths and ring density (MC 4 %) averaged for the cambial age across the thinned or unthinned Benchmarking sites.	143
Figure 5-9. Influence of the site factors on the cross-section average density. In the experimental design YC -1 denotes sites with yield class <14 m ³ /ha/yr and YC 1 yield class > 14 m ³ /ha/yr. Elev -1 is elevation under 280 m and Elev 1 elevation >280 m. East -1 <300 km east from the OS Grid datum and East 1 >300 km. North -1 is sites with <600 km north from OS Grid datum and North 1 >600 km. Spacing -1 signifies a stocking of <2500 stems/ha Spacing 1 >2500 stems/ha. Thinning -1 indicates no thinning and Thinning 1 that thinning has been carried out.	144
Figure 5-10. Two-way interactions influencing the cross-section average density in the Benchmarking experiment. In the experimental design YC -1 denotes sites with yield class <14 m ³ /ha/yr and YC 1 yield class > 14 m ³ /ha/yr. Elev -1 is elevation under 280 m and Elev 1 elevation >280 m. East -1 <300 km east from the OS Grid datum and East 1 >300 km. North -1 is sites with <600 km north from OS Grid datum and North 1 >600 km. Spacing -1 signifies a stocking of <2500 stems/ha Spacing 1 >2500 stems/ha. Thinning -1 indicates no thinning and Thinning 1 that thinning has been carried out.	145
Figure 5-11. Histograms to illustrate the spread of sites in relation to the some of the factors in the original factorial design. Vertical red line marks the level divide.	146
Figure 5-12. DBH variation between-sites from different yield class levels in the factorial design. Mean for the sites within a factor level is indicated with the dashed grey line.	147
Figure 5-13. Relationship between the yield class factor levels and yield classes estimated from the ESC data.	147
Figure 5-14. Relationship between original stocking obtained from the database and stand density calculated for the unthinned sites from the field data.	148

Figure 5-15. Diagnostic plots (left) and model predictions against the measured data for the model using the continuous variables of the original factors (excluding yield class).	149
Figure 5-16. Diagnostic plots (left) and model predictions plotted against measured data (right) for the growth rata model developed using the original factors as continuous variables (excluding yield class).	150
Figure 5-17. Selected correlated variables in the Benchmarking data.	151
Figure 5-18. Influence of site and tree variables on juvenile wood density. Density and ring width were measured at 4% moisture content. Dashed red line is the LOWESS curve fitted to the data and the solid grey line is the linear regression.	152
Figure 5-19. Random effects affecting the intercept once no model was fitted (left) and when the final model was fitted (right).	153
Figure 5-20. Diagnostic plots for the final model for predicting average juvenile wood density (left). Predictions of the final juvenile wood density model (right) plotted against the measured values. Red dashed line shows the regression line fitted to the data.	154
Figure 5-21. Influence of tree and stand variables on the mature wood density (determined at 4% moisture content).	155
Figure 5-22. Random effects for mature wood when no model (left) and when the final model was fitted (right).	156
Figure 5-23. Diagnostic plots for the final mature wood density model (left). Predicted mature wood density plotted against the measured density (right).	157
Figure 5-24. Influence of tree and site variables on the outerwood density (determined at 4% moisture content).	158
Figure 5-25. Diagnostic plots for the final outerwood density model (left). Measured outerwood density plotted against the predicted density. Dashed red line is the regression line drawn to the data (right).	158
Figure 5-26. Random effects in outerwood average density when no model (left) and the final model (right) was fitted to the data.	159
Figure 5-27. Influence of site and tree variables on the cross-section average density (determined at 4% moisture content). Dashed red line is the LOWESS curve fitted to the data and solid grey line linear regression.	160
Figure 5-28. Average wood density random effects when no model (left) and final model (right) were fitted to the data.	161
Figure 5-29. Diagnostic plots for the final cross-section average density model (left). Final cross-section average density model prediction plotted against the measured data (right).	162
Figure 5-30. Influence of site and tree variables on cross-section average density (MC 4%) at thinned and unthinned Benchmarking sites.	163
Figure 5-31. Diagnostic plots for the models developed for the dataset split according the thinning treatment.	165
Figure 5-32. Density, determined at 4% moisture content, plotted against the ring number for different social classes of trees. Dashed line is the LOWESS curve fitted to the data.	166
Figure 5-33. Influence of site and tree variables on density in dominant trees. Dominance was calculated by DBH/stand mean DBH and the upper quartile of dominance values were considered as dominant trees. Grey line is the regression line fitted to the data and the dashed red line is the lowess curve.	167
Figure 5-34. Influence of site and tree variables on density in co-dominant trees. Dominance was calculated by DBH/stand mean DBH and the 2nd quartile of dominance values were considered as co-dominant trees. Grey line is the regression line fitted to the data and dashed red line is the lowess curve.	167
Figure 5-35. Influence of site and tree variables on density in non-dominant trees. Dominance was calculated by DBH/stand mean DBH and the 3rd quartile of dominance values were considered as non-dominant trees. Grey line is the regression line fitted to the data and the dashed red line is the lowess curve.	168

Figure 5-36. Influence of site and tree variables on density in suppressed trees. Dominance was calculated by DBH/stand mean DBH and the lowest quartile of dominance values were considered as suppressed trees. Grey line is the regression line fitted to the data and the dashed red line is the lowess curve.	168
Figure 5-37. Diagnostic plots for cross-section average density models developed for different dominance classes of trees. ccc is the concordance correlation coefficient.	170
Figure 5-38. Influence of the measured variables on density at Northern Benchmarking sites.....	172
Figure 5-39. Influence of the measured variables on density at Southern Benchmarking sites.....	172
Figure 5-40. Diagnostic plots for the cross-section average density model developed for the Northern and Southern sites.	173
Figure 5-41. Model predictions against the measured values using Clocaenog (left) and Kershope (right) parameters. Dashed red line is the regression line fitted to the data, the R^2 -values for the regression were 0.34 and 0.30 for Clocaenog and Kershope parameters, respectively.	175
Figure 5-42. Lowess curves for each of the Benchmarking site plotted together.....	175
Figure 5-43. Within site variation in the ring density values at selected Benchmarking sites.	176
Figure 5-44. Density predictions for the reparameterised model plotted against the measured values. The dashed red line is the regression line fitted to the data. The R^2 -value for the regression was 0.48.....	176
Figure 5-45. Alpha values across the Benchmarking sites with the horizontal lines marking the mean values across Benchmarking experiment, at Kershope and Clocaenog sites.	178
Figure 5-46. Influence of site and tree variables on α_1 in the entire Benchmarking dataset. Dashed red line is the LOWESS curve fitted to the data and the solid grey line is the linear regression.	179
Figure 5-47. Diagnostic plots and fitted values plotted against measured values for α_1 modelled from the entire dataset (top) and separately for thinned (middle) and unthinned sites (bottom). On the right side dashed line is the linear regression line fitted to the data.	181
Figure 5-48. Influence of site and tree variables on the α_2 in the entire Benchmarking dataset. Dashed red line is the LOWESS curve fitted to the data and the solid grey line is the linear regression.	182
Figure 5-49. Diagnostic plots and fitted values plotted against measured data for models predicting α_2 from the entire dataset (top) and for thinned (middle) and unthinned (bottom) sites separately. On the right side dashed line is the linear regression line fitted to the data.	184
Figure 5-50. Influence of site and tree variables on the α_3 parameter. Dashed red line is the LOWESS curve fitted to the data and the solid grey line is the linear regression.	185
Figure 5-51. Diagnostic plots and predicted values plotted against measured values for models predicting α_3 from the entire dataset (top) and thinned (middle) and unthinned (bottom) sites separately. On the right side dashed line is the linear regression line fitted to the data.	187
Figure 5-52. The influence of site and tree variables on the α_1 values at the felled benchmarking sites. Solid black line is the regression line fitted to the data and the dashed red line the lowess curve.	189
Figure 5-53. The influence of site and tree variables on the α_2 values at the felled benchmarking sites. Solid black line is the regression line fitted to the data and the dashed red line the lowess curve.	190
Figure 5-54. The influence of site and tree variables on the α_3 values at the felled benchmarking sites. Solid black line is the regression line fitted to the data and the dashed red line the lowess curve.	190

Figure 5-55. Model predictions plotted against the measured data (left) and the diagnostic plots for the residuals (right).	192
Figure 6-1. Tree marked for felling at the Loch Tummel site. A window with bark removed cut at the breast height for grain angle assessment.	202
Figure 6-2. Schematic presentation of the locations where disks were extracted from trees with three sample disks (left) and from the subset of trees with five disks (right).	203
Figure 6-3. Radial density curves for the Level II sites.	207
Figure 6-4. Ring density model predictions for the Coalburn site using a) Clocaenog coefficients, b) Kershope coefficients, c) coefficients derived using the model based on the pooled Benchmarking data and d) using coefficients derived using a model developed for unthinned sites using the Benchmarking data. Dashed grey line is the regression line fitted to the data and ccc denotes the concordance correlation coefficient.	209
Figure 6-5. Ring density model predictions for the Loch Awe site using a) Clocaenog coefficients, b) Kershope coefficients, c) coefficients derived using the model based on the pooled Benchmarking data and d) using coefficients derived using a model developed for unthinned sites using the Benchmarking data. Dashed grey line is the regression line fitted to the data and ccc denotes the concordance correlation coefficient.	210
Figure 6-6. Ring density model predictions for the Loch Tummel site using a) Clocaenog coefficients, b) Kershope coefficients, c) coefficients derived using the model based on the pooled Benchmarking data and d) using coefficients derived using a model developed for thinned sites using the Benchmarking data. Dashed grey line is the regression line fitted to the data and ccc denotes the concordance correlation coefficient.	211
Figure 6-7. Ring density model predictions when using sub-models from felled Benchmarking sites to derive site specific model coefficients. Dashed grey line is the regression line fitted to the data and ccc notes the concordance correlation coefficient between the measured and predicted densities.	213
Figure 6-8. Autocorrelation in the ring density data from the three Level II sites prior to fitting an autocorrelation function (left) and once ARMA autocorrelation function was added (right). The dashed line marks the level of significance (0.05).	215
Figure 6-9. Model residuals (kg/m^3) plotted against ring number (top) and ring width (bottom).	216
Figure 6-10. Radial density model predictions plotted against the measured values (left) and model diagnostics plots (right) for each of the Level II sites. The radial density model was fitted separately for each site and weights and ARMA autocorrelation structure added.	217
Figure 6-11. Random effect plots for the alpha values at each of the Level II sites. These illustrate how individual trees differ from the site average values for the coefficients.	218
Figure 6-12. The predictions of the average juvenile wood density model derived from the Benchmarking data plotted against the measured values at the level II sites (left) Dashed gray line is the regression line fitted to the data and ccc denotes the concordance correlation coefficient. Model diagnostics plot (right).	219
Figure 6-13. Juvenile wood density model predictions against the measured values separately for each of the Level II sites. Dashed gray line is the regression line fitted to the data and ccc denotes the concordance correlation coefficient.	219
Figure 6-14. The predictions of the average mature wood density model derived from the Benchmarking data plotted against the measured values at the level II sites (left) Dashed gray line is the regression line fitted to the data and ccc denotes the concordance correlation coefficient. Residuals (measured-predicted density) plotted against density (right).	220
Figure 6-15. Mature wood density model predictions against the measured values, separately for each of the Level II sites. Dashed gray line is the regression line fitted to the data and ccc denotes the concordance correlation coefficient.	221

Figure 6-16. The predictions of the cross-section average wood density model derived from the Benchmarking data plotted against the measured values at the level II sites (left). Residuals (measured-predicted density) plotted against density (right).	222
Figure 6-17. Cross-section average wood density model predictions against the measured values separately for each of the Level II sites. Dashed gray line is the regression line fitted to the data and ccc denotes the concordance correlation coefficient.	222
Figure 6-18. Predictions of the average density model developed for unthinned sites from Benchmarking data plotted against the measured values at the Coalburn and Loch Awe sites. Dashed gray line is the regression line fitted to the data and ccc denotes the concordance correlation coefficient.	223
Figure 6-19. Predictions of the average density model developed for thinned sites from Benchmarking data plotted against the measured values at the Loch Tummel site. Dashed gray line is the regression line fitted to the data and ccc denotes the concordance correlation coefficient.	224
Figure 6-20. The prediction of cross-section average density models developed for different dominance classes from the Benchmarking data plotted against the measured density values for the social classes from the three Level II sites. Dashed gray line is the regression line fitted to the data and ccc denotes the concordance correlation coefficient.	225
Figure 6-21. The predictions of cross-section average density model developed for northerly and southerly sites (dividing line as grid ref 650 000) against the measured density values. Coalburn qualified as a southern site whereas the Loch Awe and Loch Tummel data were pooled for the northern site predictions. Dashed gray line is the regression line fitted to the data and ccc denotes the concordance correlation coefficient.	226
Figure 6-22. Density (at 4% MC) plotted against ring number for each disk taken at proportional heights along the stem from Coalburn (CB) and Loch Tummel (LT) sites. Dashed red lines are the LOWESS curves fitted to the data.	228
Figure 6-23. Ring width plotted against ring number for disks taken at proportional heights along the stem. Dashed red line is the LOWESS curve fitted to the data.	228
Figure 6-24. Changes in sample area-weighted density with disk height for the two sites. Density values are derived at 4% moisture content. Dashed grey line indicates the average for the site.	229
Figure 6-25. Variation in juvenile wood density with disk height at the two sites. Density was determined at 4% moisture content. Dashed grey line indicates the mean for each site.	230
Figure 6-26. Influence of azimuthal direction on the radius length and sample area-weighted density. Density and ring width were determined at 4% moisture content. Dashed grey line indicates the mean for each site.	231
Figure 6-27. Examples (two trees from the Loch Tummel site) of the detrending procedure with a spline function in dplr package.	234
Figure 6-28. Raw ring width and density data pooled from the three Level II sites. Dashed grey line represents the LOWESS curve fitted to the data.	235
Figure 6-29. Detrended tree ring variables plotted against the ring number for the Loch Tummel site. Dashed red line is LOWESS curve fitted to the data.	235
Figure 6-30. Ring density (top) and width (bottom) indices for Loch Tummel and Coalburn plotted against calendar year. Solid red line represents the mean site chronology.	237
Figure 6-31. Earlywood (top) and latewood (bottom) width indices for Loch Tummel and Coalburn plotted against calendar year. Solid red line represents the mean site chronology.	238
Figure 6-32. Earlywood (top) and latewood (bottom) density indices for Loch Tummel and Coalburn plotted against calendar year. Solid red line represents the mean site chronology.	238

- Figure 6-33. Latewood percentage (top) indices and maximum (middle) and minimum (bottom) density indices plotted against calendar year. Solid red line represents the mean site chronology.....239
- Figure 6-34. Examples of auto-correlation detected in the Loch Tummel weather variables. Dashed line corresponds to $r=0.335$241
- Figure 6-35. Remaining autocorrelation in the average tree ring chronologies at the Loch Tummel site.....242
- Figure 6-36. Loch Tummel tree ring width indices plotted against the individually significant weather variables for the current year. Solid line represents the tree ring width indices and the dashed red line the weather variable in question. Horizontal line marks the reference level for the tree ring width indices. The P-value reported refers to individual comparisons. The selected α -level was 0.05. To achieve an overall α -level of 0.05 the limit for individual comparisons would be adjusted (Curtin and Schulz, 1998) to approximately 0.0009.....243
- Figure 6-37. Loch Tummel tree ring width indices plotted against the individually significant weather variables for the previous year. Solid line represents the tree ring width indices and the dashed red line the weather variable in question. Horizontal line marks the reference level for the tree ring width indices. The P-value reported refers to individual comparisons. The selected α -level was 0.05. To achieve an overall α -level of 0.05 the limit for individual comparisons would be adjusted (Curtin and Schulz, 1998) to approximately 0.0009.....244
- Figure 6-38. Loch Tummel tree ring density indices plotted against the individually significant weather variables of the current year. Solid line represents the tree ring density indices and the dashed red line the weather variable in question. Horizontal line marks the reference level for the tree ring density indices. P-value reported refers to individual comparisons. The selected α -level was 0.05. To achieve over all α -level of 0.05 the limit for individual comparisons would be adjusted (Curtin and Schulz, 1998) to approximately 0.0009.....245
- Figure 6-39. Loch Tummel tree ring density indices plotted against the individually significant previous year weather variables. Solid line represents the tree ring density indices and the dashed red line the weather variable in question. Horizontal line marks the reference level for the tree ring density indices. P-value reported refers to individual comparisons. The selected α -level was 0.05. To achieve over all α -level of 0.05 the limit for individual comparisons would be adjusted (Curtin and Schulz, 1998) to approximately 0.0009.....246
- Figure 6-40. Loch Tummel earlywood density (EWD) indices plotted against the individually significant current and previous year weather variables. Solid line represents the earlywood density indices and the dashed red line the weather variable in question. Horizontal line marks the reference level for the earlywood density indices. P-value reported refers to individual comparisons. The selected α -level was 0.05. To achieve over all α -level of 0.05 the limit for individual comparisons would be adjusted (Curtin and Schulz, 1998) to approximately 0.0009.247
- Figure 6-41. Loch Tummel earlywood width (EWW) indices plotted against the individually significant weather variables of the current and previous year. Solid line represents the earlywood width indices and the dashed red line the weather variable in question. Horizontal line marks the reference level for the earlywood width indices P-value reported refers to individual comparisons. The selected α -level was 0.05. To achieve over all α -level of 0.05 the limit for individual comparisons would be adjusted (Curtin and Schulz, 1998) to approximately 0.0009.248
- Figure 6-42. Loch Tummel latewood density (LWD) indices plotted against the individually significant weather variables of the current year. Solid line represents the latewood density indices and the dashed red line the weather variable in question. Horizontal line marks the reference level for the latewood density indices. P-value reported refers to individual comparisons. The selected α -level was 0.05. To achieve over all α -level

of 0.05 the limit for individual comparisons would be adjusted (Curtin and Schulz, 1998) to approximately 0.0009. Continued next page.	249
Figure 6-43. Continued Loch Tummel latewood density (LWD) indices plotted against the individually significant weather variables of the current year continued.	250
Figure 6-44. Loch Tummel latewood density (LWD) indices plotted against the individually significant weather variables of the previous year. Solid line represents the latewood density indices and the dashed red line the weather variable in question. Horizontal line marks the reference level for the latewood density indices. P-value reported refers to individual comparisons. The selected α -level was 0.05. To achieve over all α -level of 0.05 the limit for individual comparisons would be adjusted (Curtin and Schulz, 1998) to approximately 0.0009.....	250
Figure 6-45. Loch Tummel latewood width (LWW) indices plotted against the individually significant weather variables of the previous year. Solid line represents the latewood width indices and the dashed red line the weather variable in question. Horizontal line marks the reference level for the latewood width indices. P-value reported refers to individual comparisons. The selected α -level was 0.05. To achieve over all α -level of 0.05 the limit for individual comparisons would be adjusted (Curtin and Schulz, 1998) to approximately 0.0009.....	251
Figure 6-46. Loch Tummel latewood percentage (LW%) indices plotted against the individually significant weather variables of the current and previous year. Solid line represents the latewood percentage indices and the dashed red line the weather variable in question. Horizontal line marks the reference level for latewood percentage indices. P-value reported refers to individual comparisons. The selected α -level was 0.05. To achieve over all α -level of 0.05 the limit for individual comparisons would be adjusted (Curtin and Schulz, 1998) to approximately 0.0009.	252
Figure 6-47. Loch Tummel maximum density (MaxD) indices plotted against the individually significant weather variables of the current year. Solid line represents the maximum density indices and the dashed red line the weather variable in question. Horizontal line marks the reference level for the maximum density indices. P-value reported refers to individual comparisons. The selected α -level was 0.05. To achieve over all α -level of 0.05 the limit for individual comparisons would be adjusted (Curtin and Schulz, 1998) to approximately 0.0009. Continued next page.	253
Figure 6-48. Continued Loch Tummel maximum density (MaxD) indices plotted against the individually significant weather variables of the current year continued.	254
Figure 6-49. Loch Tummel maximum density (MaxD) indices plotted against the individually significant weather variables of the previous year. Solid line represents the maximum density indices and the dashed red line the weather variable in question. Horizontal line marks the reference level for the maximum density indices. P-value reported refers to individual comparisons. The selected α -level was 0.05. To achieve over all α -level of 0.05 the limit for individual comparisons would be adjusted (Curtin and Schulz, 1998) to approximately 0.0009.	255
Figure 6-50. Loch Tummel minimum density (MinD) indices plotted against the individually significant weather variables of the current and previous year. Solid line represents the minimum density indices and the dashed red line the weather variable in question. Horizontal line marks the reference level for the minimum density indices. P-value reported refers to individual comparisons. The selected α -level was 0.05. To achieve over all α -level of 0.05 the limit for individual comparisons would be adjusted (Curtin and Schulz, 1998) to approximately 0.0009.	255
Figure 6-51. Selected cross-correlograms between climate and tree ring variables from the Loch Tummel site.	257
Figure 6-52. Non optimal detrending that occurred in some Loch Tummel samples that had a peculiar radial ring width pattern due to change in growth rate around ring 20-21.....	258
Figure 6-53. Remaining autocorrelation in the average tree ring chronologies at the Coalburn site.	259

- Figure 6-54. Coalburn ring width (RW) indices plotted against the individually significant weather variable of the current year. Solid line represents the tree ring width indices and the dashed red line the weather variable in question. Horizontal line marks the reference level for the tree ring width indices. P-value reported refers to individual comparisons. The selected α -level was 0.05. To achieve over all α -level of 0.05 the limit for individual comparisons would be adjusted (Curtin and Schulz, 1998) to approximated 0.0009.....260
- Figure 6-55. Coalburn ring density (RD) indices plotted against the individually significant weather variables of the current year. Solid line represents the tree ring density indices and the dashed red line the weather variable in question. Horizontal line marks the reference level for the tree ring density indices. P-value reported refers to individual comparisons. The selected α -level was 0.05. To achieve over all α -level of 0.05 the limit for individual comparisons would be adjusted (Curtin and Schulz, 1998) to approximately 0.0009.....261
- Figure 6-56. Coalburn ring density (RD) indices plotted against the individually significant weather variables of the previous year. Solid line represents the tree ring density indices and the dashed red line the weather variable in question. Horizontal line marks the reference level for the tree ring density indices. P-value reported refers to individual comparisons. The selected α -level was 0.05. To achieve over all α -level of 0.05 the limit for individual comparisons would be adjusted (Curtin and Schulz, 1998) to approximately 0.0009.....261
- Figure 6-57. Coalburn earlywood density (EWD) indices plotted against the individually significant weather variables of the current and previous year. Solid line represents the earlywood density indices and the dashed red line the weather variable in question. Horizontal line marks the reference level for the earlywood density indices. P-value reported refers to individual comparisons. The selected α -level was 0.05. To achieve over all α -level of 0.05 the limit for individual comparisons would be adjusted (Curtin and Schulz, 1998) to approximately 0.0009.262
- Figure 6-58. Coalburn earlywood width (EWW) indices plotted against the individually significant weather variables of the current year. Solid line represents the earlywood width indices and the dashed red line the weather variable in question. Horizontal line marks the reference level for the earlywood width indices. P-value reported refers to individual comparisons. The selected α -level was 0.05. To achieve over all α -level of 0.05 the limit for individual comparisons would be adjusted (Curtin and Schulz, 1998) to approximated 0.0009.....263
- Figure 6-59. Coalburn latewood density (LWD) indices plotted against the individually significant weather variables of the current year. Solid line represents the latewood density indices and the dashed red line the weather variable in question. Horizontal line marks the reference level for the latewood density indices. P-value reported refers to individual comparisons. The selected α -level was 0.05. To achieve over all α -level of 0.05 the limit for individual comparisons would be adjusted (Curtin and Schulz, 1998) to approximately 0.0009.....264
- Figure 6-60. Coalburn latewood density (LWD) indices plotted against the individually significant weather variables of the previous year. Solid line represents the latewood density indices and the dashed red line the weather variable in question. Horizontal line marks the reference level for the latewood density indices. P-value reported refers to individual comparisons. The selected α -level was 0.05. To achieve over all α -level of 0.05 the limit for individual comparisons would be adjusted (Curtin and Schulz, 1998) to approximately 0.0009.....265
- Figure 6-61. Coalburn latewood width (LWW) indices plotted against the individually significant weather variables of the current and previous year. Solid line represents the latewood width indices and the dashed red line the weather variable in question. Horizontal line marks the reference level for the latewood width indices. P-value reported refers to individual comparisons. The selected α -level was 0.05. To achieve over all α -level of 0.05 the limit for individual comparisons would be adjusted (Curtin and Schulz, 1998) to approximately 0.0009.....266

Figure 6-62. Coalburn latewood percentage (LW%) indices plotted against the significant weather variables of the current year. Solid line represents the latewood percentage indices and the dashed red line the weather variable in question. Horizontal line marks the reference level for the latewood percentage indices. P-value reported refers to individual comparisons. The selected α -level was 0.05. To achieve over all α -level of 0.05 the limit for individual comparisons would be adjusted (Curtin and Schulz, 1998) to approximated 0.0009.....	267
Figure 6-63. Coalburn maximum density (MaxD) indices plotted against the individually significant weather variables of the current year. Solid line represents the maximum density indices and the dashed red line the weather variable in question. Horizontal line marks the reference level for the maximum density indices. P-value reported refers to individual comparisons. The selected α -level was 0.05. To achieve over all α -level of 0.05 the limit for individual comparisons would be adjusted (Curtin and Schulz, 1998) to approximately 0.0009.....	268
Figure 6-64. Coalburn maximum density (MaxD) indices plotted against the individually significant weather variables of the previous year. Solid line represents the maximum density indices and the dashed red line the weather variable in question. Horizontal line marks the reference level for the maximum density indices. P-value reported refers to individual comparisons. The selected α -level was 0.05. To achieve over all α -level of 0.05 the limit for individual comparisons would be adjusted (Curtin and Schulz, 1998) to approximately 0.0009.....	269
Figure 6-65. Coalburn minimum density (MinD) indices plotted against the individually significant weather variables of the current year. Solid line represents the minimum density indices and the dashed red line the weather variable in question. Horizontal line marks the reference level for the minimum density indices. P-value reported refers to individual comparisons. The selected α -level was 0.05. To achieve over all α -level of 0.05 the limit for individual comparisons would be adjusted (Curtin and Schulz, 1998) to approximately 0.0009.....	269
Figure 6-66. Selected cross-correlograms between climate and tree ring variables from the Coalburn site.	271
Figure 6-67. Raw (left) and prewhitened (right) precipitation variables plotted against latewood density form the Loch Tummel site. Dashed blue lines represent the level of significance for individual comparisons ($\alpha=0.05$). Dashed red line represents multiple comparisons (21) adjusted α' (0.761) that will give an overall α of 0.05.....	274
Figure 6-68. Raw (left) and prewhitened (right) precipitation variables plotted against maximum density form the Loch Tummel site. Dashed blue lines represent the level of significance for individual comparisons ($\alpha=0.05$). Dashed red line represents multiple comparisons (21) adjusted α' (0.761) that will give an overall α of 0.05.....	275
Figure 6-69. Initial autocorrelation in the weather variables that were significant at the Loch Tummel site.	275
Figure 6-70. Raw (left) and prewhitened (right) March precipitation and maximum temperature variables plotted against latewood density and maximum density form the Coalburn site. Dashed blue lines represent the level of significance for individual comparisons ($\alpha=0.05$). Dashed red line represents multiple comparisons (21) adjusted α' (0.761) that will give an overall α of 0.05.....	276
Figure 6-71. Initial autocorrelation in the weather variables that were significant at the Coalburn site.	277
Figure 7-1. Schematic representation of microfibril angle in the S2 layer of a xylem cell.	284
Figure 7-2. Illustration of the use of ST300 time-of-flight tool. The probes inserted into the stem and the wireless datalogger that will record the time required for the sound pulse to travel between the probes as the lower one is tapped with a hammer.	287
Figure 7-3. Ultrasonic scanner developed at the University of Canterbury, Christchurch, New Zealand analysing a radial sample of Sitka spruce.....	287

Figure 7-4. The influence of model coefficients a, b and d on the behaviour of the radial stiffness curve.....	289
Figure 7-5. Radial acoustic velocity (left) and density (right) data for the studied sites with a smoothing LOWESS curve in red.	290
Figure 7-6. Radial trend in acoustic velocity for each of the studied trees at two sites.	291
Figure 7-7. Radial trend in density for each of the studied trees at two sites.	292
Figure 7-8. Density and acoustic velocity curves for the tree number 20 from the Coalburn site. The dashed vertical line marks the end of juvenile wood (ring 10). A section of compression wood detectable in the North radius where acoustic velocity drops and density increases.	293
Figure 7-9. Radial profiles of density and acoustic velocity for the tree number 23 from the Coalburn site. The dashed vertical line marks the end of juvenile wood (ring 10).	294
Figure 7-10. Radial profiles of density and acoustic velocity for the tree number 49 from the Loch Awe site. The dashed vertical line marks the end of juvenile wood (ring 10)....	295
Figure 7-11. Radial profiles of density and acoustic velocity for tree number 50 from the Loch Awe site. The dashed vertical line marks the end of juvenile wood (ring 10).	296
Figure 7-12. LOWESS curves of density and acoustic velocity for all data (top) and for juvenile (middle) and mature wood (bottom) sections of the radius separately plotted as a function of distance from the pith (left) and ring number (ring). 10 th ring was considered as the limit between juvenile and mature wood.	297
Figure 7-13. Relationship between acoustic velocity, density and stiffness in the studied trees. The coloured area is defined by the values encountered in the data and the colours represent the scale of MoE.	298
Figure 7-14. Influence of tree social status on the shape of the radial stiffness curves plotted a function of distance from the pith. LOWESS curve fitted to the data drawn on graphs in red.	300
Figure 7-15. Influence of tree social status on the shape of the radial stiffness curves plotted as a function of ring number. LOWESS curve fitted to the data drawn on graphs in red.	300
Figure 7-16. Influence of azimuth on the shape if stiffness curves at the Coalburn site. LOWESS drawn in red.	301
Figure 7-17. Radial variation in the Stiffness with all directions plotted separately for both sites against the ring number.	301
Figure 7-18. Average speed (top), density (middle) and stiffness (bottom) for the each direction at the two sites.	302
Figure 7-19. 95% confidence intervals for the comparisons between directions in acoustic velocity, density and stiffness using analysis of variance with the Tukey HSD test. Top row presents the results for Coalburn and bottom for Loch Awe site.	303
Figure 7-20. The pooled stiffness data plotted against ring number (left) and distance from the pith (right). Dashed red line is the lowess curve fitted to the data.	304
Figure 7-21. Average stiffness model predictions against the measured data for all data (top), Coalburn (middle) and Loch Awe (bottom) including tree effect (left) and using average coefficients only (right). Dashed line is the regression line fitted to the data.	306
Figure 7-22. Tree specific random effects for the average stiffness model fits and diagnostic plots for Coalburn (top) and Loch Awe data (bottom).	307
Figure 7-23. MoE (circles) plotted against the explanatory variables included in the final model fitted to all acoustic data. Solid grey line represents the linear regression fitted to the data and dashed red line the LOWESS curve.	308
Figure 7-24 MoE (circles) plotted against the explanatory variables included in the final model fitted to the Coalburn data. Solid grey line represents the linear regression fitted to the data and dashed red line the LOWESS curve.	308
Figure 7-25. MoE (circles) plotted against the explanatory variables included in the final model fitted to the Loch Awe data. Solid grey line represents the linear regression fitted to the data and dashed red line the LOWESS curve.	308

Figure 7-26. Juvenile wood MoE model predictions plotted against the measured data for the 2 sites. In the graphs on the left the random effects were included whereas on the right the predictions were calculated using the fixed effects only. Dashed red line is the linear regression fitted to the data.	310
Figure 7-27. Tree specific random effects and juvenile wood MoE model diagnostic plots for Coalburn (top) and Loch Awe (bottom) sites.	311
Figure 7-28. Influence of the explanatory variables on juvenile wood stiffness at the Coalburn site.	311
Figure 7-29. Influence of the explanatory variable on the juvenile wood stiffness at the Loch Awe site.	312
Figure 7-30. Outerwood MoE model predictions against the measured value (top) and diagnostic plots on residuals (middle) and random effects (bottom).	313
Figure 7-31. Influence of selected explanatory variables in the final outerwood stiffness model developed for the Coalburn site (left) and Loch Awe (right). Regression line is marked in grey and lowess curve in red.	314
Figure 7-32. Tree average acoustic velocity model predictions against the measured data (top), model diagnostic plots (middle) and random effects (bottom).	315
Figure 7-33. Influence of the explanatory variables on the sample average acoustic velocity at Coalburn site.	316
Figure 7-34. Influence of the explanatory variables on the sample average acoustic velocity at the Loch Awe site.	316
Figure 7-35. Average radial stiffness curves for the Coalburn and Loch Awe sites plotted against the distance from the pith, mm (top) and ring number (bottom).	317
Figure 7-36. Average ring stiffness curves for the Coalburn and Loch Awe sites.	318
Figure 7-37. Radial Stiffness model predictions including tree effect (left) and using only fixed effects (right) for the Coalburn (top), Loch Awe (middle) and all data combined (bottom). Dashed line is the regression line fitted to the data and ccc is the concordance correlation coefficient.	319
Figure 7-38. Diagnostic plots for the radial stiffness model fitted to Coalburn (top), Loch Awe (middle) and all data combined (bottom).	320
Figure 7-39. Relationship between the dynamic MoE (GPa) measured with the ultrasonic scanner and the ST300 standing tree tool at the two sites. Dashed line is the one to one line and solid black line a regression line fitted to the data.	325
Figure 7-40. Relationship between ST300 standing tree MoE and juvenile wood MoE measured by the ultrasonic scanning method. On the top row juvenile MoE calculated from North sections only was plotted against the ST300 measurements. Dashed line is the linear regression line fitted to the data. R^2 values are not presented since the slope was insignificant.	326
Figure 7-41. Relationship between the juvenile wood stiffness and outerwood stiffness. Outerwood stiffness was calculated for the outermost 2 cm of the stem. A dashed line is the regression line fitted to the data.	326
Figure 7-42. Relationship between the acoustic velocity (km/s) measured with the ultrasonic scanner and the ST300 standing tree tool at the two sites. Dashed line is the one to one line and solid black line a regression line fitted to the data.	327

Acknowledgement

First of all I would like to thank the Forestry Commission and WestChem graduate school for making this PhD project possible by funding it. Many thanks to my supervisors Dr. Mike Jarvis (Glasgow University) and Prof. Barry Gardiner (Forest Research) for support and advice through the project. Regarding advice on the operation of ITRAX, use of WinDENDRO and sample processing I am thankful to Dr. Paul McLean and Dr. Clemens Altaner. I wish to thank Mr. Michael Beglan for solving countless technical issues of varied kinds throughout the PhD project.

I am grateful for the chance to collaborate with Dr. John Moore and Mr. Andrew Lyon from Edinburgh Napier University and for being able to take part in the benchmarking study designed by Dr. John Moore. Thanks to Gregory Searles for good spirited sampling company whilst collecting samples from the 64 benchmarking sites regardless of the rain and midges. Thanks to Shaun Mochan, Colin Campbell and Bill Riddick for felling trees for me at the Level II sites. For further help at the Level II sites I thank Dr. Clemens Altaner, Mr. Dave Auty, Mr. Michael Beglan, Dr. Annabelle Caron, Dr. Susan Fawley and Miss Mathilde Leonardon. Further thanks to Shaun, Dave and Miss Kate Beauchamp for help in cutting the disks. Special thanks to Graeme Johnstone and Chanisa Maneekul for processing and analysing samples from the Loch Tummel and Coalburn sites. This enabled me to include the height variation section to my thesis which would have otherwise been impossible due to time restrictions.

I'm greatly indebted to Dr. Axel Wellpott for help in setting up the dendrometer system, and for writing programmes for processing the raw data as well as help with the analysis. Many thanks also to Dr. Sigrid Dengel and Miss Kate Beauchamp for help with fieldwork at Griffin and in organising transport to get there. Furthermore, I wish to thank Dr. Rob Clement for the access to Edinburgh University monitoring data from the Griffin site. Warm thank you to Dr. Cyrille Rathgeber for the opportunity to analyse the Griffin microcore samples at the INRA Nancy laboratory and COST E50 for funding the trip.

I wish to thank Dr. Clemens Altaner, Dr Shakti Chauhan and Prof. John Walker for possibility of carrying out acoustic measurements at the University of Christchurch, New Zealand and COST E50 again for the funding for this visit.

For the help in regarding statistical analysis and learning to use the R software package I would like to thank Dr. John Moore. I also wish to thank Dr. Tom Connolly and Prof. Marian Scott for other statistical advice.

I would like to thank the Zonta-women (The Zonta Club of Helsinki II ry.) for the bursary that allowed me to take part on the tree ring course in Istanbul, Turkey. I thank the NFZ-summer school for the opportunity to take part on the Forest Modelling Course in Le Tholy France and for the bursary to cover the costs.

For receiving ESC data I would like to thank Dr. Duncan Ray. For Level II monitoring data I am thankful to Dr. Nadia Barsoum and Dr. Rona Pitman. For enabling an isotope pilot study at SUERC I thank Prof. Tony Fallick and Mr Terry Donnelly.

For general mental health and words of encouragement I would like to thank Pedro Molina Sanchez and my colleagues at the Environmental Chemistry Department.

Author's Declaration

I assure that the work in this PhD thesis has been my own unless otherwise stated. Details on work that has been done by other people have been reported in the relevant chapters.

Abbreviations

- ARMA** autoregressive moving average
- AT** accumulated temperature sum (day-degrees above 5°C)
- CONT** continentality index
- CW** Compression wood
- CCC** concordance correlation coefficient
- DAMS** Detailed Aspect Method of Scoring
- DBH** diameter at breast height (1.3 m)
- dplR** Dendrochronology Program Library in R
- EW** earlywood
- EWD** earlywood density (kg/m^3)
- EWL** earlywood width (mm)
- GYC** General yield class ($\text{m}^3/\text{ha}/\text{yr}$)
- JW** juvenile wood
- LOWESS** locally weighted scatterplot smoothing
- LVDT** linear variable displacement transducer
- LW** latewood
- LWD** latewood density (kg/m^3)
- LWL** latewood width (mm)
- MC** moisture content (%)
- MD** moisture deficit (mm)
- MFA** microfibril angle (degrees)
- MoE** Modulus of Elasticity (GPa)
- MoR** Modulus of Rupture (GPa)
- MW** mature wood
- NLME** Linear and Nonlinear Mixed Effects Models
- NLS** nonlinear least-squares

OW outerwood

QCI Queen Charlotte Islands

R an open source statistical software

REML restricted maximum likelihood

RD ring density (kg/m^3)

RH relative humidity

RW ring width (mm)

SS stem straightness (score 1-7)

YC yield class ($\text{m}^3/\text{ha}/\text{yr}$)

Glossary

Autocorrelation correlation within the variable itself eg. periodic fluctuation in a time series.

Basic density measure of timber density determined as the green volume per dry mass.

Bonferroni correction is applied to adjust the significance threshold, α' -value, for the individual comparisons to retain a given α -value (eg. 0.05) for the whole experiment when multiple comparisons are carried out.

COFECHA commonly used programme for the tree ring series cross-dating and validation.

Compression wood is formed on the under side of branches and on the leeward side of the stems. Its function is to straighten the stem or to push the branches upwards. CW is characterised with high density and lignin content but low strength properties.

Concordance correlation coefficient reproducibility index that assesses the agreement between two readings by measuring the deviation from one to one line (Lin, 1989). This allows considering location and scale shift as well that would not be detected by Pearson correlation.

Dendrometer a device for monitoring tree growth.

Detailed Aspect Method of Scoring windiness score that is calculated using windiness map, elevation, topex and aspect. The score (range 3 to 36) describes the physiologically constraining effect of wind on tree growth.

Earlywood xylem formed in the beginning of the growing season characterised by wide lumens and thin cell walls.

ESC Ecological Site Classification system developed at the Forestry Commission Forest Research.

Furnival function algorithm for calculating R^2 -value for mixed effects models.

Grain angle the helical angle of the longitudinal axis of wood cells around the axis of a tree stem.

General Yield Class the measure of forest growth commonly used in the UK. It expresses the timber produced in $\text{m}^3 \text{ha}^{-1} \text{yr}^{-1}$.

Juvenile wood type of wood formed in young trees and in the crown of mature trees. In Sitka spruce the juvenile wood is characterised by high density and microfibril angle. The extend of juvenile core will vary based on the timber property used to define it. Here juvenile core was defined as the first 10 annual rings according to the density data.

Latewood xylem formed towards the end of the growing season characterised by narrower cell diameter and thicker cell wall than earlywood.

LME a function from the NLME R package for fitting linear mixed effects models.

LOWESS (locally weighted scatterplot smoothing) curve is drawn using a weighted linear least squares regression. It can be used to investigate trends in scatter plots.

Mature wood is of wood formed in lower parts of the stem in mature trees. Here ring numbers >10 from the pith were considered as mature wood.

Microfibril angle The angle at which the bundles of cellulose, called microfibrils, are organised with respect to the cell axis in the secondary cell wall of wood tracheids. It is dominated by the angle in the S2-layer due its much greater thickness than the S1 and S3. Microfibril angle influences the MoE and longitudinal shrinkage and is therefore an important timber quality indicator.

Modulus of Elasticity measure of wood stiffness which describes the resistance to deformation under a load. Dynamic MoE can be calculated from acoustic velocity and density measurements. Static MoE can be measured in tensile or bending tests.

MoR (Modulus of Rupture) measure of timber strength that is derived in destructive bending tests.

NLME package a code package for the R statistical software to fit linear and nonlinear mixed-effects models.

Outerwood a term used here for the outermost part of the radius where the standing tree acoustic measurement signal would travel.

Prewhitening a method of removing autocorrelation by reducing residuals to white noise.

Provenances segments of a species that differ in some characteristics due to evolutionary selection under particular growing conditions within the species range (Zobel and van Buijtenen, 1989).

Robust bi-weight mean method that reduces the influence of potential outliers on the mean by applying biweight transformation of the values and hence deriving a robust mean.

S1 layer a constituent layer of the secondary cell wall, typically 0.1-0.3 μm thick. It characterised by lack of organisation of the cellulose microfibrils.

S2 layer a constituent layer of secondary cell wall, typically 1-5 μm thick. In this layer the cellulose microfibrils are ordered at angle respect to the cell axis. Due to the thickness it will dominate the microfibril angle of the cell wall.

S3 layer a constituent layer of secondary cell wall, typically 0.1 μm thick.

Slenderness approximate measure of stem taper. It is calculated as the height (m)/DBH (m).

Small clears test pieces of timber cut to standard dimensions and clear of any defects, such as knots, used to assess timber stiffness in bending tests.

Spiral grain corkscrew-like longitudinal alignment of cells around the stem (Kubler, 1991).

Stem straightness score variable describing the straightness of the lower part of the tree stem according to the scoring system developed by Macdonald et al. (2001).

Topex score measure of geomorphic shelter.

Tracheid conifer wood cell.

WinDENDRO an image analysis software for tree ring and density analysis.

Yield class measure of the average timber volume produced annually ($\text{m}^3/\text{ha}/\text{yr}$).

1 Introduction

Trees form an important part of the terrestrial ecosystem. They function as a habitat for numerous species, especially in the case of natural old growth forests. Plantation forests yield raw materials that can be considered as carbon neutral if the areas are replanted or left to regenerate. Furthermore, forests act as carbon stores, the size of which depends on the species, management and rotation length. Globally forests store an equivalent of 4 500 Gt of CO₂ (Forestry Commission, 2007). Tree growth is governed by climate, site conditions, competition and genetics in a complex manner with all of these factors interacting with one and another. In case of a plantation forest, growth is further influenced by silvicultural practices such as planting density, thinning and possible fertiliser applications (Macdonald and Hubert, 2002).

1.1 Tree growth

In order to grow trees, like all plants, require light, water, carbon dioxide and mineral nutrients. In the process of photosynthesis the trees use the energy of sunlight to convert water and carbon dioxide to sugars and oxygen. Photosynthesis takes place in green leaves or needles in the crown. This requires large quantities of water to be transported from the roots up to the crown. On the other hand for root growth sugar is needed far away from the crown where it was formed. To redistribute these crucial materials, an efficient transport system is needed.

Water first enters the transport system in the roots, which seems to be the rate limiting step (Kramer and Kozlowski, 1960) and after that it is transported upwards relatively quickly. In softwoods several of the most recently formed rings participate in water transport. Water travels in dead xylem tracheids and moves from one tracheid to the next through bordered pits (Petty, 1970). The column of water is pulled upwards by the negative water potential in the needles which forms as water is used in photosynthesis and lost in transpiration. This is aided by cohesion of water molecules which holds them together as a continuous chain. The process where air bubbles enter and destroy this chain is called cavitation, and greatly reduces the transport efficiency (Koch et al., 2004; Ryan and Yoder, 1997). In the leaves carbon dioxide enters through stomata (Thomas, 2000), which are specialised structures for gas exchange. To obtain carbon dioxide the stomata need to open but once they are open water vapour is lost through them simultaneously (Thomas, 2000). The rate of water loss is influenced by the temperature (Penman, 1948) and windiness (Penman, 1948; Satoo,

1960), causing the loss to be greatest on a warm day. The effect of wind is slightly more complicated as it works to increase the water vapour pressure deficit in the surrounding air by transporting away the moisture that has left the stomata. The vaporisation of water simultaneously cools the leaves. In any case the tree needs to balance the gains in photosynthesis against losses due to excessive transpiration while the stomata are open. Usually the transpiration losses cause stomata to close in the afternoon, which then restricts photosynthesis but allows replenishment of water reserves (Kramer, 1957). In the tree water is mainly stored in phloem and bark (Milne, 1989; Zweifel et al., 2000) although a contradictory view exists that defines xylem as a water reserve (Offenthaler et al., 2001). The reserves can be used to support transpiration during high demand in the early afternoon and in the winter time when the losses are small but when frozen soil prevents replenishment. Changes in internal water reserves cause daily fluctuations in tree diameter (Downes et al., 1999; Milne, 1989; Zweifel and Häslér, 2001; Zweifel et al., 2000; Zweifel et al., 2001). The minimum is recorded in the afternoon when large amounts have been used in photosynthesis and lost in transpiration. The maximum is reached during the night after stomatal closure allows replenishment (Downes et al., 1999; Zweifel and Häslér, 2001; Zweifel et al., 2000).

In the spring, the trees break dormancy when suitable conditions are reached. In regions with a cold season this is dependent of temperature, whereas in the tropics the variation in growth is less systematic. In temperate regions growth commences with bud burst when a threshold temperature sum is reached. The absolute value of accumulated temperature required to trigger the onset varies with latitude, with Northern trees starting at lower values (Seo et al., 2008). There are differences between-trees from continental and oceanic climates. The latter usually need higher temperature sum as a safety factor since the spring weather is less stable (Leinonen, 1996; Murray et al., 1989). In Sitka spruce bud burst is strongly temperature dependent (Cannell and Smith, 1983; Cannell and Smith, 1986; Murray et al., 1989).

Height growth at the stem apex starts first as the apical bud is believed to control the onset of growth. The plant hormone auxin, which stimulates growth, is produced in the apical bud. Auxin is then gradually transported down the stem causing the initials of the secondary cambium to divide and hence start radial growth.

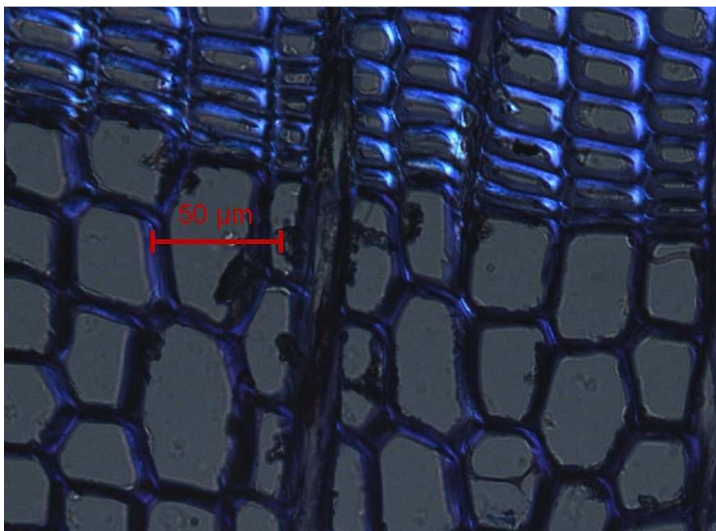


Figure 1-1. Microscope view of Sitka spruce earlywood tracheids with wide lumina and narrow latewood tracheids. The red scale bar is 50 μm .

In the spring when growth has just started, xylem production proceeds quickly and earlywood characterised by cells with wide lumina and thin walls

(Vaganov et al., 2006) is formed (Figure 1-1). These cells ensure efficient water transport in the newly formed xylem (Thomas, 2000). As the season progresses the radial growth rate will decrease and cells with smaller diameter and thicker cell wall are produced (Thomas, 2000; Vaganov et al., 2006). This type of wood is called latewood or summerwood. There is a characteristic density difference between these types, although the transition occurs gradually. The boundary is also apparent visually and forms the annual rings observed in the stem cross-section. The ring width will vary depending on the conditions during the growing season. A wider ring is produced when the conditions for growth are optimal, whereas adverse conditions such as a cold summer or drought can restrict the growth severely or even prevent it, leading to narrow or missing rings. To a degree the ring width can also depend on the conditions during previous growing seasons. Trees build food reserves that can be used for respiration during winter and also for growth early on in the spring (Hoch et al., 2003). Furthermore, leaf area index is influenced by past growth as the needles are retained for 6-8 years in Sitka spruce (Cannell, 1987). Therefore poor reserves could possibly have implications on growth the following year. Certain plant diseases or insect outbreaks that damage the needles of coniferous trees can influence the growth for several years. The relative proportions of earlywood and latewood can vary between years. Latewood production is thought to be induced by water deficit in Red pine (*Pinus resinosa*) (Whitmore and Zahner, 1966). There is also evidence that growth is synchronised with day length at high latitudes (Rossi et al., 2006c) which guarantees that sufficient time remains for cell maturation after cell divisions have ceased.

At cellular level growth takes place in several steps that overlap in time. First the cambial initials divide and produce two daughter cells, one of which will continue functioning as a cambial initial. The other one will start differentiating either into xylem or phloem cell,

forming wood or bark, respectively. The formation of xylem cells is much more frequent than the formation of phloem cells (Bäucker et al., 1998; Farmer, 1967; Gričar and Cufar, 2008; Plomion et al., 2001), which occurs only approximately once for every eight xylem cells produced (Jane, 1970). The xylem cell will then experience a phase of enlargement during which the cell reaches its full dimensions. Then lignification of the cell wall begins. This usually starts in the corner of the cells (Timell, 1964). Lignin functions as sort of a cementing agent in the cell wall. Once the cells have developed fully they will die and become part of the water transport system in the outer part of the stem, called sapwood. In sapwood water is transported upward from roots to the leaves, where it will be used in photosynthesis and lost in transpiration. Spiral grain ensures that water is distributed to all parts of the crown even if only part of the root system is functional (Kubler, 1991). Sugars are transported down to the lower parts of the tree in the phloem (Farmer, 1967; Kramer and Kozlowski, 1960). Newly formed xylem cells remain part of the sapwood for several years and young trees only contain sapwood. When sufficient new rings have been produced the innermost rings cease to take part in water transport and become part of the heartwood that is found in the centre of the tree. Heartwood is drier as it does not take part in water transport. It functions as a support structure and it may contain high levels of resins and other extractives, thought to protect it from rotting. In Sitka spruce the extractives content is fairly low in all parts of the cross-section (Cahalan, 1987). Caron-Decloquement (2010) found Sitka to contain 1.3 – 1.7 % of extractives in sapwood and 1.5 – 2.9 % in heartwood. The width of sapwood varies with age and species. There are also considerable differences between individuals of same species even within a site.

The main constituents of a coniferous tracheid are cellulose (40-50 %), hemicellulose (20-35 %) and lignin 15-35 % (Plomion et al., 2001; Saranpää, 1994; Timell, 1964). The cellulose chains in the cell wall are bundled together forming structures called microfibrils. The microfibrillar cellulose is formed of such a precise structure of hydrogen bonds within and between the cellulose chain that it is largely crystalline (Plomion et al., 2001). Plants can control the space and size of growing cells as well as the mechanical performance of tissues with the orientation of cellulose microfibrils (Burgert and Fratzl, 2009). For example high microfibril angle makes juvenile trees more flexible and better streamlined hence reducing the mechanical impact of wind on them (Burgert and Fratzl, 2009). Hemicellulose group include non-cellulosic polysaccharides such as glucomannan, galactoglucomannan, arabinogalactan, glucuronoxylan, galactan and arabinan (Plomion et al., 2001). Lignin is a phenolic polymer that has been formed from hydroxycinnamyl alcohols that are called monolignols. These include in conifers *p*-coumaryl alcohol and coniferyl alcohol (Plomion et al., 2001). The respective types of lignin formed are *p*-

hydroxyphenyl (H) and guaiacyl (G). In conifers G lignin is found in normal wood and H associated with compression wood (Savidge, 1996). Lignin makes the wood tissue more rigid as well as constitutes the hydrophobic surface required for water transport (Plomion et al., 2001; Savidge, 1996). The microfibrils are embedded sheathing hemicelluloses and surrounded by a matrix that contains lignin and hemicelluloses (Altaner et al., 2006). For the performance of cell wall, also the interactions between cellulose microfibrils, hemicelluloses, lignin and pectin are important (Burgert and Fratzl, 2009).

The angle of the cellulose microfibrils with respect to the cell axis has important consequences for timber properties. The structure of the secondary cell wall can be divided into three main layers; S1, S2 and S3, which differ on composition and thickness. In a typical softwood tracheid the S1 layer is 0.1 -0.3 μm , S2 1-5 μm and S3 0.1 μm thick (Timell, 1964). The S2-layer dominates the microfibril angle effect due to its thickness (Plomion et al., 2001). However, also the S1 and S3 layers have important functions to withstand axial compressive loads and radial tensile stresses (Burgert and Fratzl, 2009).

Furthermore, wood produced in young and old trees differ in properties. Wood produced during the early years of growth is commonly called juvenile wood (Saranpää, 1994) and wood produced later is called mature wood (Figure 1-2). However, juvenile wood is also produced in the crown of mature trees, therefore some authors (Lasserre et al., 2004; Mason, 2008) prefer corewood as a more accurate description. In this thesis the term juvenile wood is used. The point of transition from juvenile to mature wood depends on the species and the timber property considered. For Sitka spruce the 10th (McLean, 2007) or 12th (Brazier and Mobbs, 1993) ring has been used in previous work as the end of juvenile core based on ring density. In this study the limit of 10th ring was adapted. In juvenile wood of Sitka spruce the density is initially higher, decreases towards a minimum and then increases slowly and reaches a steady level (Mitchell and Denne, 1997).

The microfibril angle is high in juvenile wood and the growth rings are wide. When the tree matures the ring width gradually decreases. This is thought to be due the fact that the wood needs to be laid down around an increasingly large circumference. Therefore more material would be required to produce a given ring width and the rings become narrower. If ring area is the criterion of growth rate, a decrease in growth rate still takes place but later (Alteyrac et al., 2005; Thomas, 2000). From the timber properties point of view juvenile wood is considered to be inferior to mature wood for all end-uses (Macdonald and Hubert, 2002).

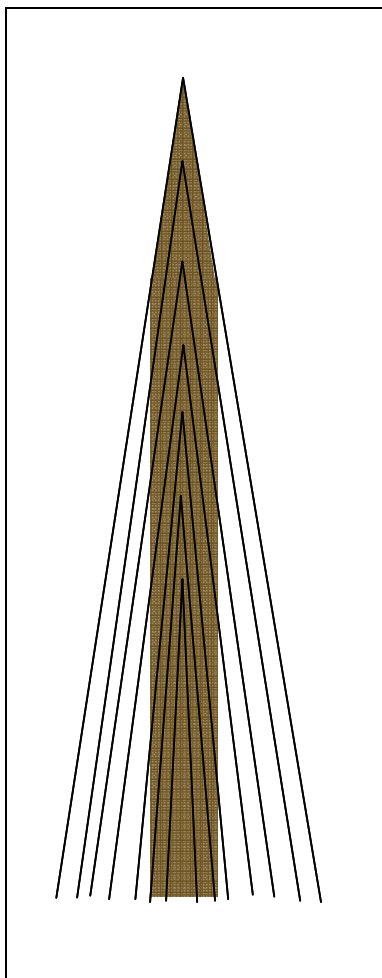


Figure 1-2. Formation of juvenile wood (brown) and mature wood within a stem.

The pattern of tree growth leads to large variation in some key wood properties within the stem. For example, density has been found to vary considerably from pith to bark in Sitka spruce (McLean, 2007; Mitchell and Denne, 1997; Saranpää, 1994). McLean (2007) found that microfibril angle was on average 28 degrees in juvenile wood and then decreased to approximately 12 degrees in mature wood. Furthermore, wood properties will vary with height since juvenile wood is still produced in the crown of old trees. There may also be azimuthal variation in timber properties arising from the formation of reaction wood in leaning stems. In conifers the reaction wood is called compression wood as it forms on the underside of leaning stems (Dunham and Cameron, 2000; Macdonald and Hubert, 2002) or branches or on the leeward side away from the prevailing wind (Macdonald and Hubert, 2002). The function of compression wood is to straighten the stem. Compression wood has lower hydraulic conductivity (k_s) than opposite wood which indicates that compression wood has a mechanical function in the tree (Mayr and Cochard, 2003). Compression wood is characterised by higher density, higher lignin content, shorter tracheids, higher microfibril angle and lower strength. The high density of compression wood causes some complications as density in normal wood is considered as a good indicator of strength whereas in compression wood the elevated density is accompanied by reduction in strength (Macdonald and Hubert, 2002). Therefore, it needs to be avoided in samples used for density analysis. Some authors have avoided sampling in the direction of the prevailing wind and the opposite side (Gardiner et al., 2010; Gardiner et al., 2002; Simpson and Denne, 1997) or in the direction of the lean (Moore et al., 2009c) in leaning stems.

Spiral grain describes how wood and bark cells are aligned around the axis of the tree. It results from a corkscrew-like orientation of longitudinal cells around the stem (Kubler,

1991). In the majority of conifer species left handed spiral grain is formed during early stages of growth (Brazier, 1967; Kubler, 1991). At the age of 10-30 years the spiral changes to the right handed direction which is usually maintained for the lifetime of the tree (Kubler, 1991; Thomas, 2000). More vigorously growing trees were found to have greater grain angle than slow-growing trees of comparable age and the grain angle decreased with age (Brazier, 1967). Spiral grain ensures that water flowing up from roots and carbohydrates flowing down from the crown are evenly distributed in the tree (Kubler, 1991; Thomas, 2000). For example, if one side of the root system is damaged the whole crown will still receive water as the transpiration stress of a branch pulls water from several roots (Kubler, 1991). This was illustrated as only a small decrease in growth occurred during an experiment in which half of the root system of Sitka spruce seedlings was placed in dry soil (Coutts, 1982).

Plantation grown trees do not approach the natural limit to growth or enter the stage of senescence, but the principles of growth limitation processes may reveal information that is applicable to earlier stages as well. A hydraulic limitation to height growth was proposed by Ryan and Yoder (1997). They describe how the increasing height and wood produced during slower growth form a limit to water transport and hence on the height growth itself. Water evaporates from the leaves, which lowers their water potential and causes water to be pulled from roots through xylem to the leaves. The flow is a function of the difference in water potential between the leaves and roots divided by the hydraulic resistance along the pathway of the flow. As trees grow taller water needs to travel a longer path from root to crown, which increases the hydraulic resistance (Ryan and Yoder, 1997). Flow may be hindered further by denser, slow growing wood. Therefore higher tension (lower water potential) is required in the xylem to maintain the flow, and this increases the risk of cavitation. To prevent cavitation the stomata will close, which lowers the rate of photosynthesis and the quantity of materials available for growth (Ryan and Yoder, 1997).

1.2 Sitka spruce in UK forestry

Large scale afforestation with coniferous species took place after World War I all over Great Britain (Adam, 1999). Sitka spruce was selected for its fast growth. In UK the mean annual increment is 6-24 m³/ha/yr (Malcolm, 1987). The most suitable variety of Sitka spruce for Great Britain has been thought to be the progeny from the Queen Charlotte Islands (QCI) in Canada (Hubert and Lee, 2005). The Queen Charlotte Islands are located

between 52 -54° N latitude and 131 - 133° E longitude. The climate is characterised by mild winters, cool summers and a high frequency of strong winds (Roche and Haddock, 1987). Precipitation is approximately 1400 mm at lower elevation (Malcolm, 1987).

The root system of Sitka spruce is based on extensive lateral roots (Mackie-Dawson et al., 1995). Depending on soil conditions Sitka spruce can form shallow or deep root systems (Blyth and Macleod, 1981a). Sitka spruce can tolerate poor drainage (Blyth and Macleod, 1981a). Sitka spruce is a moderately shade tolerant species (Cannell, 1984). In its origin under natural conditions Sitka commonly lives 700-800 years, reaching in excess of 60 m in height and 3 m in DBH (Silim et al., 2001).

In 1997 there was over 600 000 ha of Sitka spruce plantations (Figure 1-3) in the UK which constituted 28% of the forested area of the country (Mitchell and Denne, 1997). Currently, Sitka spruce plantations are the commonest woodland type (Adam, 1999). Sitka was widely used in afforestation of upland areas during the 1960s and 1970s (Worrell and Malcolm, 1990b).



Figure 1-3. Sitka spruce plantations extending into distance on the hill sides near Crianlarich.

The recent trend in silviculture to enhance growth and reduce rotation times could lead to undesired changes in anatomical and technical properties of wood (Mäkinen et al., 2002b). According to the EU, the strength classification C16 of timber is the minimum requirement for structural uses (Hubert and Lee, 2005). To penetrate the market British timber needs as

an absolute minimum to meet the requirements for C16 (Brazier and Mobbs, 1993). If C24 grade Sitka spruce timber could be grown reliably it could substitute foreign imports as sources of material for construction industry (Hubert and Lee, 2005).

1.3 Timber quality

Wood density is a very significant trait of wood quality (Anon., 2001; Lindström, 1996a) and determines the suitability of timber for different end-uses (Mäkinen et al., 2002b). Density affects strength, drying behaviour, machining and nail holding (Brazier, 1970a). Collapse during drying has been thought to arise due to low earlywood density (Brazier, 1970b). Mechanical behaviour can be predicted based on the density (Hacke et al., 2001). Density is also an indicator of pulp quality through its relationship with fibre properties like cell wall thickness (Saranpää, 1994). Furthermore, basic density is related to pulp yield and paper properties (Lindström, 1996b). Basic density was predicted by factors such as volume increment, stand density and thinning regime that regulate crown development (Lindström, 1996c). Cell wall width and lumen diameter affect the density (Rozenberg et al., 2004). Year rings show a seasonal pattern of increasing tracheid wall thickness from early to latewood (Denne and Smith, 1971).

Another important quality attribute is the microfibril angle (MFA), which measures the average angle of the cellulose microfibrillar helix in the S_2 layer of the cell wall (Evans et al., 1999). Microfibril angle is an important quality trait for sawn timber as it influences mechanical behaviour and dimensional stability (Macdonald and Hubert, 2002). Higher microfibril angle, found typically in juvenile and compression wood, causes greater longitudinal shrinkage (Jane, 1970). Microfibril angle has a strong influence on timber stiffness in Sitka spruce (Cowdrey and Preston, 1966; Macdonald and Hubert, 2002). Density was found to account for 70 % and microfibril angle (MFA) 86 % of the variation in modulus of elasticity in *Eucalyptus delegatensis* (Evans and Ilic, 2001). Together these factors accounted for 96 % of the variation (Evans and Ilic, 2001). In *Eucalyptus nitens* an inverse relationship was detected between density and microfibril angle (Evans et al., 1999).

Juvenile wood, which constitutes a large fraction of the stem volume in fast growing Sitka spruce, has poor strength and stiffness as it is characterised by low density, short tracheids, high grain angle and high microfibril angle (Evans et al., 1999; Macdonald and Hubert,

2002). Stem form, the presence of spiral grain and the distribution and size of branches can indicate other aspects of timber quality (Brazier, 1967). Large grain angle results in lumber that twists on drying and is of lower strength (Brazier, 1967; Harris, 1989). Compared to timber with straight grain, a 10-degree grain angle leads to 20 percent loss in performance and a 20 degree grain angle leads to about 50 percent loss. Furthermore, stem straightness is an important quality parameter for construction uses (Macdonald et al., 2001).

Timber strength can be measured in terms of modulus of elasticity (MoE) and modulus of rupture (MoR). MoE describes the bending stiffness whereas MoR quantifies the bending strength (Cahalan, 1987; Macdonald and Hubert, 2002). Stiffness is a measure of timber's resistance to deflection under load. It can be defined in terms Young's modulus (Equation 1):

Equation 1

$$E = \frac{\text{Stress}}{\text{Strain}} = \frac{F * L_0}{A_0 * \Delta L}$$

Where, E is the Young's modulus (N/mm²), F the force applied (N) to the object, L₀ the original length of the object (m), A₀ the original cross-sectional area through which the force was applied (mm²), ΔL is the change in the length of the object (m). The moduli can be tested with three or four point bending tests. In the case of modulus of rupture the force required to break a piece of timber is measured to derive MoR value in (N/mm²). For calculating the moduli from the bending test results, an adapted form of the Young's modulus equation will be applied (for details see eg. Dinwoodie (2000)). For timber properties MoE is considered more important since boards rarely break in normal use (Watt et al., 2006) and MoE is typically determined in longitudinal direction (Dinwoodie, 2000).

For mechanical stress grading of timber, the European Union uses a 9 point classification scheme for conifers and poplar that extends from C14 to C40 (Macdonald and Hubert, 2002). To penetrate the timber-frame construction market British timber needs as an absolute minimum to meet the requirements for C16 (Brazier and Mobbs, 1993; Hubert and Lee, 2005). For substitution of foreign imports as the major source of timber for the construction industry, it has been suggested that a reliable supply of C24 grade Sitka spruce timber is needed (Hubert and Lee, 2005). However, C16 timber is suited for general construction work and partial load-bearing end uses such as wall studs or framework

(Mochan et al., 2008). To qualify as C16 grade material, in terms of density, MoE and MoR, timber needs to have a fifth percentile bending strength of 16 N/mm^2 , mean bending stiffness of 8 kN/mm^2 or mean density of 370 kg/m^3 or higher (CEN, 2003). For C24 these threshold values are 24 N/mm^2 , 11 kN/mm^2 and 420 kg/m^3 , respectively (CEN, 2003).

The strength of battens can be tested at sawmill. However, it would be beneficial to be able to predict wood quality accurately prior to harvesting and preferably even prior to planting. If sufficient information on the factors affecting wood quality can be obtained then suitable locations for growing construction grade timber could be pinpointed. Other areas could be used for growing timber for pulping. This would have significant economic implications. Therefore, it is important to acquire more information on the influence that site factors and climate have on tree growth and on the quality of timber produced.

1.4 Factors influencing the timber quality

Genetics, site factors, silvicultural treatment, climate and microsite effects all influence the properties of timber produced at a given site. Their influences are often highly correlated; for example temperature sum and moisture deficit both decrease with altitude. Low temperature will limit growth in temperate regions whereas moisture deficit could restrict it in warmer regions (Fritts, 1976; Mäkinen et al., 2002a; Schweingruber, 2007). There may also be temporal shifts in the interrelationships (Downes et al., 1999; Mäkinen et al., 2002a). Furthermore, many of these factors influence timber quality via their effect on growth rate (Bergès et al., 2008; Guilley et al., 2004; Mäkinen et al., 2007). This section aims to review previous findings on the factors influencing tree growth and the resulting timber quality. The main focus of timber quality is on density and microfibril angle although stem straightness, knottiness and grain angle will receive some attention as well. The review of different influences is arranged under the broad headings of climate, site factors and management after which the relationship between growth and density is addressed in more detail and lastly the vast topic of climate change is touched upon, very briefly. The division remains a slightly artificial one due to the interlinked nature of the factors investigated.

1.4.1 Climate and growth

Allison et al. (1994) compiled a 1 km² resolution GIS based model for Sitka spruce yield classes in Scotland. Higher yield classes are found in the southwest of Scotland, where the Gulf Stream impacts the climate, and in the Central Lowlands. General yield class (GYC) declined with elevation. Temperature was found to impact the GYC estimates more than rainfall.

Blyth and Macleod (1981a) found that the growth of Sitka spruce was positively correlated with soil temperature during the growing season and winter rainfall. Worrell and Malcolm (1990a) concluded that growing season temperature sum and the tatter rate that measures site windiness were suitable for predicting site productivity. By using the process based model (3-PG) in diagnostic mode to study growth limitation on the Scottish Sitka spruce plantations, Waring (2000) found that variations in solar radiation due to differing topography accounted for nearly half of the differences between plantations whereas drought and vapour pressure deficit did not restrict growth significantly.

Mäkinen et al. (2002a) found that in general growth was limited by temperature at high-latitude and high-altitude sites whereas the importance of rainfall was more pronounced at low altitudes and further south. At intermediate altitudes a strong effect from weather variables was not detected and growth determining variables were assumed to vary between years at these altitudes. Furthermore, radial growth of Norway spruce was found to be negatively related to the temperature of the previous summer (Mäkinen et al., 2001). Bouriaud et al. (2005) suggested that in Norway spruce this negative relationship could explain the positive effect of temperature on density found in previous studies.

Also, the effects of soil water depletion and water regime on density are consistent with their negative impact on radial growth (Bouriaud et al., 2005). When Whitmore and Zahner (1966) studied xylem development in young Red pine trees (*Pinus resinosa*) under three different treatments, irrigation, imposed drought and bud removal, it was found that the formation of flattened and thick-walled tracheids of latewood started earlier in the drought treatment. Diameter growth was also significantly lower in the drought treatment than in the irrigation and bud removal treatments. In agreement with these findings Bouriaud et al. (2005) observed that in rainy years the period of rapid growth extended further into the growing season than drier years. Decreases in growth rate corresponded to increased soil water reserve deficits, which in turn limited transpiration (Bouriaud et al., 2005). However the degree of impact may vary depending on the initial conditions. Laurent et al. (2003)

found that in a dry stand of Norway spruce the water supply affected growth immediately whereas in a more humid stand, the climatic effect was delayed.

Wind damage is a serious problem in many forests in UK (Dunham and Cameron, 2000). Leading shoots can be damaged by strong winds (Blyth and Macleod, 1981a), which results in one of the side shoots becoming dominant (Blyth and Macleod, 1981a) leading to problems with stem straightness and compression wood. Thinning of young stands can be used to mitigate the risk of damage from wind and snow in later stages of development. Selective thinning could be carried out in that stage to remove individuals likely to contain compression wood such as leaning trees and trees with asymmetric crowns (Dunham and Cameron, 2000).

1.4.2 Site factors and growth

In transect studies across latitudinal gradients in central and northern Europe it was concluded that the relative importance of different environmental factors on growth of Norway spruce changes gradually according to the altitude and latitude (Mäkinen et al., 2002a). Blyth and Macleod (1981b) found in a regression analysis of data from 54 test plots in six forest areas in North-East Scotland that the most useful predictors of tree growth in Sitka spruce were soil physical properties and physiographic properties such as elevation and position-on-slope.

Soil chemical properties vary over such short distance that they are not of value in predicting yields (Blyth and Macleod, 1981b). Soils under conifer plantations may have been ameliorated with drainage systems and fertilisation applications, which may leave organic or mineral character as the only distinction between what have originally been quite different soils (Allison et al., 1994; Worrell and Malcolm, 1990b). This could be a reason why clear effects of soil type were not detected by Allison et al. (1994) for Sitka spruce. Worrell and Malcolm (1990b) found brown earths to be the most productive soil type. This was supported by the findings of Blyth and Macleod (1981a). After brown earths they found the productivity to decrease in order podzol > gleyed podzol > gley. Sitka spruce can tolerate poor drainage, and depending on soil conditions, it can form shallow or deep root systems. However, the growth rate of Sitka spruce was significantly lower on poorly drained soils than on freely or imperfectly drained ones (Blyth and Macleod, 1981a).

During the period from beginning of 1970s to the late 1980s forest growth increased by approximately 30% in Europe and Kauppi et al. (1992) concluded that this may have been due to a fertilisation effect by deposited nitrogen. Similarly Cannell et al. (1998) calculated that up to half of the increase in GYC in Britain would be due to joint effects of increases in N deposition, CO₂ and temperature. In support of the possible effect from N deposition are the findings by Blyth and Macleod (1981a) that total N in the organic horizon showed the strongest correlation with growth of Sitka spruce on 73 study plots in Northeast Scotland. Waring (2000) also found that soil fertility significantly limited growth on a number of Sitka spruce plantations across Scotland.

Growth of Sitka spruce was negatively correlated with elevation (Blyth and Macleod, 1981a). In the UK 100 m increase in altitude was accompanied on average with 4.3 m³ha⁻¹y⁻¹ reduction in wood production in Sitka spruce (Worrell and Malcolm, 1990a). Higher yield classes at a given elevation were found on relatively sheltered inland sites than on the coast (Worrell and Malcolm, 1990a). It was reported for Radiata pine in New Zealand that wood density decreased by about 0.1 g/cm³ with each increase in degree of latitude but increased by about 0.01 g/cm³ with each 100 m increase in altitude (Zobel and van Buijtenen, 1989). In a study on Douglas fir it was reported that the average specific gravity was 0.55 for trees growing under conditions characterised by low elevation and dry summers whereas for high elevation with wet summers it was 0.44 (Zobel and van Buijtenen, 1989). In Loblolly pine high specific gravity was reported in the southern part of its range and lower specific gravity in the northern part. Attempts to grow southern seeds in the north lead to wood densities similar to the northern population or lower (Zobel and van Buijtenen, 1989). Based on theoretical calculations regarding transport of water, a reduction in density was predicted with increase in latitude and altitude (Roderick and Berry, 2001). Furthermore, locations at high altitude were associated with greater taper and increased risk of leader damage in Sitka spruce (Blyth and Macleod, 1981a).

However, the relationship between-tree growth and elevation is a complex one since many other factors, such as temperature, moisture deficit, windiness and soil properties, that could impact growth, vary with elevation (Worrell and Malcolm, 1990a). Lower temperatures at high elevation may reduce the duration of metabolically active period. Windiness may also decrease tissue temperatures, increase evaporation and cause physical damage (Worrell and Malcolm, 1990a). Furthermore, in an oceanic climate excess soil moisture and reduced light intensities are encountered at higher elevation due to high level of cloudiness and precipitation (Worrell and Malcolm, 1990a). Therefore it is difficult to deduce which factors influence the growth at sites at higher altitude.

Based on research on conifers in alpine regions Rossi et al. (2007) concluded that temperature was the most important factor influencing growth at high elevation. They found that at the alpine tree line the thermal limit to wood formation was 6-8°C in terms of air temperature. Even if photosynthesis can take place in temperatures below 4-5°C, xylem growth was inhibited (Rossi et al., 2008). The maximum growth rate then coincided with maximum day length, which was thought to be a safety factor to guarantee that the trees will have enough time to complete cell wall lignification before the temperature decreased again (Rossi et al., 2006c). However, in temperate regions the maximum growth rate might be more dependent on temperature as suitable growing temperatures extend further into the autumn than in cold alpine regions.

The fact that Worrell and Malcolm (1990a) found higher GYC Sitka spruce stands on higher ground in sheltered locations in Scotland suggests that exposure is an important factor in reducing growth in the UK. However, they did not investigate timber properties so the influence on density at these sites is not known.

Growth of Sitka spruce was not correlated with aspect and slope (Blyth and Macleod, 1981a). Possible growth gains due to more southern aspect can be overturned by the effect of wind, which was the most important factor determining growth rate in the study of Worrell and Malcolm (1990a). In addition to elevation Blyth and Macleod (1981a) found the growth of Sitka spruce to be correlated with position-on-slope and the geomorphic shelter measurement, *topex*. Growth was found to increase by 0.3-0.4 m³ha⁻¹y⁻¹ for an increase of 10 points in *topex* value (Worrell and Malcolm, 1990a). However, field based *topex* measurements are problematic since shelter provided by distant hills is often overestimated if no distance threshold is applied (Quine and White, 1998).

1.4.3 Management and growth

Growth rate can be modified by silvicultural practices such as thinning, pruning, fertilizing and spacing (Brazier, 1970b). These treatments will impact density through their effect on growth (Mäkinen et al., 2002b). In a Sitka spruce spacing trial in Northern Ireland, the density decreased from 0.42 g/cm³ to 0.38 g/cm³ as the spacing increased from 1.9 m to 5.6 m but a large part of the difference was due to between-tree variation (Savill and Sandels, 1983). Also, Brazier (1970a) found a considerably higher volume of low-density timber in Sitka spruce plots with wider spacing. The structural performance of sawn wood was

decreased at large spacing (Brazier and Mobbs, 1993) as increased growth rate leads to formation of a large juvenile core with unstable properties such as twisting and warping during sawing (Savill and Sandels, 1983). Respacing at age of 8-11 years from 2000 stems/ha to 1500, 1000 and 500 stems/ha did not lead to significant differences in height or volume (Deans and Milne, 1999).

At wider spacing the stem straightness score decreases whereas knot number and knot size increase (Brazier and Mobbs, 1993; Deans and Milne, 1999). For high quality timber production, measures of branch size reduction such as brashing might be required. However, brashing increases costs significantly and might impair productivity (Deans and Milne, 1999). Also stem taper increased with spacing. This effect was most pronounced at higher altitudes (Deans and Milne, 1999). Macdonald and Hubert (2002) summarised the effects of wider spacing as increased knot size and reduced density as a result of the large juvenile core that develops when trees can grow vigorously without much competition.

The conventional practice of carrying out production thinning from age 20 has caused windthrow in Upland Britain. This has led to a practice of clear felling stands since windthrow tends to spread to adjacent areas and “no thin” practice has been established at many plantations to avoid this reduction in rotation length and hence timber volume (Deans and Milne, 1999). A small reduction in the latewood proportion was found at breast height in thinned stands of Norway spruce (Jaakkola et al., 2005). However, based on these findings it was estimated that at the thinning intensities current in Fennoscandia no significant reduction in density would occur.

Fertilisation increased growth rate and the production of stem wood (Anttonen et al., 2002). Mäkinen et al. (2002b) found a three fold increase in radial growth accompanied by 20% reduction in density in Norway spruce in a fertilisation experiment at the Flakaliden experimental forest in Sweden. This was due to a change in latewood proportion as well as a decrease in absolute wood density across the whole annual ring (Mäkinen et al., 2002b). Latewood proportion of Norway spruce decreased by 62 % (Kostiainen et al., 2004). Fertilisation treatment decreased the mean ring density, earlywood density and latewood density by 15%, 14% and 12%, respectively. Nutrient optimisation had changed the wood anatomy since in fertilized stands there was a larger number of thin-walled cells (Mäkinen et al., 2002b). Nutrient optimisation at the Flakaliden experiment also affected the chemical composition of wood as lignin content increased by 7% (Anttonen et al., 2002). Consistent with the inverse relationship between density and growth rate, the annual ring width increased due to fertilisation (Kostiainen et al., 2004). Increasing radial growth in

Norway spruce was mainly due to increase in earlywood width (Mäkinen et al., 2002b). Differences in ring width were caused by differing tracheid number, as tracheids in wider rings did not differ in size from those found in narrower rings (Mäkinen et al., 2003b).

Wang et al. (2006) studied the CO₂ 'fertilization' effect in white spruce in Canada by comparing annual rings of fast growing young trees to those formed during the early period of growth in currently mature trees. Systematically more growth was detected in young trees than estimated purely based on temperature and rainfall data, which could indicate a 'fertilisation' effect of increasing CO₂ levels. However in boreal forests, and other N limited forest ecosystems, the shortage of nitrogen in soil may prevent the increase in growth under elevated CO₂ concentration since it was found that elevated CO₂ concentration affected the wood properties only to a very limited degree whereas fertilisation had more pronounced impact (Kostiainen et al., 2004).

Production of denser timber by using silvicultural methods requires that trees are grown more slowly to minimise the size of the juvenile core. This can be attained with closer spacing at planting followed by thinning at the canopy closure stage (Hubert and Lee, 2005). However, currently the interest is on faster production. The discrepancy might be overcome by plant breeding. A further advantage of breeding is that the effects will be retained whereas silvicultural treatments need to be repeated for each rotation (Hubert and Lee, 2005). As there is heritable variation in wood characteristics that affect the technical behaviour these can be improved by selective breeding (Brazier, 1967). Selection for higher density traits was not found to have any detrimental effect on tracheid length (Brazier, 1967). It seemed to favour trees with high minimum earlywood density and also ones with narrow cells, although the effect was less pronounced.

Livingstone et al. (2004) found in a study on 24-year-old Sitka spruce progenies with differing growth rates that the fastest growing ones had larger branches and less latewood than the slow growing progenies or the control from Queen Charlotte Islands (QCI). Lower latewood proportion led to decreased density although the difference was not statistically significant. Fast growing progenies also produced more compression wood than the QCI control or slower growing progenies. Improved planting stock of QCI has been developed starting from 1960s (Hubert and Lee, 2005). As a result, a General Breeding Population (GBP) of 240 top-ranked plus Sitka spruce trees has been developed to improve diameter growth and stem form without compromising wood density (Hubert and Lee, 2005; Lee, 1999a; Lee, 1999b).

1.4.4 Density and growth

Conflicting results on the effects of environment and silvicultural practices on density may be due to the fact that both tracheid diameter and wall thickness affect it (Mitchell and Denne, 1997; Rozenberg et al., 2004), but these factors are under separate physiological control (Denne, 1979). A negative correlation was found between ring width and basic density in Sitka spruce (Brazier, 1967) and Norway spruce (Lindström, 1996c). In another study, a bimodal pattern between wood density and growth rate was found. Initially wood density was not affected by growth rate. This was followed by a period during which they correlated closely (Bouriaud et al., 2005). Tree height correlated positively and the stem taper negatively with basic density (Lindström, 1996c).

Mitchell and Denne (1997) found that in Sitka spruce the wood density was at maximum close to the pith and then decreased to a minimum, after which it either stayed constant or increased towards the bark. Minimum wood density is supposed to coincide with canopy closure (Mäkinen et al., 2002b). Wood density is also highly sensitive to water deficit. Bouriaud et al. (2005) observed that water deficit lead to a local reduction in cell size which corresponded with a decline in radial growth. Mäkinen et al. (2003b) observed tracheids with smaller diameter during a dry period and Wimmer et al. (2002) detected a decrease in wood density in drought -affected *Eucalyptus nitens* trees after a soil water deficit was released by irrigation treatment.

A considerable reduction in density was found in vigorously growing Sitka spruce (Brazier, 1970b). At breast height the mean density of the ring was related to ring width and the proportion of latewood (Mäkinen et al., 2002b). In fast growing trees the earlywood width was increased which led to a decrease in latewood proportion as no corresponding increase in latewood width was detected (Brazier, 1970b; Debell et al., 1994). This led to an decrease in overall density (Brazier, 1970b). Decreasing earlywood density in Norway spruce was associated with increasing fibre and lumen diameter. It was also closely related to the proportion of cell wall in the cross-section of the annual ring (Mäkinen et al., 2002b). Growth rate did not impact latewood density significantly in Western hemlock, therefore wood density could be improved without compromising the growth rate if latewood width could be manipulated (Debell et al., 1994). In a Norway spruce nutrient optimisation trial it was observed that increased growth took place in earlywood and hence lead to reduction in density (Mäkinen et al., 2002b). However in Western hemlock the negative relationship between growth and ring density was strongest at young age and became insignificant after ring 30 (DeBell et al., 2004). In *Pinus pinaster*

it has been shown that ring density had a high genetic control ($h^2=0.63$) and that the heritabilities increased from pith outward (Gaspar et al., 2008). However, in this species earlywood density has higher heritability than latewood.

Brazier (1967) found no statistically significant relationship between density and tracheid length in Sitka spruce. The cell width however correlated significantly with density, therefore selection for narrow cells could improve density (Brazier, 1967). In Sitka spruce 67% and 82% of the variation in density was accounted for by radial tracheid diameter and wall thickness, respectively (Mitchell and Denne, 1997). Density variation in juvenile wood was more closely associated with tracheid diameter and in mature wood cell wall thickness was the more important factor (Mitchell and Denne, 1997).

1.4.5 Climate change

In the future, an increase of 2-3°C in temperature is expected in the UK by 2080 with the magnitude of change being lower in the Northern part of the country (1-2°C in northern Scotland). Furthermore, the number of frost days will decrease markedly (Broadmeadow, 2000). Summer rainfall is forecast to decrease in the south-east (by 20%), where the moisture deficits are greatest at the moment. In the north the rainfall may increase by 5%. Winter rainfall is predicted to increase (10-20%) over the whole country. A small increase in average wind speed is expected; by the 2080s the increase in the northern Scotland is predicted to be 7%. Furthermore, the frequency of extreme events will increase (Broadmeadow, 2000; Broadmeadow, 2002). Climate change can potentially influence several aspects of Sitka spruce growth such as timing of bud break, growth rate and levels of pathogens (Broadmeadow, 2000). However, the impact of rising temperature on bud burst timing may be limited by the high chilling requirement of Sitka spruce (Cannell and Smith, 1986; Murray et al., 1989). Cannell and Smith (1986) estimated that with a 2 °C increase in temperature, bud break will occur only 5 days earlier in Sitka spruce in Scotland. Higher wind speed might increase compression wood formation, which would negatively impact timber quality. Rising CO₂ and increasing temperatures in the future are predicted to increase the average yield class of Sitka spruce from YC 14 to YC 16 (Ray et al., 2008). Macdonald and Hubert (2002) concluded that fast growth reduces timber density in Sitka spruce irrespective of the cause of more vigorous growth. The same has been found for Norway spruce (Mäkinen et al., 2007).

1.4.6 Climatic signal

Ring width and ring density variables are influenced by climate where the tree is grown as described above. Therefore, tree ring width series can be applied to study past climates. In addition to ring width and density variables, stable isotopes of carbon can be used to isolate a climatic signal (Brooks et al., 1998; Dupouey et al., 1993; Leavitt and Long, 1982; Loader and Switsur, 1996; Panek and Waring, 1997; Saurer and Siegenthaler, 1989). ^{13}C is fractionated during the photosynthesis as CO_2 containing the lighter ^{12}C isotope will diffuse more quickly into the stomata (Farquhar et al., 1982; O'Leary, 1988; O'Leary et al., 1992). It is further discriminated by the Rubisco enzyme (Farquhar et al., 1982; O'Leary et al., 1992) in the assimilations step which decreases the $\delta^{13}\text{C}$ to approximately -28‰ in C_3 plants (O'Leary, 1988). When trees are subjected to moisture deficit the stomata close, preventing the replenishment of CO_2 , and the existing $^{13}\text{CO}_2$ present inside the leaf will be assimilated as the $^{12}\text{CO}_2$ is eventually used up. This leads to less negative $\delta^{13}\text{C}$ during periods of moisture stress which allows this parameter to be used as an indicator of moisture stress (O'Leary, 1981; O'Leary, 1988; Silim et al., 2001). Stable isotopes of carbon could therefore provide an additional variable to help pinpoint the cause of certain growth responses in complex oceanic climate. Other stable isotopes commonly used in climate work include hydrogen (McCarroll, 2005; McCarroll and Loader, 2004; Switsur, 1996) and oxygen (McCarroll, 2005; McCarroll and Loader, 2004; Switsur, 1996). Multiple isotope analysis has also been applied as a method to isolate climatic signals in oceanic climate in Scotland (Loader et al., 2008).

For the climate signal analysis, the tree ring or other climate proxy series needs to be detrended to remove any age related trends (Fritts, 1976) such as the decrease in ring width or the characteristic density distribution across the radius in Sitka spruce. Common ways of detrending tree ring series include a cubic spline function (Cook and Kairiukstis, 1990; Cook and Peters, 1981). Other possible detrending functions are a negative exponential or a straight line. The trend is subtracted from the tree ring series and the observations converted to tree ring indices which represent the fluctuations around the long term trend. These indices can then be linked to climate data for the year of wood formation. Variables from the previous year are commonly also included in the analysis as trees may use reserves formed during the previous season (Hoch et al., 2003) and limited needle growth during a given year may influence growth for several years.

1.5 Aims of this study

The aim of this PhD study was to assess how site factors and climate influence the timber properties of Sitka spruce in the UK. The main timber quality indicator used was X-ray density but some results on acoustic velocity were also included. Both average values across the radii of trees and the patterns of density and acoustic velocity within the radius were investigated. To achieve these aims three experiments were adopted, called here Benchmarking, Level II and the Griffin dendrometer experiment.

The Benchmarking experiment compared 68 sampling sites (Figure 1-4) across Scotland and Northern England in a fractional factorial design taking into account six site factors. The aim of this experiment was to quantify the influence of different site factors on timber density. Problems related to the sample collection method prevented reliable dating of annual rings within the samples as the core ends were often damaged. Therefore, ring-based climate analysis was not possible in this experiment.

The Level II experiment was set up to investigate the influence of climate. For this experiment disk samples were collected from felled trees which allowed the accurate dating of the outer ring for ring-based analysis of climatic effects. From the vicinity of three Level II sites a total of 90 Sitka spruce trees were felled. Sample disks were collected from different heights along the stem. These samples were also used to study effect of height and azimuth on density and ring width. Breast height samples from the Loch Awe and Coalburn sites were further scanned ultrasonically to derive stiffness values and to study the relationship between sound velocity and density along the radius. The material from this experiment was also used to test the radial models of density developed on the Benchmarking data.



Figure 1-4. Numbered trees at a Benchmarking plot.

In the Griffin experiment point dendrometers, which continuously measure a tree's radius, were used to study short term (intra-ring) variation in tree growth. Increment cores from these trees were also analysed for density and the ring width measurements taken by the point dendrometers at different stages of growth season allowed an approximate dating of the density profile for that year. Therefore, any anomalies in density could potentially be related to changes in weather.

The experiments included in this PhD project allowed the quantification of environmental and climatic factors that influence tree growth and the resulting timber quality in terms of timber density. The Benchmarking experiment allowed the assessment of site factors over a wide geographical range. In addition, the Level II experiment yielded more detail concerning within-tree variation and the climatic signal contained in plantation grown Sitka spruce. The dendrometer experiment reduced the scale of measurement further to intra annual variation in growth rate and density. Hence, this project synthesised information on the scales of stand, tree, tree ring and section of tree ring to produce a holistic understanding of mechanisms governing the xylem formation and the resulting timber properties.

2 Density and Tree Ring Analysis

For the purposes of this study high resolution ring width and ring density data were required. The ring density and width analyses were carried out using an ITRAX X-ray densitometer (Cox Analytical Systems) for sample scanning and the WinDENDRO software package (Regent Instruments) for image analysis. This chapter details the methods related to sample preparation and to the use of these instruments.

2.1 Sample Preparation for the Analysis

The ITRAX X-ray densitometer consists of an X-ray source, a movable sample rack and a line camera. The source uses a flat-beam geometry to minimise radiation scattering and off-axis image distortion.



Figure 2-1. Sample preparation for the density analysis. Disks drying in the kiln (top). Drawing the radial section cutting patterns on the disks (middle). Some cut radial sections (bottom).

Samples are scanned line by line as they move in the beam when the sample rack lifts up. Resolution on the resulting radiographic images can be as high as 10-20 microns (Cox Analytical Systems). The resulting greyscale images can be analysed in the WinDENDRO Software to obtain the ring width and density variables.

Thin radial strips are required for the analysis using the Cox ITRAX X-ray densitometer. Both increment cores and disk samples were processed in this study.

The disks collected in the field were approximately 15-20 cm thick to prevent cracking during drying (Figure 2-1). The

disks were then kiln dried at 100°C and 56% humidity for 11 days.

This was done to prevent the growth of mould on the disks that can sometimes occur if they are stored in green condition. The disks were cut in half using a Woodmizer portable sawmill before finally being cut into radial sections oriented on the cardinal compass directions using a band saw. A cross-shaped cutting pattern (Figure 2-1) that ensures a fraction of the pith is present in each of the sections (McLean, 2007) was used. In the next stage approximately 2 mm strips were accurately milled from the radial sections using a computer controlled twinblade saw (Sherline Products Inc.). The exact thickness of the samples was measured to 0.001 mm at 4 points along the strip with an electronic digital micrometer (Betts). The four measurements were averaged and the value obtained used as input information for the WinDENDRO image analysis.

In this study 12 mm increment cores were also used. After extraction the cores were stored in a conditioning chamber at 60% relative humidity and 25°C until processing. For the milling of 2 mm strips, the cores were mounted on sample holders using wood glue (Unibond exterior wood glue) (Figure 2-2).



Figure 2-2. Left: a milled increment core sample on a purpose made sample holder. Right: Sample strips ready for analysis on the ITRAX X-ray densitometer.

2.2 Scanning with an ITRAX X-ray Densitometer

Inside the ITRAX densitometer the samples were mounted on the mobile sample rack by fixing them on the sample needles with double sided tape. During the scan the sample rack will move to allow each of the samples in turn to pass through the X-ray beam. The X-ray beam is attenuated as it passes through the samples and the attenuation is proportional to the density and path length (Hoag and Krahmer, 1991). The line camera produces a grey

scale image of the sample (Figure 2-4) in which the shades correspond to the density variation along the strip.



Figure 2-3. Wood samples mounted on needles on the ITRAX sample rack. The rack will move forward to bring each needle in turn in front of the x-ray beam. To scan each sample the rack lifts up step by step as defined by the step size.

The instrument was fitted with a Cu K α X-ray tube. The settings used for the analysis were 10 mA, 20kV, with 40 second

exposure time and 50 μm resolution. These settings had previously been found most suitable (McLean, 2007) for these kind of samples. Along with each set of samples a cellulose propionate calibration wedge (Walesch Electronic) of known density steps was scanned. The cellulose propionate has been selected since it has more uniform properties than wood. The calibration wedge had an X-ray density of 1073 mg/cm^3 . It consists of six steps of known thickness that have been specified to 0.0001 mm by the manufacturer (Walesch Electronic). Using the step thickness and density information WinDENDRO relates the light intensity of the grey levels to the corresponding wood density per mm of wood thickness ($\text{g}/\text{cm}^3/\text{mm}$). Once a sample strip was analysed the exact thickness of the sample was entered which allowed the calculation sample density (g/cm^3).



Figure 2-4. ITRAX greyscale image.

As wood density is dependent on the moisture content (Dinwoodie, 2000), ideally the equipment should be placed in a temperature and humidity controlled laboratory. However, in this case, accurate temperature and humidity control was not achieved. To avoid any bias caused by moisture the ITRAX chamber was kept as dry as possible by blowing in dry air with a Jun Air 2000 compressor fitted with Dominick Hunter CO₂ R280 drier unit. The variations in conditions were monitored with an Oakton RH/TempLog that records temperature (± 0.6 °C) and humidity ($\pm 3\%$). To establish a suitable working range of humidity an experiment was set up. The results indicated that no significant changes in practical terms were caused by air humidity

fluctuations in the low ranges of air humidity (Chapter 3). For scanning, the air humidity was always left to stabilise to values below 15%. Prior to scanning the samples were left to equilibrate with this low air humidity for a minimum of 3 hours. The moisture content of 2 mm thin strips was found to change rapidly (McLean, 2007). Additional sources of analytical error such as slight variation in sample angle on the rack due to bending or poor adhesion to the needle were studied (Chapter 3).

Furthermore, density can be influenced by the presence of extractives (Anon., 2001) and many coniferous species require extraction treatment prior to the X-ray density determination. However, Sitka spruce has a very low extractives content (Caron–Decloquement, 2010) and therefore extraction was concluded to be unnecessary.

2.3 Tree Ring Analysis with WinDENDRO

The grey scale images were analysed using the WinDENDRO Software package (Regent Instruments). The density of the cellulose propionate calibration wedge was related to the wood density using a six point light calibration that uses the known thickness of each step in the wedge to relate the gray scale values to wood density.

In WinDENDRO, paths are drawn from pith to bark and the programme will identify the ring boundaries as well as the division between earlywood and latewood. The 50% maximum density value was used to define the earlywood-latewood boundary (Figure 2-5). This and the ring boundary can also be corrected manually if there are inaccuracies in the automatic detection due to the presence of compression wood or any other anomalies. Two paths were drawn on each image and the path width used was 2 mm. To cope with non-circular rings multisegment paths that can be aligned with variable ring orientation were used (Figure 2-6).

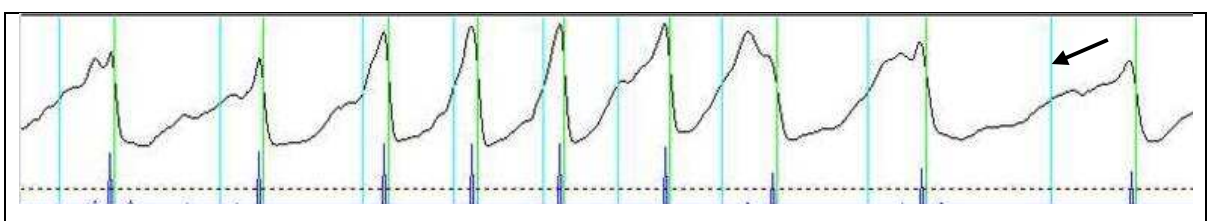


Figure 2-5. WinDENDRO ring density profile. Earlywood boundary (arrow) is set to 50% of the slope from minimum density at the beginning of the growing season and the maximum latewood density at the end of the ring. The green line marks the end of annual ring.

In addition to ring width, ring density and early/latewood proportions, WinDENDRO will calculate early/latewood, maximum and minimum densities. It can also convert the data into the Tucson decadal format that is compatible with dendrochronological programmes.

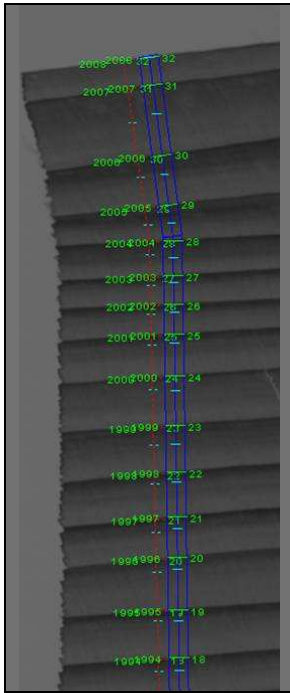


Figure 2-6. A section of analysed WinDENDRO image with two paths on it. The type of path used was a multisegment path that allows the reorientation of the path if the ring direction changes as can be seen in the upper part of the sample.

Furthermore, it will produce a density value for each pixel along the path in a separate output file. The pixel based output is accompanied by a column that labels the calendar years and earlywood/latewood separation. In this study the pixel based output was used mainly for deriving a compatible data format for the acoustic scanning study (Chapter 7) and to study the intra-ring density variation at the Griffin site (Chapter4).

3 Magnitude and sources of experimental errors in density analysis

This chapter quantifies the variation between individual paths that are drawn on the X-ray images in WinDENDRO to analyse tree rings from pith to bark (see chapter 2 for details of the analysis). This chapter also investigates the importance of measurement errors due to fluctuations in moisture content or variation in sample alignment. It will then establish recommended analysis conditions used throughout the density analysis in this PhD project. In addition, equations for correcting the X-ray density and ring dimensions to gravimetric density at different moisture contents will be derived.

3.1 Introduction

In a hygroscopic material such as wood, moisture influences both mass and volume (Anon., 2001; Dinwoodie, 2000). This occurs below the fibre saturation point (approximately 30% moisture content) as water enters the cell walls and alters the cell dimensions as well as the mass (Dinwoodie, 2000). Dinwoodie (2000) formulated an approximation that 1% increase in moisture content causes 0.5% increase in density when timber is below the fibre saturation point. Above the fibre saturation point water is stored in the cell cavity and the volume no longer changes, which leads to a more rapid increase in density (Dinwoodie, 2000). In the stems of living Sitka spruce, on average, the heartwood has a moisture content of 50% and the sapwood of 131% (Dinwoodie, 2000).

Timber samples analysed for density are below the saturation moisture content and therefore changes in relative humidity during the analysis could influence both ring dimensions and density. Therefore, for density measurements the moisture content has to be specified (Anon., 2001). Variation in moisture content during the analysis might distort the earlywood (EW) to latewood (LW) ratio as earlywood dries faster (Watanabe et al., 2008). Increase in moisture will also cause expansion of the annual rings. The degree of expansion will vary depending on the type of wood (Leonardon et al., 2010). To prevent these types of complications, X-ray analysis is traditionally carried out under standardised conditions of 20°C and 65 % relative humidity (Jaakkola et al., 2005; Jyske et al., 2008; Mäkinen et al., 2002b). These conditions will result the timber having a moisture content of approximately 12 % (Gaspar et al., 2008; Gerendiain, 2009; Ikonen et al., 2008;

Jaakkola et al., 2005; Jyske et al., 2008; Mäkinen et al., 2007; Mäkinen et al., 2002b). Lack of accurate climate control at the Glasgow X-ray laboratory raised a concern on the acceptability of the density data. The relative humidity in the ITRAX chamber is maintained low by blowing in dry air (see Chapter 2 for details) and the conditions monitored with an Oakton datalogger. Initially, the aim was to operate the ITRAX with 0% relative humidity in the chamber but this condition was seldom achieved and rarely maintained for the long period required for completion of each scan. During the operation moister air would enter the chamber through the opening in the bottom that is closed only with a set of brushes (Figure 3-1) to allow movement of the sample tray. Fans for cooling the electronics were located underneath the opening which caused an inflow of air once the X-ray densitometer was switched on. Typically the relative humidity would still fluctuate from 0% -20% and the temperature from 17°C-21°C. Under this kind of temperature and relative humidity regime the wood moisture content should remain between 5%-6% (Dinwoodie, 2000). However, an experiment was designed to study the influence of moisture under the typical conditions encountered.



Figure 3-1. Brushes inside ITRAX chamber that separate the samples from outside air conditions.

There were also concerns expressed by Moschler and Winistorfer (1990) on the effect of cell alignment to the X-ray density. Slight variation in the sample angle can easily occur during the analysis due to the mounting method of fixing the radial strips on sample holder sticks from their edge with tape. Additionally, variation in angle could be caused by slight bending of the samples. Also, the variation

between individual paths on the same samples was quantified.

In previous work (McLean, 2007) a discrepancy between the results of Glasgow University X-ray densitometer results and the gravimetric density was detected. McLean (2007) suspected that inadequacies in humidity and temperature control were causing this difference. However, the cause was never proven and McLean used regression equations to correct the X-ray density to gravimetric density. During this PhD project the cause was finally traced to an erroneous calibration wedge density value that had been saved in the

configuration file. The values were corrected for future analysis, which should lead to much better agreement between X-ray and gravimetric density. However, the results of this study also had to be corrected and regression equations similar to those used by McLean were developed for that purpose.

3.2 Materials and Methods

3.2.1 Humidity

A set of five samples from different Benchmarking sites were used in this experiment. The increment cores were processed for density analysis as described in Chapters 2 and 5. The samples were scanned on the X-ray densitometer repeatedly under varying relative humidity (Table 3-1). On each image 5 paths were drawn in WinDENDRO to obtain a measure of variability due to variation within the strip under the same moisture conditions. The location of the paths on the strip was carefully noted to avoid variation between runs due to different path locations. Furthermore, the first and last ring analysed in this experiment were removed from the data as they are most likely to contain variations in ring dimensions due to slight differences in the path starting or ending points.

Ring width and density variables obtained from the WinDENDRO analysis were investigated for influence of moisture. A weighted average density was calculated for all the paths and a mixed effects model was used to assess whether relative humidity could be the cause of variation.

Table 3-1. Relative humidity (%) in the ITRAX chamber during different scans of the selected samples.

	Sample number				
	55-28	72-15	130-19	140-15	243-19
Run A	4.5	4.5	4	3.5	4
Run B	0	0	0	0	0
Run C	7	7	5.5	3	6.5
Run D	0	0	0	0	0
Run E	28	28	28	28	28
Run F	18	18	15	15	17
Run G	10	10	9	9	10
Run H	5	5	5	5	5

3.2.2 Sample alignment

To address the concerns related to sample alignment prior to the analysis of the main bulk of the samples, experiments were designed to quantify these effects. To assess the effect of the sample angle, radial strips with well aligned year rings were analysed at a sequence of angles to the beam. The selected 3 samples were from the Kershope site used by McLean (2007). The range of angles used was 88, 89, 90, 91, 92, 93, 94, 95, 96, 97, 98, 99, 100 and 105 degrees to the beam. This set up involved keeping the samples straight in vertical direction but turning them to right or left with respect to the X-ray beam direction (Figure 3-2). This simulated the slight variation in the sample alignment when it was fixed onto the side of the sample needle with double sided tape. Some of the angles investigated here were considerably higher than was expected to occur during the analysis.

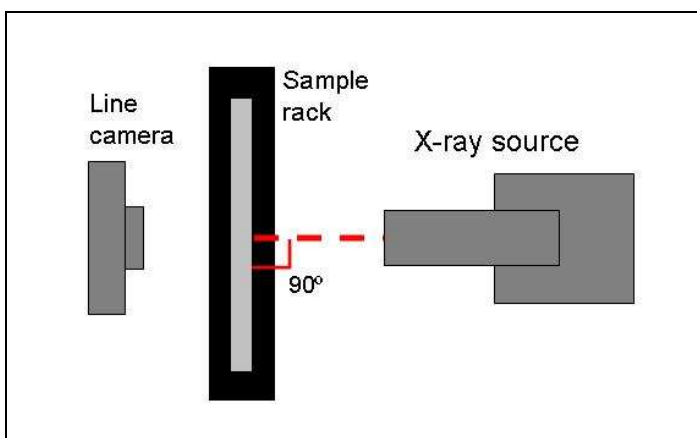


Figure 3-2. Schematic presentation (top view inside the ITRAX chamber) of a sample facing 90 degrees to the X-ray beam (dashed red line). The samples were then turned to the right with respect to the X-ray beam direction to obtain angles 91-105° and for consistency angles 88 and 89° were scanned as well, turning the samples to the left. Throughout, the samples were held straight in the vertical direction.

In the second stage, the effect of tilting the sample in the vertical direction was investigated (Figure 3-3). Control samples (Vertical) presented the normal setup during the analysis. Samples were then analysed tilted approximately 3° away from the beam in the vertical direction. This simulated the effect of bending the sample strip, which was sometimes observed to occur during the conditioning stage as the samples lost moisture. Additionally, samples were analysed when fixed on the front of the sample holder in order to bring them slightly nearer to the X-ray source. This would make it possible to discern whether any effect potentially detected in the tilted analysis might be caused by differences in distance rather than angle. Tilted samples were also scanned when turned to face the beam at different angles as described above. In this case the range of angles was narrower, 88-96°, since this was deemed sufficient to cover angles that could potentially occur in practice.

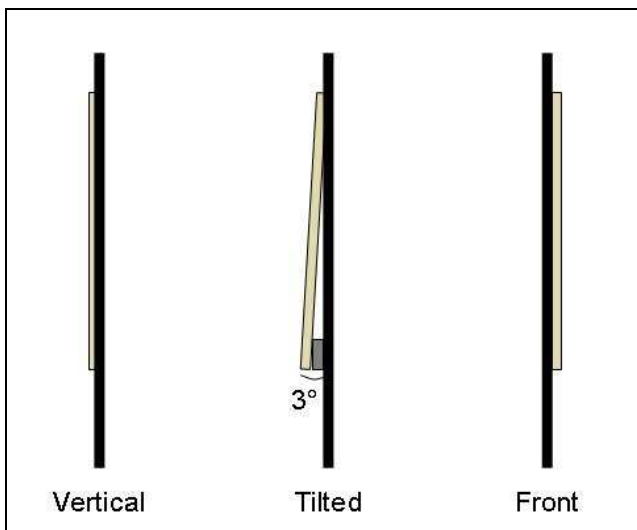


Figure 3-3. The setup of samples (side view to the samples holders) to quantify the potential variation caused by tilting the sample in vertical direction or placing it slightly nearer to the X-ray beam (Front). Normal analysis conditions (Vertical) functioned as the point of comparison.

3.2.3 X-ray density conversion

WinDENDRO analysis uses the step thickness and material density of a calibration wedge to calculate wood density. This does not directly correspond to the gravimetric density of wood because X-ray absorption depends on elemental composition and particularly on C:O ratio, which differs slightly between typical spruce wood and the cellulose propionate calibration wedge (Walesch, Effretikon, Switzerland) that was used. Therefore, to obtain absolute values of timber density across the Sitka spruce plantations or to compare the results to other studies a conversion factor is required. Concerns regarding the relationship between X-ray density and gravimetric density were raised by McLean (2007) as a result of his PhD study using the same instrument. The differences were considerable and were thought to be caused at least partially by the lack of climate control when operating the X-ray scanner. Here, a subset of 10 radial strips that had been scanned with the ITRAX and analysed in WinDENDRO were selected to calculate a conversion factor between the ITRAX density and gravimetric density under the moisture conditions used. The samples were dried overnight in the oven (110° C), cooled in a desiccator and then weighed to four decimal places on an analytical balance. Immediately after weighing, the strip thickness was measured at four points along the sample. The length of strip and the width at 2 cm intervals were carefully measured with a ruler. The values were then used to calculate gravimetric density in the oven dry state. As a quality control on the sample width measurements on which the density correction would be based, half of the samples (5) were used in a further measuring trial. On these samples the width was measured twice at 2 cm intervals, either starting from the end of the sample or 1cm from the end. Each measuring point was numbered and 4 means were calculated by using both sets of

measurements and by averaging the odd or even measurements from the 2 sets. Analysis of variance was used to test if there were significant differences between the means.

The samples were then placed in the ITRAX chamber with the dry air system fitted. They were left to equilibrate overnight and then the same weighing and measuring procedure was repeated to derive gravimetric density at ITRAX operating conditions. From the weight differences the moisture contents of the samples were also obtained.

During the investigation into discrepancies between X-ray density and gravimetric density a suspicion arose that the WinDENDRO configuration values could be the cause of the difference. It was discovered that as the default value for the calibration wedge density the material density (1.24 g/cm^3) had been inserted whereas the X-ray density (1.073 g/cm^3) should have been used (Walesch, Effretikon, Switzerland). This may explain some of the problems encountered by McLean (2007). For purposes of relating the density obtained in this study, a conversion factor was still required since the error was discovered too late to change the calibration input values.

Once the gravimetric densities had been calculated, regression analysis was carried out in R statistical package (R Development Core Team, 2007) to derive the coefficients for the equation converting the X-ray density to gravimetric density. Gravimetric densities at ITRAX operating conditions were then converted to 12% moisture content (MC) values for comparability to other studies. For this conversion, the ring widths were also adjusted as the increase in moisture will also influence the dimensions of the ring as described in the Results section.

3.3 Results

3.3.1 Humidity

The effect of humidity was studied on 5 samples during eight ITRAX scans with varying air humidity. This section reports the influence of humidity on ring density as well as area-weighted average density. Similarly, it reports the effects on ring width and path length. Furthermore, the variability between individual paths on the same samples is reported.

3.3.1.1 Ring Density

Ring density varied between the scans but not systematically according to the moisture levels (Figure 3-4). Even though run E, with the most extreme relative humidity (28%), mostly showed the highest ring density values that was not always the case. Furthermore, runs B and D that had the lowest relative humidity (0%) did not often correspond to lowest density values.

In the path average densities there seemed to be an upward trend with the moisture content (Figure 3-5). However, for sample 130-39 the average densities at 28% relative humidity were more similar to 0% relative humidity than the intermediate ones.

The results were then analysed by fitting a mixed effects model with restricted maximum likelihood (REML) in R statistical package. Initially Humidity and Sample and their interactions were included as fixed effects. Random effects had a nested structure and the model fitted was of the form:

Equation 2

$$y = \mu + \varphi_h * \tau_s + R_i + S_{j(i)} + P_{k(ij)} + A_{l(ijk)}$$

Where, y is the tree ring variable being investigated (eg. density (kg/m^3) or ring width (mm)), μ is the overall mean, φ_h the fixed effect due to humidity and τ_s the fixed effect of the sample. The humidity and sample interaction are also included. R_i is the random effect due to the i^{th} run, $S_{j(i)}$ the random effect of the j^{th} sample within the i^{th} run. $P_{k(ij)}$ is the random effect of k^{th} path within the j^{th} sample within the i^{th} run. $A_{l(ijk)}$ is the random effect of annual ring within k^{th} path within the j^{th} sample within the i^{th} run. This same model structure was used to study all the ring width and ring density variables.

When the model was fitted to the ring density data both, humidity and humidity:sample interaction remained non significant. The humidity:sample interaction term was removed. Humidity (Table 3-1) remained insignificant, whereas there were significant differences between the samples (Table 3-2).

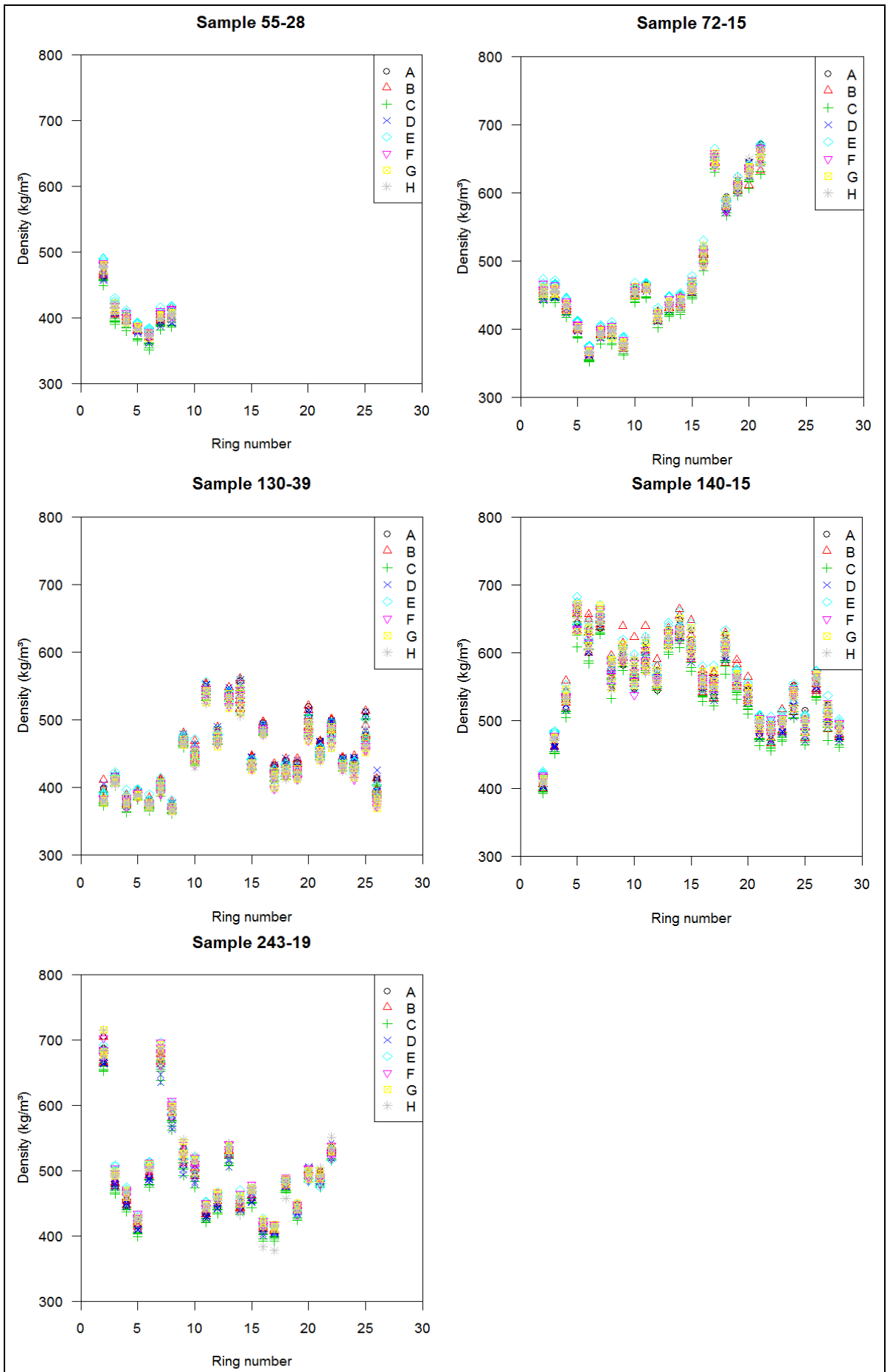


Figure 3-4. Variation in ring density during different scans (A-H)

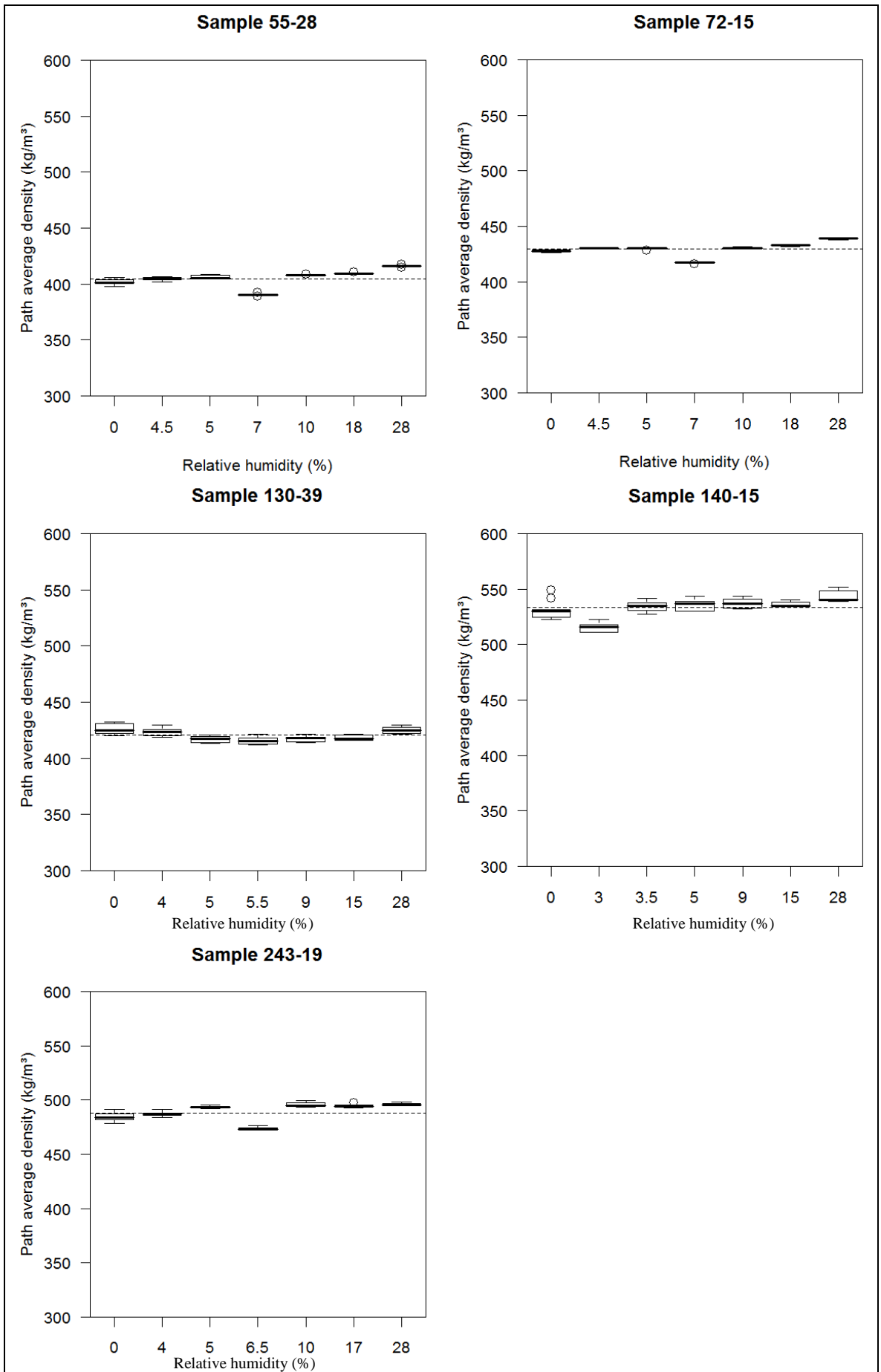


Figure 3-5. Variation in path average density against relative humidity of the run.

Table 3-2. R output for the fixed effects in the fitted humidity model for ring density

Fixed effects: Ring density ~ Humidity + SampleID					
	Value	Std.Error	DF	t-value	p-value
(Intercept)	440.19	3.103	3721	141.88	0.000
Humidity	0.32	0.206	27	1.55	0.133
Sample 140-15	110.43	2.935	27	37.62	0.000
Sample 243-19	52.85	3.200	27	16.52	0.000
Sample 55-28	-37.67	4.524	27	-8.33	0.000
Sample 72-15	35.78	3.199	27	11.19	0.000

The random effect of Run, not accounted for by the relative humidity associated with it, was very small (Table 3-3). Also, when sample was entered as a fixed effect and there was no remaining random effect once the model was fitted. Variation between paths was so small that it did not explain any of the random variation. By far most of the variation was between annual rings as could have been expected.

Table 3-3. Variance components in humidity data when humidity fitted as fixed effect.

	StdDev	% of variation
Run	4.22	0.4
Sample in Run	0.00	0
Path in Sample in Run	0.00	0
Ring in Path in Sample in Run	66.86	99.6

Influence of humidity on the path average density was also looked at. The model fitted was of the same form but lacked the ring width in the path since the values for individual rings were averaged out when the path average densities were calculated. When the model with Humidity:Sample interaction was fitted the humidity remained non-significant but the sample: humidity interaction terms were significant. A main effect cannot be removed from a model before its interaction term and therefore the model was refitted without the interaction term. In this case a significant effect of moisture was detected (Table 3-4).

Table 3-4. R output for the fixed effects in the fitted humidity model for path average density.

Fixed effects: Path average density ~ Humidity + SampleID					
	Value	Std.Error	DF	t-value	p-value
(Intercept)	417.34	2.795	156	149.30	0.000
Humidity	0.45	0.207	27	2.19	0.037
SampleID 140-15	112.19	1.808	27	62.05	0.000
SampleID 243-19	67.32	1.817	27	37.06	0.000
SampleID 55-28	-16.70	1.813	27	-9.21	0.000
SampleID 72-15	7.96	1.816	27	4.38	0.000

Table 3-5. Output for the ring density model fitted to the humidity data in a more realistic operating range (<28%).

Fixed effects: Ring density ~ Humidity + SampleID					
	Value	Std.Error	DF	t-value	p-value
(Intercept)	441.17	3.573	3266	123.49	0.000
Humidity	0.23	0.388	23	0.59	0.563
SampleID 140-15	109.39	3.149	23	34.74	0.000
SampleID 243-19	52.43	3.416	23	15.35	0.000
SampleID 55-28	-38.81	4.856	23	-7.99	0.000
SampleID 72-15	35.05	3.444	23	10.18	0.000

When the highest humidity run (E with 28% RH) was excluded to obtain a more realistic range of relative humidity, the effect of humidity was no longer significant for either ring (Table 3-5) or path average (Table 3-6) density. Even when considering the regression for full range of humidity values the effect of humidity remained small, causing at the maximum range of analysis conditions (15% RH) an error of approximately 1% on the ring density and 1.5% on the path average density (Table 3-7).

Table 3-6. R output for the path average density model fitted to density data obtained in relative humidity <28%.

Fixed effects: Path average density ~ Humidity + SampleID					
	Value	Std.Error	DF	t-value	p-value
(Intercept)	417.63	3.309	3403	126.22	0.000
Humidity	0.53	0.383	23	1.38	0.181
SampleID 140-15	111.30	1.975	23	56.36	0.000
SampleID 243-19	66.82	1.981	23	33.73	0.000
SampleID 55-28	-17.87	2.004	23	-8.90	0.000
SampleID 72-15	7.07	1.996	23	3.54	0.002

Table 3-7. Size of a measurement error caused depending on the density variable and relative humidity range considered.

	Relative humidity (%)		
	5 %	10 %	15 %
Ring density	0.35 %	0.70 %	1.05 %
Ring density (RH < 28 %)	0.25 %	0.50 %	0.75 %
Path average density	0.50 %	1.00 %	1.50 %
Path average density (RH < 28 %)	0.58 %	1.16 %	1.74 %

3.3.1.2 Ring width

When observing individual ring widths during the different runs, the results seem fairly consistent (Figure 3-6). No systematic effect was observable for the runs with lowest RH (B and D with 0%) or the one with highest RH (E with 28%). However, when the total path lengths were compared across the humidity values there appears to be an increasing trend with humidity (Figure 3-7). In statistical analysis it was confirmed that humidity did not have a significant effect on individual ring widths when looking at the full range of humidity (Table 3-8) or only the practical working range (Table 3-10). On the other hand humidity influenced the total path length significantly in both ranges of analysis (Table 3-9 and Table 3-11). Albeit being statistically significant the effect remained very small. In the worst case scenario (RH 15%) likely to be encountered during analysis the humidity would cause approximately 1% error in the measurements (Table 3-12).

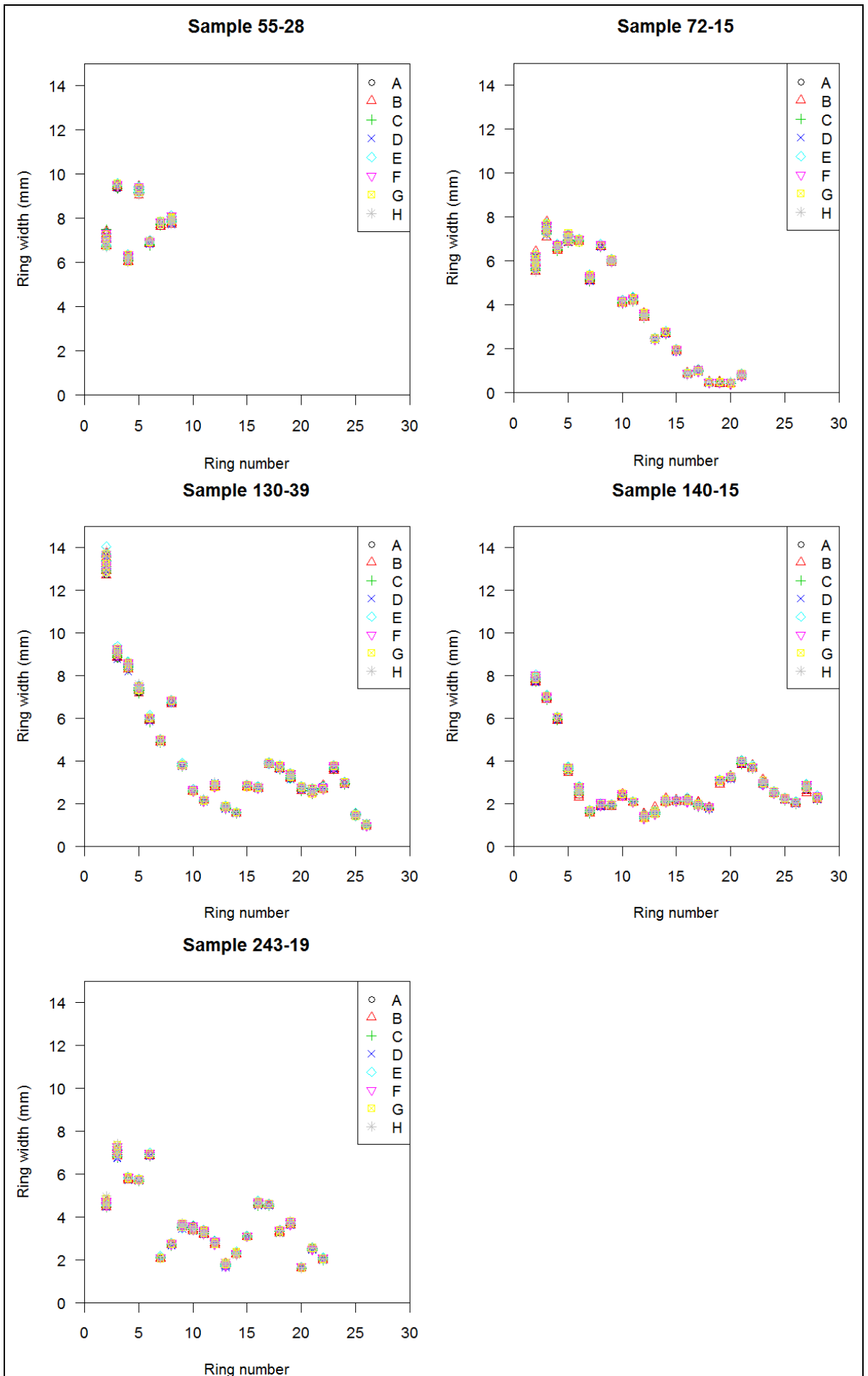


Figure 3-6. Variation in ring width during ITRAX scans under different relative humidity.

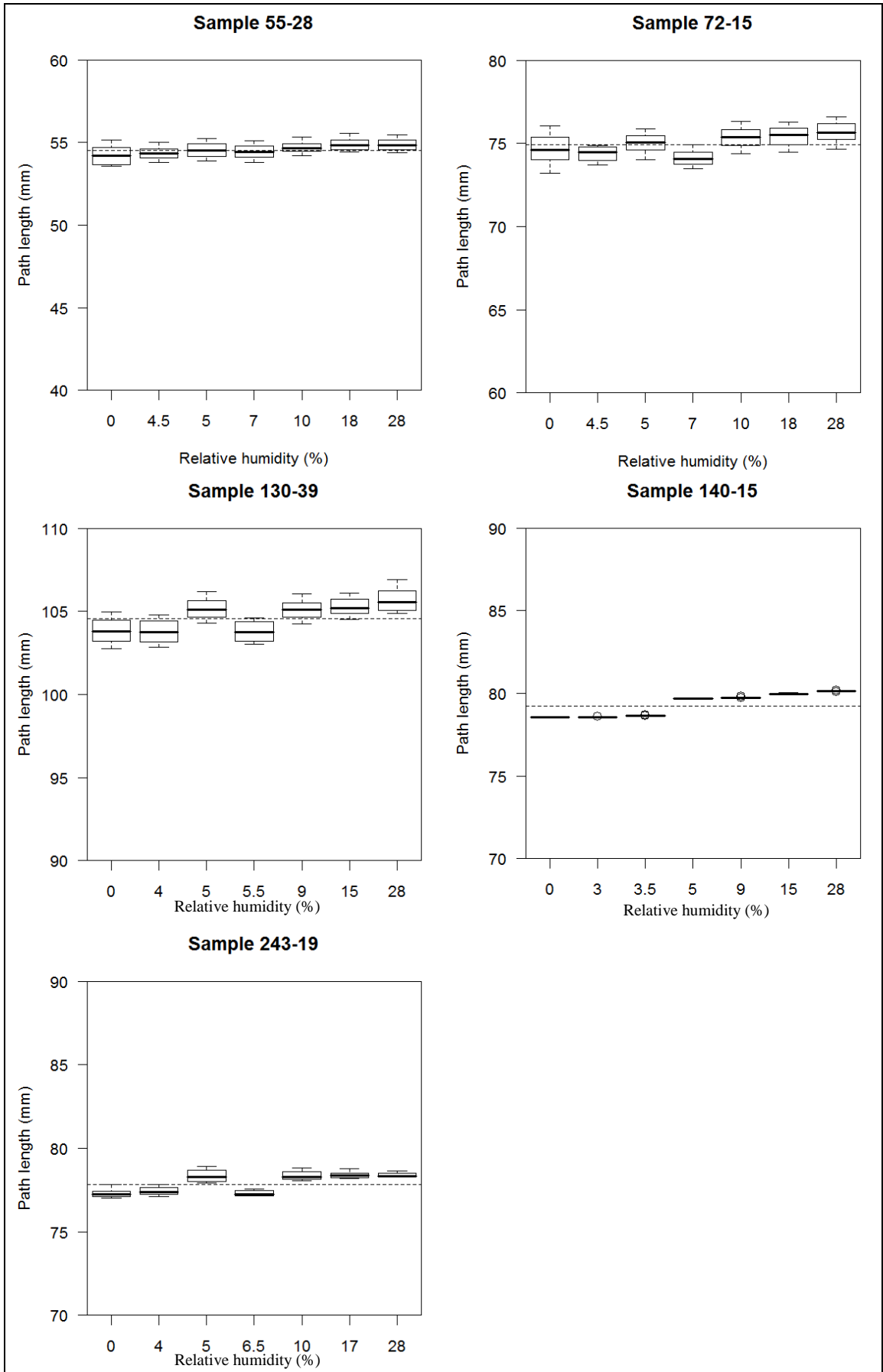


Figure 3-7. Variation in total path length with humidity.

Table 3-8. R output for the ring width model fitted to the humidity experiment data.

Fixed effects: Ring width ~ Humidity + SampleID					
	Value	Std.Error	DF	t-value	p-value
(Intercept)	4.162	0.075	3721	55.80	0.000
Humidity	0.002	0.004	27	0.65	0.521
SampleID 140-15	-1.247	0.094	27	-13.34	0.000
SampleID 243-19	-0.477	0.102	27	-4.68	0.000
SampleID 55-28	3.607	0.144	27	25.03	0.000
SampleID 72-15	-0.439	0.102	27	-4.31	0.000

Table 3-9. R output for the fixed effects in the fitted humidity model for the average path length.

Fixed effects: Path Length ~ Humidity + SampleID					
	Value	Std.Error	DF	t-value	p-value
(Intercept)	104.175	0.190	156	548.25	0.000
Humidity	0.047	0.014	27	3.37	0.002
SampleID 140-15	-25.315	0.127	27	-199.86	0.000
SampleID 243-19	-26.729	0.129	27	-206.86	0.000
SampleID 55-28	-50.063	0.127	27	-394.25	0.000
SampleID 72-15	-29.700	0.128	27	-232.39	0.000

Table 3-10. R output for the ring width model fitted to the humidity data in the operating range <28% relative humidity

Fixed effects: Ring width ~ Humidity + SampleID					
	Value	Std.Error	DF	t-value	p-value
(Intercept)	4.156	0.081	3266	51.30	0.000
Humidity	0.004	0.007	23	0.54	0.592
SampleID 140-15	-1.247	0.100	23	-12.47	0.000
SampleID 243-19	-0.475	0.108	23	-4.40	0.000
SampleID 55-28	3.605	0.154	23	23.45	0.000
SampleID 72-15	-0.439	0.109	23	-4.03	0.001

Table 3-11. R output for the average path length analysis in relative humidity <28%

Fixed effects: Path Length ~ Humidity + SampleID					
	Value	Std.Error	DF	t-value	p-value
(Intercept)	104.091	0.209	3403	498.52	0.000
Humidity	0.056	0.024	23	2.33	0.029
SampleID 140-15	-25.273	0.126	23	-200.75	0.000
SampleID 243-19	-26.646	0.127	23	-210.46	0.000
SampleID 55-28	-49.958	0.130	23	-384.26	0.000
SampleID 72-15	-29.655	0.128	23	-232.46	0.000

Table 3-12. Size of the measurement error depending on the ring width variable and relative humidity range considered.

	Relative humidity (%)		
	5 %	10 %	15 %
Ring width	0.02 %	0.03 %	0.05 %
Ring width (RH < 28 %)	0.02 %	0.05 %	0.07 %
Path length	0.30 %	0.60 %	0.91 %
Path length (RH < 28 %)	0.36 %	0.72 %	1.08 %

3.3.1.3 Variation between the paths

Path constituted only a very minor fraction of the random variation when the ring was included in the model. However, the variation between rings is large and therefore the random effect of the path location could still cause an important amount of variation. The density variation between paths was also studied to assess the feasibility of using only one path in WinDENDRO analysis.

To look at the contribution of the minor variation in path location to the measurement error Run B (with RH 0%) was selected. The variation between the paths (Figure 3-8) was quantified by subtracting ring density for each path from the mean and calculating root mean square errors (RMSE) for each path in turn, within the sample (Table 3-13) and pooled across the samples. The RMSE was approximately twice as large for sample 140-15 as for the other four samples. There were the remains of a branch on the edge of the sample 140-15. The defect was avoided as well as possible but these results indicate that the paths nearest to it must have been affected even if in visual observation it seemed that the defect was avoided. In the dataset as whole the RMSE was 7.14 kg/m^3 which corresponded to 1.6 % of the pooled average density.

Table 3-13. Root mean square errors for the individual paths and the samples in average in the X-ray density (kg/m^3) measurements.

RMSE	Sample ID				
	55-28	72-15	130-39	140-15	243-19
Path 1	5.19	7.49	6.62	14.25	6.21
Path 2	1.62	4.18	4.00	19.86	5.08
Path 3	2.80	4.76	8.73	10.44	3.77
Path 4	1.97	3.48	8.34	6.35	5.11
Path 5	4.97	4.26	7.85	11.92	7.36
Average	4.39	5.03	7.31	13.33	5.64
% of sample mean	1.1 %	1.2 %	1.7 %	2.5 %	1.2 %

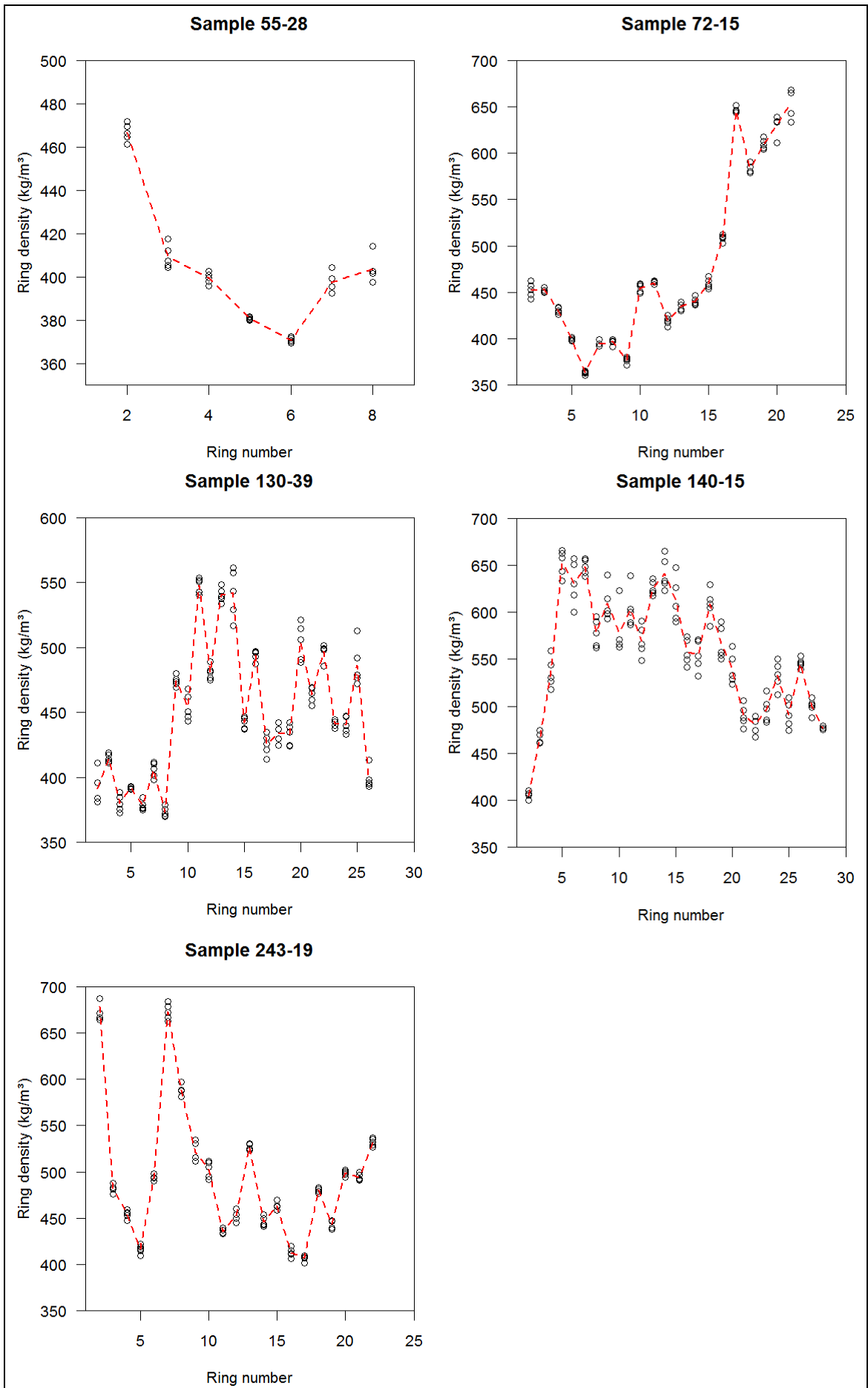


Figure 3-8. Variation in the ring density due to the differences in the path location. Average across the paths marked with the dashed red line.

3.3.2 Sample alignment

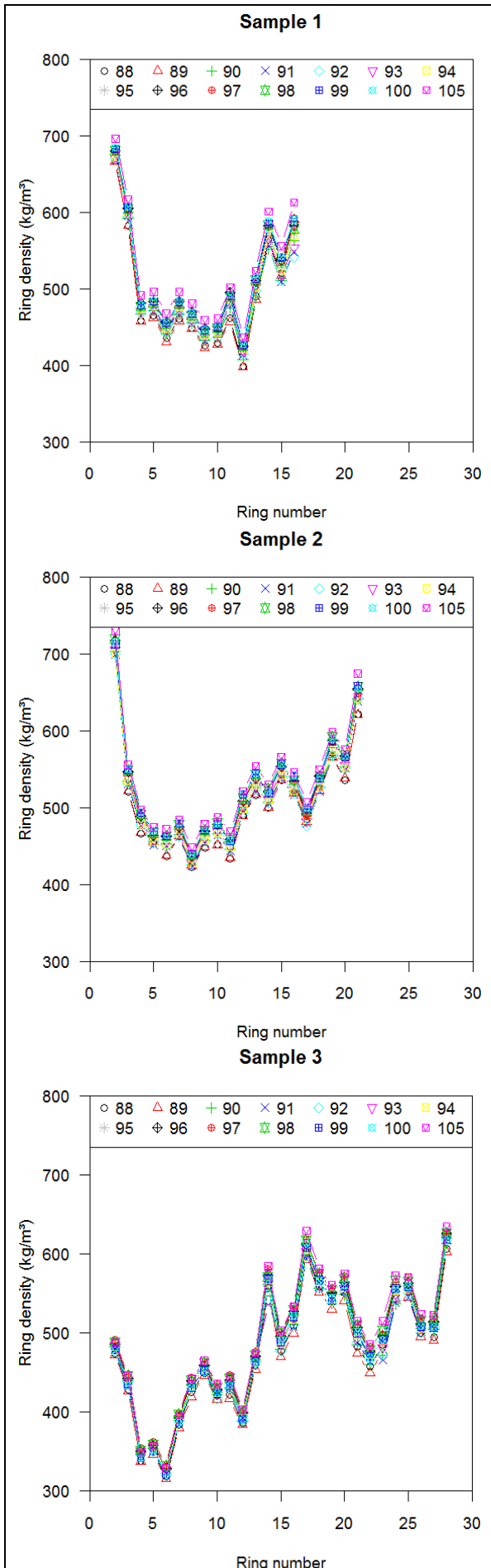


Figure 3-9. Ring density plotted for the 3 radii analysed in vertical position at the different angles.

Three samples with well aligned rings from the Kershope site were used in this experiment. In the sample alignment experiment one WinDENDRO path per sample was used for each scan. There was variation in ring densities with the sample angle (Figure 3-9) and in most cases the highest angle (105°) seemed to yield the highest density values, whereas 89° corresponded to lowest values. Looking at the vertically tilted samples (Figure 3-10) the differences were not so systematic but there was variation between different angles. At a given angle, positioning the sample in front of the sample holder or tilting it vertically did not cause much variation in ring density in the case of sample 1 (Figure 3-11). For sample 3 tilted positions always yielded slightly lower density values.

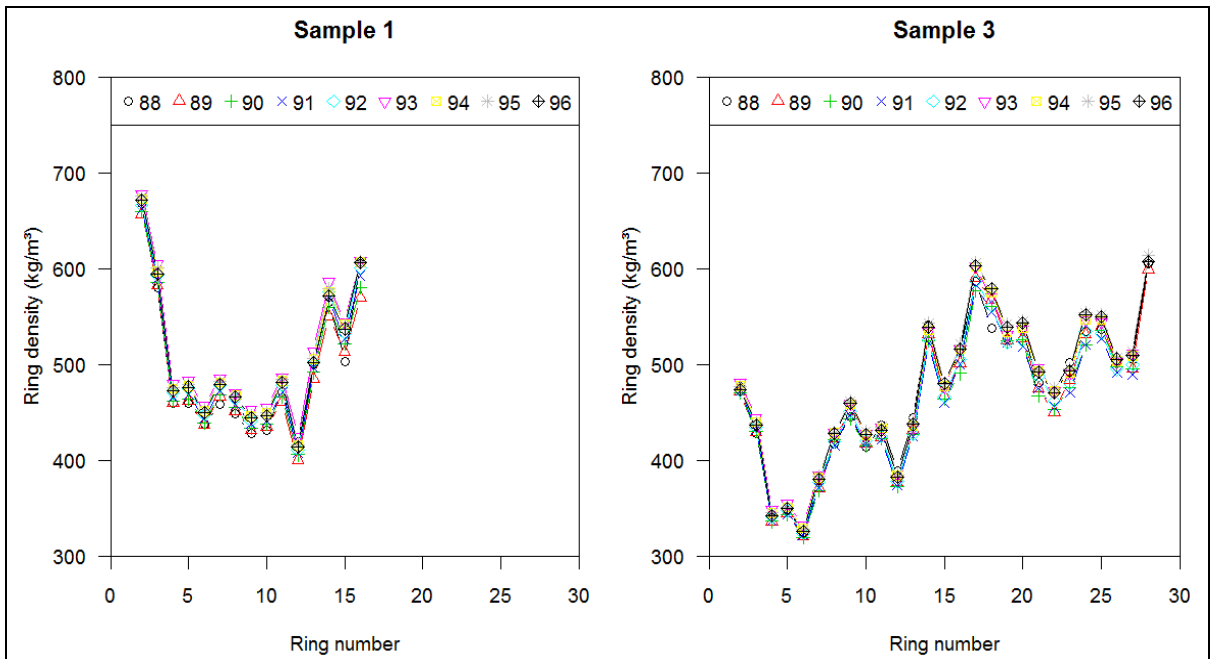


Figure 3-10. Influence of sample angle on the ring density of the vertically tilted radii.

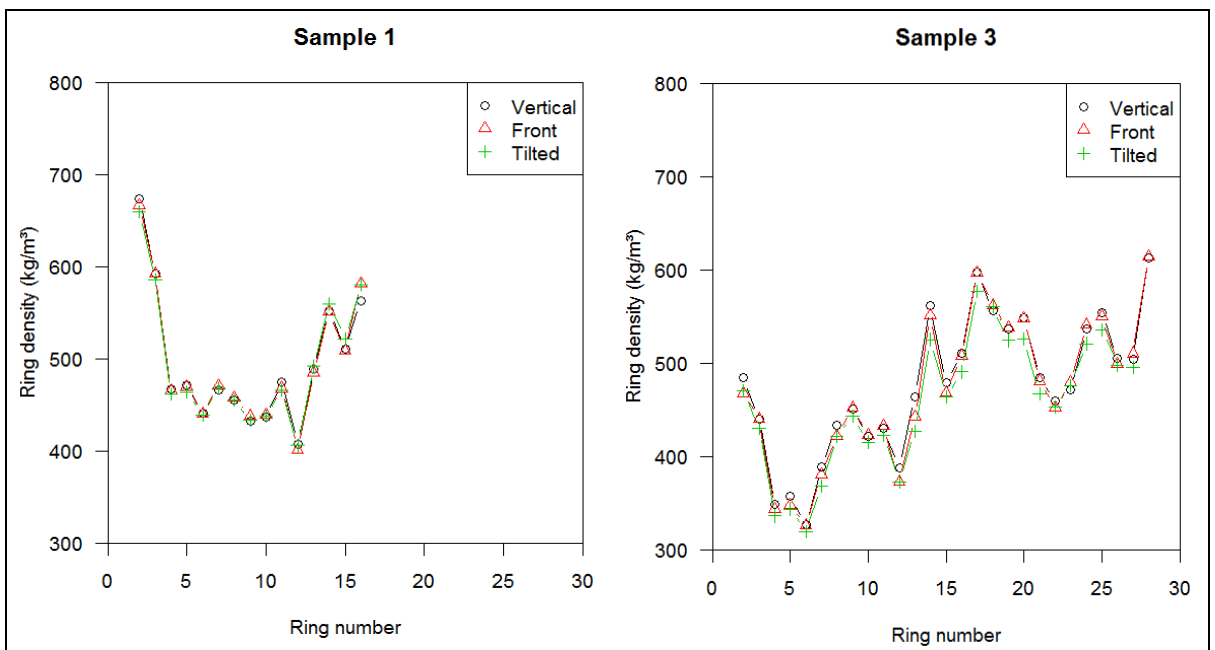


Figure 3-11. Influence of sample positioning on the ring density at 90° angle to the beam.

When the sample average densities were compared (Figure 3-12), there seemed to be an increasing trend in the average densities in both vertical and tilted samples when the angle increased beyond 90°. Curiously, in all the cases except for the tilted sample 3, a decrease in density was observed when the samples were turned to the left (angles 89 and 88°). In the case of sample 1 the vertical and tilted position yielded comparable results across different angles (Figure 3-13) whereas for sample 3 the density at the tilted position was consistently lower from 90° onwards.

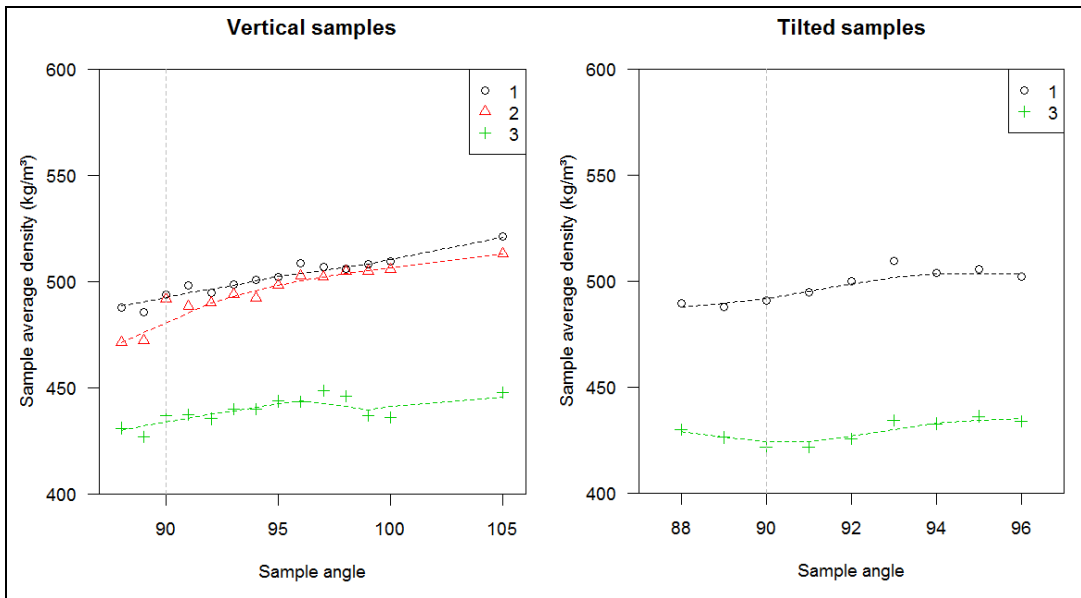


Figure 3-12. Influence of analysis angle on the average density of samples mounted vertically (left) and tilted (right). Dashed lines are the LOWESS curves.

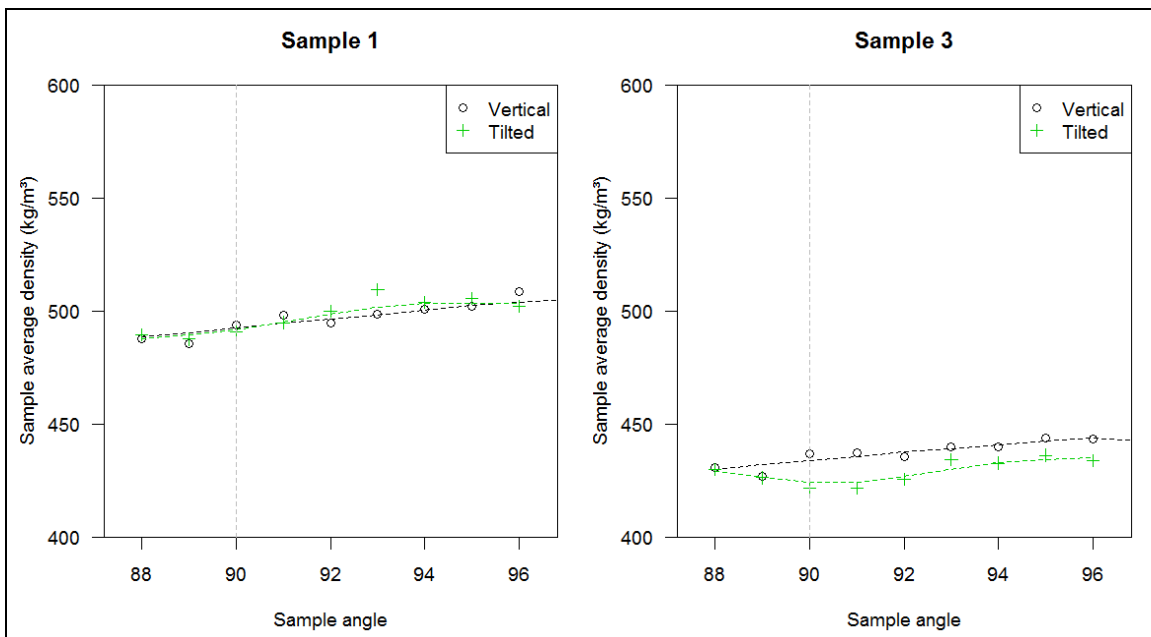


Figure 3-13. Comparison between vertical and tilted samples at different analysis angles. Dashed lines are the LOWESS curves.

When samples are not perpendicular to the X-ray beam, the length of the path that X-ray passes along inside the sample is increased. This could artificially increase density results as the path length for the X-ray beam is assumed to be equal to the value of sample thickness inserted by the user to WinDENDRO. Therefore, the increase in the X-ray beam path length with angle was calculated for 1.97 mm and 2 mm samples (Figure 3-14). In calculating the increase in the path travelled by the beam in the sample as the sample angle to the beam increases, it is important to note that WinDENDRO only takes the width information in 2 decimal places. Therefore, in case of both samples the input width

information would in practice only change once the sample angle reached 95 degrees. Therefore, the increase in path length within the normal operating conditions should not decrease the level of accuracy obtainable from the WinDENDRO density analysis. At 95 degree angle the change in the path length alone would cause approximately 0.5% error (Figure 3-14) in the density values whereas the average total error at that angle was 2.2% (Table 3-14). This indicates that the error arising from cell alignment had larger contribution than the slight increase in path length. In practical terms the errors remained small.

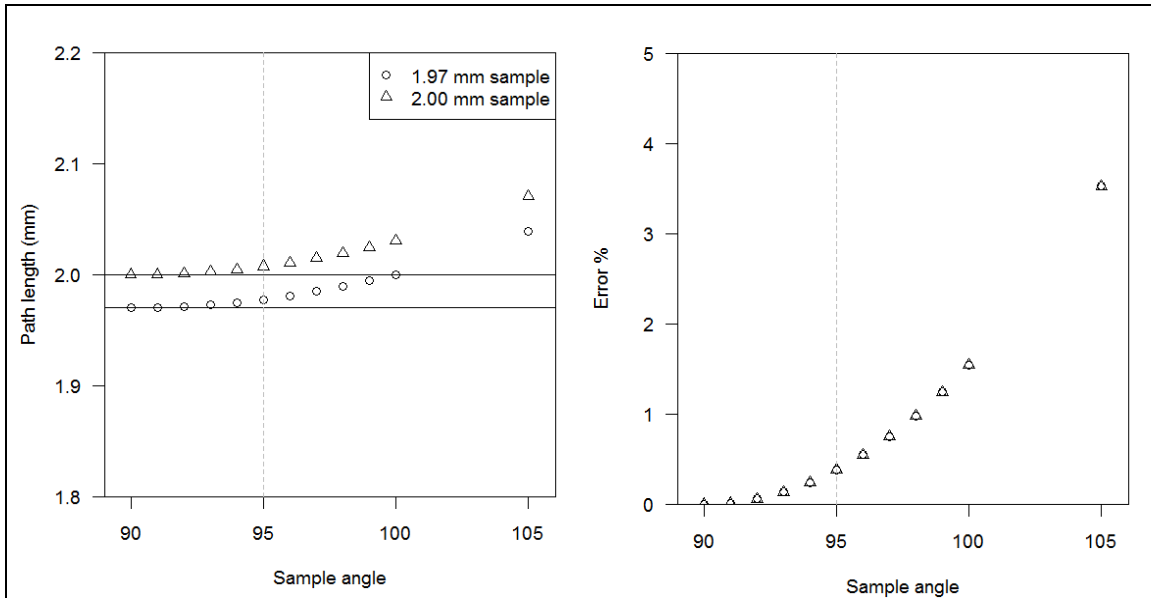


Figure 3-14. Calculated length of the path that x-ray beam travels through the sample strips at different angles (left) and the resulting percent increase in the path length due to the angle (right). The dashes vertical line marks the 95 degree sample angle which is considered the upper limit below which the sample angles should lie in normal operating conditions.

Table 3-14. RMSE for density measurement at different angles in the realistic working range compared to the 90 degrees to the beam.

	Sample 1	Sample 2	Sample 3	Average	% of average 90° density
91 degrees	6.46	3.94	7.30	5.90	1.2 %
92 degrees	6.65	3.13	3.50	4.43	0.9 %
93 degrees	7.87	2.88	6.59	5.78	1.2 %
94 degrees	10.03	2.24	7.51	6.59	1.4 %
95 degrees	11.88	7.31	12.02	10.40	2.2 %

3.3.3 Conversion from X-ray density to gravimetric density

For all the samples very similar values were obtained for the mean sample width by all the measuring methods (Figure 3-15). There were no significant differences between the measurements (Table 3-15). Therefore, the measurement procedure was deemed reliable and the data acceptable for the development of regression equation for the density value correction.

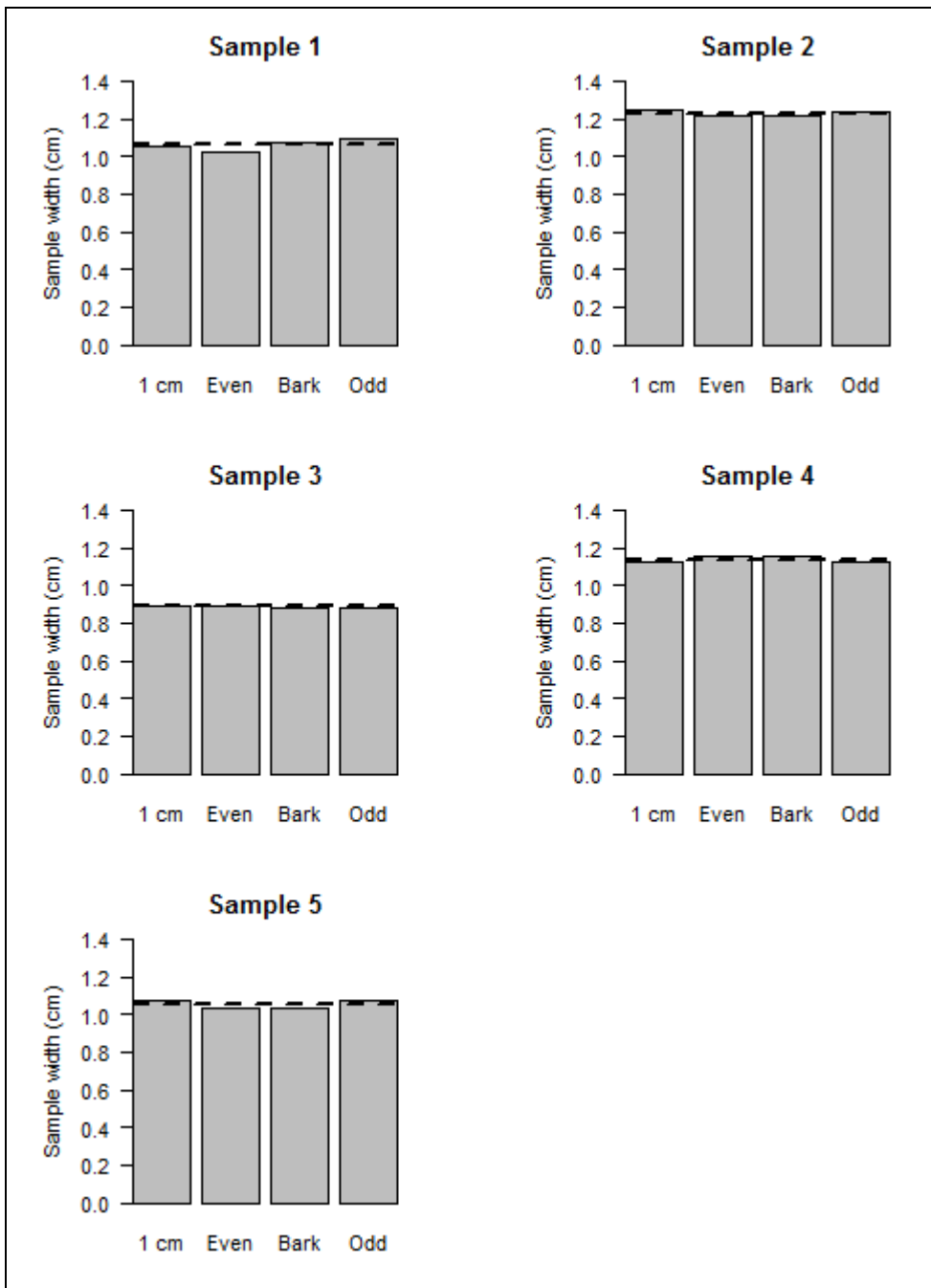


Figure 3-15. Sample widths determined by the four different measurements. Sample width was measured at one centimetre intervals along the samples strips and each measurement point was numbered. Sample widths were calculated using measurements starting from the end of the sample (Bark), one centimetre from the edge (1 cm) and derived by averaging odd (Odd) or even (Even) numbered measurements. Dashed line represents the mean across the methods.

Table 3-15. P-values for comparing the measurement methods for each sample.

Sample number	p-value for the comparison
1	0.283
2	0.978
3	0.856
4	0.576
5	0.873

Linear regression (Figure 3-16 and Table 3-16) was used to derive the conversion from ITRAX density to oven dry density.

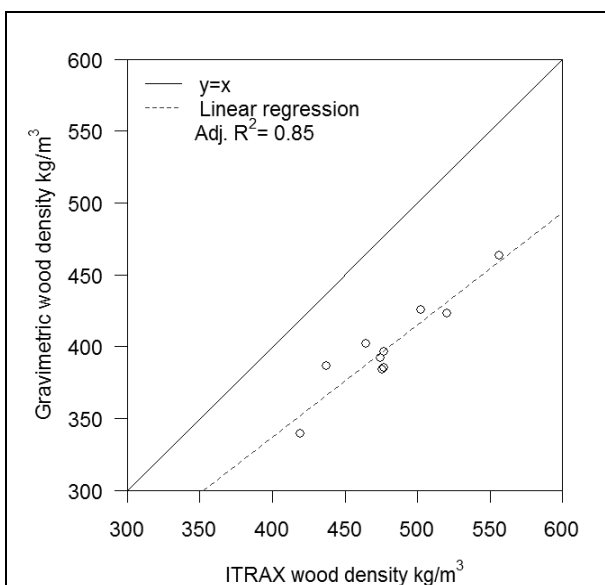


Figure 3-16. ITRAX wood density plotted against the oven dry gravimetric density.

Table 3-16. Regression equation for converting ITRAX density to oven dry wood density.

Coefficients:				
	Estimate	Std. Error	t value	Pr(> t)
(Intercept)	24.526	51.251	0.48	0.645
ITRAXdens.kg	0.781	0.106	7.35	8.03*10 ⁻⁰⁵ ***

Signif. codes: 0 '***' 0.001 '**' 0.01 '*' 0.05 '.' 0.1 ' ' 1

Residual standard error: 12.49 on 8 degrees of freedom
 Multiple R-squared: 0.8709, Adjusted R-squared: 0.8547
 F-statistic: 53.94 on 1 and 8 DF, p-value: 8.035e-05

The equation for converting ITRAX density expressed in kg/m³ to over dry wood density was of the form:

Equation 3

$$\text{Wood density}_{\text{dry}} \text{ (kg/m}^3\text{)} = 24.5263 + 0.7813 * \text{ITRAX density (kg/m}^3\text{)}$$

This is well in line with previous findings by McLean (2007) who derived values of 20.6 for the intercept and 0.778472 for the slope, based on the same assumptions.

Based on regression analysis of ITRAX density and gravimetric density of samples conditioned in the ITRAX chamber (Figure 3-17 and Table 3-17) an equation correcting the values to gravimetric density under typical scan conditions was derived (Equation 4).

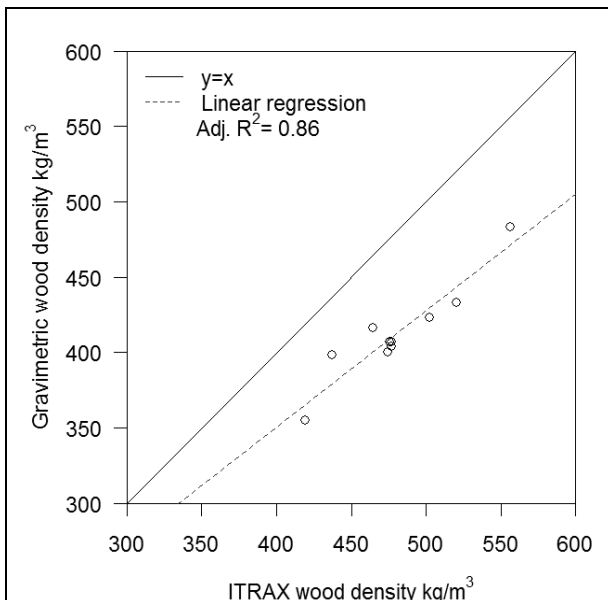


Figure 3-17. ITRAX density plotted against gravimetric density at moisture content of a typical scan.

Table 3-17. Regression equation for converting ITRAX density to gravimetric density under the scan moisture content.

Coefficients:											
	Estimate	Std. Error	t value	Pr(> t)							
(Intercept)	40.9949	49.0179	0.84	0.427							
ITRAXdens.kg	0.7738	0.1017	7.61	6.27*10 ⁻⁰⁵ ***							

Signif. codes:	0	'***'	0.001	'**'	0.01	'*'	0.05	'.'	0.1	' '	1
Residual standard error: 11.94 on 8 degrees of freedom											
Multiple R-squared: 0.8785, Adjusted R-squared: 0.8633											
F-statistic: 57.85 on 1 and 8 DF, p-value: 6.269e-05											

Equation 4

$$\text{Wood density}_{\text{scan}} \text{ (kg/m}^3\text{)} = 40.9949 + 0.7738 * \text{ITRAX density (kg/m}^3\text{)}$$

Mean moisture content of the samples conditioned in the ITRAX chamber for 24 hours was approximately 4 % (3.99%, with standard deviation of ±0.44). In ambient conditions the mean moisture content was approximately 7.4% (st.dev ±0.41). Both values are slightly lower than those predicted by the relative humidity, temperature, moisture content graphs in Dinwoodie (2000). Samples that had lower moisture content under ambient conditions also had lower moisture content under ITRAX conditions (Pearson’s correlations coefficient 0.78, Figure 3-18).

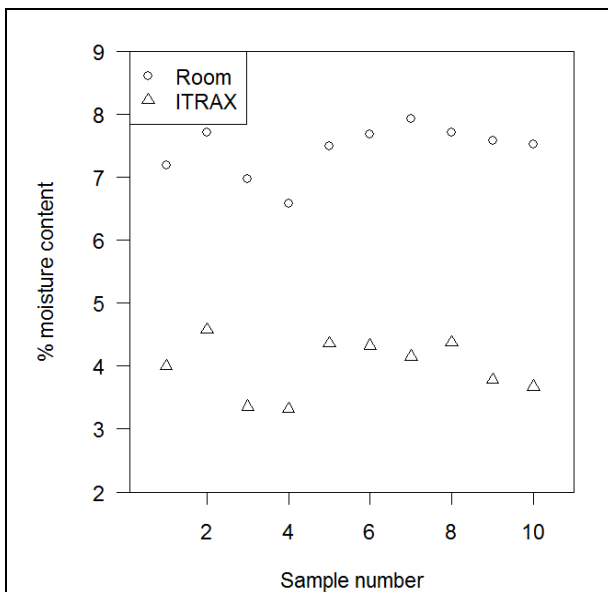


Figure 3-18. Moisture contents of the samples in room and ITRAX chamber conditions.

The experimental density was then corrected to 12% moisture content according to Simpson (1993). In the equations 4 and 5 MC stands for moisture content, RW for ring width and dens for density.

Equation 5

$$\text{Density}(Dens, MC1, MC2) = \frac{1 + \frac{MC1}{100}}{1 + \frac{MC2}{100}} \left[1 + \frac{0.009 * (MC2 - MC1) * \frac{Dens}{\left(1 + \frac{MC2}{100}\right)}}{1 + 0.009 * (30 - MC2) * Dens} \right] * Dens$$

Furthermore, the ring width was then adjusted to 12% moisture content:

Equation 6

$$RW(RW_{MC2}, MC1, MC2) = (1 + ((MC1 - MC2) * 4.3/30/100)) * RW_{MC2}$$

This conversion assumed linear increase in ring width in all parts of the ring as well as linearity of the increase between 0% moisture content and the fibre saturation point (MC 30%).

3.4 Conclusions

The influence of humidity on density was statistically significant only for the path average density when the entire humidity range (0-28%) was considered. If the highest humidity scan was removed the effect became non-significant. Individual ring widths were not significantly influenced by humidity but the total paths lengths were. However, the effect on total path lengths was small in practical terms (approximately 1% error). It was decided that for the X-ray measurements relative humidities below 15 % would be a suitable working range, which according to Dinwoodie (2000) would result in 5% moisture content in the wood under the typical operating temperature range. The models developed here were linear whereas the change in moisture content of wood is not linear when relative humidity reaches higher levels (Dinwoodie, 2000). Therefore, these models should not be applied outside the relative humidity range studied here.

Variation between paths within a sample was low, ranging from 1.1 % to 2.5 % of the sample average density measurement. As a defect was present in the sample 140-15 that yielded the highest value, the RMSE in normal samples is likely to be approximately 1.5 %. In this light, one path could yield satisfactory data. However, addition of second path on the image does not require much additional time and allows effective quality control of data. When the two paths are plotted against each other mistakes in, for example, ring detection and sample width are easily observed. If only one path was used it would require more complicated screening of the data to detect mistakes. This would be especially risky when there was only 1 sample per tree. Therefore, two paths were used throughout the tree ring analysis in this study. Sample alignment was calculated to cause a 2.2 % error in density values if the samples were tilted as much as 5 degrees off perpendicular. To avoid

sample tilting on that scale the double sided tape was changed regularly to ensure proper adhesion.

The variation caused in density by humidity was in the range 1-1.5%, which is similar to that caused by random variation in path location even when every effort is made to place the paths optimally. Since the variation due to moisture was not significantly larger than the unavoidable variation due to path location it is concluded that the current method of climate control by dry air produced density measurements of satisfactory quality. Hoag and Krahmer (1991) recommended that the moisture content of samples should not vary by more than 2%. In the low range of air humidity used here (0-15%) the variation in wood moisture content with humidity is small (Dinwoodie, 2000) and should satisfy the conditions set by Hoag and Krahmer (1991).

The quality of width measurement in building the regression equation for density corrections was deemed satisfactory. All the density and ring width data were converted to 12% MC values but for the major part of the analyses the 4% MC values were used preferentially. This was due to the assumptions in ring width conversion where an increase in width was assumed to occur equally in earlywood and latewood, which after all have different properties (Leonardon et al., 2010). Due to this, the unconverted ring widths were preferred and they were then matched with the density data corrected with the empirical regression equation.

4 Tree growth dynamics in Sitka spruce

This chapter reports the findings xylem growth monitoring from Griffin dendrometer experiment for the year 2008. The results section first reports the thermal expansion correction calculations for the dendrometers as well as presents the growth curves detected by the dendrometers (4.3.1). In the following section (4.3.2) the difficulties of microcore analysis and the implications for future sample collection are addressed. Then, the tree growth detected by the point dendrometers is compared to values measured from microcores collected during the site visits (4.3.3). The influence of climatic variables on radial increments is then studied using correlation analysis (4.3.4). Finally, density measurements of the 2008 ring from the studied trees are linked to the radial increment data (4.3.5).

4.1 Introduction

In a temperate climate, tree growth takes place over the summer months and the timber properties are the end result of varying growing conditions over the growing season. In addition, each tree ring will be influenced by the conditions of the previous year, as trees can use reserves for growth (Hoch et al., 2003) and needles are retained for several years (Cannell, 1987). At the beginning of the growing season growth is fast and wide diameter earlywood cells are produced. Later in the season the growth rate slows and a transition to latewood production takes place. The timing of growth onset, the growth rate and the latewood transition are influenced by the weather conditions. Measuring radial growth in real time allows detailed information to be obtained on the timing of growth initiation as well as relating anomalies in growth to specific weather events.

Onset of growth in temperate climate depends most strongly on the accumulated temperature sum (Cannell and Smith, 1983). Whereas the growth rate may be influenced both by temperature and rainfall during the growing season (Grace and Norton, 1990; Mäkinen et al., 2002a). In the UK conditions, bud burst is thought to occur between end of March and the end of May and wood production is estimated to end between July and November (Denne, 1977). Sitka spruce has a high chilling requirement and therefore the temperature sum required for the growth onset is also impacted by winter temperatures (Cannell and Smith, 1983; Cannell and Smith, 1986; Murray et al., 1989).

Knowledge on how weather influences the growth rate and pattern will aid the prediction of wood properties (Downes et al., 1999). However, precision instruments are required for studies on short-term growth response (Clark et al., 2000). A dendrometer is a device for measuring tree diameter either by detecting increment in circumference (band dendrometer) or in radius (point dendrometer). Band or point dendrometers can be applied to monitor short term changes in radius (Mäkinen et al., 2003b) and yield information on the seasonal activity of the vascular cambium (Bouriaud et al., 2005). Modern dendrometers fitted with dataloggers can collect high resolution measurements of the tree radius at short time intervals ranging typically from a few seconds (5 s (Zweifel et al., 2000; Zweifel et al., 2001) to a few minutes (10-20 min (Milne, 1989; Milne et al., 1983; Offenthaler et al., 2001; Wimmer et al., 2002; Zweifel and Häsler, 2000; Zweifel and Häsler, 2001). Measurements are then typically averaged for 10 min (Zweifel et al., 2000; Zweifel et al., 2001), 15 min (Offenthaler et al., 2001) to 1 hour (Mäkinen et al., 2008; Milne, 1989).

However, the use of these datasets for radial growth monitoring is confounded by other factors that influence the tree radius such as water reserves (Zweifel and Häsler, 2001). Elastic tissues in the cambial region may swell after rainfall as transpiration ceases and root water uptake continues (Downes *et al.*, 1999). Diurnal changes in stem radius take place as transpiration causes a water flow through the tree and a depletion of stored water (Zweifel and Häsler, 2001). It has been found that the shrinkage phase starts in the morning and the diameter recovers during an expansion phase that starts in the evening (Downes et al., 1999; Zweifel and Häsler, 2000; Zweifel and Häsler, 2001). The maximum shrinkage has been found to be reached at times of rapid transpiration in the early afternoon (Milne et al., 1983). In mature Norway spruce of 150-250 years of age the water induced fluctuations of the bark, which was assumed to be the stem water storage location, exceeded the increase in diameter due to growth (Zweifel and Häsler, 2001). In slow growing trees the water related diameter fluctuation may prevent the detection of xylem formation (Mäkinen et al., 2003b). The detection of growth onset in the spring is particularly difficult in these conditions (Zweifel and Häsler, 2001).

There are different views on which tissues take part in water storage and hence cause the reversible fluctuations in stem diameter (Mäkinen et al., 2003b). When a clear diurnal pattern in stem diameter was detected with point dendrometers the fluctuations were concluded to take place in xylem since phloem and bark had been removed prior to the installation of the dendrometers (Offenthaler et al., 2001). Zweifel et al. (2000) on the other hand assumed that at normal water potential the contribution from xylem was

minimal and even when water withdrawal occurred, the xylem maintained its size. They found that the elastic tissues like cambium, phloem and parenchyma almost solely contributed to stem contraction (Zweifel et al., 2000). Furthermore, changes in radius closely followed the bark water content (Zweifel et al., 2000). Similarly, Milne (1989) reported that in Sitka spruce, phloem and bark constituted the main water storage in the stems. Diurnal fluctuations in diameter were largest near the crown and lowest near the base of the stem (Offenthaler et al., 2001; Zweifel and Häsler, 2001). Dendrometer measurements could also be influenced by fluctuations in cambium width during a growing season (Wimmer et al., 2002). The problems are thought to be more severe in band dendrometers, the type used by Mäkinen et al. (2003b; 2008) as slack often remains in the band before the tree growth pushes it tight and therefore newly installed band dendrometers detect less growth (Keeland and Sharitz, 1993). However, Mäkinen et al. (2008) installed the band dendrometers 1.5 years prior to the study period.

Due to these interferences, some authors (Mäkinen et al., 2003b; Mäkinen et al., 2008; Zweifel and Häsler, 2001) have concluded that dendrometers alone are not sufficient for detailed monitoring of radial growth, especially due to problems in detecting the onset of xylem formation. To overcome the problem, the dendrometer measurements can be supplemented with microsampling of the xylem either by pinning (Mäkinen et al., 2008; Seo et al., 2007) or microcoring (Bäucker et al., 1998; Forster et al., 2000; Mäkinen et al., 2008; Rossi et al., 2006a; Rossi et al., 2006b). In the former method a needle is inserted to the cambium to cause diagnostic damage that can be detected in the wood samples (Seo et al., 2007). Pinning is carried on at regular intervals during the growing season and at the end of the study period the trees are either felled or wood samples containing the pinnings extracted with a chisel. The pinning canals, identified by wound tissue, will then be used to deduce the stage of growth at the pinning date. In the latter method small increment cores, typically a few mm in diameter and 1-2 cm in length (Bäucker et al., 1998; Rossi et al., 2006a; Rossi et al., 2006b; Zweifel et al., 2006), are collected from the trees at regular intervals during the growing season. The samples can be used to measure the width of xylem developed, count the cells formed or even to distinguish between different stages of development when the samples are stained.

This study used linear variable displacement transducer (LVDT) point dendrometers complemented with microcore sampling to monitor the growth of Sitka spruce. The trees selected for the experiment were vigorously growing plantation trees. The mean annual increment in the Griffin forest was estimated to be $0.7 \pm 1.0 \text{ cm tree}^{-1} \text{ yr}^{-1}$ (Wingate, 2003). Therefore, the problems particular to slow growth (Mäkinen et al., 2003b; Zweifel and

Häsler, 2001) should not apply to these sample trees. The purpose of the monitoring was to establish the timing of growth onset as well as to study the seasonal variation in growth rate and to attempt to connect the growth data to observed values of timber density.

4.2 Materials and Methods

4.2.1 Site and Tree Selection

Griffin experimental forest near Aberfeldy, Scotland (56°37'N, 3°48'W), was selected for the experiment. The site has been used for long term monitoring by Edinburgh University as a part of the CARBOEUROFLUX network (Wingate, 2003). Therefore, previous and current data exists for example on different fractions of radiation, temperature at different heights in the canopy, tree stems and soil, wind and rainfall. The site is located in a fairly isolated forest area which decreases the possibility of the public interfering with the monitoring devices.



Figure 4-1. Road leading to the Griffin experimental site where the dendrometer experiment was established in April 2008.

The forest is located at 340 m altitude. The soil types at the site are peaty gley and podsol. The site receives, on average, 1200 mm of precipitation annually and experiences a mean temperature of 8.2°C. The site was previously moorland and the Sitka spruce stand was planted in 1981 at approximately 2200 stems/ha stocking (Wingate, 2003). The stand has been row thinned. In the thinning every 5th row was removed.

A rectangular sampling plot (35 m * 21 m) was established at the Griffin experimental forest. The DBH of all trees (97) inside the plot was measured and the trees divided into quartiles. 5 dominant trees without any visible defects were randomly selected as the sample trees (Table 4-1).

Table 4-1. The selected sample trees at the Griffin site and their DBH and height at the time of plot establishment April 2008.

Tree number	Dendrometer number	DBH (cm)	Height (m)
08	3	30.4	18.8
15	4	28	18.7
43	2	27.6	17.9
48	1	36.7	20.6
66	5	26	15.7

4.2.2 Dendrometers

Point dendrometers were mounted on the North side of the selected trees. The dendrometer setup consists of 5 LVDT (Linear Variable Displacement Transducer) probes for recording variations in the tree diameter. The LVDT dendrometers are fixed on the trees using two stainless steel beams. The first beam is mounted on the tree with a screw on the East or West side. The second beam is fixed to the first at a 90 degree angle to support the dendrometer on the North face of the tree (Figure 4-2). The beam supporting the dendrometer was further fitted with a spirit level to detect any displacement of the beam. The beams were thermally insulated with Styrofoam.



Figure 4-2. Point dendrometer on a tree at the Griffin site, Aberfeldy, Scotland.

Furthermore, two thermistor temperature sensors were fitted on each tree to monitor the temperature changes of the metal and the wood. One was fixed on the metal beam and the

other was inserted into the tree trunk by drilling a small hole to fit the sensor. The hole was then covered with blue tack to fix the sensor in place as well as prevent the air temperature from interfering with the measurement. The thermistor measurements allowed the calculation of thermal expansion of the metal fixture and of the trees themselves, which could interfere with the radial growth measurements. Probes for monitoring the air temperature, air humidity and soil moisture were also connected to the datalogger system (Campbell Scientific, CR23X). Axel Wellpott from Forest Research (currently at Cranfield University) wired the dendrometers and developed programmes for running the dendrometers and formatting the data.

The datalogger setup (Figure 4-3) recorded the tree diameter measurements every 2 minutes and the measurements were then averaged for 15 minutes. Thermistor, air temperature, air humidity and the soil moisture values were recorded every 15 minutes. The site was visited 2-3 weekly to change batteries and to download data.

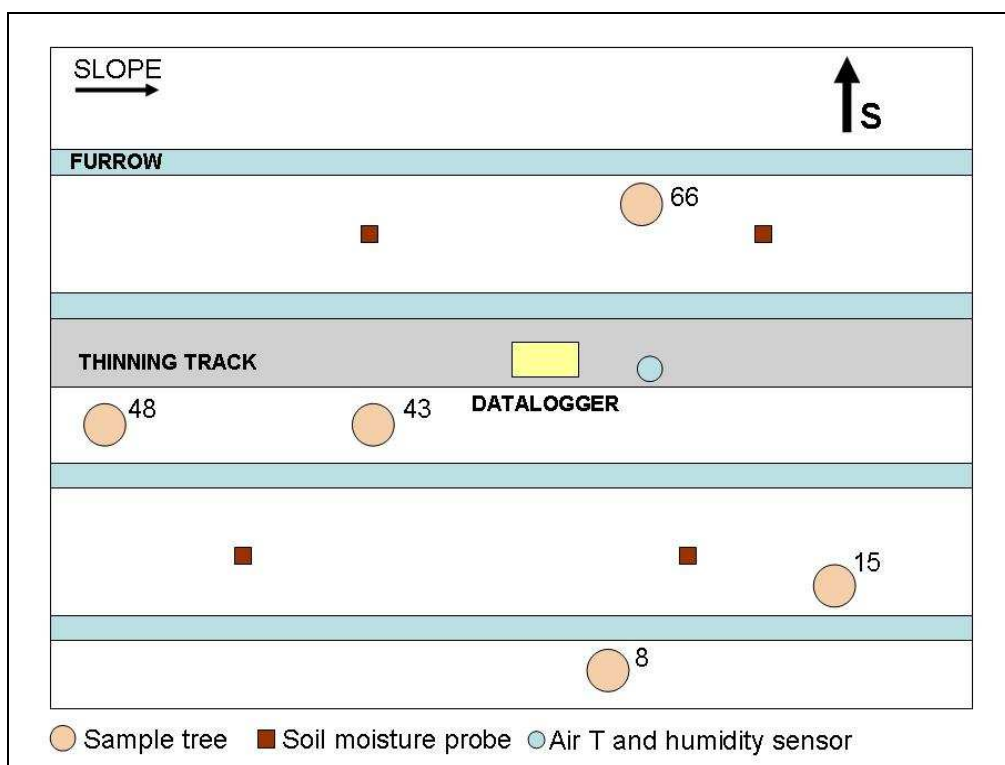


Figure 4-3. Location of the dendrometer trees and soil moisture probes on the sample plot established at the Griffin site.

The measurements of the radius were divided into 3 phases according to Downes et al. (1999). The phases used were shrinkage, recovery and increment (Figure 4-4). The same three phases were also used in studies of *Abies balsamea*, *Picea abies*, *Pinus cembra* and *Larix decidua* (Deslauriers et al., 2007; Deslauriers et al., 2003) and *Picea mariana* (Turcotte et al., 2009).

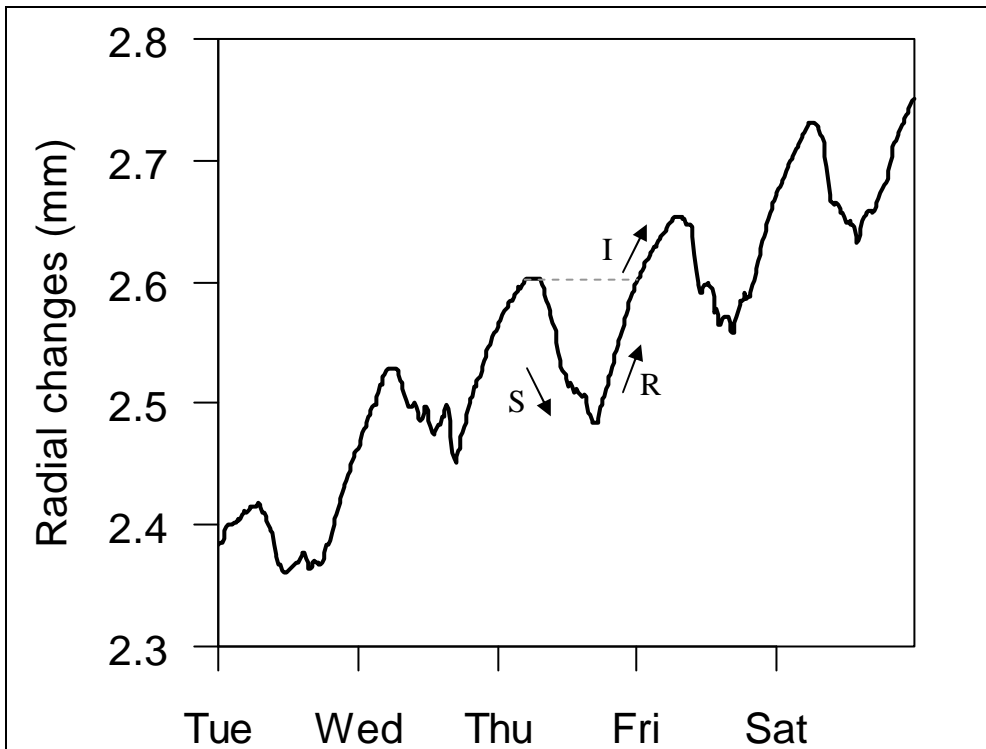


Figure 4-4. Graphical illustration of the shrinkage (S), recovery (R) and increment (I) phases defined by Downes et al. (1999). Shrinkage will take place from previous day maxima (dashed line) until the afternoon minima. This is followed by a recovery phase which is considered to last until the radius reached the maximum value of the previous day and any increase after that is recorded as radial increment.

Thermal expansion corrections were calculated using the linear thermal expansion coefficient for wet wood $14.8 \cdot 10^{-6} \text{ K}^{-1}$ (Sevanto et al., 2005) and for stainless steel $17.3 \cdot 10^{-6} \text{ K}^{-1}$. Thermal expansion of the wood material will increase the radius measured as it will press the end of the LVDT (Figure 4-5). Expansion of the steel bar perpendicular to the LVDT has the opposite effect since it will move the LVDT further away from the trunk and hence release the spring in the tip.

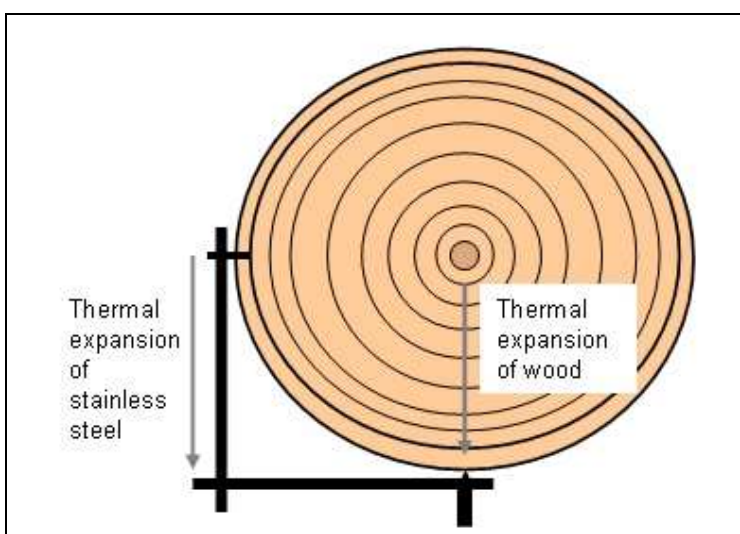


Figure 4-5. Influence of thermal expansion of wood and thermal expansion of stainless steel on the dendrometer measurements.

4.2.3 Microcoring

On each visit to the site two microcore samples were collected from each sample tree. The cores were taken from the North side of the tree because the data was used to validate the radial growth detected by the dendrometers. Furthermore, the microcore analysis allows separation between different cell development stages which would yield additional information on the xylem formation dynamics.

Modified medical needles (Figure 4-6) of 2 mm diameter were used for the coring. The needles were sharpened prior to each sampling occasion since quality of the cross-sections cut from the microcores is directly influenced by the sharpness of the cutting tool (Rossi et al., 2006a). Deep cracks or flakes may form on the surface of the cores as a result of inadequate tool sharpness (Rossi et al., 2006a). The cores were extracted from the needles by pushing with a metal rod from the pith side to avoid compressing the newly formed xylem cells. The cores were allowed to dry inside the needles for about two days prior to this to ease the extraction. Approximately 3 cm was left between the sampling point and previous holes to avoid growth anomalies caused by the coring (Bäucker et al., 1998; Forster et al., 2000).



Figure 4-6. Modified medical needles used to take the microcore samples (left). A microcore and a biocassette used in the paraffin impregnation (right).

The microcore analysis was carried out at the INRA Nancy laboratory where state-of-the-art equipment for sample processing was available. The microcores were observed under light microscope and the transversal side was marked with pencil to allow correct orientation when the samples were fixed in the paraffin blocks. The samples were then enclosed in biocassettes (Figure 4-6) for the automated paraffin impregnation sequence. As the samples had been stored dry they were immersed in 50% alcohol solution overnight

prior to starting the impregnation sequence (Table 4-2). During the sequence the water was gradually excluded from the cells by increasing the concentration of ethanol and D-limonene. The cells were filled with hot paraffin in the final step.

Table 4-2. Paraffin impregnation sequence

Solvent	Time (min)
Ethanol (70%)	120
Ethanol (70%)	120
Ethanol (90%)	90
Ethanol (90%)	90
Ethanol (95%)	90
Ethanol (100%)	90
Ethanol (100%)	90
D-limonene	90
D-limonene	90
D-limonene	90
Paraffin	120
Paraffin	120

After the sequence the microcores remained in hot paraffin for several hours to ensure proper impregnation. The samples were then fixed into paraffin blocks with the orientation mark facing up. Once the paraffin block had cooled and solidified sufficiently excess paraffin was removed. This was done by cutting thin sections with a rotary microtome (Microm, HM355) until the surface of the core was reached. The samples were immersed in water at least

overnight to facilitate the cutting. Thin sections (7-10 μm) were then sliced from the cores with the microtome (Figure 4-7). Sections were transferred to a warm (approximately 40° C) water bath from which they were collected onto microscope slides and left to dry on a hot plate set at 50° C. Microscope slides that had a surface layer of albumin were used to ensure strong adhesion. In addition to that, the sample slides were left in the 50° C oven for a minimum of 4 hours. The purpose of the heat treatments was to melt the paraffin surrounding the thin wood sections to prevent them sliding off the glass during the coloration step.

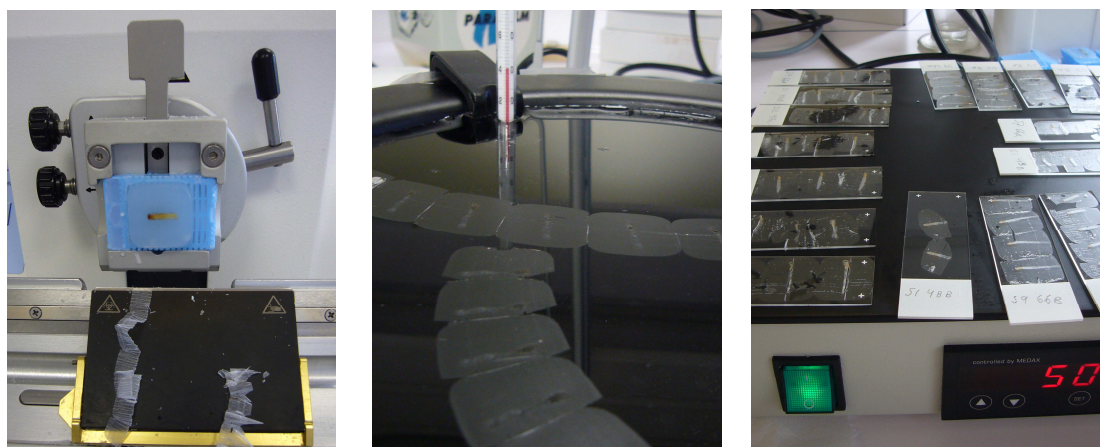


Figure 4-7. Microcore samples from the Griffin site were cut into thin sections with a rotary microtome (left), lifted out of a water bath (middle) and collected on albumin coated microscope slides that were placed on a hotplate (right).

The sections were then stained for detection of different growth stages. Staining was carried out by immersing the sections on the slides in four consecutive solutions; HistoClear (Flowgen Bioscience Ltd.) (20 min), Ethanol 96% (20 min), Cresyl violet acetate (20 min) and distilled water (6 min). After this, the sections were dried by gently pressing the surface of the slide with paper. Two drops of fixing agent were added on the top of the sections, then they were enclosed underneath a plastic cover slip and left to dry overnight.

Cresyl violet acetate produces a violet colour in unligified cell wall and blue in the mature cell wall (Rossi et al., 2006b) therefore it allows the lignification stage and mature cells to be distinguished. On the other hand, mature cells and those in the cell wall thickening stage will naturally shine under polarised light due to the arrangement of microfibrils in the cell wall (Rossi et al., 2006b). The cells in the enlargement stage lack this property which allows separation between these stages. Stained samples (Figure 4-8) were inspected under light microscope fitted with a light polariser.

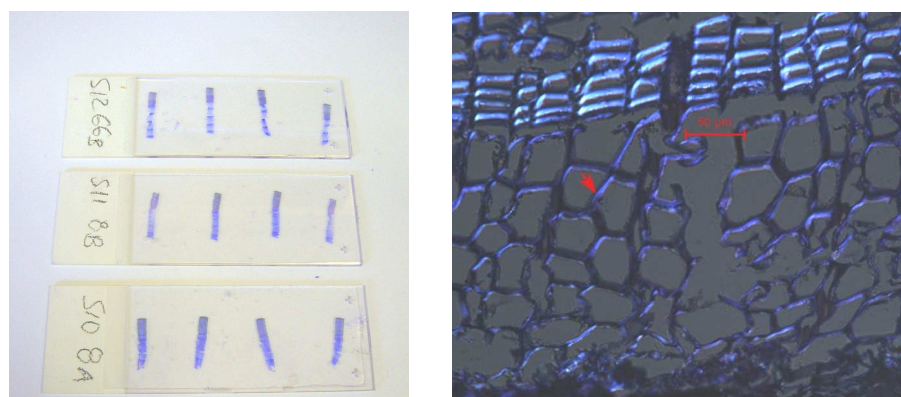


Figure 4-8. Coloured thin sections of Griffin microcores (left). Stained thin section observed under polarised light (right). Earlywood going through the wall thickening stage was characterised by glowing (arrow). Scale bar is 50 μ m.

4.2.4 Density determination

Increment cores (6 mm in diameter) were collected from the sample trees for density analysis. This was done during the growing season 2009 when it was certain that some growth had already taken place. Including some part of the 2009 ring in the sample ensured more accurate detection of the end of 2008 year ring in the WinDENDRO analysis. The samples were prepared the same way as described for the larger Benchmarking increment cores in Chapter 5. Pixel based output from WinDENDRO was used to produce detailed density curves of the 2008 growth for these five trees.

4.2.5 Data analysis

The dendrometer and microcore results of tree growth onset, determination and the final ring width were compared. Growth increments in different months were calculated. The relationship between different weather variables and the xylem increment was investigated using a 40 day moving correlation (Downes et al., 1999). The dendrometer data were used to connect the density measurements to an approximate date (Wimmer et al., 2002).

4.3 Results

4.3.1 Dendrometers

As the thermal expansion coefficients of wet wood (Sevanto et al., 2005) and stainless steel were of the same order of magnitude but impact the measurements to opposite directions, the influence of temperature on the radial measurements was expected to be small. The calculated values for the effect of temperature proved to be minimal (Figure 4-9) and the raw measurements were used in the following analyses.

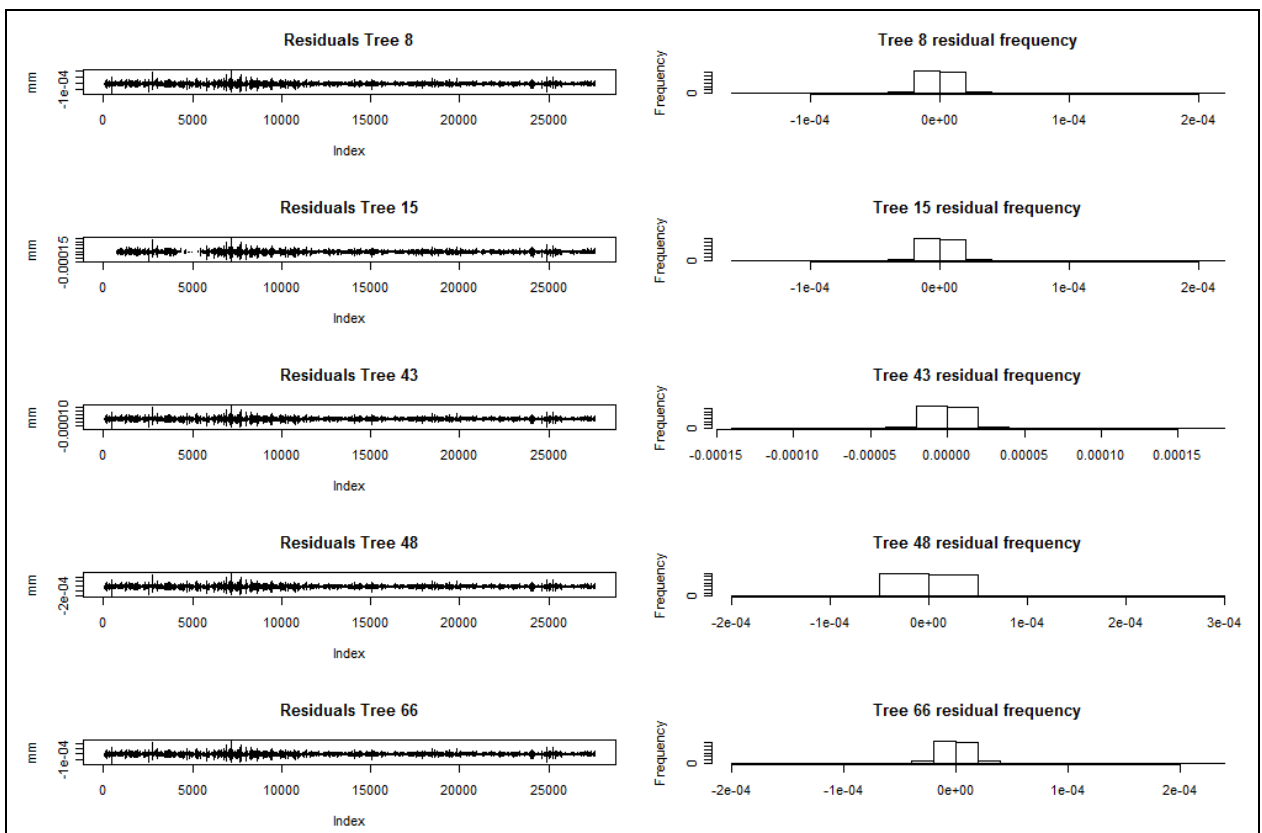


Figure 4-9. The residuals of LVDT measurements and thermal expansion corrected data for each of the studied trees (left) and the frequency distribution of the residual (right).

In most cases except for tree 66, the dendrometers were already detecting diameter increase in April (Figure 4-10). The period of fast growth extended from early May to the beginning of August except in tree 66 where the period of growth started later and finished earlier. A change to slower growth seems to coincide with the minimum values of soil moisture. Periods of relatively high temperature during the winter when also the relative humidity was lower seemed to be accompanied by shrinkage of the tree stems.

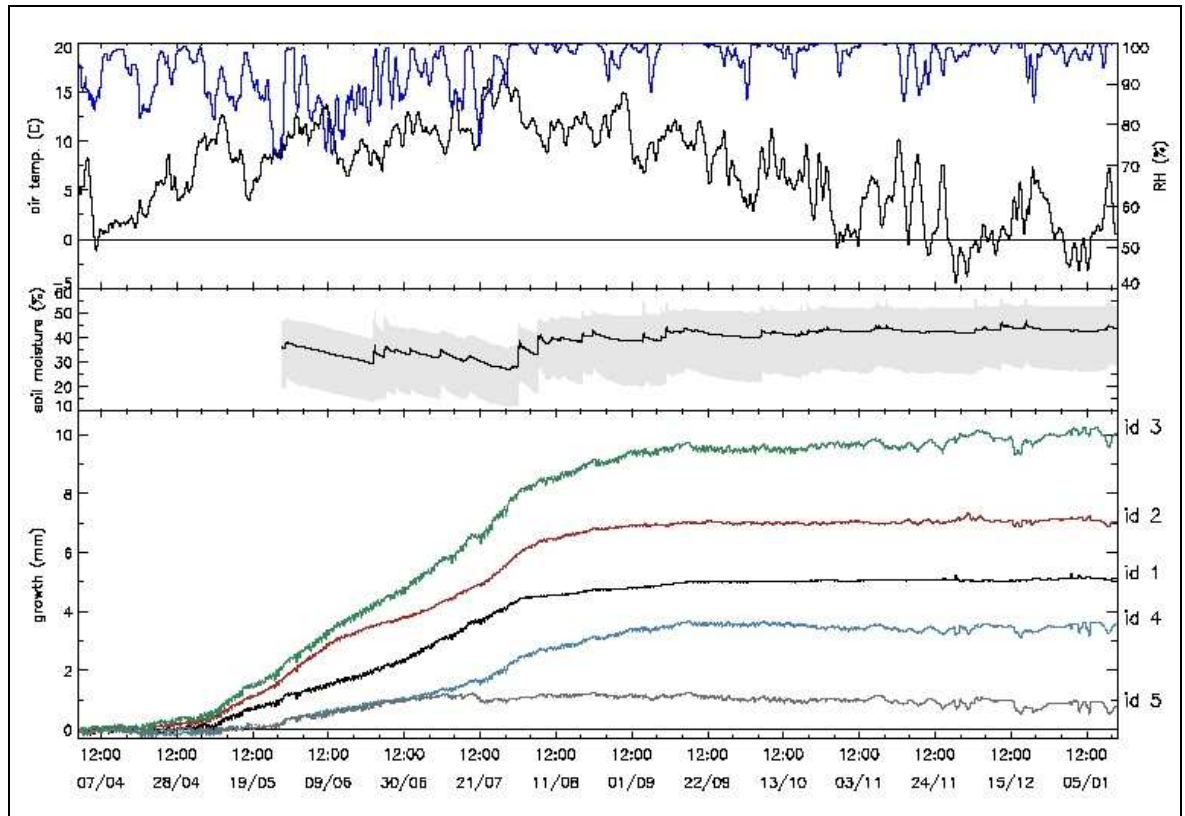


Figure 4-10. Air temperature (black) and relative humidity (blue) for the Griffin site (1st April 2008-13th January 2009) are shown in the top part of the graph. Soil moisture is plotted in the middle graph, where the black line illustrates the mean and the grey area measurements by the individual soil moisture probes. Radial growth detected by the LVDTs is shown at the bottom. LVDTs were fitted as follows; id 1 = tree 48, id 2 = tree 43, id 3 = tree 8, id 4 = tree 15 and id 5 = tree 66.

4.3.2 Microcores

During the analysis of microcore sections under microscope it was observed that the cells in the enlargement stage had been destroyed. This was clear under polarised light, which differentiates between cells in the enlargement stage and in the stage of cell wall thickening (Figure 4-11). Only very rarely were a few individual cells in the enlargement stage detected in the sections. More often, all the cells visible were in the cell wall thickening stage which was indicated by the glowing of the cell wall under polarised light.

The destruction of enlarging cells must delay the detection of growth onset in the microcore samples.

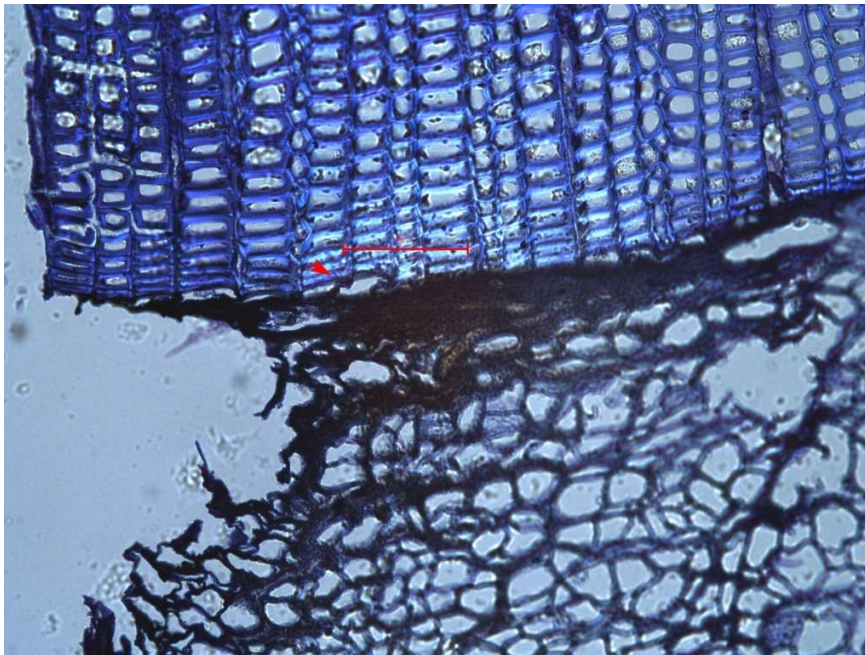


Figure 4-11. Latewood from previous year glowing under polarised light. Shrinkage is visible at the cambial region resulting into a funnel shape. Scale bar 100 μ m

It was thought that the enlarging cells were most probably destroyed during the stage of sample storage. The samples were left to dry inside the medical needles to ease extraction and were then stored dry. Microscope observations showed a funnel shape near where the cambial region would be located (Figure 4-11) which indicated a substantial amount of tangential shrinkage. During drying, these fragile cells would have also undergone a similar amount of shrinkage in the radial direction, which seems to have caused them to collapse. Otherwise, the sections were in relatively good condition which indicated that the sample extraction by medical needles was less likely to be the cause of the problems. In fact, the needles had been sharpened before each sampling trip to avoid damaging the wood material and causing cracking on the surface of the core (Rossi et al., 2006a). Based on these findings the sampling method was revised. During the 2009 growing season the needles containing the samples were immersed in 50% alcohol in the field and once back in the laboratory they were extracted from the needles. The samples were stored in 50% alcohol at 5° C until analysis following the storage conditions used by Rossi et al. (2006a; 2006b).

Furthermore, the staining to separate mature cells from those still undergoing the lignification stage was unsuccessful as there seemed to be no distinction between the colours. Depending on light wavelength, violet was observed either throughout the cell

wall or nowhere. There was no conclusion on what might have caused the failure in staining as the problem occurred in both batches of samples stained on different days. Due to this it was impossible to conclude the ring maturation stage from the cell development phases.

4.3.3 Comparing the core and dendrometer measurements

For this comparison a daily average of the dendrometer data was calculated for each date when microcores were collected. As expected, based on previous studies (Mäkinen et al., 2008) the dendrometers detected growth earlier than the microcores (Figure 4-12). This could be partly explained by the destruction of enlarging cells but the differences were too large to be caused by that alone. During the period of fastest growth in July-August the microcore observations were consistently lower than the dendrometer measurements. But the timing of fastest growth was fairly consistent between the methods.

To compare the total ring widths, the final ring widths detected by the microcores were calculated by averaging the final 6 measurements of the season, which were thought to represent the period when the radial growth has ceased and the ring had reached its final dimensions. Similarly the LVDT ring width was derived from the daily average values on these microcoring days to allow the most valid comparison. Ring width information from WinDENDRO ring based output was used as such. The pixel based output was modified to exclude the high density values in the beginning of the ring and the downward drifting density values at the end of the ring that are due to the definition of ring boundary (50% of the slope) used in WinDENDRO. This caused the ring width calculated from the pixel based data to differ from those reported in the ring based output. When the final ring width derived by all the different measurement methods, were compared, there was no consistent pattern in the differences between the methods (Figure 4-13). In most cases the ring width detected by the dendrometers was larger than the one measured from the microcores. Tree 66 was the exception to this. More variation is expected in the microcore data since they presented widths of different radii as they are extracted in slightly different locations whereas the dendrometer measures the same radii continuously. Furthermore, occasionally, cracks and other defects caused difficulties in measuring the ring widths under microscope on the microtome strips cut from the microcores. This may have caused some inaccuracy in the ring determination. ITRAX results on the other hand present just one radius but at a certain distance from the dendrometer in order to avoid causing any wound tissue

formation in the vicinity of the dendrometer. There were considerable variations in numbers of cell and hence ring width around the tree circumference (Gričar, 2007; Rathgeber, 2009). The differences in sampling location may have caused some of these differences in ring dimensions.

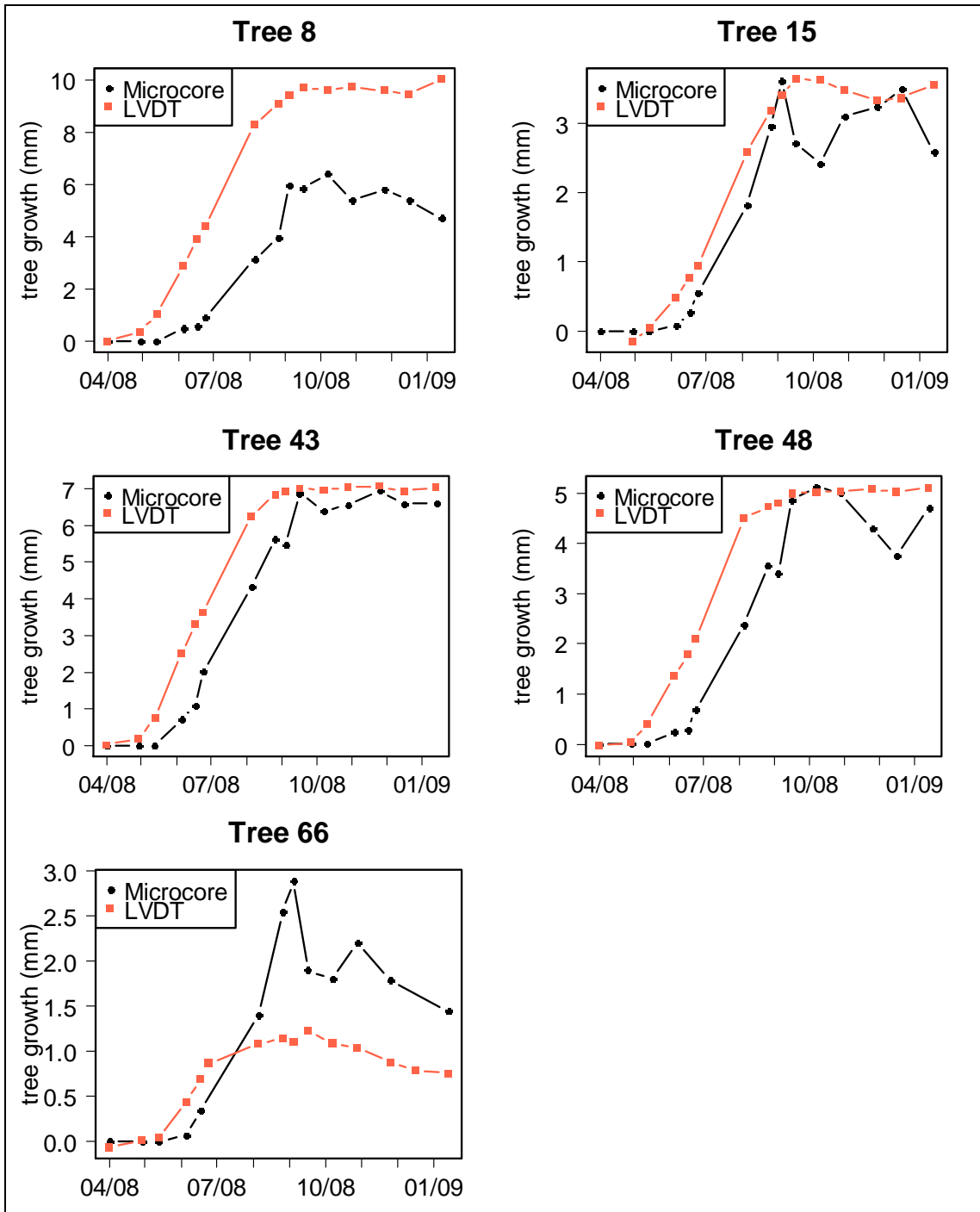


Figure 4-12. The tree growth measured on microcore samples compared to the growth detected by the LVDT dendrometers at different stages of the growing season.

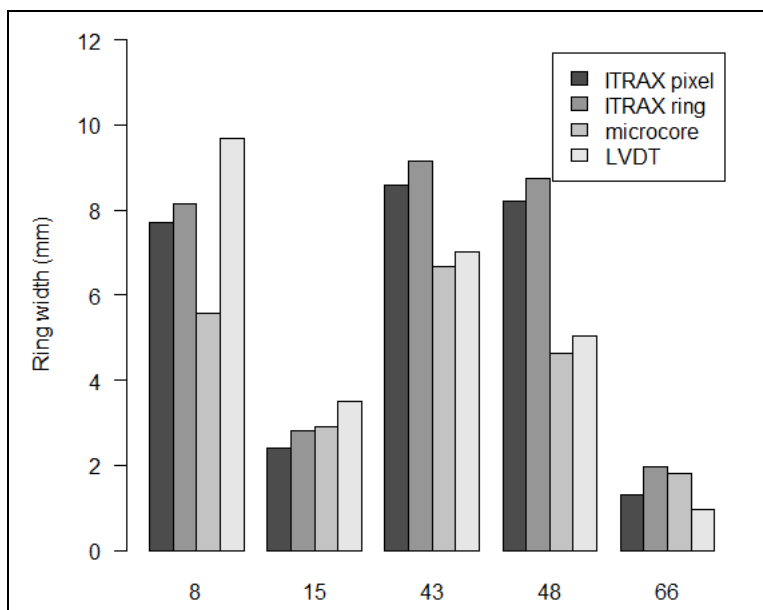


Figure 4-13. Measured ring width for 2008 by ITRAX, microcore and LVDT. The pixel based ITRAX data were modified to remove high density values in the beginning of the ring and decreasing density values at the end of the ring that result from the ring boundary definition. This caused the two ITRAX based readings to differ.

4.3.4 Linking growth to climatic data

The climatic data collected with the datalogger at the site were compared with UK Meteorological Office (2009) data from the Aberfeldy Dull weather station to validate the field measurements. Aberfeldy Dull weather station (N 5.621° E -3.924°) is located approximately 10 km from the Griffin site at 100 m altitude. Temperature variation at the site followed the same pattern as observed for the Aberfeldy Dull data (Figure 4-14) but the amplitude seemed to be larger at the Griffin site. The minimum temperatures measured at the Griffin site were best correlated with the minimum grass temperature at the Aberfeldy Dull weather station. This might be due to the fact that the sensor at the Griffin site was relatively near the ground (about 1.3m height). The two locations differ in altitude and therefore difference in the measured temperatures could be expected. However, the similarity in the pattern of variation indicated that the temperature sensor at Griffin was functioning correctly and the data obtained could therefore be used in the analysis.

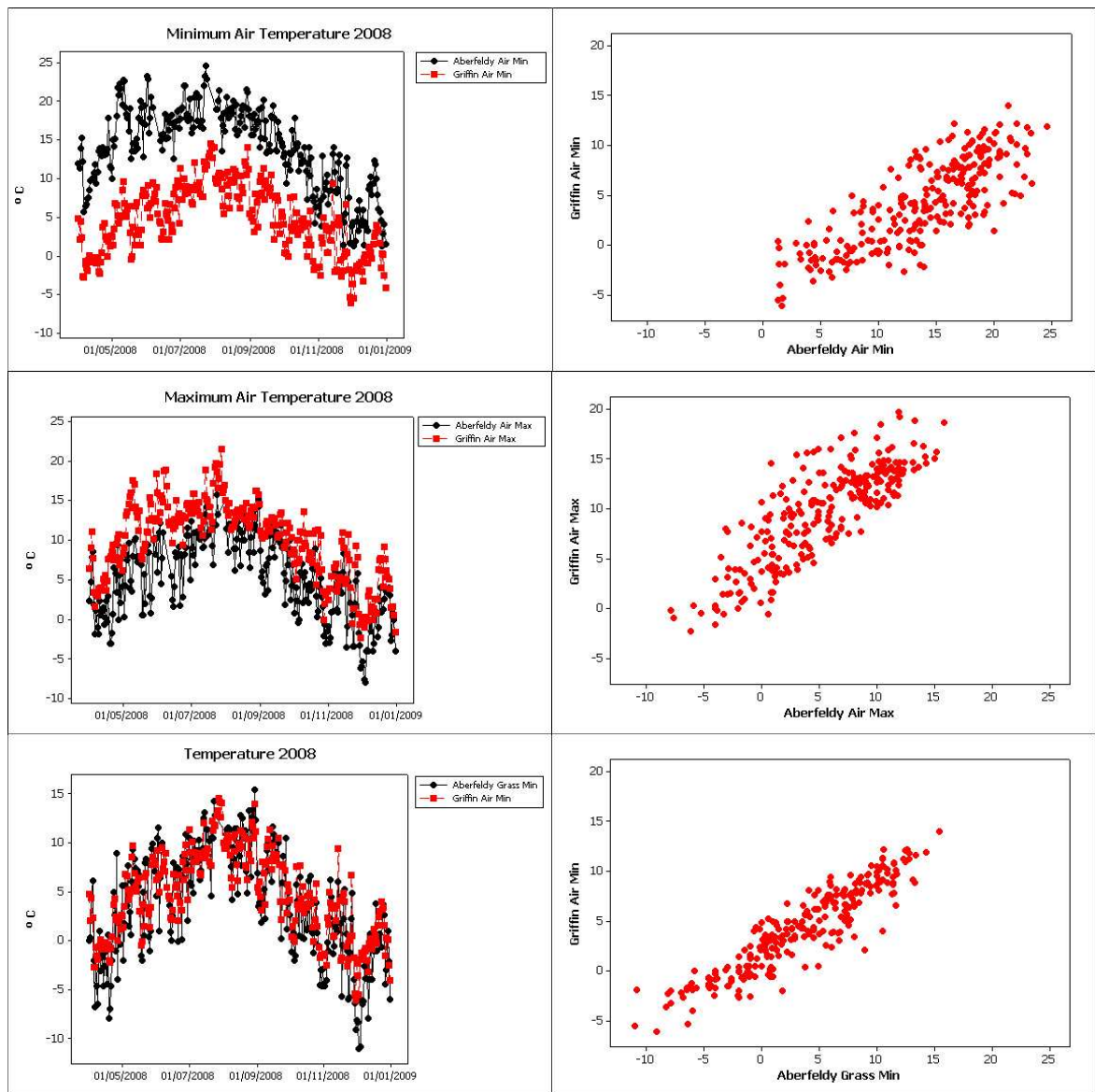


Figure 4-14. Comparison of the temperature data measured at the Griffin site with the Met Office Aberfeldy Dull weather station.

When the monthly increments in diameter measured by the dendrometers were observed, a substantial fraction of the radial expansion was measured in all of the trees in May (Figure 4-15), whereas no growth was detected in the microcore samples. According to the dendrometer measurements May, June, July and to a lesser extent August accounted for most of the xylem growth. However, with this method radial increments were also detected during the autumn and winter months of September, October, November and December. Some growth might potentially take place in September even though it does not appear likely in the light of Figure 4-10, where the growth curves clearly level off to a plateau by late August. Therefore, the increments detected in September and after are deemed to present an artefact of the method as expansion beyond previous day minima was defined as increment. During the winter period it might take trees several days to recover from severe shrinkage (Figure 4-10) and some of that recovery would be registered as increment. This

problem is not applicable to the period of fast growth since the radial increment was so large that shrinkage events persisting over extended periods would be much less likely to occur. However, in the following studies the method for defining increment might have to be adjusted if there was interest in studying the winter period in more detail from the tree water reserves point of view.

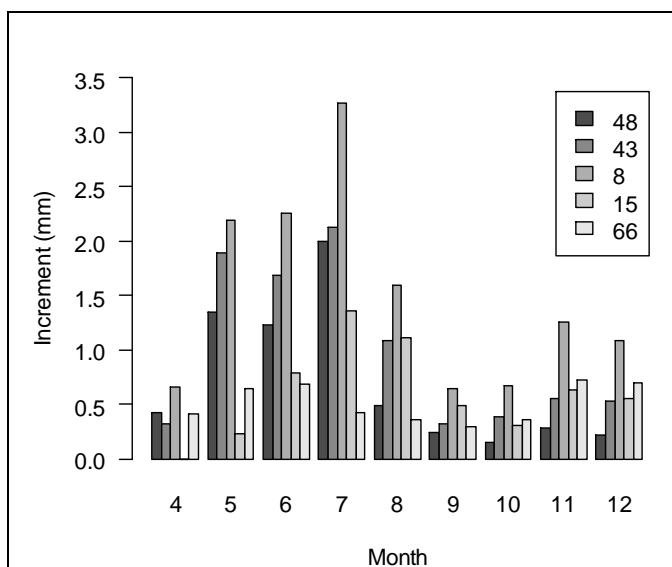


Figure 4-15. Monthly increments measured by the dendrometers during the 2008.

The influence of climatic variables measured on the datalogger setup or obtained from Edinburgh University flux tower measurements was studied using a 40 day moving correlation (Downes et al., 1999). In these correlations daily increments in different trees were related to the weather variables. In this approach 20 day long period of daily increments to either direction from a given day was correlated with a climatic variable. The window would then move forward by one day producing a correlation centred on the following day, hence producing an overlapping moving correlation that would allow detection of any changes in the relationship between radial increment and a given climatic variable. The Edinburgh University monitoring weather variables included in the study are listed in Table 4-3.

Table 4-3. Details of the climatic variables obtained from the Edinburgh University monitoring data.

Variable	Abbreviation	Units	Measurement details
Air temperature	T	°C	
Rainfall	-	mm	Half-hour total recorded
Soil moisture content	TDR _{tower}	-	Volumetric soil moisture
Global incoming shortwave radiation above canopy	RG	W/m ²	
Global incoming Photosynthetic Photon Flux Density (PPFD) above canopy	PPFDg	μmol/m ² /s	Photosynthetically active radiation
Diffuse PPFD above canopy	PPFDd	μmol/m ² /s	Photosynthetically active diffuse radiation
Wind	-	m/s	From the Eddy Covariance data
Soil temperature	Soil T	°C	6 sampling locations, 4 depths
Bole temperature	Bole T	°C	From 3 trees, 3 heights (0.5 m, 1 m, 3 m), 2 types of measurements (internal and near surface)

Until mid September trees 43, 8 and 15 have a consistently positive correlation with temperature (Figure 4-16). For tree 48 the positive correlation with temperature extends even further into the autumn but there is a section in the middle of growing season (from early/mid May to mid Jun) where this relationship disappears. This period is visible as slower growth in tree 48 (Figure 4-10). In tree 66 there was no strong relationship with temperature. As will be discussed in relation to other climatic variables as well, the behaviour of tree 66 differed from all of the other sample trees. There was a short period of positive correlation with temperature which lasted from early May to early June. This approximately corresponds to the period of growth detected in tree 66 (Figure 4-10).

The correlations using the temperature measurements from the datalogger setup (Figure 4-17) gave results that agreed closely with the tower temperature measurements as would be assumed if both systems functioned correctly.

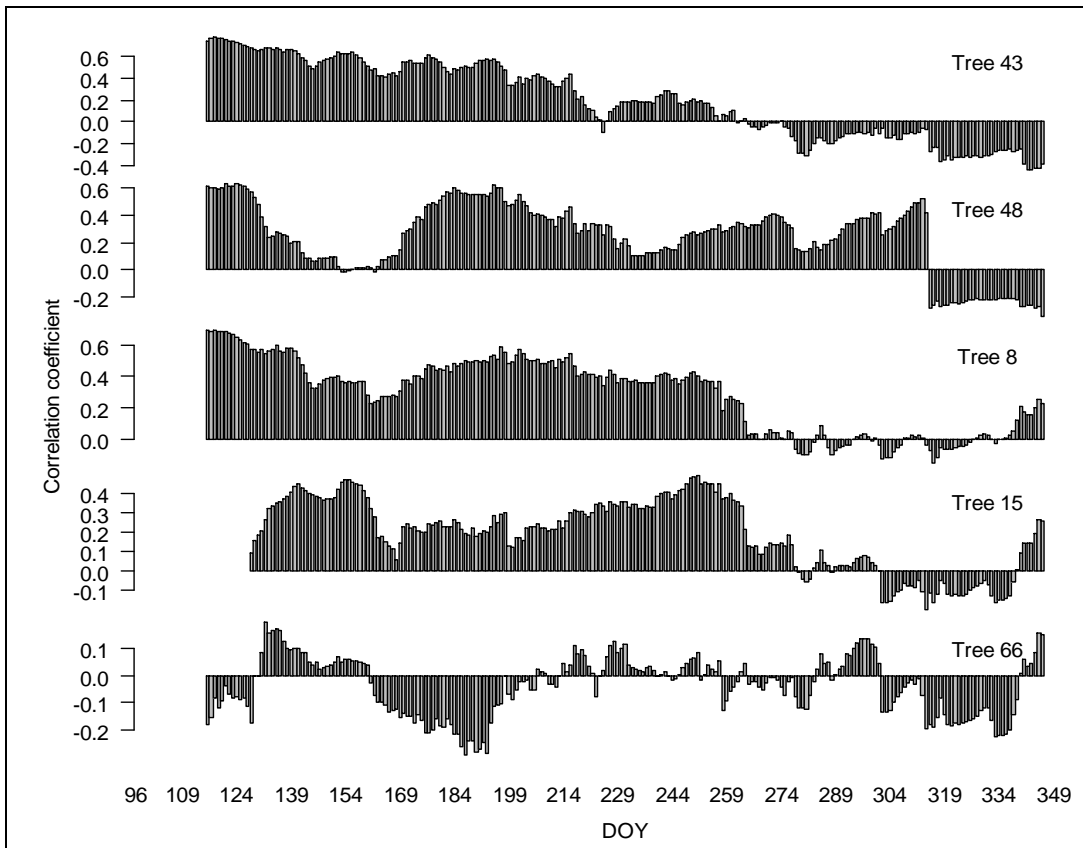


Figure 4-16. Forty day moving correlation between daily mean temperature from the flux tower measurements and daily radial increments in the dendrometer trees.

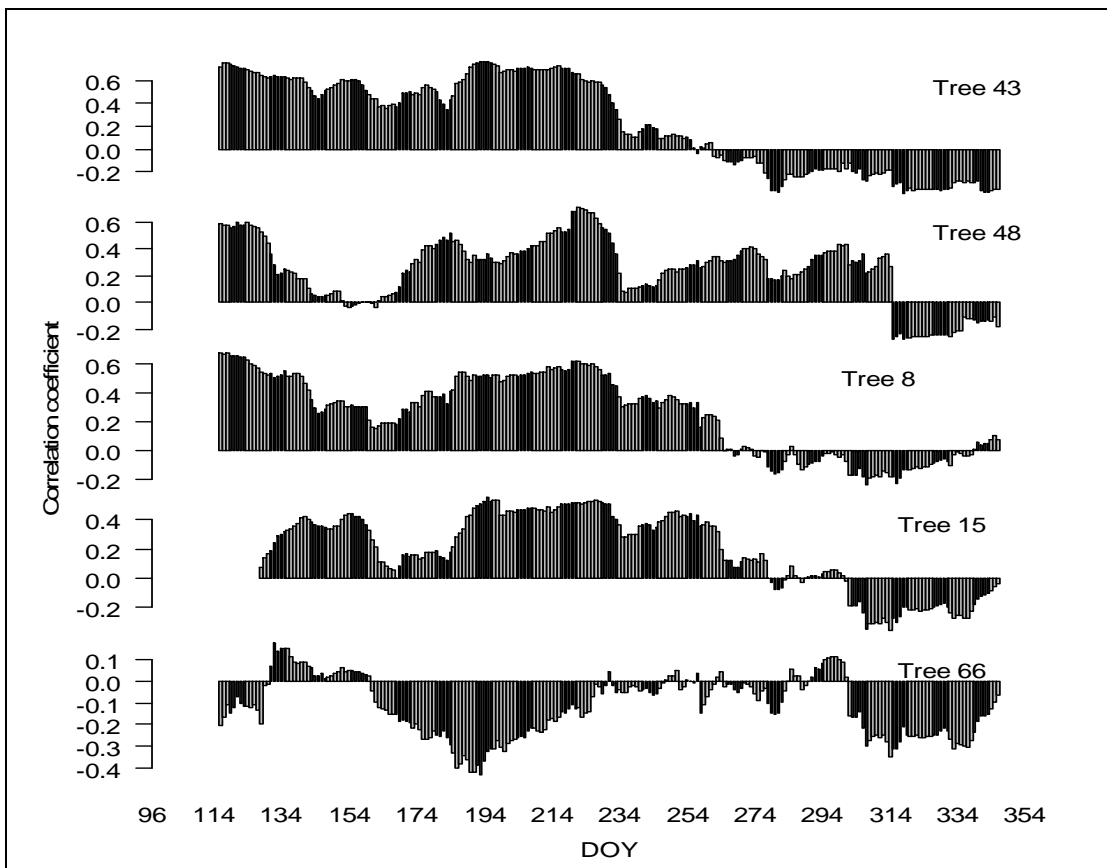


Figure 4-17. Forty day moving correlation between daily mean temperature from the datalogger measurements and daily radial increments in the dendrometer trees.

For air humidity the relationship with radial increment varied more during the year (Figure 4-18). Mainly in June and early July there was a positive correlation between air humidity and daily diameter increments. In tree 43 this was not detected. In tree 66 the positive correlation persisted until end of October, which might indicate that swelling during more humid conditions, might have controlled the changes in radius after growth ceased in June. Furthermore, in June and early July, temperature was positively correlated with humidity (Figure 4-31) and the effect of temperature on tree growth might explain some of the positive correlation detected between growth and humidity. Humidity was also negatively correlated with wind. Grace et al. (1975) have shown with wind tunnel experiment on seedlings of Sitka spruce that the stomata are sensitive to vapour pressure deficit. When relative humidity decreases the stomata start to close progressively, which increases leaf diffusive resistance and restricts growth in Sitka spruce.

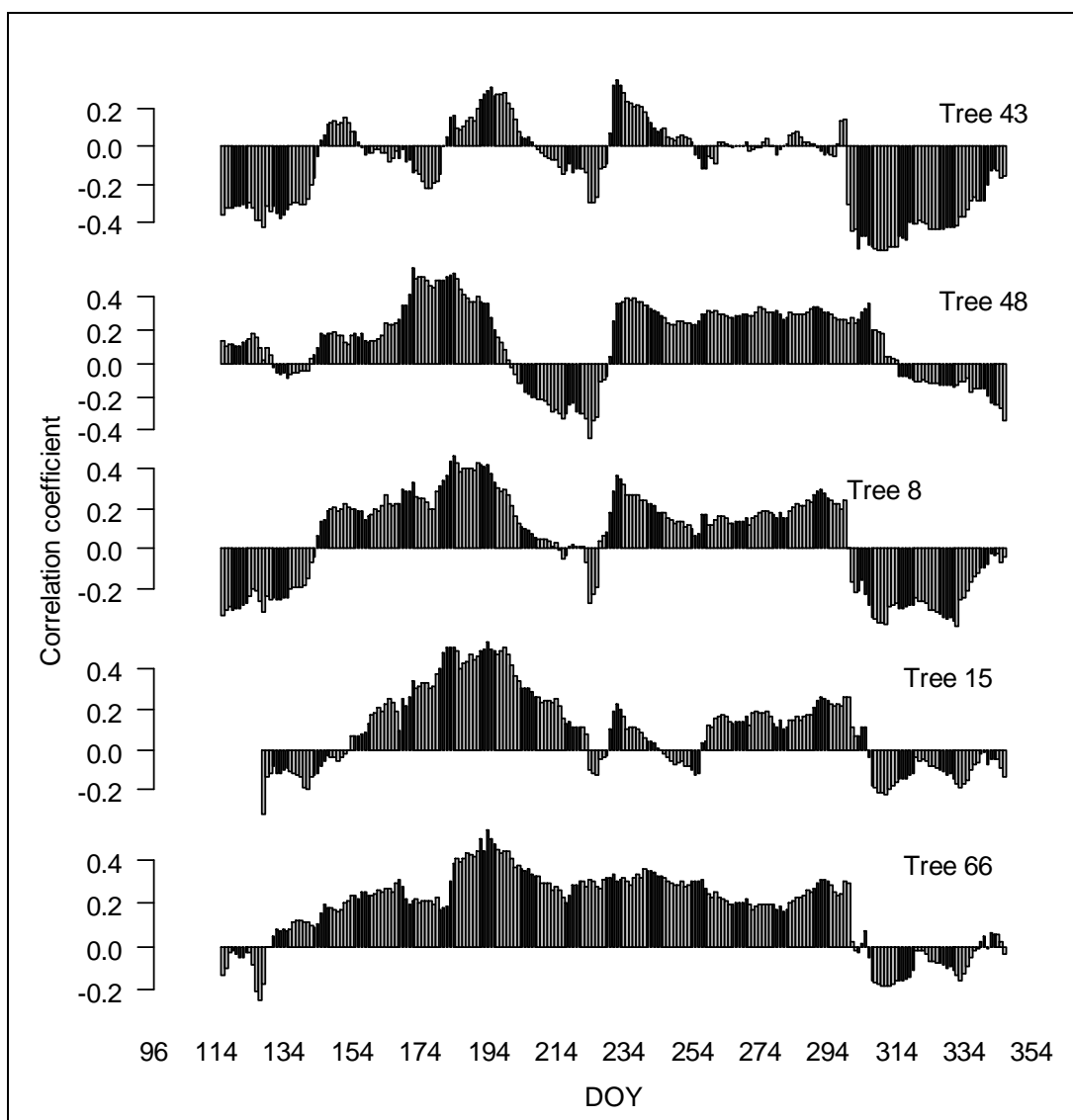


Figure 4-18. Forty day moving correlation between daily mean air humidity from the datalogger measurements and daily radial increments in the dendrometer trees.

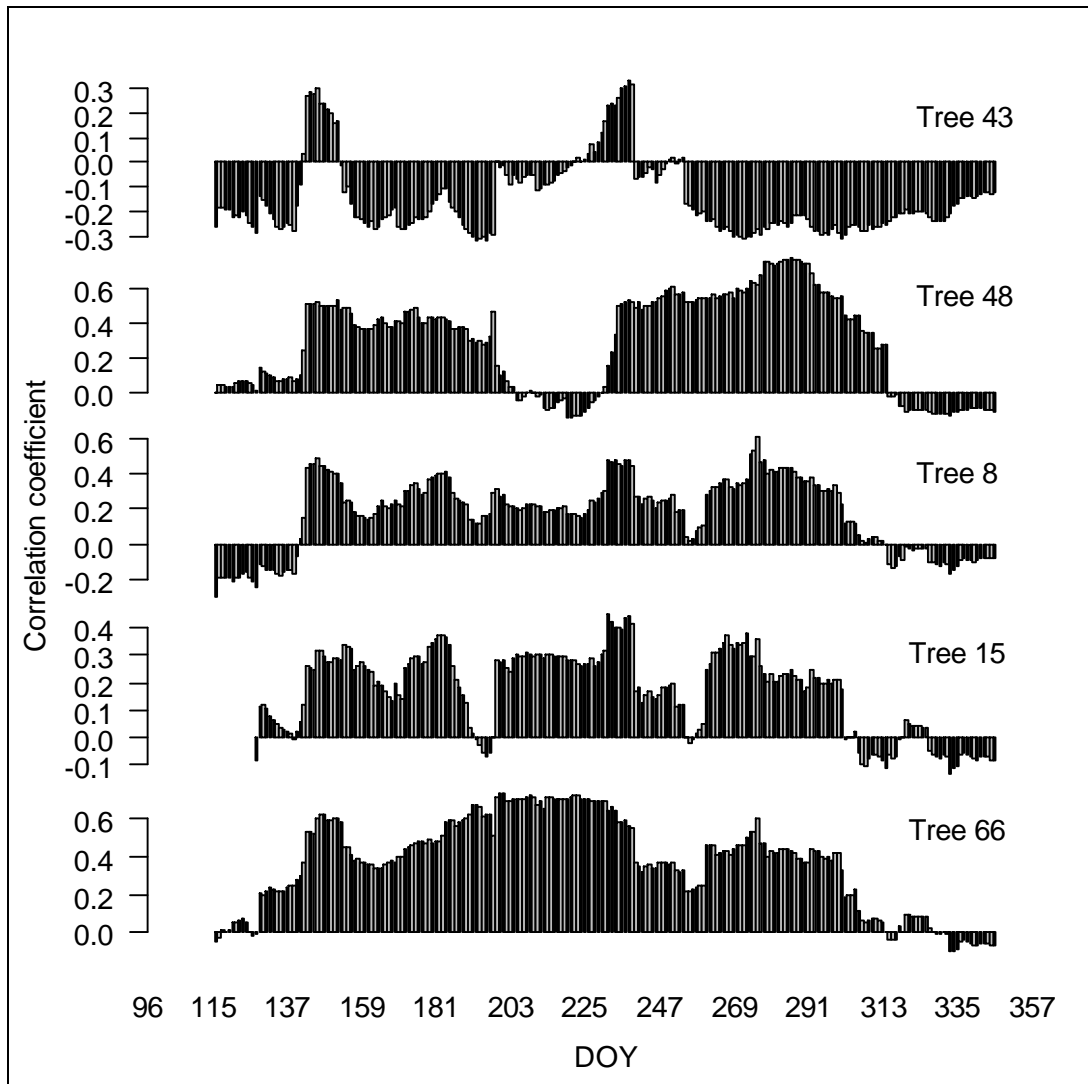


Figure 4-19. Forty day moving correlation between daily rainfall (mm) and daily radial increments in the dendrometer trees.

In comparison to air humidity there was a stronger and more consistent positive correlation between growth and rainfall (Figure 4-19). However, the graphs did also resemble each other to some degree. In trees 48, 8 and 15 the positive correlation between growth and rainfall was observed from mid May until the end of October but in tree 48 this relationship disappeared from late June to early August. Consistent with the findings regarding air humidity, the positive correlation between rainfall and radial expansion in tree 66 persisted well into the autumn even though growth ceased much earlier. This lends further support to the hypothesis that the dimensions were largely controlled by water status in that tree in the later part of the growing season, which could explain its obscure behaviour. In other trees the simple swelling of the stem would be masked by growth. In tree 43 the correlation with rainfall was largely negative except for two short periods of positive response. The end of the first positive relationship coincides with the change in growth rate visible on the Figure 4-10. The slow growth rate lasts for approximately 40-50 days and then increases again. The timing of increase in growth rate coincided with the

second positive correlation between growth and rainfall. This positive relationship seemed to persist until the growth ceased a couple of weeks later.

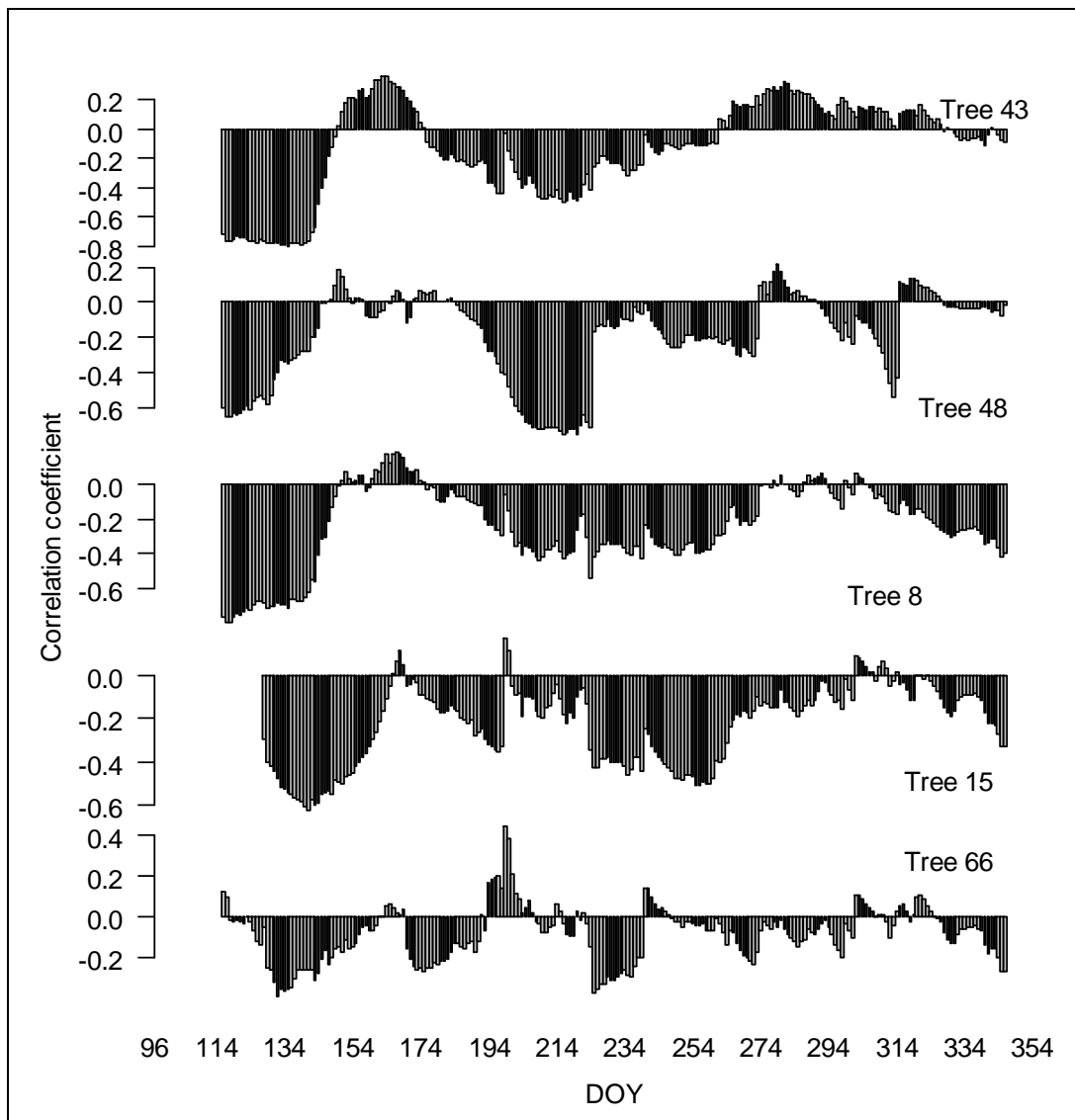


Figure 4-20. Forty day moving correlation between daily volumetric soil moisture (Edinburgh University) and daily radial increments in the dendrometer trees.

The soil moisture measurements differed considerably, with the datalogger setup showing much smaller amplitude in values. The soil moisture probes related to the datalogger setup were placed on the elevated area between the furrows and would not be subjected to accumulation of pools of water that took place in the furrows. Therefore, these soil moisture probes might detect shorter periods of elevated soil moisture as the water would drain under gravity from these more elevated locations. However, the tree response derived from these different sets of data was fairly consistent (Figure 4-20 and Figure 4-21). When comparing these graphs it is worth noting that the soil moisture measurements made with the data logger system only commenced on day 148 and therefore correlation values are

only available from day 168 to accommodate the correlation window around the central date.

According to both of the graphs the correlation between soil moisture and tree growth was negative for most part of the growing season (May-September). Looking at the datalogger data (Figure 4-21) the negative relationship was more consistent than in the Edinburgh University measurements (Figure 4-20). It has been postulated that a little rainfall that might be insufficient to influence tree growth via soil water could release the low water potential in the crown simply by wetting the leaves and hence allow the expansion of already formed xylem cells (Zweifel et al., 2006). This would decouple radial growth and soil water (Zweifel et al., 2006). In October a positive correlation between radial increment and soil water content was observed (Figure 4-21), which could indicate filling of water reserves before the winter. Slight positive correlations were detectable during the same period in the other dataset as well (Figure 4-20).

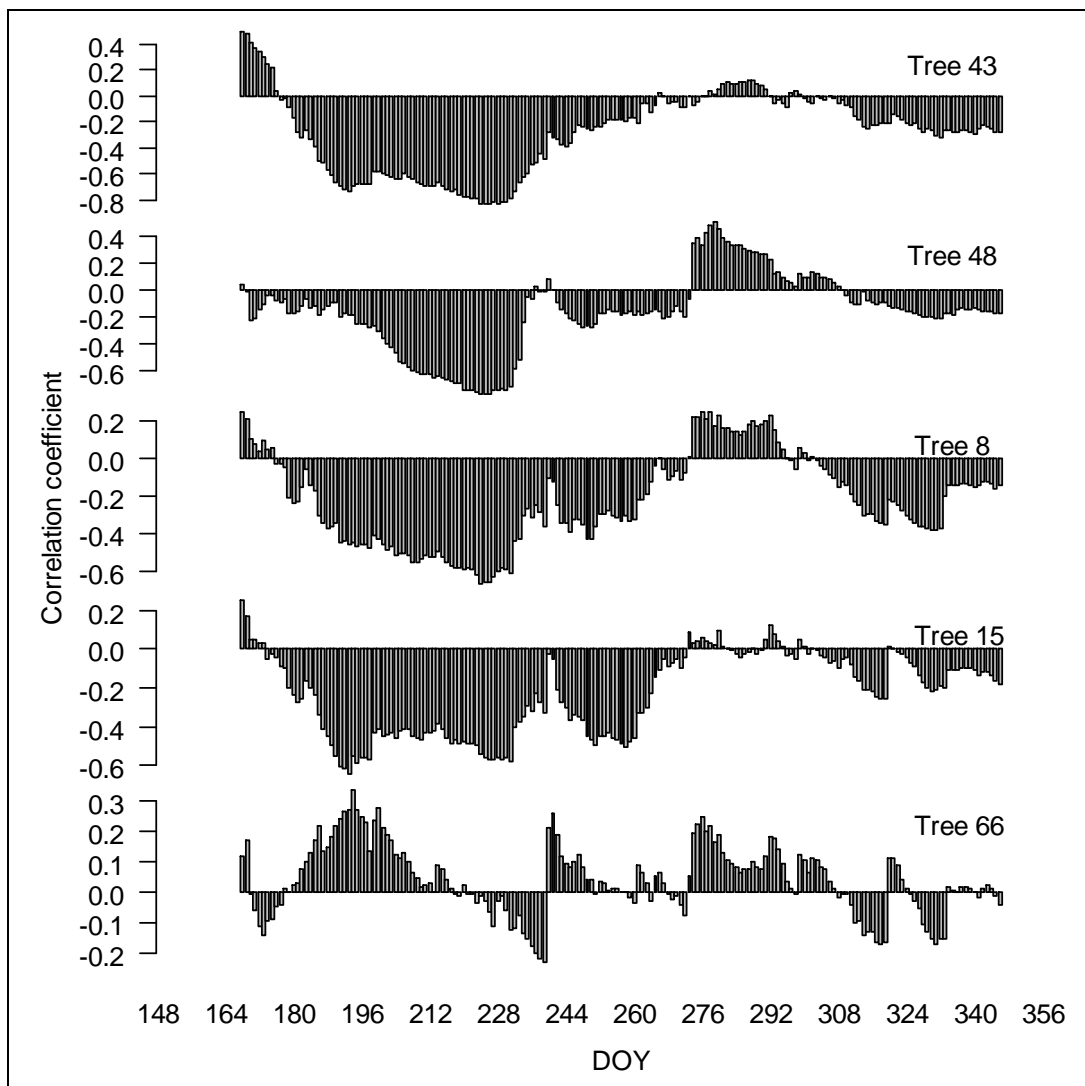


Figure 4-21. Forty day moving correlation between daily soil moisture % (datalogger setup) and daily radial increments in the dendrometer trees.

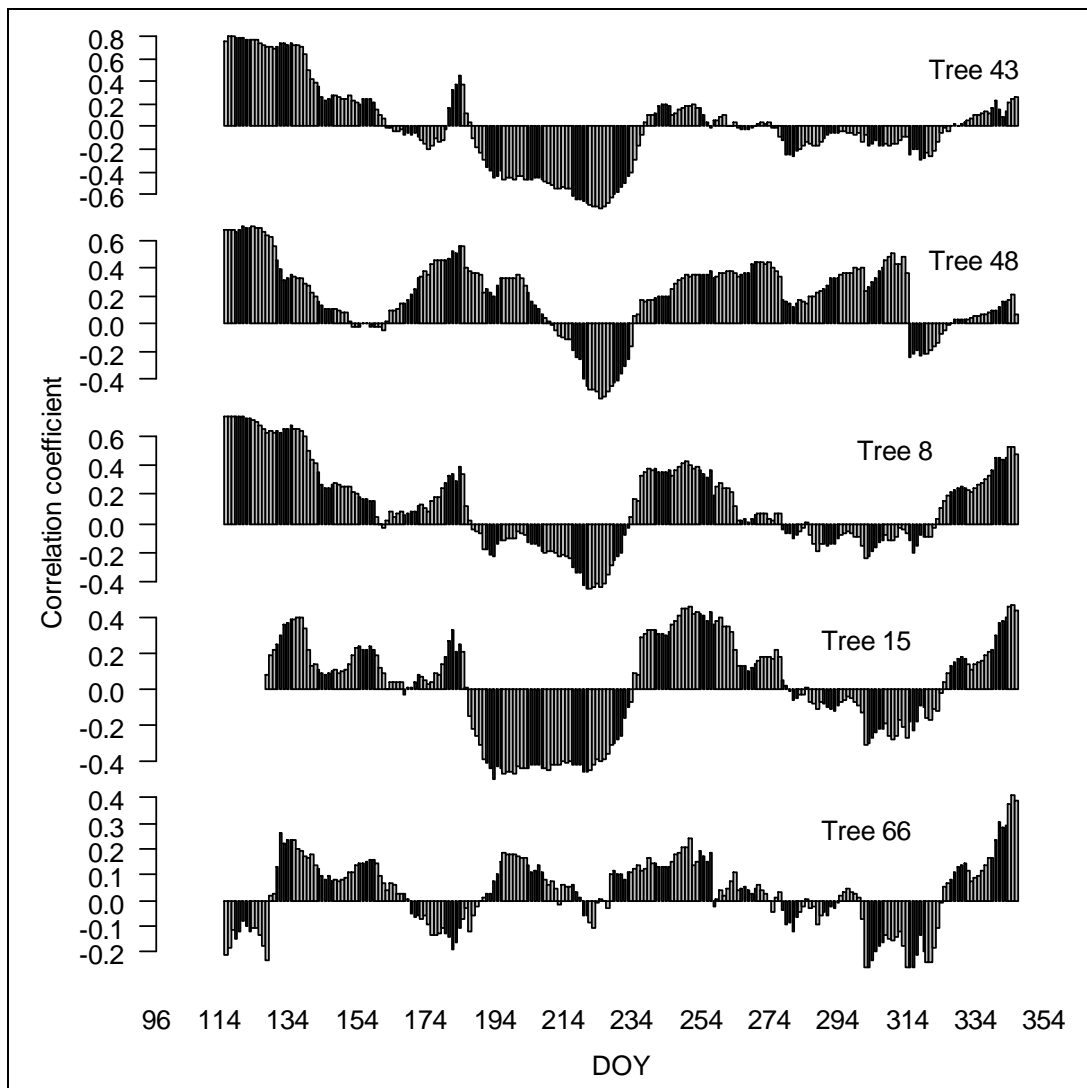


Figure 4-22. Forty day moving correlation between daily mean surface soil (depth 2.5 cm) temperature and daily radial increments in the dendrometer trees.

The tree responses to temperature followed a similar pattern throughout the soil profile, so here only the upper (Figure 4-22) and lower (Figure 4-23) measurements are shown. During the period from July to early August high soil temperature seemed to be associated with slower growth (Figure 4-22 and Figure 4-23). However, based on these data it cannot be deduced whether the soil temperature was the cause or whether it simply coincided with the end of the growing season.

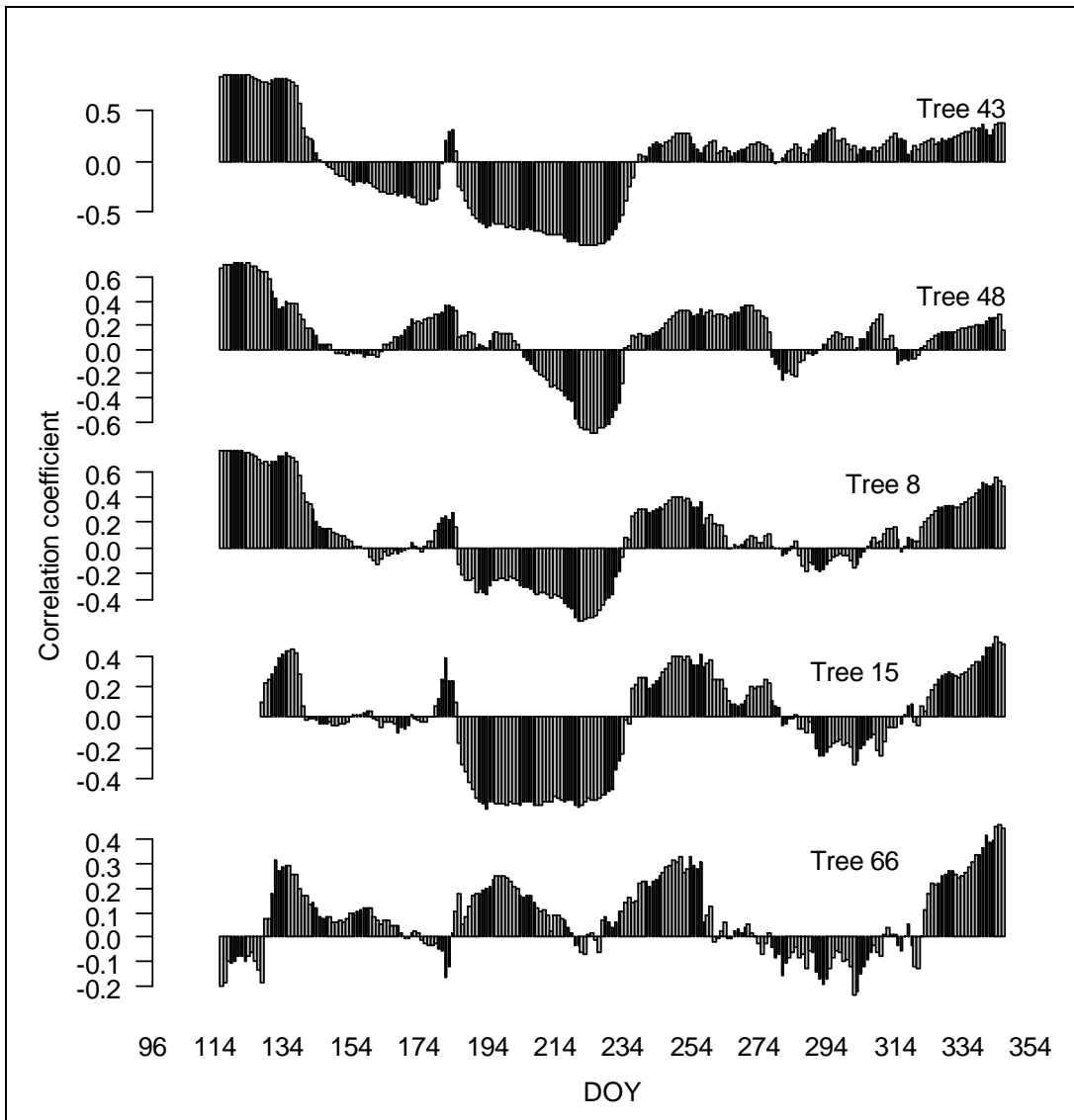


Figure 4-23. Forty day moving correlation between daily mean soil temperature in the lower part of the profile (depth 20-40 cm depending on the sampling location) and daily radial increments in the dendrometer trees.

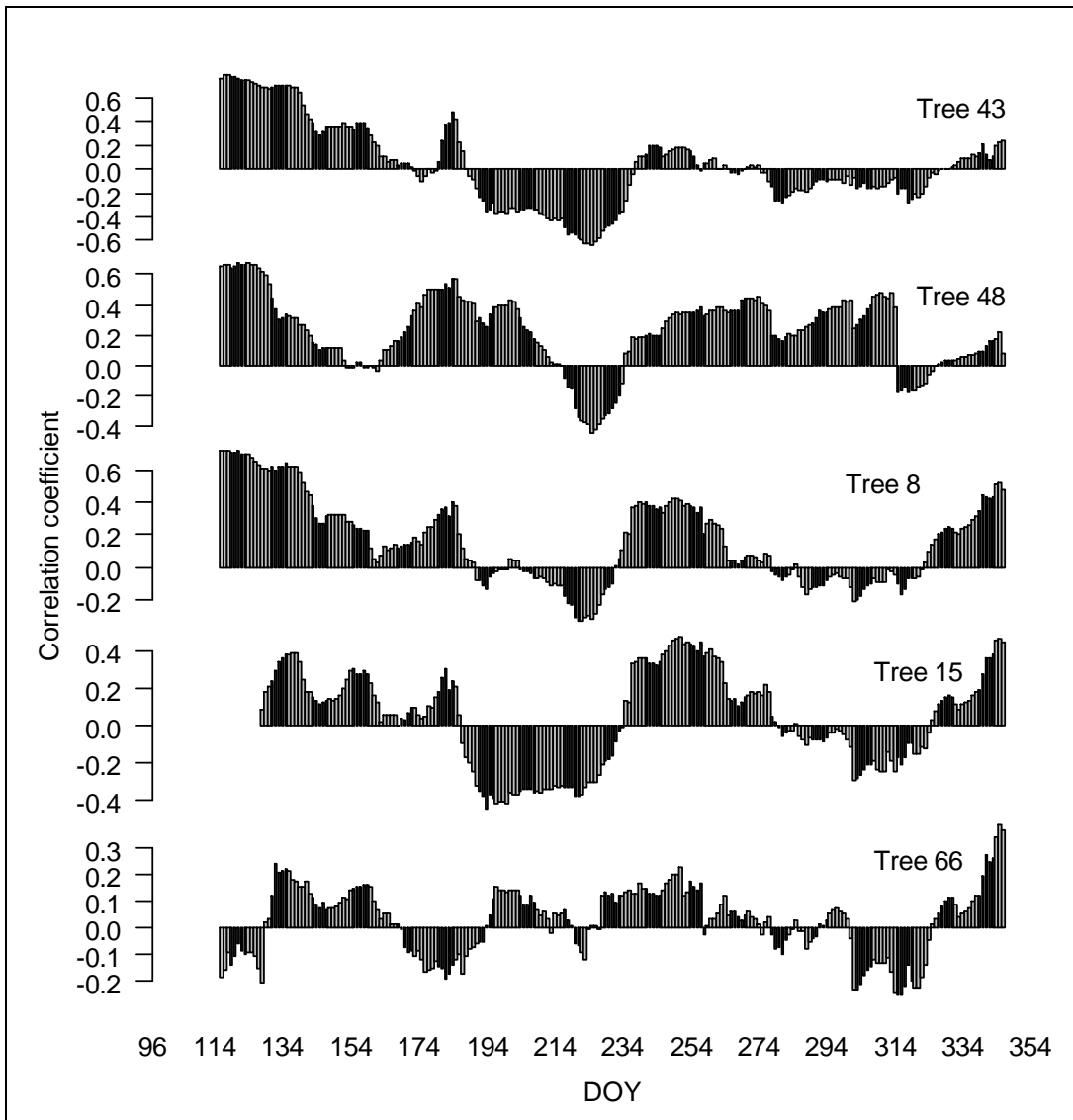


Figure 4-24. Forty day moving correlation between daily mean internal bole temperature at 0.5 m height and daily radial increments in the dendrometer trees.

Bole temperature at 0.5 m height inside the stem (Figure 4-24) and near the surface (Figure 4-25) showed a similar pattern. Furthermore, temperature measurements taken at 1 m and 3 m heights (data not shown) showed similar patterns. At the beginning of the growing season daily increment was positively related to bole temperature in all trees but in tree 66 the positive relationship appeared later, coinciding with the growth onset. Similarly, there was a positive relationship between soil temperature (Figure 4-22 and Figure 4-23) and increment at the beginning of the growing season and the two sets of graphs largely resemble each other; also in the case of the negative relationship apparent from July to early August. The positive relationship in the beginning of the growing season might simply occur since naturally the temperature increases towards summer and tree growth will commence and reach fast rate as the season advances. Both soil and bole temperatures were strongly correlated with air temperature (Appendix 1). The correlation coefficients

for soil temperatures ranged from 0.725 for the deepest layers to 0.901 for surface soil and for bole temperatures 0.908-0.925 depending on position.

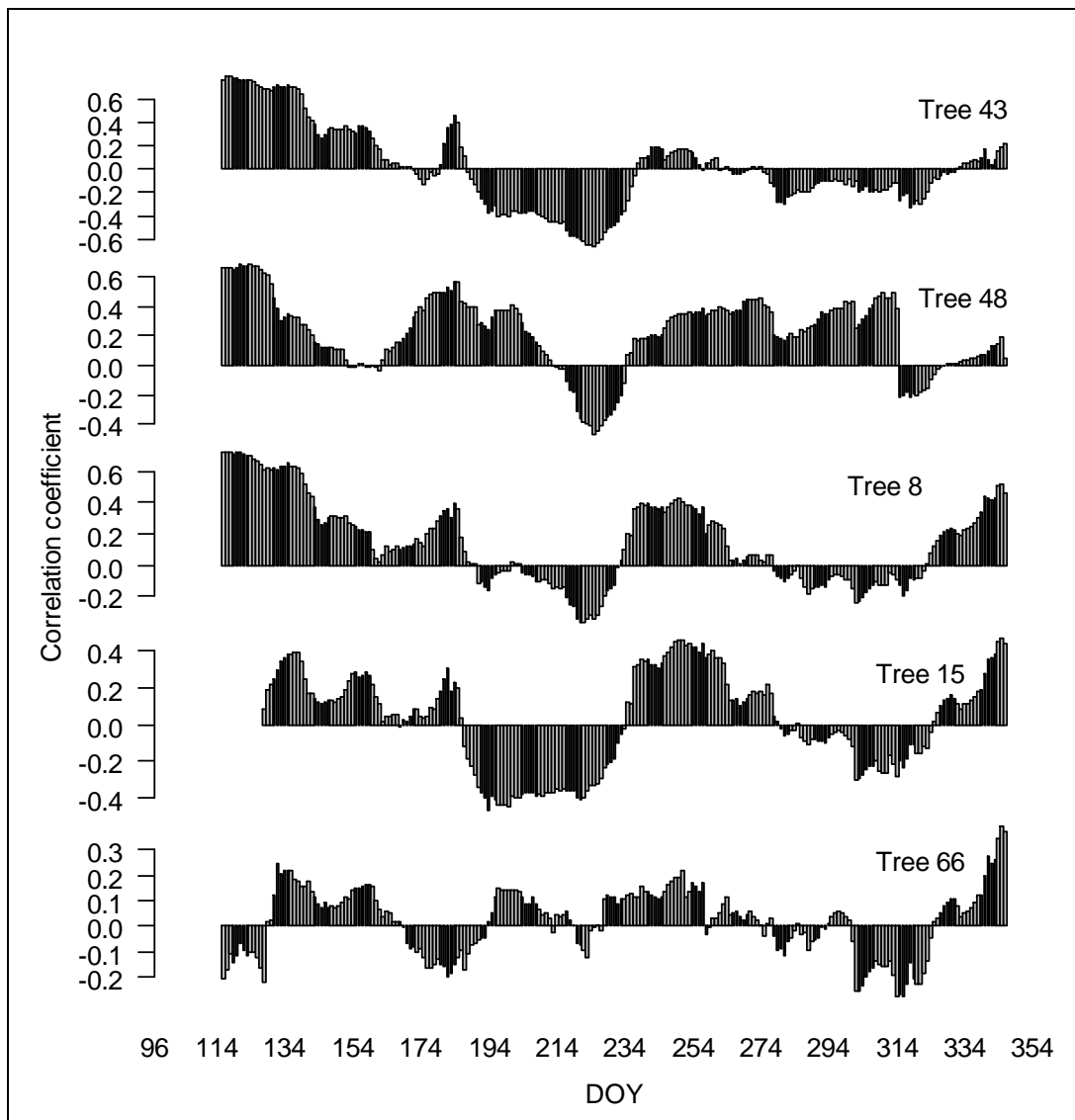


Figure 4-25. Forty day moving correlation between daily mean surface bole temperature at 0.5 m height and daily radial increments in the dendrometer trees.

When comparing wind speed and radial increment, trees 66 and 48 showed a pattern that differed from the others (Figure 4-26). In trees 43, 8 and 15 the relationship between wind and daily increment was mainly a negative one which might be due to windy conditions being associated with reduction in relative humidity (Figure 4-34) which in turn was positively related to increment.

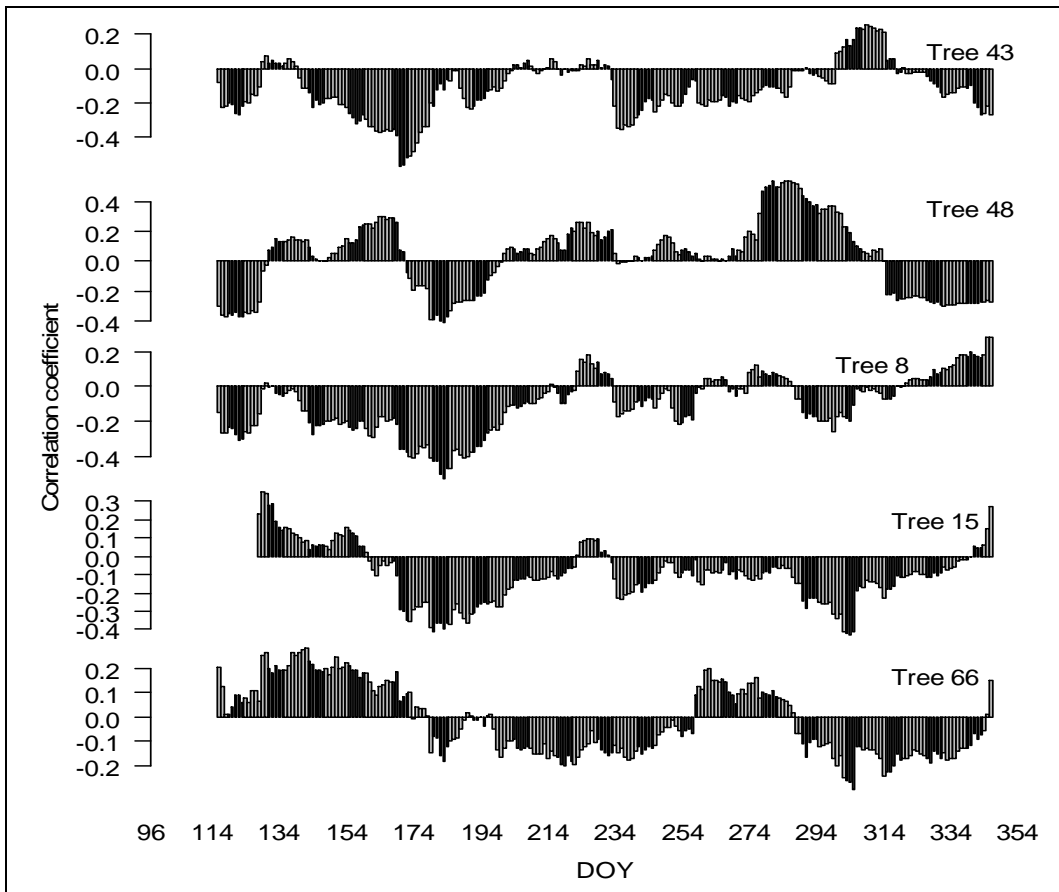


Figure 4-26. Forty day moving correlation between daily mean wind speed (m/s) and daily radial increments in the dendrometer trees.

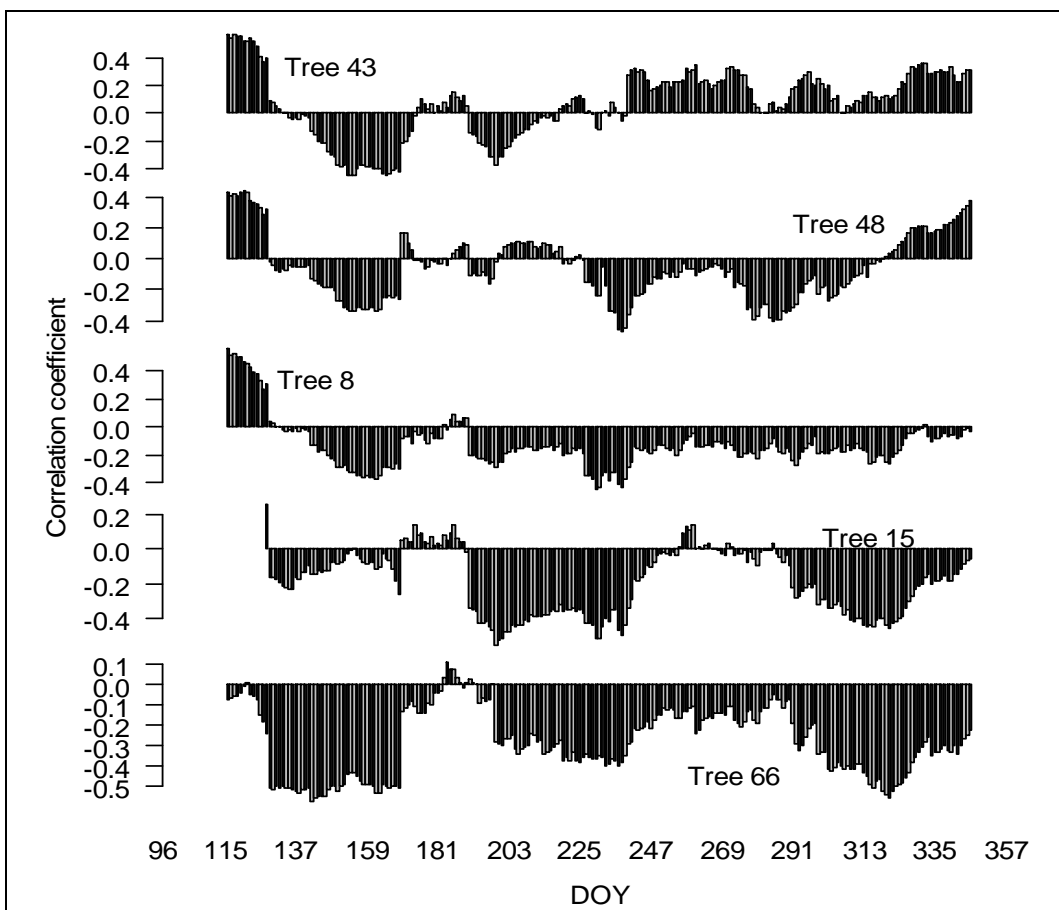


Figure 4-27. Forty day moving correlation between daily mean PPFDd diffuse radiation above canopy ($\mu\text{mol}/\text{m}^2/\text{s}$) and daily radial increments in the dendrometer trees.

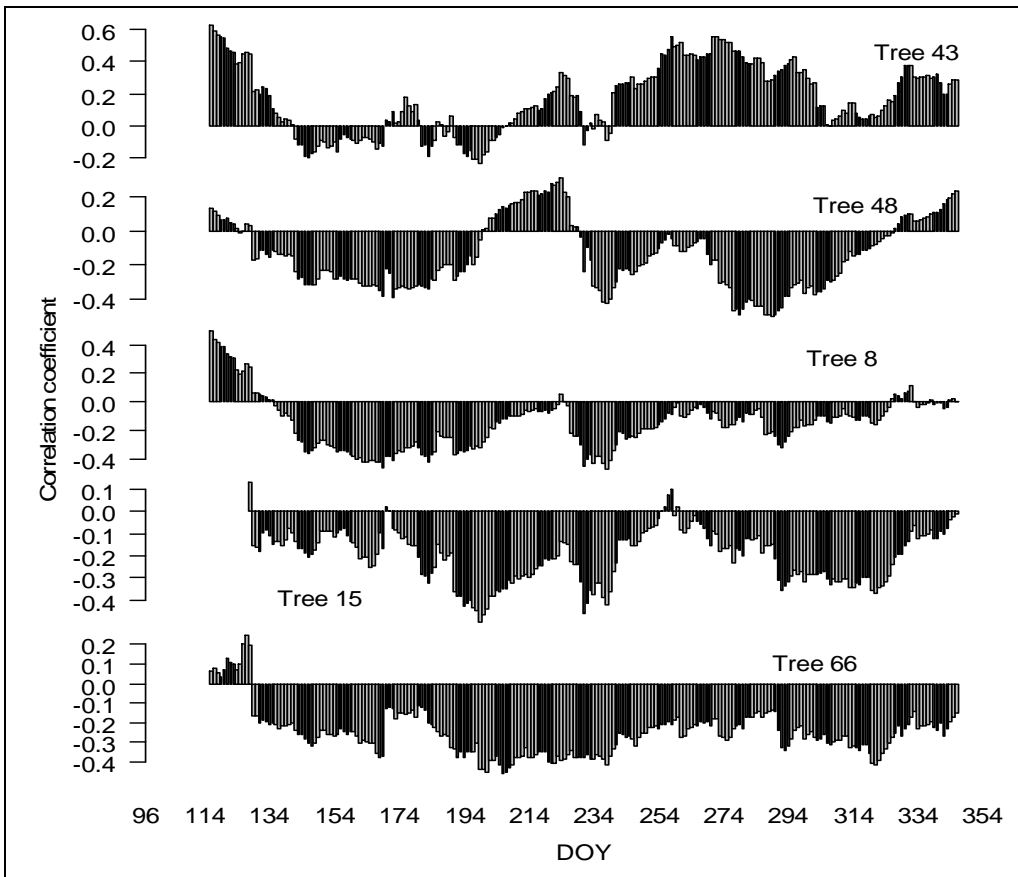


Figure 4-28. Forty day moving correlation between daily mean global incoming PPFDg above canopy ($\mu\text{mol}/\text{m}^2/\text{s}$) and daily radial increments in the dendrometer trees.

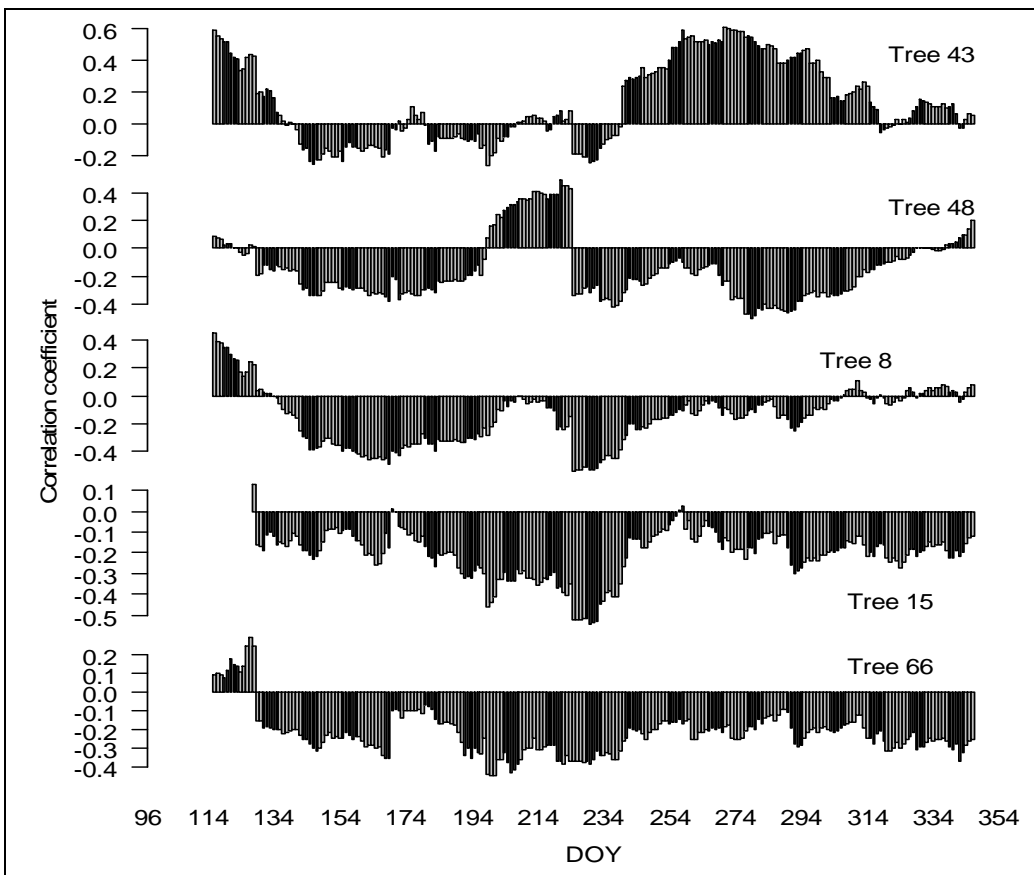


Figure 4-29. Forty day moving correlation between daily mean global incoming shortwave radiation RG (W/m^2) and daily radial increments in the dendrometer trees.

Growth increment seemed to be negatively correlated with the different radiation variables studied (Figure 4-27, Figure 4-28 and Figure 4-29). Furthermore, the relationship between temperature and radiation was observed to be very weak (Figure 4-31 and Figure 4-32), which seems counter intuitive. Perhaps relating daily mean radiation to daily increment was not an optimal approach as the mean also includes low values measured during the night.

Some of the unexpected growth responses might be explained by the complex relationships and interactions between the climate variables themselves. Therefore, similar correlation analysis was carried out on the pairs of climate variables to assess seasonal changes in the relationships (simple correlations between the time series are listed in Appendix 1).

Between May and the end of August there was a weak negative correlation between air temperature and rainfall (Figure 4-31). However, since both temperature and rainfall were individually positively related to tree growth, the decrease due to lower temperature on rainy days is likely to remain small. In June, high temperature was linked to higher soil moisture and air humidity. This was no longer observed in July or August except for TDR_{tower} data in the very beginning of July.

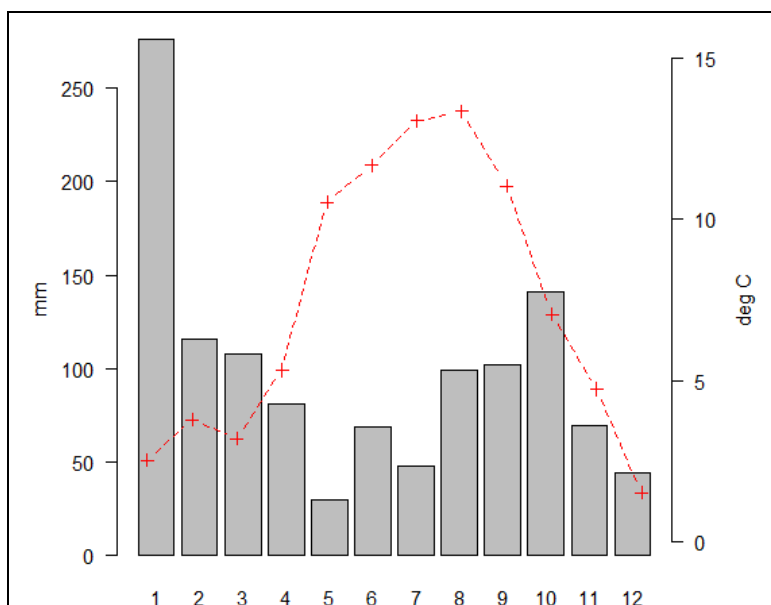


Figure 4-30. Monthly precipitation and mean temperature (dashed line) at the Griffin site 2008.

During the growing season until August higher wind speed was related to cooler temperature (Figure 4-31), whereas in the winter the reverse was observed. In October and November higher wind speed was also associated with higher rainfall. Precipitation was always negatively related to all radiation variables (Figure 4-31 and Figure 4-32). As

precipitation was positively correlated with humidity, these radiation variables were negatively related to humidity as well. Wind was negatively correlated with humidity throughout the observation period (Figure 4-33). In May-June, temperature was negatively correlated with wind which could explain the positive correlation found between temperature and humidity. However, the relationship between temperature and wind was a fairly weak one.

The radiation variables were strongly and positively interrelated (Figure 4-33 and Figure 4-34) as would be expected. However, an interesting point to note was that the correlations were weaker in the early summer (May-July) for the RG-PPFDd and PPFDg-PPFDd pairs (Figure 4-35).

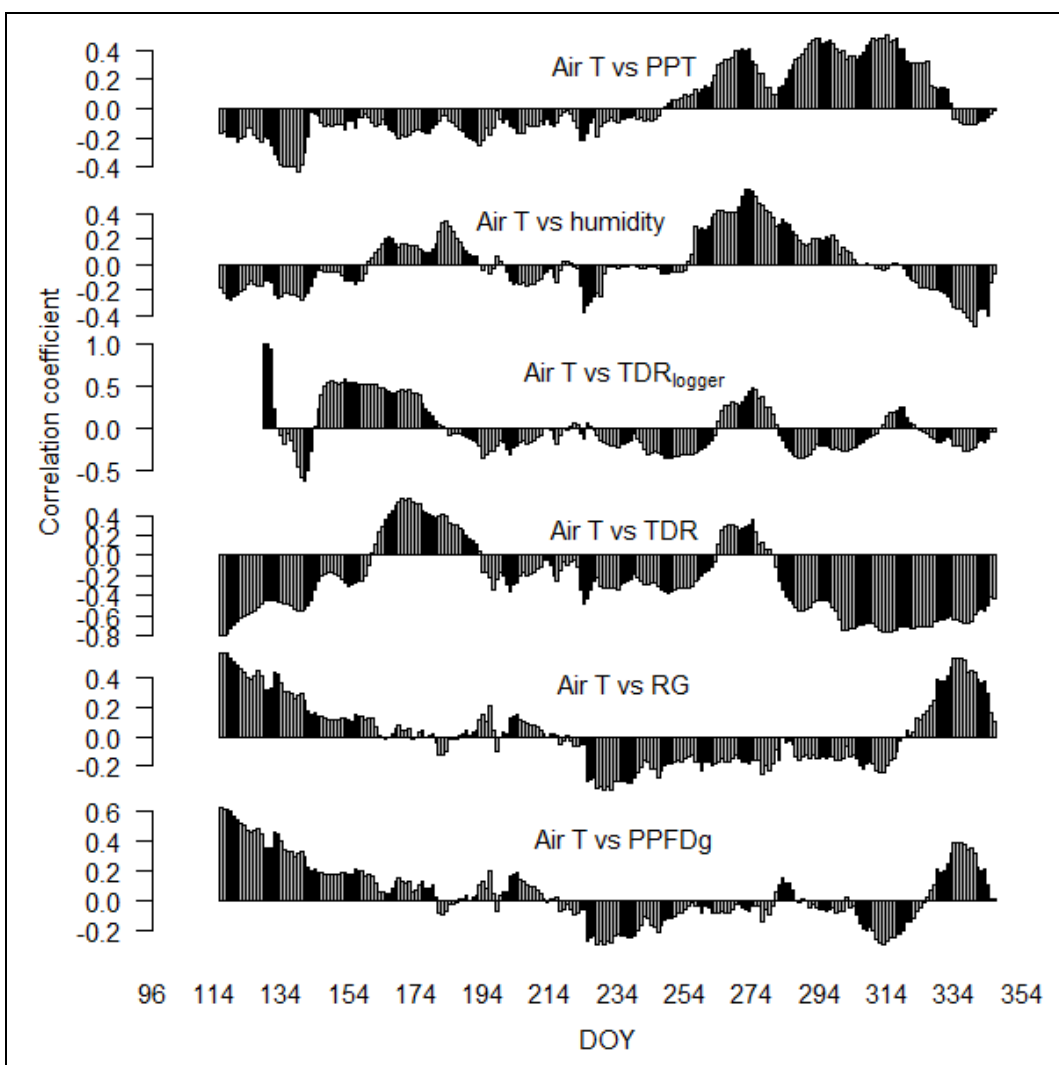


Figure 4-31. Inter correlations between climate variables tested with the forty day moving correlation window. Continued on following pages.

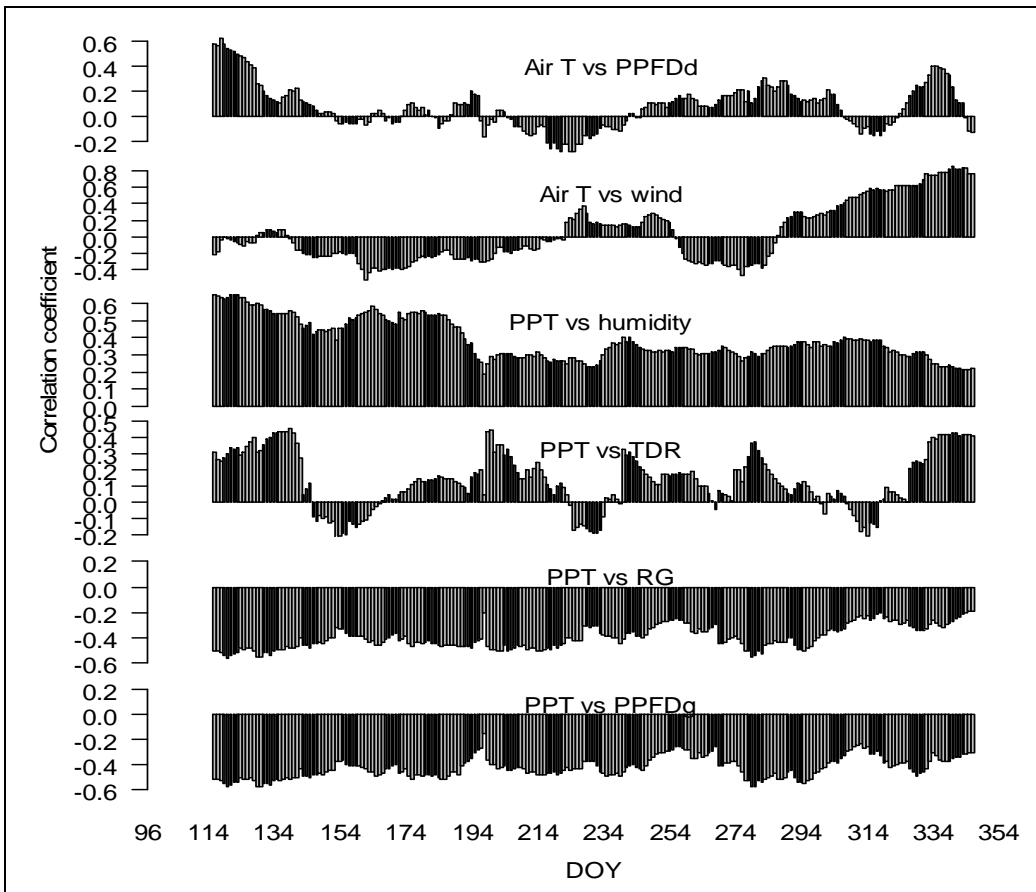


Figure 4-32. Inter correlations between climate variables tested with the forty day moving correlation window. Continued above and on following pages.

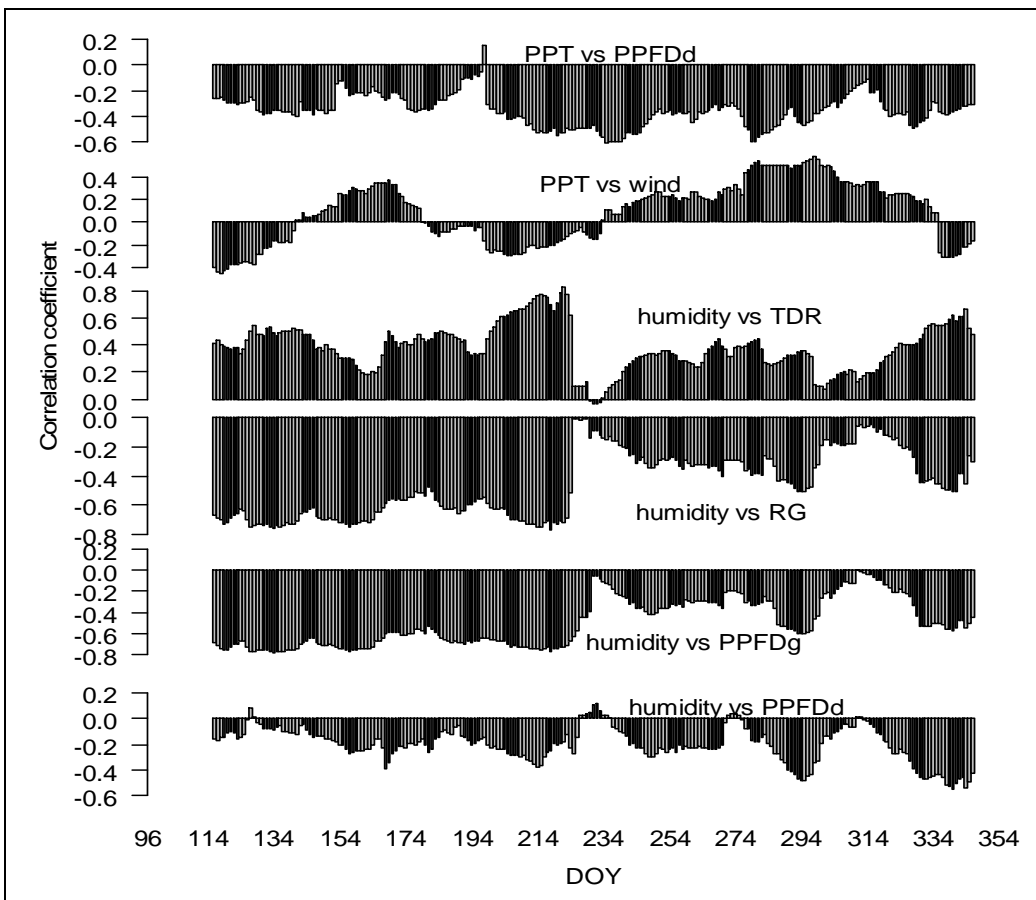


Figure 4-33. Inter correlations between climate variables tested with the forty day moving correlation window. Continued above and on following pages.

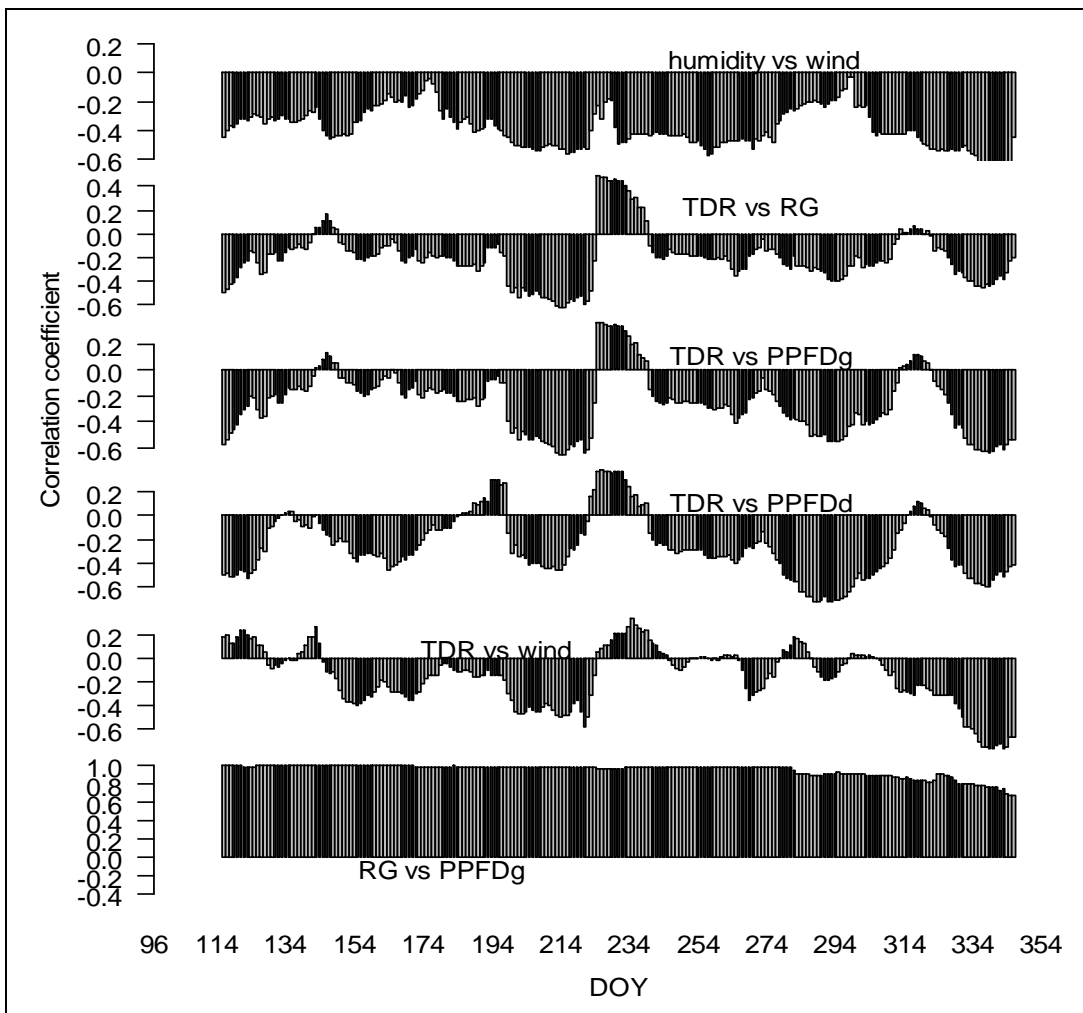


Figure 4-34. Inter correlations between climate variables tested with the forty day moving correlation window. Continued above and the following page.

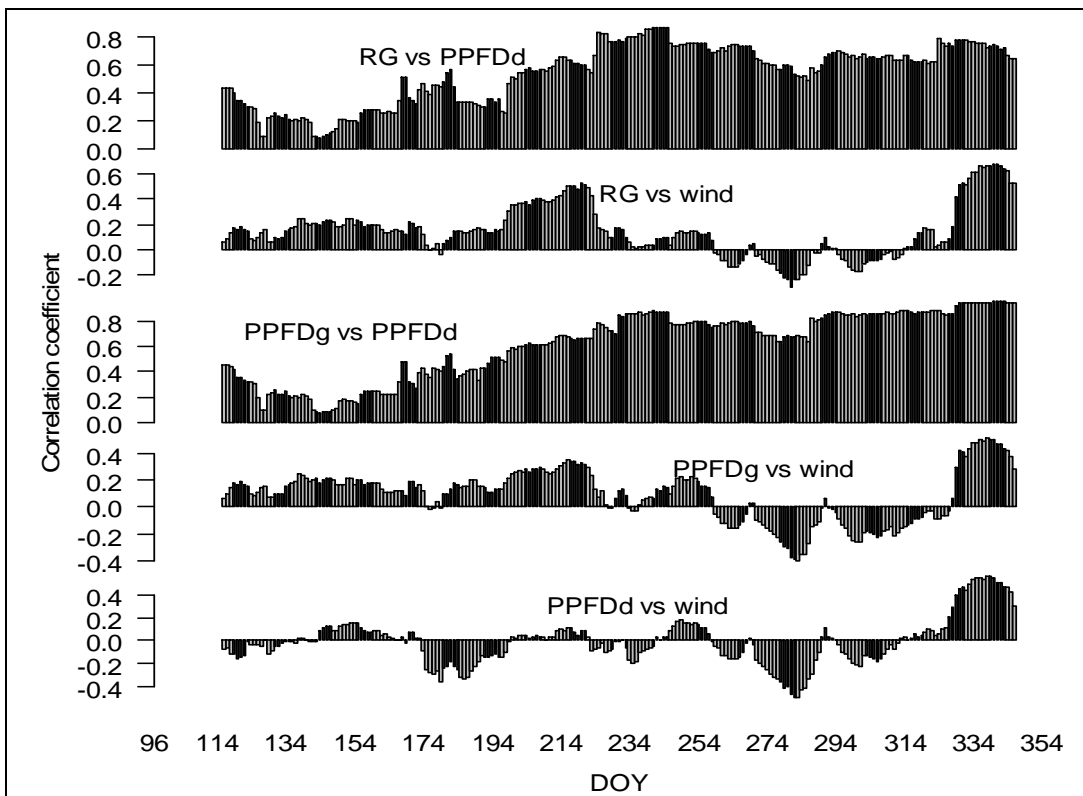


Figure 4-35. Inter correlations between climate variables tested with the forty day moving correlation window. Continued from above.

4.3.5 Density variation within the tree ring

Ring densities varied between the trees with the slow-growing tree 66 being markedly different from the other sample trees (Table 4-4). It had the largest proportion of latewood but also the earlywood was markedly denser than in other trees. Tree 48 had the lowest earlywood density but its latewood density was similar to trees 43 and 15.

Table 4-4. WinDENDRO results for 2008 growth rings from the Griffin dendrometer experiment. Density and ring dimensions reported at 4% moisture content.

	Ring width (mm)	Ring density (kg/m ³)	EW width (mm)	EW density (kg/m ³)	LW width (mm)	LW density (kg/m ³)	LW %
Tree 8	8.16	339	7.20	308	0.95	572	11.7
Tree 15	2.81	374	2.10	327	0.70	515	25.0
Tree 43	9.16	364	7.23	324	1.93	514	21.1
Tree 48	8.74	313	7.38	277	1.36	515	15.5
Tree 66	1.95	498	1.13	424	0.83	598	42.3

The detailed density curves plotted from the pixel based WinDENDRO output (50 μm resolution for density determination) showed that during the growing season there was fluctuation in density values (Figure 4-36) for trees 8, 43 and 48. However, in trees 15 and 66 the density increased steadily as the growing season advanced with each new layer of cells being denser than the previous ones. The sections with higher density in earlywood indicated changes in some aspects of xylem formation which are likely to have taken place via alteration of growth rate. These changes might have been linked to particular weather conditions that prevailed during the formation of those rows of cells. If the timing of formation was known these features could be linked to weather data.

The linking of density data to calendar days by using distance into the ring (mm) as a common axis (Wimmer et al., 2002) was attempted. However the discrepancies in the ring widths measurement with the dendrometers and the ITRAX pixel based data seemed to be more severe than those in the example by Wimmer et al. (2002). Approximately the first and last 5 pixels (pixel size = 0.05 mm) of each ring were removed to remove the high density values in the beginning of the ring and the downward tail in density at the end of the ring (Figure 4-36) as these arise due to the WinDENDRO definition of ring boundary that was set as 50% of the slope. Data on cell dimensions of these rings, as used to rescale dendrometer measurements in *Eucalyptus* spp. (Downes et al., 2009; Drew and Downes,

2009) were not available in this experiment. Furthermore, it was not considered desirable to use periods of slower growth to rescale density as the purpose of combining the growth and density data was to see if these features did indeed coincide.

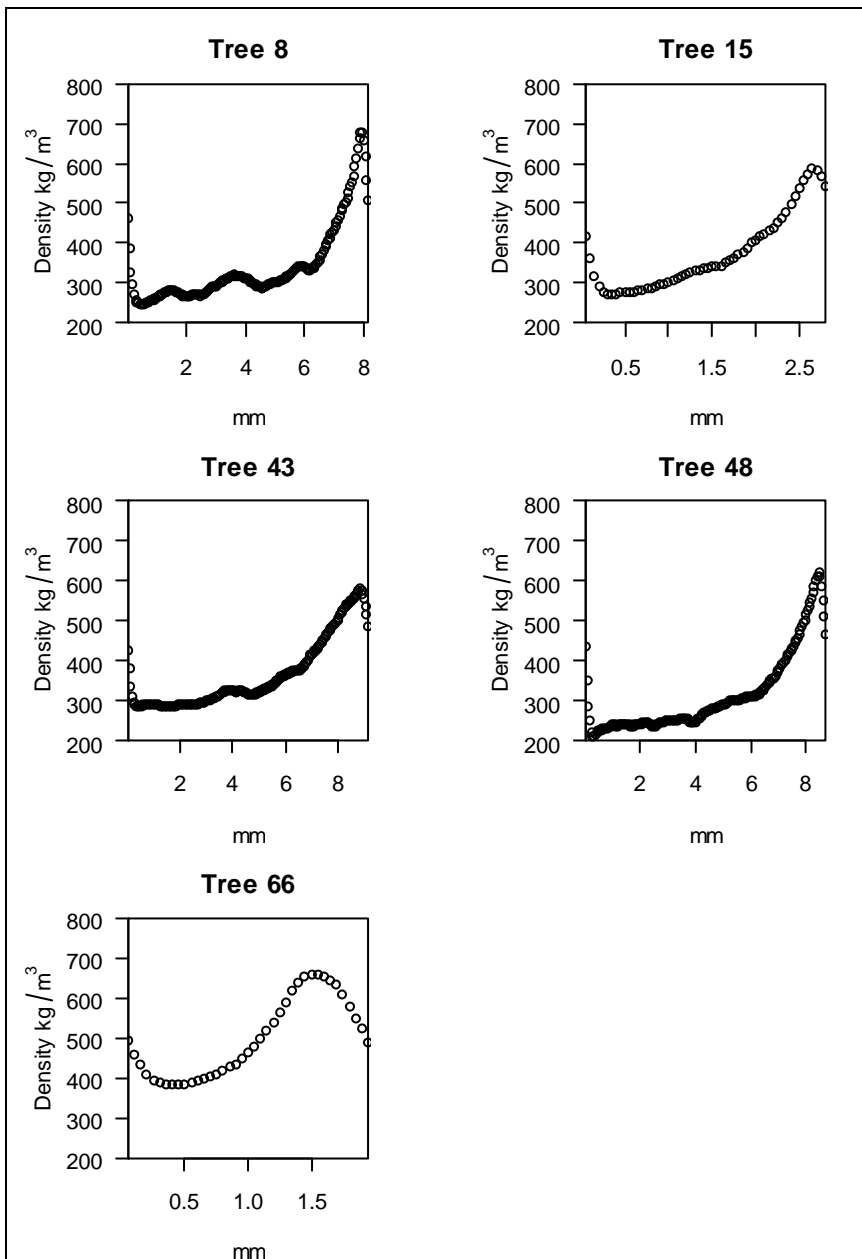


Figure 4-36. Density profiles for the 2008 growing season for the monitored trees at the Griffin site. Density values were defined at 4% moisture content.

Due to the large difference between ring widths measured by the LVDT dendrometers and by X-ray density analysis of the increment core, and the lack of additional information on xylem formation, the alignment of density and date remained tentative. To illustrate the difficulties experienced, ring width measured by both methods are included in the graphs with absolute scales in millimetres (Figure 4-38, Figure 4-39, Figure 4-40, Figure 4-41 and Figure 4-42). However, the two x-axes could also be perceived in terms of percentage of

ring formed which would justify connecting certain density values to approximate dates (date of the year (DOY)) via the dendrometer curve. The growth rates of the trees varied during the growing season, with the growth curves showing 3-4 different slopes. Tree 66 was an exception to this as it showed very little variation in growth rate and also intra ring density differences were absent. In tree 48 the growth rate increased at the end of June (approximately DOY 180) and it grew faster for approximately 35 days, after which the rate of increment decreased dramatically. In tree 43 the growth rate decreased at day 170 and increased again at day 205. Finally, from day 230 onwards, the growth rate lowered markedly before ceasing completely. In tree 8 there were 3 periods with differing growth rates; the first lasting until day 180. After this the growth rate increased between days 180-275 and then lowered towards cessation. Tree 15 experienced a change in growth rate at day 205 and the increase in the rate lasted until day 220 after which the rate started decreasing again. All the trees apart from tree 66 seemed to be characterised by a period of faster growth towards the end of growing season. In tree 15 that had a fairly narrow annual ring, there was a period of surprisingly fast increment between days 205-220. During those two weeks the radius increased by 0.88 mm, which corresponds to $\frac{1}{4}$ of the ring according to the dendrometer measurements. However, after the period of fastest growth the radial increment could also be more easily influenced by water reserve related swelling and in a tree with small ring width, the effect of swelling would be more marked.

Interestingly in trees 48, 43 and 8 there were some intra annual density bands with the most pronounced one occurring at 2.5-3.5 mm, 3 – 4.4 mm and 2.6- 4 mm in to the ring according to the ITRAX ring width data, respectively. According to the rough dating from the dendrometer data this corresponded to the period from day 160 to 180 (i.e. approximately 10th of June to end of June). If the approximate dating was correct then there should have been some changes in the weather conditions during that period as well. This was investigated by plotting rainfall, air temperature, humidity and soil moisture for a period starting two weeks before the approximate date of the density band and ending some weeks after (Figure 4-37). In fact, a period of warmer and drier weather (drier in terms of both rainfall and relative humidity) was observed around day 160. Between days 160-180 the site received some precipitation, the temperature decreased and the relative humidity started increasing. However, the strong decline in soil moisture persisted until approximately day 170. In the correlation analysis, radial increment was positively correlated with temperature (Figure 4-16), humidity (Figure 4-18) and rainfall (Figure 4-19) and negatively with soil moisture (Figure 4-20). Therefore, if the density band was caused by growth rate reduction this could have been mediated mainly by decrease in temperature and air humidity. However, it is also interesting to note that even though there

were two other sections of higher density in tree 8 before and after the day 180, there was no change in the slope of the growth curve at these points. In tree 48 and 43 there was an increase in growth rate at day 180 and 170, respectively, which would coincide with the period when the potentially restrictive weather conditions were relaxed.

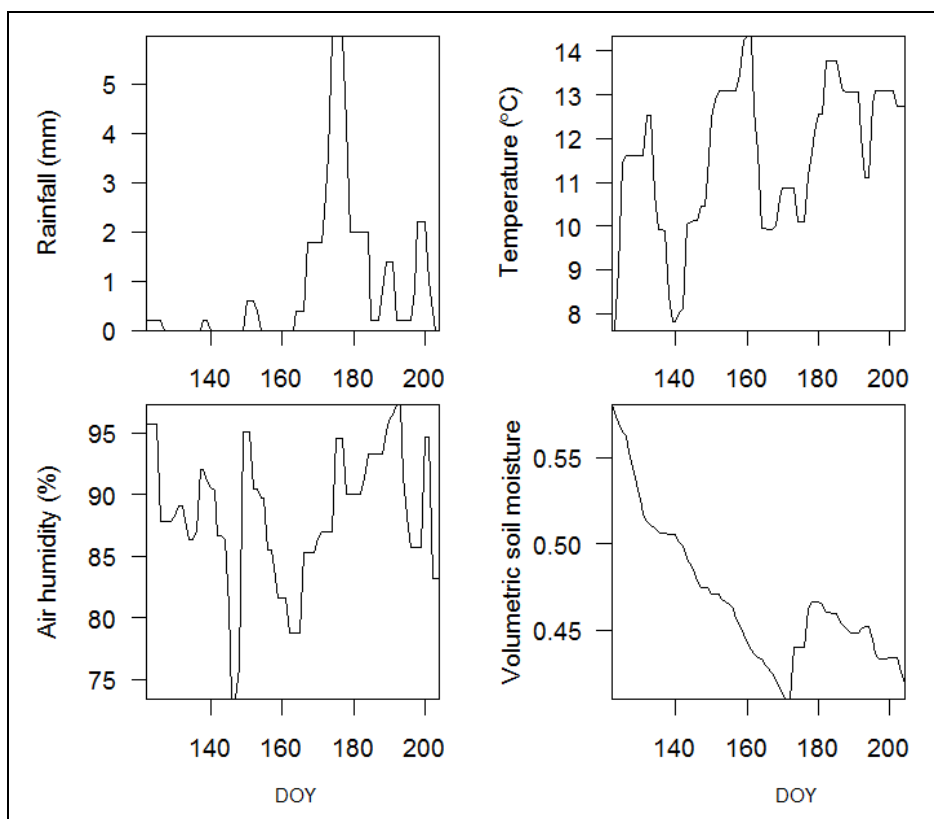


Figure 4-37. Comparison of the key weather variables during the estimated period of intra-annual density band formation in trees 48, 43 and 8 and the surrounding weeks. The curves were smoothed with a three day moving median for easier observation.

In trees 48 (Figure 4-38) and 43 (Figure 4-39) the point of latewood formation detected in the WinDENDRO analysis did not correspond with the change of growth rate observed in the dendrometer data, which might indicate that the alignment of the curves was not successful or that perhaps differences caused by the location where the samples were extracted were quite large. In trees 8 (Figure 4-40) and 15 (Figure 4-41) the onset of latewood formation coincided with a change in growth rate. In tree 66 the growth rate remained the same throughout the season and ceased early (Figure 4-42). After growth cessation there were large fluctuations in the radius of tree 66 which made the alignment difficult.

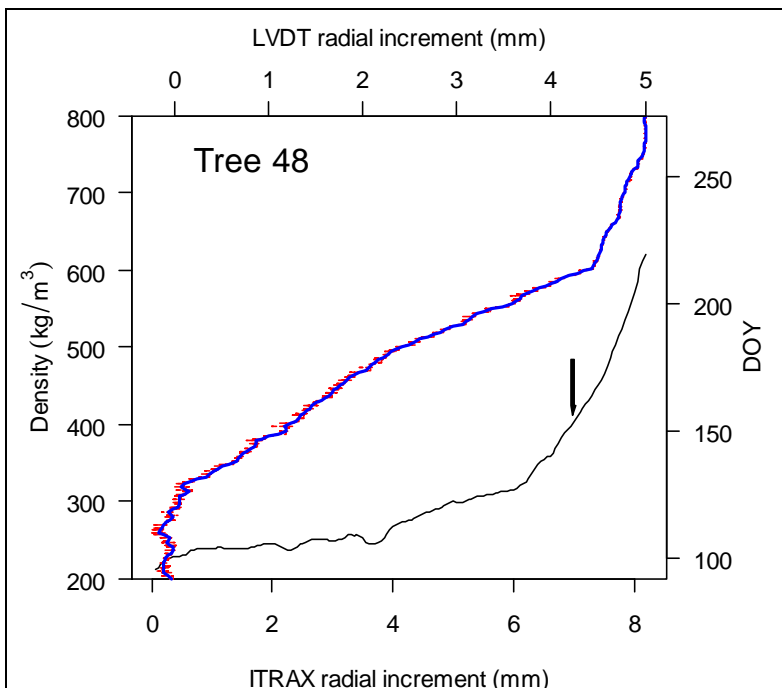


Figure 4-38. The ITRAX density (black) and day of the year (DOY) in tree 48 plotted against the respective radial increment. The dendrometer measurements were smoothed with a LOWESS curve (blue) and the original measurements showing the diurnal variation are plotted in red. The black arrow indicates the onset of latewood formation.

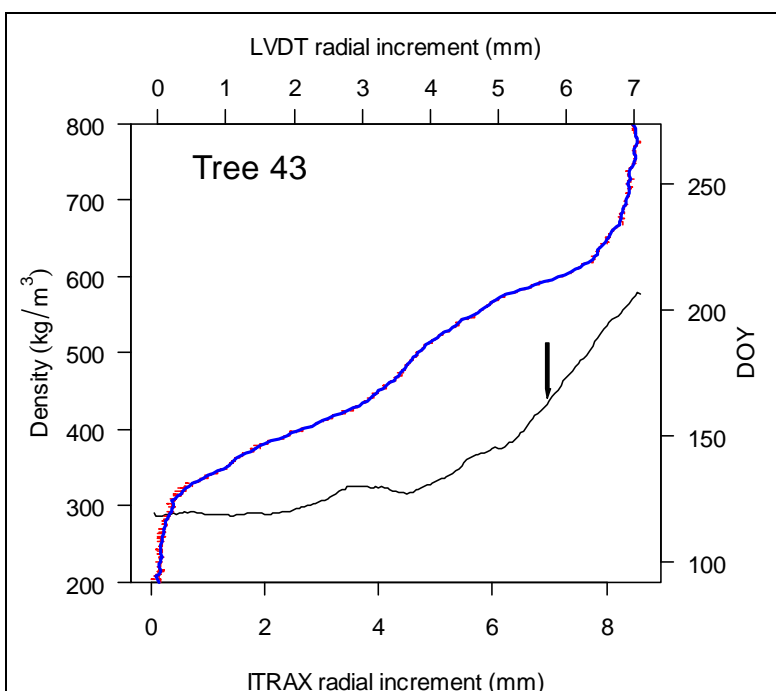


Figure 4-39. The ITRAX density (black) and day of the year (DOY) in tree 43 plotted against the respective radial increment. The dendrometer measurements were smoothed with a LOWESS curve (blue) and the original measurements showing the diurnal variation are plotted in red. The black arrow indicates the onset of latewood formation.

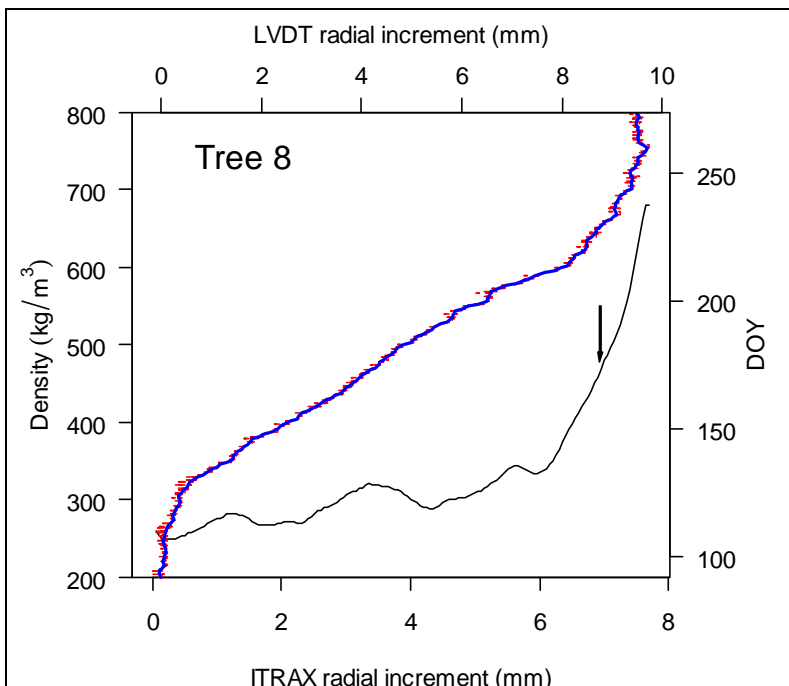


Figure 4-40. The ITRAX density (black) and day of the year (DOY) in tree 8 plotted against the respective radial increment. The dendrometer measurements were smoothed with a LOWESS curve (blue) and the original measurements showing the diurnal variation are plotted in red. The black arrow indicates the onset of latewood formation.

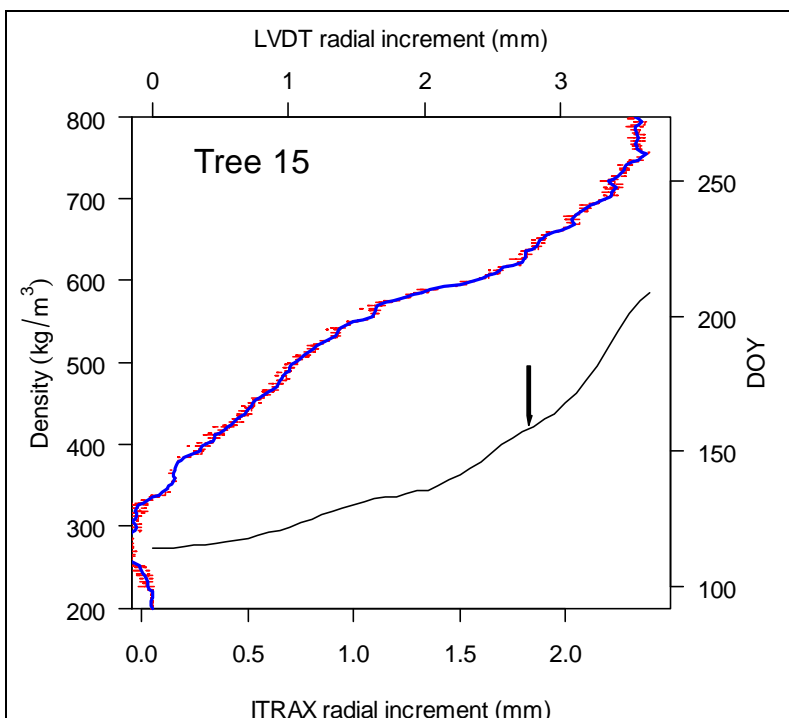


Figure 4-41. The ITRAX density (black) and day of the year (DOY) in tree 15 plotted against the respective radial increment. The dendrometer measurements were smoothed with a LOWESS curve (blue) and the original measurements showing the diurnal variation are plotted in red. The black arrow indicates the onset of latewood formation.

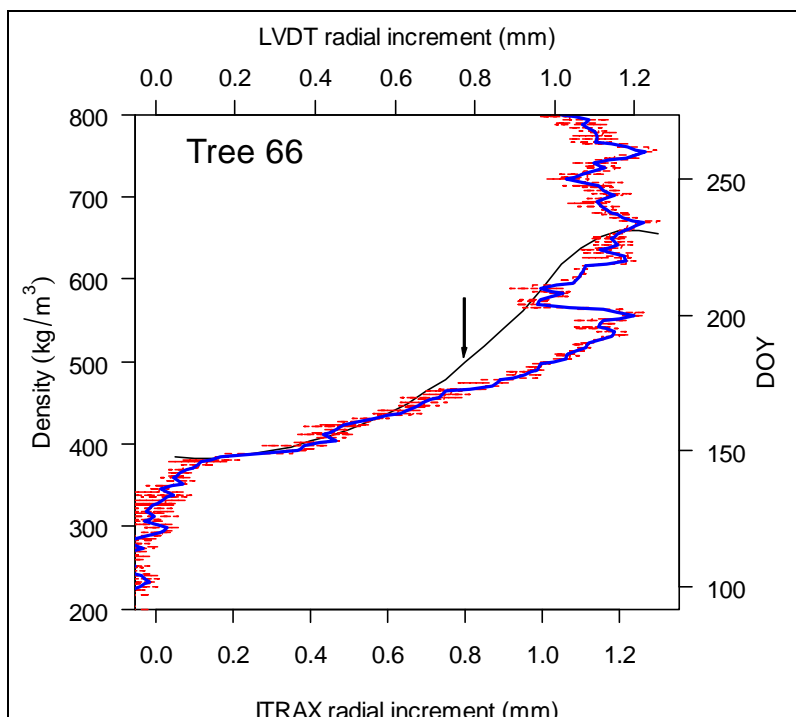


Figure 4-42. The ITRAX density (black) and day of the year (DOY) in tree 66 plotted against the respective radial increment. The dendrometer measurements were smoothed with a LOWESS curve (blue) and the original measurements showing the diurnal variation are plotted in red. The black arrow indicates the onset of latewood formation.

4.4 Discussion

Information on how growth depends on climatic variables at different stages of growing season is needed to understand how growth dynamics might change under future climatic conditions. This study looked at growth increment data for one growing season (2008) but the experiment will continue over several years which will allow comparison of different growing seasons and defining factors that govern the onset of radial growth.

At the Griffin site, the dendrometers detected growth earlier than the microcores. On the 29th of April the dendrometers measured 0.012-0.357 mm of growth depending on the tree, except in tree 15 where a negative value (-0.0144 mm) for the average ring dimension of the day was obtained. However, the dendrometer in tree 15 was only installed that day due to a technical difficulty on the previous visit. Therefore, the dendrometer only recorded values from noon onwards, which would not have included high values in the early morning before the shrinkage phase commenced. Due to this, the measurement for tree 15 was not comparable to other trees. According to the dendrometer data a sizeable fraction of the radial increment occurred in May whereas the microcores only detected growth in one tree (tree 48) in mid May. Growth was detected by microcores in all trees on the 5th of

June. Several factors are likely to have contributed to this discrepancy. First of all, the destruction of enlarging cells will have delayed the detection of growth in the microcores. Secondly, there was a large gap between the sampling occasions when growth was only detected in one tree (13th of May) and when considerable amount of growth (0.06-0.7 mm depending on the tree) was observed in all trees (5th of June). An additional set of microcore samples between these dates would have improved the resolution of the microcore data and the estimation of growth onset. In addition to the problems related to microcore sampling, dendrometer measurements may have been influenced by the filling of water reserves (Herzog et al., 1995; Mäkinen et al., 2003b; Zweifel and Häsler, 2001; Zweifel et al., 2001), expansion of cambium (Wimmer et al., 2002) and phloem growth (Antonova and Stasova, 2006; Antonova and Stasova, 2008). All of these could contribute to radial increment being detected by the dendrometers before xylem growth actually took place. Several authors have observed that in the spring, stem expansion that is related to filling of water reserves takes place. Zweifel et al. (2000) reported in Norway spruce that the stem radius changes were closely linked to bark water content. They reported that from green conditions to air dry state the phloem of Norway spruce disk samples contracted to approximately half (from 1648 μm to 886 μm). In living trees the degree of water loss would naturally be less severe. Zweifel and Häsler (2001) reported that maximum shrinkage of bark could reach 2 mm annually. However, these trees were of considerable age; 150-250 years.

In this study only the outer flakes of bark that typically form in Sitka spruce had been removed but otherwise the bark had been left in place in order to avoid causing damage to the cambium as the focus of the study was to monitor the xylem formation. Therefore, bark swelling could contribute to the increment detected. During the period of fast growth the daily amplitude of radius dimensions was quite insignificant in proportion to the growth (Figure 4-10) as the rings formed were wide. In comparison the mean growth ring width in the Norway spruce trees studied by Zweifel and Häsler (2001) was 0.75 mm and by Mäkinen et al. (2003b) 1.16 mm. The xylem formation was verified by microcore measurements and X-ray analysis even though exact matches of ring width were not always obtained by the different methods.

Before the onset of growth the cambial initials divide and the cambium increases in width (Gričar, 2007). This could further contribute to the growth detected in the beginning of the growing season. Gričar (2007) reported that in spruce and fir, the width of dormant cambium was 7-9 cells. But the number of cells varies between species as well as individuals of different age and vigour (Gričar, 2007). Bäucker et al. (1998) observed in

43-year-old Norway spruce that the number of cell files in the cambium varied from 5 in dormant stage to 11 at the peak of activity. However, the trees investigated both by Gričar (2007) and Bäucker et al. (1998) were less vigorously growing than the sample trees in this study. Therefore, the width of the cambium might be wider but the contribution to ring width should still remain small.

As bark and phloem were left intact the phloem growth could contribute to the observations here as well. For Siberian larch the annual phloem growth was found to be 273 μm (Antonova and Stasova, 2008). In Norway spruce it was reported that the phloem ring was 5-6 cells, which in those trees corresponded to 1/3 of the xylem ring width (Bäucker et al., 1998). For both Siberian larch (Antonova and Stasova, 2008) and Scots pine (Antonova and Stasova, 2006) it was found that phloem growth started earlier than xylem growth which could explain some of the discrepancy between onset data detected by dendrometer and microcores observed here. However, in contrast to these findings in Norway spruce and Silver fir, the xylem and phloem growth was found to start and stop simultaneously (Gričar, 2007; Gričar and Cufar, 2008). In long term monitoring any increase in the width of the bark might cause difficulties in interpreting the data. However, the increase in the bark width is fairly slow as older phloem cells collapse and older layers of bark are lost from the surface (Gričar and Cufar, 2008).

Problems in matching growth observations from different methods have been experienced in other studies as well. Similar results for the total number of tracheids developed during the growing season were obtained by microcoring and pinning methods (Mäkinen et al., 2008; Seo et al., 2007) but the microcore samples indicated a later cessation date. Dendrometer results differed from both of these methods especially regarding the onset of radial growth. At the Griffin site the true timing of radial growth onset is likely to have occurred between early May and the beginning of June. Denne (1977) estimated that the bud burst and the onset of height growth takes place between end of March and end of May in the UK.

In the trees at the Griffin site, the period of fast growth ended in the first week of August, apart from tree 66 where the growth rate was very slow and had ceased already in late July. Tree 66 showed a shorter growing period than the other trees; starting later and ending earlier. This has been observed in suppressed trees (Bäucker et al., 1998). By mid September the growth ring was completed in all trees based on both microcore and dendrometer observations (Figure 4-12). However, in trees 48 and 43 growth had

practically ceased a couple of weeks earlier, according to the dendrometer curves (Figure 4-10).

In the case of trees 15, 43 and 48, similar values for the width of xylem formed were measured by both methods at the end of the growing season. In the case of trees 15 and 48 there was quite large variation between sampling occasions towards the end of the year. The ring width can vary around the circumference (Gričar, 2007), therefore large variations like observed here can occur simply as the sampling location on the trunk was changed slightly on each visit. In the trees 66 and 8, good agreement between dendrometer and microcore measurements was not reached in the end of the growing season.

Some periods of shrinkage were observable in the dendrometer curves during the winter. These could be due to transpiration losses during warm periods (Mäkinen et al., 2003b) or alternatively to drying of bark during cold periods ($<-5^{\circ}\text{C}$) (Zweifel and Häsler, 2000). During the early winter of 2008 the temperature was not observed to fall below -5°C and the shrinkage was observed to occur on warm days, therefore transpiration was a more likely cause. Further indication that the trees were transpiring and taking up water during the winter period was that the daily fluctuation in diameter was observed throughout the year. In cold climates this pattern was absent during the winter (Turcotte et al., 2009; Zweifel and Häsler, 2000). However, some of the shrinkage periods coincided with temperatures below 0°C indicating that perhaps temporary freezing of soil might have interrupted water uptake. Continuous replenishment of water reserves by Sitka spruce at the Griffin site further indicates that an extensive period of spring rehydration as described by Turcotte et al. (2009) in boreal conditions may not be required. This would decrease the confounding effect on detection of the onset of growth in UK grown Sitka spruce.

The growth rate was found to vary during the growing season with typically 3-4 periods with different growth rate. Mäkinen et al. (2003b) also found in Norway spruce several periods of differing growth rates. They found that after spring and in early summer the growth rate increased and then gradually decreased towards the end of growing season.

Correlation analysis with the forty day moving correlation window indicated that both temperature and rainfall during the growing season were positively related to radial increment in most trees. However, soil moisture content was negatively correlated with radial increment. The soil moisture probes related to the datalogger setup were located on the elevated area between the furrows. Therefore, when high soils moisture readings were detected parts of the deeper root system could be experiencing much wetter conditions

which might restrict the growth. Negative correlations between soil and bole temperatures and the daily increment were observed in July-August.

The sample storage protocol was changed in order to prevent the destruction of enlarging cells. Microcore samples from 2009 and the coming years will be analysed in future work and if the new sample storage method proves to preserve the samples better this will allow more accurate estimation of growth onset. Furthermore, with growth data from several growing seasons the dependence of growth onset set on climatic conditions and the consistency of the correlations between climatic variables and the radial increment can be tested. In addition to this, sap flow monitoring was started at the site in 2009 and there would be scope for comparing the diameter fluctuations with sap flow data in order to separate the growth from water related dynamics more efficiently. In addition, predicting sap flow from xylem diameter fluctuation (Sevanto et al., 2008) could be attempted in Sitka spruce.

The thin sections of microcores used here to measure ring width (mm) at different points during the growing season could be used further to study the cell dimensions. This would make it possible to determine whether faster growth and increased ring width is due to higher numbers of cells, larger cell diameter or a mixture of these effects. The density results from tree 66 that was slowest growing indicate that smaller ring width was due to decreased cell size since the timber was denser in this tree. To assess the potential contribution of phloem growth to the dendrometer measurements in the future analysis of the microcores the width of the phloem ring could also be measured.

5 Wood quality survey – “The Benchmarking Experiment”

This chapter reports the findings of the wood quality survey that was carried out over a wide range of sites. This survey will be called the Benchmarking experiment throughout this thesis. The results section first reports (5.3.1) some general findings on the density data such radial density pattern in the radius of Sitka spruce, between-site differences in density, influence of thinning or tree social status on density and finally reports the results of factorial analysis and the problems related to it. In the following sections continuous variables of the factors and other site and tree variables were used to model average density in juvenile wood (5.3.2), mature wood (5.3.3), outerwood (5.3.4) and the whole cross-section (5.3.5). In the sub sections of the sections of 5.3.5 it was investigated if the average density predictions could be improved by grouping the sites according to the silvicultural treatment (5.3.5.1) or geographical location (5.3.5.3) or by grouping trees into social classes (5.3.5.2). However, these divisions proved not to improve the models.

The behaviour of density in the radius was modelled in section (5.3.6). The model fitted to the data when it was reparameterised. Attempts of modelling the model parameters from the site and tree data in the entire dataset (end of section 5.3.6) or data from Benchmarking sites selected for felling (5.3.6.1) were not very successful.

5.1 Introduction

At stand level, tree growth is influenced by climate, silvicultural practices and site factors. In addition, individual trees are influenced by genetics, microsite effects and competition. Site factors and climate are interlinked in complex ways as discussed in the main introduction (Chapter 1).

By using a factorial design, the influence of each site factor and their interactions can be quantified. The Benchmarking experiment was planned to study the timber properties across Scotland and northern England due to concerns regarding the quality of future timber quality following changes in silvicultural practice that had taken place in past decades (Anon., 2006). The experiment follows a fractional factorial design. It was designed by Dr. John Moore from Napier University. Six site factors with two levels

(Table 5-1) are included in the experiment. According to the fractional factorial design this yielded 32 different combinations. Each combination was replicated yielding 64 sites. Due to some additional replicates, in total 68 sites were sampled. The sites were located in Scotland and northern England (Figure 5-1). This study was a collaborative project between Napier University, Forest Research (Northern Research Station, NRS) and Glasgow University. Other data arising from the extensive field campaigns have been used in other theses (Caron–Decloquement, 2010) and published (Moore et al., 2009a).

The samples from this experiment were used to study cross-section average densities in the whole stem and separately in juvenile and mature wood. In addition, the data were used to model the density curve along the radius (that is, the curve of the mean densities for every annual ring). Initially, the aim was to use dated tree ring data from these sites in a large scale climatic analysis, but difficulties caused by the sampling procedure prevented reliable dating of the outer year ring in many samples. This arose when increment cores were extracted through the whole diameter in a north-south direction, whereupon at the south ends of the cores some outer rings were often damaged or lost. For these reasons the ring-level climatic analysis was carried out on the samples collected from the Level II sites (chapter 6).

Table 5-1 Site factors used in the Benchmarking experiment

Factors	Levels
Yield class	<14, >14
Thinning	Unthinned, thinned
Elevation	<280 m, >280 m
Spacing	<2500 trees ha ⁻¹ , >2500 trees ha ⁻¹
Latitude	North, South
Longitude	East, West

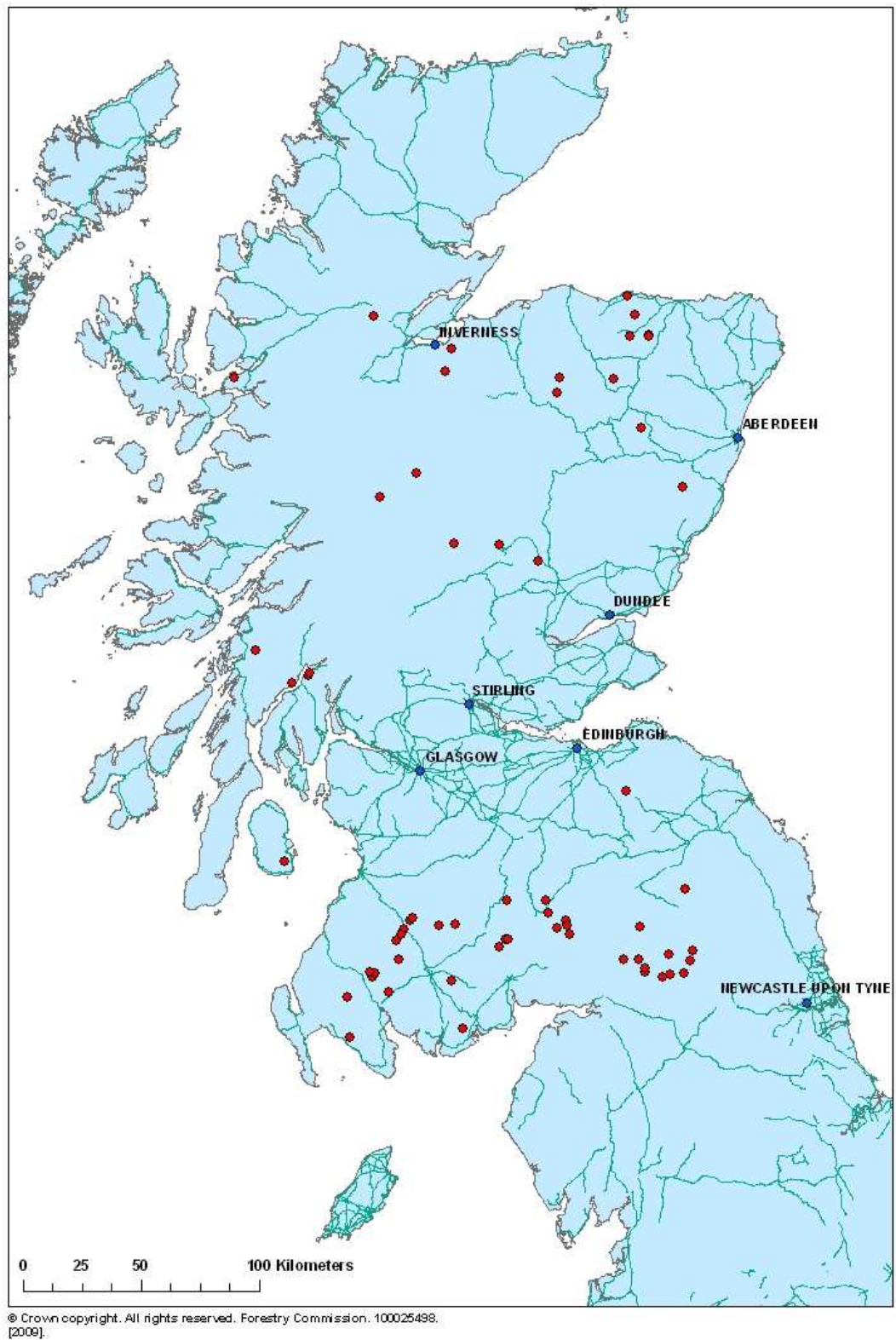


Figure 5-1. Map showing the locations of the Benchmarking experiment sampling sites.

5.2 Materials and Methods

5.2.1 Sampling

The sampling sites matching to each combination of factors were selected from the list of sites used in a stem straightness study (Macdonald et al., 2001; Stirling et al., 2000) and amended from the forestry commission database or from forests owned by Tillhill Corporation. In addition to the factors incorporated in the design, information on slope, and aspect were collected.

At each site, an 8 m radius (slope adjusted) sampling plot was established. This yielded an area of 0.02 ha. All trees on the plot were measured for DBH and assessed for stem form (Moore et al., 2009c) and stem straightness (Macdonald et al., 2001). For stem straightness, scores from 1-7 were allocated to the trees according to the straightness of the first 6 m of the trunk. A grade 1 tree will yield no usable timber whereas from a grade 7 tree, at least 5 m long logs can be cut. In stem form, deviation from normal growth such as broken tops, double leaders and ramicorn branches are noted. In total 2824 trees were measured.

At each site, ten randomly selected trees were tested acoustically (data not included in this thesis) and cored with a TrecorTM tree corer (CSIRO, Australia) to obtain 12 mm diameter increment cores. The coring was done at breast height from bark to bark in north-south direction. The direction was selected to avoid compression wood that is most likely to form on the leeward side, away from the prevailing wind (SW). North cores were retained by Napier University. The south cores were used for the purposes of this thesis and they were processed and analysed for density on an ITRAX X-ray densitometer as described in Chapter 2. Some core samples contained defects such as branches that prevented the density analysis. Some samples were lost due to difficulties during the sawing process which caused the strips to break. Strips broken into a couple of relatively large pieces were analysed as it is possible to allow for cracks and gaps in the WinDENDRO analysis. However, some samples were broken into a large number of smaller pieces that could not be reassembled reliably. In total, density data were obtained for 578 trees.

5.2.2 Area-weighted density analysis

Density data were used to calculate different average density variables. These included average density across the whole radius, juvenile wood density, mature wood density and outerwood density. Outerwood density was calculated to allow comparison with the acoustic measurements and it was defined as the outer most 5 cm of the stem. Average, juvenile and mature wood densities were calculated from the ring density values as a weighted average by using the ring areas as the weights. The outerwood density was calculated from the pixel based WinDENDRO output.

As the experiment was set out according to a fractional factorial design, factorial analysis could be used to analyse the data. This was initially done in Minitab. However, practical limitations caused complications in following the factorial analysis in an ideal way. For example there were great difficulties in finding high elevation sites that would meet some of the other criteria. That was especially the case when high elevation and high yield were required. Therefore, in practice some high and low elevation sites were very close on either side of the limit set to separate the levels of elevation factor. Also, some northern sites were very close to the dividing line and some considerably further north. Factorial analysis would simply treat these sites as equal representatives of their factor level. Hence, carrying out factorial analysis alone would not have been sufficient to separate out the influence of the different site factors. The factors were therefore converted into continuous variables whenever possible based on the data collected in the field. Mixed effects models (Pineiro et al., 2008) in the statistical package R (R Development Core Team, 2007) were used to explain the variation in density. Calculating average densities and modelling them from the site factors has the advantage that these explanatory variables such as DBH (diameter at breast height 1.3 m), stand density, and age are standard forest mensuration data, which are readily available.

In addition to the variables measured in the field further information on site conditions was obtained from the Ecological Site Classification (ESC) database (Pyatt et al., 2001; Ray, 2001). ESC is a decision support tool that assesses the site suitability eg. for certain species. Based on site coordinates and altitude, values for accumulated temperature (AT), moisture deficit (MD), windiness (DAMS) and continentality index were derived. Accumulated temperature in ESC is based on the mean monthly temperature values that exceed 5 degrees multiplied by the number of days in that month. These values were then summed over a 30-year-period (1961-1990) and divided by the monitoring period to obtain annual values. The resolution of data is 10 km grid squares. To produce a value for a

specific location ESC uses a multiple regression model. The same observation period and resolution has been used to calculate the moisture deficit values. Mean maximum moisture deficit (mm) values have been calculated from the difference between excess evaporation and rainfall. Detailed Aspect Method of Scoring (DAMS) to classify the windiness of a site has been described by Quine and White (1993). Calculation of continentality index in ESC (For details see Conrad (1946)) is based on the average annual temperature range over the 30 year period, latitude, longitude and altitude. Also estimated yield values (ESCyield) were derived. A complete list of site and tree variables collected or derived for the Benchmarking sites is in Table 5-2.

Table 5-2. Stand and tree variables used in the Benchmarking experiment.

	Type	Unit	Source	Sample size	Minimum value	Maximum value
Stand variables						
Northing	Factor + Continuous	OS National Grid	Field	68	551367	866426
Easting	Factor + Continuous	OS National Grid	Field	68	181914	375062
Yield class	Factor + Continuous	m ³ /ha/yr	FC data	68	-1	1
Elevation	Factor + Continuous	m	Field	68	73	558
Thinning	Factor	-	FC data / Field	68	-1	1
Original stocking	Factor + Continuous	Stems /ha	FC data	62	1710	7990
Trees per plot	Continuous	no of trees	Field	68	13	84
Stand density	Continuous	Stems /ha	Calc from Field	68	650	4180
Slope	Continuous	degrees	Field	67	0	31
Age	Continuous	yr	FC data		35	50
Site mean ring count	Continuous	No of rings	Calc from Field	68	21	49
Site mean DBH	Continuous	cm	Calc from Field	68	14.1	35.5
Site mean SS	Category	Score 1-7	Calc from Field	68	1.3	6.2
Accumulated Temp Sum	Continuous	Degree days	ESC	68	731	1388
Moisture deficit	Continuous	mm	ESC	68	0	128
DAMS *	Continuous		ESC	68	10	19
Continentality *	Continuous		ESC	68	3	8
Site mean height	Continuous	m	Field	59	14.7	31.8
Tree variables						
Juvenile DBH	Continuous	cm	Calc from Field	578	2.9	20.9
DBH	Continuous	cm	Field	578	7.6	43.7
Growth rate	Continuous	mm/yr	Calc from Field	576	2.1	16.8
Juvenile growth rate	Continuous	mm/yr	Calc from Field	578	2.9	20.9
Dominance Index	Continuous	-	Calc from Field	578	0.36	1.85
SS	Category	Score 1-7	Field	578	1	7

* obtained from the Ecological Site Classification (ESC).

For the data analysis the open source statistical package R (R Development Core Team, 2007) was used, apart from the initial analysis that was done in Minitab (Minitab 15 for Windows). The relationships between the variables were studied using scatter plots and correlation analysis. Linear mixed effects models (Pinheiro and Bates, 2000) were used to study the influence of site factors and tree parameters on the timber density (Table 5-2). First, a saturated model was built using selected variables based on scatter plots and correlation analysis. The data included both categorical (eg. Thinning with levels 1 and -1) and continuous variables. Furthermore, the data were unbalanced in nature and contained missing values. Therefore, mixed effects modelling in the statistical package R (Pinheiro et al., 2008; R Development Core Team, 2007) was selected as a method. Mixed effects models can cope with datasets of that kind. Furthermore, in mixed effects modelling the nested structure of data can be allowed for to avoid pseudoreplication, where the number of degrees of freedom is inflated by observations that are not truly independent; eg. trees from the same site. With analysis of variance, using a large dataset such as this, the possibility of detecting a significant difference where one does not exist becomes very large, especially if the structure of the data is not acknowledged to remove pseudoreplication. Trees within a site are not independent observations since they are all influenced by the same climate and other factors specific to the site. Therefore, site needs to be included as a grouping factor in the analysis to allow for this. Mixed effects models can allow for the nested structure of the data with minimum loss in the degrees of freedom and without the need of losing information by averaging out the pseudoreplication. The model developed was fitted with the REML (Restricted Maximum Likelihood), which is a more robust method for a dataset with missing values. The p-values for the significance were used to exclude parameters one by one to derive a model where all the explanatory variables are significant.

5.2.3 Radial density modelling

Furthermore the radial profiles for ring density (RD) and ring width (RW) were studied. An existing wood density model (Equation 7) developed by Gardiner et al. (2010) that predicts ring density based on ring width and ring number was fitted to the data and reparameterised. The aim of this part of work was to test this unpublished model and explore the possibilities of improving it. As this model predicts density based on ring number and ring width it can be linked to existing ring width and growth models that are in use at Forest Research. This supports the current aim of integrating the existing timber properties models.

Equation 7

$$SG = e^{\alpha_1 / RingNumber} (\alpha_2 + \alpha_3 / RingWidth)$$

To improve the fit of the model to stands that it has not been calibrated on, the model parameters (α_1 , α_2 and α_3) were modelled to find site factors that could be incorporated into the model equation to improve the values of α_1 , α_2 and α_3 . The fit of the models developed was assessed using a concordance correlation analysis (Lin, 1989; Stevenson et al., 2009). R^2 -values for the models were derived using a furnival function written by S. M. Garber and modified by J. R. Moore (Napier University). Furnival functions has been developed to calculate R^2 -values for mixed effects models.

5.3 Results

This section reports the results of the Benchmarking experiment focusing first on density variation in terms of growth rate. Then results on variation within and between-sites are reported. Factorial analysis carried out in Minitab is compared to models using continuous variables of the factors in R (5.3.1). Then, the results of modelling area-weighted density in juvenile wood (5.3.2), mature wood (5.3.3), outerwood (5.3.4) and whole cross-section (5.3.5) from site and tree parameters are reported. The latter includes subsections on models developed for different groups of sites (thinned vs non thinned, north vs south) or trees (based on dominance class) separately. The following section (5.3.6) includes the results of a ring density model fit to the data. Finally, the possibility of improving the radial density model by deriving alpha values using additional tree variables from felled Benchmarking sites was investigated (5.3.6.1).

5.3.1 Density variation

When the density data (Figure 5-2) were plotted against the ring number, the density curve characteristic for Sitka spruce was obtained. There, the density initially decreases until a minimum is reached at about ring 10 (McLean, 2007), which is often regarded as the changing point from juvenile to mature wood. Density will then increase and eventually level off. In this study the density does not appear to level off but there are markedly fewer data points after ring number 35. The trend in density in the later rings is much less reliable as it is based on fewer measurements. Ring width (Figure 5-2) decreased from the pith

outwards. Initially ring width decreased at a faster rate until approximately ring number 20 and thereafter considerably more slowly. In some trees also some rings nearest to the pith were narrower than the following rings causing an initial increase in the ring width that was not tracked by the LOWESS curve.

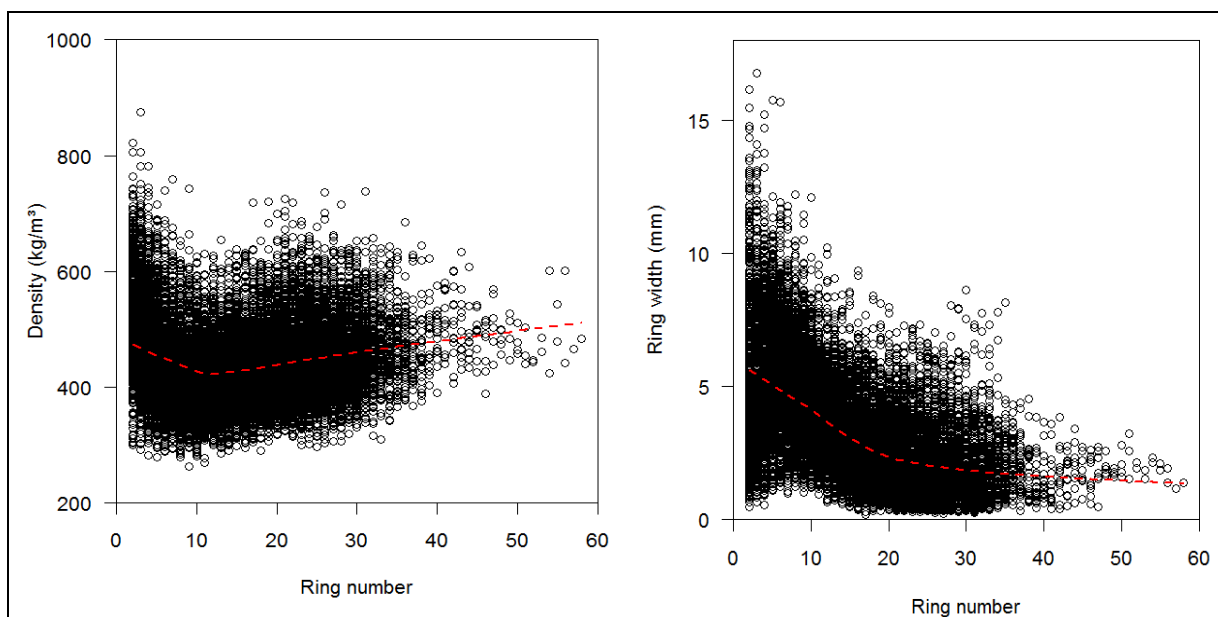


Figure 5-2. Ring density (left) and ring width (right) data at 4 % moisture content from all the Benchmarking sites plotted against ring number. LOWESS curve marked with a dashed red line.

On average there was a fairly strong and significant (p -value < 0.001) negative correlation between ring width and ring density. The correlation was stronger in mature wood (-0.61) than in juvenile wood (-0.54). However, the values varied considerably between-sites (See Appendix 2 for full list of correlation coefficients) and at a few sites the correlation was not significant. The relationship between ring density and ring width in mature wood is illustrated for each Benchmarking site in Figure 5-4. DeBell et al. (2004) on the other hand found that the negative relationship between ring width and ring density decreased in strength with age in western hemlock in Oregon becoming insignificant at age 30.

Repola (2006) found that in Norway spruce the tree rings in dominant trees were denser than predicted based on the width only, whereas the suppressed trees were less dense than predicted from the width. These findings were not supported in this experiment (Table 5-3). The density/ring width ratio decreased linearly from the suppressed to the dominant quartile (Figure 5-3).

Table 5-3. Average ring widths and ring densities for different dominance groups in the Benchmarking data. Trees were divided into quartiles according the DBH at each site.

	Average ring width (mm)	Average ring density (kg/m ³)
Whole dataset	3.37	447
Dominant quartile	4.21	419
Intermediate quartiles	3.31	448
Suppressed quartile	2.68	471

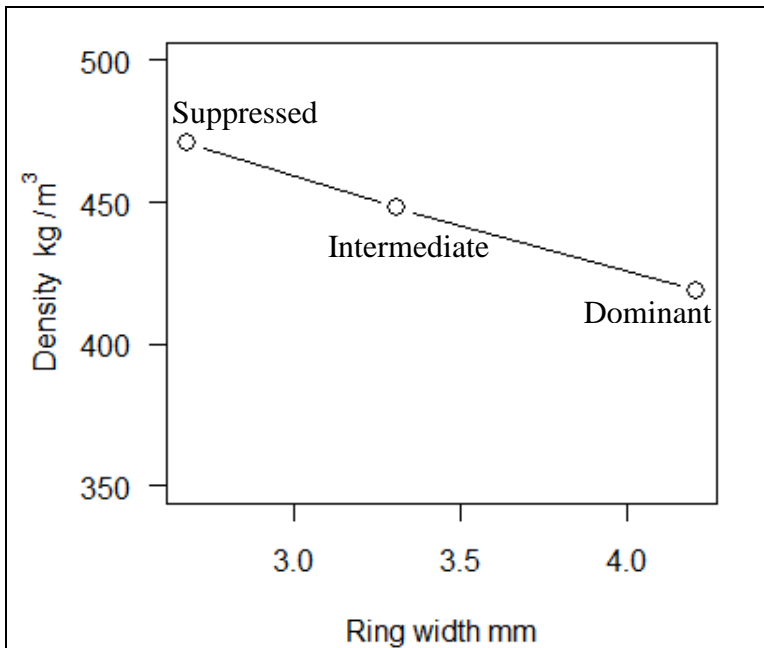


Figure 5-3. Average ring densities plotted against the average ring widths for different dominance groups in Table 5-3.

Initially, area-weighted densities for different parts of the cross-section were calculated. There was a wide range of densities within the experiment (Table 5-4). The density could also vary widely within a site (Figure 5-5). The between-tree variation seemed to be most pronounced in the juvenile wood (defined as first 10 rings). Pearson's correlation coefficient between juvenile and mature wood density was 0.600 (p-value <0.001) which indicates that trees with dense juvenile wood tended to form denser mature wood as well.

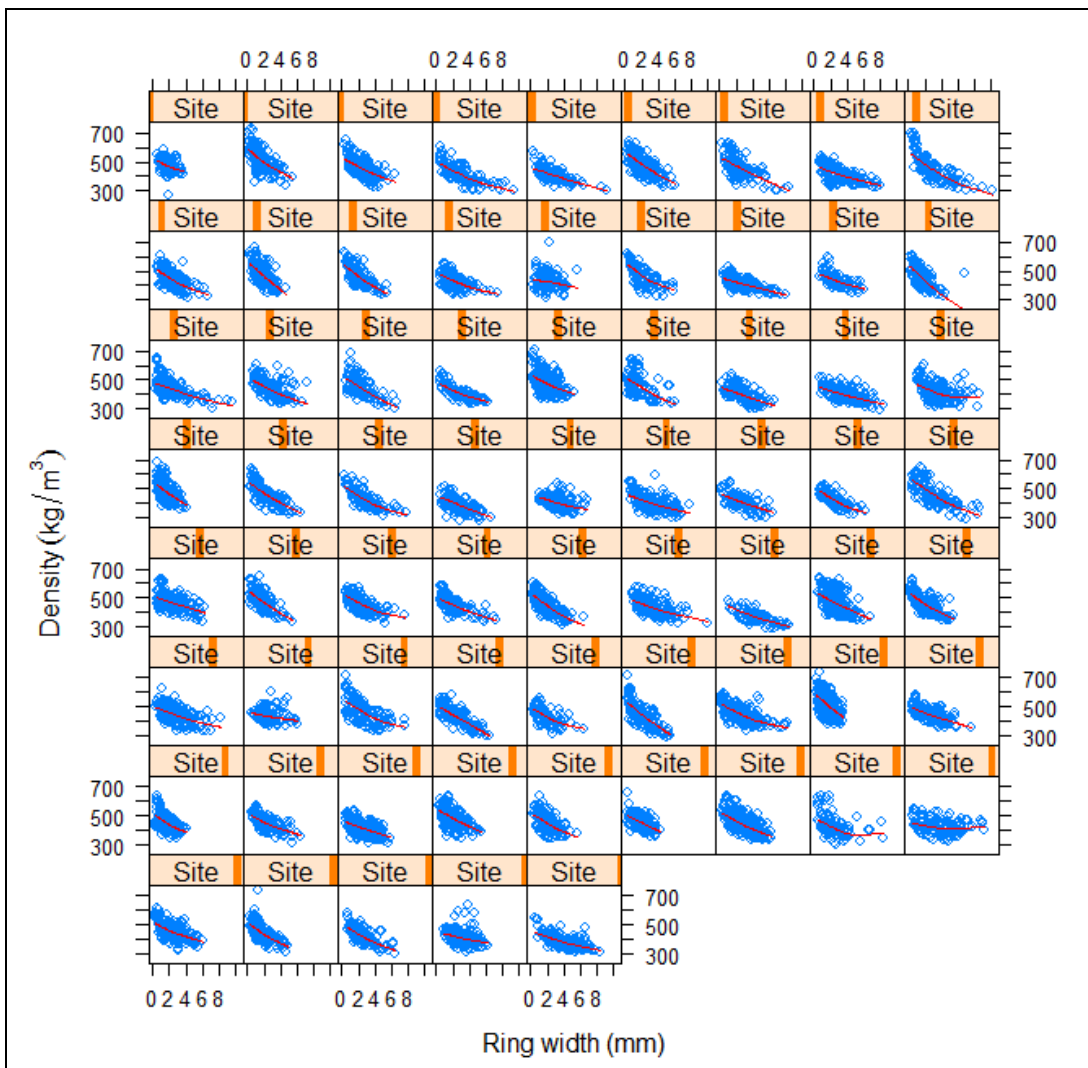


Figure 5-4. Relationship between ring width and ring density in the mature part of the radius (ring number >10) for all the Benchmarking sites. Red line is the LOWESS curve fitted to the data.

Table 5-4. Range of density values in the Benchmarking dataset.

Measurement type	Density (kg/m ³) MC 4 %		Density (kg/m ³) MC 12 %	
	Minimum	Maximum	Minimum	Maximum
Ring	263	876	279	899
Cross-section average	312	626	330	651
Juvenile wood (JW) average	302	646	319	671
Mature wood (MW) average	307	629	325	654
Outerwood (OW) average	307	619	324	643
Site cross-section average	368	512	387	535
Site JW average	375	534	395	558
Site MW average	360	509	380	532

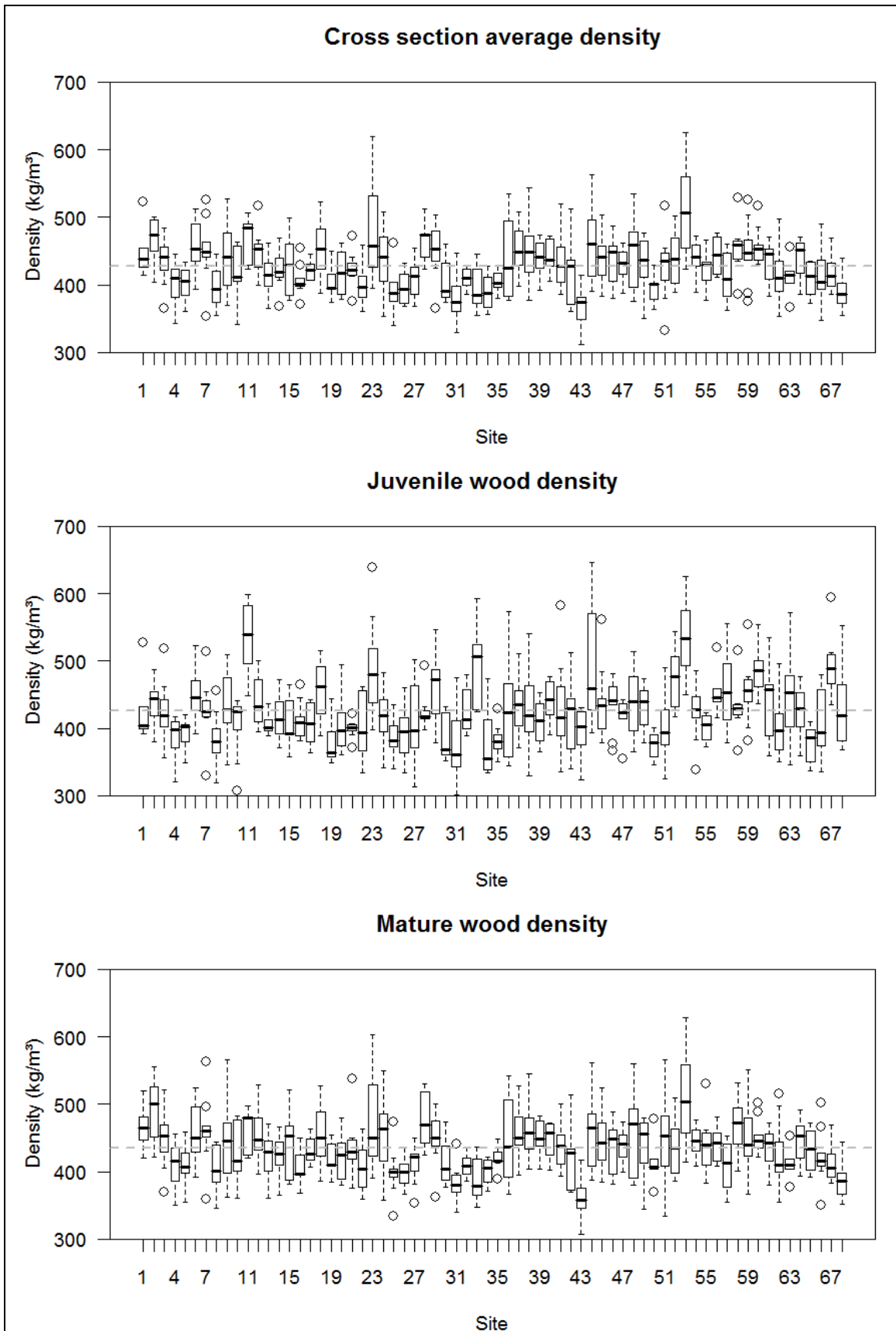


Figure 5-5. Cross-section average density, juvenile wood density and mature wood density determined at 4% moisture content at the Benchmarking sites. Dashed grey line marks the mean across the sites.

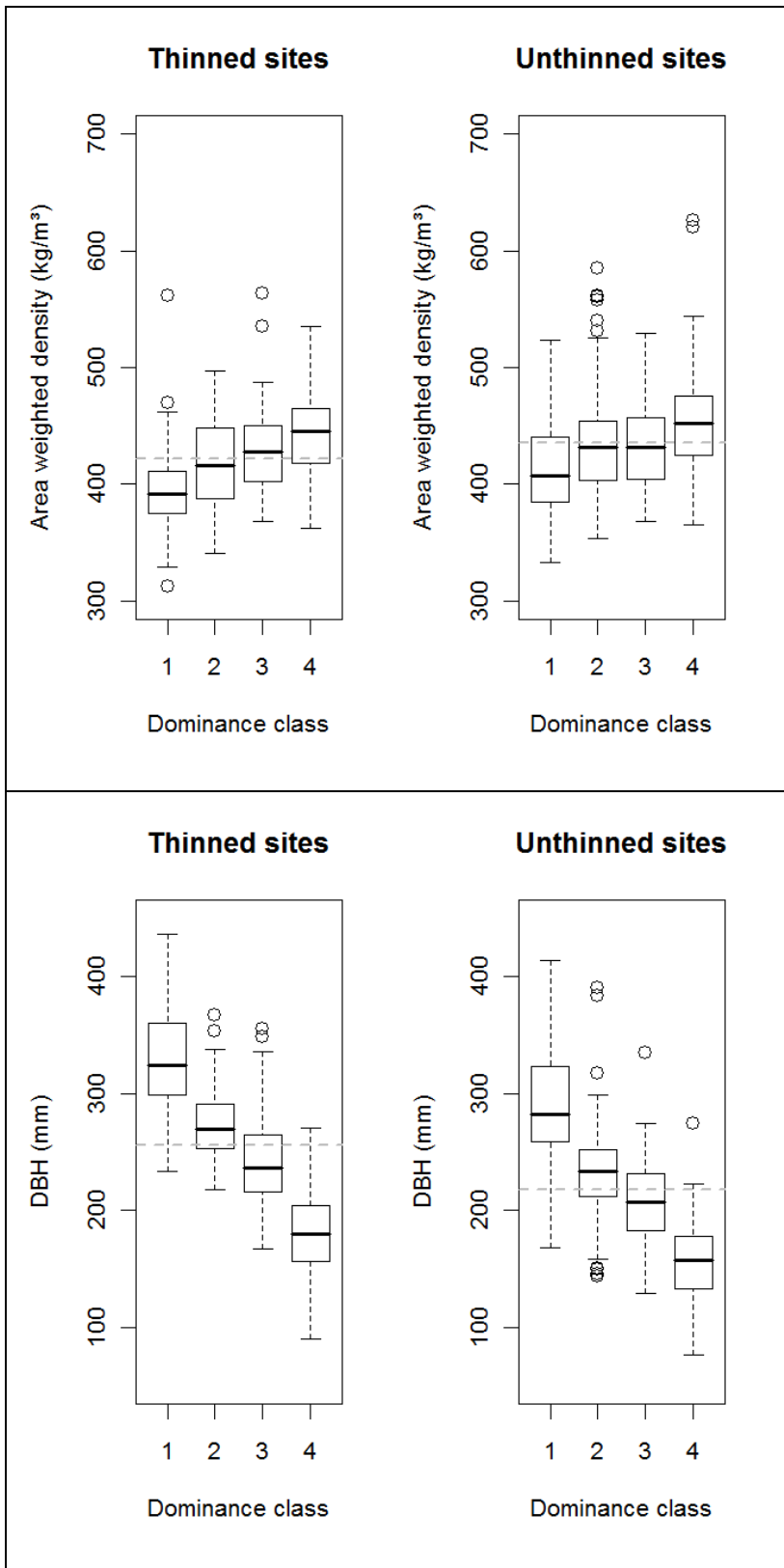


Figure 5-6. Area-weighted density of different dominance classes at thinned (left) and unthinned (right) sites. The mean is marked with a dashed grey line. Density determined at 4% moisture content.

When the area-weighted density was compared between thinned and unthinned sites and across dominance classes it was found that, the thinned and unthinned sites differed in area-weighted average density (423 kg/m³, 436 kg/m³). The difference was significant

($p < 0.001$) but the size of the effect was relatively small (Figure 5-6). However, at both thinned and unthinned sites, similar trends in density were found with the tree social status. The dominant trees (class 1) tended to have lower density than more suppressed individuals. In the pooled data there were significant differences ($p < 0.001$) between all the other quartiles except the co-dominant and non-dominant. However, comparing the ring width curves for each dominance class at thinned and unthinned sites (Figure 5-7) it appeared that part of the effect was due simply to the removal of suppressed individuals of higher density from the thinned sites. This can be concluded since density differs already in the juvenile part of the curve, whereas typically, thinning is carried out at stand age of 15. The thinning operation has removed most of the suppressed individuals with narrower rings and therefore the ring width curves have shifted upward, as the dominance classification was only a relative one comparing the DBH of an individual tree to the stand average. Hence, the reduction in average density and increase in ring width were not necessarily and certainly not solely due to growth response after the thinning treatment. Looking at individual ring width series from the thinned sites (data not shown), a growth response to thinning was not apparent. A further point to note about the graphs (Figure 5-7) was that all of the sites containing trees over 40 years were at the thinned sites, which is likely to increase the area-weighted density and hence decrease the difference between the two groups. This also influenced the shape of the LOWESS curves causing them to plateau. To separate the effects of pushing the average up by removing suppressed trees and of a genuine growth response, average ring widths and densities for each cambial age were plotted for thinned and unthinned sites separately (Figure 5-8). As observed in the previous graphs there was an initial difference in ring width due to the removal of suppressed trees. This initial difference was absent for ring density until about ring number 5, probably due to the huge variation in juvenile wood density near the pith. Approximately at ring number 15 there is an increase in the differences which in turn must be due to the thinning effect. The start of the effect at breast height age of 15 years corresponds to the typical timing of thinning.

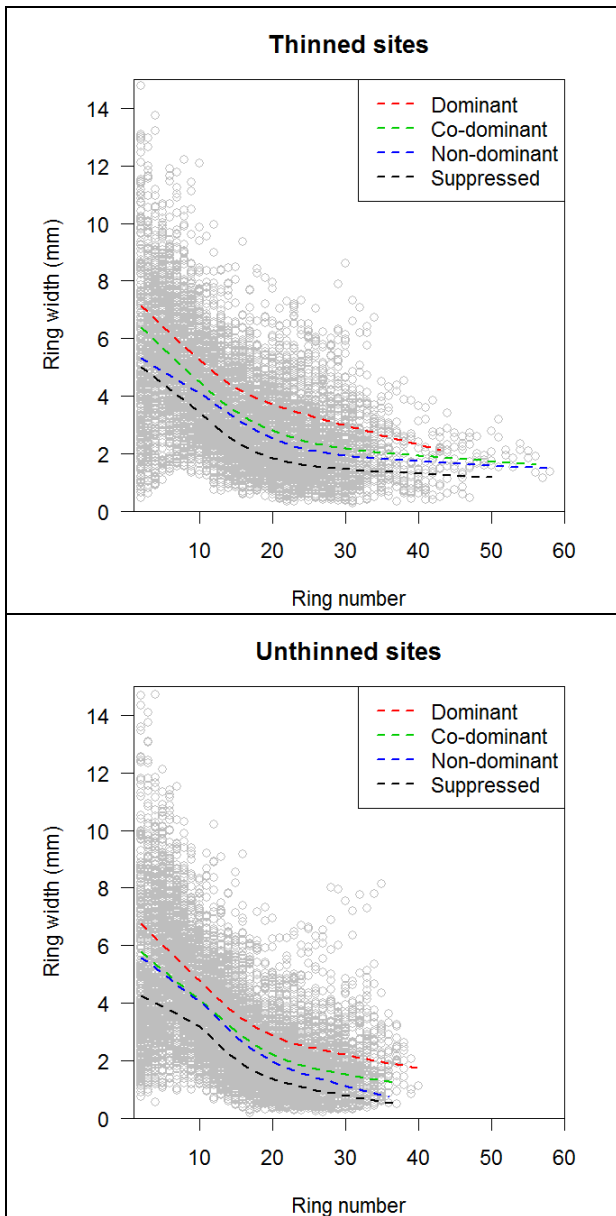


Figure 5-7. Shape of ring width curves at thinned (top) and unthinned (bottom) benchmarking sites. Dashed lines mark the LOWESS curves for each dominance quartile.

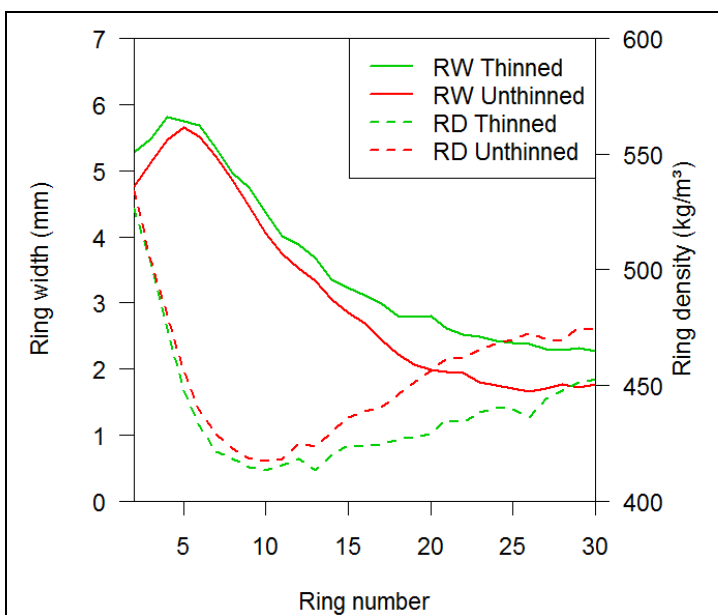


Figure 5-8. Influence of thinning on ring widths and ring density (MC 4 %) averaged for the cambial age across the thinned or unthinned Benchmarking sites.

The area-weighted averages were used in the factor analysis (MINITAB) to determine the influence of the site factors the experiment was designed to assess. When looking at the main effects (Figure 5-9) it was found that density was decreased by thinning treatment, higher yield class, lower stocking and higher elevation ($p < 0.05$). Easting and Northing did not have a significant effect on density ($p > 0.05$). The 2-way interactions were also looked at (Figure 5-10) and two significant ones and one in borderline to significance were detected. The Yield class*Spacing interaction was significant ($p\text{-value} < 0.05$) with the density-reducing effect of low stocking being more pronounced for the high yield class stands. Northing*Elevation interaction ($p\text{-value} < 0.01$) led to larger reduction in density with increase in latitude at the low elevation site. Elevation*Thinning interaction ($p\text{-value} = 0.051$) indicated that the thinning treatment reduced density more at the high elevations sites than at the low elevation ones. Higher order interactions were not investigated

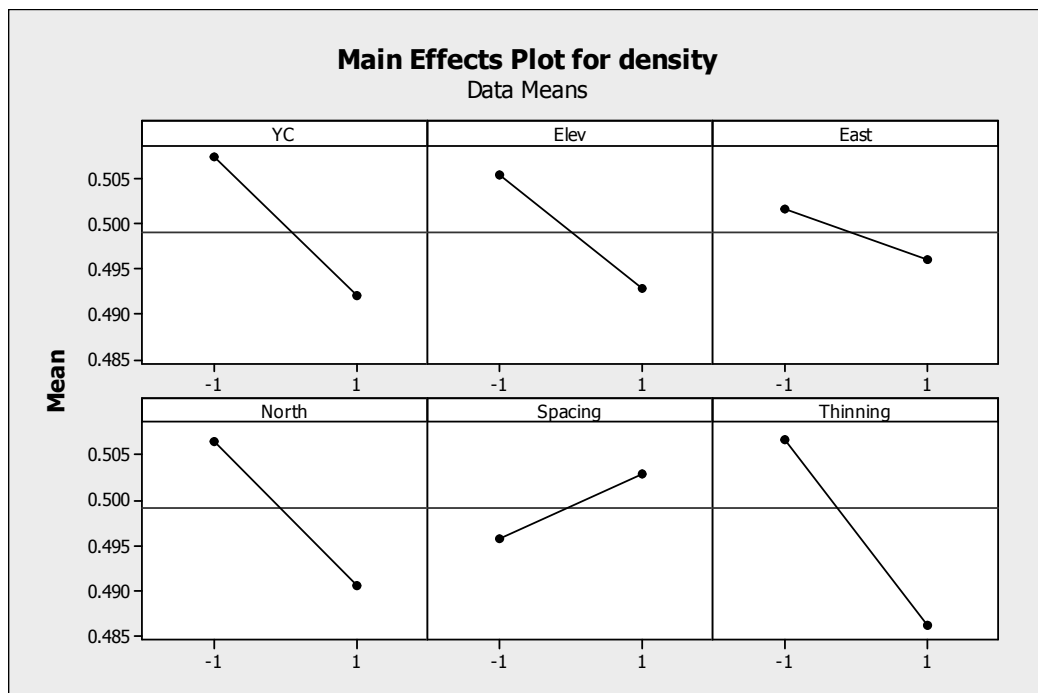


Figure 5-9. Influence of the site factors on the cross-section average density. In the experimental design YC -1 denotes sites with yield class $< 14 \text{ m}^3/\text{ha}/\text{yr}$ and YC 1 yield class $> 14 \text{ m}^3/\text{ha}/\text{yr}$. Elev -1 is elevation under 280 m and Elev 1 elevation $> 280 \text{ m}$. East -1 $< 300 \text{ km}$ east from the OS Grid datum and East 1 $> 300 \text{ km}$. North -1 is sites with $< 600 \text{ km}$ north from OS Grid datum and North 1 $> 600 \text{ km}$. Spacing -1 signifies a stocking of $< 2500 \text{ stems}/\text{ha}$ Spacing 1 $> 2500 \text{ stems}/\text{ha}$. Thinning -1 indicates no thinning and Thinning 1 that thinning has been carried out.

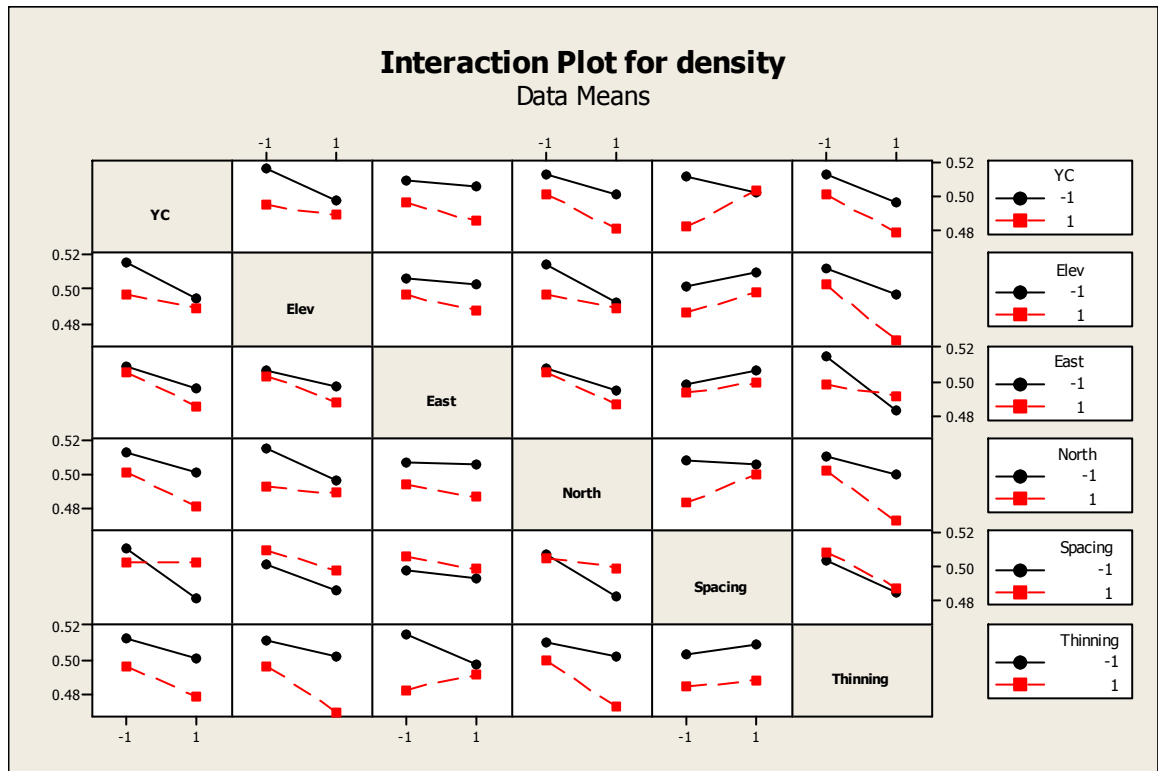


Figure 5-10. Two-way interactions influencing the cross-section average density in the Benchmarking experiment. In the experimental design YC -1 denotes sites with yield class <math> < 14 \text{ m}^3/\text{ha/yr}</math> and YC 1 yield class > 14 $\text{m}^3/\text{ha/yr}</math>. Elev -1 is elevation under 280 m and Elev 1 elevation >280 m. East -1 <300 km east from the OS Grid datum and East 1 >300 km. North -1 is sites with <600 km north from OS Grid datum and North 1 >600 km. Spacing -1 signifies a stocking of <2500 stems/ha Spacing 1 >2500 stems/ha. Thinning -1 indicates no thinning and Thinning 1 that thinning has been carried out.$

The concerns regarding the north/south divide and low/high altitude divide raised earlier, were investigated in more detail. The histograms (Figure 5-11) illustrated very clearly shortcomings of the north/south divide as the southern sites were geographically clustered very close together whereas the northern sites were spread over a wider range. A further problem was that the southernmost ‘northern’ sites were located very near the southern sites. These sites were in fact much closer to the southern sites than to many of the northern sites further north. Therefore, it could be argued that regarding this variable, these sites would have more in common with southern sites and would not present their factor level successfully. This latter problem was also observed in the case of easting and especially elevation which showed a high frequency of sites in the immediate vicinity of the limit value of 280 m. The yield class information (Figure 5-12) on the other hand showed signs of inaccuracy as some sites classed in the high yield class had lower DBH values than some sites in the low yield category. The problem was further illustrated plotting ESC yield estimates against the factor levels. In both categories there was variation beyond the level limit (YC 14) and the effect was most severe in the high yield category where the median was just above 14. However, correlation between-site mean

DBH and ESC yield estimate was also weak 0.145 (p-value <0.001) which indicates that these estimates may not be very accurate either. The original stocking information that formed the basis of the spacing factor was assessed by plotting the original stocking values against the stand densities calculated from field measurements for the unthinned sites (Figure 5-14). Some decrease in stem numbers would be expected due to self-thinning but the data included deviations that were much greater or opposite in direction than what could have been explained by self-thinning only. Therefore, the use of data based on field measurements was preferred. Thinning status was verified in the field and it was therefore considered suitable to be used in the analysis. Apart from that, it was concluded that analysis using the continuous variables was preferred over the factorial analysis. This was carried out using linear mixed effects models in R.

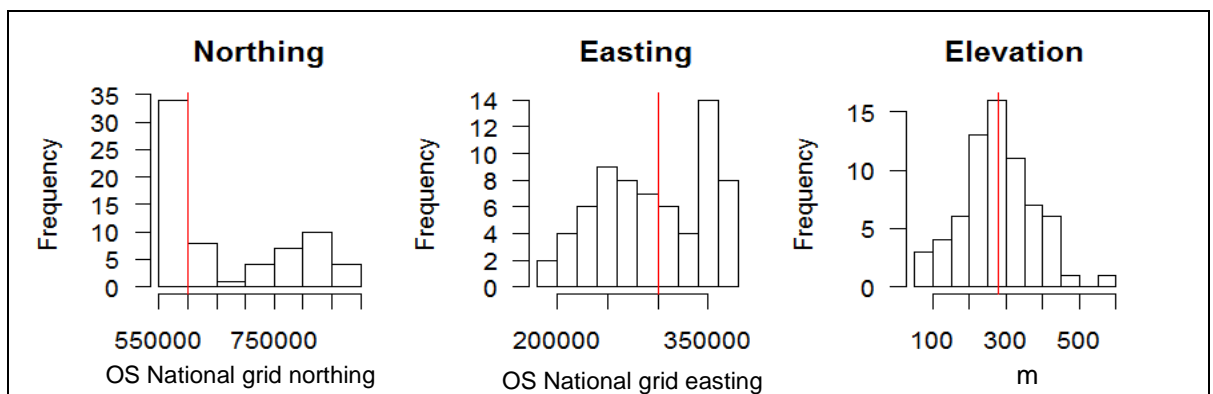


Figure 5-11. Histograms to illustrate the spread of sites in relation to the some of the factors in the original factorial design. Vertical red line marks the level divide.

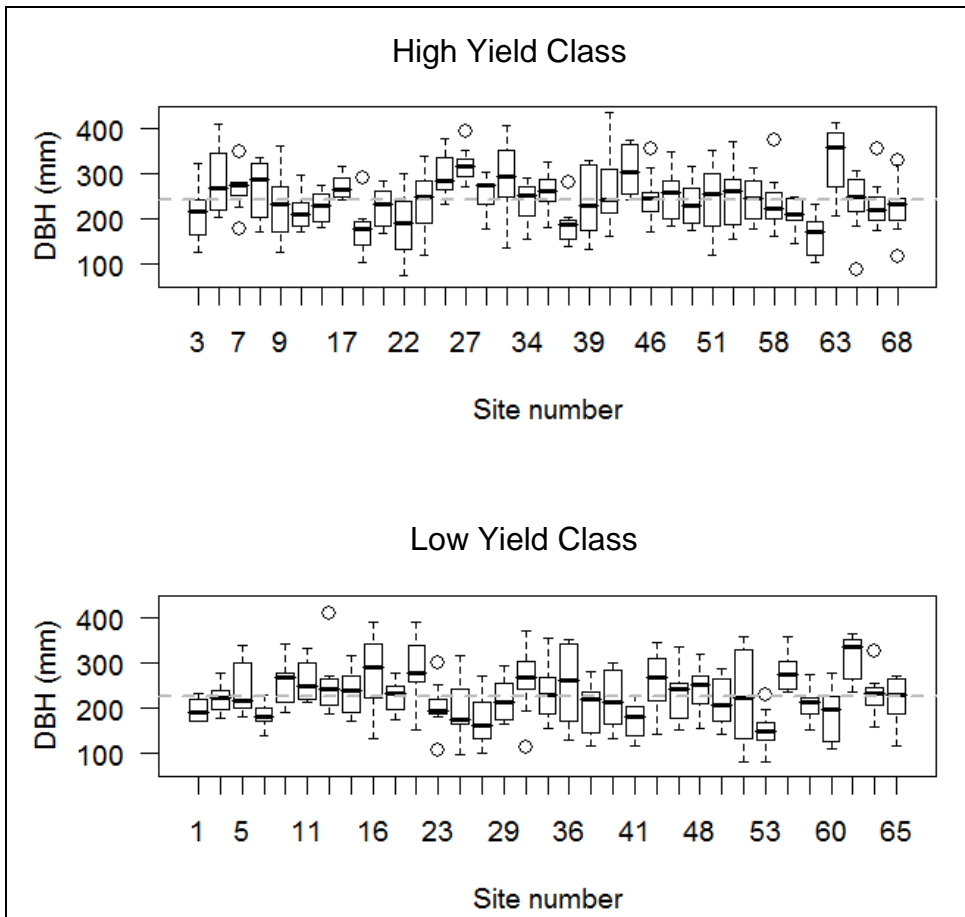


Figure 5-12. DBH variation between-sites from different yield class levels in the factorial design. Mean for the sites within a factor level is indicated with the dashed grey line.

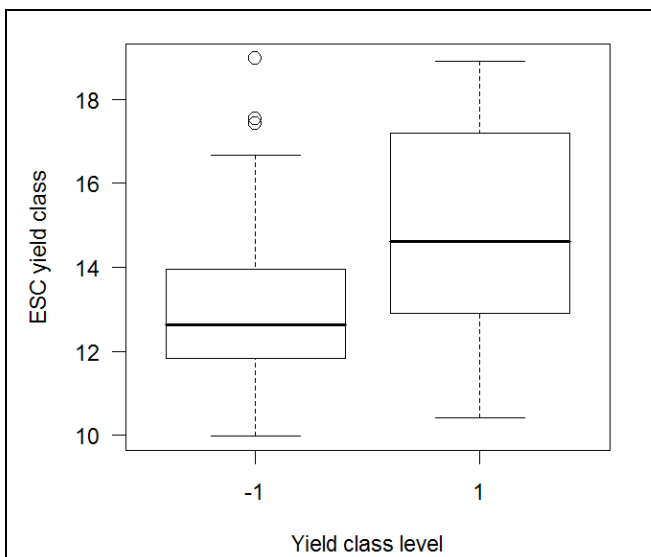


Figure 5-13. Relationship between the yield class factor levels and yield classes estimated from the ESC data.

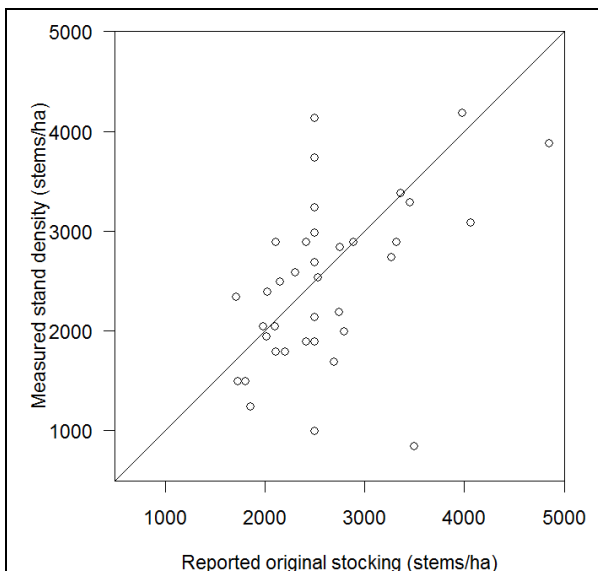


Figure 5-14. Relationship between original stocking obtained from the database and stand density calculated for the unthinned sites from the field data.

Firstly the average density variables were studied. When a model with no explanatory variables was fitted, it was clear that most of the variation was between-trees within a site and only about 25% of the variation was between the sites (Table 5-5).

Table 5-5. Partitioning of variation in density to within the site and between-site components. Density at 4% moisture content was used.

	Between-tree variation (%)	Between-site variation (%)
Juvenile wood	68.8	31.2
Mature wood	77.4	22.6
Outerwood	77.5	22.5
Average of whole radius	75.0	25.0

Initially, the cross-section average density data was analysed using the continuous variables of the original factors except for yield class where a fully reliable variable was not available (Figure 5-13). The aim was to investigate if the findings of the factorial analysis would be supported when the shortcomings of the factor divides were removed. In this case interactions were not fitted. Only stand density and elevation remained as significant explanatory variables in this model. Density increased with stand density and decreased with elevation. However, the model had poor predictive power (Figure 5-15) as it had R^2 -value of only 0.22 when random site effects were included and only 0.07 with just the fixed effects. Residuals tended to increase with the fitted values (Figure 5-15).

Table 5-6. Average density model obtained using the factors from the design as continuous variables.

Fixed effects: Average density ~ StemsPerHa + Elevation					
	Value	Std.Error	DF	t-value	p-value
(Intercept)	418.287	10.429	505	40.11	0.000
StemsPerHa	0.013	0.003	505	4.01	0.000
Elevation	-0.059	0.029	66	-2.00	0.049

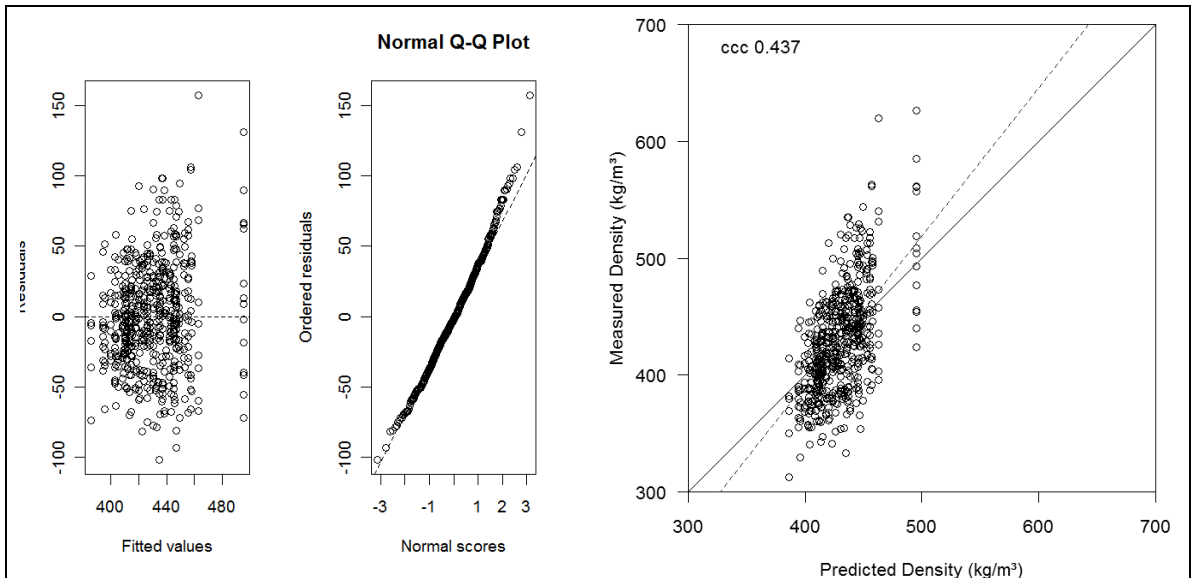


Figure 5-15. Diagnostic plots (left) and model predictions against the measured data for the model using the continuous variables of the original factors (excluding yield class).

Density and growth rate are intimately linked and therefore the influence, of the above described continuous variables, on the growth rate was also investigated. The variable that significantly influenced growth rate was stand density (Table 5-7) and as expected growth rate decreased with stand density since in a denser stand the resources available for each tree are more limited. The adjusted R^2 -values for this model were also quite poor 0.12 and 0.26 for the fixed effects and for the full model, respectively. There was a trend in residuals with residuals increasing with fitted values (Figure 5-16).

Table 5-7. Growth rate model obtained using the factors from the design as continuous variables.

Fixed effects: Growth rate ~ StemsPerHa					
	Value	Std.Error	DF	t-value	p-value
(Intercept)	9.6772	0.3390	503	28.54	0
StemsPerHa	-0.0009	0.0002	503	-5.69	0

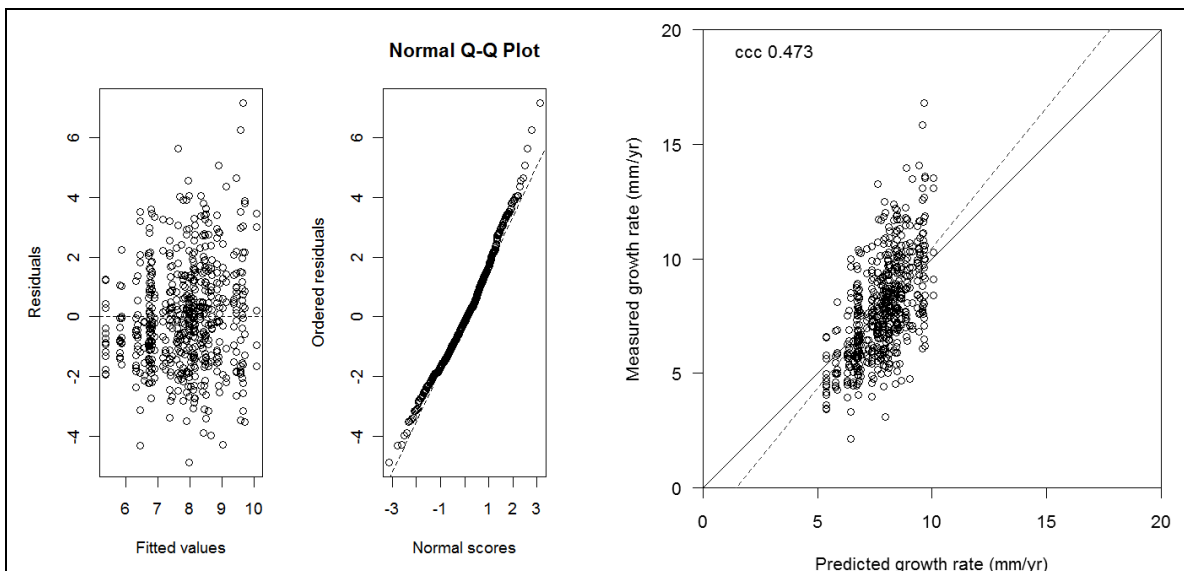


Figure 5-16. Diagnostic plots (left) and model predictions plotted against measured data (right) for the growth rate model developed using the original factors as continuous variables (excluding yield class).

As the tree cross-section consists of two types of wood with different properties; juvenile wood and mature wood, these were analysed separately in the following sections (juvenile wood 5.3.2 and mature wood 5.3.3)

5.3.2 Juvenile wood

The juvenile wood density was initially plotted against the site and tree data (Figure 5-18) to select the potential explanatory variables. Variables that seemed to have an influence on the density were considered for the full model, however only one variable was used to represent a certain feature. For example, in this case juvenile DBH was selected to represent the vigour of tree growth and therefore dominance was not entered since it had been derived from DBH measurements. This initial selection was carried out to minimise the problems arising from correlated explanatory variables in the model. The variables were then investigated for correlation that would cause problems in the model (for full correlation matrix see Appendix 3). Problematic variables (Figure 5-17) included continentality index (CONT) and easting (Pearson's correlation coefficient 0.647, $p < 0.001$), moisture deficit (MD) and accumulated temp sum (AT) (Pearson's correlation coefficient 0.868, $p < 0.001$), elevation and moisture deficit (Pearson's correlation coefficient -0.887, $p < 0.001$), and elevation and accumulated temp sum (Pearson's correlation coefficient -0.868, $p < 0.001$). Naturally correlations were also found between variables that described similar properties of trees. Site mean height was also included in

the initial model since it seemed to have some influence. It was a problematic variable because there were only a limited number of measurements due to practical difficulties of obtaining reliable measurement in a dense stand of Sitka spruce. Furthermore, there were nine sites for which there were no height measurements at all. When site mean height was included as an explanatory variable, as a consequence the model was fitted to a smaller dataset as sites with missing information were excluded.

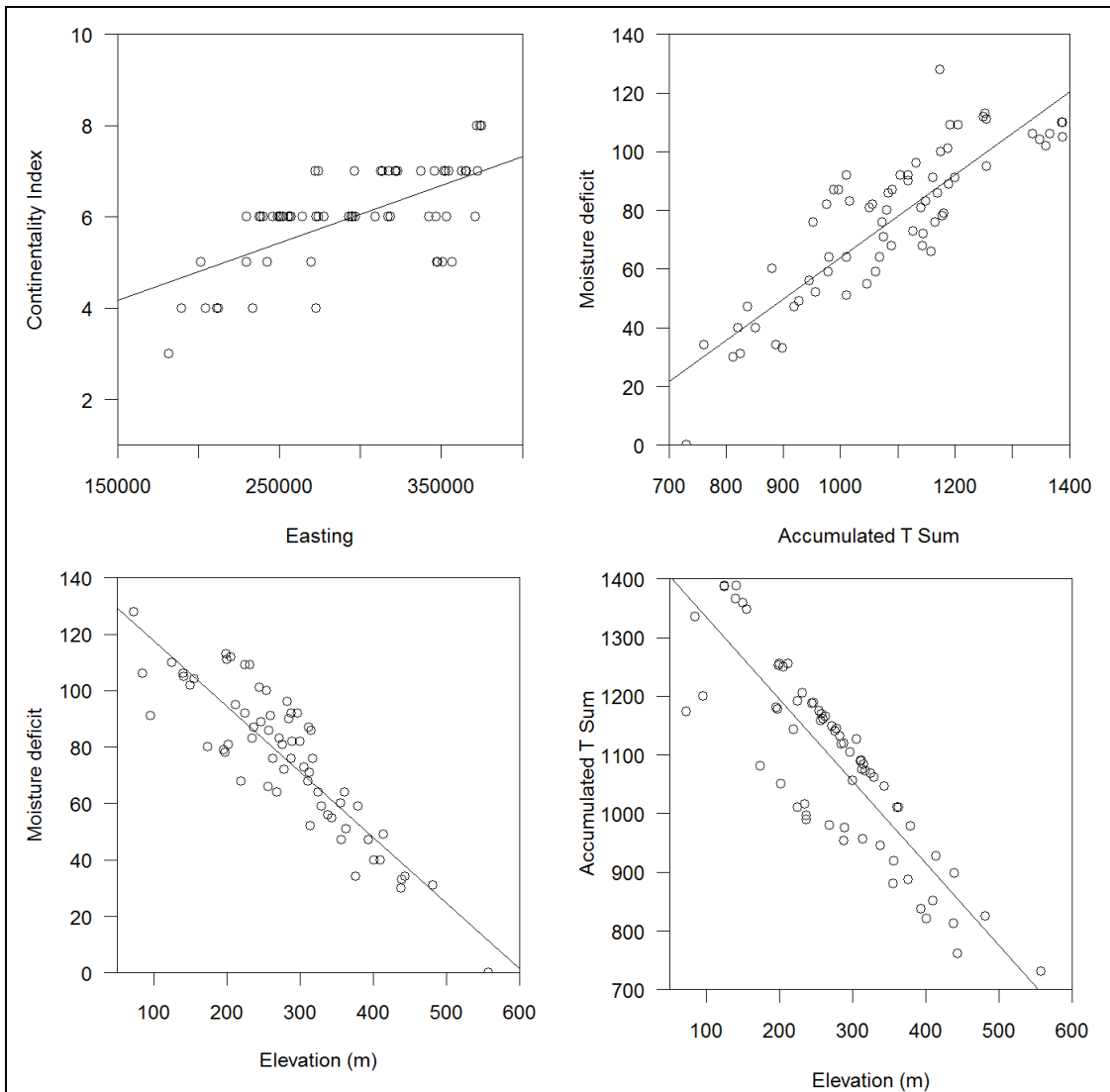


Figure 5-17. Selected correlated variables in the Benchmarking data.

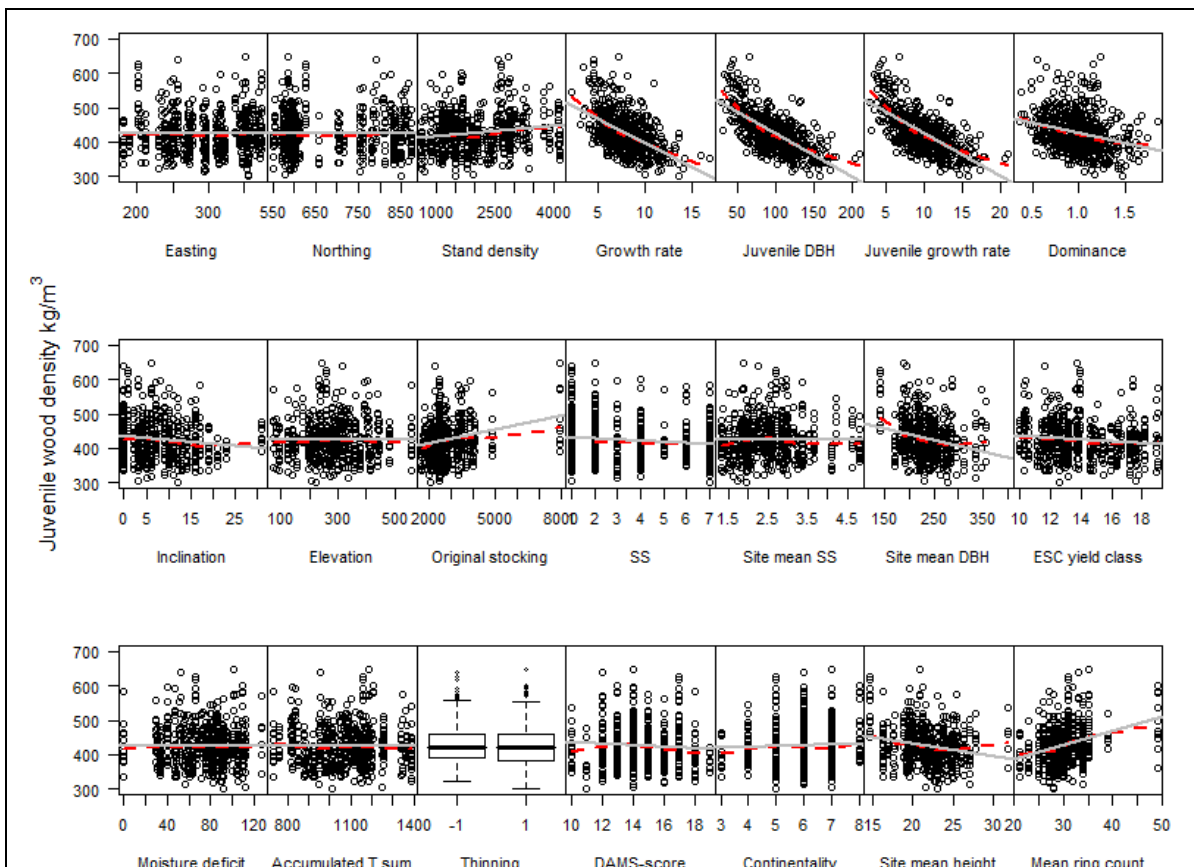


Figure 5-18. Influence of site and tree variables on juvenile wood density. Density and ring width were measured at 4% moisture content. Dashed red line is the LOWESS curve fitted to the data and the solid grey line is the linear regression.

After selection of variables the initial model had the following form:

$$\text{Juvenile wood density} \sim \text{Stand density} + \text{Juvenile DBH} + \text{Stand mean DBH} + \text{Slope} + \text{Original stocking} + \text{DAMS score} + \text{Continentality index} + \text{Site mean height}$$

Variables were then removed from the model one by one according to the p-values until only significant explanatory variables remained. The final juvenile wood density model (Table 5-8) had juvenile DBH (mm) as the only explanatory variable. Juvenile DBH was negatively correlated with juvenile density. The selected juvenile wood model explained 67 % of between-site variation and 35 % of between-tree variation. Random effects of site that were not explained by Juvenile DBH were plotted in Figure 5-19. Adjusted R^2 -values were 0.454 for the fixed effects and 0.535 including also the random tree effects. There was a departure from normality in the ordered residuals as the residual tended to increase with the fitted values (Figure 5-20). This effect was also visible when the model predictions were plotted against the measured values. The model was under predicting the higher density values.

Table 5-8. The Juvenile wood density model. Density values at 4% moisture content were used.

Fixed effects: Juvenile density ~ Juvenile DBH					
	Value	Std.Error	DF	t-value	p-value
(Intercept)	544.293	6.621	505	82.20	0
DBH10yr	-1.192	0.061	505	-19.44	0

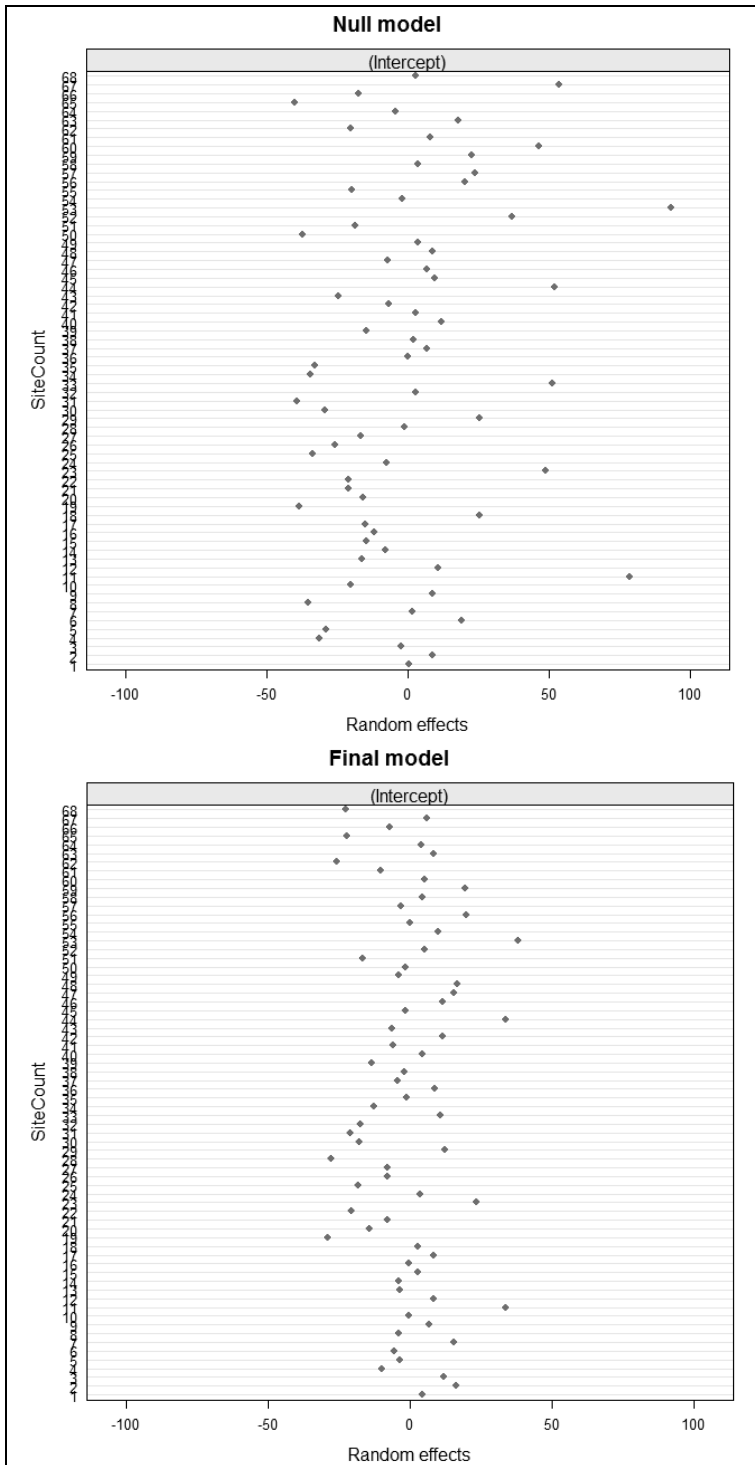


Figure 5-19. Random effects affecting the intercept once no model was fitted (left) and when the final model was fitted (right).

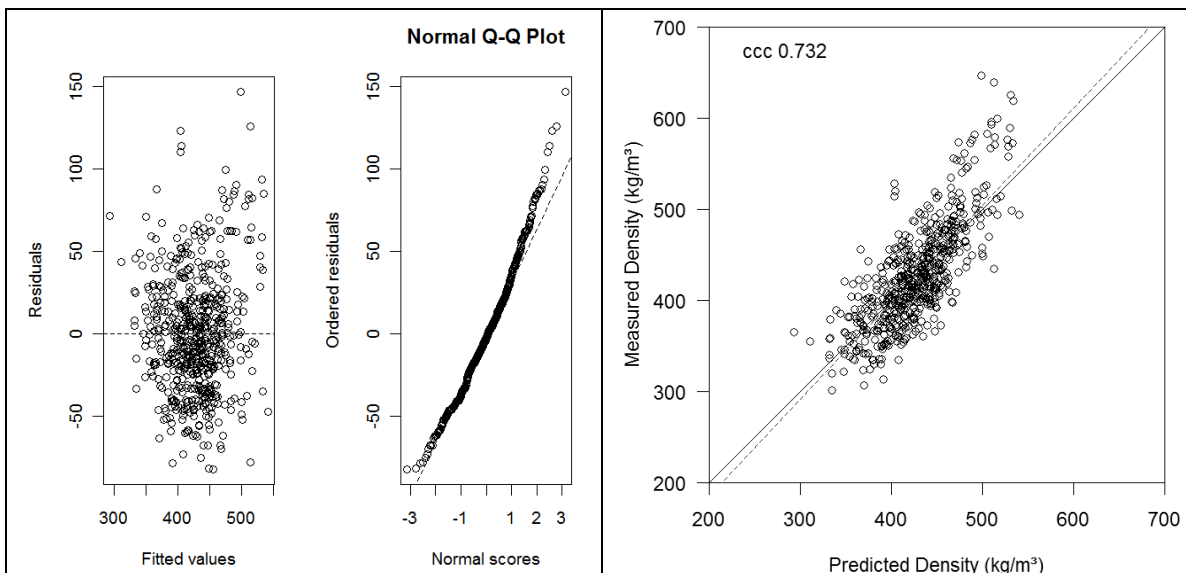


Figure 5-20. Diagnostic plots for the final model for predicting average juvenile wood density (left). Predictions of the final juvenile wood density model (right) plotted against the measured values. Red dashed line shows the regression line fitted to the data.

5.3.3 Mature wood

Similarly for mature wood, plots (Figure 5-21) were used to select variables for the initial model:

Mature wood density ~ Stand density + Growth Rate + Site Mean DBH + SS + Original Stocking + AT + Site Mean Ht + Thinning

The model was then simplified by removing variables one by one until a model with only significant variables and no disturbing correlations between them was reached (Table 5-9). In the model, growth rate decreased density and accumulated temperature sum increased density. The effect of growth rate could be expected based on previous studies (Brazier, 1967; Brazier, 1970b; Macdonald and Hubert, 2002; Saranpää, 1994). The effect of temperature sum was more unexpected as in temperate regions temperature would be expected to correlate positively with growth rate. In this data set there was no correlation between temperature sum and individual tree growth rates (0.0582, p -value > 0.05) or between the temperature sum and site average growth rate (0.0979, p -value > 0.05). Therefore, it seems that temperature sum (AT) had a direct influence on density.

The R^2 value was relatively low (0.33) for the mature wood model but in this case there was no difference whether only fixed effects were used or if the random effects were

included as well. In fact the model had decreased the random effects considerably (Figure 5-22). This indicates that the tree random effects in density were related to growth rate. However, there was departure from normality in the residuals and the model was under predicting at the higher range of density values. The relationship between density and growth rate might be more accurately described with a curve (Figure 5-21).

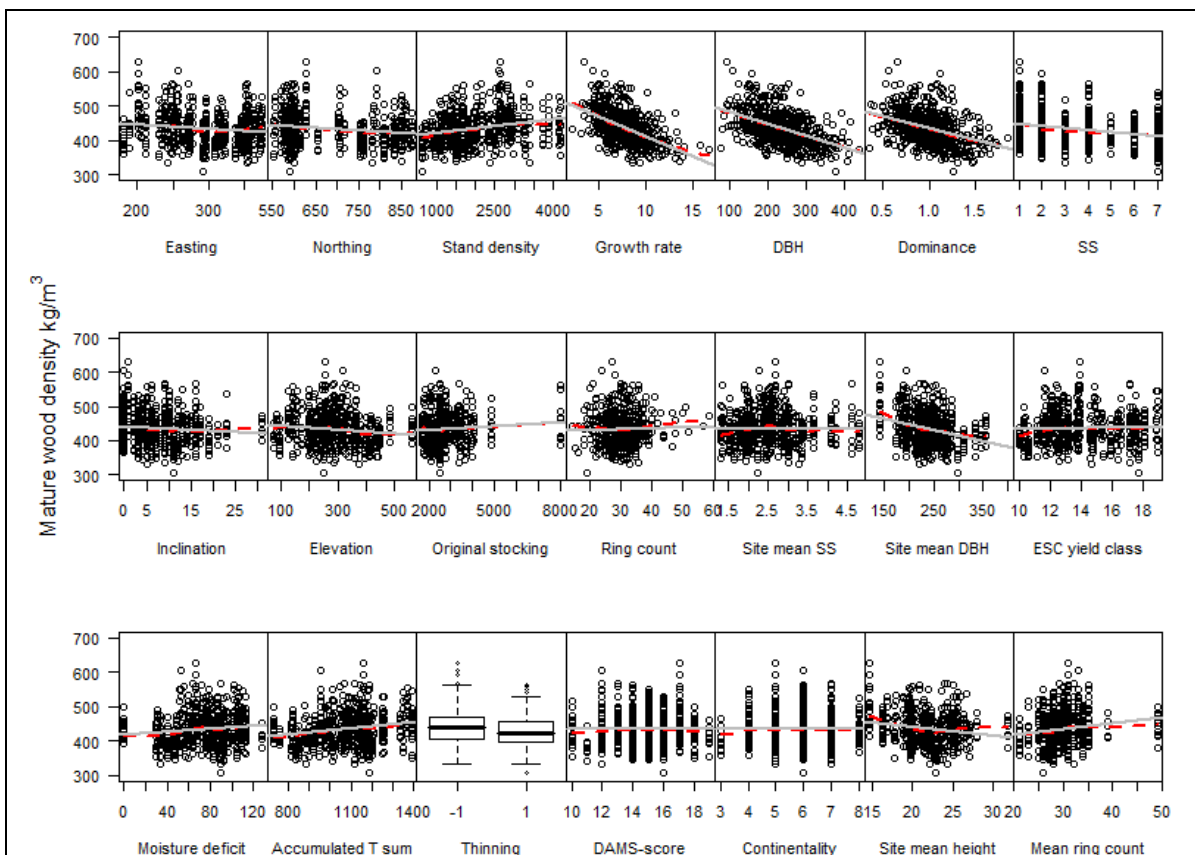


Figure 5-21. Influence of tree and stand variables on the mature wood density (determined at 4% moisture content).

Table 5-9. Values of the coefficients in the final mature wood density model

Fixed effects: Mature density ~ GrowthRate + AT					
	Value	Std.Error	DF	t-value	p-value
(Intercept)	448.862	15.251	503	29.43	0
GrowthRate	-11.313	0.787	503	-14.38	0
AT	0.070	0.013	66	5.38	0

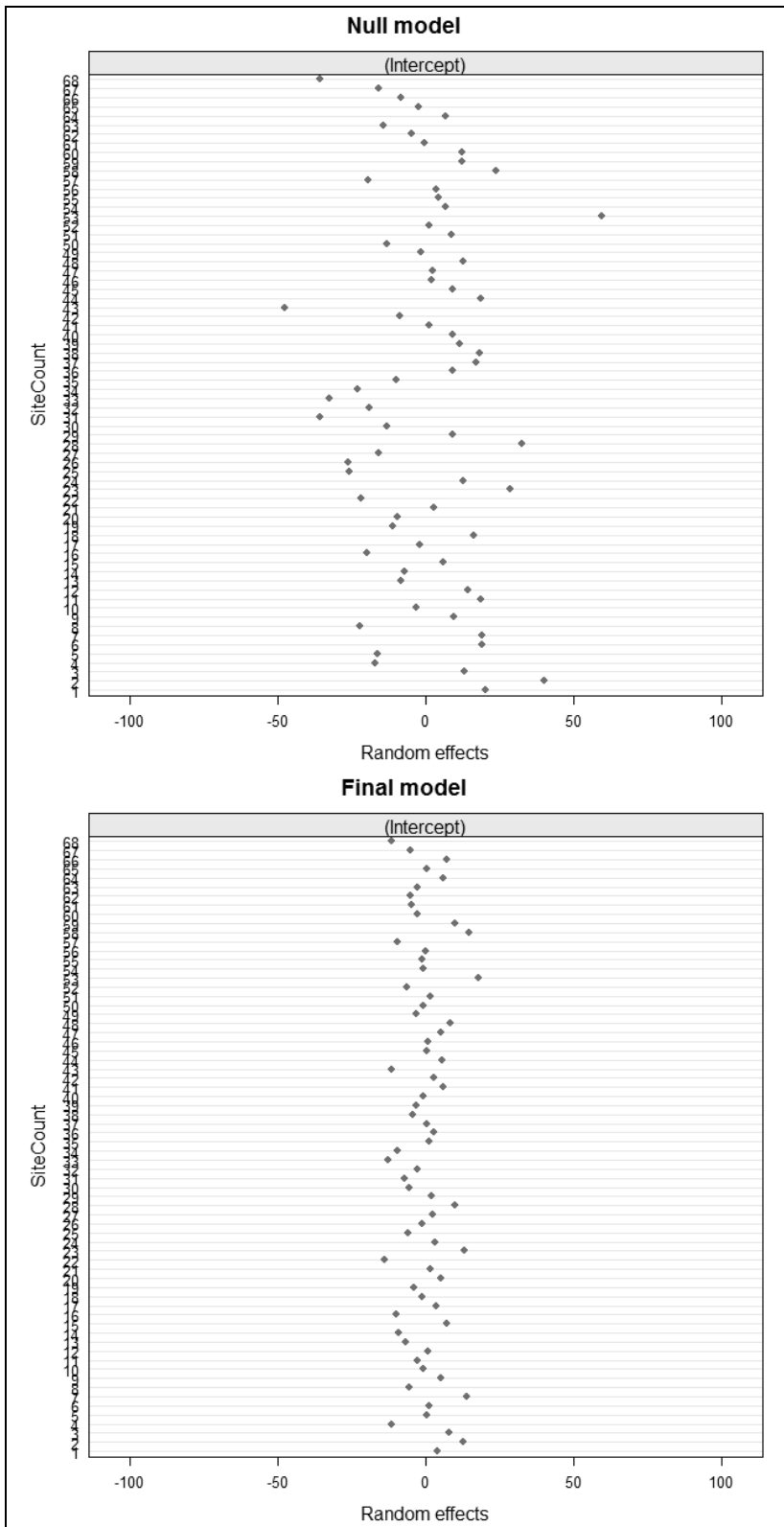


Figure 5-22. Random effects for mature wood when no model (left) and when the final model was fitted (right).

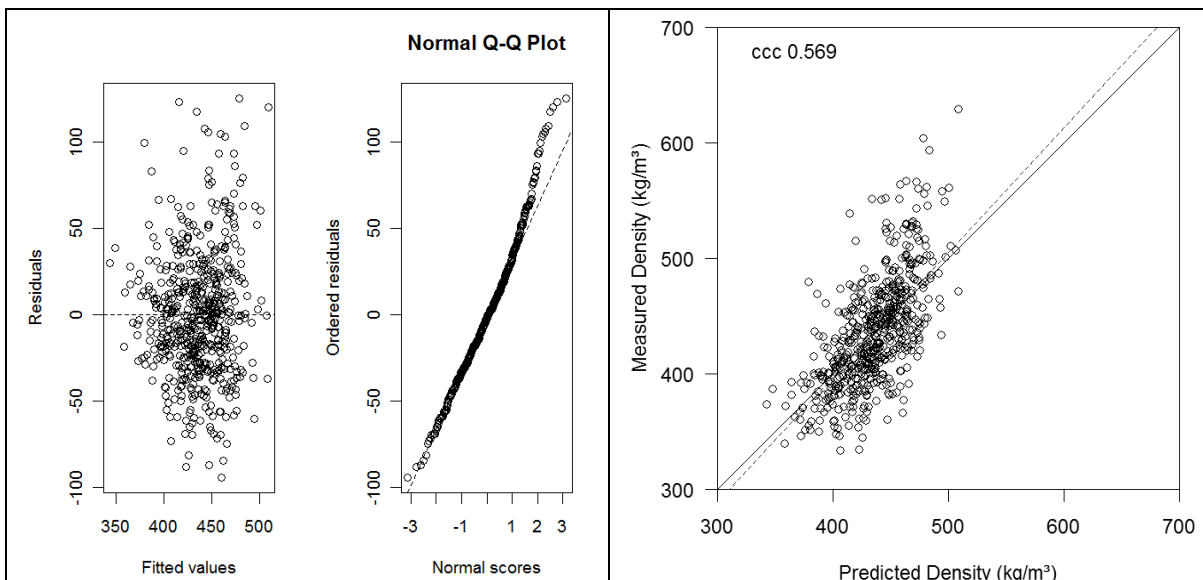


Figure 5-23. Diagnostic plots for the final mature wood density model (left). Predicted mature wood density plotted against the measured density (right).

5.3.4 Outerwood

Outerwood was defined as the outermost 5 cm of the stem. These density variables were mainly calculated to allow comparison with the (IML hammer) acoustic data collected by Napier University. The variables selected from the graphs (Figure 5-24) for the initial model included:

Outerwood density ~ Thinning + Stand density + Growth Rate + Original Stocking + Accumulated Temp Sum + Site Mean Ht + SS

Once the model was simplified, growth rate and accumulated temperature sum were left as explanatory variables (Table 5-10). These were the same explanatory variables as for mature wood as a whole. The density-decreasing effect of growth rate was smaller since the coefficient had decreased from -11.3 to -9.95. Growth rate was defined according to Repola (2006) as DBH divided by ring number, therefore it is a measure of the average growth rate over the whole radius and integrates the fast growth during the juvenile stage and slower growth in the mature stage. Therefore, growth rate is expected to have less influence in the outermost part of the stem where the local growth rate that will influence the density has decreased, but this was not documented in the overall growth rate.

Therefore, the adjusted R^2 -values were also slightly lower (0.29). Also, in this case the R^2 -values were very similar between fixed effects (0.29) and the full model (0.30), since a fair amount of random effects were explained by this model (Figure 5-26). The same problems of departure from normality and under prediction at a higher range of density (Figure 5-25) as in the mature wood model were observed.

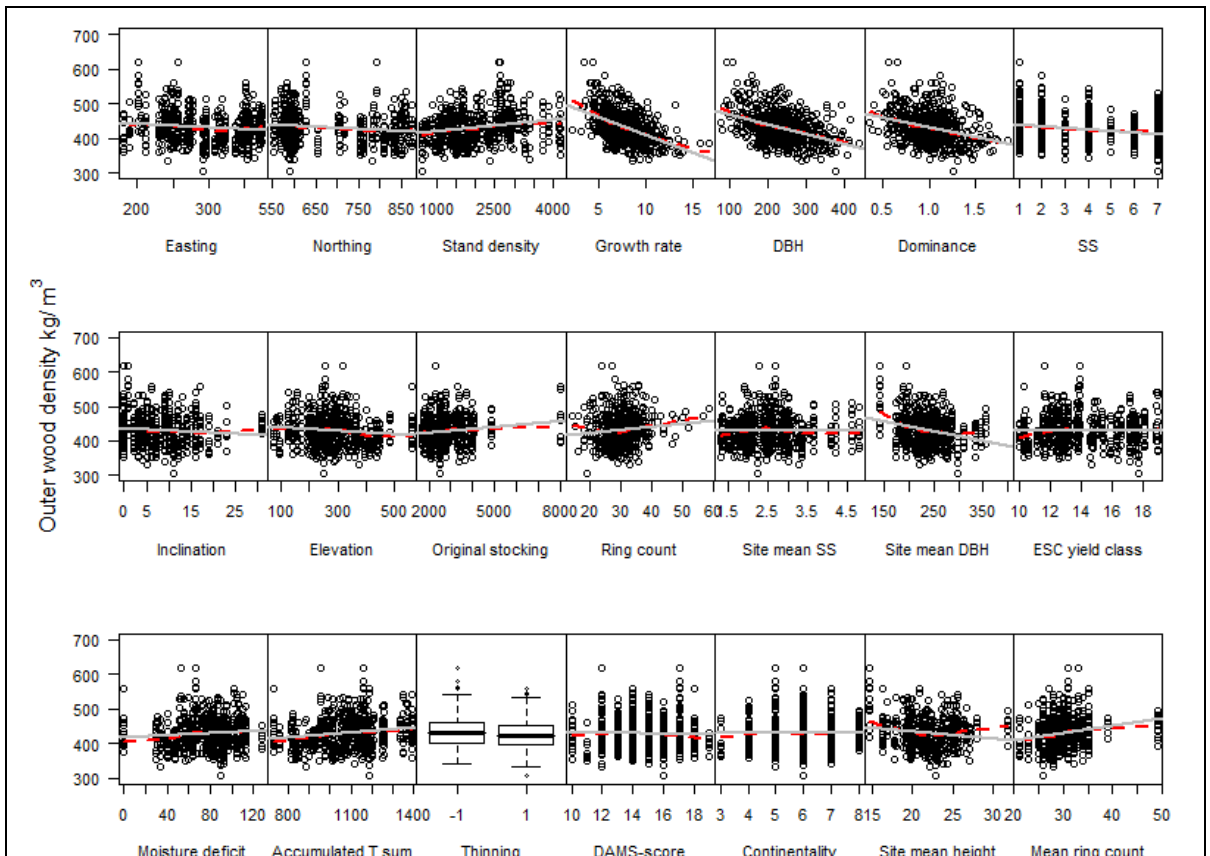


Figure 5-24. Influence of tree and site variables on the outerwood density (determined at 4% moisture content).

Table 5-10. Final outerwood model variables and the diagnostic values associated with them.

Fixed effects: Outerwood density ~ GrowthRate + AT

	Value	Std.Error	DF	t-value	p-value
(Intercept)	446.675	14.793	499	30.19	0
GrowthRate	-9.955	0.763	499	-13.04	0
AT	0.058	0.013	66	4.62	0

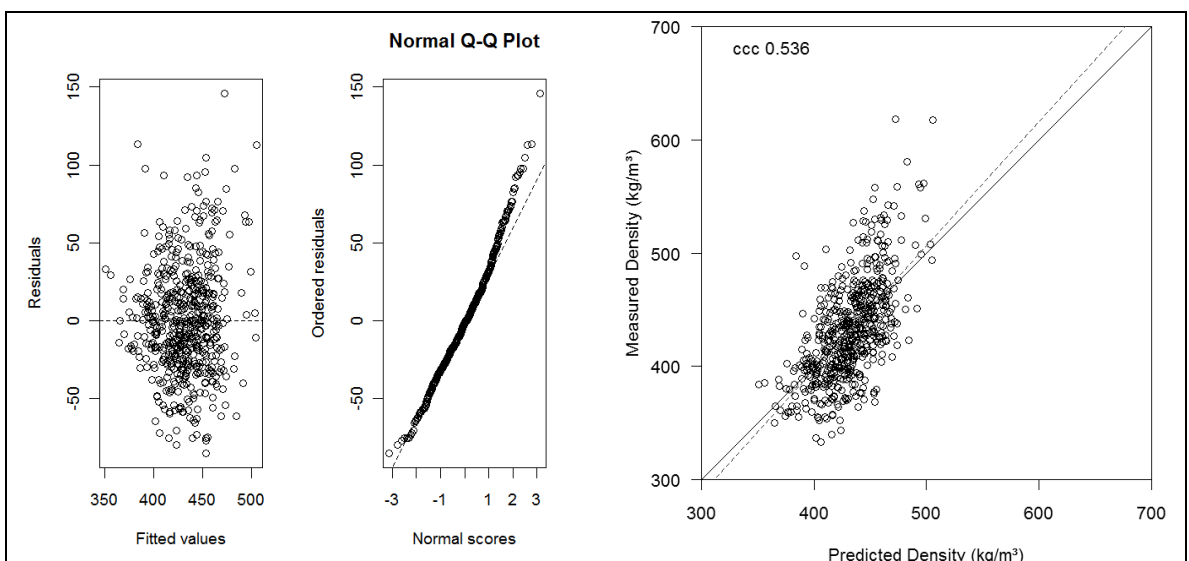


Figure 5-25. Diagnostic plots for the final outerwood density model (left). Measured outerwood density plotted against the predicted density. Dashed red line is the regression line drawn to the data (right).

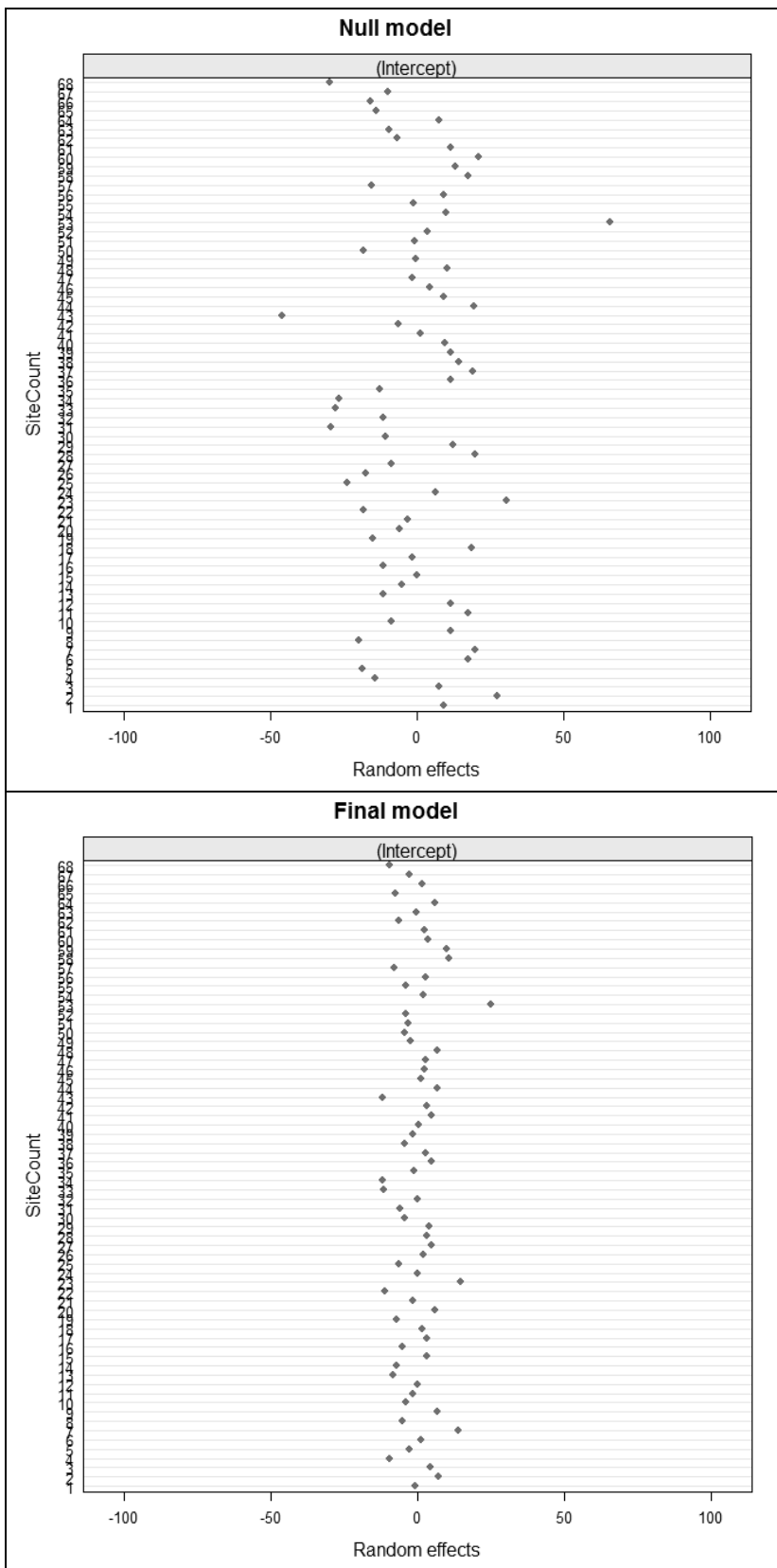


Figure 5-26. Random effects in outerwood average density when no model (left) and the final model (right) was fitted to the data.

5.3.5 Average density over the entire cross-section

Scatter plots (Figure 5-27) and correlation analysis indicated that the initial model should have the form:

$$\text{Cross-section average density} \sim \text{Thinning} + \text{Stand density} + \text{Growth Rate} + \text{Site Mean DBH} + \text{SS} + \text{Slope} + \text{Original Stocking} + \text{Accumulated Temp Sum} + \text{Site Mean Ht}$$

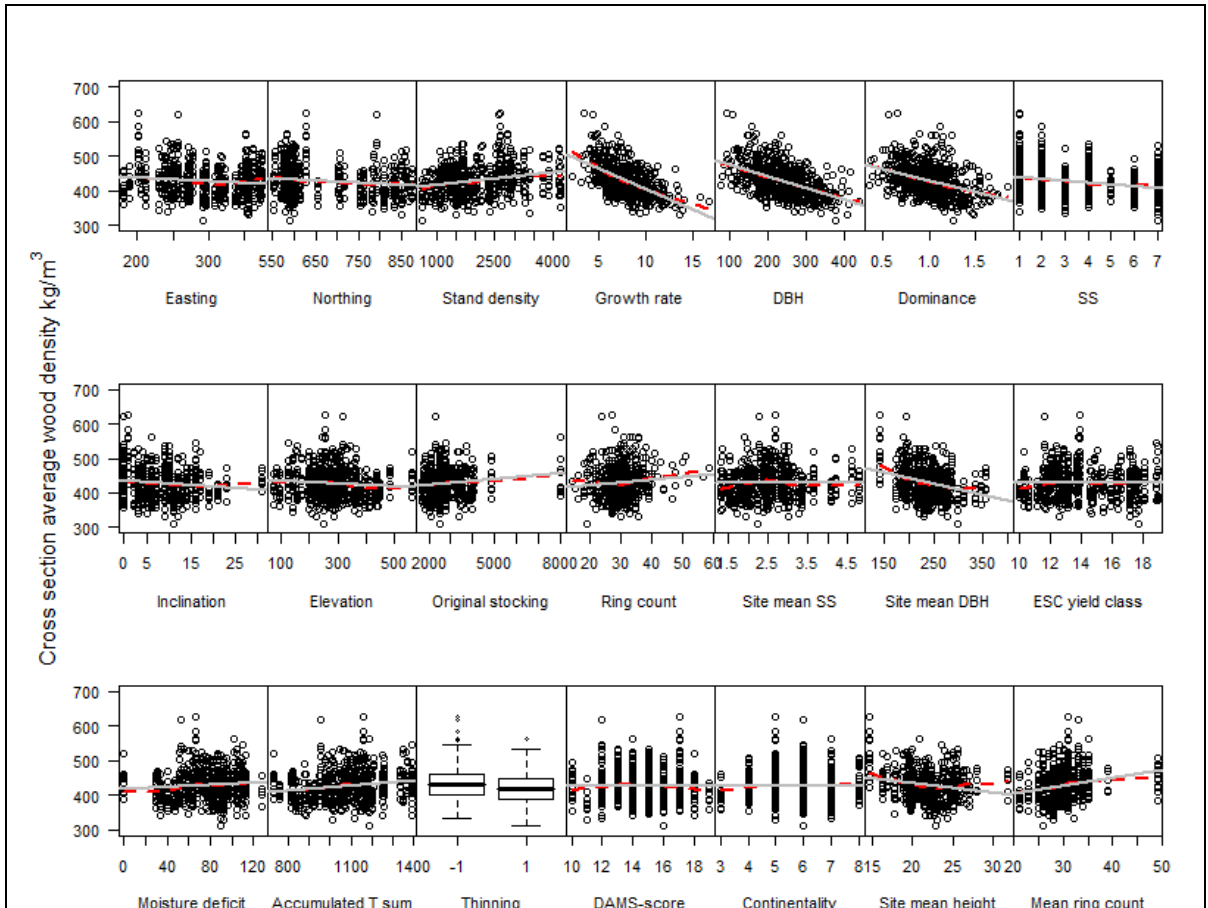


Figure 5-27. Influence of site and tree variables on the cross-section average density (determined at 4% moisture content). Dashed red line is the LOWESS curve fitted to the data and solid grey line linear regression.

The final model obtained (Table 5-11) explained 75 % of between-site variation and 24 % of within site variation. The change in random effects between the null model and the final model is illustrated (Figure 5-28). However, again a departure from normality was observed in the residuals as the spread increased with the fitted value. Due to this, the model predictions were less accurate in the high range of density values (Figure 5-29).

Table 5-11. Variables in the final average wood density model

Fixed effects: Average density ~ GrowthRate + AT					
	Value	Std.Error	DF	t-value	p-value
(Intercept)	457.699	14.504	503	31.56	0
GrowthRate	-11.433	0.721	503	-15.85	0
AT	0.057	0.012	66	4.59	0

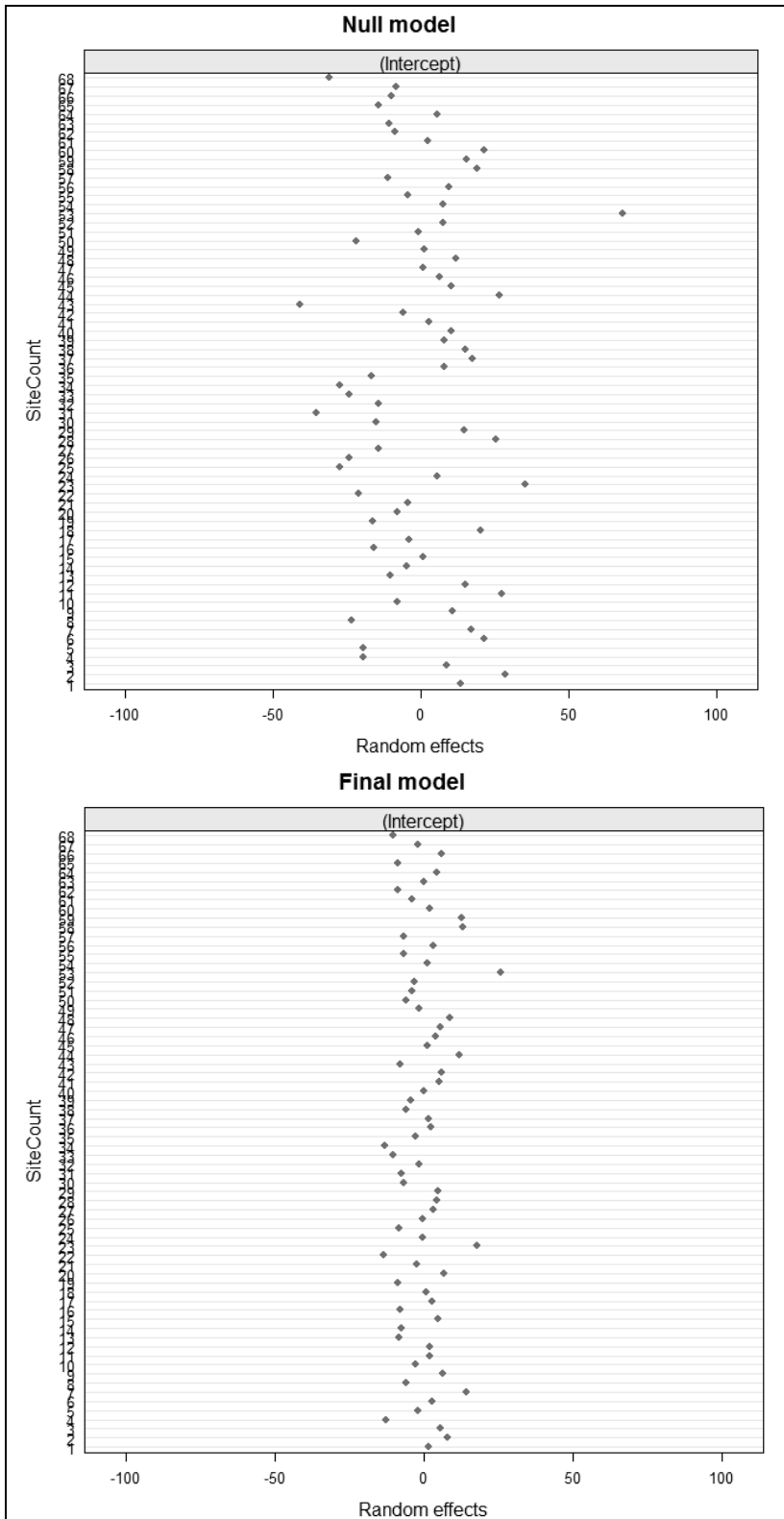


Figure 5-28. Average wood density random effects when no model (left) and final model (right) were fitted to the data.

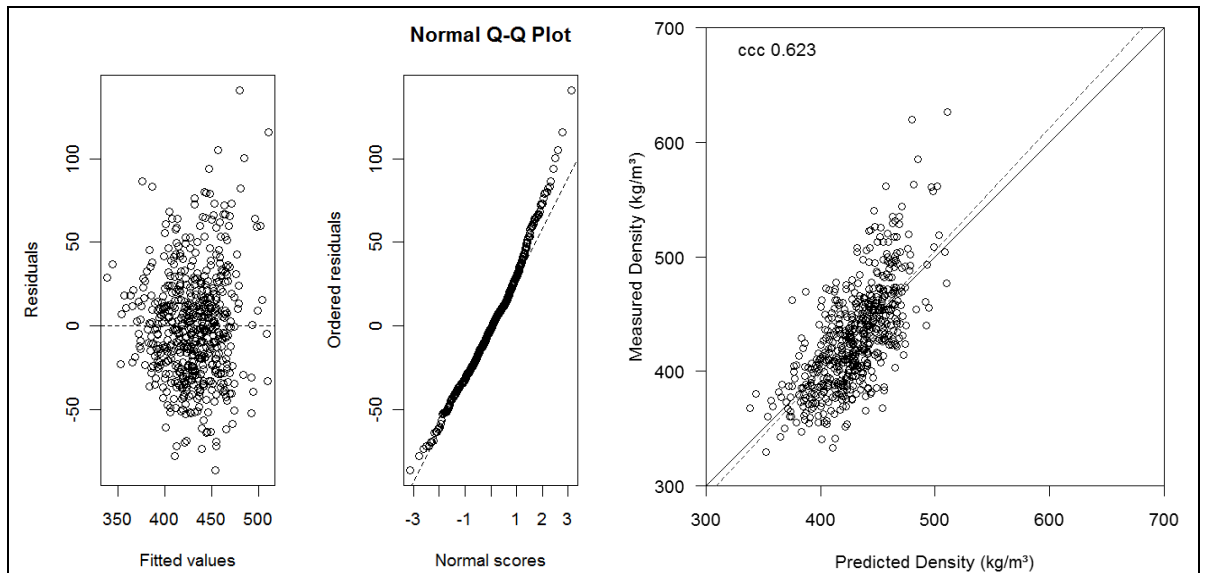


Figure 5-29. Diagnostic plots for the final cross-section average density model (left). Final cross-section average density model prediction plotted against the measured data (right).

5.3.5.1 Influence of thinning

The influence of the thinning regime was studied by analysing the two groups of data separately. An interesting point to note was that moisture deficit had no relationship with density at unthinned sites (Pearson's correlation coefficient 0.041). Furthermore, the relationship between growth rate and density appeared to be more linear when the data was split into these two sections than what was observed above.

As previously, initially a full model was fitted to the thinned:

Cross-section average density_{thinned} ~ GrowthRate + Stand density + Site Mean DBH + SS + Site Mean SS + Original Stocking + Moisture deficit + DAMS + CONT + Site Mean Ht

and unthinned sites:

Cross-section average density_{unthinned} ~ Easting + Stand density + Growth Rate + Site Mean DBH + SS + Site Mean SS + Slope + Original Stocking + ESCyield + Accumulated Temp Sum + Site Mean Ht

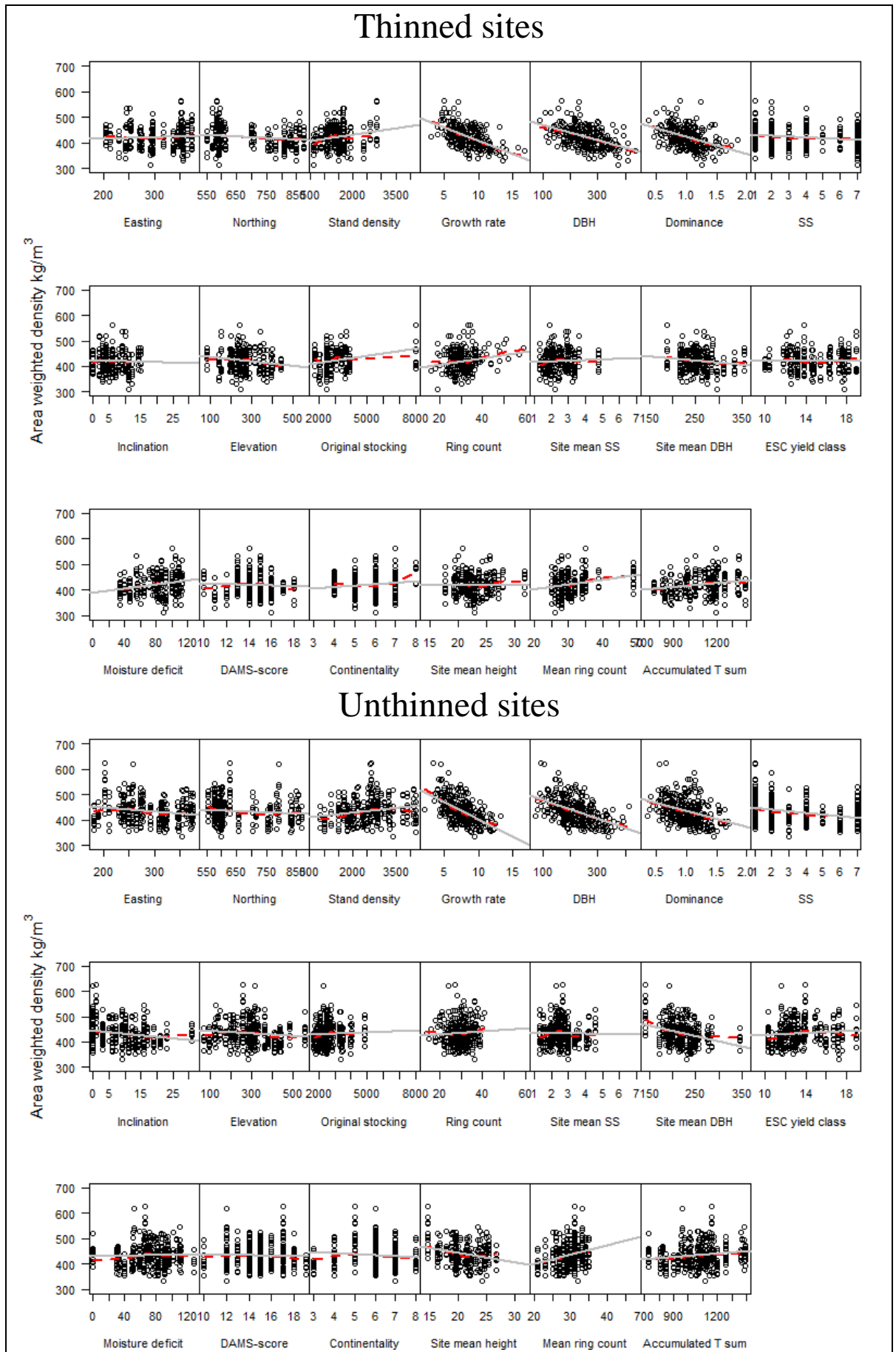


Figure 5-30. Influence of site and tree variables on cross-section average density (MC 4%) at thinned and unthinned Benchmarking sites.

The models were then simplified to derive the final models (Table 5-12). Both models included the growth rate as an explanatory variable. The average growth rate at thinned sites was 8.4 (sd. 2.26) and 7.4 (sd. 1.99) at unthinned sites. The absolute value of the coefficient and therefore the size of the effect caused by growth rate was smaller for the thinned sites, however the intercept was lower. This indicates that slower growing, denser trees had been removed and the effect of growth rate was more limited in the remaining trees.

Table 5-12. Selected explanatory variables in the model developed for the thinned and unthinned BM sites at 4% moisture content.

THINNED SITES					
Fixed effects: Average density ~ GrowthRate + OrigStock + MD					
	Value	Std.Error	DF	t-value	p-value
(Intercept)	454.756	13.256	207	34.31	0.0000
GrowthRate	-9.452	0.937	207	-10.09	0.0000
OrigStock	0.005	0.002	25	2.18	0.0387
MD	0.398	0.102	25	3.90	0.0006
UNTHINNED SITES					
Fixed effects: Average density ~ Easting + GrowthRate + Slope					
	Value	Std.Error	DF	t-value	p-value
(Intercept)	587.513	17.619	281	33.35	0.0000
Easting	-0.179	0.051	35	-3.49	0.0013
GrowthRate	-12.122	1.090	281	-11.12	0.0000
Slope	-1.187	0.381	35	-3.12	0.0036

In the case of both models there was some departure from normality in the ordered residuals (Figure 5-31). The effect was slightly smaller in case of the unthinned model. The adjusted R^2 -value for fixed effects was 0.39 for the thinned model and 0.38 for the unthinned model.

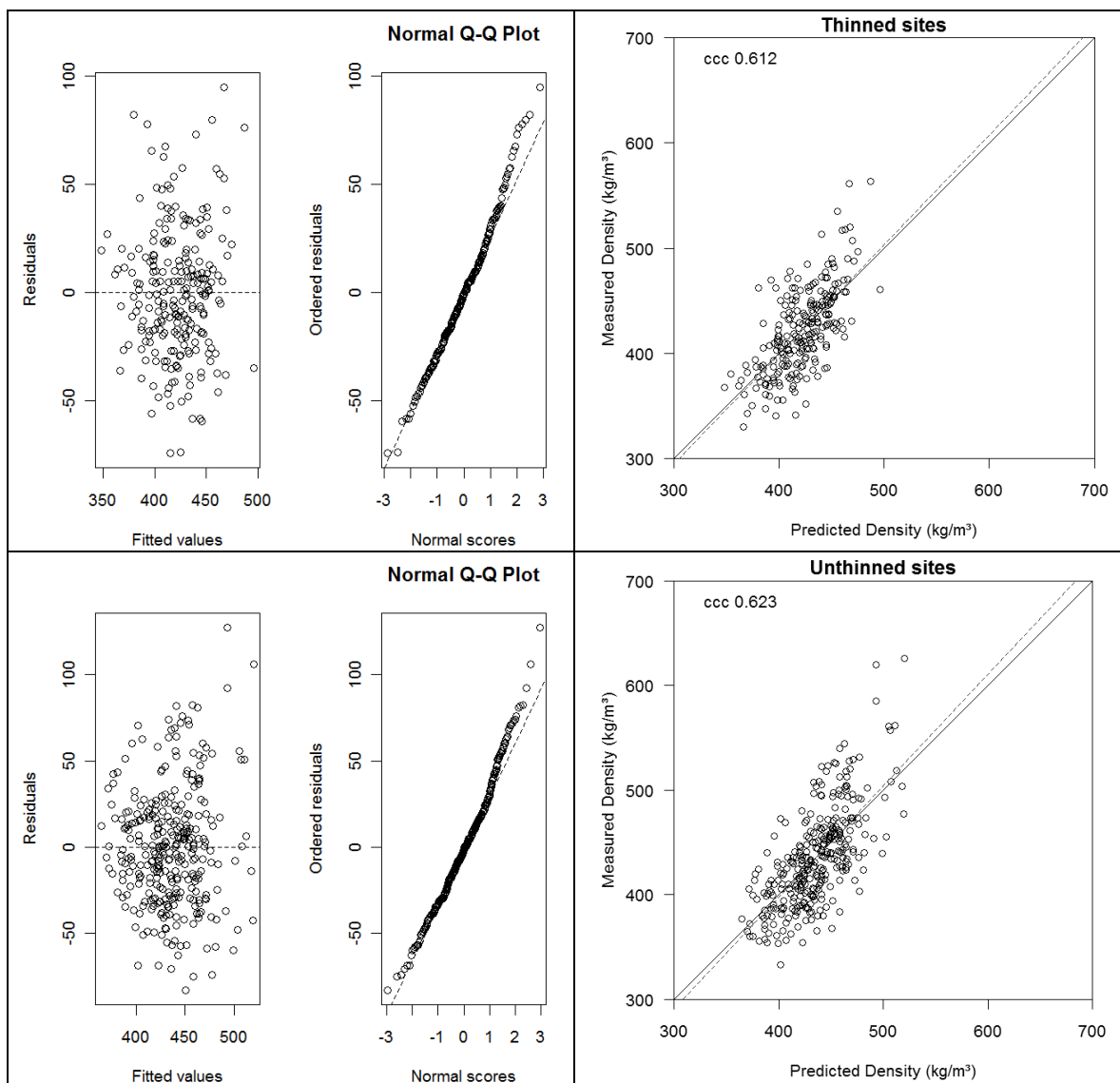


Figure 5-31. Diagnostic plots for the models developed for the dataset split according the thinning treatment.

5.3.5.2 Influence of social status

It has been found in previous studies that there are differences in timber properties between tree social classes (Kärkkäinen, 1984; Repola, 2006). When density was plotted against ring number for each of the classes separately (Figure 5-32), some differences in the LOWESS curves were apparent. The curve for dominant trees had a lower intercept and in addition, there was very little evidence of the characteristic Sitka spruce curve. In the case of the other classes there was an initial decrease in density. The minimum density was reached at approximately the 10th ring, which corresponds to findings by McLean (2007) and is in line with the juvenile wood definition chosen also for this study that uses the 10th ring as the division point between juvenile and mature wood.

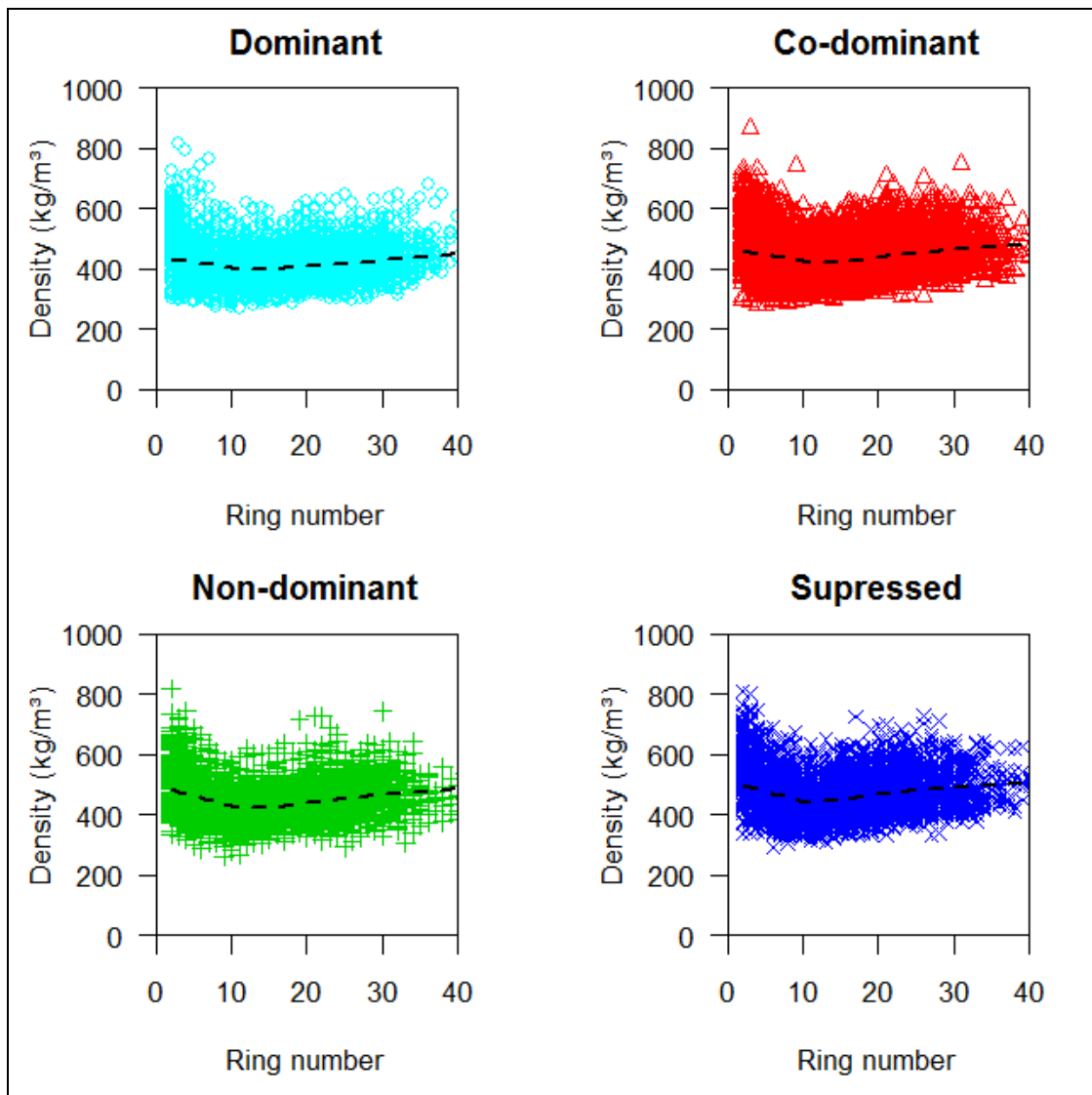


Figure 5-32. Density, determined at 4% moisture content, plotted against the ring number for different social classes of trees. Dashed line is the LOWESS curve fitted to the data.

As previously, initially a full model developed based on scatter plots (Figure 5-33, Figure 5-34, Figure 5-35 and Figure 5-36) was fitted to each of the four groups of data independently. The models were then simplified as described above to derive the final models (Table 5-13).

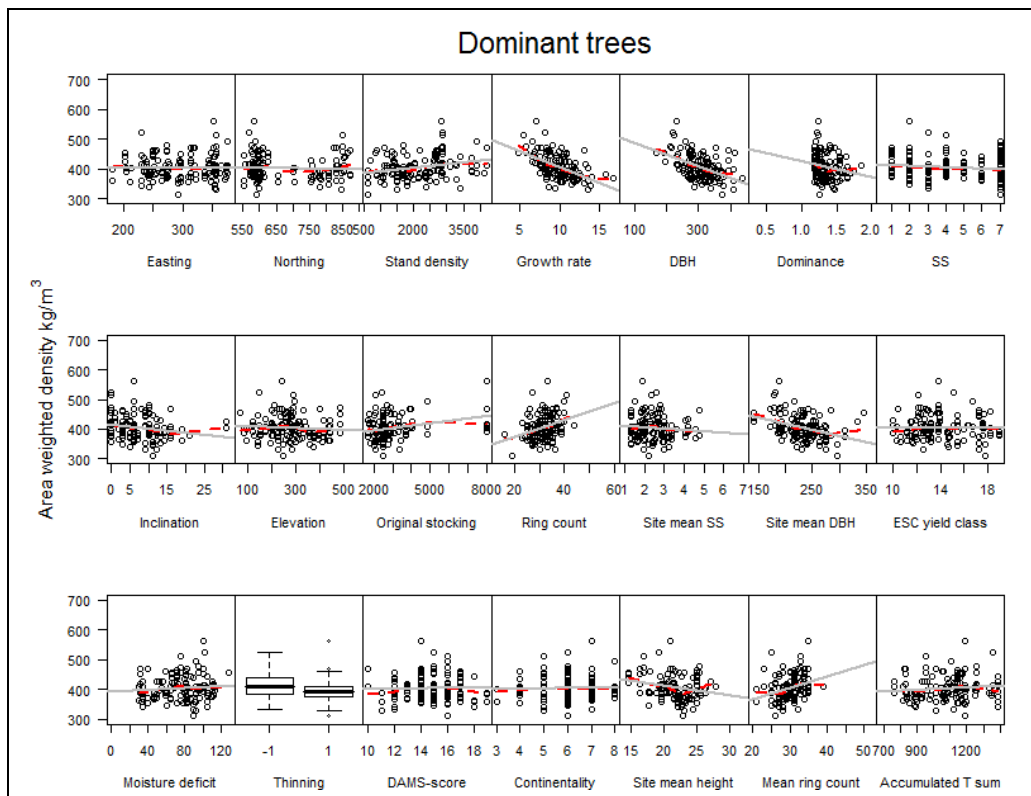


Figure 5-33. Influence of site and tree variables on density in dominant trees. Dominance was calculated by DBH/stand mean DBH and the upper quartile of dominance values were considered as dominant trees. Grey line is the regression line fitted to the data and the dashed red line is the lowest curve.

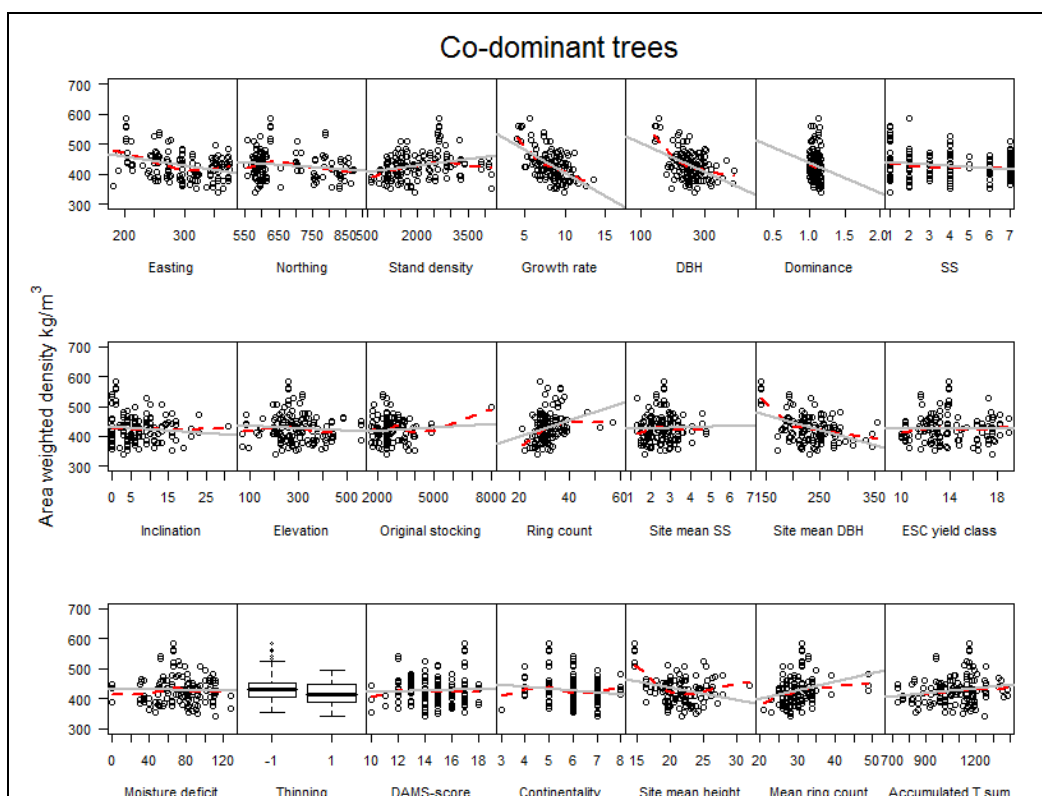


Figure 5-34. Influence of site and tree variables on density in co-dominant trees. Dominance was calculated by DBH/stand mean DBH and the 2nd quartile of dominance values were considered as co-dominant trees. Grey line is the regression line fitted to the data and dashed red line is the lowest curve.

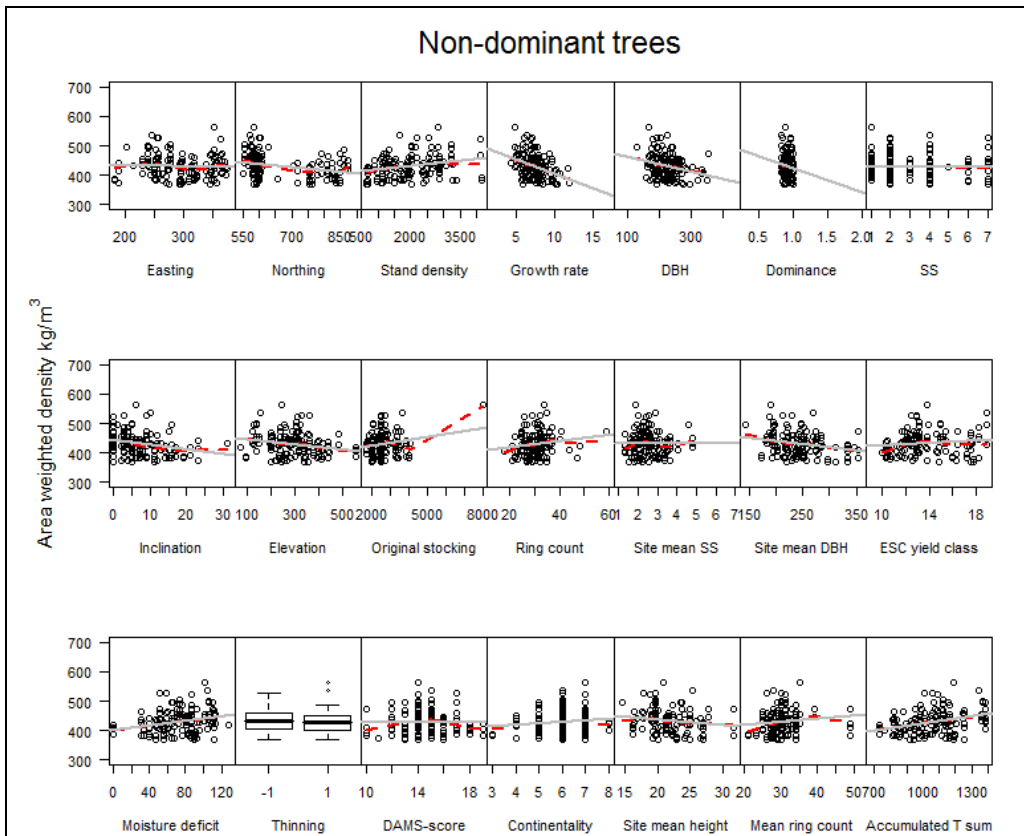


Figure 5-35. Influence of site and tree variables on density in non-dominant trees. Dominance was calculated by DBH/stand mean DBH and the 3rd quartile of dominance values were considered as non-dominant trees. Grey line is the regression line fitted to the data and the dashed red line is the lowest curve.

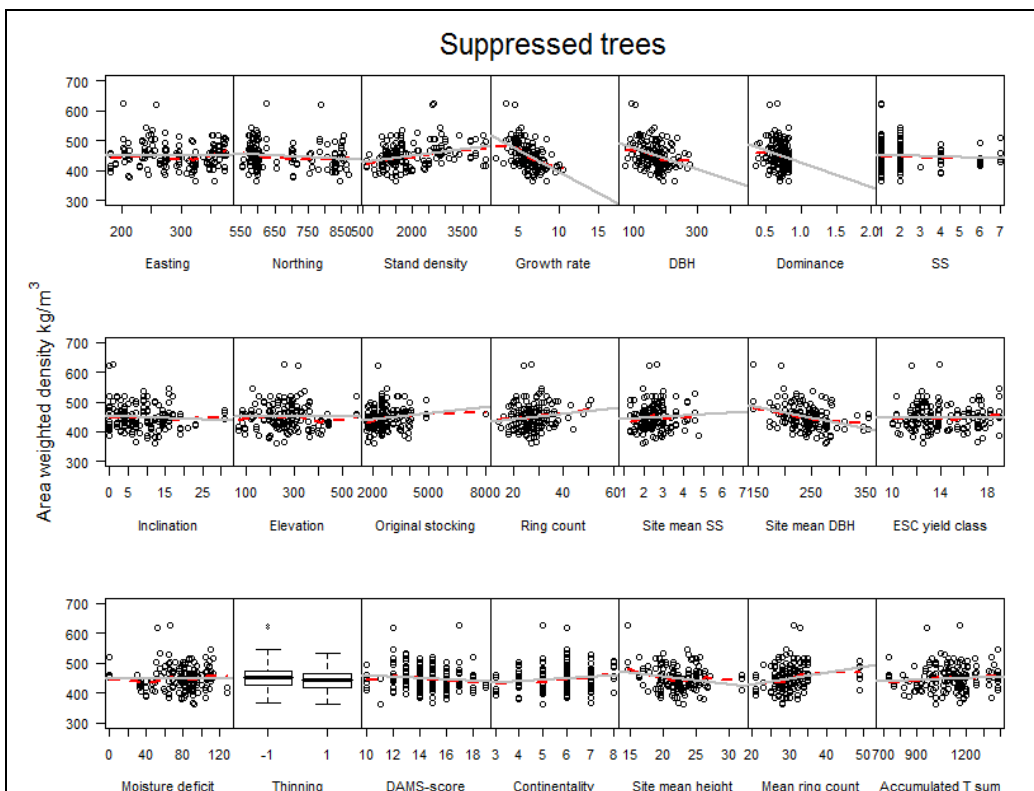


Figure 5-36. Influence of site and tree variables on density in suppressed trees. Dominance was calculated by DBH/stand mean DBH and the lowest quartile of dominance values were considered as suppressed trees. Grey line is the regression line fitted to the data and the dashed red line is the lowest curve.

Different explanatory variables were obtained for the four classes (Table 5-13). Growth rate was the only variable that remained significant in all of the models. Accumulated temperature sum was included in all the models apart from the dominant trees. The residual and normality plots (Figure 5-37) showed no severe trends in residuals or departure from normality. Adjusted R^2 –values (fixed effects) were 0.35 for dominant trees, 0.44 co-dominant, 0.27 non-dominant and 0.26 for suppressed trees.

Table 5-13. Area-weighted density models for the different dominance classes of trees. Density determined at 4% moisture content.

DOMINANT TREES					
Fixed effects: Average density ~ GrowthRate + Slope + MD					
	Value	Std.Error	DF	t-value	p-value
(Intercept)	501.006	15.770	75	31.77	0.0000
GrowthRate	-11.311	1.389	75	-8.15	0.0000
Slope	-1.138	0.485	56	-2.35	0.0226
MD	0.333	0.115	56	2.90	0.0054
CO-DOMINANT TREES					
Fixed effects: Average density ~ Easting + GrowthRate + AT					
	Value	Std.Error	DF	t-value	p-value
(Intercept)	564.806	32.417	73	17.42	0.0000
Easting	-0.249	0.058	61	-4.26	0.0001
GrowthRate	-15.212	1.792	73	-8.49	0.0000
AT	0.059	0.021	61	2.81	0.0066
NON-DOMINANT					
Fixed effects: Average density ~ Northing + GrowthRate + AT					
	Value	Std.Error	DF	t-value	p-value
(Intercept)	486.481	44.390	77	10.96	0.0000
Northing	-0.068	0.035	59	-1.93	0.0581
GrowthRate	-9.350	2.062	77	-4.54	0.0000
AT	0.055	0.023	59	2.37	0.0213
SUPPRESSED					
Fixed effects: Average density ~ GrowthRate + SiteMeanDBH + AT + CONT					
	Value	Std.Error	DF	t-value	p-value
(Intercept)	486.866	29.885	95	16.29	0.0000
GrowthRate	-12.612	2.227	95	-5.66	0.0000
SiteMeanDBH	-0.170	0.082	58	-2.06	0.0435
AT	0.046	0.019	58	2.42	0.0185
CONT	5.324	2.478	58	2.15	0.0358

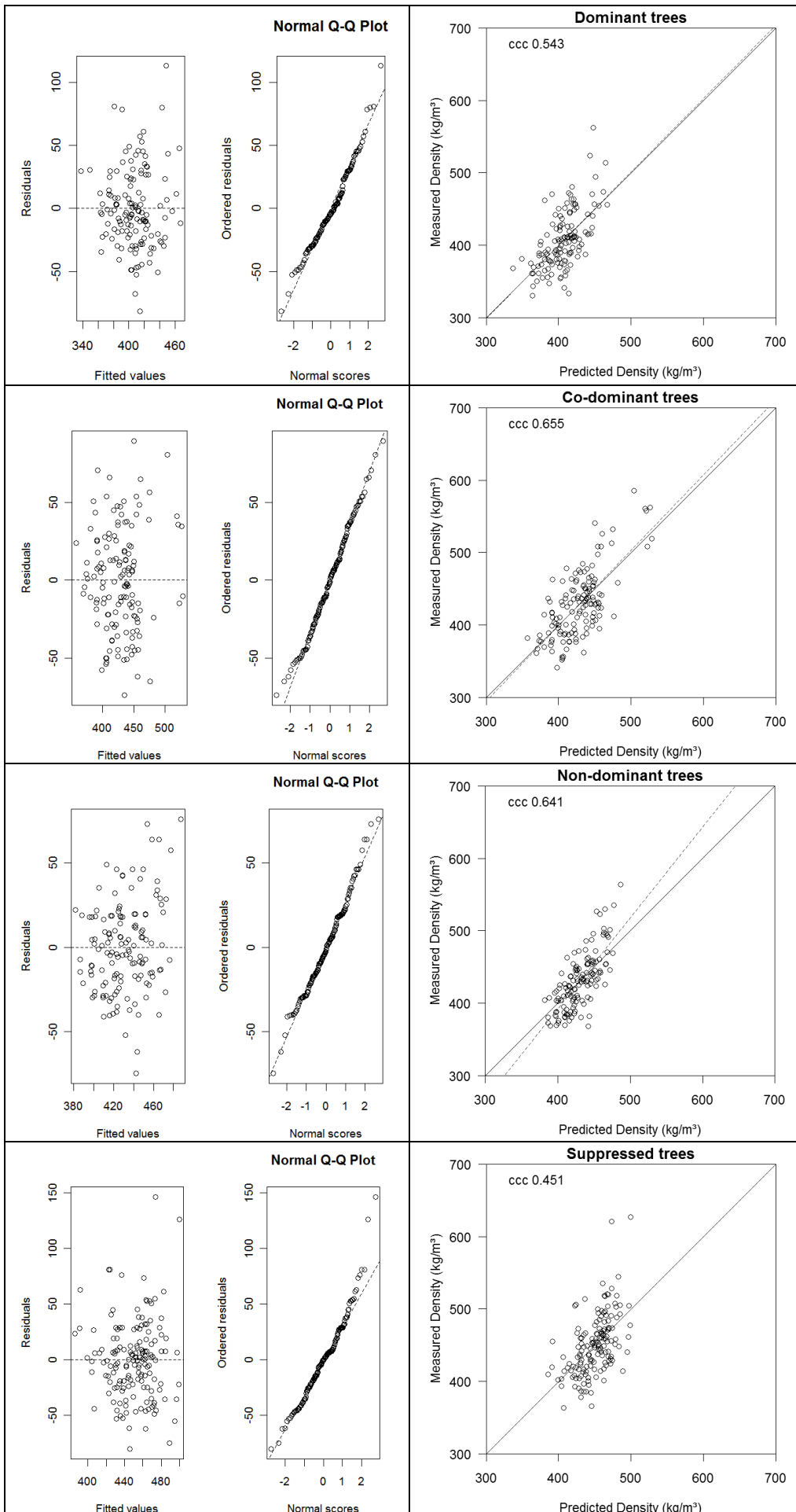


Figure 5-37. Diagnostic plots for cross-section average density models developed for different dominance classes of trees. ccc is the concordance correlation coefficient.

5.3.5.3 North vs South

Due to the concerns regarding the unbalanced divide of the Northing factor levels, the splitting of the data was not based on the factor levels. Instead the two clusters of the data visible on the histogram (Figure 5-11) were used. The sites with a Northing value less than 650 000 were considered southerly and the sites with Northing value greater than 700 000 were considered northerly. This resulted into 42 southerly sites, 25 northerly sites and 1 site that fell between these clusters was excluded from the analysis. Scatter plots (Figure 5-39) were used to derive the initial models that were simplified to obtain the final models (Table 5-14).

In both models growth rate remained a significant variable. Otherwise, the models differed in their explanatory variables. For example, in the southern model the DAMS score was significant whereas in the northern model moisture deficit was a significant variable. The residuals of the southern model showed less departure from normality than the ones of the northern model (Figure 5-40). The adjusted R²- values (fixed effects) for the models were 0.31 for the northern model and 0.41 for the southern model.

Table 5-14. Cross-section average density model for the Northern and Southern Benchmarking sites separately.

NORTHERN SITES						
Fixed effects: Average density ~ GrowthRate + MD						
	Value	Std.Error	DF	t-value	p-value	
(Intercept)	472.440	12.747	188	37.06	0.0000	
GrowthRate	-9.281	1.101	188	-8.43	0.0000	
MD	0.310	0.133	23	2.34	0.0285	
SOUTHERN SITES						
Fixed effects: Average density ~ Easting + GrowthRate + SiteMeanDBH + factor(Thinning) + DAMS						
	Value	Std.Error	DF	t-value	p-value	
(Intercept)	661.339	29.502	308	22.42	0.0000	
Easting	-0.146	0.044	37	-3.30	0.0021	
GrowthRate	-11.994	0.992	308	-12.09	0.0000	
SiteMeanDBH	-0.171	0.071	37	-2.39	0.0221	
factor(Thinning)1	9.870	4.822	37	2.05	0.0478	
DAMS	-3.398	1.342	37	-2.53	0.0157	

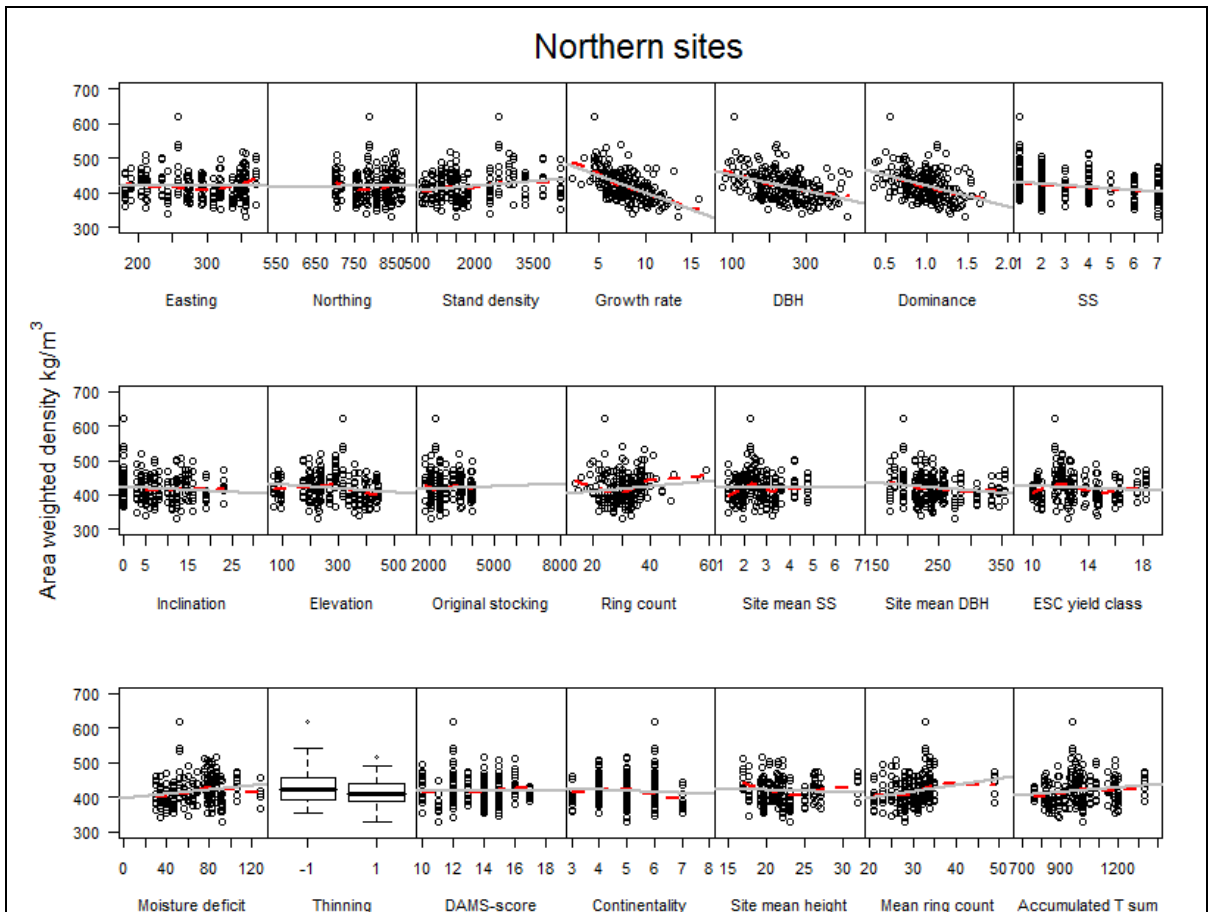


Figure 5-38. Influence of the measured variables on density at Northern Benchmarking sites.

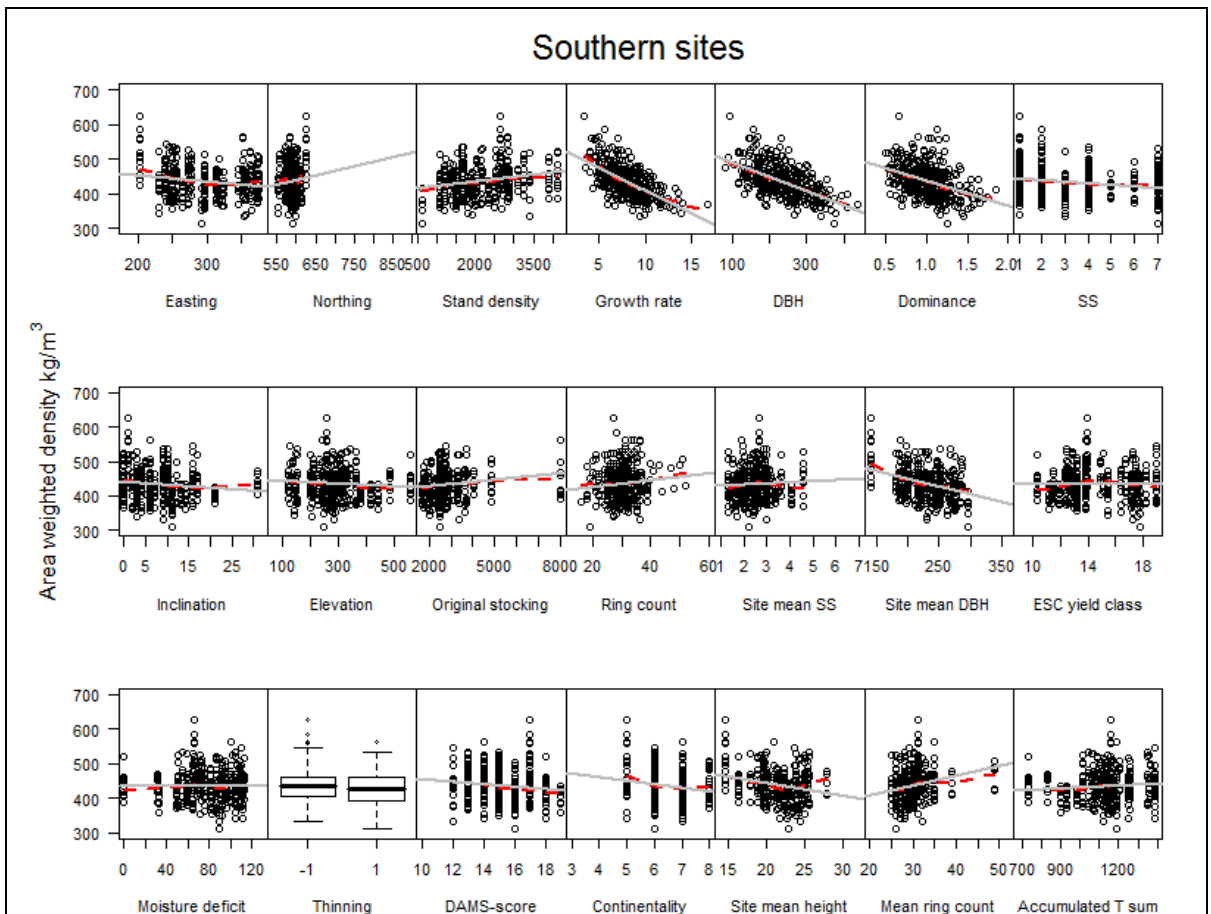


Figure 5-39. Influence of the measured variables on density at Southern Benchmarking sites.

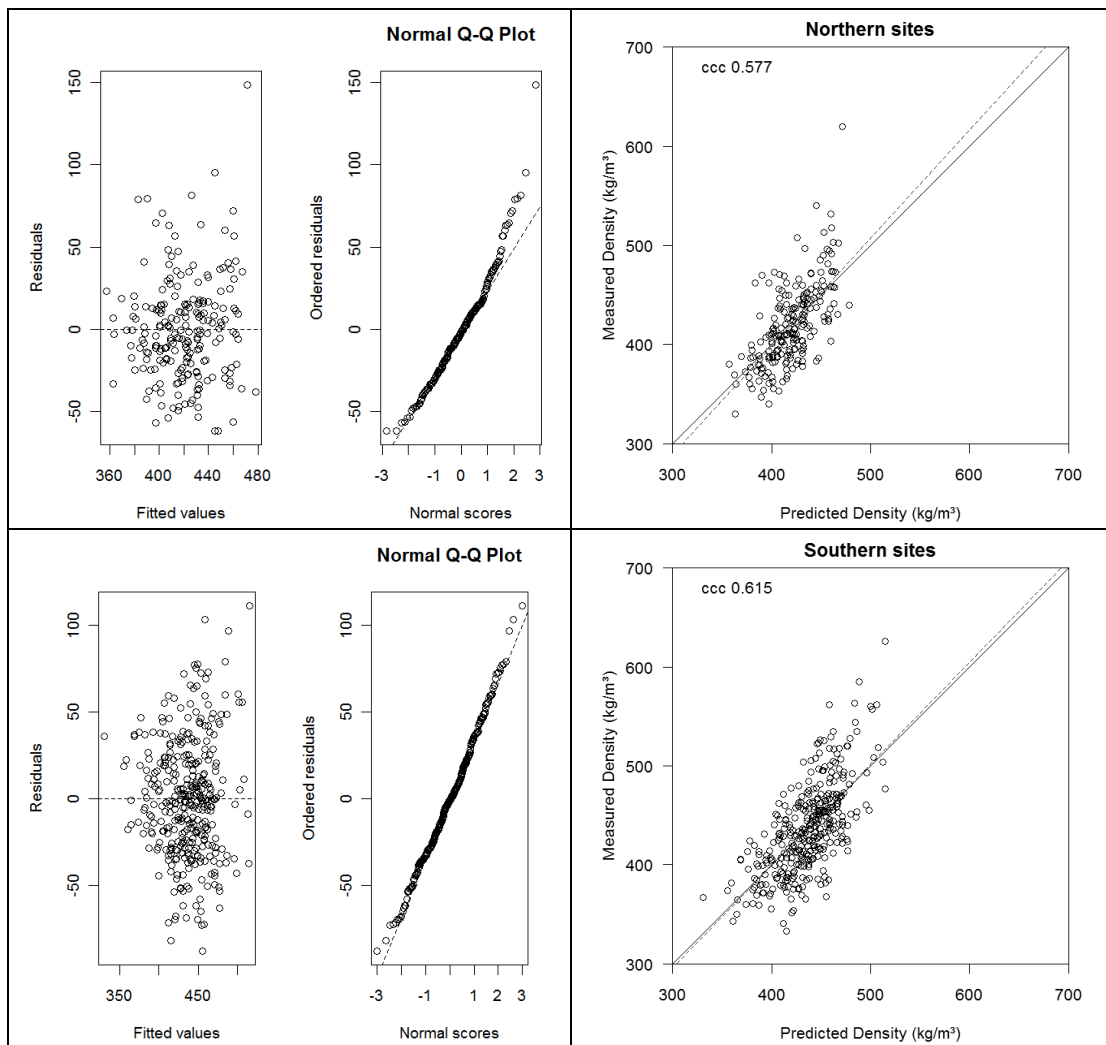


Figure 5-40. Diagnostic plots for the cross-section average density model developed for the Northern and Southern sites.

When the results of the concordance analysis, R^2 -values and amount of variance explained, were compared between all cross-section average density models (Table 5-15), it was evident that there was limited benefit in trying to develop separate models for different groups of sites.

Table 5-15. Concordance correlation coefficient, R^2 -values and variance explained for all the different models attempted for the area-weighted density.

	ccc	Adj. R^2 (fixed)	Adj. R^2	Variance explained (site)	Variance explained (tree)
All data	0.622	0.371	0.394	75 %	24 %
Thinned	0.612	0.393	0.368	87 %	30 %
Unthinned 1	0.623	0.381	0.389	77 %	23 %
Dominant	0.543	0.346	-0.161	98 %	13 %
Co-dominant	0.655	0.440	0.015	94 %	1 %
Non-dominant	0.641	0.246	0.120	65 %	- 4 %
Suppressed	0.451	0.268	- 0.223	100 %	2 %
North	0.577	0.312	0.342	70 %	18 %
South	0.616	0.413	0.367	91 %	28 %

5.3.6 Radial density profiles

The variation in the radial profiles of density and ring width were studied by fitting a mixed effects model with nested error structure, but without any explanatory variables. In this case the nested structure consisted of site, tree within the site, and ring within the tree. As expected, in both cases most of the variation was between rings, but in the case of density there was also a considerable tree effect (Table 5-16). At tree level, variation in density was higher than variation in ring width, which indicates that some of the density variation was not controlled by ring width. The model (Equation 7) predicts ring density based on ring number and ring width (Gardiner et al., 2010).

The model will predict density in mature wood more accurately if the ring width is controlling the density. The original model coefficients were developed to predict specific gravity and here these values were applied and the results converted at the end to kg/m³.

Table 5-16. Variance components in the radial profiles of density and ring width in the Benchmarking data.

	Variance components (%)	
	Ring density	Ring width
Between-sites	9.3	6.3
Between-trees	30.9	11.0
Between rings	59.9	82.7

Initially, the model was fitted to the data using the original parameters derived from Clocaenog and Kershope data by Gardiner et al. (2010) but the fit was very poor (Figure 5-41). This was thought to be due to a large variation in the shape of the radial density curves between the benchmarking sites (Figure 5-42, Figure 5-43). In addition to that, at some sites there was more between-tree variation (Figure 5-43). Improved fit was obtained when the model was reparameterised with the Benchmarking data (Figure 5-44). However, the model was still over predicting at low values and the R²-value remained low; 0.48. Furthermore, reparameterising the model to each site requires density and ring width measurements which in comparison to forest mensuration data are much more time consuming to derive. Therefore, it was attempted to relate the α parameters to site variables in order to derive sub-models that could predict suitable alpha values for different sites. If the α parameters could be predicted well, then good predictions of radial density curves could be modelled for sites for which no density data existed.

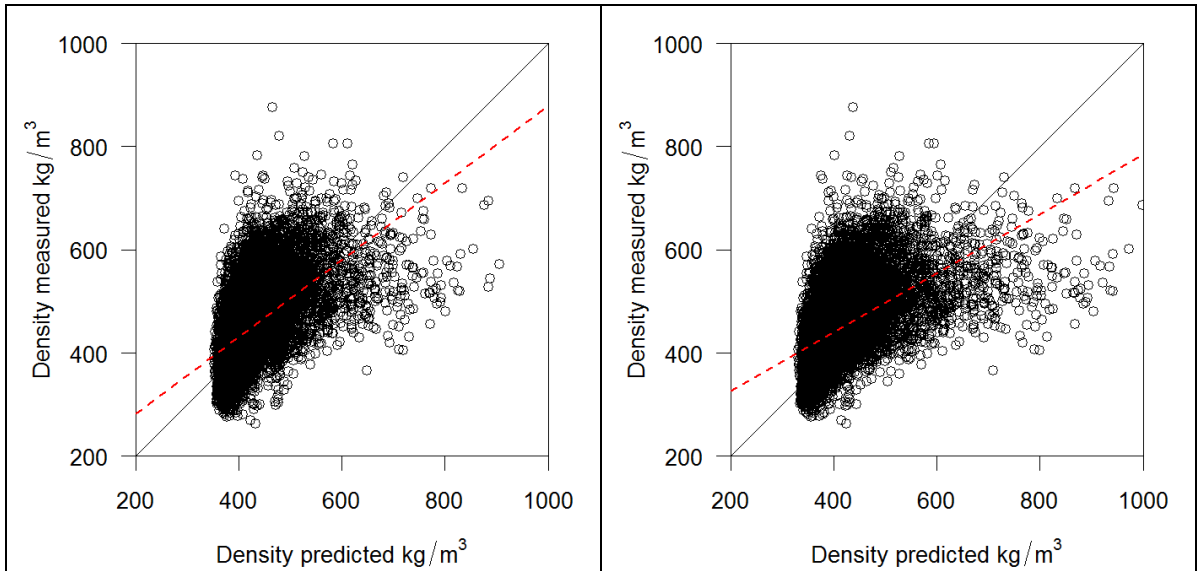


Figure 5-41. Model predictions against the measured values using Clocaenog (left) and Kershope (right) parameters. Dashed red line is the regression line fitted to the data, the R²-values for the regression were 0.34 and 0.30 for Clocaenog and Kershope parameters, respectively.

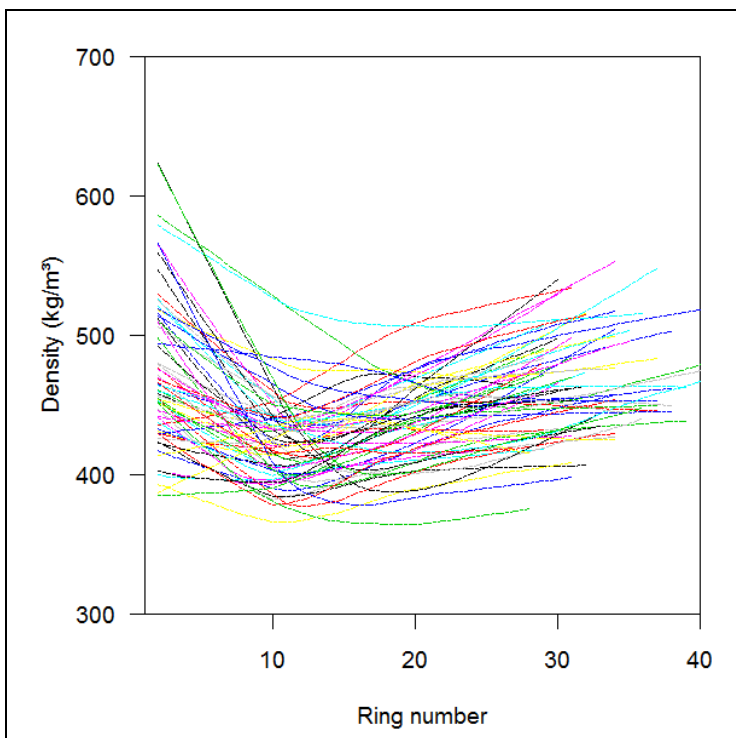


Figure 5-42. Lowess curves for each of the Benchmarking site plotted together.

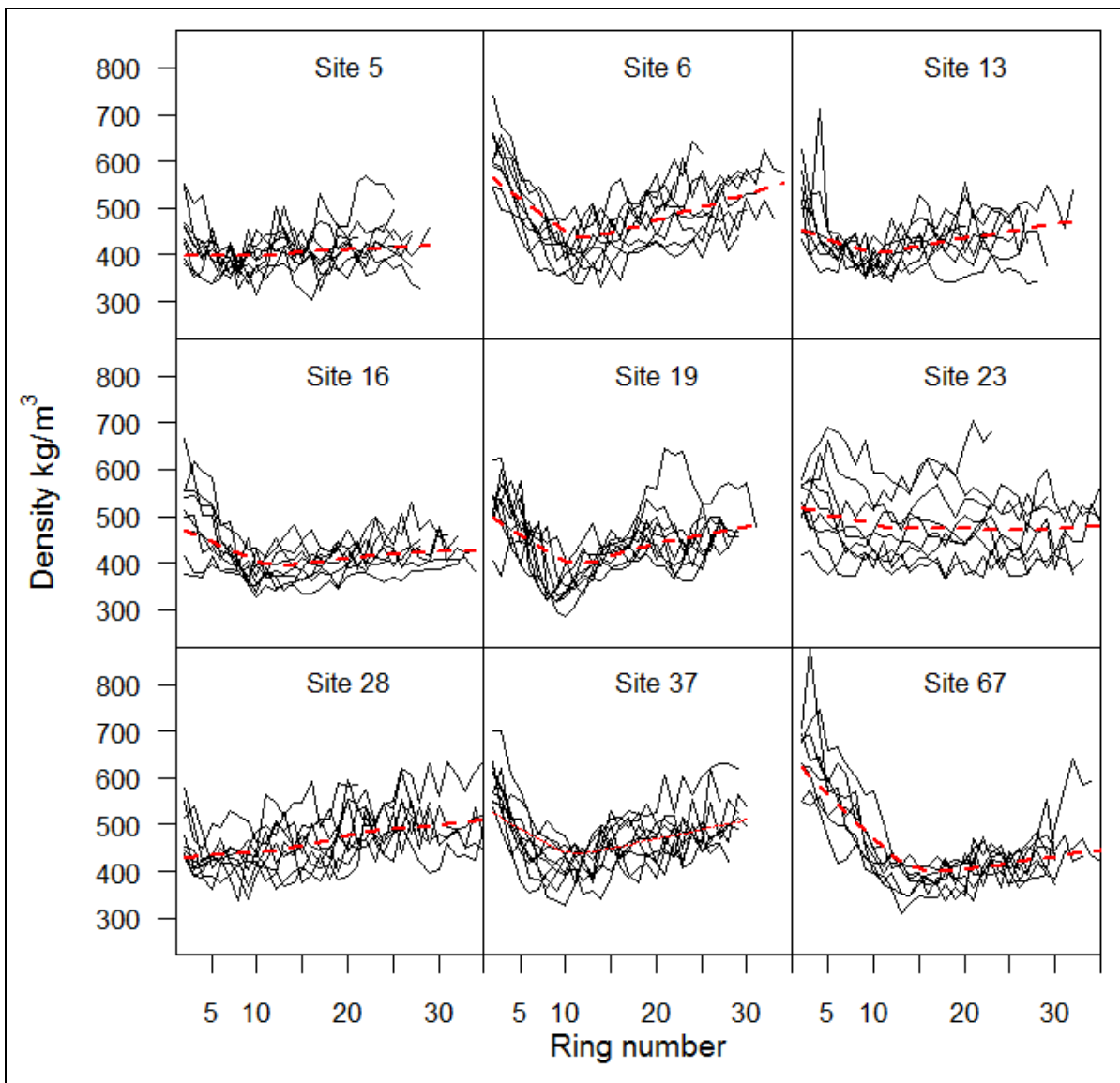


Figure 5-43. Within site variation in the ring density values at selected Benchmarking sites.

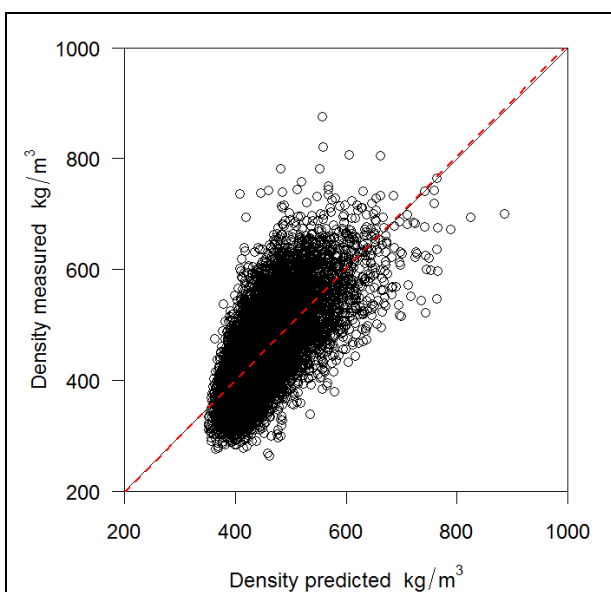


Figure 5-44. Density predictions for the reparameterised model plotted against the measured values. The dashed red line is the regression line fitted to the data. The R^2 -value for the regression was 0.48.

First, tree specific alpha parameters were derived. The average α_1 (0.6018 ± 0.407) and α_3 (0.1319 ± 0.101) values for the entire Benchmarking dataset was quite near to the Kershope and Clocaenog values but there was considerable variation between-sites (Figure 5-45). In the case of α_2 , also the mean (0.3655 ± 0.056) differed from Kershope and Clocaenog data. In the next stage, the tree specific α -values were related to tree and site variables. This was done for each parameter in turn, firstly for the entire dataset and then separately for thinned and unthinned sites. α_1 was not very strongly influenced by the site and tree variables (Figure 5-46). In all final models juvenile DBH remained a significant explanatory variable. There was a departure from normality in the residuals of all the models but in the case of unthinned sites this was less severe and the model predictions were better in the case of unthinned sites (Figure 5-47). Adjusted R^2 -values were very low: 0.14, 0.04 and 0.21 for all data, thinned and unthinned, respectively.

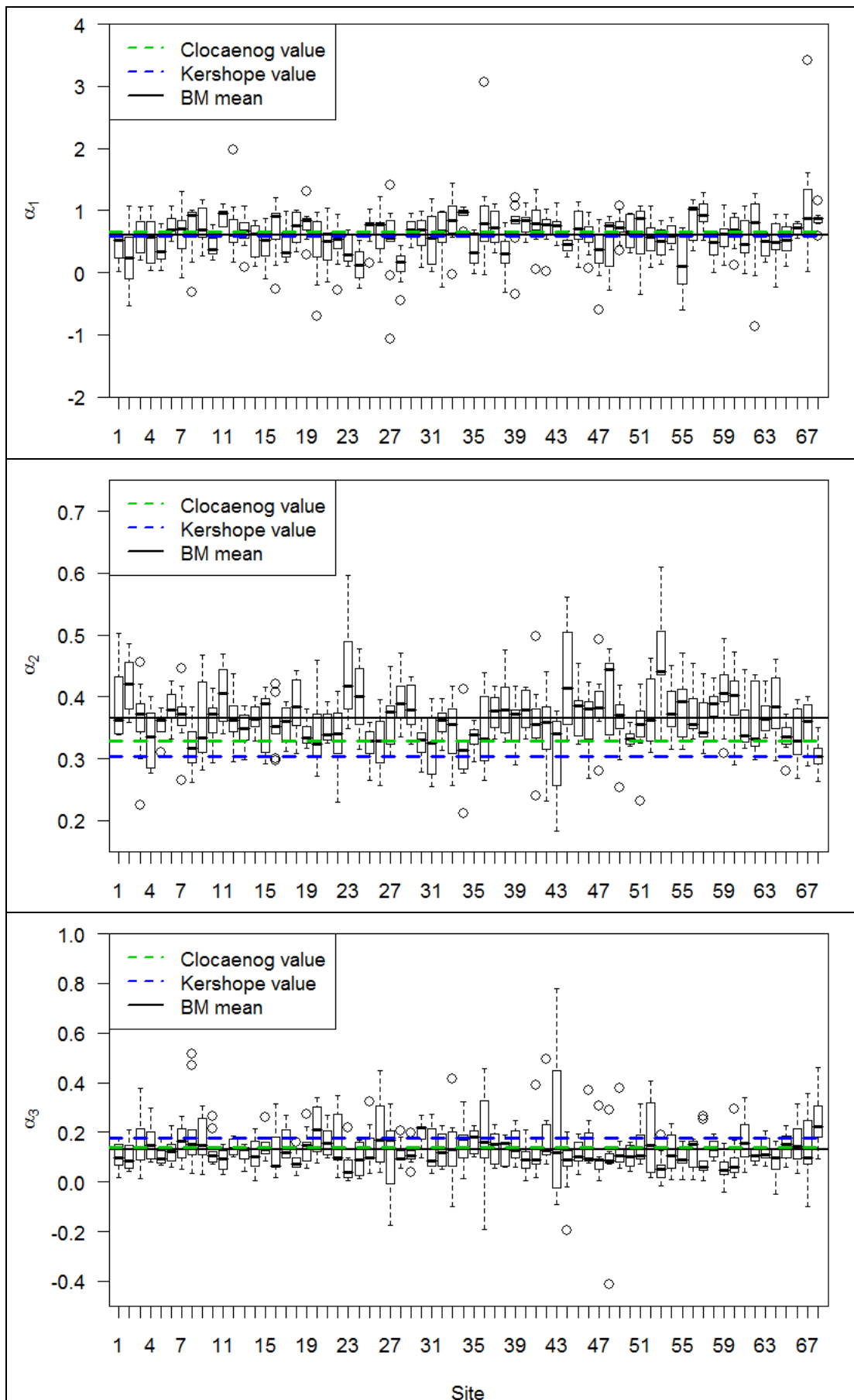


Figure 5-45. Alpha values across the Benchmarking sites with the horizontal lines marking the mean values across Benchmarking experiment, at Kershope and Clocaenog sites.

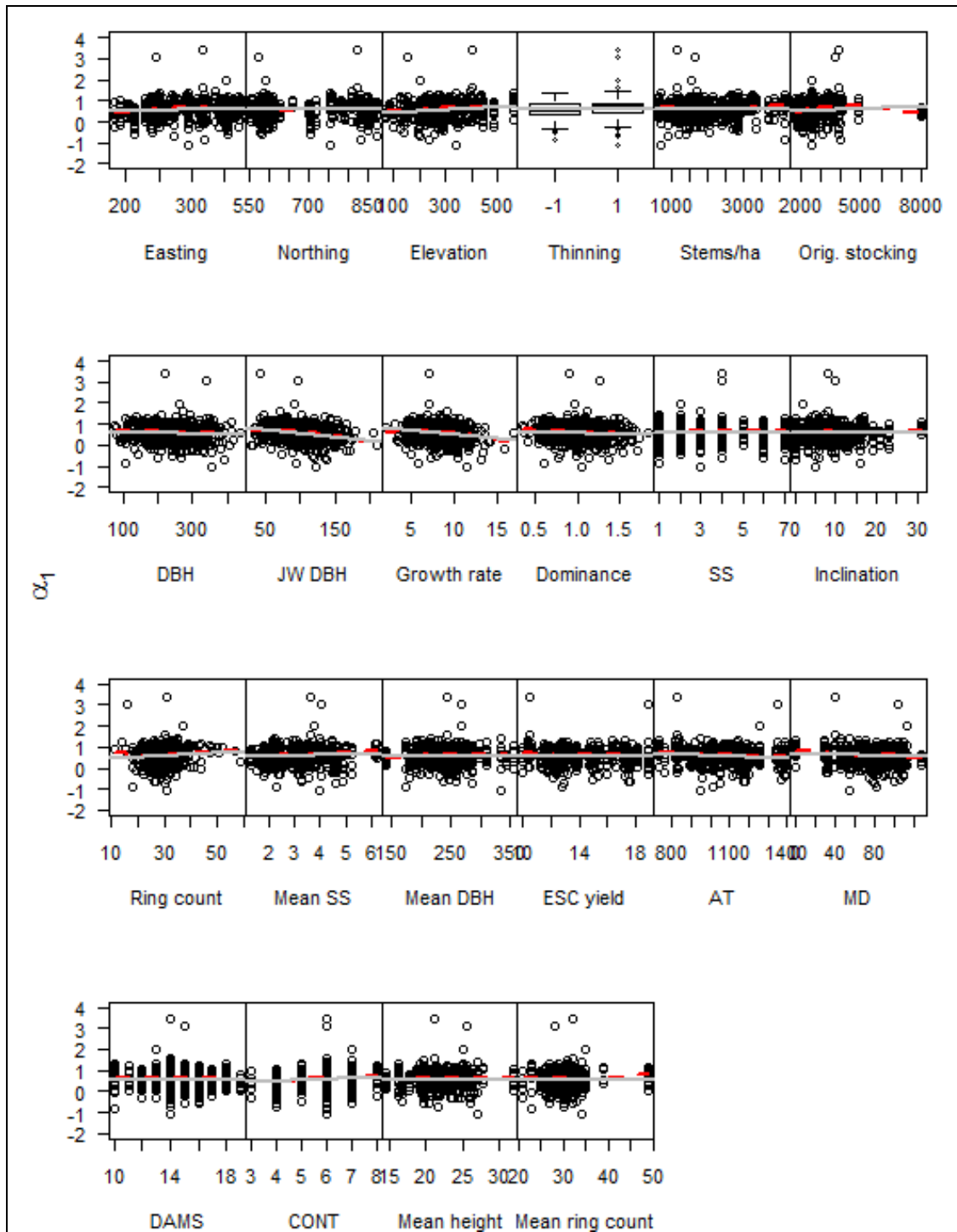


Figure 5-46. Influence of site and tree variables on α_1 in the entire Benchmarking dataset. Dashed red line is the LOWESS curve fitted to the data and the solid grey line is the linear regression.

Table 5-17. Explanatory variables and coefficients in the α_1 models. **α_1 ALL DATA**Fixed effects: $\alpha_1 \sim \text{DBH10yr} + \text{SiteMeanSS} + \text{CONT}$

	Value	Std.Error	DF	t-value	p-value
(Intercept)	0.2486	0.169	506	1.47	0.1411
DBH10yr	-0.0039	0.001	506	-7.06	0.0000
CONT	0.0888	0.021	65	4.20	0.0001
SiteMeanSS	0.0644	0.020	65	3.17	0.0024

 α_1 THINNED SITESFixed effects: $\alpha_1 \sim \text{DBH10yr}$

	Value	Std.Error	DF	t-value	p-value
(Intercept)	1.0903	0.098	224	11.11	0
DBH10yr	-0.0045	0.001	224	-4.89	0

 α_1 UNTHINNED SITESFixed effects: $\alpha_1 \sim \text{DBH10yr} + \text{RingCount} + \text{CONT} + \text{SiteMeanSS}$

	Value	Std.Error	DF	t-value	p-value
(Intercept)	-0.2056	0.250	280	-0.82	0.4123
DBH10yr	-0.0038	0.001	280	-5.68	0.0000
RingCount	0.0092	0.004	280	2.18	0.0301
CONT	0.1074	0.029	35	3.69	0.0008
SiteMeanSS	0.0758	0.029	35	2.60	0.0135

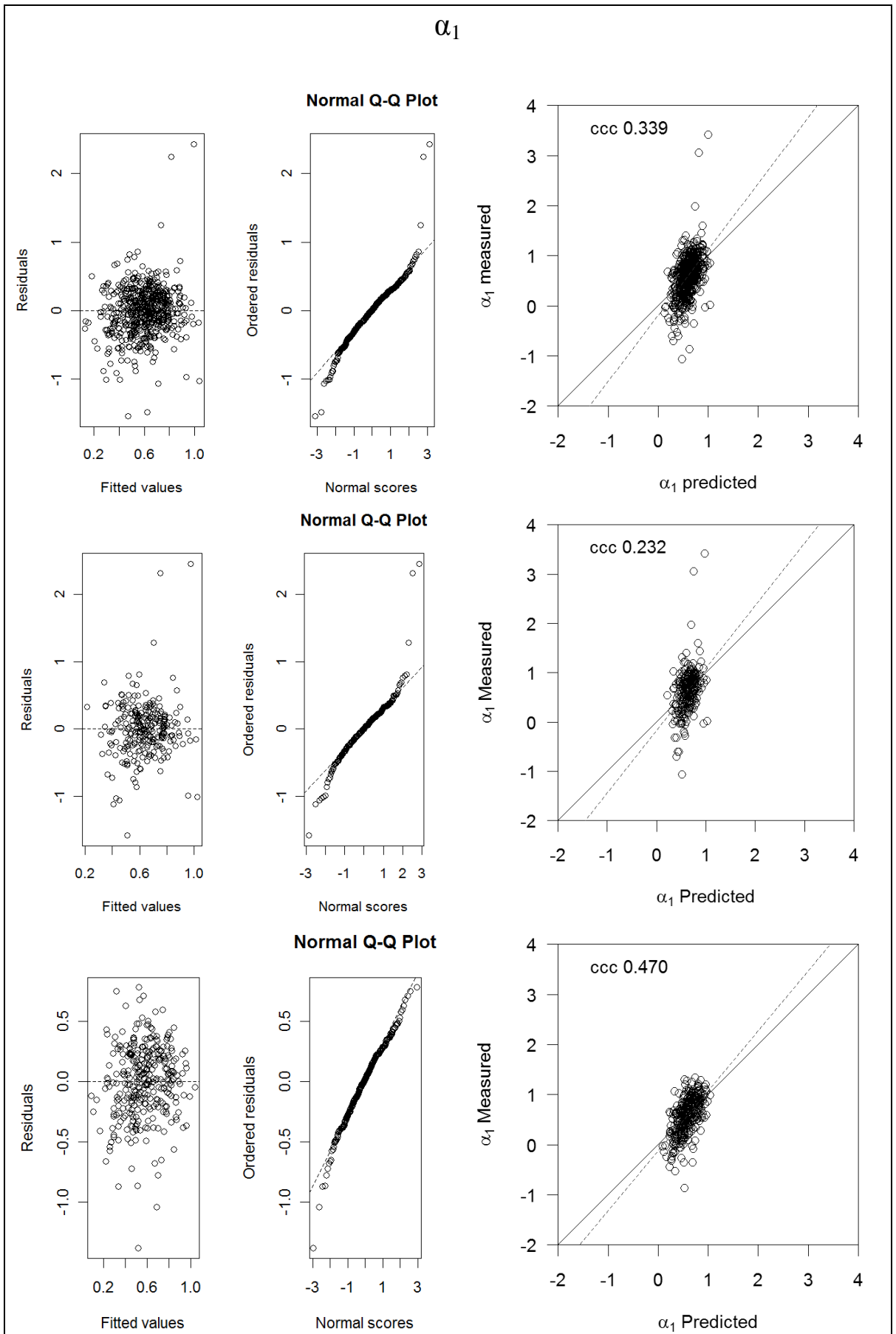


Figure 5-47. Diagnostic plots and fitted values plotted against measured values for α_1 modelled from the entire dataset (top) and separately for thinned (middle) and unthinned sites (bottom). On the right side dashed line is the linear regression line fitted to the data.

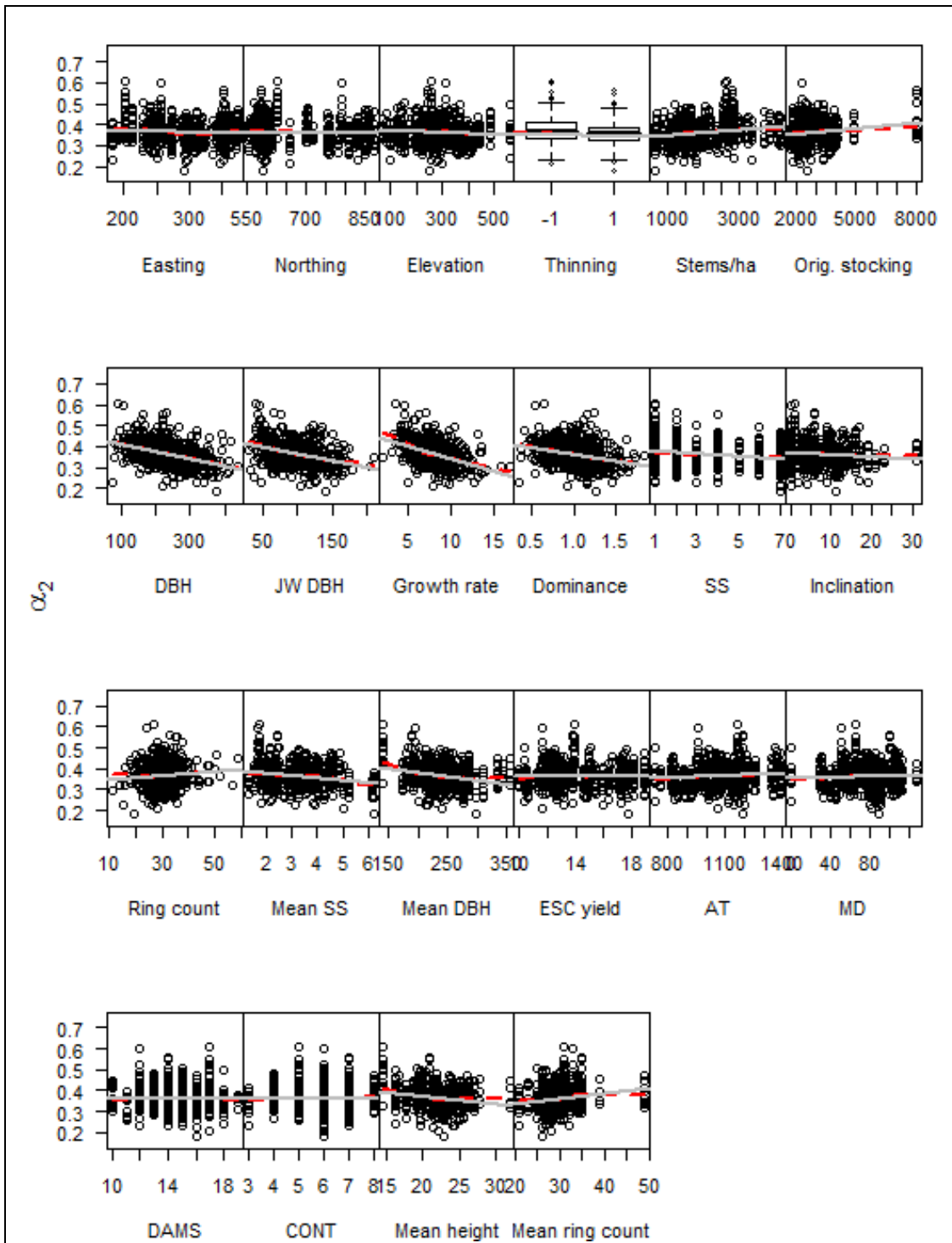


Figure 5-48. Influence of site and tree variables on the α_2 in the entire Benchmarking dataset. Dashed red line is the LOWESS curve fitted to the data and the solid grey line is the linear regression.

Compared with α_1 , α_2 was much more influenced by growth variables such as DBH, juvenile DBH, growth rate and mean height (Figure 5-48). Growth rate also remained in all alternative models (Table 5-18). Model predictions were slightly better than for α_1 and the departure from normality in residuals less severe (Figure 5-49). The adjusted R^2 -values were: all data 0.15, thinned 0.14, and unthinned 0.27.

Table 5-18. Explanatory variables and coefficients in the α_2 models

α_2 ALL DATA					
Fixed effects: $\alpha_2 \sim$ AT + GrowthRate + OrigStock + SiteMeanHt					
	Value	Std.Error	DF	t-value	p-value
(Intercept)	0.404129	0.022629	408	17.86	0.0000
AT	0.000051	0.000016	52	3.21	0.0023
GrowthRate	-0.009484	0.001032	408	-9.19	0.0000
OrigStock	0.000008	0.000003	52	3.00	0.0041
SiteMeanHt	-0.001941	0.000863	52	-2.25	0.0287
α_2 THINNED SITES					
Fixed effects: $\alpha_2 \sim$ MD + GrowthRate + OrigStock					
	Value	Std.Error	DF	t-value	p-value
(Intercept)	0.38243	0.017854	207	21.42	0.0000
MD	0.00027	0.000130	25	2.09	0.0472
GrowthRate	-0.00909	0.001359	207	-6.69	0.0000
OrigStock	0.00001	0.000003	25	3.58	0.0014
α_2 UNTHINDED SITES					
Fixed effects: $\alpha_2 \sim$ FieldEast + AT + GrowthRate + SS + SiteAveRC + SiteMeanHt					
	Value	Std.Error	DF	t-value	p-value
(Intercept)	0.406566	0.05393	217	7.54	0.0000
Easting	-0.000166	0.00007	25	-2.27	0.0324
AT	0.000067	0.00003	25	2.40	0.0243
GrowthRate	-0.007750	0.00175	217	-4.43	0.0000
SS	-0.004353	0.00169	217	-2.58	0.0106
SiteAveRC	0.003426	0.00141	25	2.42	0.0229
SiteMeanHt	-0.004364	0.00135	25	-3.23	0.0035

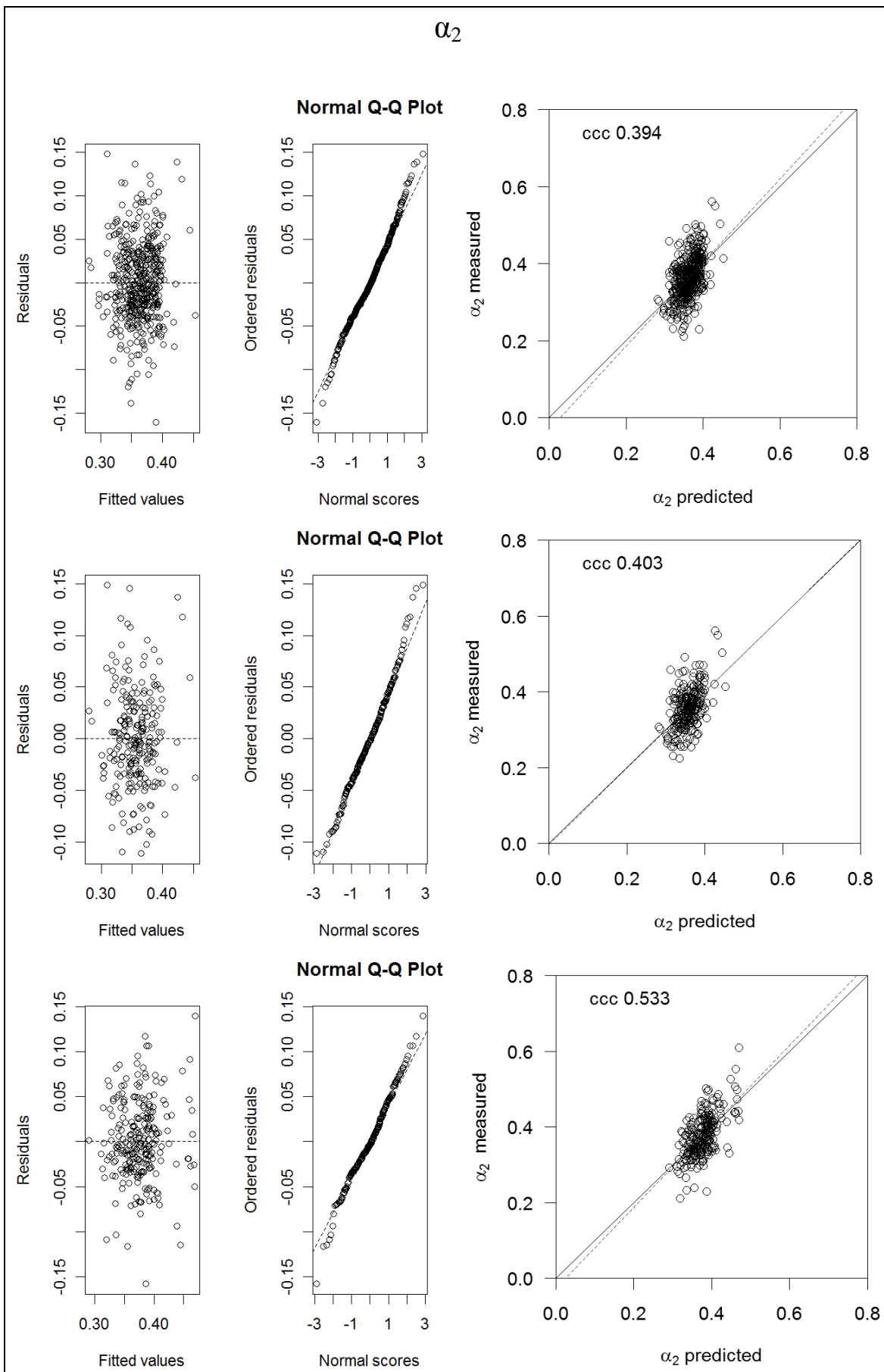


Figure 5-49. Diagnostic plots and fitted values plotted against measured data for models predicting α_2 from the entire dataset (top) and for thinned (middle) and unthinned (bottom) sites separately. On the right side dashed line is the linear regression line fitted to the data.

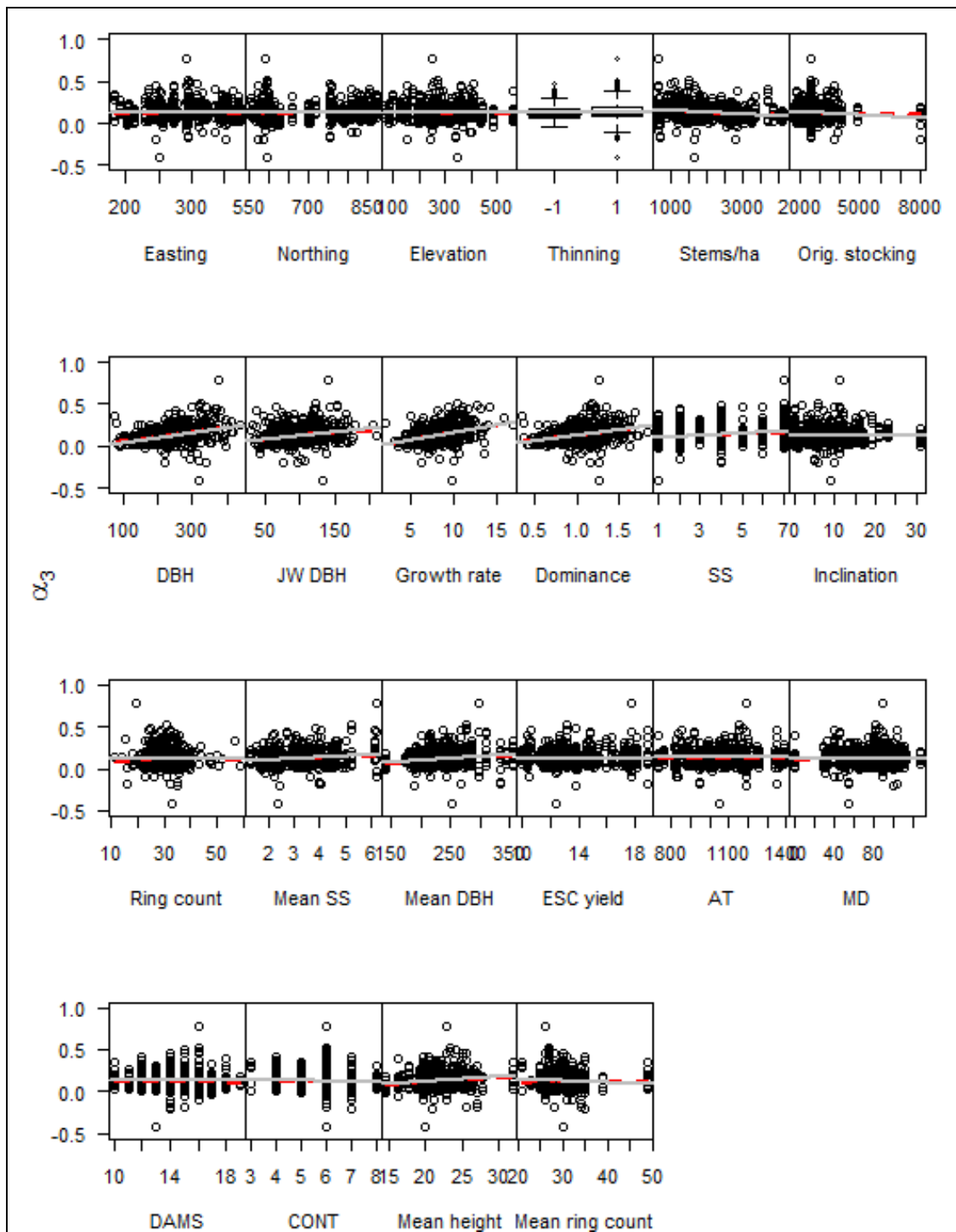


Figure 5-50. Influence of site and tree variables on the α_3 parameter. Dashed red line is the LOWESS curve fitted to the data and the solid grey line is the linear regression.

α_3 also was most strongly influenced by growth variables (Figure 5-50). Growth rate was included in two of the models and DBH in one (Table 5-19). Departure from normality in the residuals was quite severe, especially in the case of all data and data from thinned sites (Figure 5-51). Adjusted R^2 -values were 0.15, 0.06 and 0.28 for all data, thinned and unthinned, respectively.

Table 5-19. α_3 models.

α_3 ALL DATA					
Fixed effects: $\alpha_3 \sim$ GrowthRate + SS					
	Value	Std.Error	DF	t-value	p-value
(Intercept)	-0.0157	0.015	502	-1.07	0.2876
GrowthRate	0.0168	0.002	502	8.81	0.0000
SS	0.0047	0.002	502	2.48	0.0135
α_3 THINNED SITES					
Fixed effects: $\alpha_3 \sim$ GrowthRate					
	Value	Std.Error	DF	t-value	p-value
(Intercept)	-0.021	0.026	221	-0.80	0.4275
GrowthRate	0.019	0.003	221	6.41	0.0000
α_3 UNTHINNED SITES					
Fixed effects: $\alpha_3 \sim$ DBH + SS					
	Value	Std.Error	DF	t-value	p-value
(Intercept)	0.0023	0.01494	280	0.15	0.8778
DBH	0.0005	0.00007	280	6.75	0.0000
SS	0.0049	0.00224	280	2.18	0.0303

All in all, the alpha parameter modelling was most successful in the case of unthinned sites. There were significant differences in the values of α_2 and α_3 between the thinned and unthinned sites (Table 5-20).

Table 5-20. The average alpha values for thinned and unthinned Benchmarking sites with standard deviation in parentheses. P-value indicates the difference between thinned and unthinned sites.

	Thinned	Unthinned	p-value
α_1	0.6338 (0.448)	0.5764 (0.370)	0.0999 ns
α_2	0.3574 (0.055)	0.3719 (0.057)	0.0021 **
α_3	0.1431 (0.123)	0.1230 (0.079)	0.0241 *

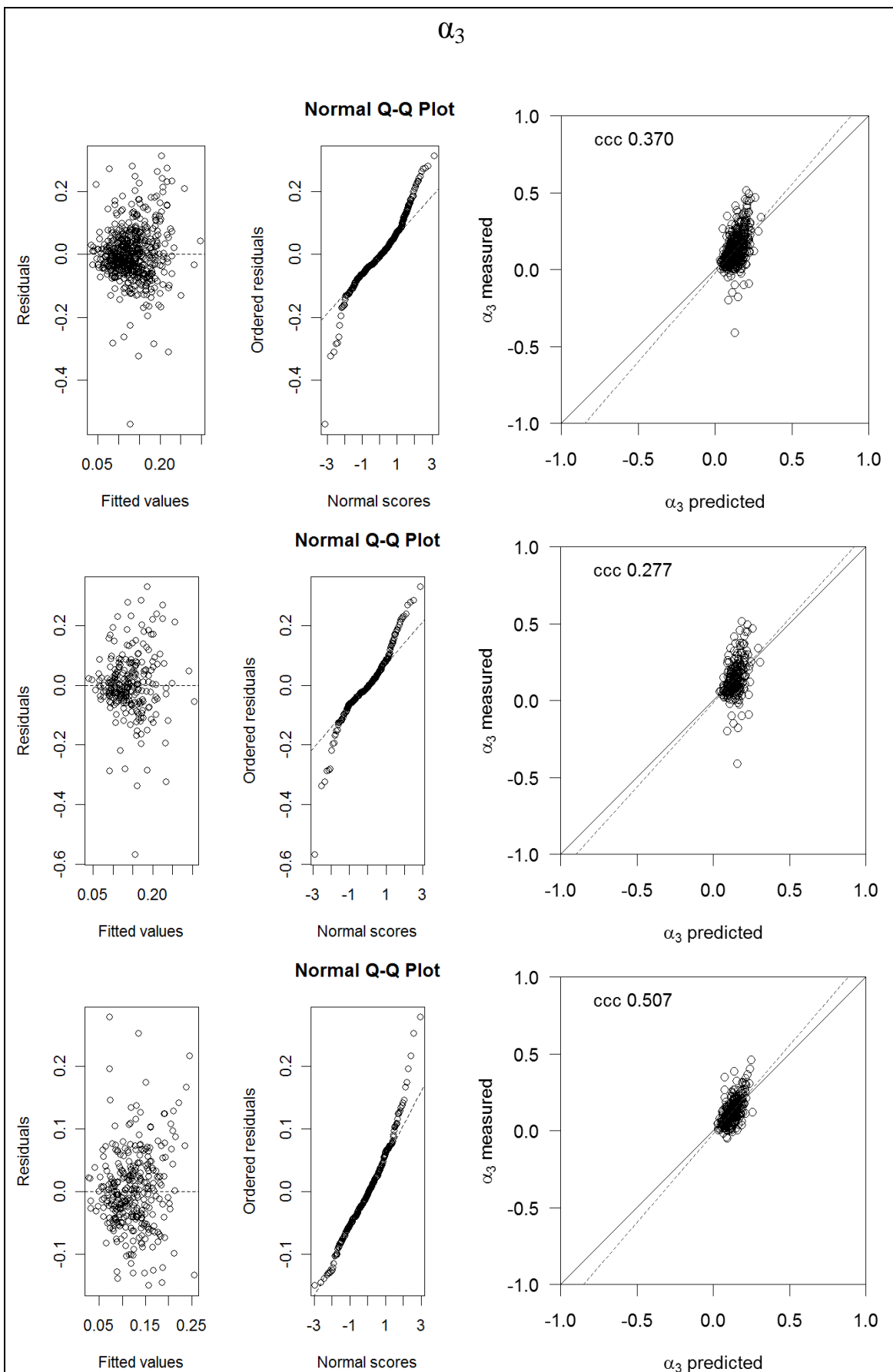


Figure 5-51. Diagnostic plots and predicted values plotted against measured values for models predicting α_3 from the entire dataset (top) and thinned (middle) and unthinned (bottom) sites separately. On the right side dashed line is the linear regression line fitted to the data.

5.3.6.1 Predicting alphas using additional data from the felled Benchmarking sites

The models derived above for the α -values were used to predict site specific alpha values for each of the 3 Level II sites (Chapter 6). These coefficients were then used to predict radial density values for these sites using the density model described above. However, the predictions were poor (see Figure 6-4, Figure 6-5 and Figure 6-6 in Chapter 6). This was thought to arise because most of the variation in the parameters was between-trees, whereas most of the explanatory variables were site level variables. A selected set of the Benchmarking sites were felled for further testing by Napier University. The 12 sites selected for felling represented the range of acoustic velocity measurements obtained using the IML hammer standing tree tool. At each of these sites, the 10 trees that had been randomly selected for coring were felled. However, if these trees were too small to yield logs for the Napier University study alternative ones were randomly selected. On the felled trees the height, lowest living branch and whorl were measured. Allowing for the substituted trees and samples lost during core preparation for density analysis a total of 74 trees were obtained for which both density and crown dimension measurements existed. It was thought that including these tree level variables could potentially improve the predictions.

First of all the potential explanatory variables from these felled sites were plotted against the tree specific α -values, to screen for potentially influential variables, since the full model would not converge due to problems with singularity.

In the case of α_1 , the variables selected for inclusion in the model, based on the plots (Figure 5-52) and correlation analysis included Easting, elevation, growth rate, ring count, original stocking, and thinning. On the plots it was observed that continentality also influenced the α_1 . Continentality is correlated with Easting since the climate is drier in the Eastern part of the country. This was also found here with the Pearson's correlation coefficient being 0.61. Continentality seemed to have a poor spread since 7 of the 12 sites scored 6. Two sites scored 4 and only 1 site fell into scores 3, 5 and 7. Therefore, Easting was selected as a potential explanatory variable in the initial model. However, the coefficient for Easting gave the opposite sign from that expected, which indicates collinearity problems in the model. Easting was correlated with elevation (0.677) and it was removed from the model. The correlation between Easting and elevation indicates that the higher altitude sites were clustered in the eastern part of the study area. The differences

in elevation will explain some of the easting-accumulated temperature sum correlation as well, since sites at higher elevation will have lower temperature sum.

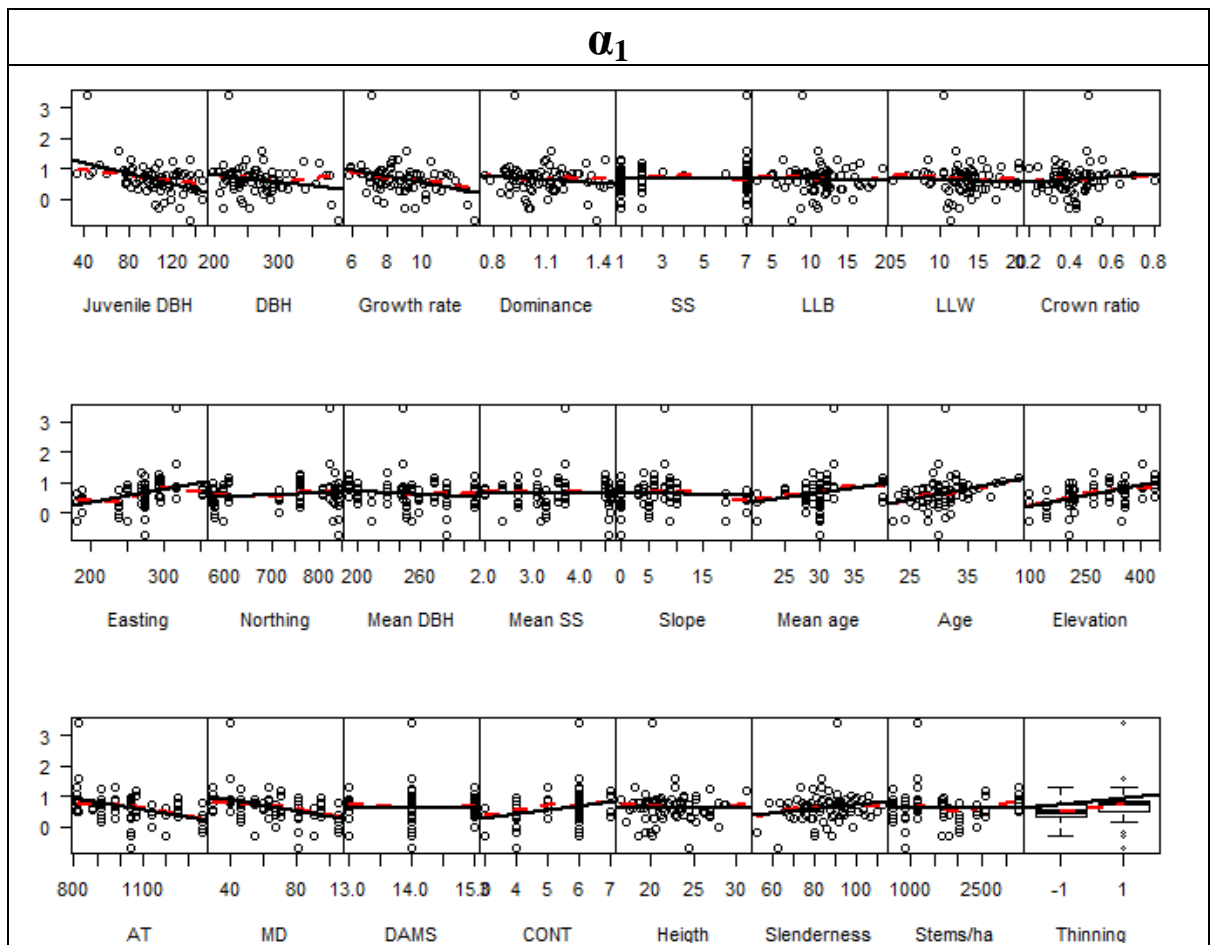


Figure 5-52. The influence of site and tree variables on the α_1 values at the felled benchmarking sites. Solid black line is the regression line fitted to the data and the dashed red line the lowest curve.

The initial α_1 model did not include any of the new crown variables and therefore improvement was regarded as unlikely. This would effectively remain just as a modelling exercise on a subset of the data. The final α_1 model (Table 5-21) was left with two explanatory variables, growth rate and original stocking. The Adjusted R^2 -values were poor (0.27) when fixed effects only were considered and even lower (0.14) when random effects were included. This indicates that the inclusion of random effects did not improve the prediction much and since the adjusted R^2 penalises additional terms that are not contributing markedly in explaining the variation, the resulting value was lower than for the fixed effects alone. In fact the R^2 -values were identical for both options.

Most of the variation (81%) was between-trees within a site which would be included in the random term unless explained by growth and original stocking in the final model. Only 11.6 % of the between-tree variation was explained by the model.

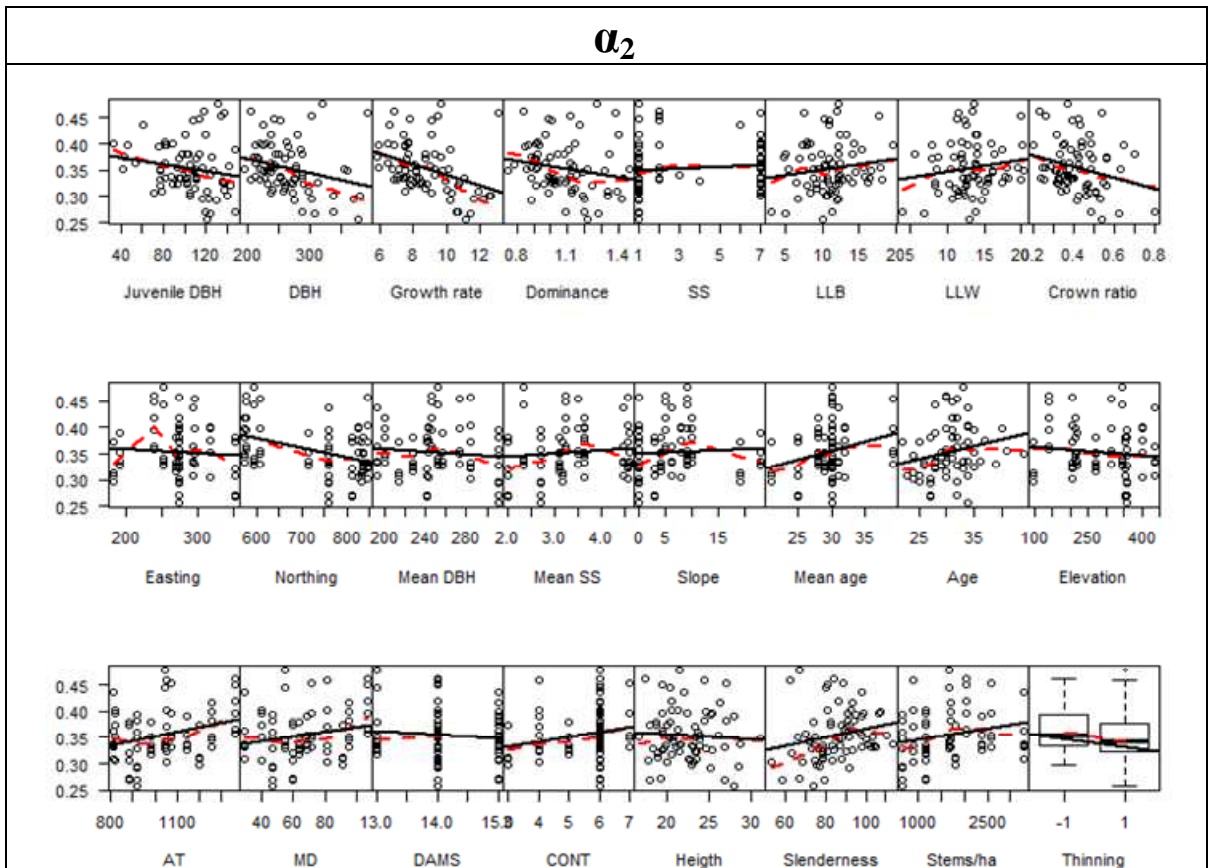


Figure 5-53. The influence of site and tree variables on the α_2 values at the felled benchmarking sites. Solid black line is the regression line fitted to the data and the dashed red line the lowest curve.

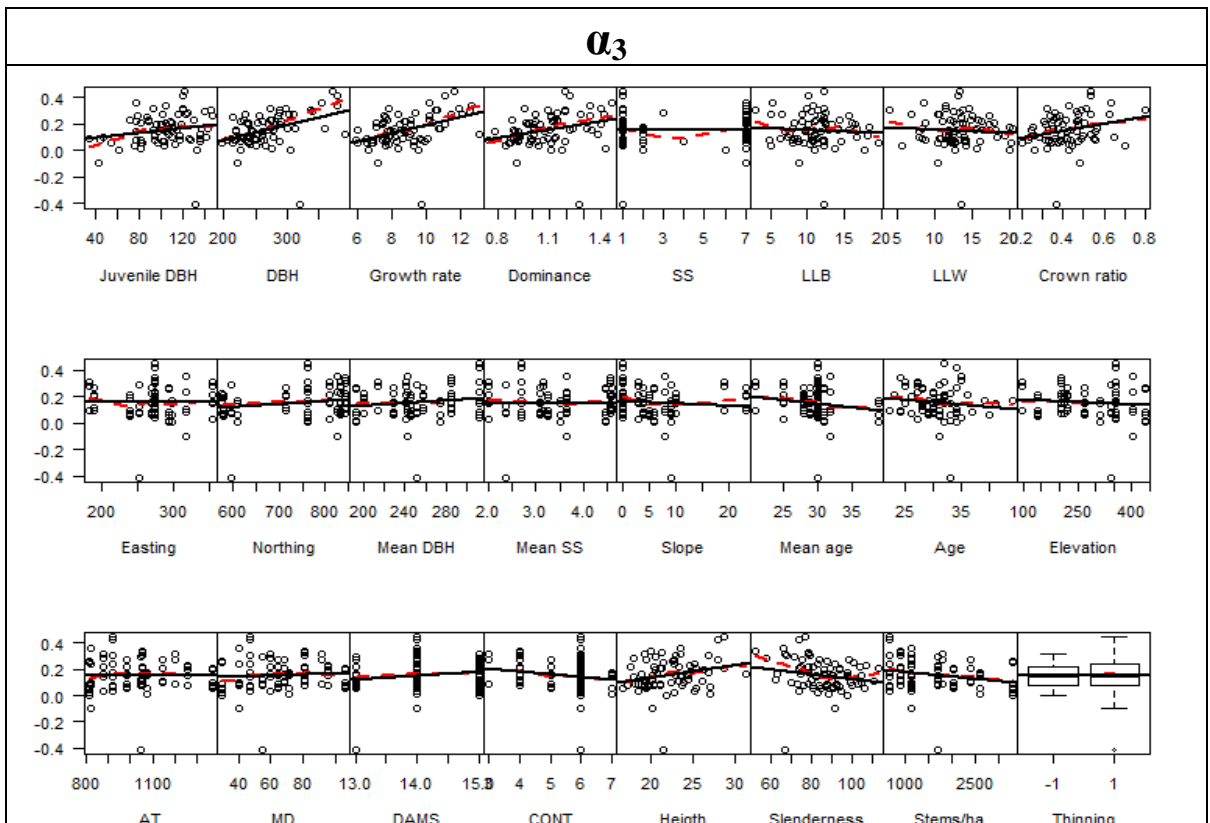


Figure 5-54. The influence of site and tree variables on the α_3 values at the felled benchmarking sites. Solid black line is the regression line fitted to the data and the dashed red line the lowest curve.

Table 5-21. The explanatory variables and coefficients in the model for predicting the alphas at the felled Benchmarking sites. Density at moisture content 4 %.

α_1					
Fixed effects: a1 ~ GrowthRate + OrigStock					
	Value	Std.Error	DF	t-value	p-value
(Intercept)	0.1042	0.4505	57	0.23	0.8179
GrowthRate	-0.0686	0.0316	57	-2.17	0.0341
OrigStock	0.0004	0.0001	9	4.07	0.0028
α_2					
Fixed effects: a2 ~ AT + GrowthRate					
	Value	Std.Error	DF	t-value	p-value
(Intercept)	0.35728	0.04267	61	8.37	0.0000
AT	0.00008	0.00003	10	2.58	0.0276
GrowthRate	-0.00983	0.00299	61	-3.28	0.0017
α_3					
Fixed effects: a3 ~ GrowthRate + HT					
	Value	Std.Error	DF	t-value	p-value
(Intercept)	-0.2858	0.110	60	-2.59	0.0120
GrowthRate	0.0286	0.008	60	3.74	0.0004
HT	0.0085	0.004	60	2.03	0.0469

Most of the potential variables had an influence on α_2 (Figure 5-53). Visually, DBH, growth rate, lowest living branch, crown ratio, northing, mean ring count (mean age), elevation, accumulated temp sum, moisture deficit, continentality, DAMS-score, slenderness, stand density and thinning were considered as potential explanatory variables. To avoid correlation problems one variable per class was selected. Accumulated temperature was selected as the climatic variable and the mean ring count to describe the site age. Northing was also included. Growth rate and crown ratio were selected to represent the tree vigour since the regression line had a steeper slope than that for DBH and lowest living branch, respectively. The initial model had the form:

$$\alpha_2 \sim \text{AT} + \text{Northing} + \text{GrowthRate} + \text{SiteAveRC} + \text{CrownRatio}$$

This model was simplified until only significant variables remained and as in the case of α_1 none of the additional variables obtained for the felled trees remained in the final α_2 model (Table 5-21). The explanatory power of the model remained poor (Figure 5-55) and the adjusted R^2 for the fixed effects was 0.16. The model explained 100 % of between-site variation but only 16 % of the overall variation was between-sites, therefore the explanatory power of the model remained poor since it failed to explain the variation between-trees within the sites (3.8% explained).

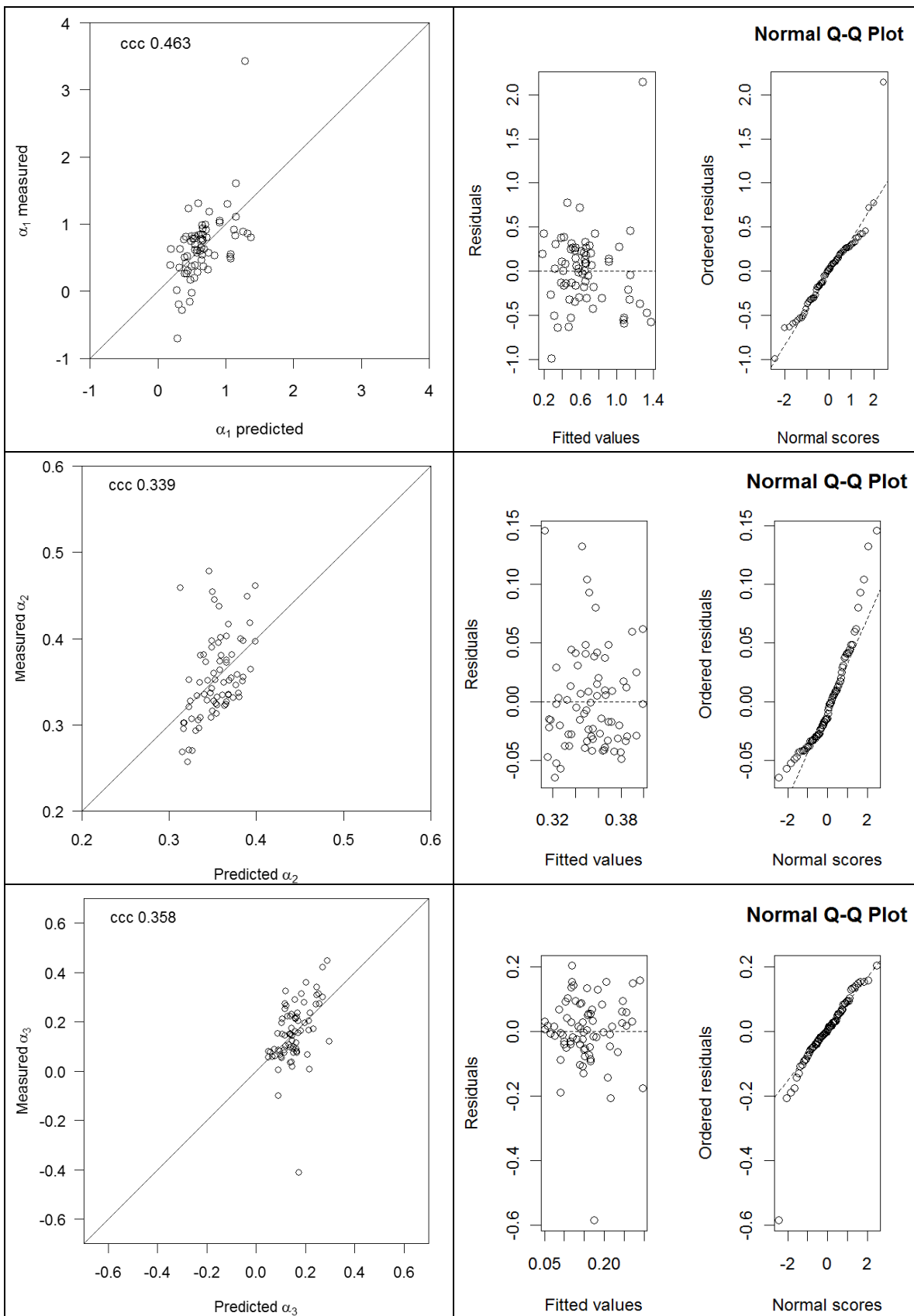


Figure 5-55. Model predictions plotted against the measured data (left) and the diagnostic plots for the residuals (right).

Based on the graphs (Figure 5-54) and correlation analysis, only growth rate, crown ratio and tree height were included in the initial α_3 model. One of the additional tree variables,

tree height, was retained in the final α_3 model (Table 5-21), however the model fit remained poor (Figure 5-55) and the adjusted R^2 -value for the fixed effects was 0.18. Also, in the case of α_3 , only 1.5% of the variation was between the sites. Therefore, the coefficients of determination remained poor although in this case 19% of the between-tree variation was explained in addition to the 100% of the between-site variation.

The mean α -values determined from the felled sites are listed in Table 5-22. These figures are similar to the α -values derived for thinned sites (Table 5-20).

Table 5-22. Mean values of the coefficients and standard deviations at the felled Benchmarking sites.

	Mean	Standard deviation
α_1	0.6538	0.512
α_2	0.3540	0.048
α_3	0.1548	0.124

5.4 Discussion

A strong negative correlation was observed between ring width and density across the Benchmarking sites. In only three of the 68 sites was the relationship not significant when the whole radius was observed. When the radii were divided into juvenile and mature parts, the negative correlation was stronger in mature than in juvenile wood. At only one site was the relationship not significant in mature wood whereas in juvenile wood this occurred at eight sites. However, at all sites the relationship was significant for at least some part of the radius (Appendix 2). As the Benchmarking experiment included a wide variety of sites over quite an extensive geographical area this provides strong evidence that an increase in growth is indeed normally accompanied by a reduction in density in Sitka spruce. Previous studies have also reported this in Sitka spruce (Brazier, 1967; Brazier, 1970b; Macdonald and Hubert, 2002; Petty et al., 1990; Simpson and Denne, 1997). Furthermore, there is evidence for it in; Norway spruce (Jyske et al., 2008; Lindström, 1996a; Lindström, 1996c; Mäkinen et al., 2007; Petty et al., 1990; Saranpää and Repola, 2000), Black spruce

(Koubaa et al., 2000), more generally in *Picea* sp. (Saranpää, 1994), and Western hemlock (Debell et al., 1994). Petty et al. (1990) found that the relationship was strong in Sitka and weak in Norway spruce. Similarly Saranpää and Repola (2000) reported that the negative correlation was not strong in Norway spruce. So, such a relationship is not a new discovery but the most interesting observation was its consistency over different site types and tree social classes. However, in absolute terms there was large variation in density between-sites and trees within sites and therefore there is scope for selecting trees producing higher density for the development of seed source. Rozenberg et al. (2001) found in Douglas-fir that incorporating a genetic effect in the density models improved the predictions and decreased the residuals. Based on their findings, they reported that most of the variability in the density-growth relationship was genetic. In the present experiment, genetic variation between the sites and between-trees within the sites was unknown. Much of the seed is likely to be of Queen Charlotte Island provenance but it is likely to be from open pollinated seed sources and therefore genetic variation could be high within the stand, which could explain the high between-tree variation observed (69-78% depending on the section of radius observed). Also, in previous studies, a considerable amount of random, between-tree, variation has been found in wood density (Mäkinen et al., 2007). Hedenberg et al. (2004) reported a large tree effect (63%) in basic density of Sitka spruce, which they attributed to genetic factors. Guilley et al. (2004), working with oak models based on region, site quality and silvicultural practice, found that fixed effects explained 48-50% of the variation, the random tree effect was 29-31% and the remainder was residual variation. Tree breeding projects have aimed to find genotypes where high density is retained and improved planting stocks have been developed for the UK (Hubert and Lee, 2005; Lee, 1999a; Lee, 1999b).

To assess whether any of the site or climatic factors had a direct influence on timber density or impacted it simply through growth rate, the data could be analysed further by holding the ring width constant statistically (Bergès et al., 2008; Guilley et al., 2004). Guilley et al. (2004) found for oak in France that region (5 French regions), silviculture (coppice with standards vs high forest) or site quality (three classes) did not impact ring density significantly when ring width and cambial age were held constant. Bergès et al. (2008) found a slight direct effect of ecological factors on oak density. For example, altitude had a significant direct influence on oak density in addition to its effect through latewood proportion. From experiments on Norway spruce grown in long term monitoring plots with comparisons of thinning, fertilisation, nutrient optimisation and fast-growing clones it was also concluded that changes in wood and tracheid properties were in their entirety related to growth rate (Mäkinen et al., 2007). However, direct effects of elevated

temperature and CO₂ were reported in a whole tree chamber experiment on Norway spruce since wood properties were altered even if the treatment did not affect the growth rate (Kostiainen et al., 2009). In closed chamber studies, elevated temperature was found to increase mean and earlywood density in Scots pine (Kilpeläinen et al., 2005). In Radiata pine studies it was reported that density was not related to growth traits such as height, DBH and sapwood area (Nyakuengama et al., 1998) and in a fertiliser trial that ring width and density were only weakly related (Nyakuengama et al., 2003). In Radiata pine, site mean outerwood basic density was increased by increase in site mean annual temperature (Beets et al., 2007). Here, accumulated temperature sum (AT) was found to increase mature wood and outerwood density independently of growth rate as these two variables were not correlated.

Negative effect of elevation on ring density detected in the factorial analysis has been reported by many authors. In subalpine fir, negative correlation was observed with latewood density and maximum density (Splechna et al., 2000). In Radiata pine in New Zealand, reduction in density was reported with increasing altitude and when moving southwards (Cown and Ball, 2001). In black spruce in Quebec, the growth rate and cell wall thickness decreased with latitude (St-Germain and Krause, 2008). Decrease in cell wall thickness could cause a reduction in density, however the authors also observed reduction in lumen and cell diameters as well as an increase in latewood proportion. Therefore, the influence on density remains uncertain as density itself was not investigated. In the Benchmarking experiment in the factorial analysis nothing did not influence density significantly.

The history of fertiliser usage is not known for the Benchmarking sites. Some differences between-sites may be attributable to fertiliser applications. In conifers, fertilisers have been found to decrease wood density (Kostiainen et al., 2004) and influence chemical composition (Kostiainen et al., 2004). However, since the largest proportion of variation was between-trees within a site, the fertiliser effect is not likely to have been the cause. Furthermore, the aim of the fertiliser application is to boost the tree growth so if it was successful then the increase would be incorporated into the growth rate term and the accompanying density reduction at least in part allowed for.

Due to its dominating effect on density, growth rate, or another vigour related variable such as juvenile DBH, in the case of average juvenile wood density, was always included in the final density or alpha model. The fact that in the average juvenile wood density model DBH was left as the only significant explanatory variable indicated that

environmental control was influencing the density through its impact on growth rate. When growth rate was modelled it was significantly related only to stand density, with higher stocking reducing the growth rate as competition limits light, water and other resources available per tree. However, site mean Stem Straightness was negatively correlated with stand density (-0.362) and therefore growing trees at higher stand density to increase wood density might lead to alternative timber quality issues.

Perhaps the outerwood and mature wood models could be improved by calculating separate growth rates for the respective parts of the radius alone. However, keeping practical implications in mind, it is much easier to derive an average growth rate from DBH and age, that are widely available forest mensuration data, than to carry out detailed measurements of ring widths in different parts of the radius, on core or disk samples, in order to determine local growth rates.

Using theoretical calculations based on transport of water, Roderick and Berry (2001) concluded that density should decrease with decreasing temperature in parallel with changes in the viscosity of water. In line with these predictions, larger earlywood cells were detected in Norway spruce at cool-humid sites in Germany and more latewood cells and thicker cell walls were observed at warm-dry sites (Park and Spiecker, 2005). Furthermore, an increase in earlywood cell wall thickness and wood density in Norway spruce was detected in the elevated temperature treatment in a whole tree chamber experiment (Kostiainen et al., 2009). Unusually, low temperatures during the growing season have been related to formation of cells with thinner walls in Black spruce (Wang et al., 2002). In this study accumulated temperature sum was found to have a positive relationship with density. It was significant in mature wood, outerwood and cross-section average density models as well as models derived for co-dominant, non-dominant and suppressed trees separately. Furthermore, altitude had a negative impact on density, which could be related to the temperature effect as temperature decreases rapidly with altitude. In addition to that the stem straightness score was negatively correlated with elevation (-0.219) which indicated the potential for multiple timber quality issues at high elevation.

In modelling the average density of the tree cross-section it was found unhelpful to divide the dataset into separate groups by thinning treatment, geographical location or tree social status, as the predictions were not improved. For divisions based on thinning treatment or north/south location, the adjusted R^2 -values remained fairly similar (0.342-0.389) compared to the model developed on the pooled data (Adj. R^2 0.394) but in the case of tree social class division there was a drastic reduction in the R^2 -values. The latter may indicate

shortcomings in the definition of dominance class in this experiment as it was based on an index between-tree DBH and stand average DBH. These ratios were then divided into quartiles to define the dominance classes in the pooled dataset.

The radial density model of Gardiner et al. (2010) did not predict density accurately at the Benchmarking sites when the original coefficients from the Kershope or Clocaenog site were used. When the model was reparameterised the predictions improved markedly. However, inherent problems in the predictions remained as the model tended to over predict low values of density and under predict high ones. The possibility of developing models for deriving the model coefficients (α -values) from site and tree parameters when the model was used to predict density at new sites was investigated. This was attempted based on the Benchmarking site and tree variables as well as on a smaller subset of sites for which additional tree variables were available. Tree specific α -values from the model reparameterisation were used in this task but the model derived to describe them performed poorly. The range of predicted values remained much smaller than the range of observed values, suggesting a deficiency in the structure of the model. Growth rate (or DBH) influenced the α -values as it was included as a significant explanatory variable in all the models, but the poor predictions indicated that the variables included here were not suited to explain the variation in the α -values. Alternatively, the variables here were not the correct ones as Rozenberg et al. (2001) found that the predictions of ring density from cambial age and ring width were improved by including information of the genetic relatedness in Douglas-fir.

6 Detailed inter-site density study – “The Level II Experiment”

In this chapter the results relating to data collected from the Level II sites are reported apart from the acoustic measurements that will be treated in Chapter 7. Initially, the site characteristics and density data are summarised (6.3). Then, the radial density model studied in the Benchmarking chapter (Chapter 5) was fitted to Level II data first by deriving model coefficients using model developed on entire Benchmarking dataset (6.3.1.1) and then by using felled sites only (6.3.1.2). However, best fits of the radial density model were obtained by reparameterising it (6.3.1.3).

In section 6.3.2 the models developed on Benchmarking data for predicting average density in juvenile (6.3.2.1) or mature (6.3.2.2) part of the cross-section or in the entire stem cross-section (6.3.2.3) were tested. The effects of height and direction were studied in section 6.3.3.

The climate analysis section 6.3.4 first reports the results of the detrending and presents the tree and site chronologies for both sites. In the following sections the climatic relationships at Loch Tummel (6.3.4.1) and Coalburn (6.3.4.2) sites are studied separately. The data were initially screened for climatic variables of interest using correlation analysis with α -level of 0.05 for individual comparisons. These variables were plotted and then the ones that were significant when multiple comparisons were allowed for were selected for further analysis (6.3.4.3).

6.1 Introduction

Ring level density and width information can be used to study the effect of climate on tree growth if the age related trend is removed. This would allow the investigation of annual variations in growth rate and density and their relationship to climate data. Whereas the Benchmarking experiment looked at the influence of site factors and long term average climatic conditions such as (average temperature sum, DAMS-score, average moisture deficit and continentality) this study would establish the connection between annual weather and timber properties. Determination of climatic variables that influence the timber properties is needed to understand what kind of changes might occur in timber

properties of Sitka spruce in future when the effects of climate change become more severe.

For climatic analysis it is crucial to date the tree rings correctly so that they will be related to the climatic data of the corresponding calendar year. In the Benchmarking experiment, reliable dating of the outer year was not achieved in many cases due to problems with the south ends of cores extracted through the whole tree in the north-south direction. Initially, increment core sampling was planned for three sites used in the European-wide Level II experiment as well but to ensure better dating of samples for the climate study it was decided to collect disk samples. These samples were easier to date securely, since part of the pith and bark was present on all of the samples. Furthermore, the disks yielded several samples per tree which allowed comparison between samples. The quality of available climatic data limited the analysis to the Coalburn and Loch Tummel sites.

In addition to pith to bark trend in density and annual climatic variation there might also be variation with height and azimuth (Zobel and van Buijtenen, 1989). This experiment was also used to study these effects and several samples per tree were collected from different heights and samples cut from the disks in four cardinal directions. The collected samples were also used as a test dataset for the models developed on the Benchmarking data.

Stands in the vicinity of Europe-wide Level II forest monitoring network sites were selected for this study. The Level II site network was established to study effects of air pollution and other environmental factors (Durrant, 2000). In the UK there are 4 Level II permanent monitoring plots that grow Sitka spruce; Coalburn, Loch Awe, Loch Tummel and Llynn Brienne. The Coalburn plot was located in the eastern part of the Kielder forest, the Loch Tummel plot on the northern side of Loch Tummel, the Loch Awe plot near Dalavich on the west side of Loch Awe and Llynn Brienne in Wales. The Llynn Brienne site was geographically very distant from the other Level II sites as well as from the areas sampled during the Benchmarking experiment, therefore only Coalburn, Loch Awe and Loch Tummel (Table 6-1) were included in the sampling. There are several years of monitoring data from these sites and since the monitoring started when the forest was already fairly mature the monitoring period covers rings of mature wood (Table 6-2). Monitoring activities at all of the three sites ceased in the spring of 2007. In this PhD project the Level II sampling was included to quantify annual variation in tree growth as well as variation in timber properties within the stems. Trees were sampled from different dominance classes to assess the influence of social status on the timber properties.

Furthermore, the data from the Level II sites was used to test the models developed on Benchmarking data (Chapter 5).

Table 6-1. Elevation and some average climatic parameters for the sampled Level II sites.

	Coalburn	Loch Awe	Loch Tummel
Elevation (m)	290	50	370
Slope	3	5	7
Accumulated temperature sum (AT)*	1122	1375	903
Moisture deficit (MD)*	94	113	43
Windiness score (DAMS)*	16	14	15
Continental index (CONT)*	7	4	6
Mean annual rainfall (mm) **	1200	2200	1500

* Obtained from the ESC, ** Obtained from the Level II monitoring data.

Table 6-2. Parameters sampled at the sites for Level II monitoring. Soil classification from the monitoring documents (Author: T. R. Hutchings).

	Coalburn	Loch Awe	Loch Tummel
Planting year	1974	1971	1969
Monitoring start year	1994	1995	1995
Soil type	Cambic stagnohumic gley	Stagnogley podsol	Ferric podsol (sandy)
Horizons (thickness, cm)	L (3), F (3), H (17), Ah(g) (10), Eg (13), Bg (20), 2B(g) (57)	L (1.5), F (0.5), H (1.5), Ah (8), Bs (31), BCg (15)	L (2.5), F (1.5), Ah1 (30), Ah2 (6), E (23), Bs (41)
Monitored variables (frequency)	<ul style="list-style-type: none"> - Foliar (2 yr) - Soil (10 yr) - Increment (5 yr) - Crown condition (1 yr) - Meteorology - Atm deposition (2 wks) - Air quality (monthly) - Phytopathology (2 wks) - Phenology (2 wks) - Ground flora (3 yr) - Deadwood (3 yr) - Litter fall (2-4 wks) - Soil solution (2 wks)* - Soil minerals (1997) 	<ul style="list-style-type: none"> - Foliar (2 yr) - Soil (10 yr) - Increment (5 yr) - Crown condition (1 yr) - Atm deposition (2 wks) - Phytopathology (2 wks) - Phenology (2 wks) - Ground flora (3 yr) - Deadwood (3 yr) - Soil minerals (1997) 	<ul style="list-style-type: none"> - Foliar (2 yr) - Soil (10 yr) - Increment (5 yr) - Crown condition (1 yr) - Atm deposition (2 wks) - Phytopathology (2 wks) - Phenology (2 wks) - Ground flora (3 yr) - Deadwood (3 yr) - Litter fall (2-4 wks) - Soil solution (2 wks) - Soil minerals (1997)

* only since 2002

6.2 Materials and methods

At each of the study sites 4-5 circular sampling plots with 5.6 m radius were established to collect information on the range of tree sizes. On each plot all trees were measured for diameter at breast height (DBH). The DBH values were used to divide trees into quartiles to determine the size classes to be sampled. Trees were selected from the 3 upper quartiles which represent the dominant, co-dominant and non-dominant classes (Table 6-3). The suppressed quartile was not sampled. Ten trees without any visible defects from each size class were marked for felling. The trees to be felled were selected in the same forest area, well away from the Level II monitoring plots since these plots needed to be conserved for possible reinstating of the monitoring.

Table 6-3. Measurements on the initial site visit and the sample quartiles defined.

	Coalburn	Loch Awe	Loch Tummel
Trees measured	95	83	54
Mean DBH (cm)	23.8 (± 5.58)	25.1 (± 8.49)	32.1 (± 7.95)
Dominant quartile DBH (cm)	32.0 (± 1.79)	36.25 (± 7.85)	38.9 (± 3.71)
Co-dominant quartile DBH (cm)	25.5 (± 0.76)	25.95 (± 1.74)	31.6 (± 1.56)
Non-dominant quartile DBH (cm)	21.2 (± 0.70)	20.72 (± 1.66)	26.6 (± 0.65)

Prior to felling, the trees were marked with a North line to allow identification of compass directions once the tree had been cut. The trees were assessed for stem straightness and stem form as in the benchmarking study (Chapter 5). Furthermore, grain angle was determined from North and South side of the trunk. For this, approximately 5 cm * 5 cm areas at breast height were cleared of bark using a knife (Figure 6-1). The grain angle measurement was based on deviation from the vertical axis as the wood surface was scraped downwards with a needle (Harris, 1989). The trees were also assessed acoustically with the ST300 time of flight tool. The acoustic measurements were only collected from the Coalburn and Loch Awe sites due to unavailability of the tool during the time of sampling at Loch Tummel.

Once the trees were felled, the length, lowest living branch, lowest living whorl and crown width were measured. Stem taper was determined by measuring the diameter of the trunk with callipers at 1 m intervals in North-South and East-West directions until the diameter fell below 7 cm, which corresponds to the smallest size usable for paper production.



Figure 6-1. Tree marked for felling at the Loch Tummel site. A window with bark removed cut at the breast height for grain angle assessment.

Slenderness was calculated as the tree height (m) divided by the DBH (m).

Three disks were cut from the trees; the first at breast height and the others at the same relative heights along the stem depending on the tree length. From a subset of 4 (Loch Tummel) or 5 (Loch Awe and Coalburn) trees from each size class a total of 5 disks were taken.

Additional disks were collected from the middle of the section between the first and second disk and between the second and third disk (Figure 6-2).

Disks would provide samples that contain the pith and outer year which would avoid uncertainties regarding the dating of outer year that could arise when the southern ends of the increment cores collected with the Treco corer were damaged. This occurred when the drill bored through the bark on the south side when the whole diameter was sampled in north-south direction. For this reason the climate analysis was solely carried out on samples derived from disks.

The disks were labelled with directions, site ID, tree number, disk number and disk height. After kiln drying (to decrease moisture content and reduce the growth of mould) the disks were cut into smaller sections extending into each cardinal direction according to a cutting pattern that ensures that a part of the pith will be present in each section (McLean, 2007). The samples were then further processed to 2 mm radial strips with the twin blade saw and analysed for density and ring width parameters on the ITRAX X-ray densitometer (Cox Analytical). Images were then analysed in WinDENDRO and the resulting density and tree ring data were analysed in the statistical package R. For tree ring analysis the first and last rings were removed from all the samples as they were often incomplete and only complete rings should be used to investigate relationships between ring density and ring width. Even if the rings were complete the density values would not be comparable since the first ring also includes fibrous material from the pith (McLean, 2007). Furthermore, the highest

variation between two WinDENDRO paths was detected in the first and last rings (McLean, 2007).

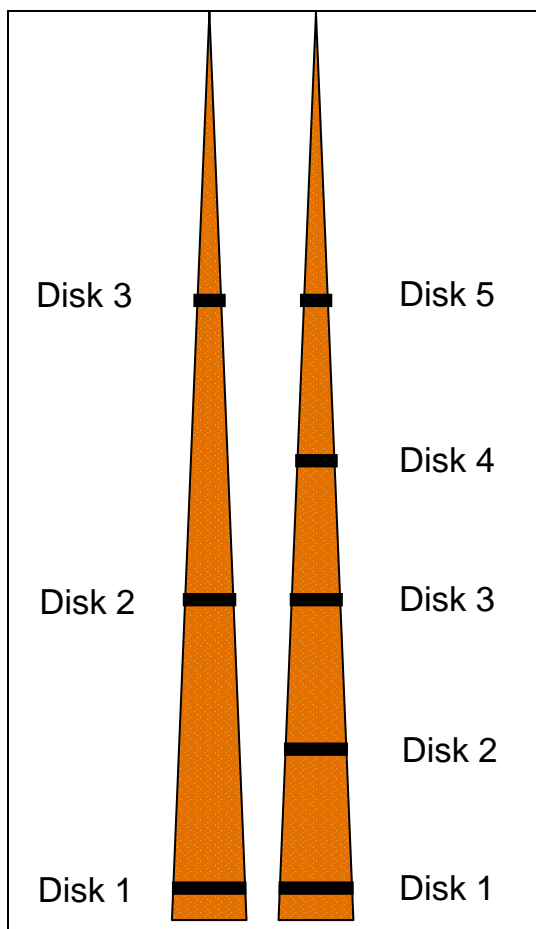


Figure 6-2. Schematic presentation of the locations where disks were extracted from trees with three sample disks (left) and from the subset of trees with five disks (right).

For these plantation sites, the planting year and hence the expected age, at breast height where the climatic samples were taken, were known. Also, the date of the outer ring was known since the samples were collected from live trees. Furthermore, these were young vigorously growing trees with ring widths of several millimetres. Therefore, the series were very unlikely to contain missing rings and the rings were dated counting backwards from the outer ring. The four radii from a given sample tree were carefully matched and any difficulties in defining rings near the pith, where bands of

severe compression wood were occasionally observed, were resolved in this way. The more traditional dendrochronology methods such as COFECHA software that are commonly used to validate tree ring dating was found unsuited due to restricted chronology lengths. Yamaguchi (1991) suggested that for samples from living trees the investigation of pointer years would be sufficient. This techniques involves identifying unusually narrow tree rings in different chronologies and using them to validate the dating.

The data from the four directions within the tree were averaged and the chronologies were then detrended using a spline function in the dplR package (Bunn, 2008). Spline functions can follow the trends in the data better since the curve is defined piecewise (Cook and Peters, 1981) and hence constitutes a good detrending method. The flexibility of the spline defines who closely it will follow the data points and hence how much of the trends it will remove. Here, the default rigidity, 0.67 of the series length (Bunn, 2008) was applied. Individual tree chronologies of different ring width and density indices were then averaged to obtain site chronologies. This was done by deriving robust bi-weight means of

prewhitened individual chronologies (Bunn, 2008). Calculating a robust bi-weight mean reduces the influence of potential outliers and prewhitening removes any remaining autocorrelation from the chronologies.

The correlation between-site chronologies and climate were investigated. This was done using multiple pairwise correlations, cross correlograms and autocorrelation plots. There were 57 climatic variables in total that were screened using these methods, therefore adjusted α' -levels to achieve an overall α -value of 0.05 were calculated according to Curtin and Schulz (1998). These included the very conservative Bonferroni correction (Equation 8) and a less stringent correction (Equation 9). Both of these corrections define a new limit value to significance (α') for the individual comparisons to achieve a given α -value (here 0.05) in over all. The new limit is derived using the number of comparisons carried out (k).

Equation 8

$$\alpha' = \text{Overall-}\alpha / k$$

Equation 9

$$\alpha' = 1 - (1 - \text{Overall-}\alpha)^{1/k}$$

MIDAS weather data (UK Meteorological Office, 2009) was collected from the nearest weather stations (Table 6-4). In the case of Loch Awe only an incomplete record covering the period from 1985-2007 was available. The data included observations of minimum and maximum daily temperature and the rainfall accumulated during the day of observation. Due to the limited range of weather data and the frequency of missing values in the Lochgilphead station data, only Coalburn and Loch Tummel sites were used in the climate analysis. Where there were any missing values they were interpolated by averaging the values of surrounding months of the same calendar year.

Table 6-4. Weather stations used in the Level II climatic effect study.

	Coalburn	Loch Awe	Loch Tummel
Station name	Kielder Castle	Lochgilphead	Faskally
Station number	289	915	214
Recording period start	1961	1985	1961
Recording period end	Current	Current	Current

The data were used to calculate monthly rainfall and degree days. Degrees days were calculated according to Equation 10 where the selected base temperature was 5°C. The daily values were then summed over the growing season which was defined as from

beginning of April to the end of September, or different parts of the growing season, or over the whole calendar year. Furthermore, the total number of days exceeding the 5 °C base temperature were counted (Equation 10) for each month, the growing season and the calendar year using daily maximum and minimum temperatures as input.

Equation 10

$$\text{Deg. Day} = (\text{Temp}_{\text{Max}} + \text{Temp}_{\text{Min}}) / 2 - 5$$

Due to time restrictions sample, processing was started from the breast height disks which were used to study the effect of climate as well as acoustic velocity in the radius (Chapter 7). To look at the influence of height at the Loch Tummel site an undergraduate student, Graeme Johnstone analysed samples from four dominant and non-dominant trees. For Coalburn site a visiting student, Chanisa Maneekul carried out a similar project. Results from these X-ray density scans and the related WinDENDRO analyses are processed further here to quantify the within-tree variation.

In addition to these tasks, the Level II density data were used to test the model developed in Chapter 5 to predict model coefficients based on site and tree factors and fit a radial density model (Gardiner et al., 2010) to new sites.

6.3 Results

The stand and tree ring characteristics for the three Level II sites were summarised in Table 6-5 and Table 6-6. There were marked differences between the sites in terms of tree size. In particular, the Loch Tummel site had the largest DBH and tree volumes. However, the trees at Loch Tummel site were also some years older and this site had been thinned which will have removed some of the more suppressed individuals. In terms of mean ring width (Table 6-6) there was not much difference between the Loch Awe and Loch Tummel sites. The ring density curve for the Coalburn site (Figure 6-3) had a much steeper initial decline in density compared to the other two sites.

Table 6-5. Average stand characteristics for each site with standard deviation in the brackets

Variable	Coalburn	Loch Awe	Loch Tummel
DBH (cm)	26.1 (± 4.56)	27.1 (± 5.97)	32.2 (± 5.50)
Height (m)	19.6 (± 1.41)	24.9 (± 3.27)	26.0 (± 1.64)
Age (yr)	29 (± 1.39)	30 (± 2.18)	34 (± 1.16)
Slenderness (m/m)	77 (± 9.94)	94 (± 15.43)	82 (± 9.08)
Lowest living branch (m)	10.5 (± 1.20)	11.5 (± 3.15)	9.9 (± 1.65)
Lowest living whorl (m)	11.6 (± 1.03)	14.1 (± 2.64)	12.2 (± 2.08)
Crown volume (m ³)	20.7 (± 9.39)	54.7 (± 45.45)	92.1 (± 60.90)
Tree volume (m ³)	0.44 (± 0.18)	0.66 (± 0.51)	0.98 (± 0.37)
ST300 velocity (m/s)	3.50 (± 0.35)	3.95 (± 0.47)	NA
ST300 MoE (GPa)	12.36 (± 2.42)	15.84 (± 3.74)	NA
Average grain angle (degrees)	2.28 (± 2.67)	0.89 (± 2.46)	1.97 (± 1.36)
Stem straightness	2 (± 1.77)	3 (± 2.12)	4 (± 2.00)
Area-weighted density (kg/m ³) MC 4 %	392 (± 29.4)	407 (± 34.7)	409 (± 40.3)
Area-weighted density (kg/m ³) MC 12 %	413 (± 30.3)	428 (± 35.6)	430 (± 41.4)
Average growing season T sum (period)*	1065 (1979-2006)	NA	1255 (1973-2006)
Average Annual T sum (period)*	1248 (1979-2006)	NA	1472 (1973-2006)
Annual Average Rainfall (mm)*	1385 (1979-2006)	NA	920 (1973-2006)

* Calculated from the MIDAS weather data

** From the Level II monitoring data

Table 6-6. Summary of average tree ring variables for the studied sites (standard deviation). Density and width reported at 4% MC.

	RW	EWV	LWW	LW%	RD	EWD	LWD	MaxD	MinD
Coalburn									
Dominant	4.98 (± 2.38)	3.95 (± 2.23)	1.02 (± 0.61)	23 (± 11.7)	396 (± 67.9)	343 (± 65.8)	569 (± 81.9)	664 (± 90.0)	277 (± 61.7)
Co-dominant	3.99 (± 2.39)	3.09 (± 2.19)	0.90 (± 0.52)	27 (± 11.5)	421 (± 72.8)	354 (± 72.2)	609 (± 73.0)	708 (± 77.3)	282 (± 67.9)
Non-Dominant	3.56 (± 2.24)	2.74 (± 2.00)	0.82 (± 0.52)	27 (± 11.6)	435 (± 77.7)	369 (± 77.0)	613 (± 75.4)	708 (± 79.3)	299 (± 74.3)
Mean	4.18 (± 2.41)	3.26 (± 2.21)	0.92 (± 0.56)	26 (± 11.7)	417 (± 74.6)	355 (± 72.5)	597 (± 79.2)	693 (± 84.9)	286 (± 68.7)
Loch Awe									
Dominant	5.40 (± 2.31)	4.45 (± 2.18)	0.95 (± 0.44)	20 (± 9.6)	401 (± 56.8)	355 (± 49.9)	583 (± 74.3)	685 (± 82.2)	281 (± 44.5)
Co-dominant	3.88 (± 2.14)	3.05 (± 1.99)	0.84 (± 0.38)	26 (± 12.2)	429 (± 60.3)	367 (± 55.3)	602 (± 64.5)	702 (± 70.4)	292 (± 57.0)
Non-Dominant	3.36 (± 1.90)	2.61 (± 1.73)	0.75 (± 0.37)	27 (± 11.7)	445 (± 62.0)	385 (± 56.3)	611 (± 70.3)	705 (± 78.9)	310 (± 55.3)
Mean	4.28 (± 2.31)	3.43 (± 2.14)	0.85 (± 0.41)	24 (± 11.6)	424 (± 62.3)	368 (± 55.1)	597 (± 70.9)	697 (± 77.9)	294 (± 53.5)
Loch Tummel									
Dominant	5.27 (± 1.61)	4.18 (± 1.44)	1.08 (± 0.56)	21 (± 9.1)	402 (± 68.8)	348 (± 66.4)	606 (± 77.4)	715 (± 80.7)	278 (± 61.4)
Co-dominant	4.26 (± 1.62)	3.31 (± 1.50)	0.96 (± 0.46)	24 (± 9.7)	421 (± 60.0)	354 (± 57.8)	630 (± 72.2)	734 (± 78.1)	284 (± 54.7)
Non-Dominant	3.52 (± 1.56)	2.64 (± 1.42)	0.88 (± 0.39)	27 (± 10.4)	461 (± 62.9)	383 (± 60.0)	664 (± 74.2)	769 (± 78.7)	307 (± 56.0)
Mean	4.32 (± 1.75)	3.35 (± 1.59)	0.97 (± 0.48)	24 (± 10.1)	429 (± 68.6)	362 (± 63.4)	634 (± 78.3)	740 (± 82.2)	290 (± 58.7)

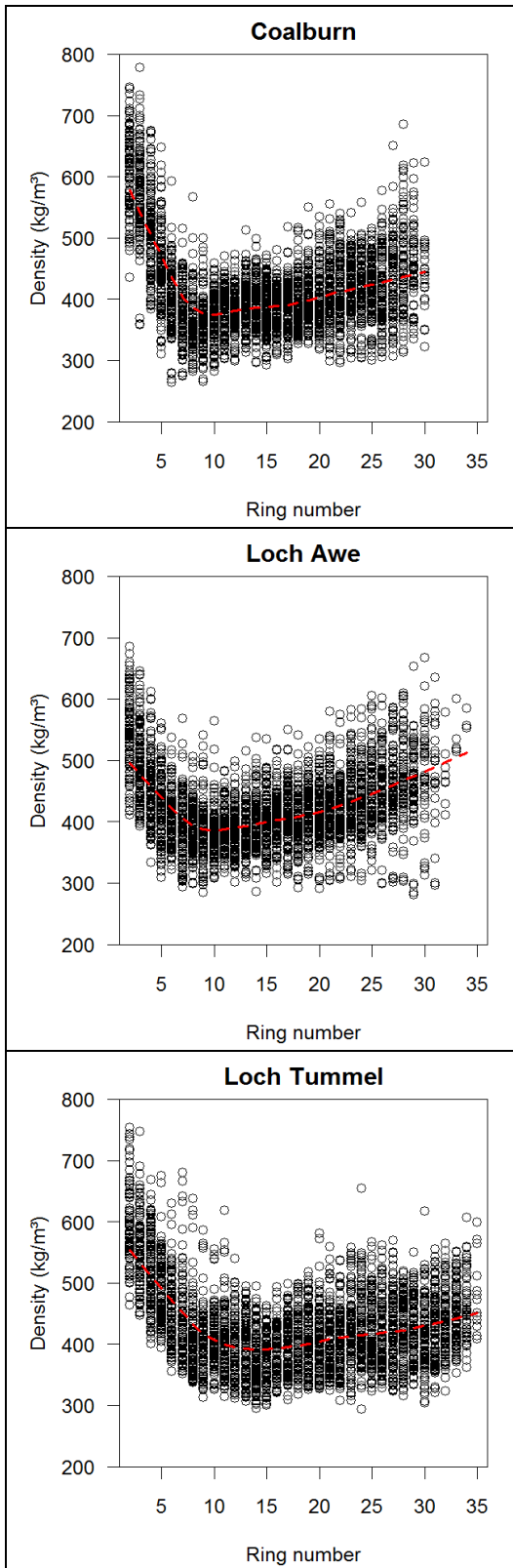


Figure 6-3. Radial density curves for the Level II sites.

6.3.1 Fitting the radial density model

In Chapter 5, the radial density model of Gardiner et al. (2010) was tested and models developed to predict site specific coefficients and thus to improve radial density predictions at different sites. These sub-models were tested on the Level II data.

6.3.1.1 Deriving coefficients using models from Benchmarking sites

The models developed to predict α -values for the radial density model (Table 6-7) were applied to derive site specific α -values for each of the Level II sites. Coalburn and Loch Awe sites had not been thinned and therefore the alpha models for unthinned sites were used to predict the coefficients. Loch Tummel site had been thinned.

Table 6-7. Model prediction the α -values for radial density model derived on the original Benchmarking data.

α_1			
ALL DATA			
0.2486 - 0.0039*DBH10yr + 0.0644*SiteMeanSS + 0.0888*CONT			
THINNED			
1.0903 - 0.0045*DBH10yr			
UNTHINNED			
-0.2056 - 0.0038*DBH10yr + 0.0092*RingCount + 0.1074*CONT + 0.0758*SiteMeanSS			
α_2			
ALL DATA			
0.4041290 + 0.0000512*AT - 0.0094842*Growth Rate + 0.0000079 *OrigStock + -0.0019412*Site Mean Ht			
THINNED			
0.3824268 + 0.0002716*MD - 0.0090861*Growth Rate + 0.0000099 *OrigStock			
UNTHINNED			
0.4066 - 0.00017*Easting + 0.000067*AT - 0.0078*Growth Rate - 0.0044*SS + 0.0034*SiteAveRC - 0.0044*Site Mean Ht			
α_3			
ALL DATA			
-0.0157 + 0.0168*Growth Rate + 0.0047*SS			
THINNED			
-0.0210 + 0.0194*Growth Rate			
UNTHINNED			
0.0023 + 0.00049*DBH + 0.0049*SS			

Table 6-8. The α -values predicted for the Level II sites using the models developed on Benchmarking data and the original Clocaenog and Kershope values. Standard deviation in brackets.

	α_1	α_2	α_3
Coalburn (all data)	0.5443 (± 0.056)	0.4990 (NA)	0.1432 (± 0.027)
Coalburn (unthinned)	0.5256 (± 0.053)	0.3635 (± 0.011)	0.1409 (± 0.025)
Loch Awe (all data)	0.3556 (± 0.093)	0.5175 (NA)	0.1491 (± 0.037)
Loch Awe (unthinned)	0.2999 (± 0.089)	0.3894 (± 0.015)	0.1499 (± 0.025)
Loch Tummel (all data)	0.6618 (± 0.072)	0.4769 (NA)	0.1616 (± 0.027)
Loch Tummel (thinned)	0.6477 (± 0.083)	0.3495 (± 0.015)	0.1614 (± 0.032)
Original coef (Clocaenog)	0.6629 (± 0.023)	0.3288 (± 0.003)	0.1377 (± 0.008)
Original coef (Kershope)	0.5831 (± 0.015)	0.3043 (± 0.002)	0.1767 (± 0.006)

The coefficients (Table 6-8) were then used in the ring density model (Equation 6, p. 136) to make predictions for the three Level II sites.

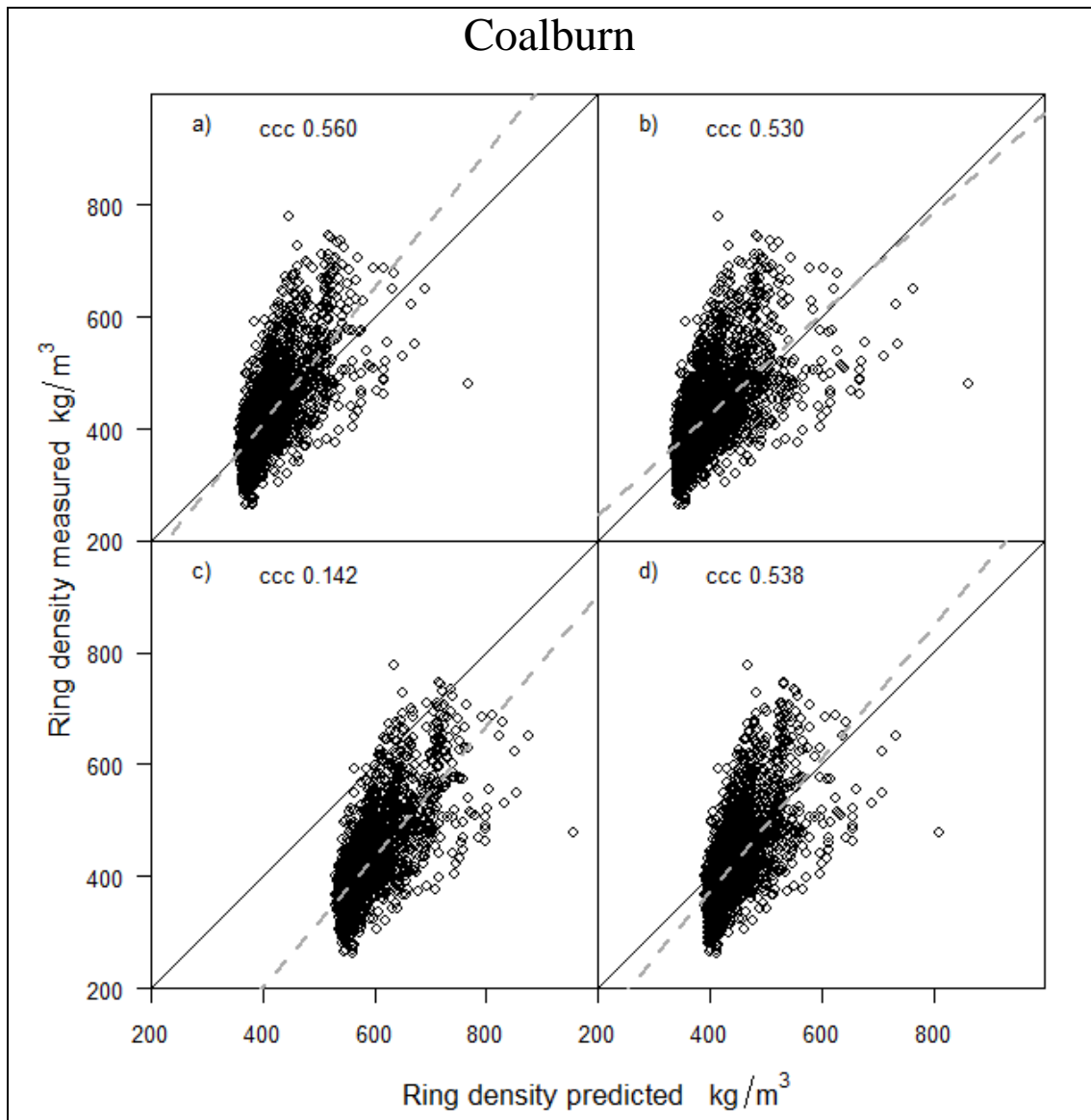


Figure 6-4. Ring density model predictions for the Coalburn site using a) Clocaenog coefficients, b) Kershope coefficients, c) coefficients derived using the model based on the pooled Benchmarking data and d) using coefficients derived using a model developed for unthinned sites using the Benchmarking data. Dashed grey line is the regression line fitted to the data and ccc denotes the concordance correlation coefficient.

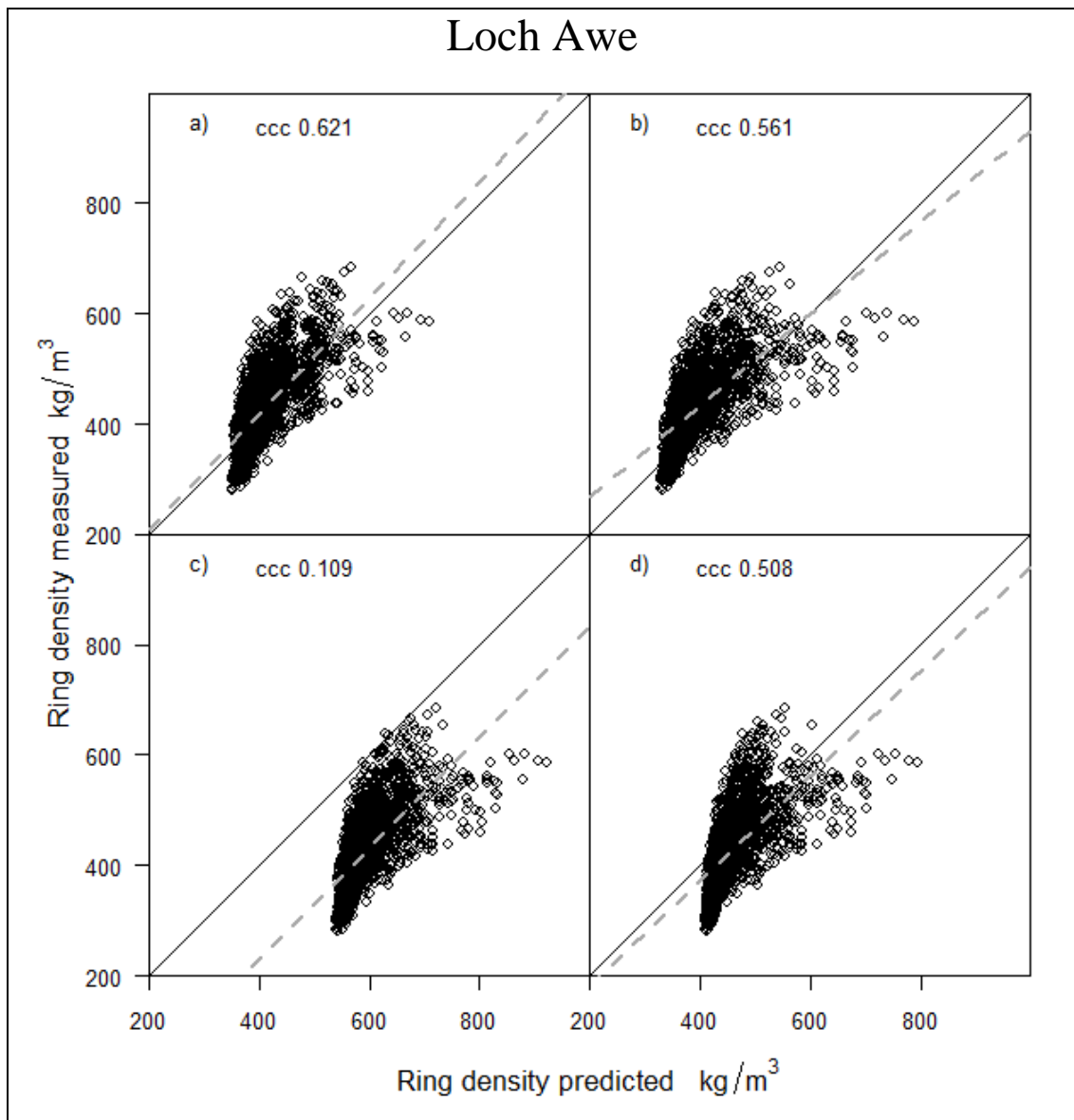


Figure 6-5. Ring density model predictions for the Loch Awe site using a) Clocaenog coefficients, b) Kershope coefficients, c) coefficients derived using the model based on the pooled Benchmarking data and d) using coefficients derived using a model developed for unthinned sites using the Benchmarking data. Dashed grey line is the regression line fitted to the data and ccc denotes the concordance correlation coefficient.

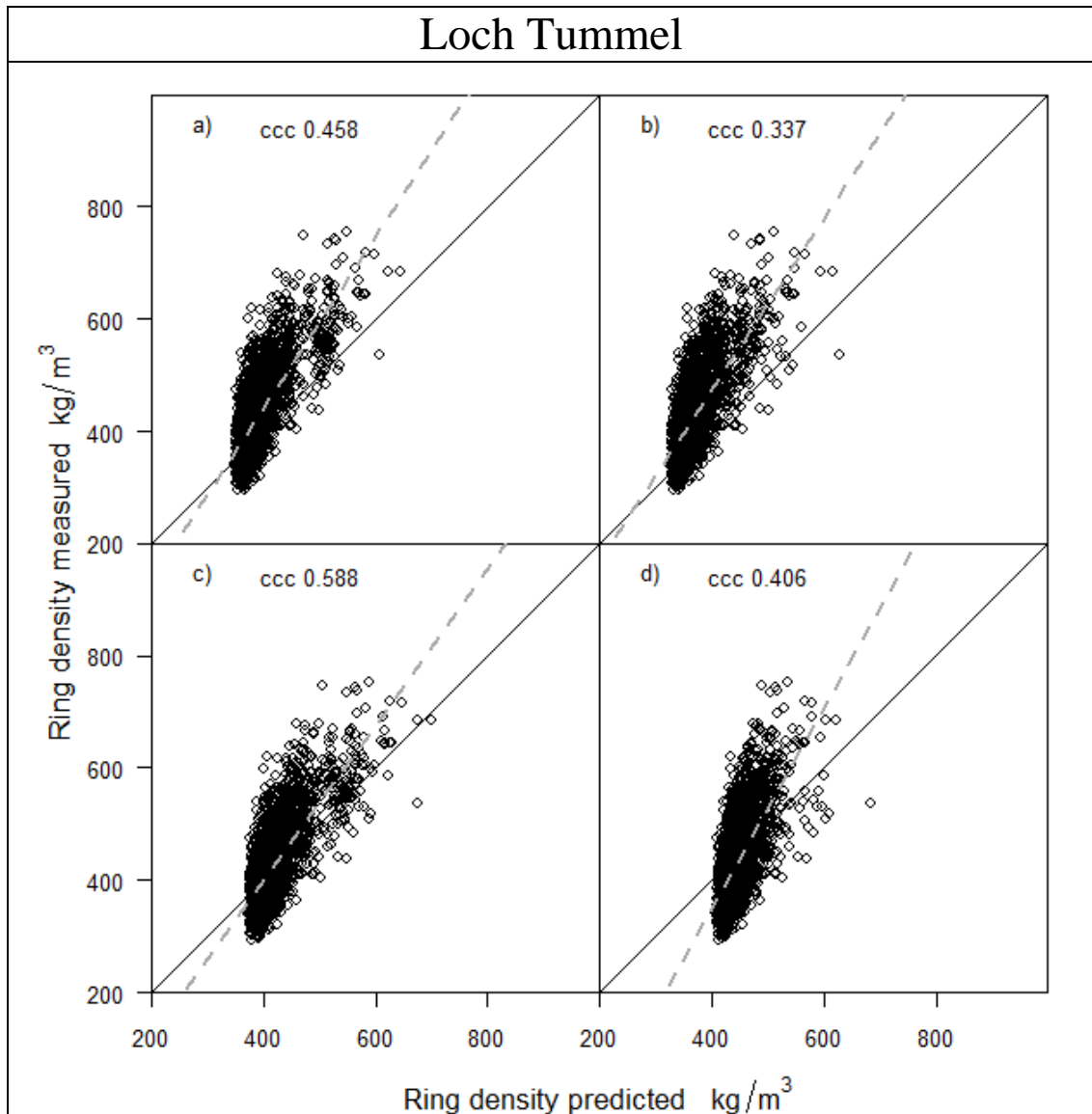


Figure 6-6. Ring density model predictions for the Loch Tummel site using a) Clocaenog coefficients, b) Kershope coefficients, c) coefficients derived using the model based on the pooled Benchmarking data and d) using coefficients derived using a model developed for thinned sites using the Benchmarking data. Dashed grey line is the regression line fitted to the data and ccc denotes the concordance correlation coefficient.

Predicting site specific α -values was not successful as the predictions did not improve compared to using the original model coefficients (Figure 6-4, Figure 6-5 and Figure 6-6). The predictions derived using models based on the pooled Benchmarking data to derive site specific alpha values for the model yielded predictions that were much worse than those obtained by using the original Clocaenog coefficients in the case of Coalburn and Loch Awe. In the case of Loch Tummel, the prediction using sub-models based on the pooled Benchmarking data to derive alpha values for the density prediction yielded slightly better predictions (ccc 0.588) than when using Clocaenog (ccc 0.458) or Kershope (ccc 0.337) coefficients in the model. Using sub-models developed for thinned or unthinned sites brought about no improvement in comparison to using Clocaenog coefficients. In the

cases of Coalburn and Loch Tummel sites, using unthinned and thinned models, respectively, to derive α -values improved the predictions in comparison to Kershope coefficients.

6.3.1.2 Deriving coefficients with models from felled Benchmarking sites

A second attempt to predict density with site specific α -values was carried out using the sub-models built on the data from felled Benchmarking sites where additional tree variables such as height and crown dimensions existed. However, only one of these additional variables remained as a significant explanatory variable in the models. This was tree height in α_3 model (Table 6-9). Since the contribution of the additional parameters was so limited the expected improvement was likely to remain low.

Table 6-9. Models to predict α -values derived using data from felled Benchmarking sites.

α_1	$0.1042 - 0.0686 * \text{Growth Rate} + 0.0004 * \text{OrigStock}$
α_2	$0.3573 + 0.00008 * \text{AT} - 0.0098 * \text{Growth Rate}$
α_3	$-0.2852 + 0.0286 * \text{GrowthRate} + 0.0085 * \text{HT}$

AT = accumulated temperature sum

The derived sub-models were used to calculate site specific alpha values (Table 6-10) which then were used in the radial density model (Equation 6, p. 136) to predict ring densities (Figure 6-7).

Table 6-10. Values of the radial density model coefficients based on the models built on the data from felled Benchmarking sites for the three Level II sites.

	α_1	α_2	α_3
Coalburn	0.5725 (± 0.096)	0.3604 (± 0.014)	0.1341 (± 0.048)
Loch Awe	0.7306 (± 0.129)	0.3794 (± 0.018)	0.1826 (± 0.071)
Loch Tummel	1.1763 (± 0.112)	0.3372 (± 0.016)	0.2050 (± 0.059)

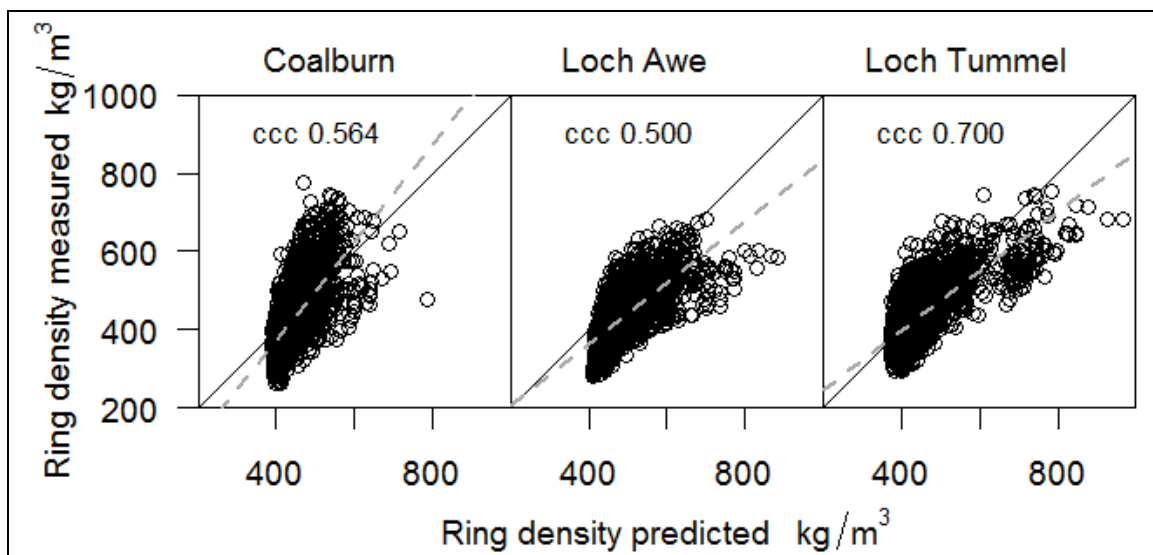


Figure 6-7. Ring density model predictions when using sub-models from felled Benchmarking sites to derive site specific model coefficients. Dashed grey line is the regression line fitted to the data and ccc notes the concordance correlation coefficient between the measured and predicted densities.

In the case of Loch Tummel, using the sub-models from felled Benchmarking sites to derive the coefficients (α -values) for the radial density models did improve the predictions (Figure 6-7) but for Coalburn and Loch Awe sites there was no improvement compared to the models used in the previous section. The benefit of using site specific α -values values was likely to be limited since a large percentage of the variation was between-trees within the site.

6.3.1.3 Reparameterising the radial density model

It was concluded that deriving improved α -values using the model developed on the Benchmarking data was unhelpful in improving the radial density predictions. The radial density model was reparameterised using non-linear least squares (nls) to fit the model (R Development Core Team, 2007). New starting values for the coefficients were derived to predict density in kg/m^3 directly instead of specific gravity as in the original model. The model fitting was done separately for each of the sites. This fit defined individual set of coefficients for each tree.

The explanatory power of the model was investigated by using an adapted S-plus code to derive coefficients of determination for the fixed effects and the fit as a whole (S-plus code written by Sean M. Garber and edited by John R Moore (Napier University, Edinburgh) to be used in R). After the estimates of starting values were refined with nls, the model was

fitted with non-linear mixed effects, nlme, (Pinheiro et al., 2008). Different random effects structures were tested by letting either all α -values or different pairs vary randomly. The model with α_1 and α_2 varying randomly was selected. Weights were added to adjust any deviations in the variance. Different autocorrelation structures were tested since density follows a pattern from pith to bark. Adding an autocorrelation structure improved the model significantly and successfully removed autocorrelation (Figure 6-8). The autoregressive moving average (ARMA) model for autocorrelation was found to be the most suited one to be used in the model. After the addition of ARMA autocorrelation structure, the random components in the α -values were reassessed and it was found the letting all the α -values vary randomly improved the model. The model development was initially done for the Coalburn site and then the same model fitted to the Loch Awe and Loch Tummel sites.

The mean α -values for each site are reported in Table 6-11. These values have been adjusted to predict density directly in kg/m^3 and therefore differ from previous sections (Table 6-10). The R^2 -values for the model (Figure 6-10) varied between the sites from 0.48-0.56 for the fixed effects and 0.66-0.75 when random effects of tree were included. From the diagnostic plots it was visible that the residuals were not normally distributed for any of the sites. The mean absolute error varied from approximately 35-40 kg/m^3 depending on the site (Table 6-12).

Table 6-11. The mean α -values of radial density model reparameterised on the Level II data. The model was fitted to each site individually. The α -values have been adjusted to predict density directly as kg/m^3

	α_1	α_2	α_3
Coalburn	1.0150	324.93	149.67
Loch Awe	0.7181	344.54	163.12
Loch Tummel	0.7060	362.78	164.88

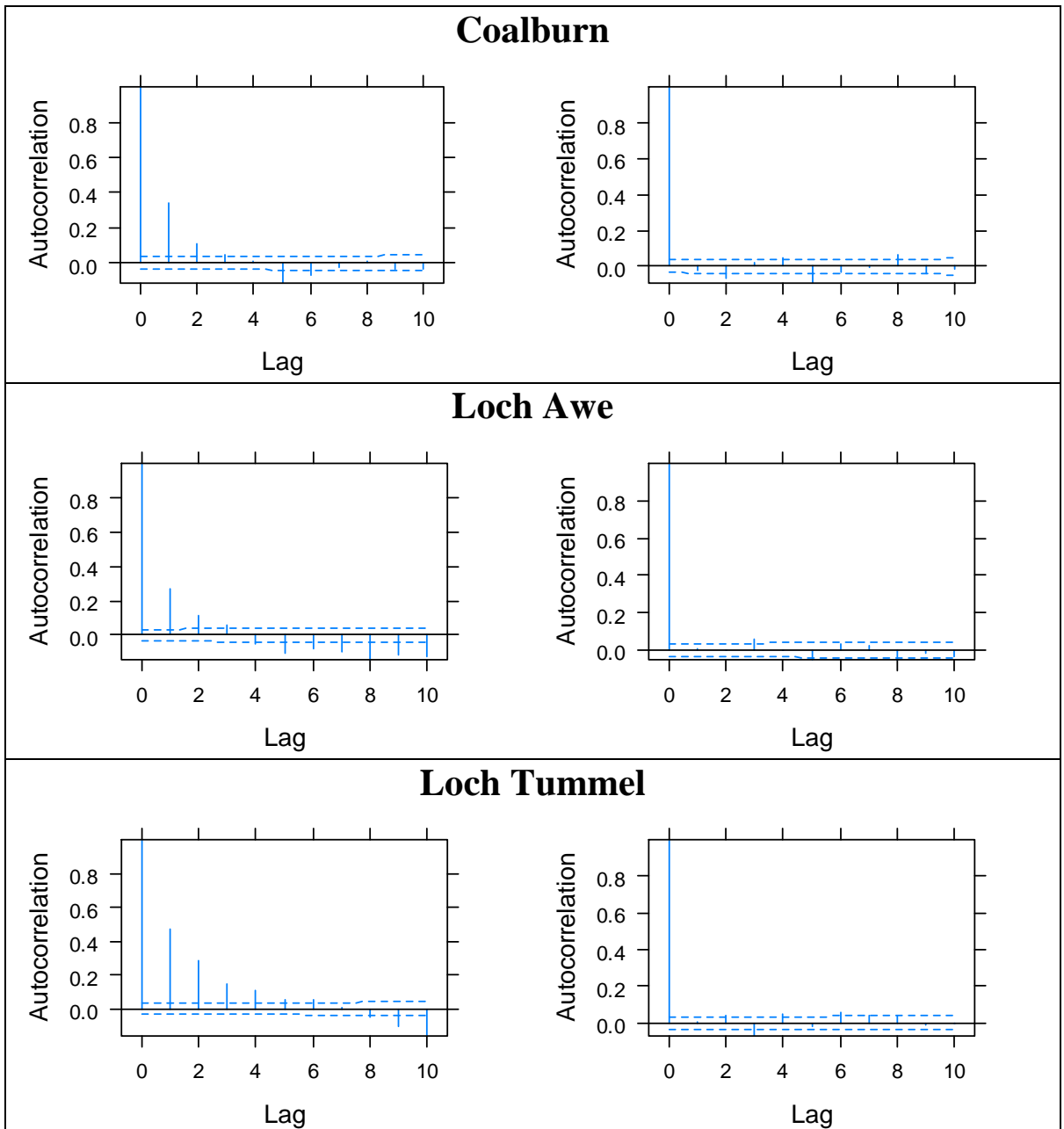


Figure 6-8. Autocorrelation in the ring density data from the three Level II sites prior to fitting an autocorrelation function (left) and once ARMA autocorrelation function was added (right). The dashed line marks the level of significance (0.05).

When the residuals were plotted against ring number or ring width (Figure 6-9), clear trends were observed. First of all, the model was not entirely successful in describing the pith to bark behaviour of the density since the characteristic shape of Sitka spruce density curve was still identifiable in the residuals. The problem was most pronounced for the Coalburn and Loch Tummel sites. In the case of Loch Awe there was only a very slight trend. With ring width all of the sites showed a similar trend in which the model was overestimating the density of widest rings.

Table 6-12. Bias in different levels of the selected final radial density model with weights and ARMA autocorrelation structure added. The model was fitted separately to each site.

	Fixed effects	Tree random effects	Sample random effects
Mean absolute error			
Coalburn	36.77	28.45	26.24
Loch Awe	34.54	23.56	22.63
Loch Tummel	39.57	31.43	31.43
RMSE			
Coalburn	48.97	38.42	35.66
Loch Awe	44.87	30.91	29.45
Loch Tummel	49.11	39.73	39.73
% residuals			
Coalburn	8.81	6.82	6.29
Loch Awe	8.15	5.56	5.34
Loch Tummel	9.23	7.33	7.33

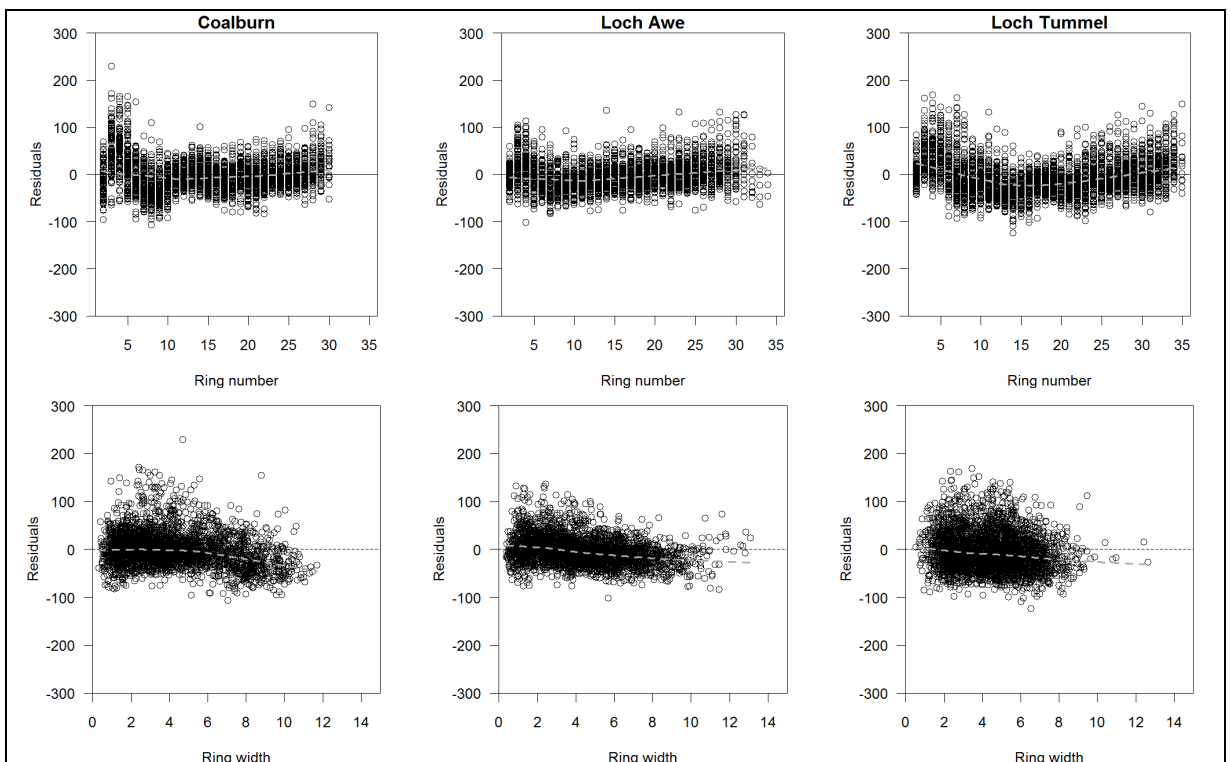


Figure 6-9. Model residuals (kg/m^3) plotted against ring number (top) and ring width (bottom).

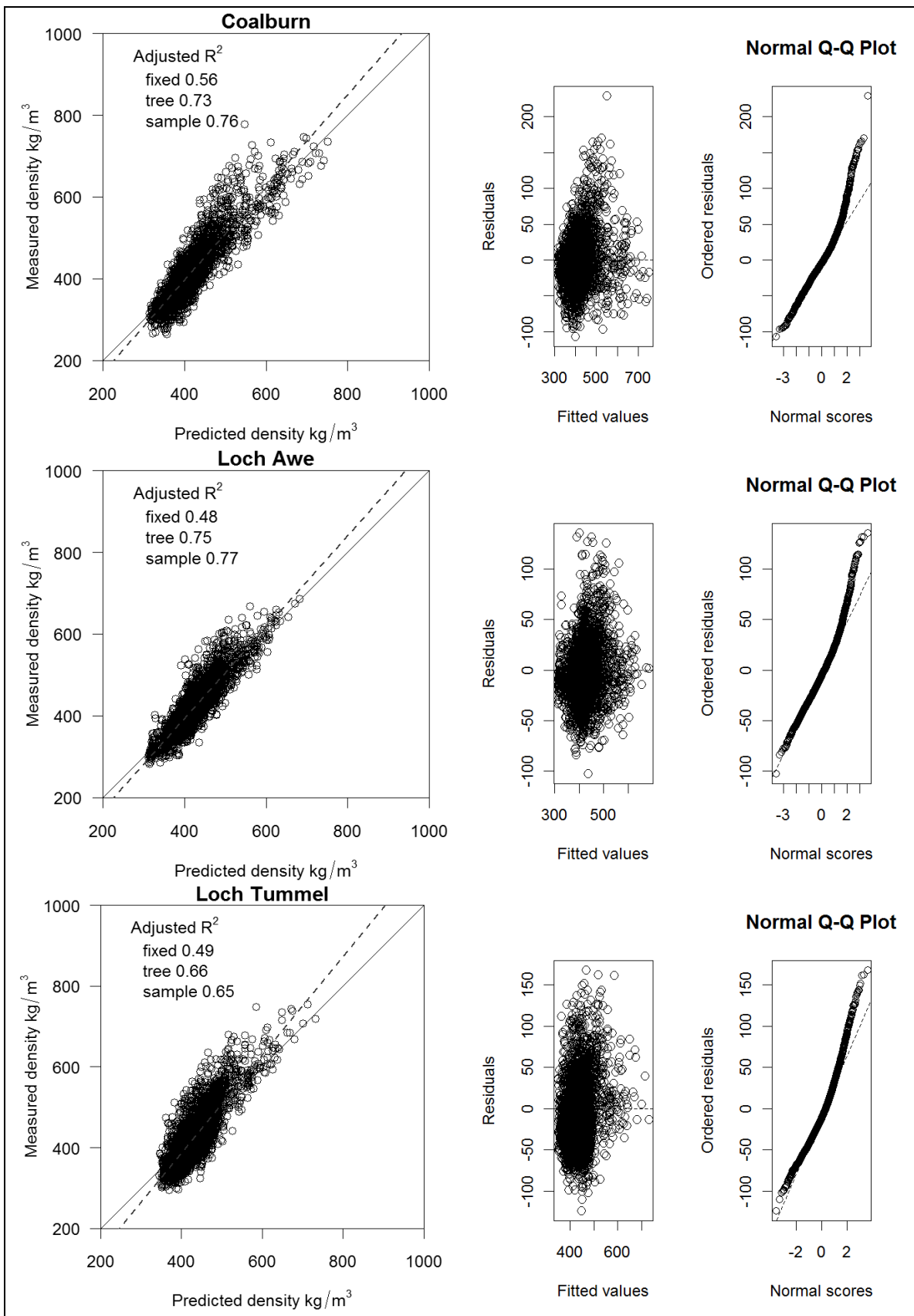


Figure 6-10. Radial density model predictions plotted against the measured values (left) and model diagnostics plots (right) for each of the Level II sites. The radial density model was fitted separately for each site and weights and ARMA autocorrelation structure added.

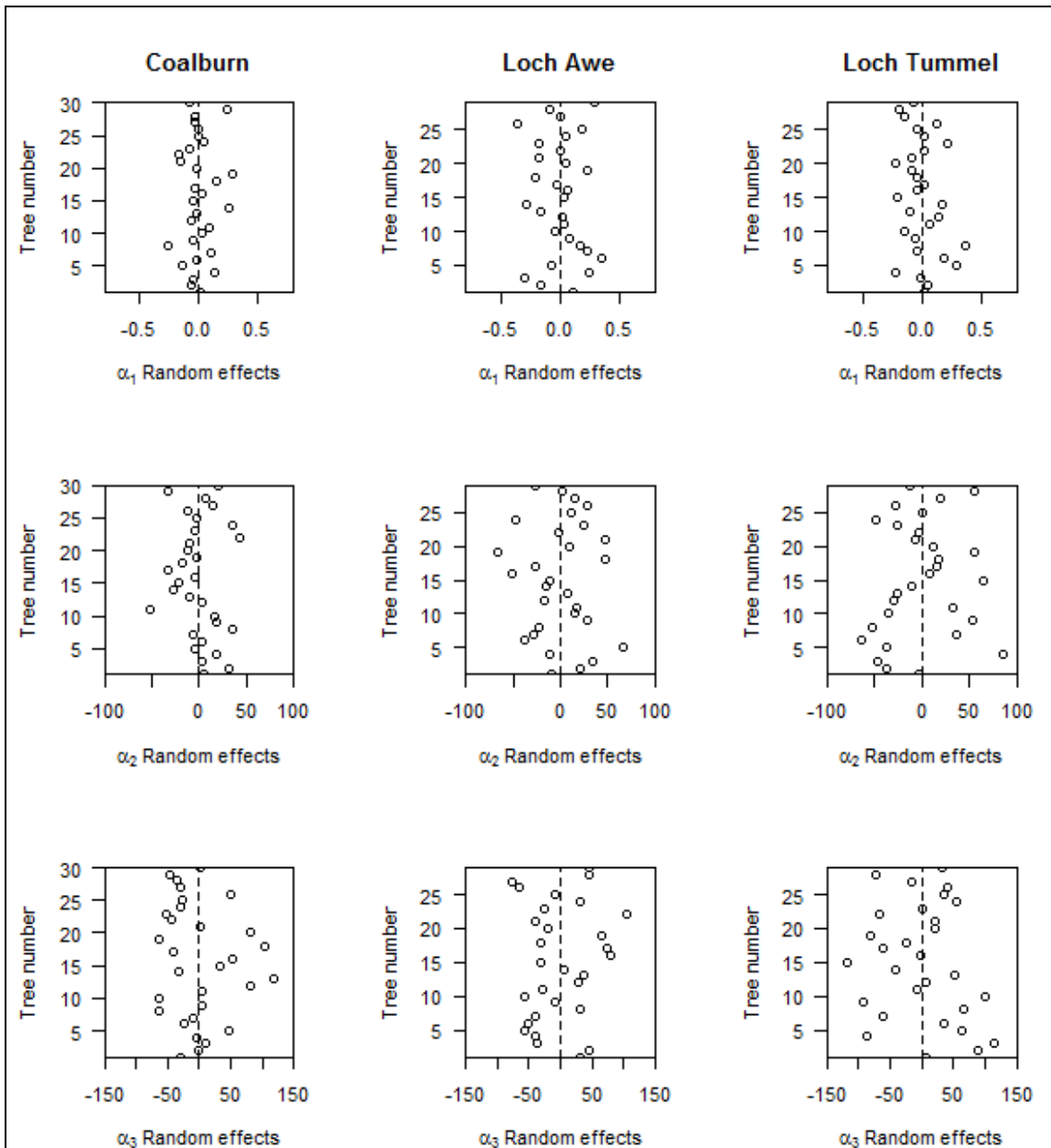


Figure 6-11. Random effect plots for the alpha values at each of the Level II sites. These illustrate how individual trees differ from the site average values for the coefficients.

There was a considerable amount of random between-tree variation in the α -parameters (Figure 6-11). Large differences between-trees will complicate the site level prediction of density curves, as the site level estimates use average values of the α -parameters. This would mean the random effects would need to be quantified for new sites unless the model was improved to explain more of the between-tree variation. It seems that the model equation should be developed further, perhaps to include some tree level variables that might explain some of the between-tree variation in α -parameters.

6.3.2 Testing average density models

In Chapter 5, a series of models predicting the average density in different sections of the radius were developed. The breast height samples from the Level II sites are used in this section to test those models.

6.3.2.1 Juvenile wood density

The model for predicting juvenile wood density, developed for the Benchmarking data (Equation 11) was tested on the Level II data.

Equation 11

$$\text{JW density (kg/m}^3\text{)} = 544.2933 - 1.1923 * \text{Juvenile DBH (mm)}$$

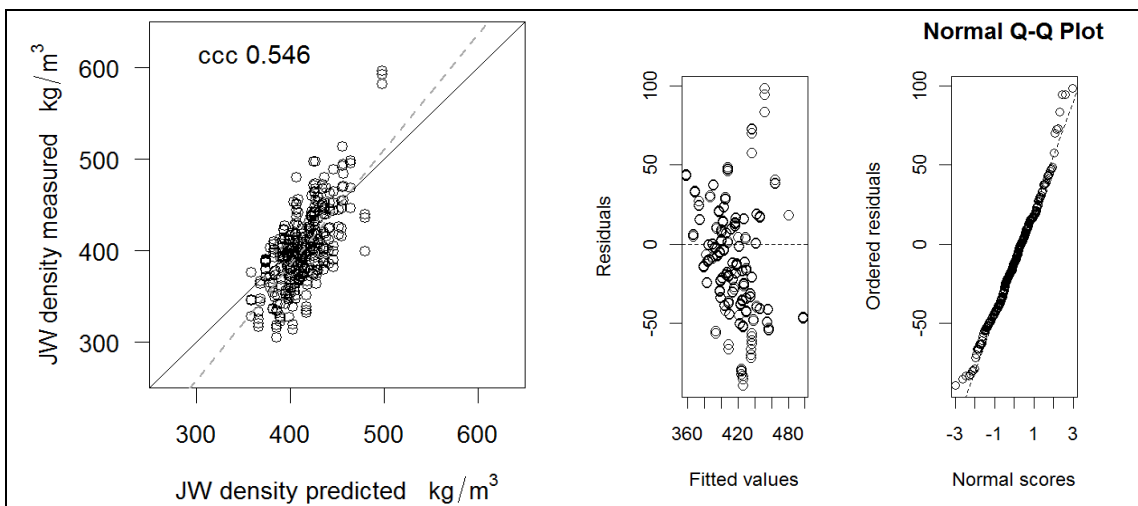


Figure 6-12. The predictions of the average juvenile wood density model derived from the Benchmarking data plotted against the measured values at the level II sites (left) Dashed gray line is the regression line fitted to the data and ccc denotes the concordance correlation coefficient. Model diagnostics plot (right).

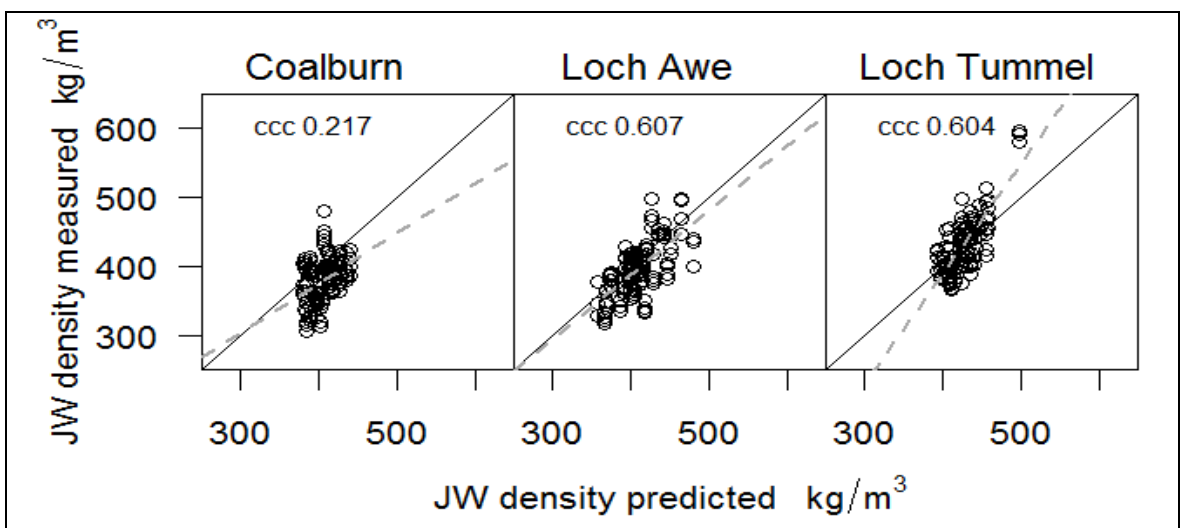


Figure 6-13. Juvenile wood density model predictions against the measured values separately for each of the Level II sites. Dashed gray line is the regression line fitted to the data and ccc denotes the concordance correlation coefficient.

The prediction of juvenile wood density for the pooled Level II sites (Figure 6-12) was relatively successful (ccc 0.546). There were some potential outliers in the higher range of density values which correspond to the different azimuthal directions from a single denser tree. Furthermore, in the lower range of density values there was a tendency for the model to over-predict density as the observations were clustered below the one to one line. When the predictions were separated by site (Figure 6-13) it is evident that the poor fit at lower density range was caused by the Coalburn site. In the case of Loch Awe the values were quite evenly distributed around the one to one line and the regression line closely followed it. The concordance correlation coefficient was fairly high as well, 0.607. Also for Loch Tummel the predictions were fairly good (ccc 0.604), even though the regression line was pulled up by the cluster of potential outliers.

6.3.2.2 Mature wood density

The model developed (Equation 12) on the Benchmarking dataset for predicting mature wood density was tested on the Level II sites.

Equation 12

Mature wood density (kg/m^3) = $448.8620 - 11.3125 * \text{Growth rate (mm/yr)} + 0.0583 * \text{Accumulated T sum}$

Where AT stands for the accumulated temperature sum. This model was used to predict the density on all Level II sites pooled (Figure 6-14) and then at each site in turn (Figure 6-15).

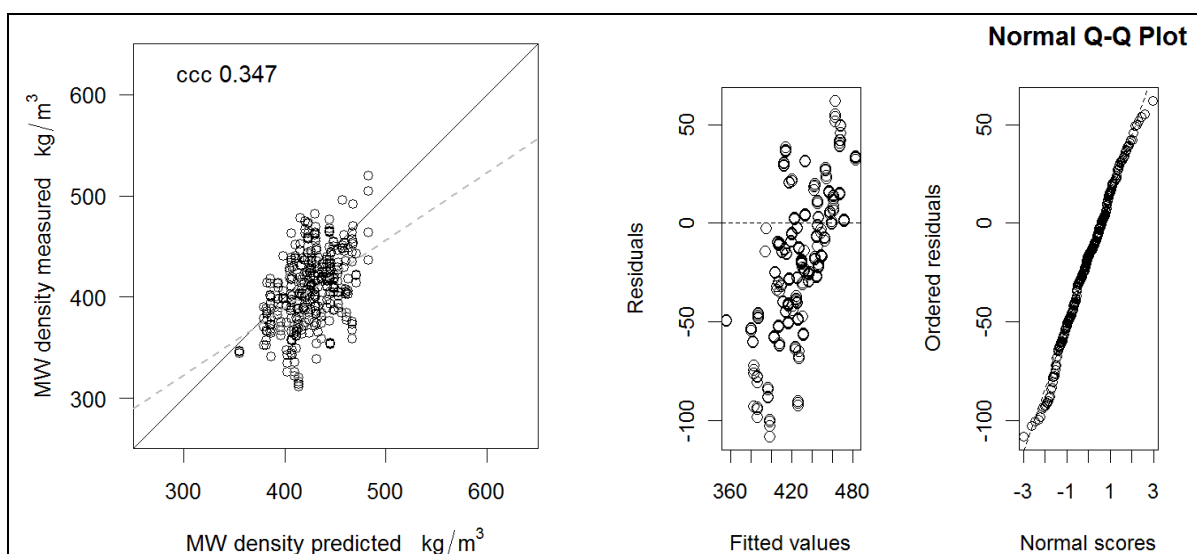


Figure 6-14. The predictions of the average mature wood density model derived from the Benchmarking data plotted against the measured values at the level II sites (left) Dashed gray line is the regression line fitted to the data and ccc denotes the concordance correlation coefficient. Residuals (measured-predicted density) plotted against density (right).

The mature wood density predictions were not very good for Coalburn and Loch Awe as the concordance correlation coefficients obtained had low values, 0.218 and 0.281 respectively. In the case of Loch Tummel the predictions were slightly better (ccc 0.562) and the data were more evenly spread around the one to one line. However, it is apparent from the shape of the data that the model failed to predict accurately the lowest and highest values of density.

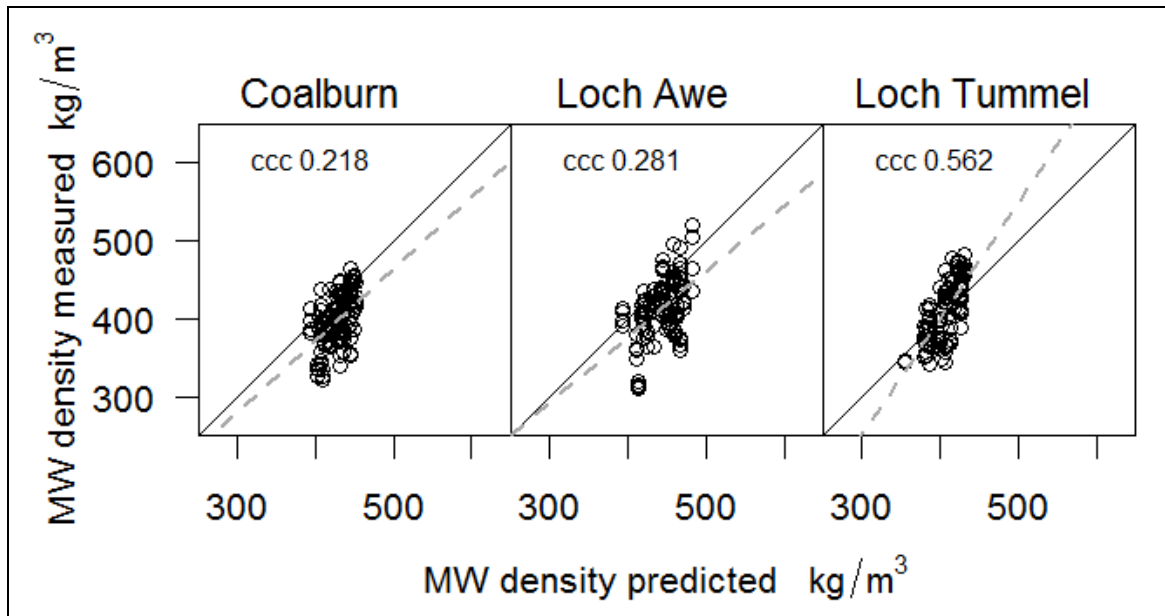


Figure 6-15. Mature wood density model predictions against the measured values, separately for each of the Level II sites. Dashed gray line is the regression line fitted to the data and ccc denotes the concordance correlation coefficient.

6.3.2.3 Cross-section average density

Initially, the general model (Equation 13) developed for predicting cross-section average density was used to predict density values for the pooled data (Figure 6-16) and for each of the Level II sites separately (Figure 6-17).

Equation 13

Cross-section average density (kg/m^3) = $457.6994 - 11.4331 * \text{Growth rate (mm/yr)} + 0.0571 * \text{Accumulated T sum}$

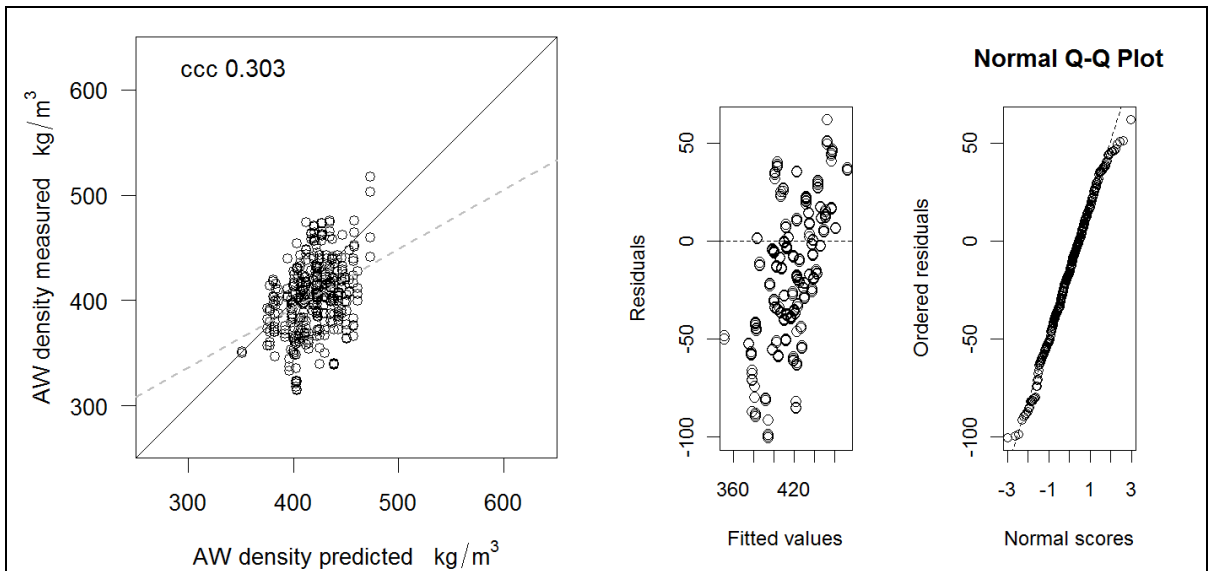


Figure 6-16. The predictions of the cross-section average wood density model derived from the Benchmarking data plotted against the measured values at the level II sites (left). Residuals (measured-predicted density) plotted against density (right).

The model predictions on the pooled data remained fairly poor (Figure 6-16), which seemed to be caused by the particularly poor fits in the case of Coalburn and Loch Awe (Figure 6-17). For the Loch Tummel site on its own, the fits seemed better (ccc 0.571) but the model failed to predict the highest values of density accurately.

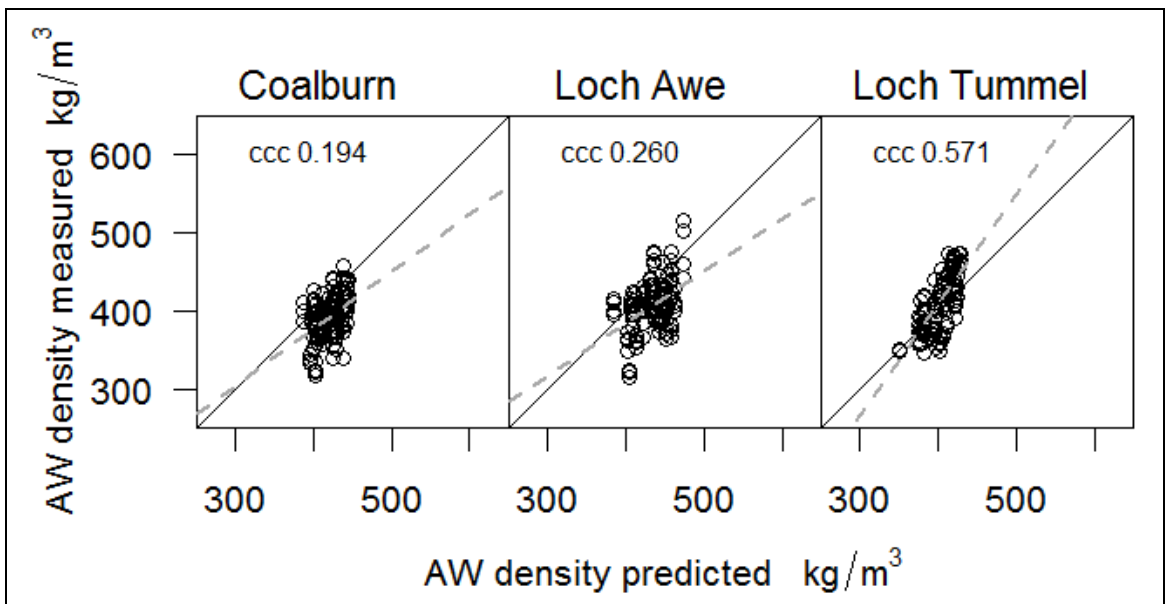


Figure 6-17. Cross-section average wood density model predictions against the measured values separately for each of the Level II sites. Dashed gray line is the regression line fitted to the data and ccc denotes the concordance correlation coefficient.

To see if taking into account the differences in thinning regime would improve the model predictions the models developed for thinned and unthinned sites were tested. For the Coalburn and Loch Awe sites the average density models for unthinned sites were fitted

with the following coefficients derived from the Benchmarking data (Equation 14, Equation 15).

Equation 14

$$\text{Average density}_{\text{unthinned}} \text{ (kg/m}^3\text{)} = 587.5133 - 0.1786 * \text{Easting} - 12.1219 * \text{Growth rate (mm/yr)} - 1.1871 * \text{Slope}$$

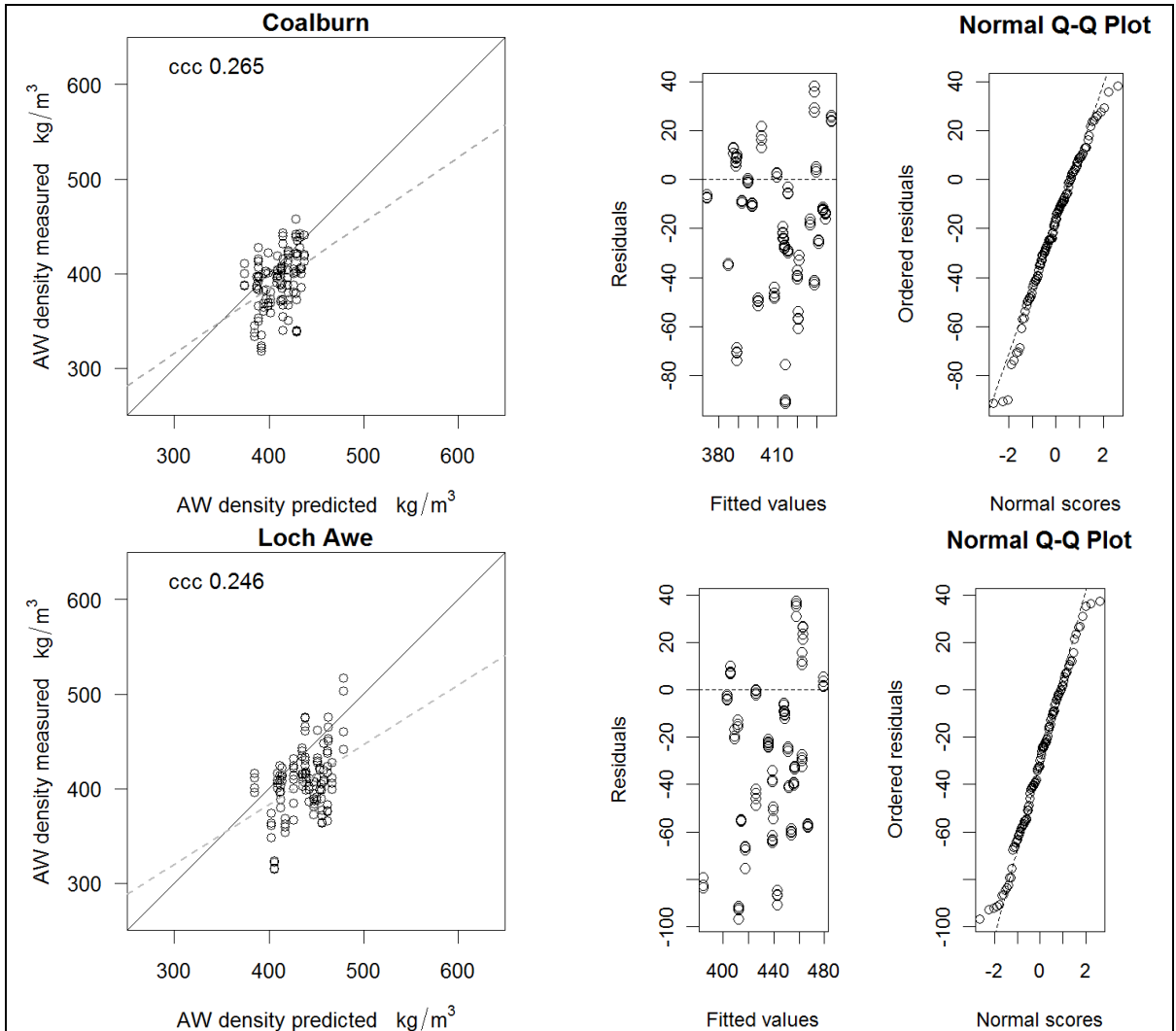


Figure 6-18. Predictions of the average density model developed for unthinned sites from Benchmarking data plotted against the measured values at the Coalburn and Loch Awe sites. Dashed gray line is the regression line fitted to the data and ccc denotes the concordance correlation coefficient.

For Loch Tummel the model for thinned sites (Equation 15) was used.

Equation 15

$$\text{Average density}_{\text{thinned}} \text{ (kg/m}^3\text{)} = 454.7555 - 9.4517 * \text{Growth rate (mm/yr)} + 0.0048 * \text{Original Stocking (stems/ha)} + 0.3977 * \text{Moisture Deficit}$$

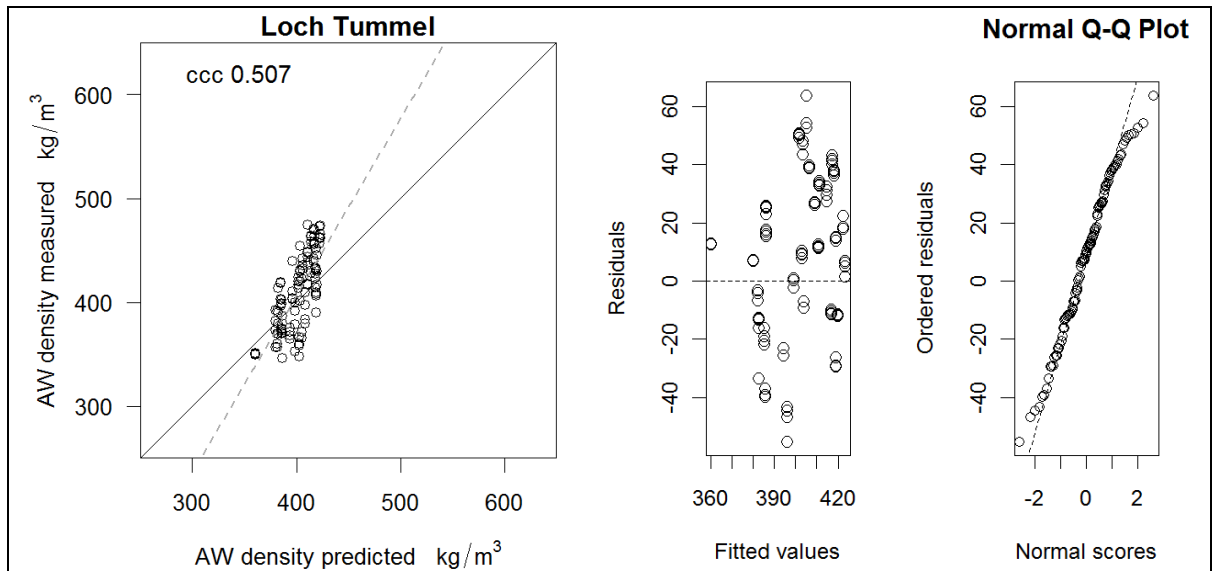


Figure 6-19. Predictions of the average density model developed for thinned sites from Benchmarking data plotted against the measured values at the Loch Tummel site. Dashed gray line is the regression line fitted to the data and ccc denotes the concordance correlation coefficient.

Using the average density model for unthinned sites improved the prediction for the Coalburn site (Figure 6-18). However, the results were still very poor (ccc 0.265). For Loch Awe (Figure 6-18) and Loch Tummel (Figure 6-19) the unthinned/thinned model fits were poorer than the general model developed for the pooled Benchmarking data.

As there was more variation between-trees within a site than between-sites, dominance class specific models were also tested. Data for all the sites was pooled and the models developed for different dominance classes (Equation 16, Equation 17, Equation 18) from the Benchmarking data were tested on these data.

Equation 16

$$\text{AW density}_{\text{dominant}} = 501.0059 - 11.3108 * \text{Growth rate (mm/yr)} * 1.1.379 * \text{Slope} + 0.3328 * \text{Moisture Deficit}$$

Equation 17

$$\text{AW density}_{\text{co-dominant}} = 564.8057 - 0.2488 * \text{Easting} - 15.2123 * \text{Growth rate (mm/yr)} + 0.0592 * \text{Accumulated T sum}$$

Equation 18

$$\text{AW density}_{\text{non-dominant}} = 486.4806 - 0.0684 * \text{Northing} - 9.3503 * \text{Growth rate (mm/yr)} + 0.0551 * \text{Accumulated T sum}$$

Using social class specific models (Figure 6-20) was not helpful at all and the model predictions were poor with ccc-values ranging from -0.185-0.058.

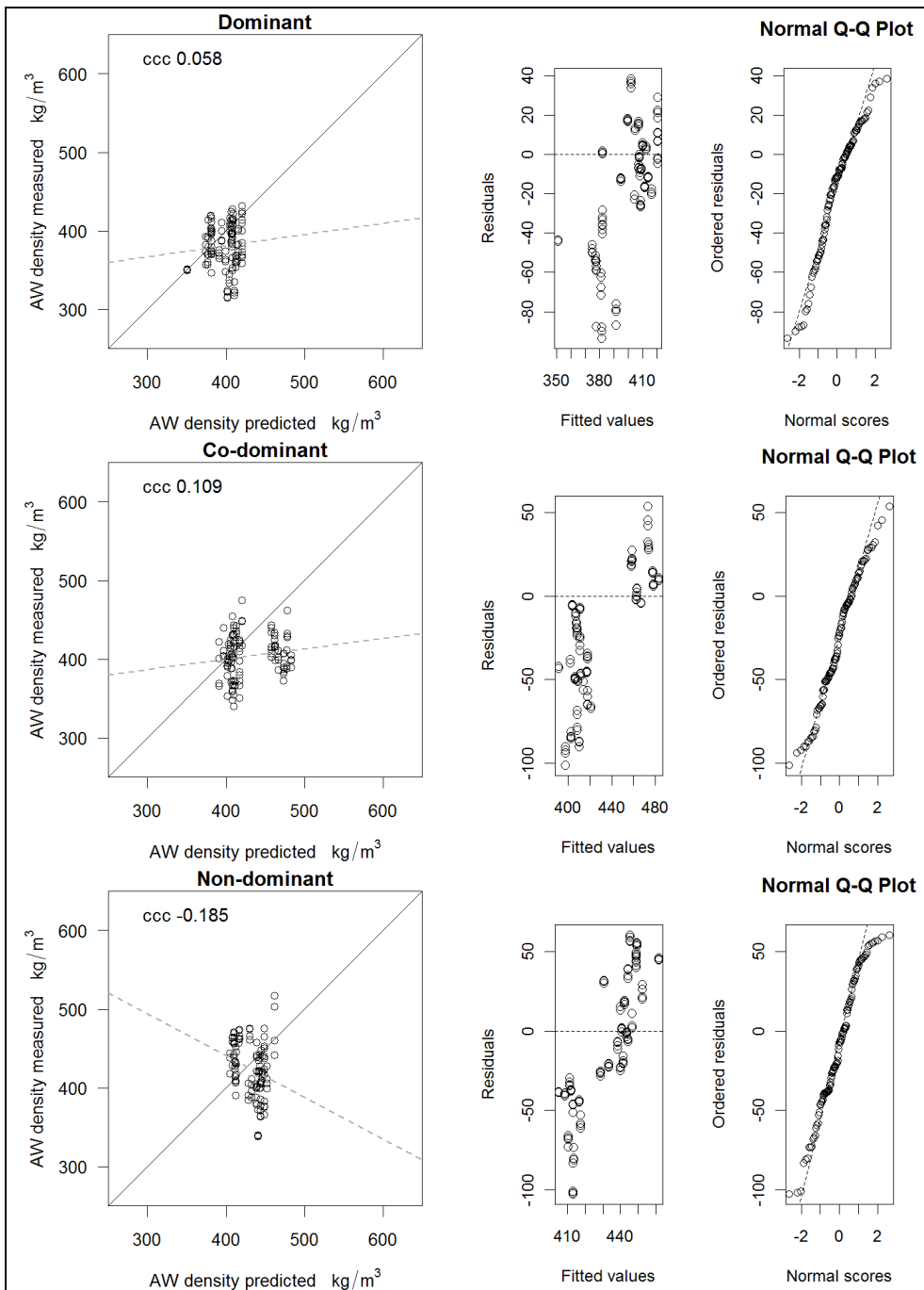


Figure 6-20. The prediction of cross-section average density models developed for different dominance classes from the Benchmarking data plotted against the measured density values for the social classes from the three Level II sites. Dashed gray line is the regression line fitted to the data and ccc denotes the concordance correlation coefficient.

Lastly, the potential for improving the model predictions by considering northern and southern sites separately was tested by testing the north (Equation 19) and south (Equation 20) models developed for the Benchmarking data.

Equation 19

$$AW\ density_{north} = 472.4404 - 9.2807 * Growth\ rate\ (mm/yr) + 0.3099 * Moisture\ Deficit$$

Equation 20

$$AW\ density_{south} = 661.3389 - 0.1463 * Easting - 11.9943 * Growth\ rate\ (mm/yr) - 0.1705\ Site\ Mean\ DBH\ (mm) + 9.8703 * Thinning - 3.3984 * DAMS$$

Using separate models for northern and southern sites did not markedly improve the model predictions either (Figure 6-21).

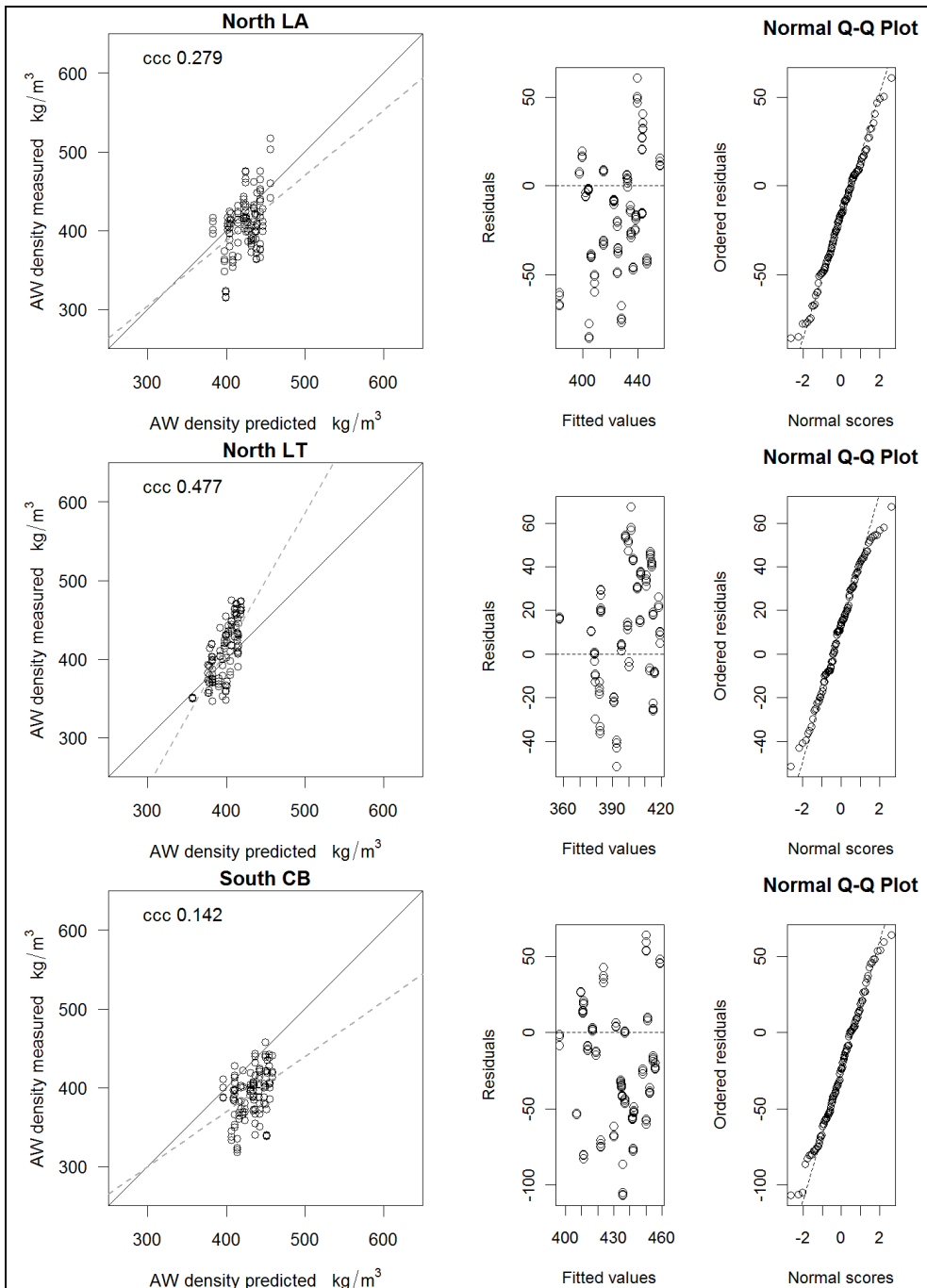


Figure 6-21. The predictions of cross-section average density model developed for northerly and southerly sites (dividing line as grid ref 650 000) against the measured density values. Coalburn qualified as a southern site whereas the Loch Awe and Loch Tummel data were pooled for the northern site predictions. Dashed gray line is the regression line fitted to the data and ccc denotes the concordance correlation coefficient.

6.3.3 Variation within the tree

Density might vary with height within a tree since juvenile wood is still being produced in the crown of mature trees. The dataset for the analysis of the effect of height consisted of four dominant and non-dominant trees sampled at the Coalburn and Loch Tummel sites. The selected trees all had 5 disks extracted in the field and samples were cut in all four cardinal directions. However, due to difficulties caused by branches and other defects, some samples were lost. The final dataset consisted of 303 samples. The samples were divided between the heights and directions according to Table 6-13 and 149 of the samples were from Loch Tummel and 154 from the Coalburn site.

Table 6-13. Distribution of sample disks from Loch Tummel and Coalburn sites to different azimuthal directions and height classes

	N	E	S	W	Total per disk height
Disk 1	15	16	15	16	62
Disk 2	15	16	16	16	63
Disk 3	13	12	14	13	52
Disk 4	16	16	15	15	62
Disk 5	16	16	16	16	64
Total per direction	75	76	76	76	303

At these two sites the patterns of ring density vs ring number were fairly similar (Figure 6-22) whereas there were marked differences in the ring width curves (Figure 6-23). At the Loch Tummel site there was much less reduction in ring width with ring number in the first 3 disks.

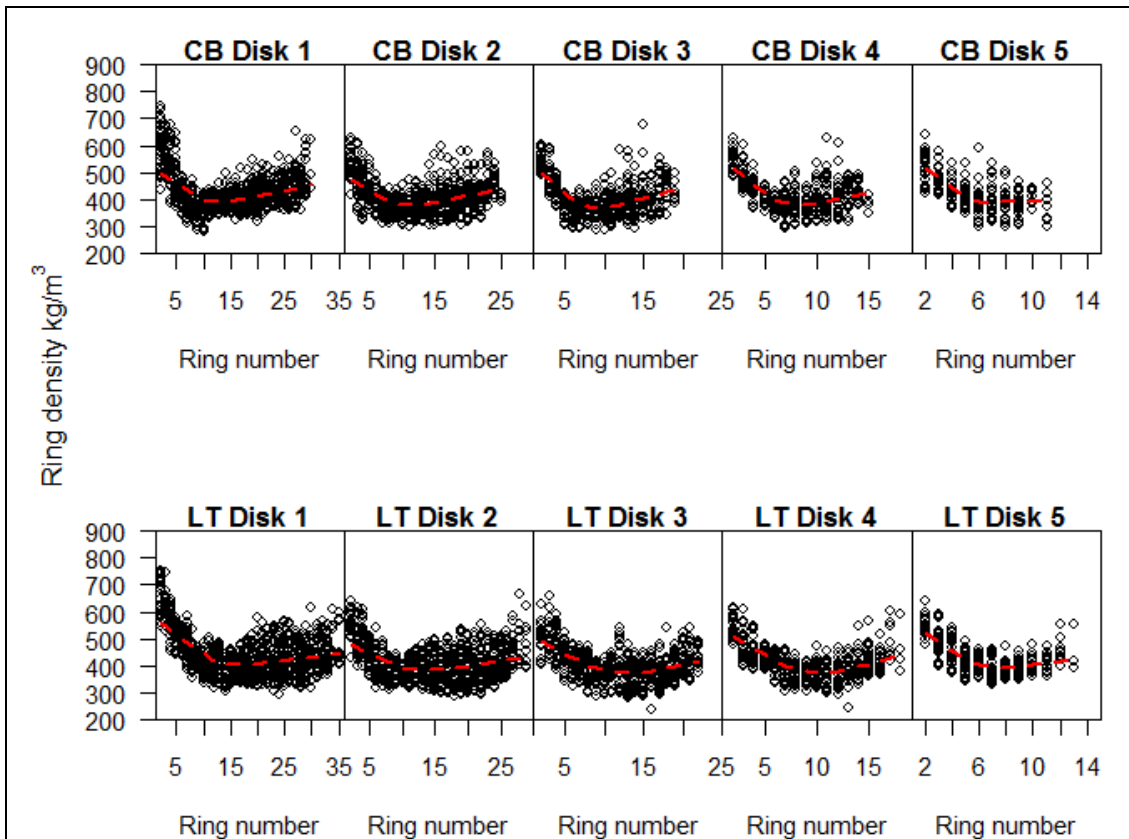


Figure 6-22. Density (at 4% MC) plotted against ring number for each disk taken at proportional heights along the stem from Coalburn (CB) and Loch Tummel (LT) sites. Dashed red lines are the LOWESS curves fitted to the data.

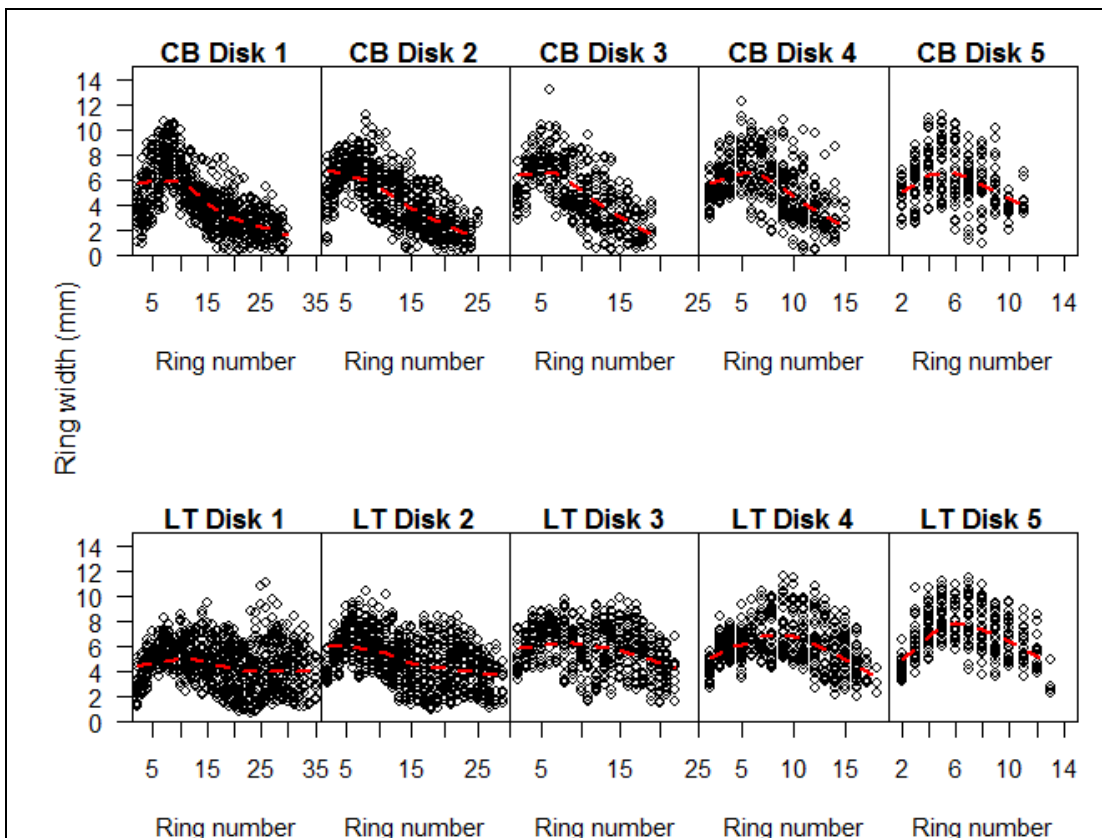


Figure 6-23. Ring width plotted against ring number for disks taken at proportional heights along the stem. Dashed red line is the LOWESS curve fitted to the data.

When the cross-section average densities at different heights were compared visually for the two sites (Figure 6-24), there was not much difference in median values for Coalburn. In the case of Loch Tummel the lowest disk differed markedly from all the others. Ring density plots (Figure 6-22) indicated that this might be due to high density near the pith. To assess this, the average juvenile wood densities were plotted against the disk number (Figure 6-25), which showed that in fact the differences between heights were much more pronounced for juvenile wood. Even for Coalburn there seemed to be a reduction in juvenile wood density at the 3rd disk height.

During the sample processing it was noted that the East and North radii seemed consistently longer than South and West at the Loch Tummel site. Longer radii can be an indication of compression wood formation. However, the increased radius was not accompanied with a rise in density (Figure 6-26) which suggested that compression wood was not present in the samples.

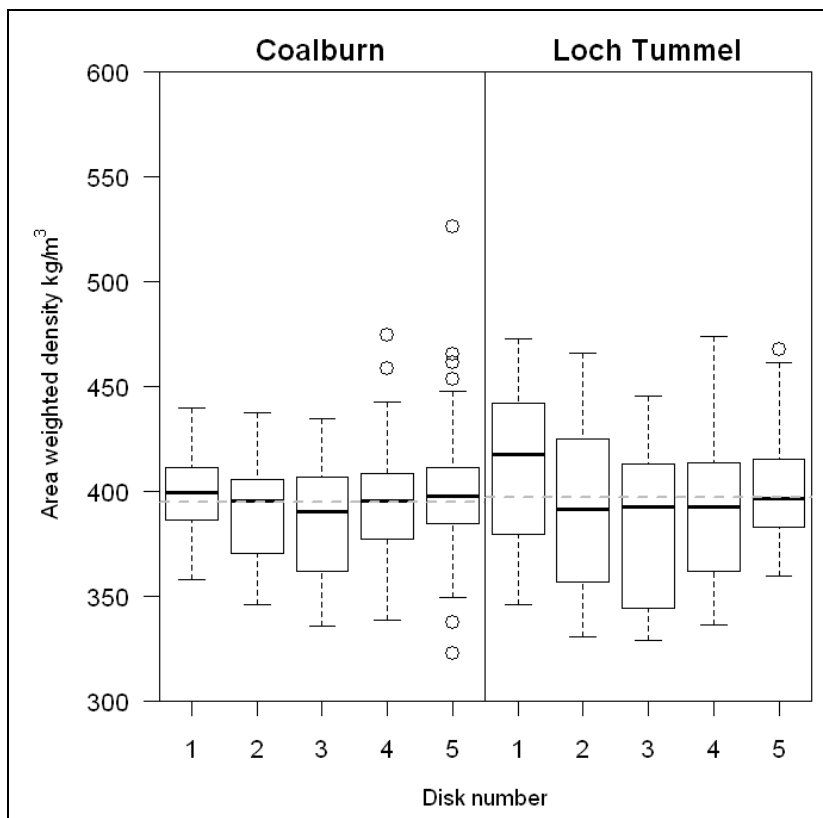


Figure 6-24. Changes in sample area-weighted density with disk height for the two sites. Density values are derived at 4% moisture content. Dashed grey line indicates the average for the site.

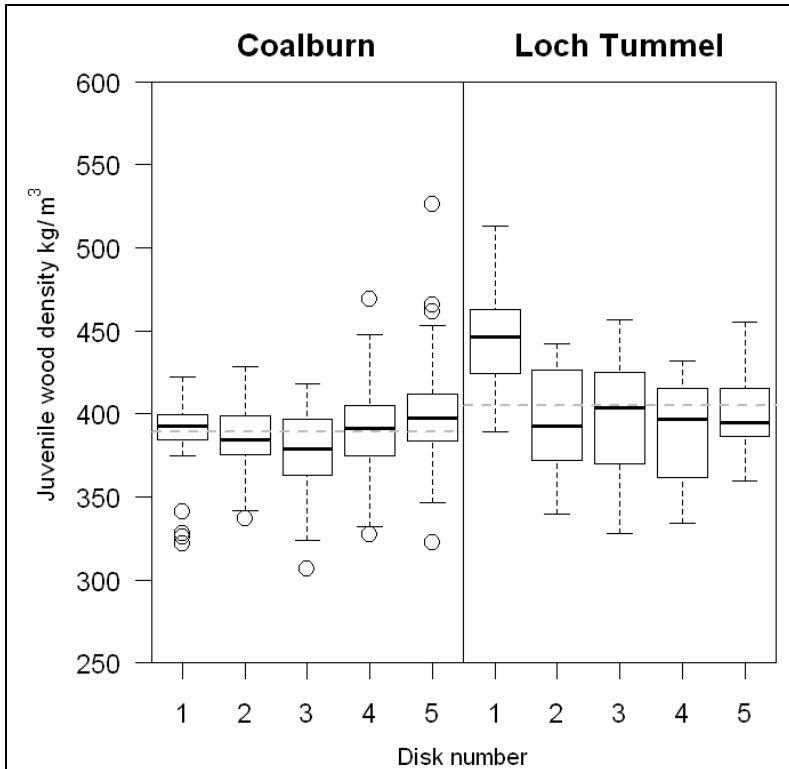


Figure 6-25. Variation in juvenile wood density with disk height at the two sites. Density was determined at 4% moisture content. Dashed grey line indicates the mean for each site.

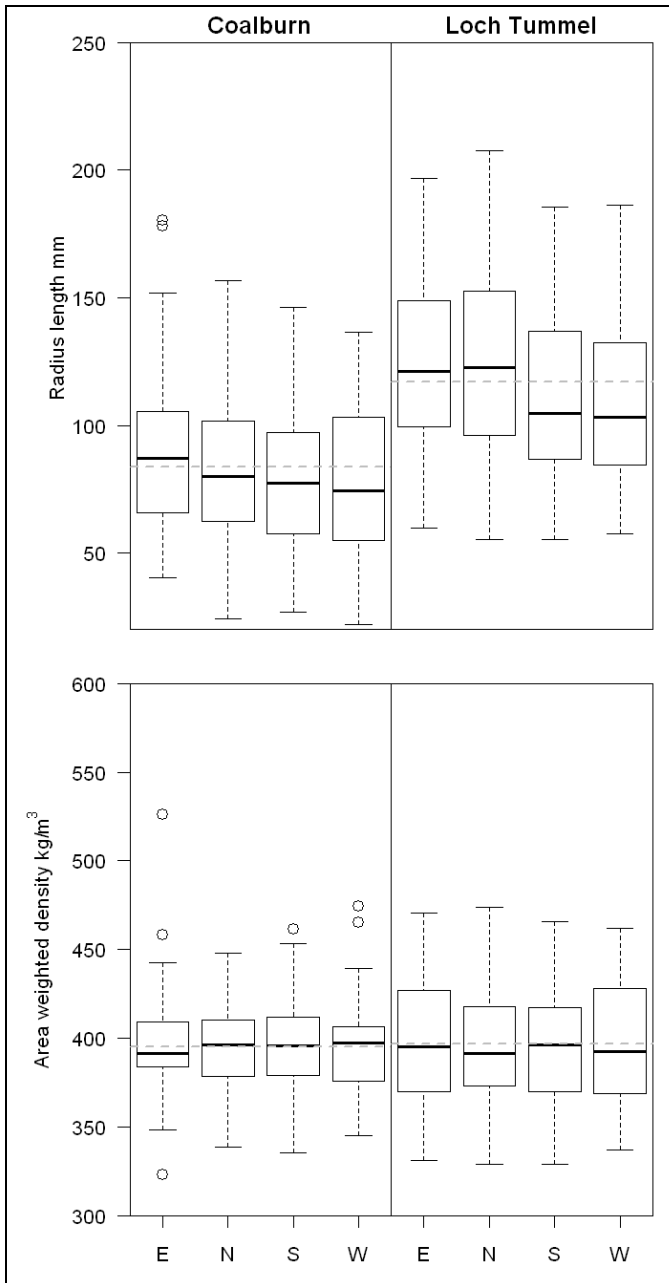


Figure 6-26. Influence of azimuthal direction on the radius length and sample area-weighted density. Density and ring width were determined at 4% moisture content. Dashed grey line indicates the mean for each site.

To quantify the variation in density along the tree, first, the area-weighted average density (corrected to 4% moisture content) was investigated. A model consisting only of random error structure was fitted to derive the variance components (Table 6-14). The same was done for ring density, which effectively meant one more level in the nested data structure (Table 6-15). When the weighted density was considered, the main bulk of the variation was between-trees within each site whereas the variation between the sites was negligible. Comparable amounts of variation were found for the

next levels of nesting; disk within a tree and direction within a disk. In the ring level data the differences between rings formed the dominant proportion of the variation (80 %) and the only other variable constituting a meaningful proportion of the variation (14 %) was trees within a site.

Table 6-14. Variance components of the area-weighted density data when the nested structure of the data was allowed for.

	Variance	% of the total
Site	$1.2 \cdot 10^{-03}$	0.0
Tree within the Site	729	64.6
Disk within the Tree	225	19.9
Direction within the Disk	175	15.5
Total	1129	100

Table 6-15. Variance components for the ring density data when the mixed effect model was fitted without explanatory variables

	Variance	% of the total
Site	$9.9 \cdot 10^{-4}$	0.0
Tree within the Site	653	14.0
Disk within the Tree	231	5.0
Direction within the Disk	33	0.7
Ring within the Direction	3749	80.3
Total	4666	100

The area-weighted density was then tested for the effects of height and direction. The height effect (as noted by disk number since the disks were collected from proportional heights) was found to be significant (Table 6-16). If the two sites were analysed separately, height had a significant effect at the Loch Tummel site, with the breast height disk being significantly different from disks 2, 3 and 4. In the case of the Coalburn site no significant effect of height was observed. Direction was found to be insignificant in the pooled data as well as in the site specific data.

Table 6-16. The effect of height in the different fractions of area-weighted density data from the Loch Tummel and Coalburn sites.

ALL DATA					
Fixed effects: AreaWtDens.MC4 ~ factor(DiskNo)					
	Value	Std.Error	DF	t-value	p-value
(Intercept)	405.97	7.529	225	53.92	0.0000
factor(DiskNo)2	-13.47	4.827	58	-2.79	0.0071
factor(DiskNo)3	-18.43	5.070	58	-3.64	0.0006
factor(DiskNo)4	-11.58	4.835	58	-2.40	0.0199
factor(DiskNo)5	-3.18	4.819	58	-0.66	0.5124
LOCH TUMMEL					
Fixed effects: AreaWtDens.MC4 ~ factor(DiskNo)					
	Value	Std.Error	DF	t-value	p-value
(Intercept)	413.05	12.743	110	32.41	0.0000
factor(DiskNo)2	-19.00	6.180	27	-3.08	0.0048
factor(DiskNo)3	-23.93	6.470	27	-3.70	0.0010
factor(DiskNo)4	-21.37	6.203	27	-3.44	0.0019
factor(DiskNo)5	-10.18	6.156	27	-1.65	0.1099
COALBURN					
Fixed effects: AreaWtDens.MC4 ~ factor(DiskNo)					
	Value	Std.Error	DF	t-value	p-value
(Intercept)	399.02	10.103	115	39.49	0.0000
factor(DiskNo)2	-8.07	7.383	27	-1.09	0.2838
factor(DiskNo)3	-12.92	7.775	27	-1.66	0.1080
factor(DiskNo)4	-2.07	7.383	27	-0.28	0.7816
factor(DiskNo)5	3.69	7.383	27	0.50	0.6210

6.3.4 Climate Analysis

Climate data from the nearest weather stations was used to calculate monthly temperature and rainfall variables (Table 6-17). The tree ring width and density data were detrended in R for the climate analysis using a cubic spline function (Figure 6-27) in the *dplR*-package (Bunn, 2008) to remove the growth related trends. Visual comparison of the raw data (Figure 6-28) and detrended data (Figure 6-29) indicated that the detrending had been successful.

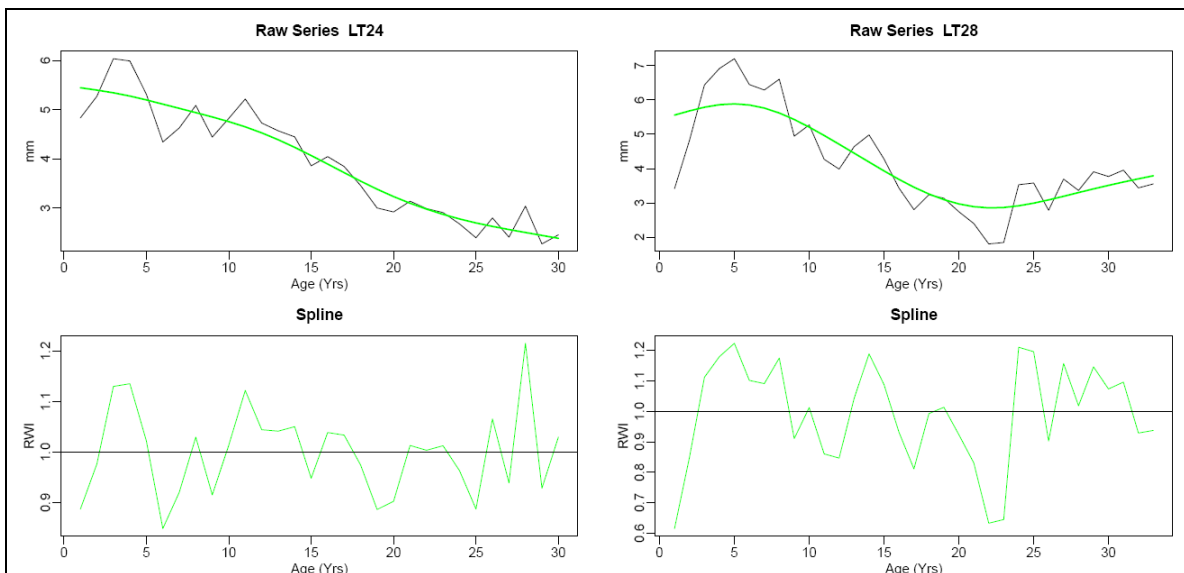


Figure 6-27. Examples (two trees from the Loch Tummel site) of the detrending procedure with a spline function in dplR package.

Table 6-17. Weather variables included in the climate influence analysis at the Level II sites.

Abbreviation	Weather variable	Calculation method
GDD _{yr}	Annual temperature sum	Temperature sum calculated for entire calendar year
GDD _{gs}	Growing season temperature sum	Temperature sum calculated for the period from April to September
GDD _{May-Aug}	Summer temperature sum	Temperature sum calculated for the period from May to August
GDD _{Jun-Aug}	Mid to late summer temperature sum	Temperature sum calculated for the period from June to August
MonthlyMaxT	Average maximum temperature for each month	Averaged for each month from the daily maximum temperature data
MonthlyMinT	Average minimum temperature for each month	Averaged for each month from the daily minimum temperature data
MonthlyMeanT	Mean temperature of each month	Daily mean temperature calculated from the daily minimum and maximum temperature data and then averaged for each month
Precip _{yr}	Annual precipitation	Sum of daily precipitation fallen during a calendar year
Precip _{gs}	Growing season precipitation	Sum of daily precipitation fallen during the period from April to September
Precip _{May-Aug}	Summer precipitation	Sum of daily precipitation fallen during the period from May to August
Precip _{June-Aug}	Mid to late summer precipitation	Sum of daily precipitation fallen during the period from June to August
Precip _{monthly}	Precipitation fallen during each calendar month	Sum of daily precipitation fallen during a calendar month

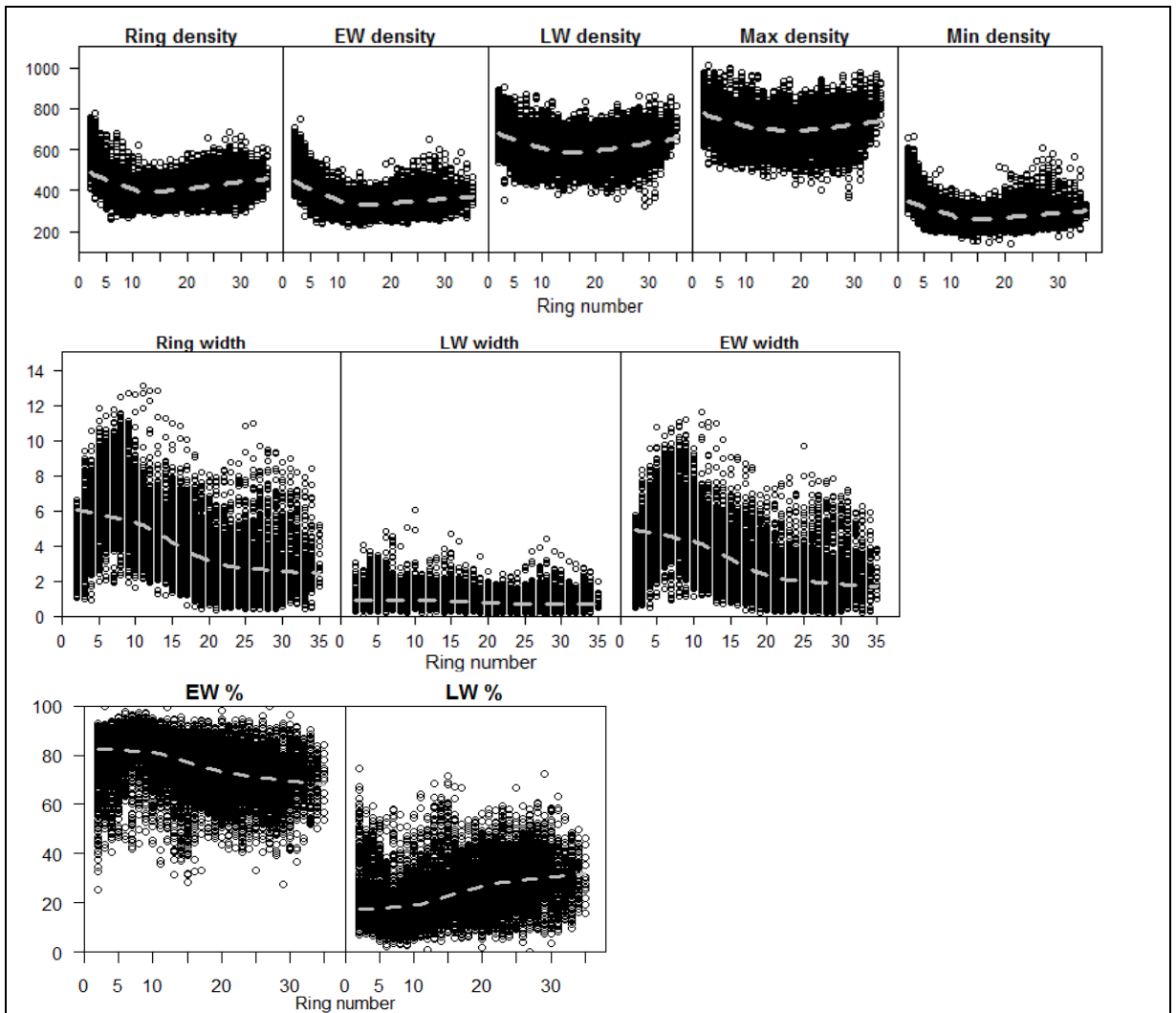


Figure 6-28. Raw ring width and density data pooled from the three Level II sites. Dashed grey line represents the LOWESS curve fitted to the data.

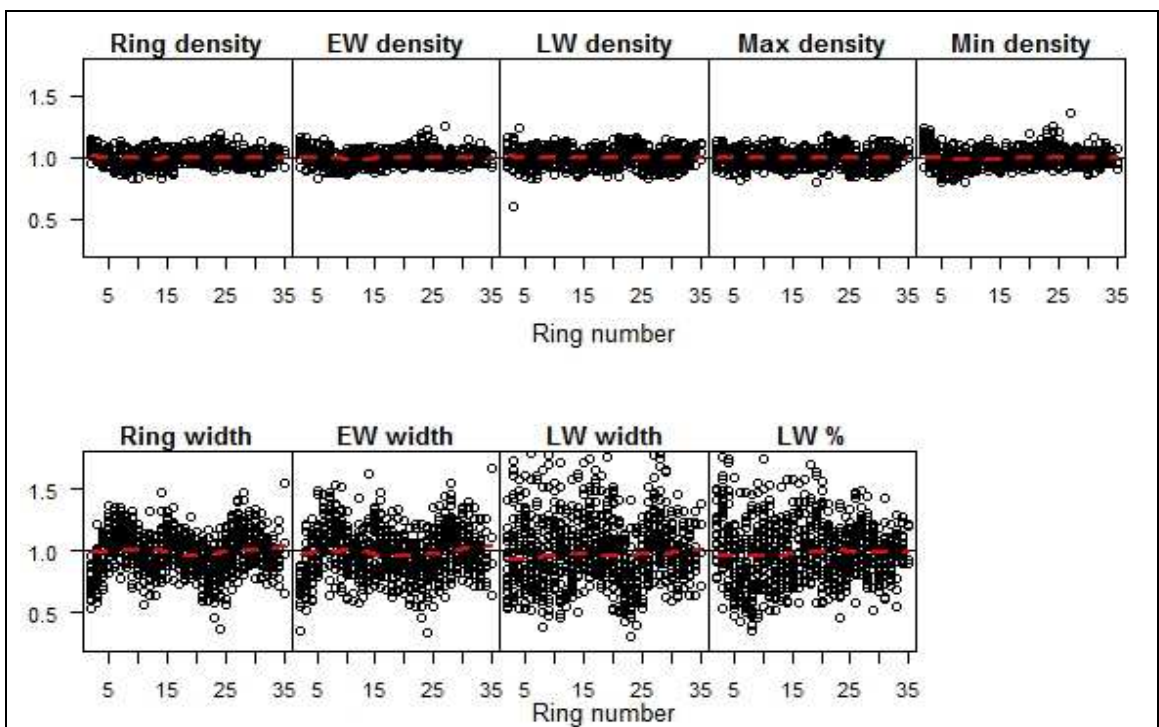


Figure 6-29. Detrended tree ring variables plotted against the ring number for the Loch Tummel site. Dashed red line is LOWESS curve fitted to the data.

The expressed population signal value (EPS, Table 6-18) describes how well the individual trees express the common site signal, which after removal of the growth related trend is believed to be the climatic signal. ESP quantifies how well the mean chronology represents a hypothetical noise free chronology that is infinitely replicated (Briffa, 1995). Usually EPS above 0.85 are deemed suitable (McCarroll, 2005; Robertson et al., 1997; Wigley et al., 1984). In these datasets the EPS values were high 0.951-0.982 for the detrended series. This was probably due to high number of samples (30) at each site. EPS is also influenced by sample number and can be applied to quantify the required number of samples for climate analysis (McCarroll, 2005; Robertson et al., 1997). Gleichläufigkeit (Table 6-18) describes the agreement between each step in pairs of chronologies in terms of direction i.e. assessing how often both chronologies are increasing or decreasing in synchrony (Schweingruber et al., 1978). Here the pairwise figures have been averaged. Sensitivity (Table 6-18) is a measure of the size of variability between years in the chronology (Fritts, 1976). It quantifies how strongly the different ring parameters react on an annual basis and hence quantifies the potential of the variable reacting to a climate related change. In comparison to the values here, Schweingruber et al. (1978) in study on *Picea abies*, *Pinus cembra* and *Larix decidua* reported the following sensitivity values: Ring width 0.115-0.173, earlywood width 0.127-0.199, latewood width 0.180-0.328, maximum density 0.080-0.124 and minimum density 0.038-0.073.

Table 6-18. Diagnostic values for the different tree ring variable chronologies from Loch Tummel and Coalburn sites

	EPS		Gleichläufigkeit		Sensitivity	
	Loch Tummel	Coalburn	Loch Tummel	Coalburn	Loch Tummel	Coalburn
RW _{raw}	0.954	0.996	0.653	0.714	0.150	0.215
RW _{detrended}	0.951	0.974	0.640	0.684	0.135	0.172
RD _{raw}	0.980	0.982	0.697	0.654	0.067	0.075
RD _{detrended}	0.967	0.980	0.683	0.669	0.056	0.063
EW _{raw}	0.957	0.995	0.650	0.704	0.188	0.273
EW _{detrended}	0.946	0.977	0.631	0.689	0.171	0.231
EWD _{raw}	0.990	0.987	0.686	0.702	0.068	0.085
EWD _{detrended}	0.960	0.974	0.676	0.688	0.054	0.068
LW _{raw}	0.946	0.980	0.691	0.691	0.287	0.328
LW _{detrended}	0.966	0.971	0.699	0.695	0.280	0.303
LWD _{raw}	0.973	0.981	0.764	0.742	0.079	0.086
LWD _{detrended}	0.979	0.982	0.775	0.729	0.076	0.079
LW% _{raw}	0.956	0.981	0.669	0.699	0.270	0.319
LW% _{detrended}	0.961	0.979	0.665	0.701	0.264	0.310
MaxD _{raw}	0.974	0.979	0.766	0.733	0.076	0.079
MaxD _{detrended}	0.981	0.982	0.775	0.718	0.074	0.072
MinD _{raw}	0.988	0.985	0.682	0.659	0.083	0.091
MinD _{detrended}	0.957	0.973	0.681	0.683	0.068	0.076

When the ring indices were plotted against the calendar year (Figure 6-30 - Figure 6-33) there were marked differences in the patterns between the sites. For example ring density at the Loch Tummel site contained a section 1984-1995 when there was very limited annual variation in the ring density indices, whereas this effect was absent in the Coalburn data. LW% (Figure 6-33) was in the most agreement between the sites.

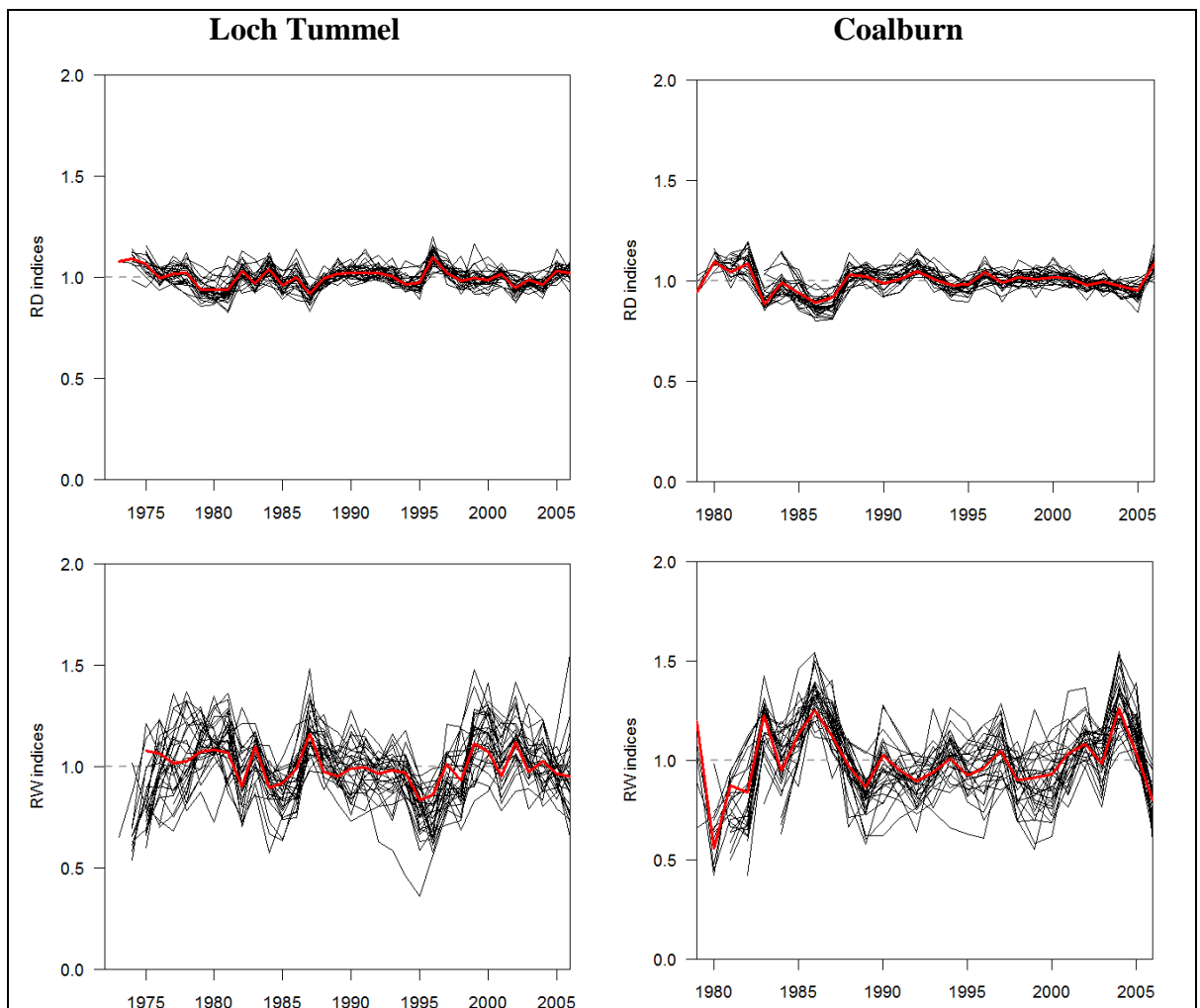


Figure 6-30. Ring density (top) and width (bottom) indices for Loch Tummel and Coalburn plotted against calendar year. Solid red line represents the mean site chronology.

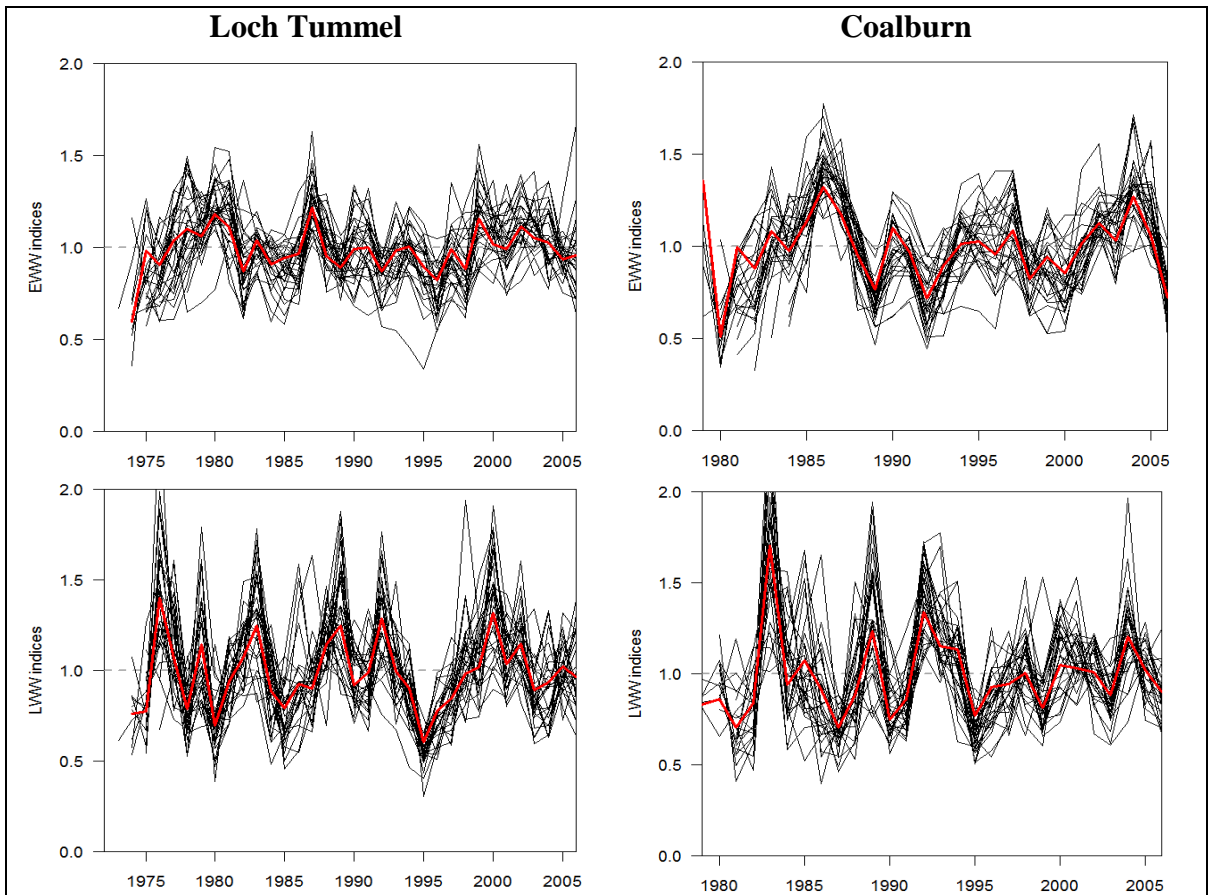


Figure 6-31. Earlywood (top) and latewood (bottom) width indices for Loch Tummel and Coalburn plotted against calendar year. Solid red line represents the mean site chronology.

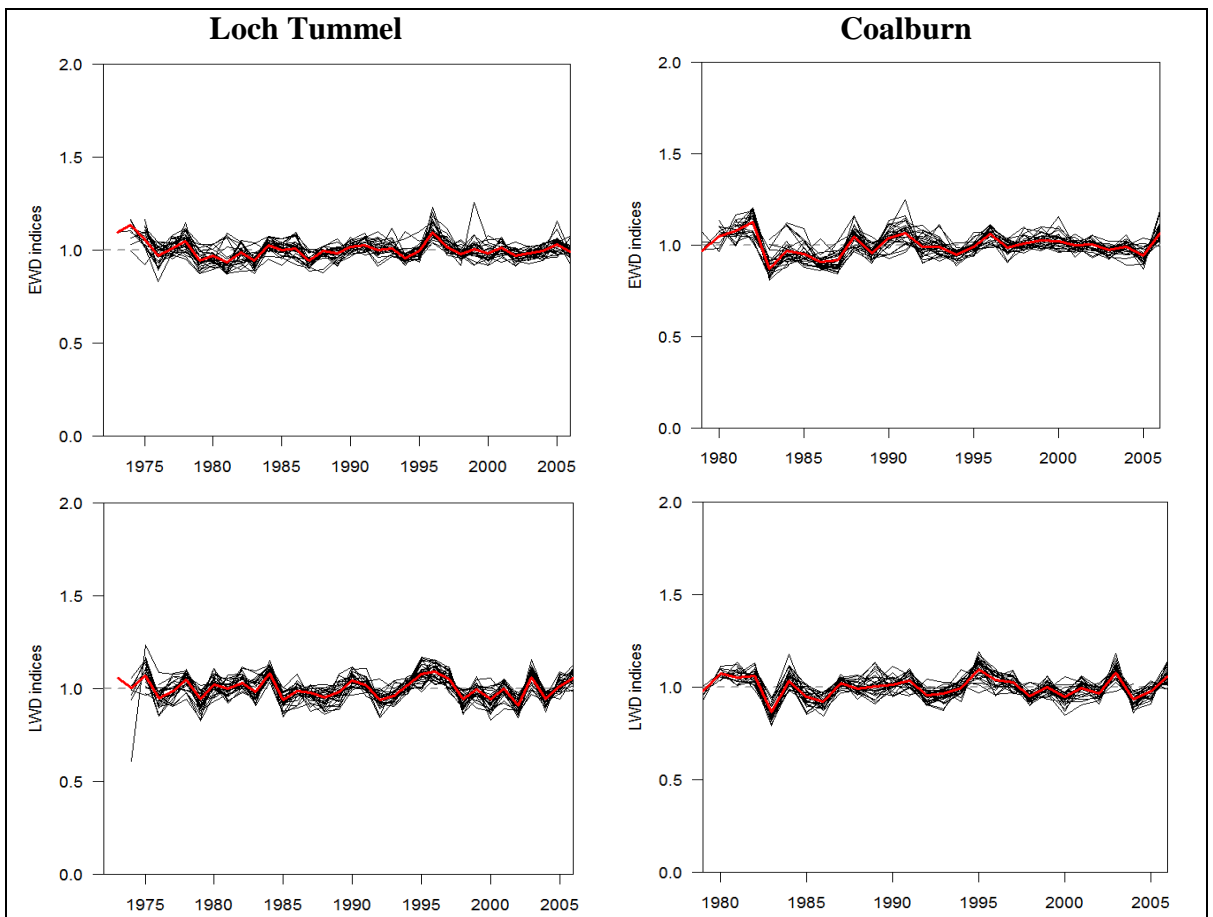


Figure 6-32. Earlywood (top) and latewood (bottom) density indices for Loch Tummel and Coalburn plotted against calendar year. Solid red line represents the mean site chronology.

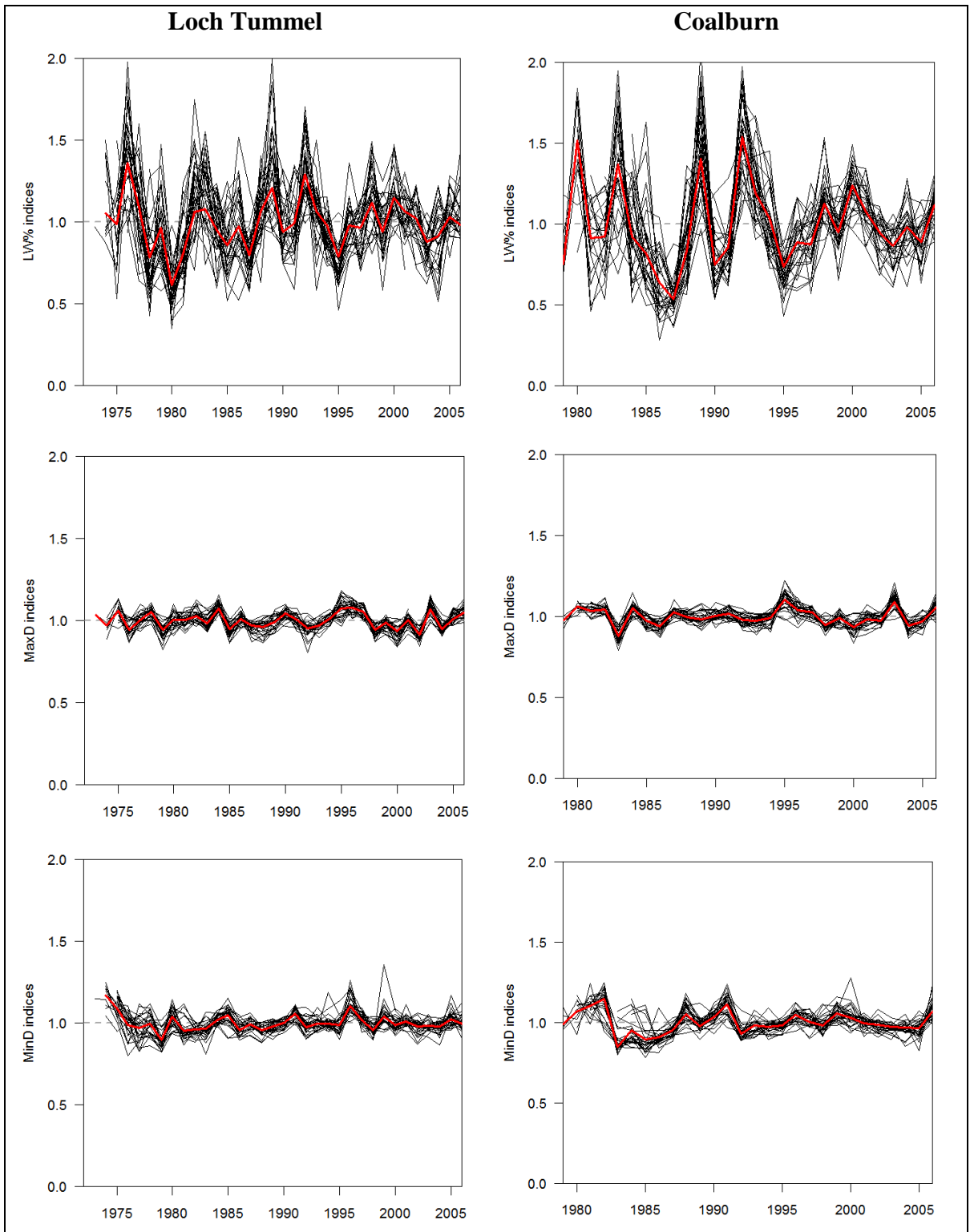


Figure 6-33. Latewood percentage (top) indices and maximum (middle) and minimum (bottom) density indices plotted against calendar year. Solid red line represents the mean site chronology.

Average site chronologies were derived by averaging all pre-whitened individual tree chronologies for each site using a robust bi-weight mean (Bunn, 2008). These site average chronologies were then compared to the climatic variables of the current and previous year. Significant correlations (individual alpha 0.05) from each sites separately (Loch Tummel 6.3.4.1 and Coalburn 6.3.4.2) were selected for further analysis (see Appendices 4, 5, 7 and

8 for full list of correlations for Loch Tummel and Coalburn with p-value <0.1). If several weather variables from the same group (eg. June maximum, minimum and mean temperature), were found to be significant then the strongest correlation was selected for further investigation. The selected climatic variables were plotted with the relevant tree ring variable.

Weather variables for which a significant correlation was detected when the multiple comparisons were allowed for ($\alpha' = 0.0009$) were included in more extensive cross-correlation analysis (6.3.4.3). This selection criterion was a fairly stringent one, therefore some of the climatic correlations with a p-value <0.05 might still be important and worth studying more at different sites.

6.3.4.1 Tree ring and weather relationships at Loch Tummel site

Only weak autocorrelation was detected in the ring variables (Figure 6-35), which was to be expected as the series had been treated to remove autocorrelation. In general the autocorrelation was low in the weather variables as well. In 28 cases out of the 57 variables examined at 14 lag positions, autocorrelations exceeding the 95% confidence interval were detected (See Appendix 6 for full autocorrelation matrix). These higher autocorrelations usually occurred just as separate peaks, as shown for June maximum temperature and July minimum temperature (Figure 6-34). Only in the case of September maximum temperature was a pattern in the autocorrelations observed (Figure 6-34), however, only lag 1 exceeded the boundaries.

In the next step, tree ring chronologies and weather variables for the same and the previous year were tested for correlations ($\alpha=0.05$ for individual pairwise comparisons) and the significantly correlated pairs were plotted.

At the Loch Tummel site the only temperature variable for the current year that influenced ring width significantly was October maximum temperature (Figure 6-36). October maximum temperature was negatively correlated with ring width. However, any significant increase in ring width during October is difficult to perceive. Several rainfall variables (May-August, May, June and October precipitation) were correlated with ring width (Figure 6-36), October precipitation negatively but all the others positively.

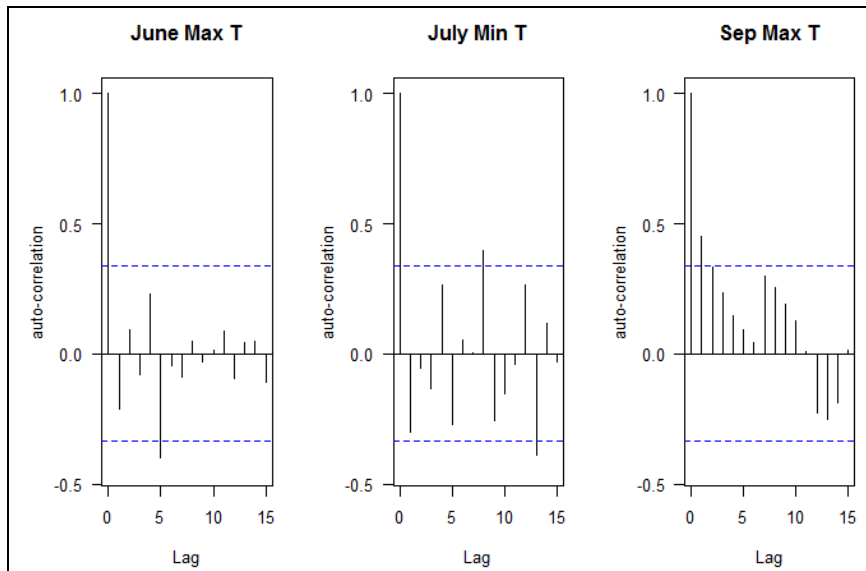


Figure 6-34. Examples of auto-correlation detected in the Loch Tummel weather variables. Dashed line corresponds to $r=0.335$.

A negative effect of October rain on ring width would be difficult to explain in physiological terms as the growth of the ring should have been completed by then. The adjusted α' -level for carrying out 57 comparisons to achieve overall α -level of 0.05 was calculated according to Curtin and Schulz (1998) and was defined as 0.000899 according the less stringent method and 0.000877 according the Bonferroni correction. These, for most practical purposes, were identical and were approximated to 0.0009. None of the correlations remained significant when the α' was adjusted.

Temperature variables from the previous year were also found to be correlated with ring width (Figure 6-37). These included June-August temperature sum, August mean and maximum temperatures. Warmer weather during the previous growing season might allow the tree to build more reserves or more photosynthetic capacity which would allow vigorous growth the following season. However, under corrected α' none of these relationships remained significant.

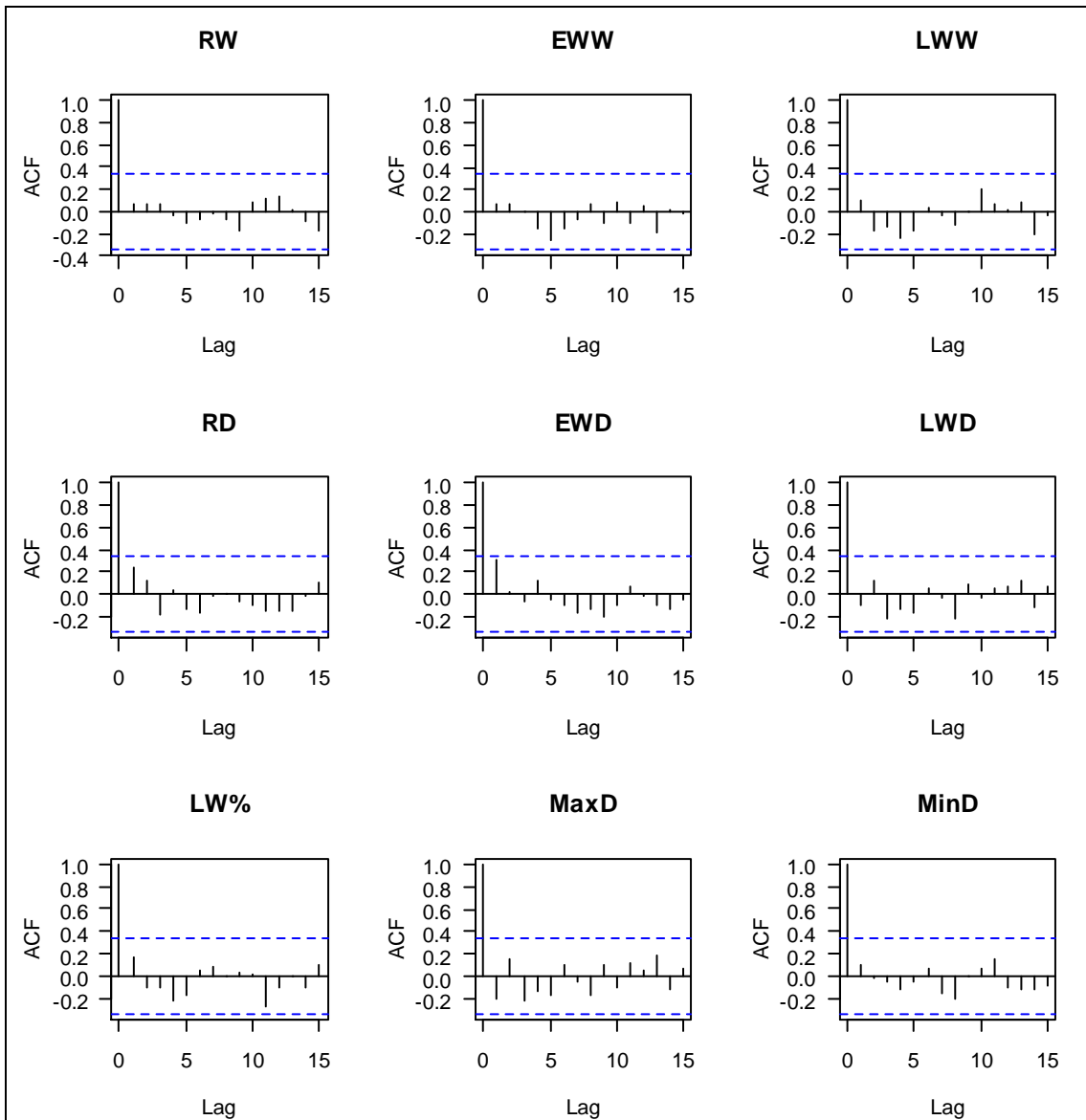


Figure 6-35. Remaining autocorrelation in the average tree ring chronologies at the Loch Tummel site.

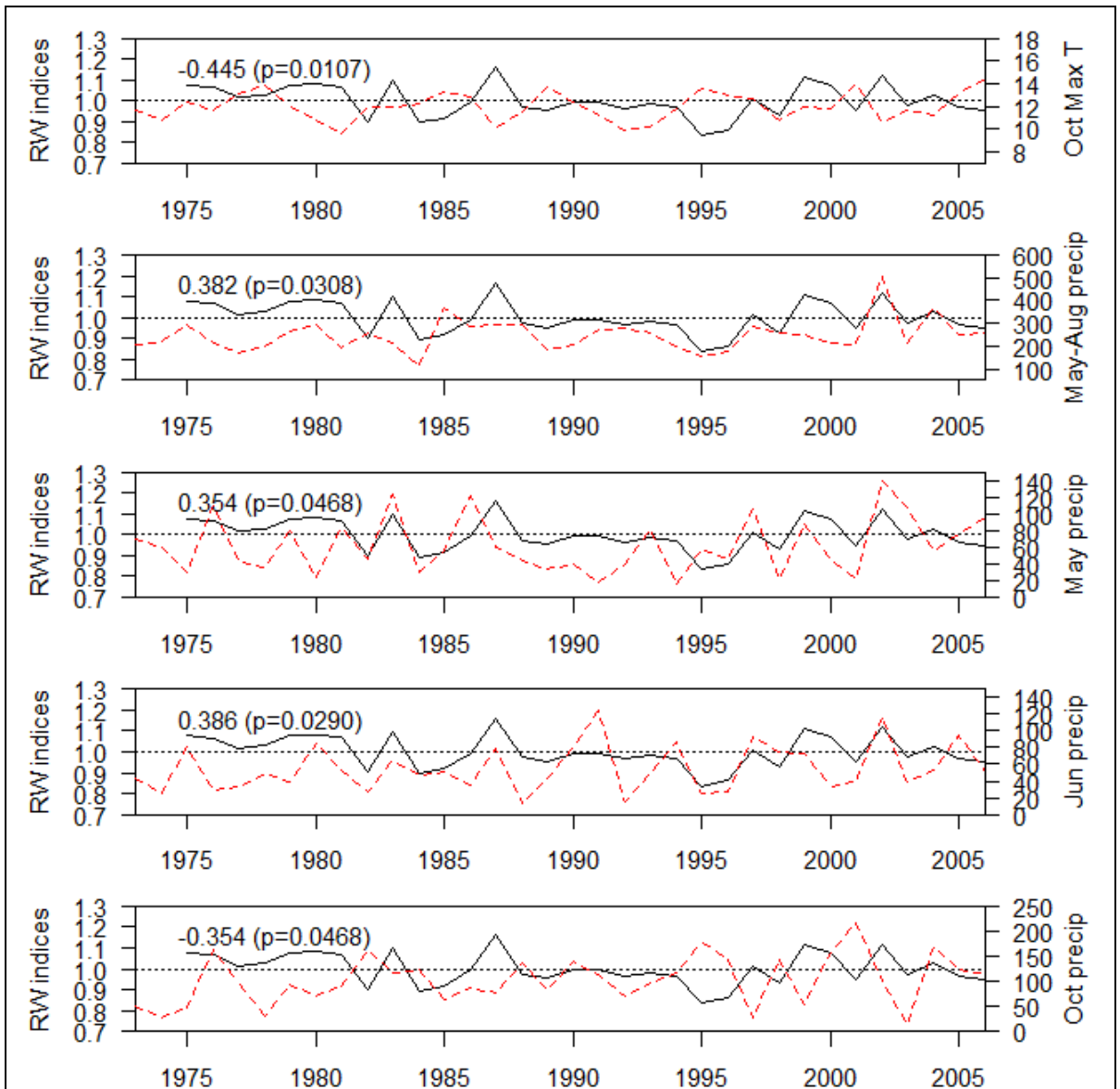


Figure 6-36. Loch Tummel tree ring width indices plotted against the individually significant weather variables for the current year. Solid line represents the tree ring width indices and the dashed red line the weather variable in question. Horizontal line marks the reference level for the tree ring width indices. The P-value reported refers to individual comparisons. The selected α -level was 0.05. To achieve an overall α -level of 0.05 the limit for individual comparisons would be adjusted (Curtin and Schulz, 1998) to approximately 0.0009.

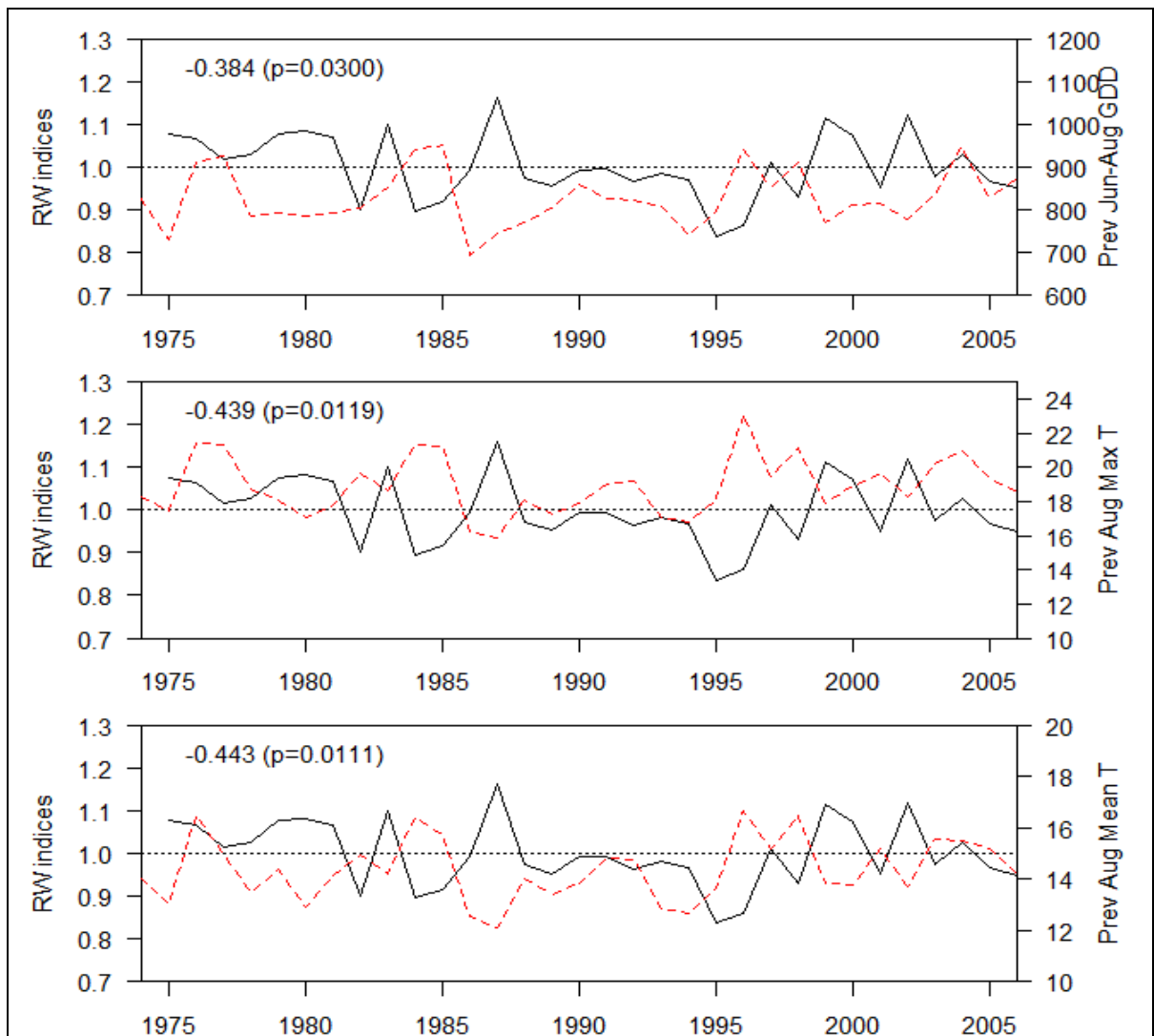


Figure 6-37. Loch Tummel tree ring width indices plotted against the individually significant weather variables for the previous year. Solid line represents the tree ring width indices and the dashed red line the weather variable in question. Horizontal line marks the reference level for the tree ring width indices. The P-value reported refers to individual comparisons. The selected α -level was 0.05. To achieve an overall α -level of 0.05 the limit for individual comparisons would be adjusted (Curtin and Schulz, 1998) to approximately 0.0009.

Ring density at the Loch Tummel site (Figure 6-38) was significantly correlated only with rainfall variables (Growing season, May-August and March precipitation), all of which had a negative effect on density. The above precipitation variables were positively correlated with ring width which is consistent with the negative relationship between rainfall and density. The climatic variables for the previous year (Figure 6-39) also included significant relationships (previous January temperatures, February and August maximum temperature and December rainfall). The strongest correlations were found for January temperature but there was also a weaker negative correlation ($p < 0.1$) between January maximum temperature and ring width, which could indicate that high temperatures in the winter increase respiration and hence consume reserves. This would slow down growth and lead to higher density. However, some other mechanisms might also govern this relationship. In

the ring density indices there is a period from 1989-1994 that contains no climatic signal (Figure 6-38 and Figure 6-39). Under adjusted α' -level none of these relationships remained significant.

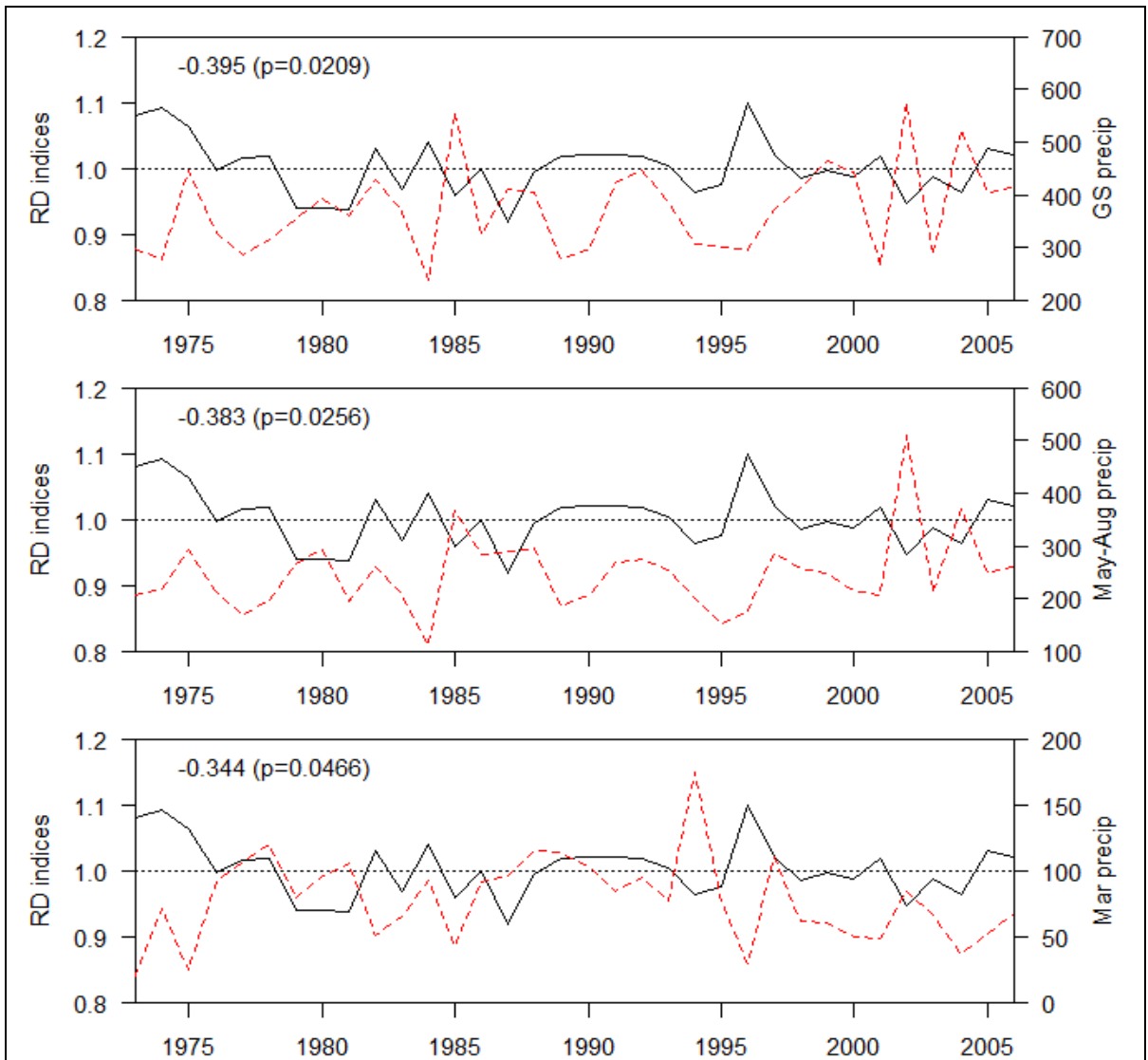


Figure 6-38. Loch Tummel tree ring density indices plotted against the individually significant weather variables of the current year. Solid line represents the tree ring density indices and the dashed red line the weather variable in question. Horizontal line marks the reference level for the tree ring density indices. P-value reported refers to individual comparisons. The selected α -level was 0.05. To achieve over all α -level of 0.05 the limit for individual comparisons would be adjusted (Curtin and Schulz, 1998) to approximately 0.0009.

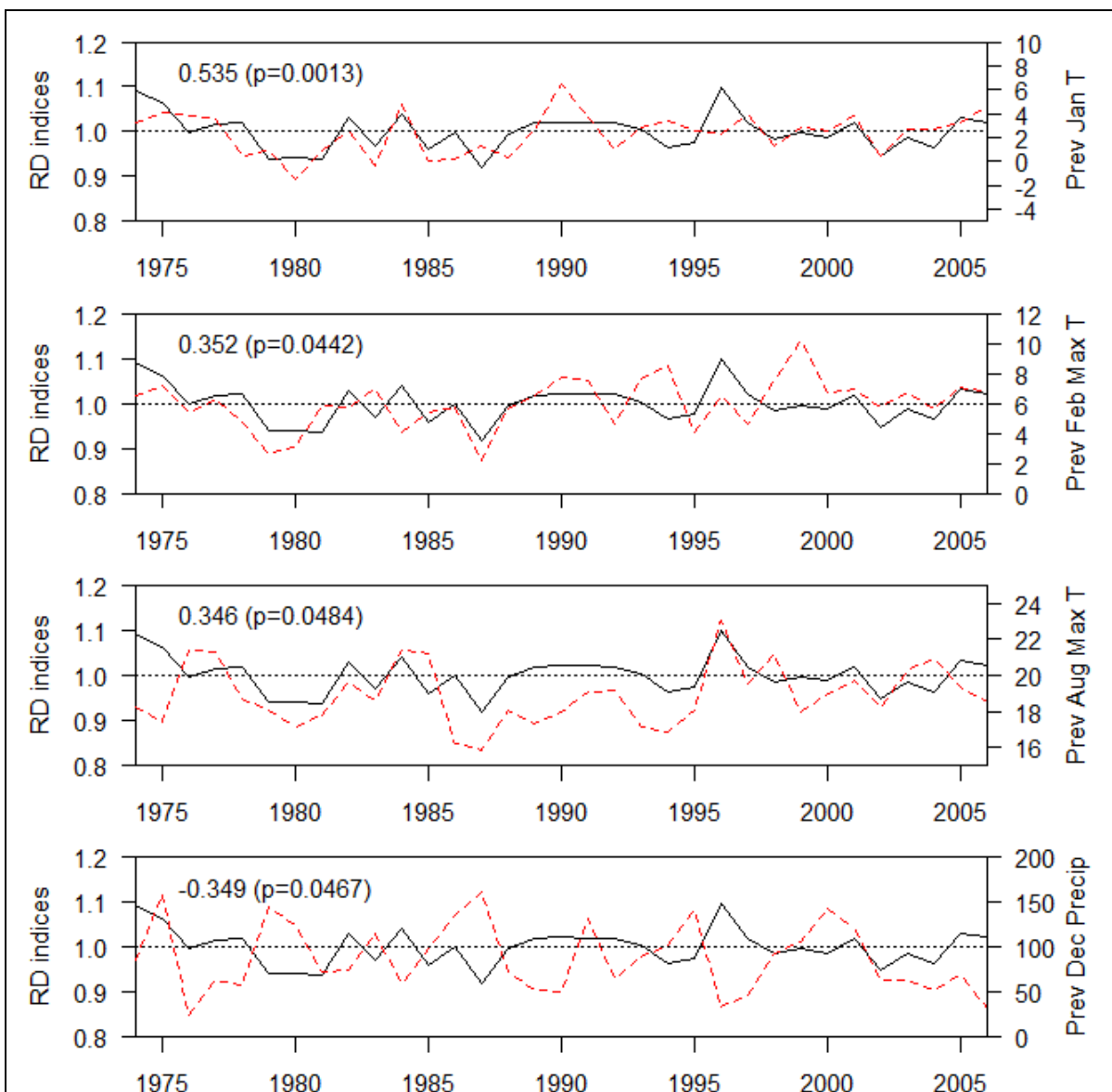


Figure 6-39. Loch Tummel tree ring density indices plotted against the individually significant previous year weather variables. Solid line represents the tree ring density indices and the dashed red line the weather variable in question. Horizontal line marks the reference level for the tree ring density indices. P-value reported refers to individual comparisons. The selected α -level was 0.05. To achieve over all α -level of 0.05 the limit for individual comparisons would be adjusted (Curtin and Schulz, 1998) to approximately 0.0009.

The earlywood density (EWD) was only significantly related to March precipitation and January temperature (mean and minimum) of the previous year (Figure 6-40). The correlation in this case was negative with rainfall and positive with temperature. It is difficult to see what would be the physiological mechanism for temperature of previous January influencing the earlywood density of the following year. Under adjusted α these relationships were non-significant.

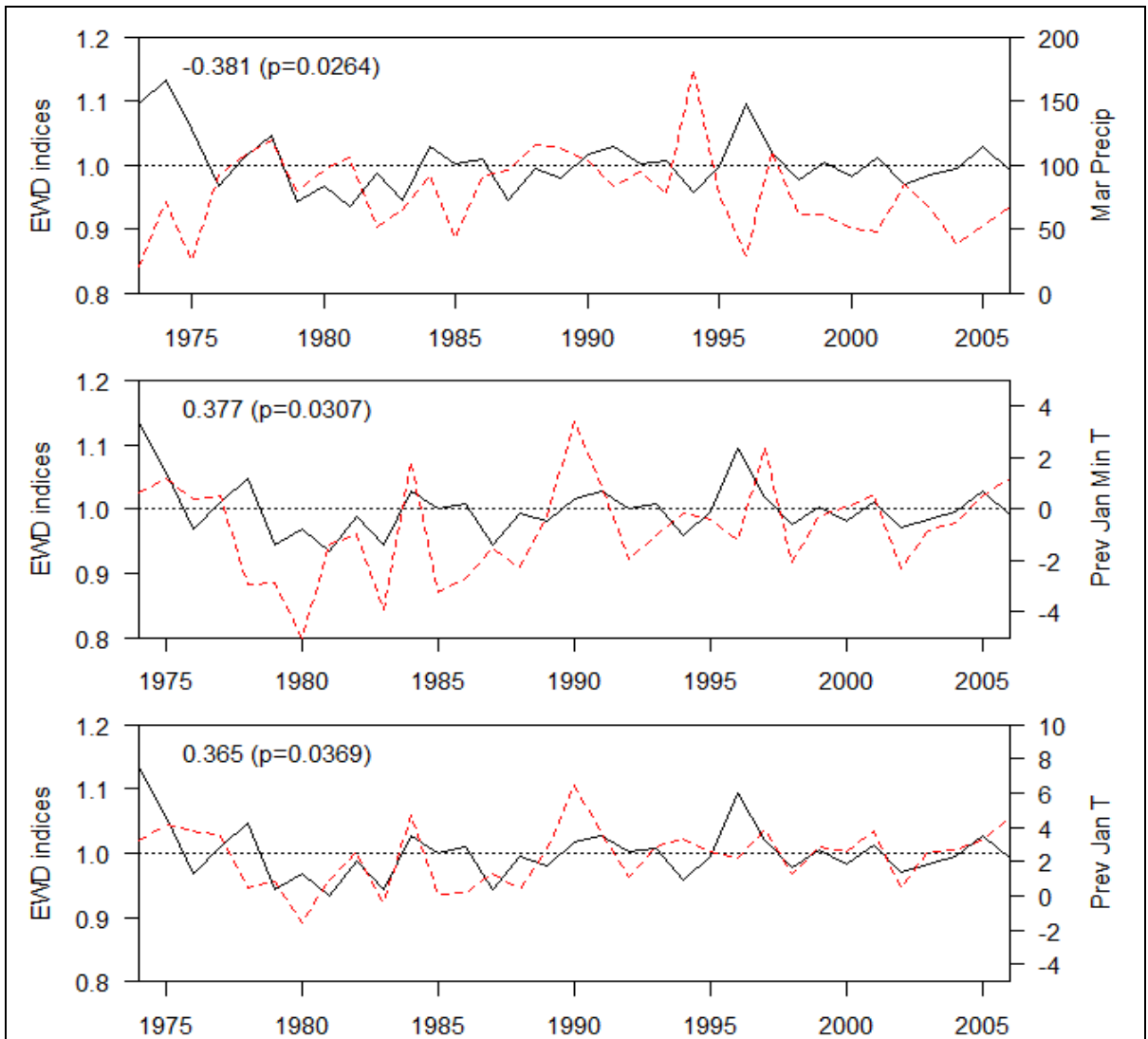


Figure 6-40. Loch Tummel earlywood density (EWD) indices plotted against the individually significant current and previous year weather variables. Solid line represents the earlywood density indices and the dashed red line the weather variable in question. Horizontal line marks the reference level for the earlywood density indices. P-value reported refers to individual comparisons. The selected α -level was 0.05. To achieve over all α -level of 0.05 the limit for individual comparisons would be adjusted (Curtin and Schulz, 1998) to approximately 0.0009.

Earlywood width (Figure 6-41) at the Loch Tummel site was positively correlated with June precipitation and negatively with June maximum temperature. June rainfall was the strongest correlation. Furthermore, previous August temperature was negatively correlated with earlywood width. All of the correlations became non-significant under adjusted α -level (0.0009).

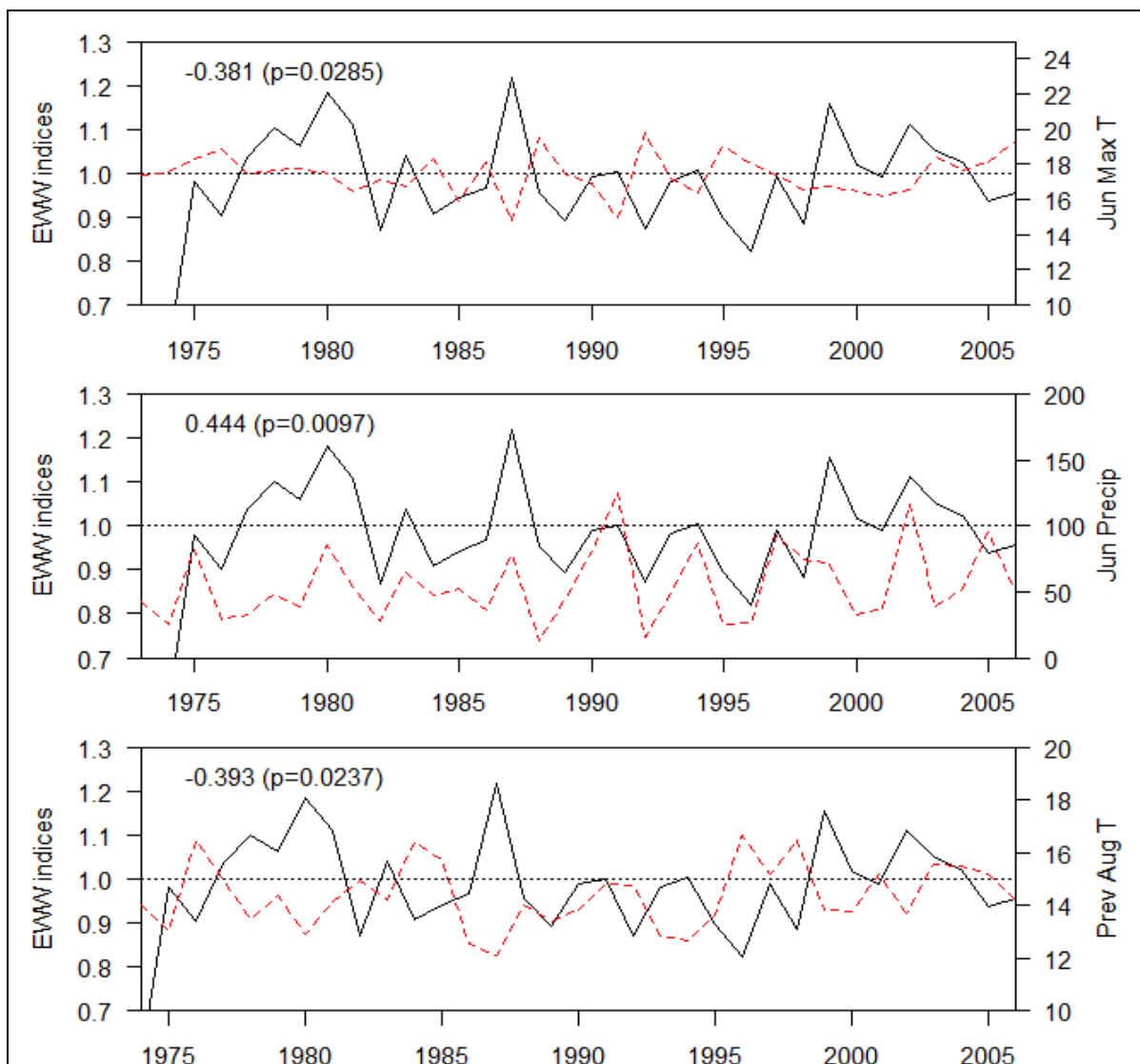


Figure 6-41. Loch Tummel earlywood width (EWW) indices plotted against the individually significant weather variables of the current and previous year. Solid line represents the earlywood width indices and the dashed red line the weather variable in question. Horizontal line marks the reference level for the earlywood width indices P-value reported refers to individual comparisons. The selected α -level was 0.05. To achieve over all α -level of 0.05 the limit for individual comparisons would be adjusted (Curtin and Schulz, 1998) to approximately 0.0009.

Latewood density indices (Figure 6-42 and Figure 6-43) were positively correlated with several temperature variables including temperature sums for different parts of the growing season, temperature variables from May, July and August as well as October mean and maximum temperature. Precipitation sums from different parts of the growing season and August precipitation were negatively correlated with the latewood density indices. In the case of May-August and whole growing season (April-September) precipitation, the correlations were strong and significant even if the strictest Bonferroni correction (Curtin and Schulz, 1998) was applied to the p-values resulting to α' -value of 0.000877 for individual comparisons. Negative correlations between precipitation variables and latewood density would be inline with the findings that precipitation typically increases the growth rate. However, temperature and rainfall were also negatively correlated in the

summer months (Table 6-19) and therefore the negative effect of rainfall could also arise through temperature. Latewood density indices were also significantly correlated with temperature variables of the previous January and May (Figure 6-44). Previous January temperature variables again seem strange candidates to influence latewood density in the year after.

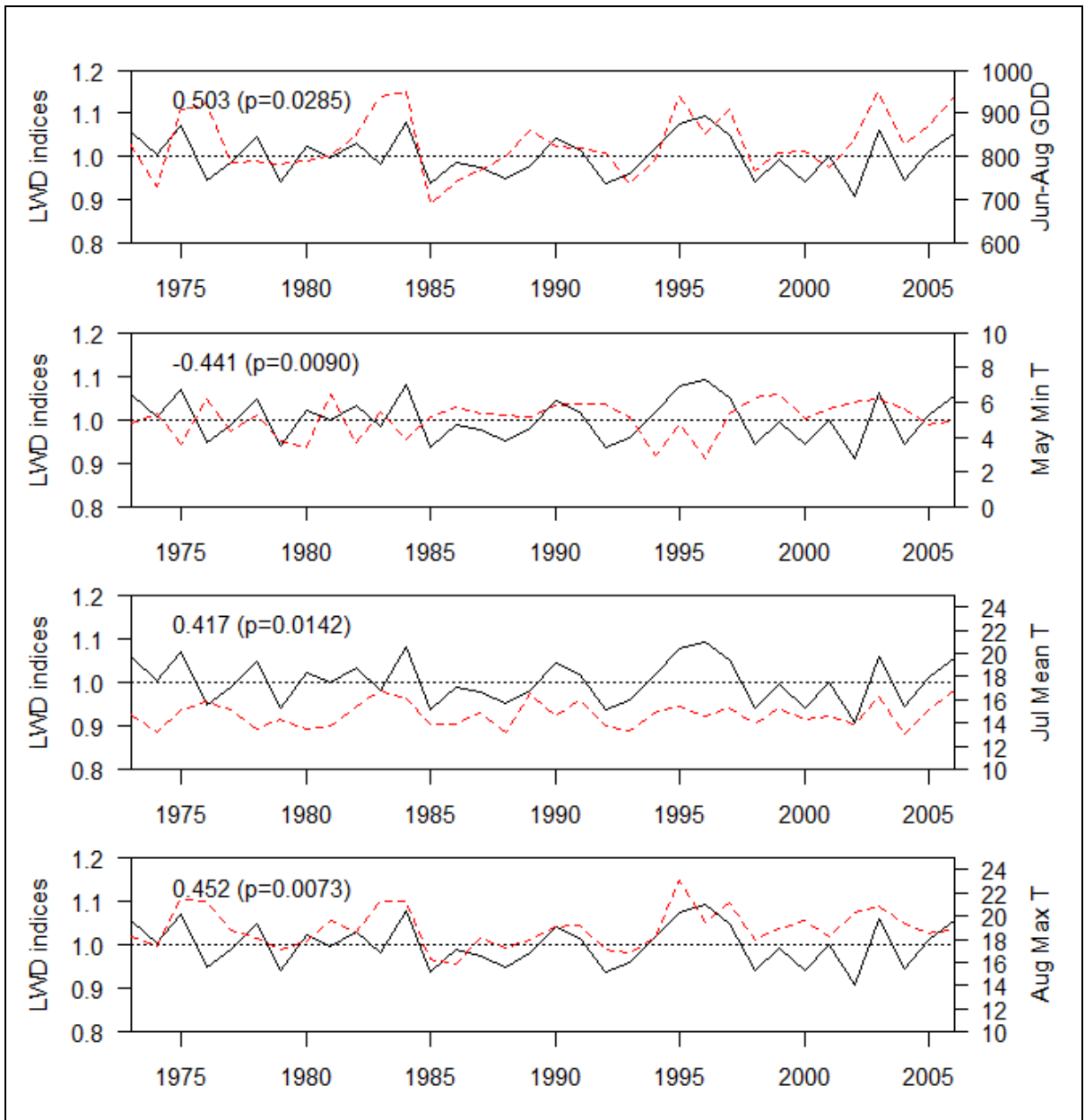


Figure 6-42. Loch Tummel latewood density (LWD) indices plotted against the individually significant weather variables of the current year. Solid line represents the latewood density indices and the dashed red line the weather variable in question. Horizontal line marks the reference level for the latewood density indices. P-value reported refers to individual comparisons. The selected α -level was 0.05. To achieve over all α -level of 0.05 the limit for individual comparisons would be adjusted (Curtin and Schulz, 1998) to approximately 0.0009. Continued next page.

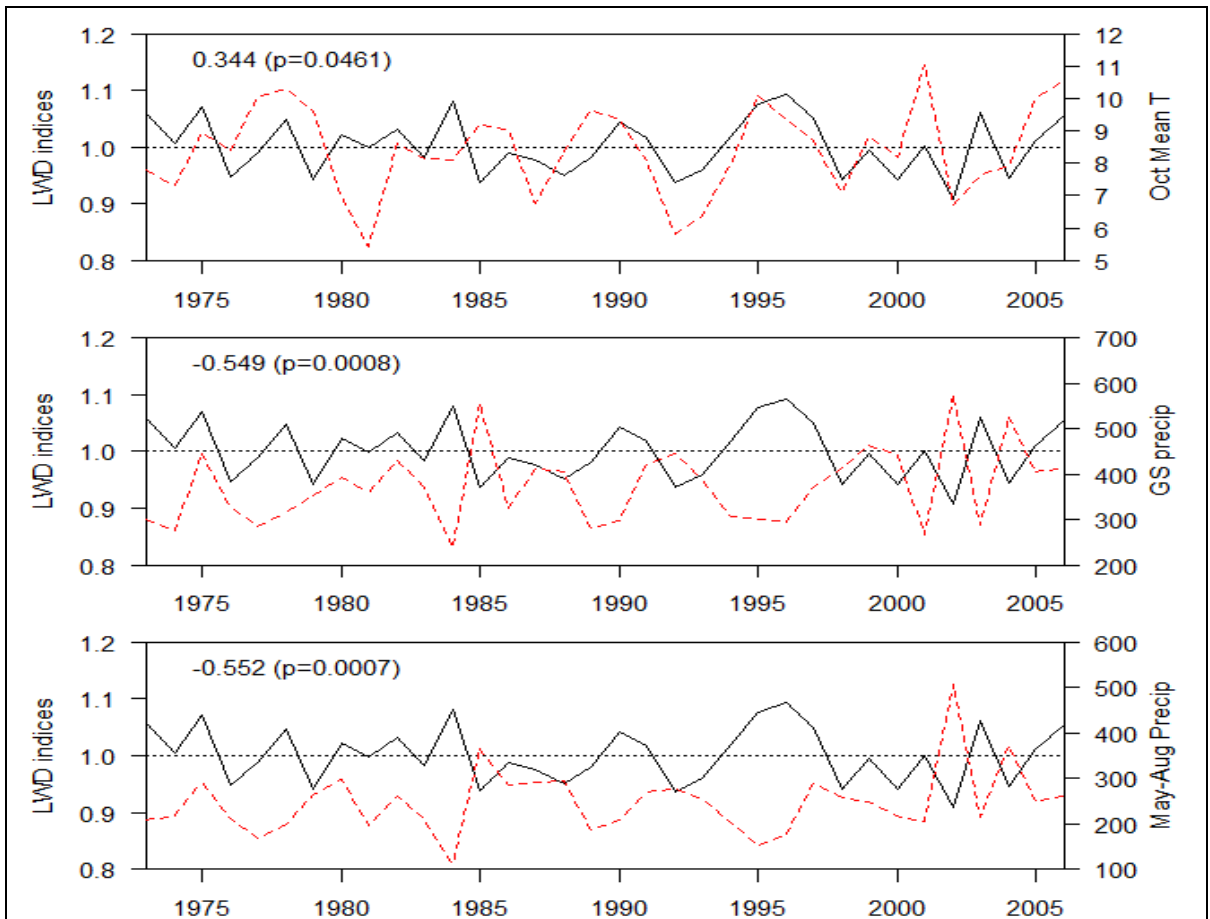


Figure 6-43. Continued Loch Tummel latewood density (LWD) indices plotted against the individually significant weather variables of the current year continued.

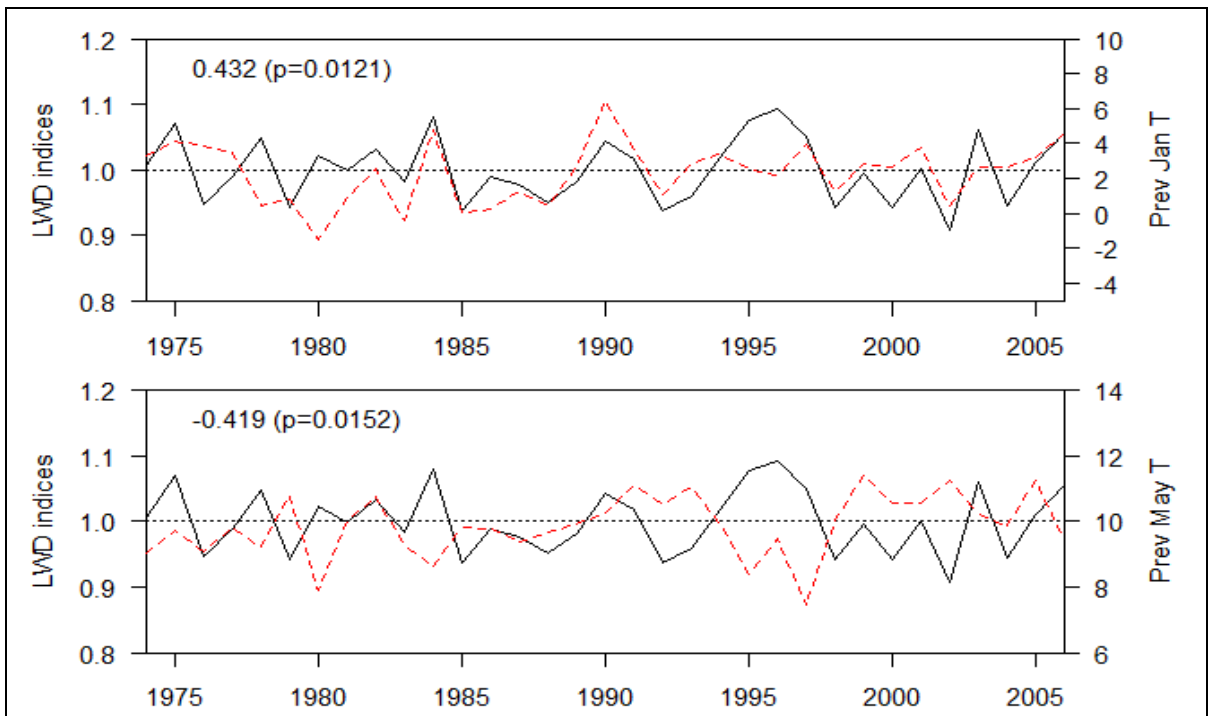


Figure 6-44. Loch Tummel latewood density (LWD) indices plotted against the individually significant weather variables of the previous year. Solid line represents the latewood density indices and the dashed red line the weather variable in question. Horizontal line marks the reference level for the latewood density indices. P-value reported refers to individual comparisons. The selected α -level was 0.05. To achieve over all α -level of 0.05 the limit for individual comparisons would be adjusted (Curtin and Schulz, 1998) to approximately 0.0009.

Latewood width (Figure 6-45) was only significantly correlated with previous year variables. These included May temperature, growing season and September precipitation but correlations were too weak to be significant when α -level was adjusted to 0.0009.

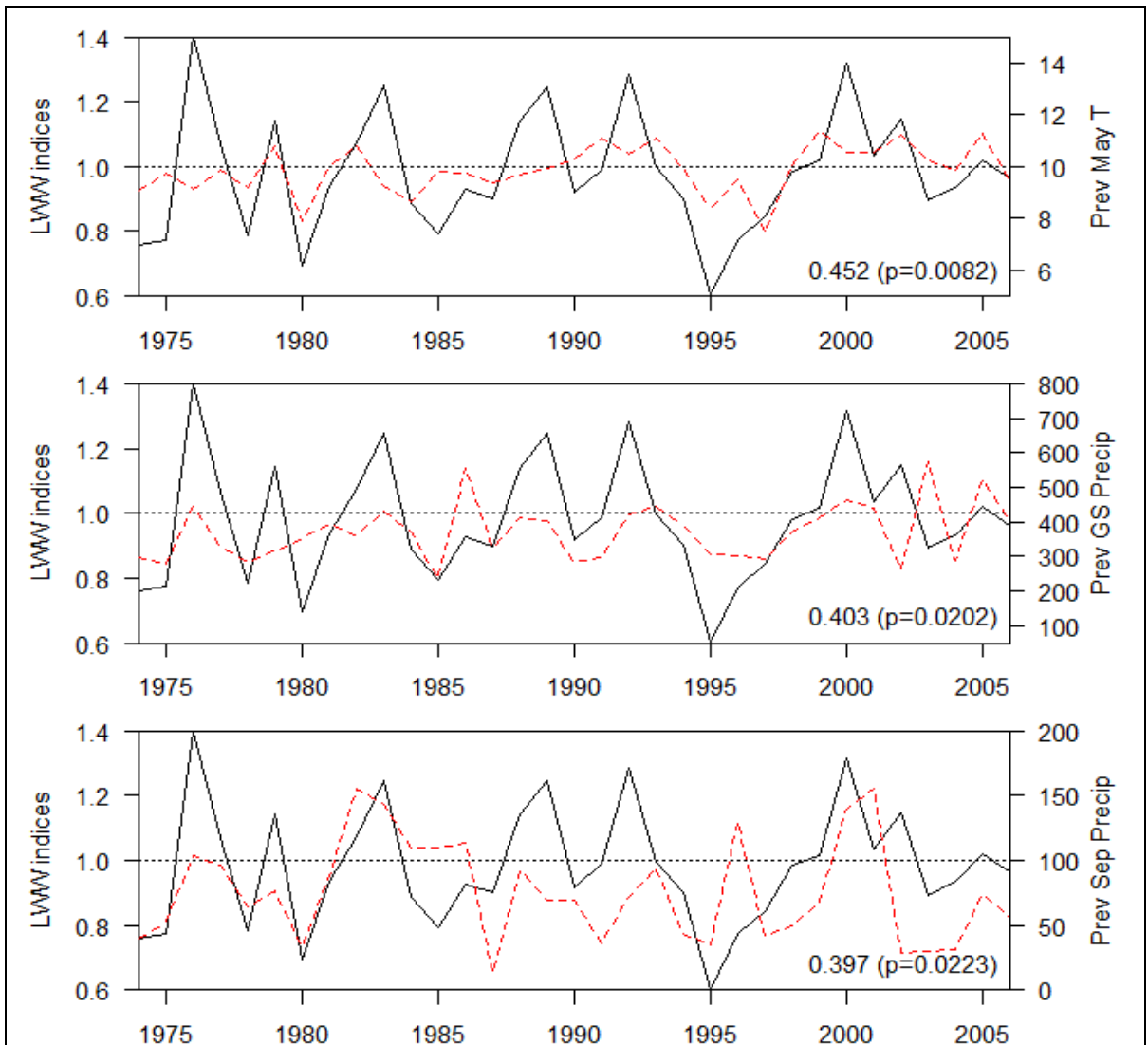


Figure 6-45. Loch Tummel latewood width (LWW) indices plotted against the individually significant weather variables of the previous year. Solid line represents the latewood width indices and the dashed red line the weather variable in question. Horizontal line marks the reference level for the latewood width indices. P-value reported refers to individual comparisons. The selected α -level was 0.05. To achieve over all α -level of 0.05 the limit for individual comparisons would be adjusted (Curtin and Schulz, 1998) to approximately 0.0009.

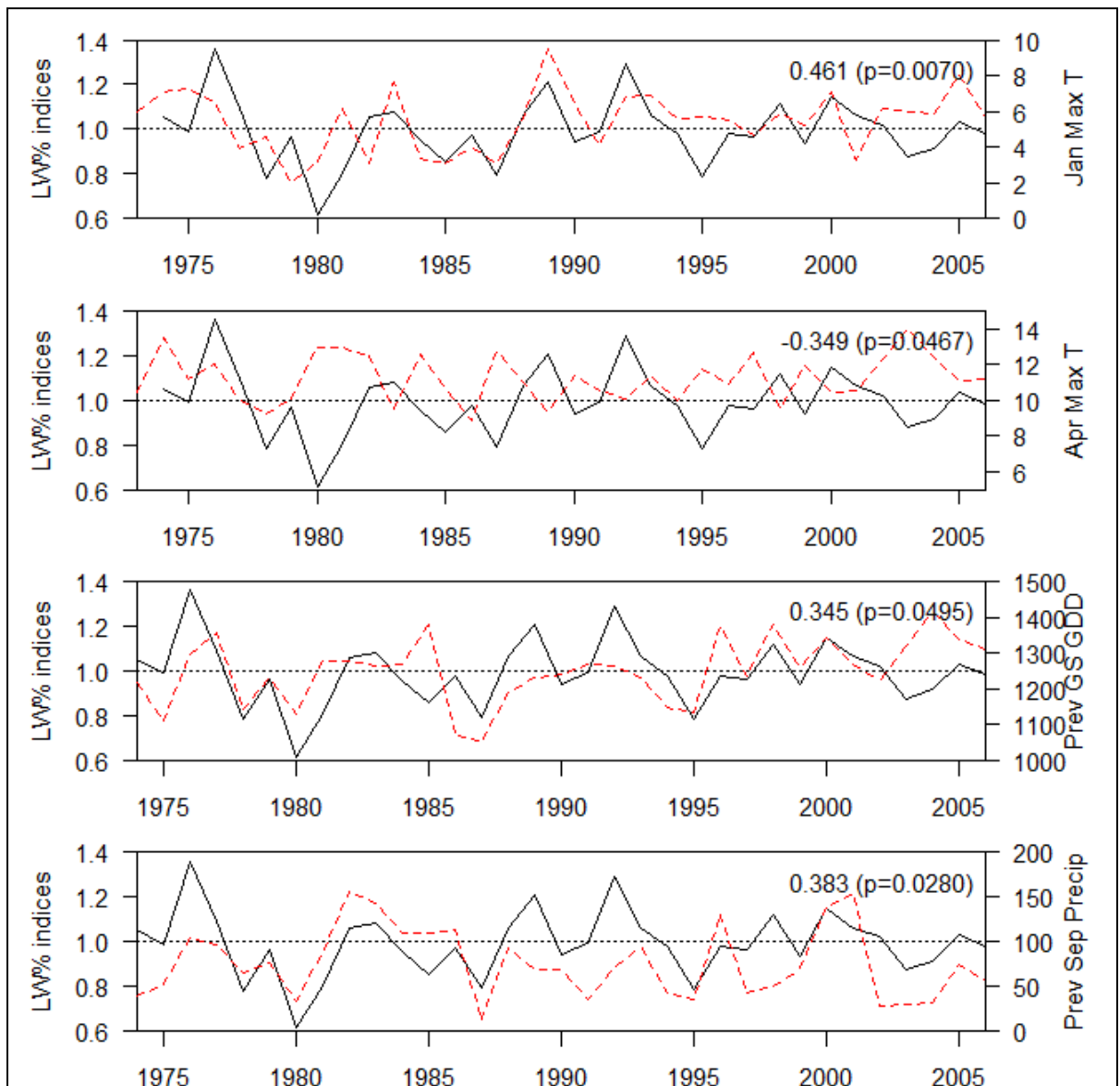


Figure 6-46. Loch Tummel latewood percentage (LW%) indices plotted against the individually significant weather variables of the current and previous year. Solid line represents the latewood percentage indices and the dashed red line the weather variable in question. Horizontal line marks the reference level for latewood percentage indices. P-value reported refers to individual comparisons. The selected α -level was 0.05. To achieve over all α -level of 0.05 the limit for individual comparisons would be adjusted (Curtin and Schulz, 1998) to approximately 0.0009.

Latewood percentage (Figure 6-46) was negatively correlated with the April maximum temperature but positively with January maximum temperature. The former correlation probably arises due to increase in earlywood formation which would reduce the percentage accounted for by latewood. January temperatures were negatively correlated with earlywood width even if the association was weaker ($r=-0.316$, $p=0.073$) and was therefore not included in these plots. However, the negative influence on earlywood width could indicate a mechanism for increasing the latewood percentage. Of the previous season's climatic variables (Figure 6-46), growing season temperature sum and September rainfall

were positively correlated with latewood percentage. Using a stricter α -level for multiple comparisons all these correlations became insignificant.

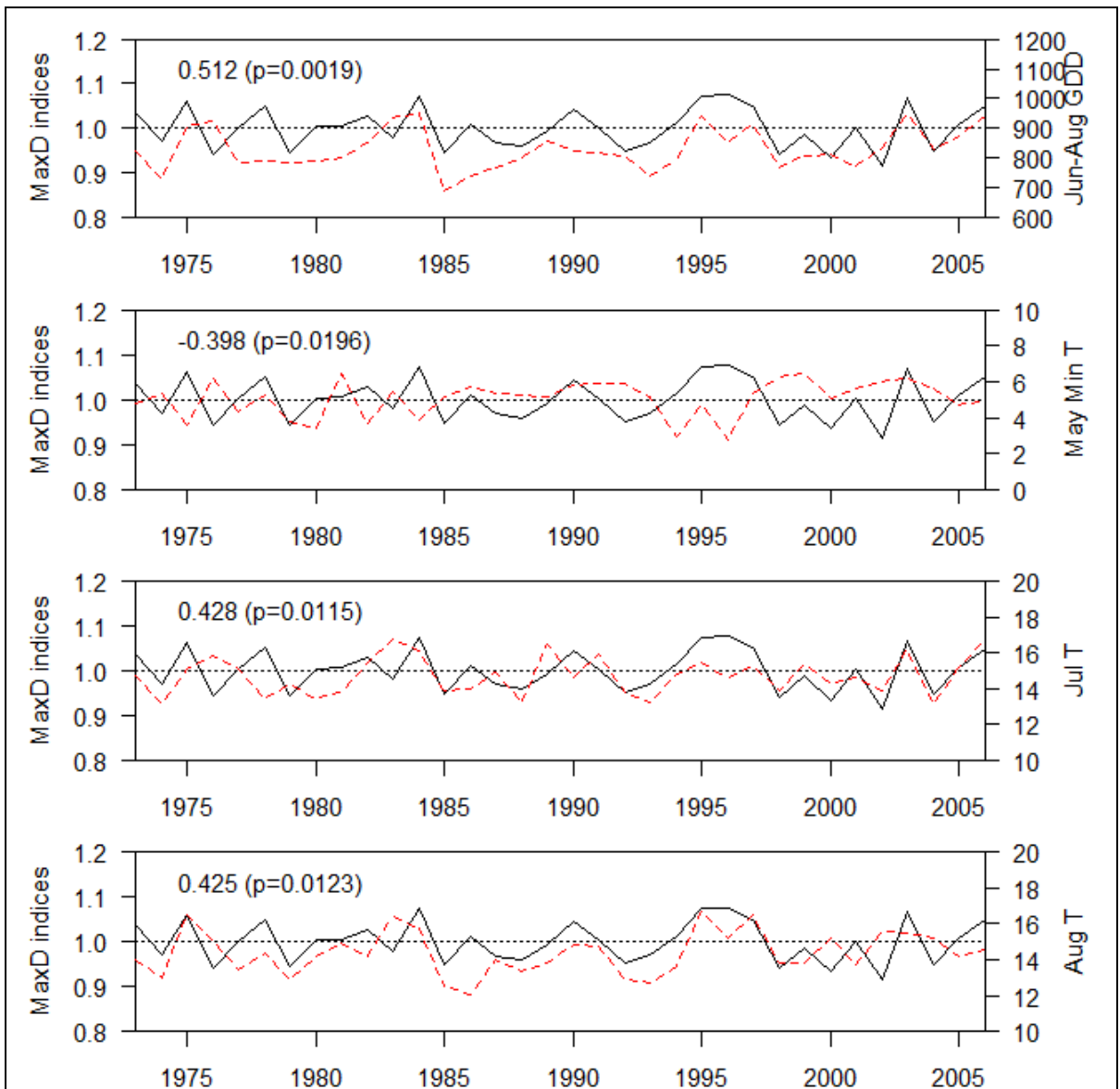


Figure 6-47. Loch Tummel maximum density (MaxD) indices plotted against the individually significant weather variables of the current year. Solid line represents the maximum density indices and the dashed red line the weather variable in question. Horizontal line marks the reference level for the maximum density indices. P-value reported refers to individual comparisons. The selected α -level was 0.05. To achieve over all α -level of 0.05 the limit for individual comparisons would be adjusted (Curtin and Schulz, 1998) to approximately 0.0009. Continued next page.

Ring maximum density (Figure 6-47 and Figure 6-48) at the Loch Tummel site was positively correlated with various temperature variables (all temperature sums, July and August temperatures, October maximum and mean and November mean temperature) and negatively with precipitation variables (all rainfall sums, August and September precipitation) of the current season. May minimum temperature with a negative correlation

with Maximum density formed an exception from the general direction of temperature correlations. Negative correlations with growing season and May-August precipitation were so strong that they would even be included under the most stringent Bonferroni correction (Curtin and Schulz, 1998) for multiple correlations (which for this dataset would give $\alpha'=0.0009$). All in all, temperature late in the summer tended to increase Maximum density whereas spring temperature (May) decreased it.

Relationships with climate of the previous year also included a positive correlation with January temperatures and negative correlations with May temperatures (maximum and mean). Again, it is difficult to imagine how temperature in the beginning of the previous year would influence the maximum density of the ring as maximum density usually occurs at the end of latewood. By using the stricter $\alpha'=0.0009$ these became insignificant.

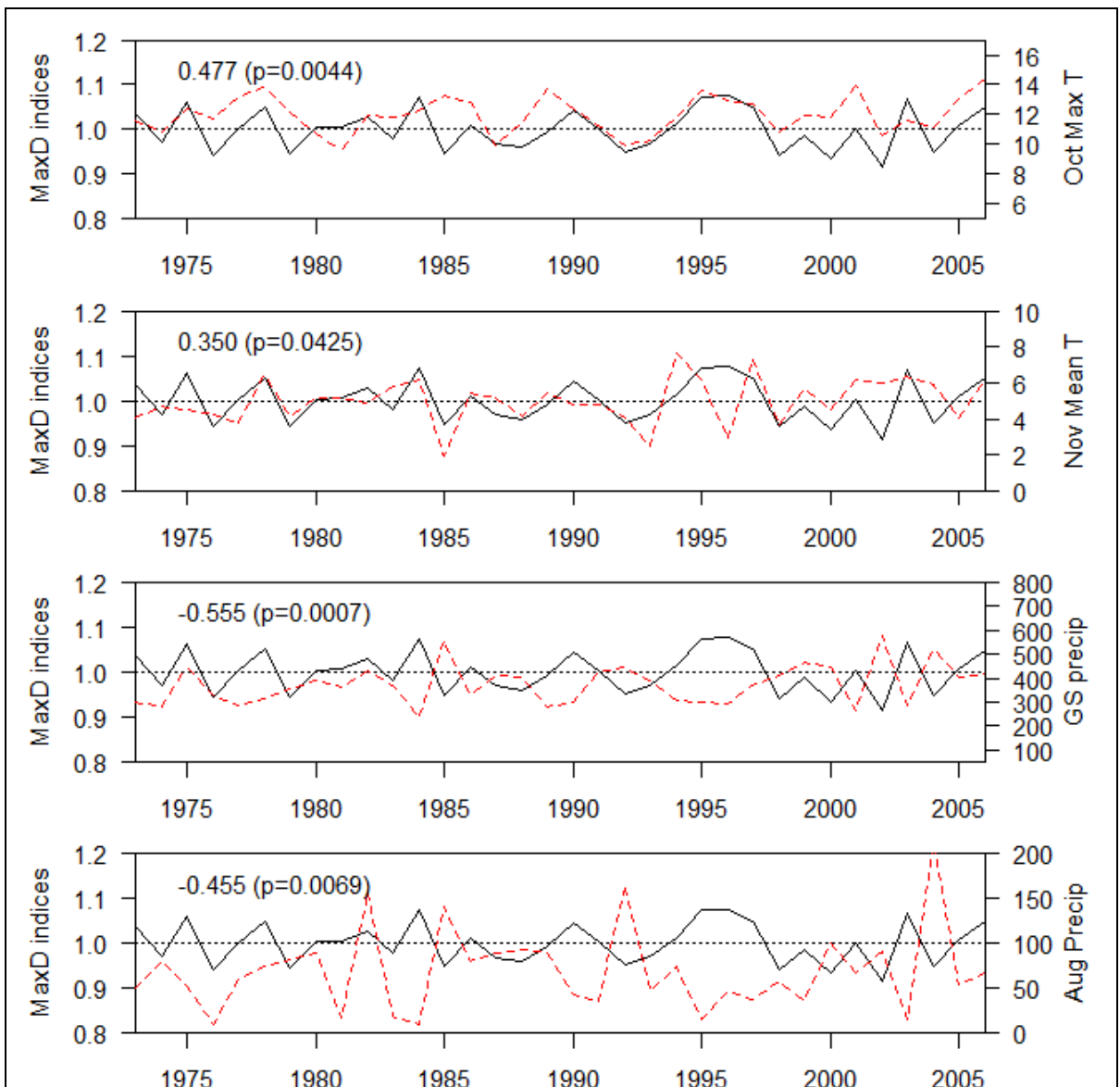


Figure 6-48. Continued Loch Tummel maximum density (MaxD) indices plotted against the individually significant weather variables of the current year continued.

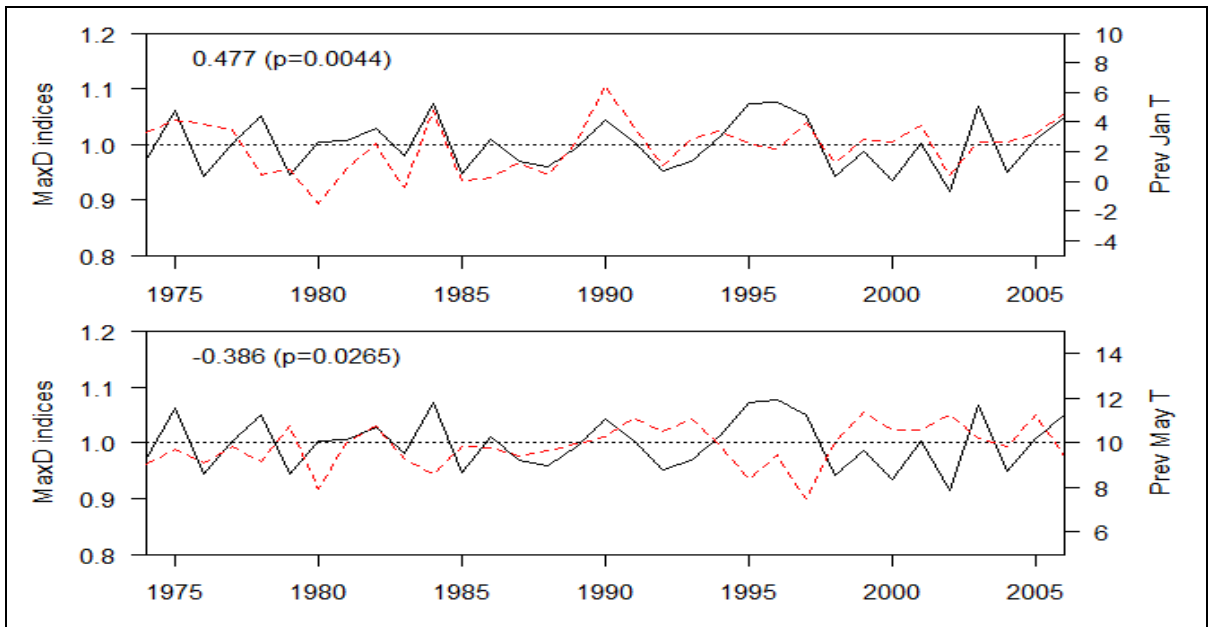


Figure 6-49. Loch Tummel maximum density (MaxD) indices plotted against the individually significant weather variables of the previous year. Solid line represents the maximum density indices and the dashed red line the weather variable in question. Horizontal line marks the reference level for the maximum density indices. P-value reported refers to individual comparisons. The selected α -level was 0.05. To achieve over all α -level of 0.05 the limit for individual comparisons would be adjusted (Curtin and Schulz, 1998) to approximately 0.0009.

Ring minimum density (Figure 6-50) was only correlated with January precipitation (positively) and previous March precipitation (negatively). Under adjusted α no correlations would remain significant.

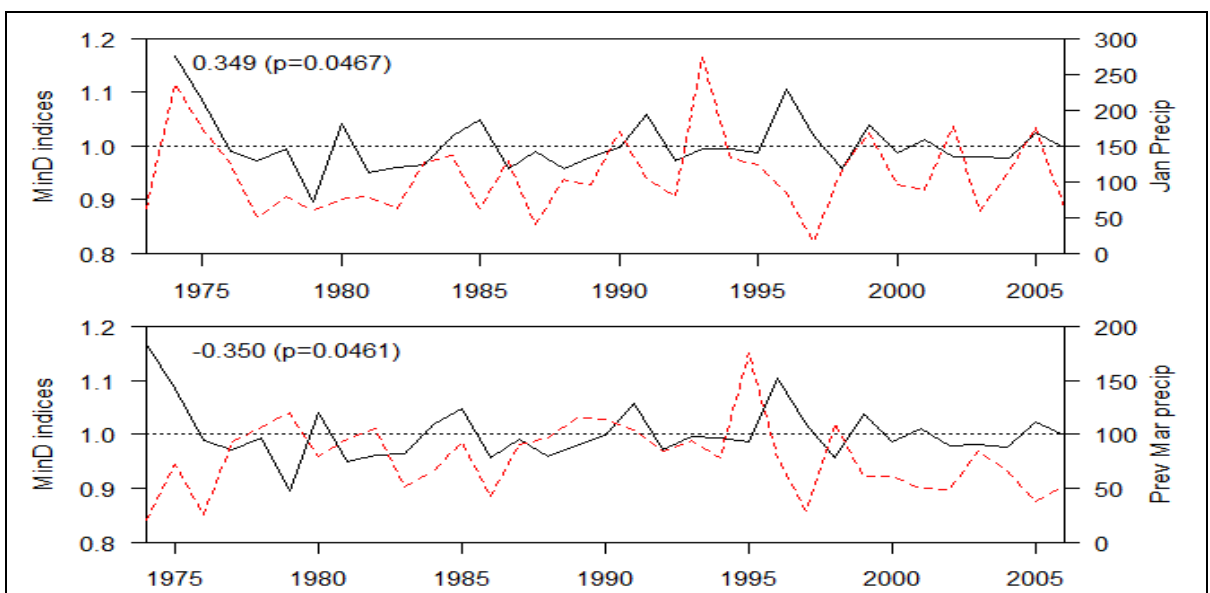


Figure 6-50. Loch Tummel minimum density (MinD) indices plotted against the individually significant weather variables of the current and previous year. Solid line represents the minimum density indices and the dashed red line the weather variable in question. Horizontal line marks the reference level for the minimum density indices. P-value reported refers to individual comparisons. The selected α -level was 0.05. To achieve over all α -level of 0.05 the limit for individual comparisons would be adjusted (Curtin and Schulz, 1998) to approximately 0.0009.

Table 6-19. Correlation between mean temperature and the rainfall of the period for Loch Tummel site.

Rainfall Period	Max T		Min T		Mean T	
	Correlation coef.	p-value	Correlation coef.	p-value	Correlation coef.	p-value
January	0.478	0.0043	0.423	0.0128	0.465	0.0056
February	0.295	0.0903	0.256	>0.1 ns.	0.283	>0.1 ns.
March	-0.053	>0.1 ns.	0.152	>0.1 ns.	0.043	>0.1 ns.
April	-0.389	0.0231	0.387	0.0236	-0.061	>0.1 ns.
May	-0.541	0.0009	0.406	0.0172	-0.175	>0.1 ns.
June	-0.554	0.0007	-0.178	>0.1 ns.	-0.436	0.0100
July	-0.543	0.0009	-0.088	>0.1 ns.	-0.424	0.0125
August	-0.506	0.0022	-0.117	>0.1 ns.	-0.402	0.0186
September	0.058	>0.1 ns.	0.445	0.0084	0.297	0.0876
October	0.169	>0.1 ns.	0.324	0.0613	0.267	>0.1 ns.
November	0.179	>0.1 ns.	0.225	>0.1 ns.	0.221	>0.1 ns.
December	0.060	>0.1 ns.	0.156	>0.1 ns.	0.119	>0.1 ns.
Year	-	-	-	-	0.123	>0.1 ns.
Growing season	-	-	-	-	0.064	>0.1 ns.
May-August	-	-	-	-	-0.201	>0.1 ns.
June-August	-	-	-	-	-0.416	0.0145

Table 6-20. Correlations between the site average tree ring chronologies of the Loch Tummel site. Level of significance ($\alpha=0.05$) is 0.348.

	RW	RD	EWV	LWW	EWD	LWD	LW%	MaxD	MinD
RW	1	-0.513	0.810	0.299	-0.452	-0.408	-0.088	-0.453	-0.161
RD	-0.513	1	-0.708	-0.130	0.887	0.533	0.357	0.480	0.622
EWV	0.810	-0.708	1	0.024	-0.619	-0.137	-0.495	-0.088	-0.419
LWW	0.299	-0.130	0.024	1	-0.426	-0.635	0.791	-0.598	-0.495
EWD	-0.452	0.887	-0.619	-0.426	1	0.477	0.050	0.396	0.798
LWD	-0.408	0.533	-0.137	-0.635	0.477	1	-0.414	0.975	0.413
LW%	-0.088	0.357	-0.495	0.791	0.050	-0.414	1	-0.398	-0.121
MaxD	-0.453	0.480	-0.088	-0.598	0.396	0.975	-0.398	1	0.273
MinD	-0.161	0.622	-0.419	-0.495	0.798	0.413	-0.121	0.273	1

Investigation of cross-correlations (Figure 6-51) between ring indices and the selected climatic variables that were significantly correlated either at lag 0 or 1 ($\alpha=0.05$) yielded some spurious correlations between ring variables and future climate (positive lags). However, so far, the detrended site mean tree ring chronologies had been related to untreated climate data. Therefore, there was a risk of detecting a relationship due to the pattern of autocorrelation (Diggle, 1990). This is particularly true for short series (Brockwell and Davis, 1996). Therefore, the correlations that were significant at $\alpha=0.0009$ were selected to be treated further by prewhitening the climate data as well (6.3.4.3).

At the Loch Tummel site there was also a potential issue with the detrending process. There was a sudden increase in tree ring width in most trees approximately at ring 20-21 depending on when the trees had reached breast height (Figure 6-52). The cause of this remains unknown as the Forestry Commission database had a record of thinning treatment only in 2004 which is much after this growth increase. There was no mention of previous thinning or fertiliser application. The spline function only partially removed the effect of these growth rate changes, which may have caused problems with the data analysis as some trends were left in the data. However, the autocorrelation plots (Figure 6-35) indicated the average site chronology did not suffer from these effects.

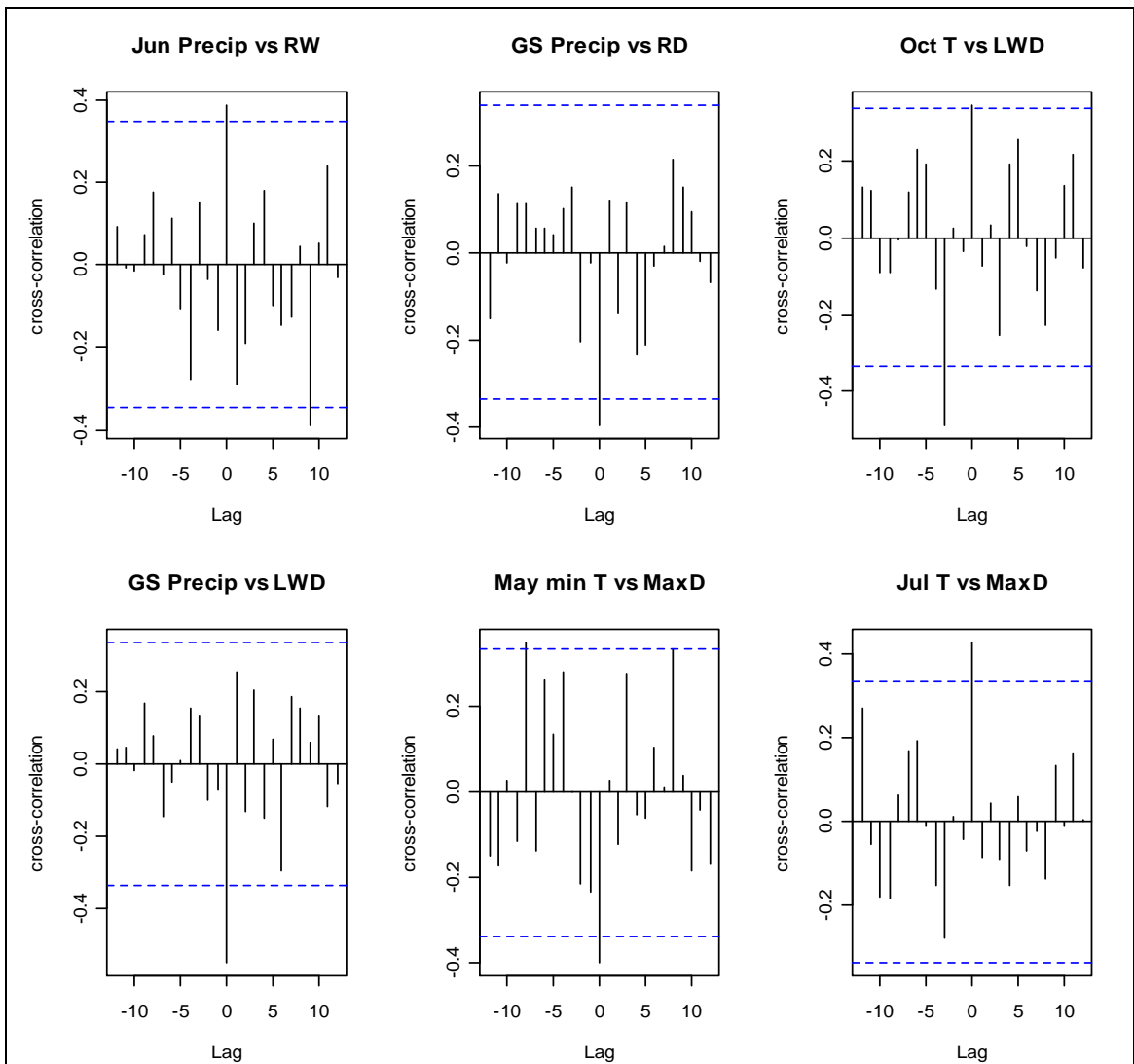


Figure 6-51. Selected cross-correlograms between climate and tree ring variables from the Loch Tummel site.

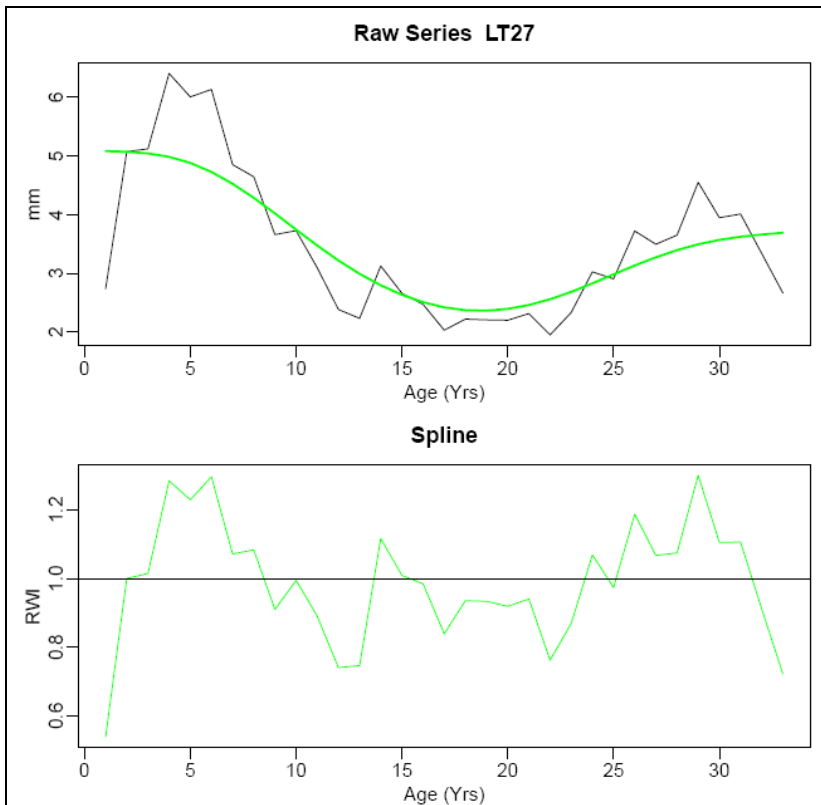


Figure 6-52. Non optimal detrending that occurred in some Loch Tummel samples that had a peculiar radial ring width pattern due to change in growth rate around ring 20-21.

6.3.4.2 Tree ring and weather relationships at the Coalburn site

The autocorrelation plots of the site tree ring chronologies (Figure 6-53) indicated that the prewhitening of the individual series had removed the autocorrelation successfully. Only in the case of latewood percentage (LW%) there was a correlation at lag 9 that exceeded the 95% confidence interval indicated by the dashed lines but there were no systematic patterns. In general, the autocorrelation was also low in the weather variables. Only in 12 cases of the 57 weather variables examined at 14 lag positions, autocorrelations that exceed the 95% confidence interval were detected (plots not shown, See Appendix 9 for full autocorrelation matrix).

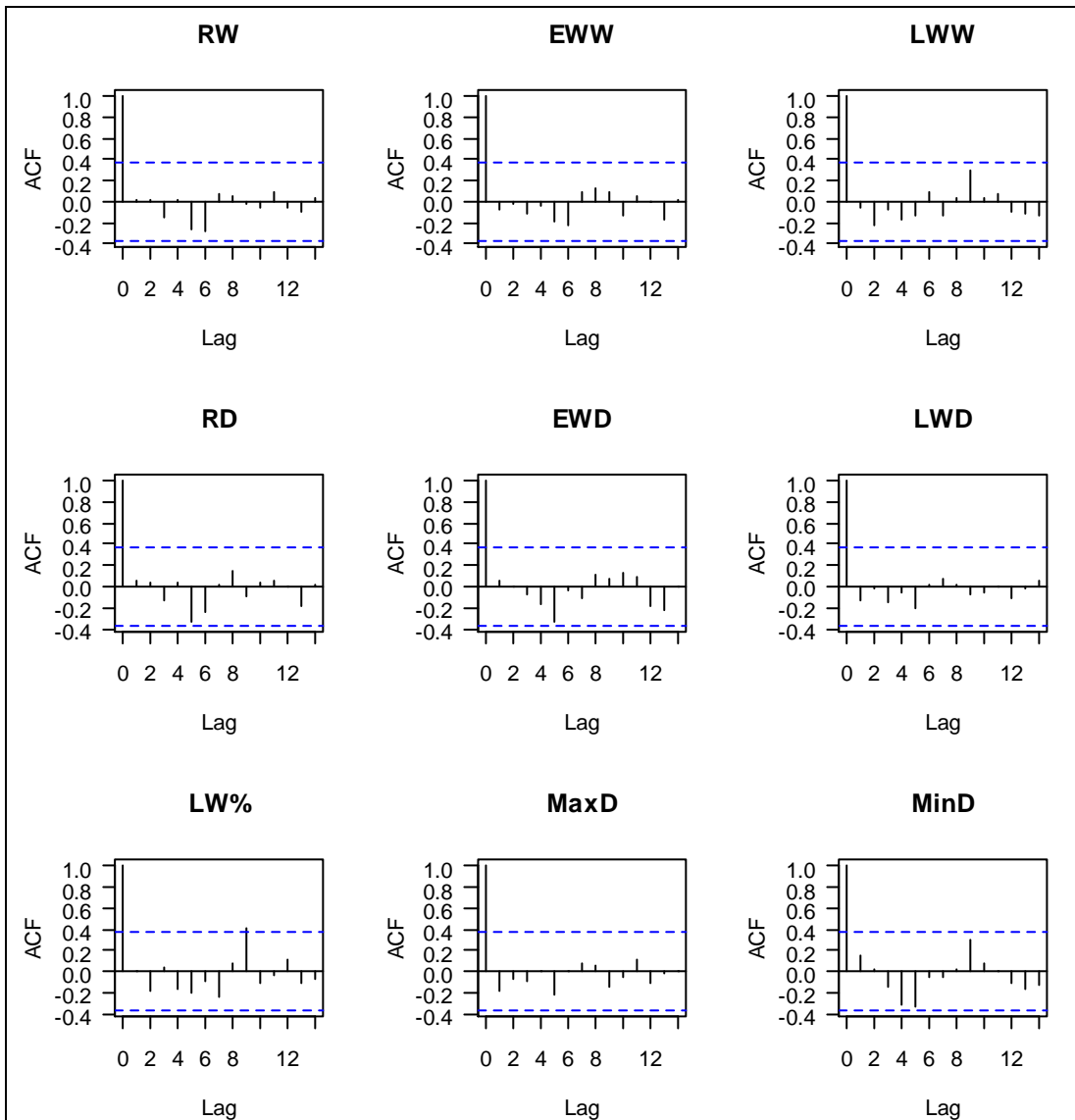


Figure 6-53. Remaining autocorrelation in the average tree ring chronologies at the Coalburn site.

At the Coalburn site, the ring width (Figure 6-54) was negatively correlated with winter (January minimum and mean T), spring (May maximum T) and autumn (September minimum and mean) temperatures. The latter makes no physiological sense since the larger part of the ring is composed of earlywood which should be formed by September. At the Coalburn site, the average latewood percentage was 26% (Table 6-6). Furthermore, the dendrometer experiment (Chapter 4) indicated that very little if any growth takes place this late in the season. Ring width was not correlated with climatic variables from the previous year. Under adjusted α' (0.0009) these correlations were non-significant.

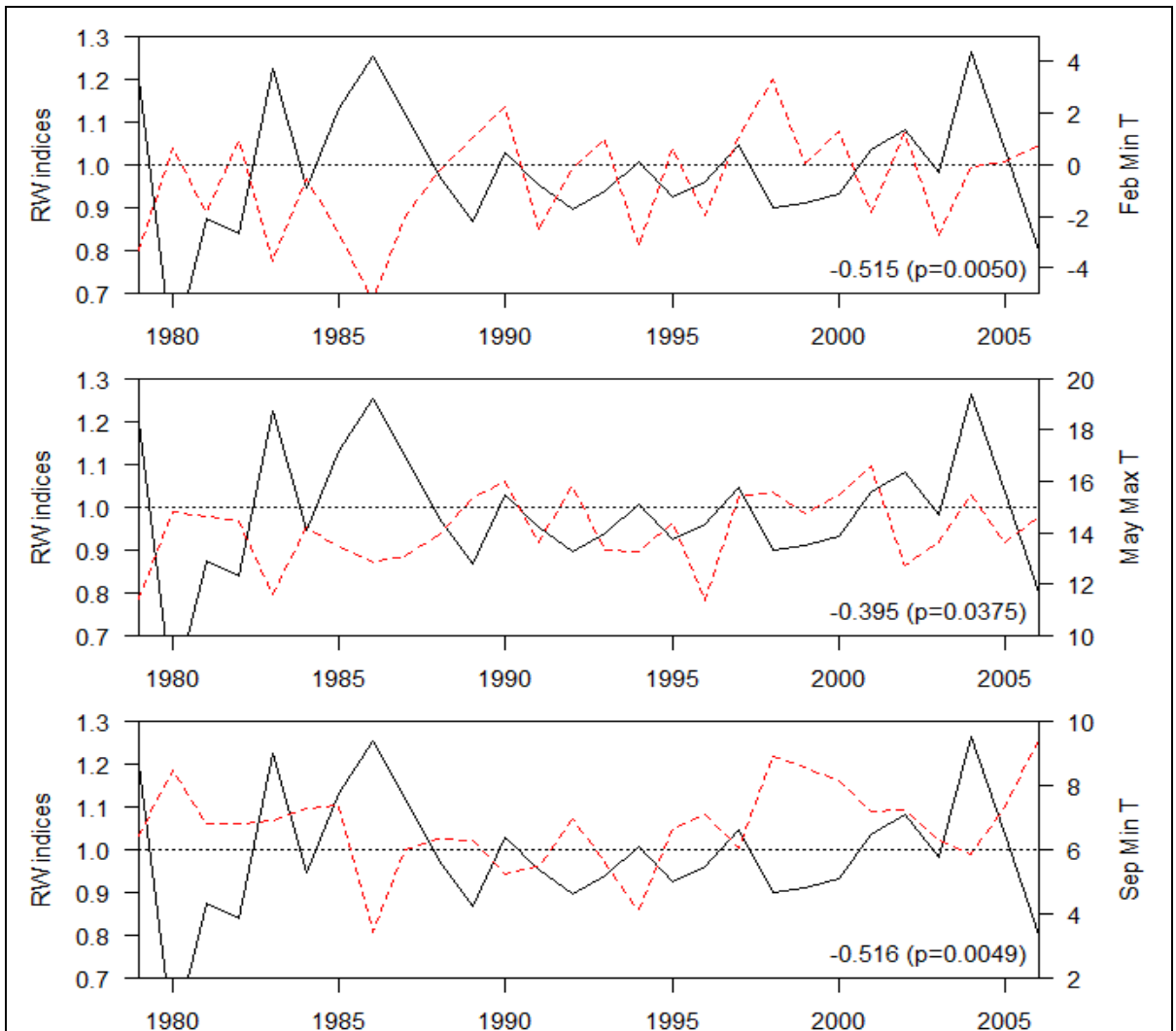


Figure 6-54. Coalburn ring width (RW) indices plotted against the individually significant weather variable of the current year. Solid line represents the tree ring width indices and the dashed red line the weather variable in question. Horizontal line marks the reference level for the tree ring width indices. P-value reported refers to individual comparisons. The selected α -level was 0.05. To achieve over all α -level of 0.05 the limit for individual comparisons would be adjusted (Curtin and Schulz, 1998) to approximated 0.0009.

Ring density (Figure 6-55) on the other hand was significantly positively correlated with winter (all February temperature variables), spring (May maximum T) and autumn (September minimum and mean T) temperatures. Furthermore, it was positively correlated with the temperature of the previous autumn (September maximum and mean). Precipitation in the previous December was negatively related to ring density (Figure 6-56). These correlations were non-significant under adjusted α' (0.0009).

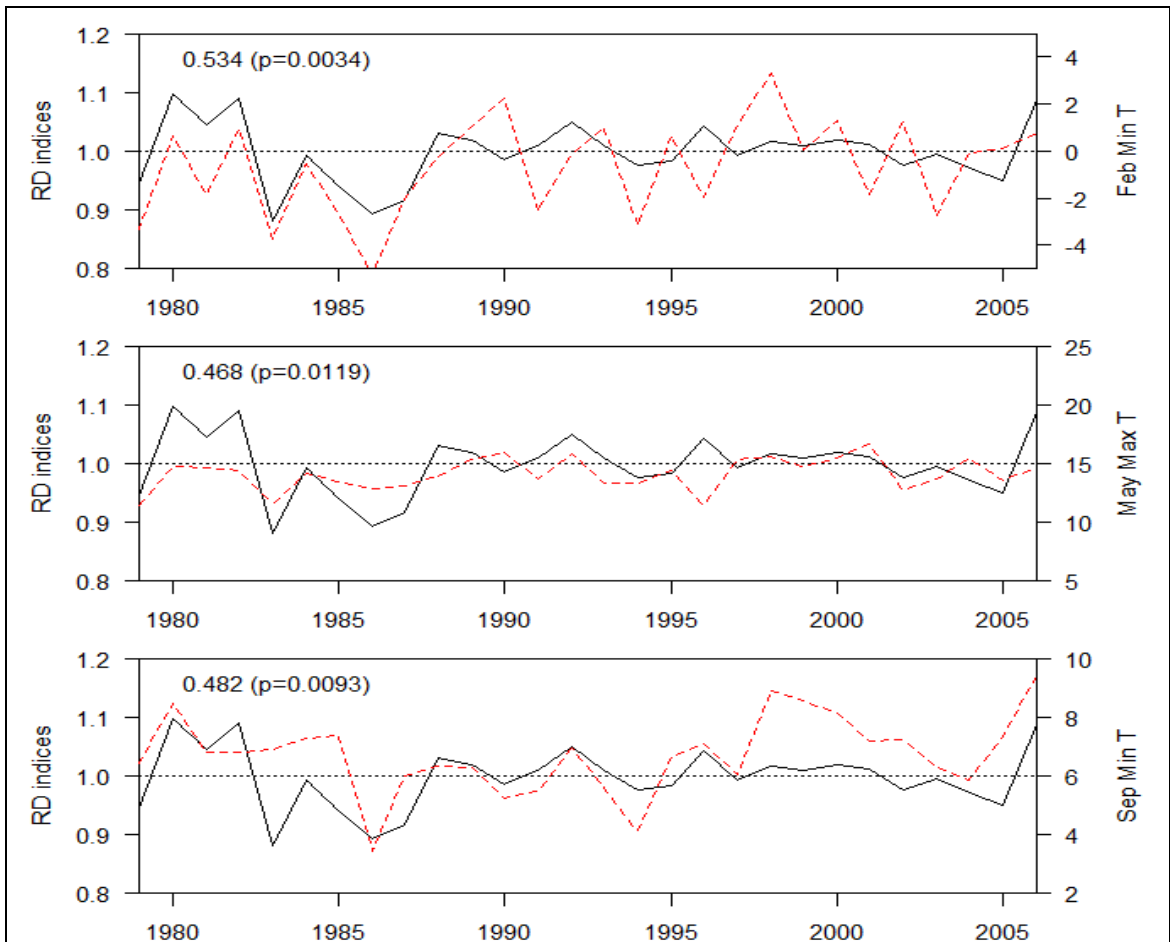


Figure 6-55. Coalburn ring density (RD) indices plotted against the individually significant weather variables of the current year. Solid line represents the tree ring density indices and the dashed red line the weather variable in question. Horizontal line marks the reference level for the tree ring density indices. P-value reported refers to individual comparisons. The selected α -level was 0.05. To achieve over all α -level of 0.05 the limit for individual comparisons would be adjusted (Curtin and Schulz, 1998) to approximately 0.0009.

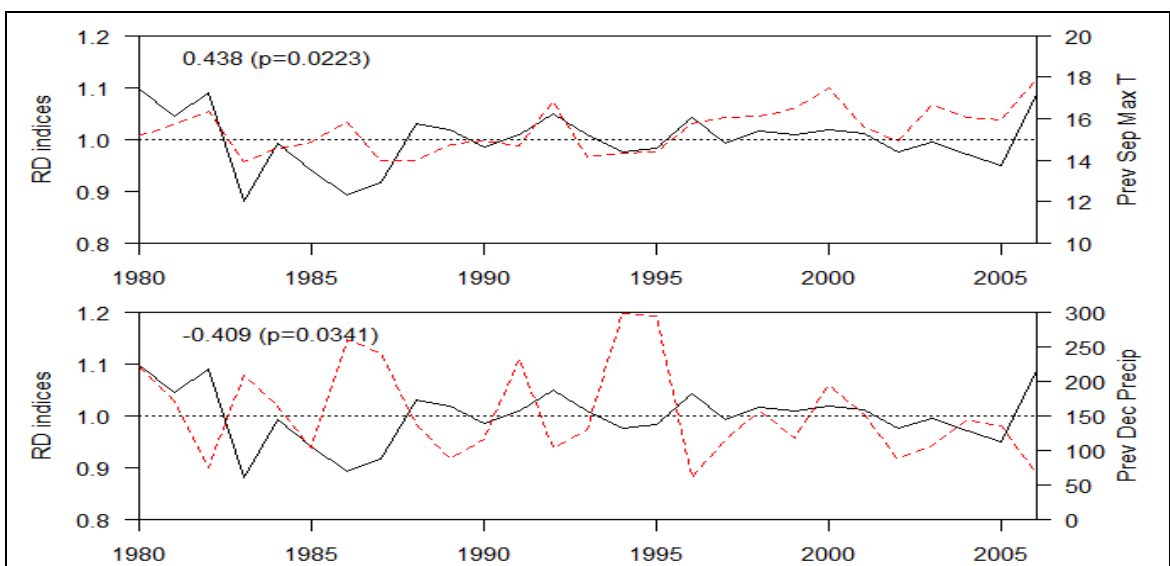


Figure 6-56. Coalburn ring density (RD) indices plotted against the individually significant weather variables of the previous year. Solid line represents the tree ring density indices and the dashed red line the weather variable in question. Horizontal line marks the reference level for the tree ring density indices. P-value reported refers to individual comparisons. The selected α -level was 0.05. To achieve over all α -level of 0.05 the limit for individual comparisons would be adjusted (Curtin and Schulz, 1998) to approximately 0.0009.

Earlywood density (Figure 6-57) at the Coalburn site was positively correlated with February temperature (minimum and mean) and September mean temperature. Winter temperatures seem to have significant correlations with many ring variables indicating that the effect is genuine. Perhaps warm temperatures in February increase respiratory losses and hence decrease growth rate in the beginning of the growing season and therefore lead to higher density. However, peculiarly December temperature of the previous year was negatively related to earlywood density but perhaps the December temperature might still be influencing when the trees enter dormancy whereas February temperature could be related to either respiratory losses, chilling requirement or the dynamics leading to release of dormancy. Using the stricter α' (0.0009) to allow for multiple comparisons, all of these relationships became non-significant.

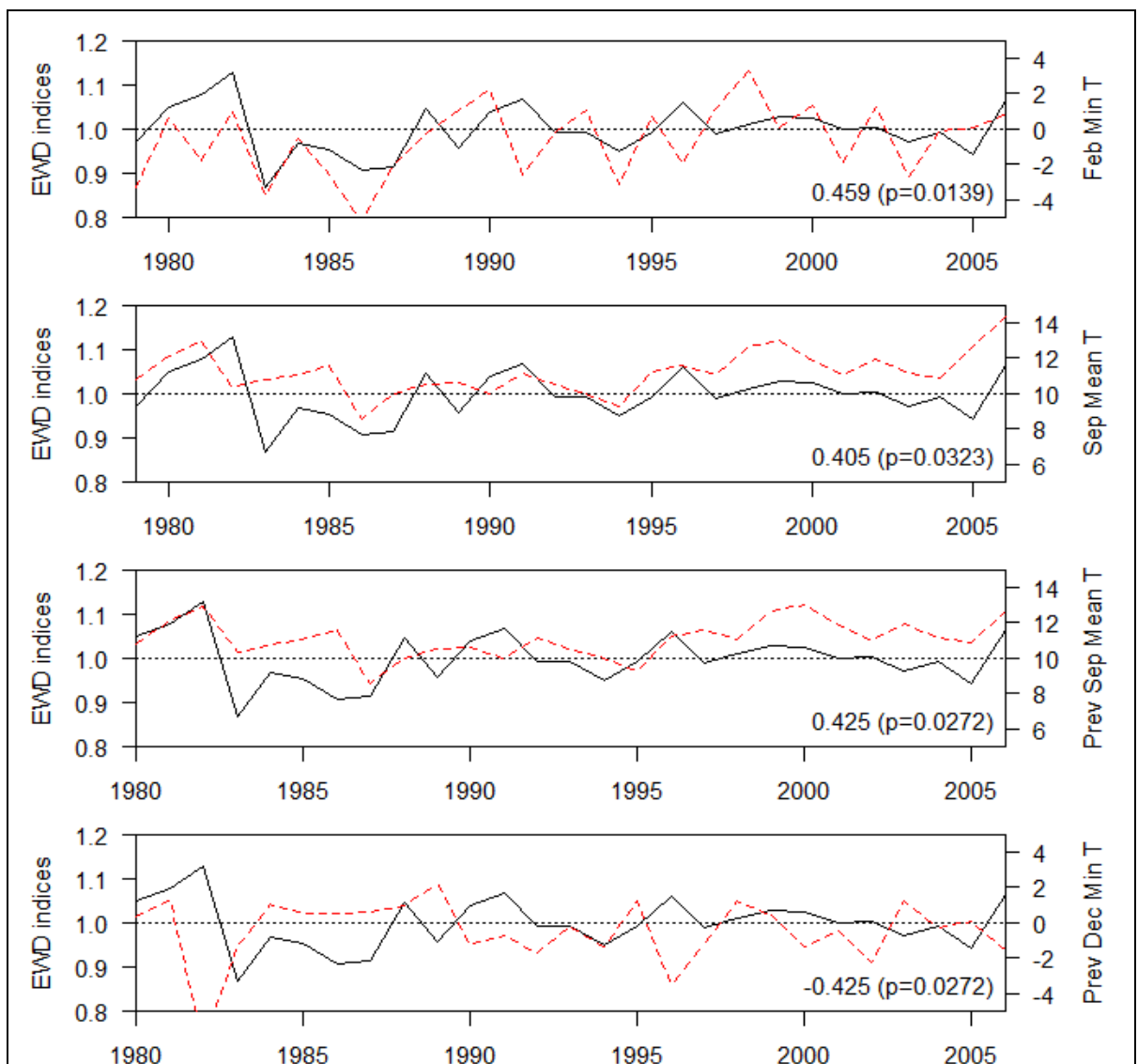


Figure 6-57. Coalburn earlywood density (EWD) indices plotted against the individually significant weather variables of the current and previous year. Solid line represents the earlywood density indices and the dashed red line the weather variable in question. Horizontal line marks the reference level for the earlywood density indices. P-value reported refers to individual comparisons. The selected α -level was 0.05. To achieve over all α -level of 0.05 the limit for individual comparisons would be adjusted (Curtin and Schulz, 1998) to approximately 0.0009.

Earlywood width (Figure 6-58) was negatively correlated with February minimum, May maximum and September minimum temperature at the Coalburn site. All of the correlations were strong but the p-values were still above the α' (0.0009). Variables of the previous year were not significantly related with earlywood width.

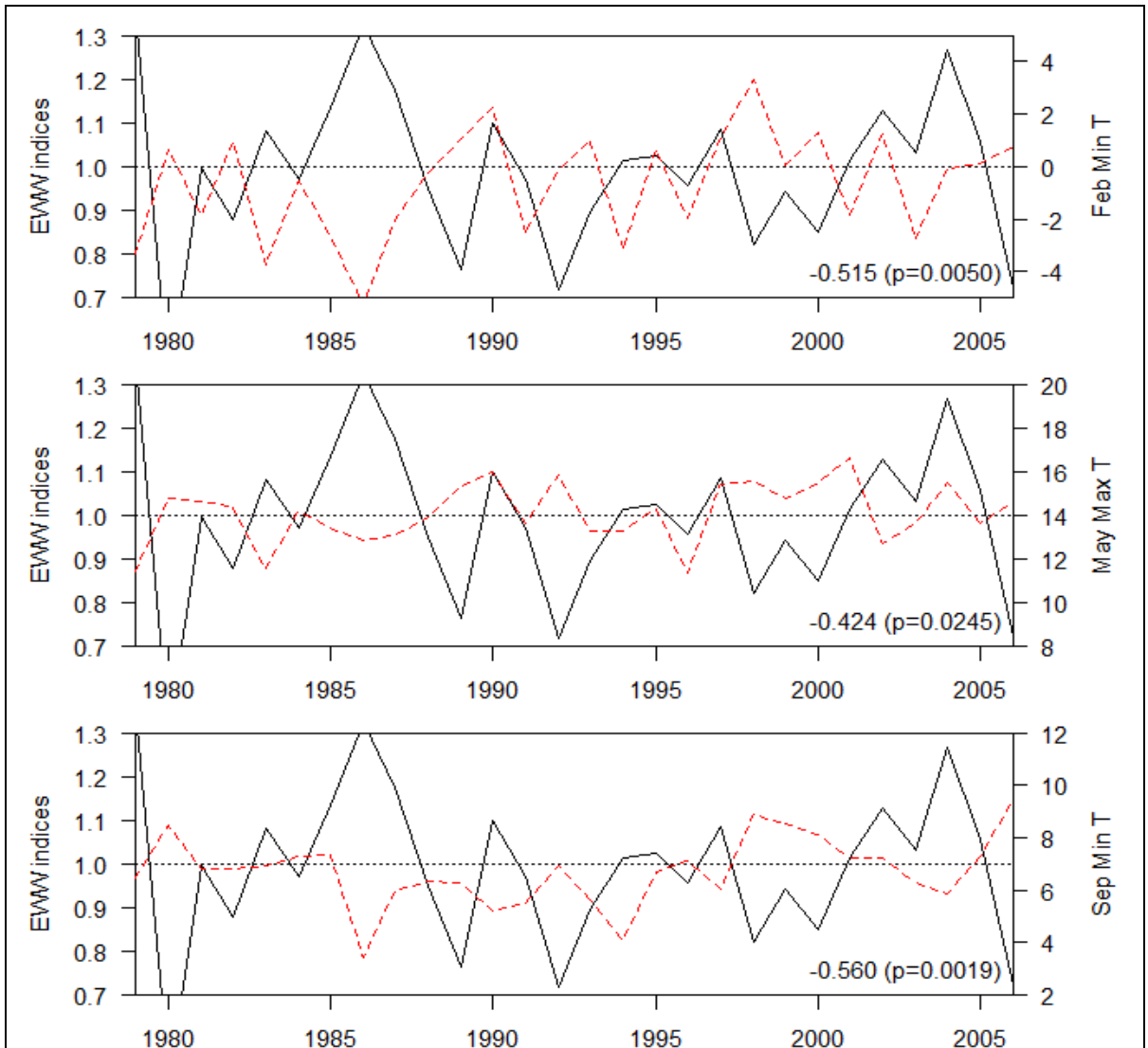


Figure 6-58. Coalburn earlywood width (EWW) indices plotted against the individually significant weather variables of the current year. Solid line represents the earlywood width indices and the dashed red line the weather variable in question. Horizontal line marks the reference level for the earlywood width indices. P-value reported refers to individual comparisons. The selected α -level was 0.05. To achieve over all α -level of 0.05 the limit for individual comparisons would be adjusted (Curtin and Schulz, 1998) to approximated 0.0009.

Latewood density (Figure 6-59) was positively correlated with April maximum temperature and negatively with the December maximum temperature. It is quite difficult to think how December temperature would influence latewood density unless some cell wall lignification continued this late into the season. Latewood density was negatively correlated with precipitation variables (growing season total, annual total and April precipitation). The correlations with April temperature and rainfall were so strong that they

would remain significant even after Bonferroni correction for multiple comparison ($\alpha' = 0.0009$). July and August minimum temperatures of the previous year had a negative correlation with latewood density (Figure 6-60) but these were not strong enough to be significant if the Bonferroni correction was used.

Precipitation variables had a negative influence on the latewood density which is expected as rainfall would increase ring width, which in turn was negatively related to the density. At the Coalburn site, latewood density was significantly correlated with latewood width indices ($r = -0.707$, Table 6-22).

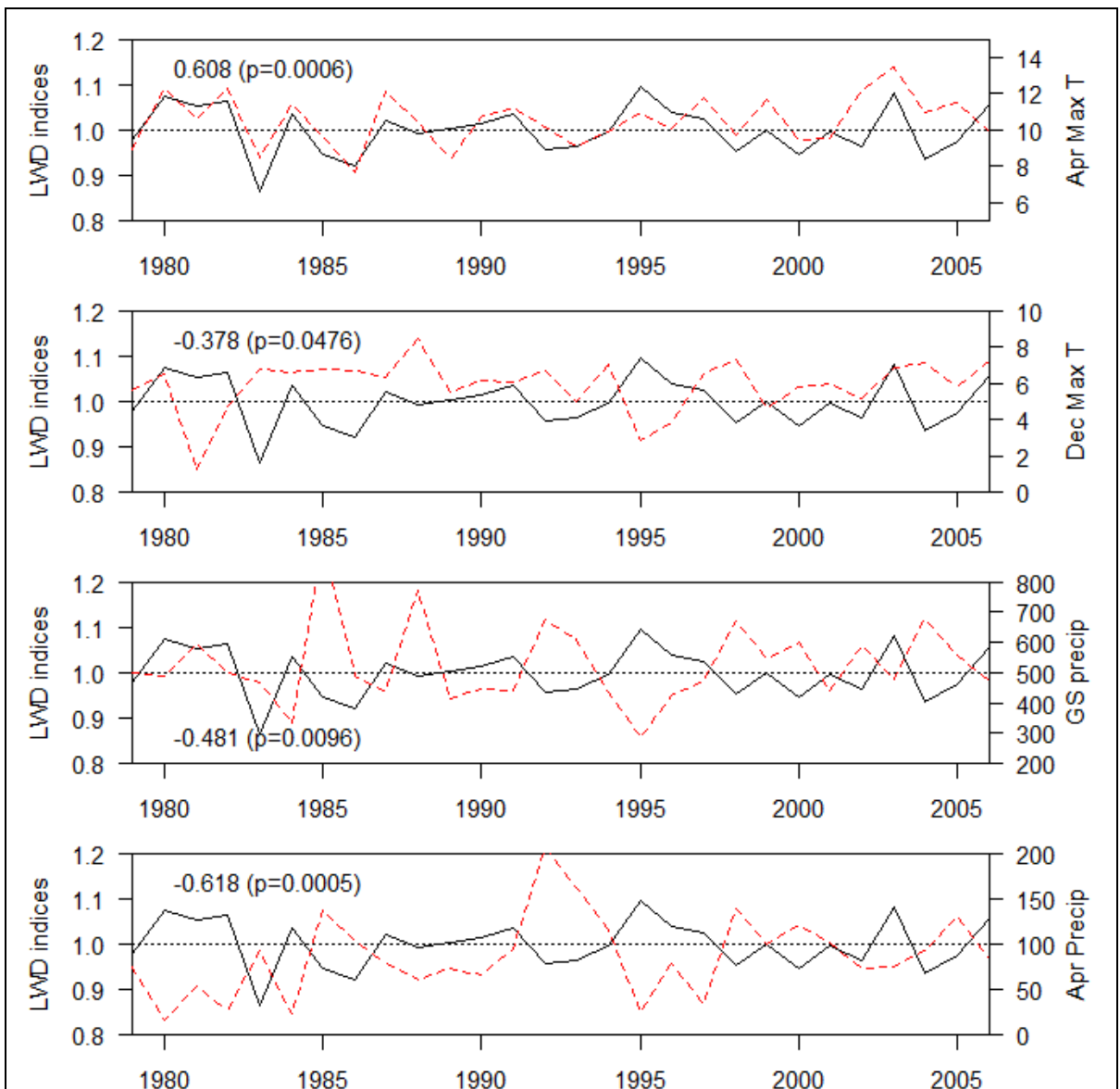


Figure 6-59. Coalburn latewood density (LWD) indices plotted against the individually significant weather variables of the current year. Solid line represents the latewood density indices and the dashed red line the weather variable in question. Horizontal line marks the reference level for the latewood density indices. P-value reported refers to individual comparisons. The selected α -level was 0.05. To achieve over all α -level of 0.05 the limit for individual comparisons would be adjusted (Curtin and Schulz, 1998) to approximately 0.0009.

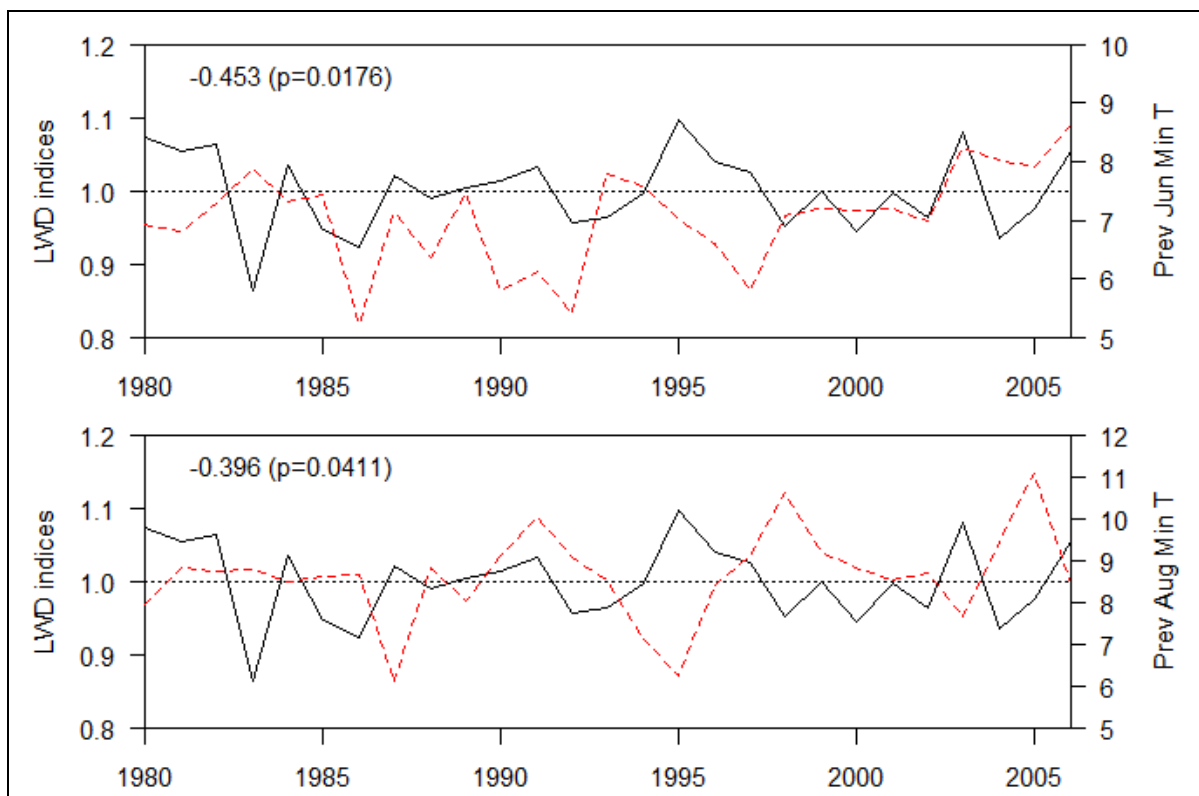


Figure 6-60. Coalburn latewood density (LWD) indices plotted against the individually significant weather variables of the previous year. Solid line represents the latewood density indices and the dashed red line the weather variable in question. Horizontal line marks the reference level for the latewood density indices. P-value reported refers to individual comparisons. The selected α -level was 0.05. To achieve over all α -level of 0.05 the limit for individual comparisons would be adjusted (Curtin and Schulz, 1998) to approximately 0.0009.

Latewood width (Figure 6-61) was also correlated with April precipitation and temperature, which follows logically from the correlation between latewood width and density. However, why April conditions would influence latewood properties rather than earlywood remains unknown. There was no significant correlation between earlywood width and latewood width ($r=-0.083$) but there was a significant correlation between earlywood density and latewood density ($r=0.562$) (Table 6-22). Furthermore, latewood width was positively correlated with January temperature variables and negatively with June precipitation. Of the previous year variables, latewood width was positively correlated with June minimum temperature (Figure 6-61). All of these correlations remained non-significant when adjusted α' (0.0009) was applied.

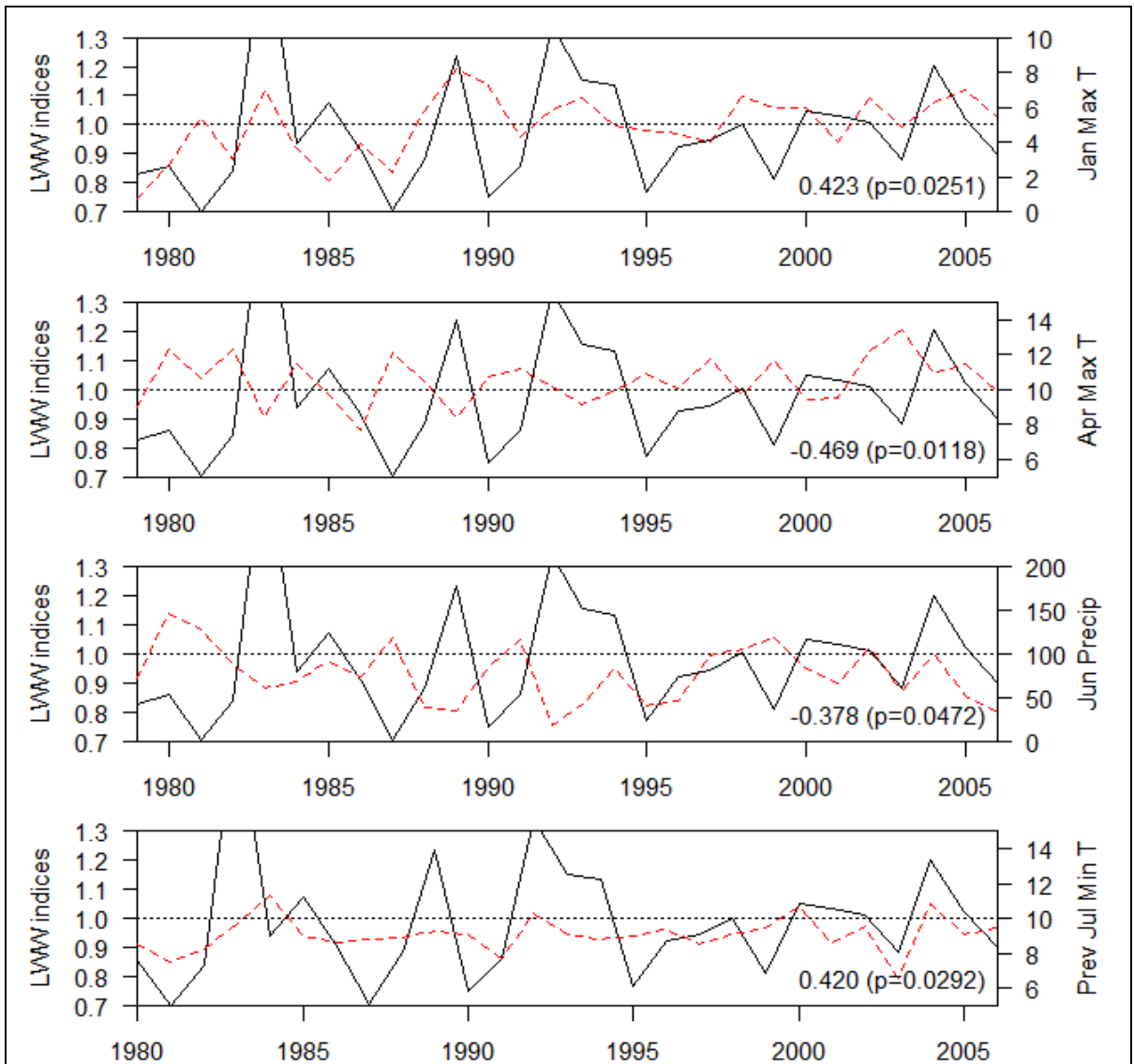


Figure 6-61. Coalburn latewood width (LWW) indices plotted against the individually significant weather variables of the current and previous year. Solid line represents the latewood width indices and the dashed red line the weather variable in question. Horizontal line marks the reference level for the latewood width indices. P-value reported refers to individual comparisons. The selected α -level was 0.05. To achieve over all α -level of 0.05 the limit for individual comparisons would be adjusted (Curtin and Schulz, 1998) to approximately 0.0009.

Only January maximum and September minimum temperatures were found to correlate significantly with latewood percentage (Figure 6-62). Both correlations were positive in direction but too weak to be included if the more stringent α' (0.0009) was used to allow for multiple comparisons (Curtin and Schulz, 1998).

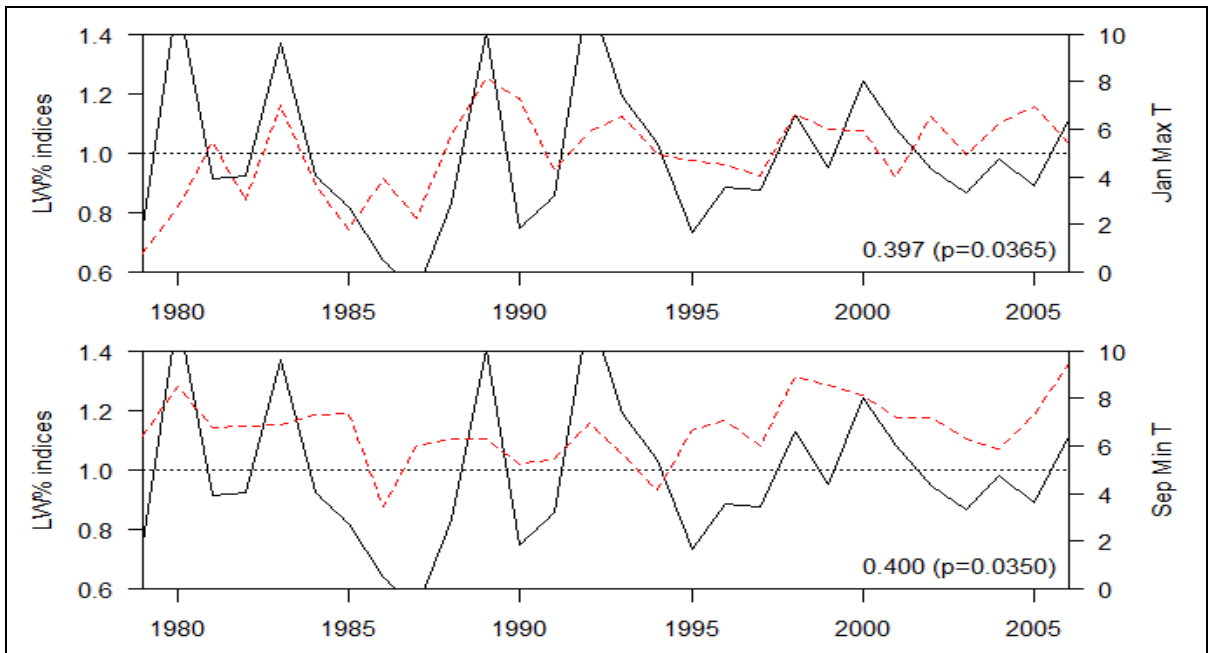


Figure 6-62. Coalburn latewood percentage (LW%) indices plotted against the significant weather variables of the current year. Solid line represents the latewood percentage indices and the dashed red line the weather variable in question. Horizontal line marks the reference level for the latewood percentage indices. P-value reported refers to individual comparisons. The selected α -level was 0.05. To achieve over all α -level of 0.05 the limit for individual comparisons would be adjusted (Curtin and Schulz, 1998) to approximated 0.0009.

Maximum density (Figure 6-63) at the Coalburn site was correlated with April maximum temperature (+ve) and precipitation of the growing season, whole calendar year and April. These followed closely the pattern found for latewood density, which is logical since maximum density under normal conditions (absence of compression wood) would occur in latewood. The correlation with April maximum temperature was strong enough to be significant even at Bonferroni corrected α' (0.0009). Previous summer temperature variables (May maximum, July minimum and August minimum) were negatively correlated with maximum density (Figure 6-64). Minimum density on the other hand (Figure 6-65) was only correlated with April maximum temperature and April precipitation, positively with the former and negatively with the latter. These correlations were too weak to be significant under stricter α' (0.0009).

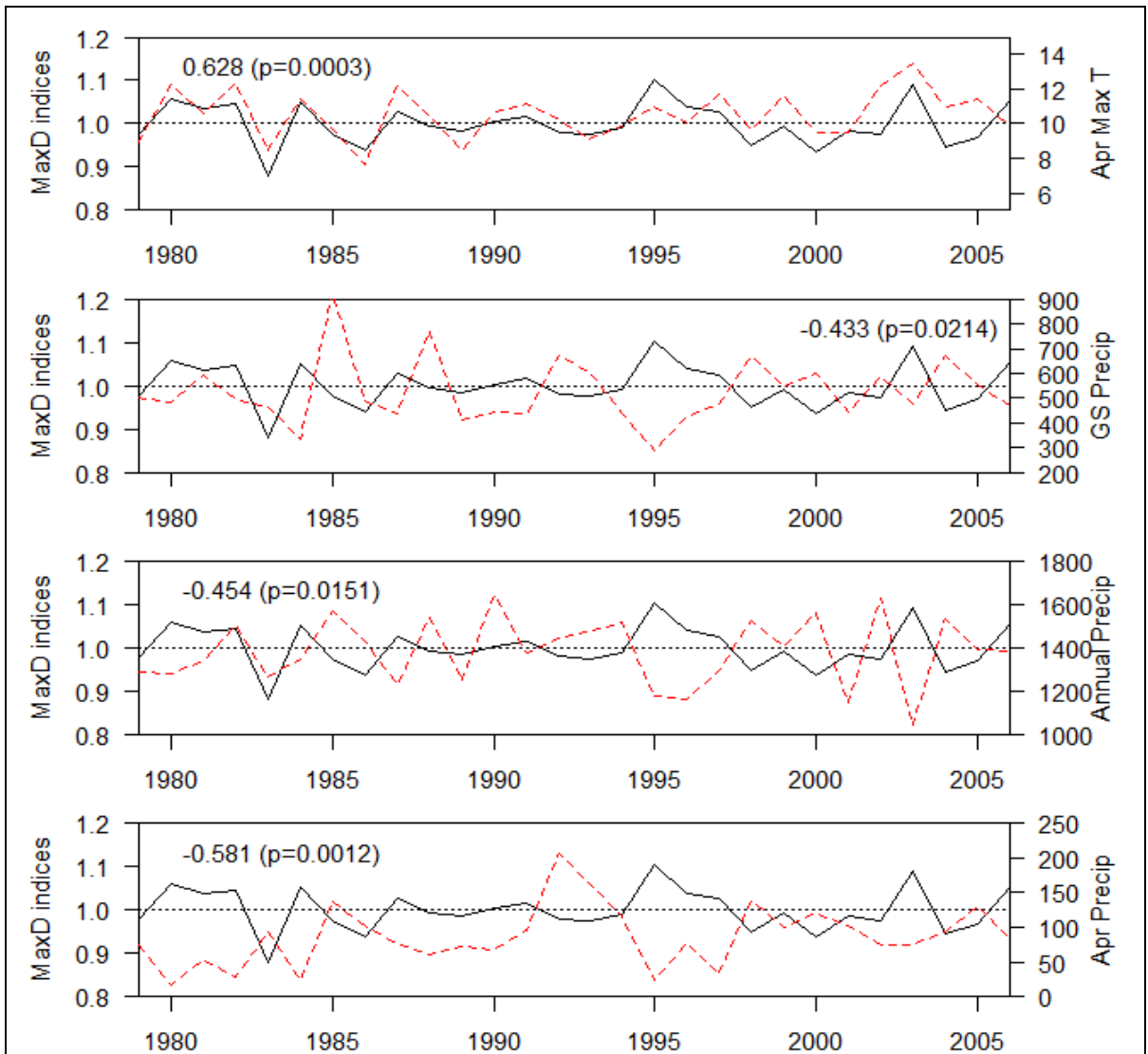


Figure 6-63. Coalburn maximum density (MaxD) indices plotted against the individually significant weather variables of the current year. Solid line represents the maximum density indices and the dashed red line the weather variable in question. Horizontal line marks the reference level for the maximum density indices. P-value reported refers to individual comparisons. The selected α -level was 0.05. To achieve over all α -level of 0.05 the limit for individual comparisons would be adjusted (Curtin and Schulz, 1998) to approximately 0.0009.

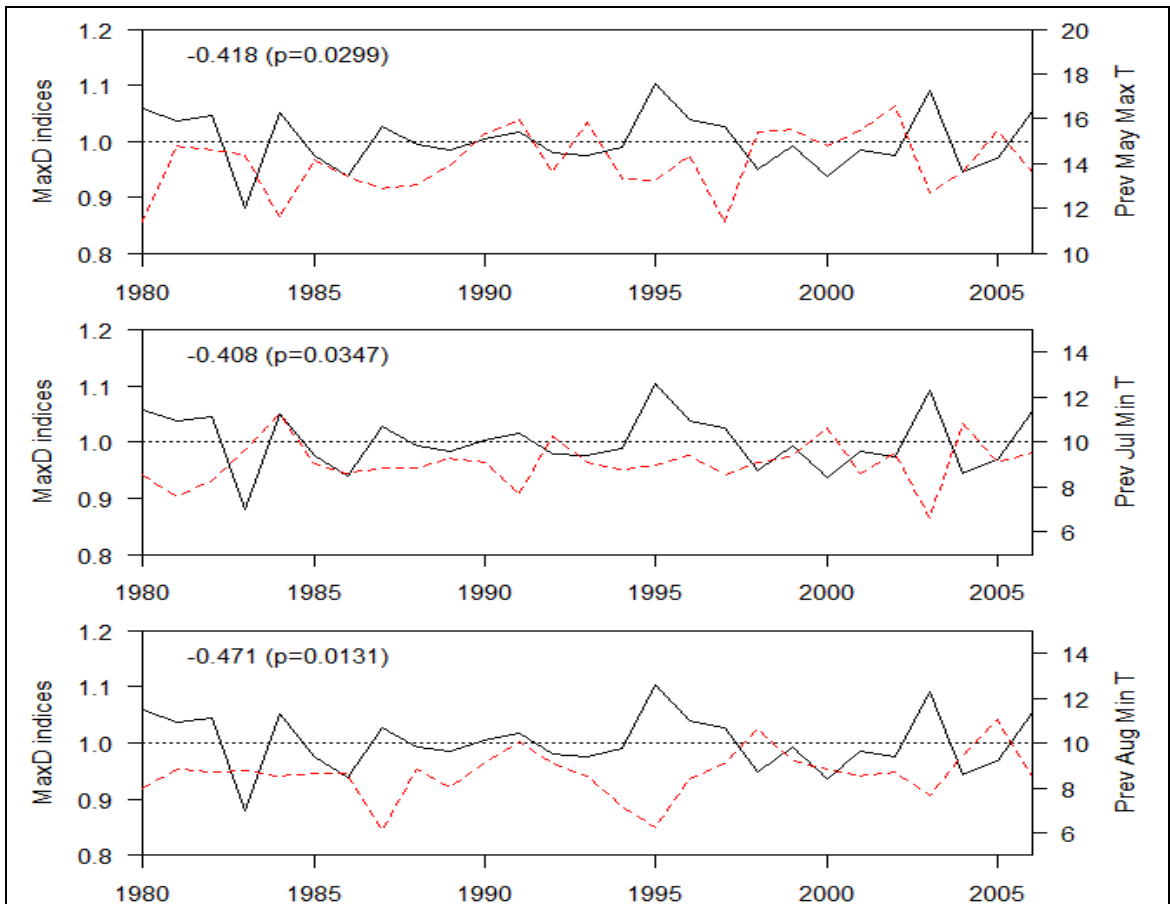


Figure 6-64. Coalburn maximum density (MaxD) indices plotted against the individually significant weather variables of the previous year. Solid line represents the maximum density indices and the dashed red line the weather variable in question. Horizontal line marks the reference level for the maximum density indices. P-value reported refers to individual comparisons. The selected α -level was 0.05. To achieve over all α -level of 0.05 the limit for individual comparisons would be adjusted (Curtin and Schulz, 1998) to approximately 0.0009.

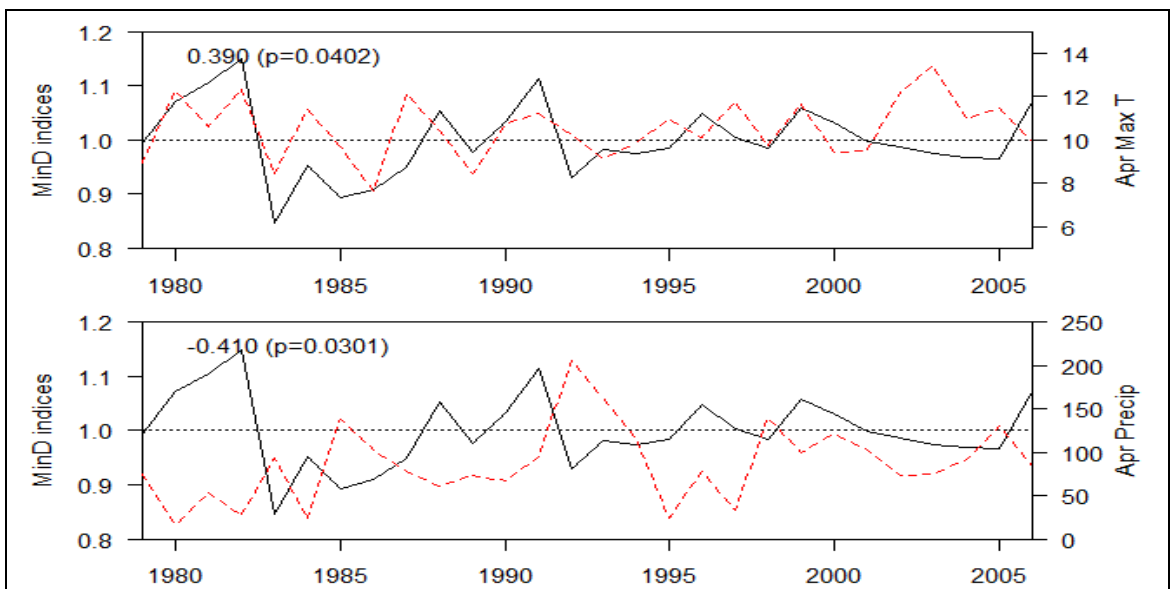


Figure 6-65. Coalburn minimum density (MinD) indices plotted against the individually significant weather variables of the current year. Solid line represents the minimum density indices and the dashed red line the weather variable in question. Horizontal line marks the reference level for the minimum density indices. P-value reported refers to individual comparisons. The selected α -level was 0.05. To achieve over all α -level of 0.05 the limit for individual comparisons would be adjusted (Curtin and Schulz, 1998) to approximately 0.0009

Also at the Coalburn site there were significant correlations between the rainfall and temperature variables (Table 6-21). In January and February rainfall was positively correlated with temperature, whereas during the spring and summer (April-August) rainfall was negatively correlated with maximum temperature. Unlike at the Loch Tummel site (Table 6-19) minimum and mean temperatures were not significantly correlated with rainfall during spring and summer at the Coalburn site.

Table 6-21. Correlation between temperature and the rainfall of the period for the Coalburn site. For periods longer than one month the temperature sum (base 5°C) was used. Significant correlations ($\alpha=0.05$) in italics.

Rainfall period	Max T		Min T		Mean T	
	Correlation coef.	p-value	Correlation coef.	p-value	Correlation coef.	p-value
January	<i>0.466</i>	<i>0.0123</i>	<i>0.416</i>	<i>0.0276</i>	<i>0.398</i>	<i>0.0357</i>
February	<i>0.440</i>	<i>0.0191</i>	<i>0.459</i>	<i>0.0140</i>	<i>0.430</i>	<i>0.0223</i>
March	-0.058	>0.1 ns.	0.003	>0.1 ns.	-0.074	>0.1 ns.
April	<i>-0.426</i>	<i>0.0238</i>	0.328	0.0879	-0.190	>0.1 ns.
May	<i>-0.387</i>	<i>0.0419</i>	0.371	0.0519	-0.154	>0.1 ns.
June	<i>-0.713</i>	<i>0.0000</i>	-0.152	>0.1 ns.	-0.323	0.0934
July	<i>-0.528</i>	<i>0.0039</i>	-0.138	>0.1 ns.	-0.320	0.0961
August	<i>-0.524</i>	<i>0.0042</i>	0.056	>0.1 ns.	-0.363	0.0578
September	0.112	>0.1 ns.	0.372	0.0511	0.351	0.0674
October	0.270	>0.1 ns.	0.309	>0.1 ns.	0.306	>0.1 ns.
November	-0.063	>0.1 ns.	0.207	>0.1 ns.	0.106	>0.1 ns.
December	0.248	>0.1 ns.	0.344	0.0731	<i>0.424</i>	<i>0.0246</i>
Year	-	-	-	-	-0.198	>0.1 ns.
Growing season	-	-	-	-	-0.114	>0.1 ns.
May-August	-	-	-	-	-0.336	0.0803
June-August	-	-	-	-	-0.339	0.0779

Table 6-22. Correlations between the detrended mean site tree ring chronologies for the Coalburn site. Level of significance ($\alpha = 0.05$) is 0.377.

	RW	RD	EWW	LWW	EWD	LWD	LW%	MaxD	MinD
RW	1	-0.869	0.919	0.271	-0.632	-0.627	-0.492	-0.550	-0.617
RD	-0.869	1	-0.798	-0.272	0.852	0.591	0.427	0.509	0.765
EWW	0.919	-0.798	1	-0.083	-0.464	-0.343	-0.735	-0.281	-0.396
LWW	0.271	-0.272	-0.083	1	-0.502	-0.707	0.648	-0.670	-0.615
EWD	-0.632	0.852	-0.464	-0.502	1	0.562	0.047	0.462	0.928
LWD	-0.627	0.591	-0.343	-0.707	0.562	1	-0.214	0.971	0.641
LW%	-0.492	0.427	-0.735	0.648	0.047	-0.214	1	-0.259	-0.057
MaxD	-0.550	0.509	-0.281	-0.670	0.462	0.971	-0.259	1	0.496
MinD	-0.617	0.765	-0.396	-0.615	0.928	0.641	-0.057	0.496	1

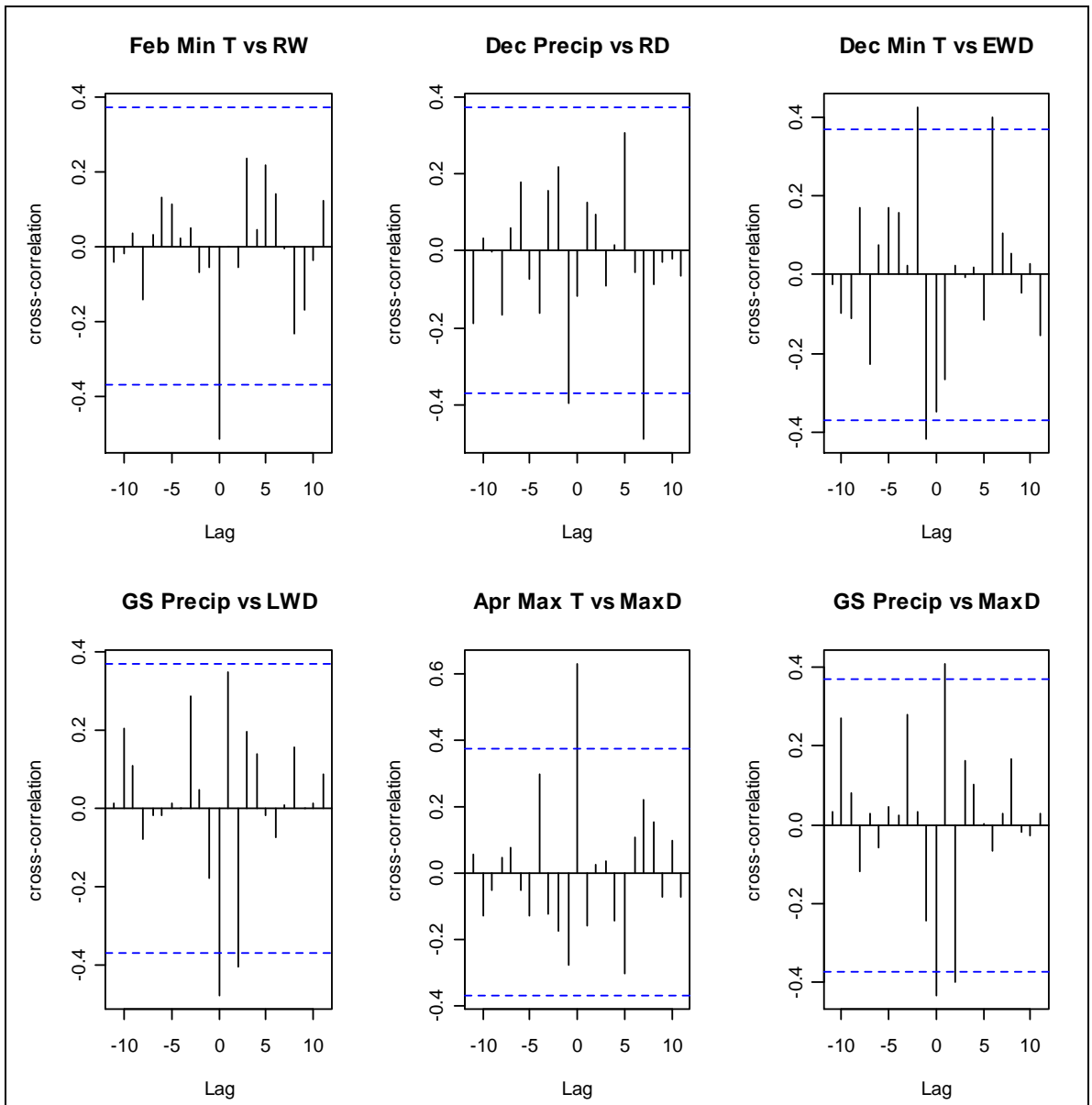


Figure 6-66. Selected cross-correlograms between climate and tree ring variables from the Coalburn site.

Also, in the case of Coalburn site, some significant cross-correlations were detected that would have to be spurious, such as correlations between-tree rings variables and the future climate (Figure 6-66). However, as discussed above for Loch Tummel, these observations use raw climate data and might therefore be influenced by any patterns in it. Examples of prewhitened climate data from both sites are investigated in section 6.3.4.2.

There were marked differences in the correlations found between-tree ring and climate variables (non prewhitened) for the two sites. Of the current year variables (Table 6-23), only the positive correlation between January maximum temperature and latewood proportion was detected at both sites. Furthermore, growing season and annual total rainfall was negatively correlated with latewood density and maximum density at both

sites. On overall it seems that the winter/spring temperatures were more important at the Coalburn site whereas the summer temperatures were more influential at the Loch Tummel site. Precipitation seemed to have a lesser role at the Coalburn site in comparison to Loch Tummel as fewer precipitation terms were significantly correlated with ring variables (p-value for individual comparisons <0.05). Also, in the case of the weather of the previous year, there were only two responses common to both sites; negative effect of May maximum temperature on maximum density and negative effect of December precipitation on ring density. The fact that the similarities were so few indicates that the effect of December rainfall might be an important climate variable to investigate further.

Table 6-23. Significant correlations ($\alpha=0.05$) between ring indices and weather variables of the current year at the Loch Tummel and Coalburn sites. The sign in front of the ring variable indicates the direction of the correlation. Correlations common to both sites are highlighted in bold.

Weather	Loch Tummel	Coalburn
GDD yr	+LWD, +MaxD	
GDDgsTot	+LWD, +MaxD	
GDD May-Aug	+LWD, +MaxD	
GDD Jun-Aug	+LWD, +MaxD	
JanMaxT	+LW%	+LW%, +LWW
JanMinT		+LWW
JanMeanT	+LW%	+LWW
FebMaxT		+RD, -EWW
FebMinT		-RW, +RD, +EWD, -EWW
FebMeanT		-RW, +RD, +EWD, -EWW
AprMaxT	-LW%	+LWD, -LWW, +MaxD, +MinD
MayMinT	-LWD, -MaxD	
JunMaxT	-EWW	
JulMaxT	+LWD, +MaxD	
JulMinT	+MaxD	
JulMeanT	+LWD, +MaxD	
AugMaxT	+LWD, +MaxD	
AugMinT	+LWD, +MaxD	
AugMeanT	+LWD, +MaxD	
SepMinT		-RW, +RD, -EWW, +LW%
SepMeanT		-RW, +RD, +EWD, -EWW
OctMaxT	-RW, +LWD, +MaxD	
OctMeanT	+LWD, +MaxD	
NovMeanT	+MaxD	
DecMaxT		-LWD
GS Precip	-RD, -LWD, -MaxD	-LWD, -MaxD
Yr Precip	-LWD, -MaxD	-LWD, -MaxD
May-Aug Precip	+RW, -RD, -LWD, -MaxD	
Jun-Aug Precip	-LWD, -MaxD	
JanPrecip	+MinD	
MarPrecip	-RD, -EWD	
Apr Precip		-LWD, +LWW, -MaxD, -MinD
MayPrecip	+RW	
Jun Precip	+RW, +EWW	-LWW
Aug Precip	-LWD, -MaxD	
OctPrecip	-RW	

Table 6-24. Significant correlations ($\alpha'=0.05$) between ring indices and weather variables of the previous year at the Loch Tummel and Coalburn sites. The sign in front of the ring variable indicates the direction of the correlation. Correlations common to both sites are highlighted in bold.

Weather	Loch Tummel	Coalburn
GS deg day no	+LW%	
GDD Jun-Aug	-RW	
JanMaxT	+RD, +LWD, +MaxD	
JanMinT	+RD,+EWD, +LWD, +MaxD	
JanMeanT	+RD, +EWD, +LWD, +MaxD	
FebMaxT	+RD	
MayMaxT	-LWD, +LWW, -MaxD	-MaxD
MayMeanT	-LWD, +LWW, -MaxD	
JunMinT		+LWW, -MaxD
JulMinT		-LWD
AugMaxT	-RW, +RD, -EWW	
AugMinT	-EWW	-LWD, -MaxD
AugMeanT	-RW, -EWW	
SepMaxT		+RD
SepMeanT		+RD, +EWD
DecMaxT		-EWD
DecMinT		-EWD
DecMeanT		-EWD
GS Precip	+LWW	
MarPrecip	-MinD	
Sep Precip	+LW%, +LWW	
DecPrecip	-RD	-RD

6.3.4.3 Investigating the strongest correlations further

The correlations significant at $\alpha'=0.0009$ were selected for further investigation (Table 6-25). The climate variables were prewhitened with an autoregressive moving average (ARMA) model in R tseries package (Trapletti and Hornik, 2009). The cross-correlations between the model residuals and the selected tree ring variables were investigated and these were compared to the ones created using raw climatic variables. The prewhitening seemed to enhance the correlation at lag 0 at the Loch Tummel site (Figure 6-67 and Figure 6-68) and decrease it (Figure 6-70) at the Coalburn site but the effects were very slight. This was probably due to the fact that the amount of autocorrelation in the raw climate series was low (Figure 6-70) and only in April precipitation, some high bars that extended near the boundaries were observed (Figure 6-71).

The cross-correlograms present 21 comparisons and hence are subjected to the increased probability of detecting false positive results that applies to multiple comparisons. Once the boundaries (dashed blue lines) in the cross-correlograms were widened to allow for multiple comparisons (dashed red lines), the correlations of interest at lag 0 were no longer

significant. The new boundaries were calculated using the Bonferroni correction with $k=21$ (Curtin and Schulz, 1998).

Table 6-25. Tree ring – climate variable pairs with significant correlations under Bonferroni correction for multiple comparisons ($\alpha' = 0.0009$).

Climate variable	Tree ring variable	r	p-value
<i>Loch Tummel</i>			
Growing season precipitation	Latewood density	-0.549	0.000766
May-August precipitation	Latewood density	-0.552	0.000706
Growing season precipitation	Maximum density	-0.555	0.000661
May-August precipitation	Maximum density	-0.547	0.000813
<i>Coalburn</i>			
April maximum temperature	Latewood density	0.608	0.000606
April precipitation	Latewood density	-0.618	0.000455
April maximum temperature	Maximum density	0.627	0.000351

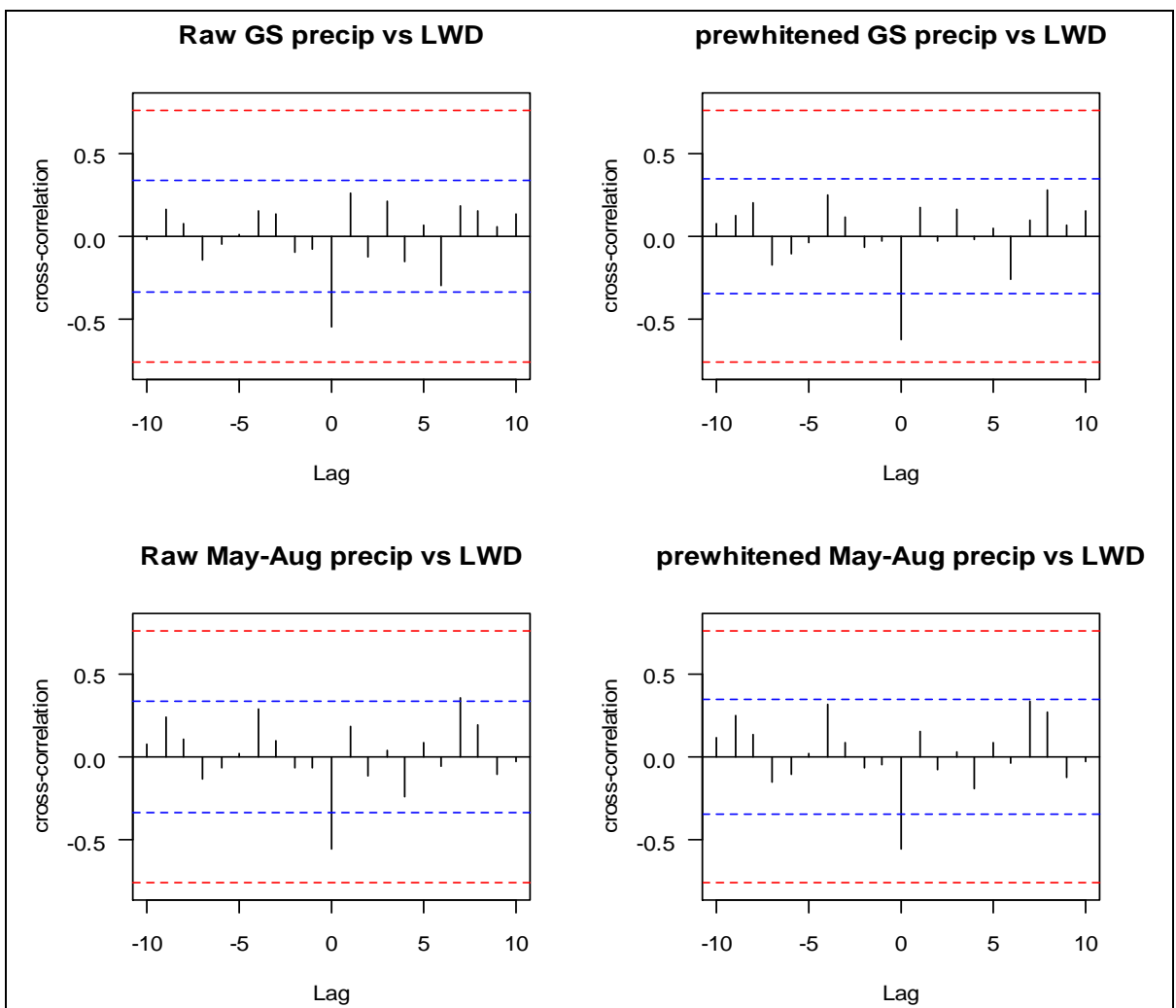


Figure 6-67. Raw (left) and prewhitened (right) precipitation variables plotted against latewood density from the Loch Tummel site. Dashed blue lines represent the level of significance for individual comparisons ($\alpha=0.05$). Dashed red line represents multiple comparisons (21) adjusted α' (0.761) that will give an overall α of 0.05.

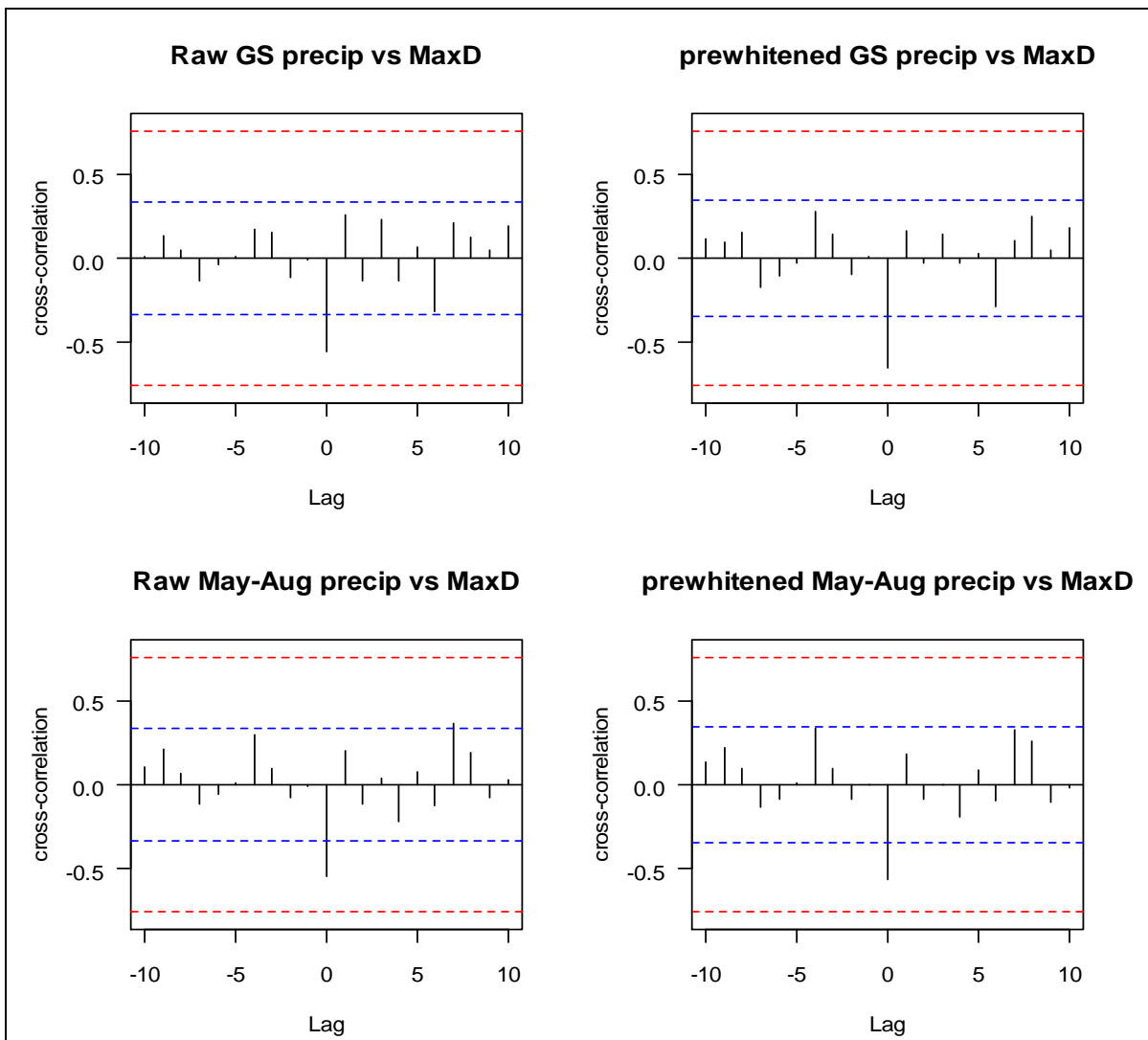


Figure 6-68. Raw (left) and prewhitened (right) precipitation variables plotted against maximum density form the Loch Tummel site. Dashed blue lines represent the level of significance for individual comparisons ($\alpha=0.05$). Dashed red line represents multiple comparisons (21) adjusted α' (0.761) that will give an overall α of 0.05.

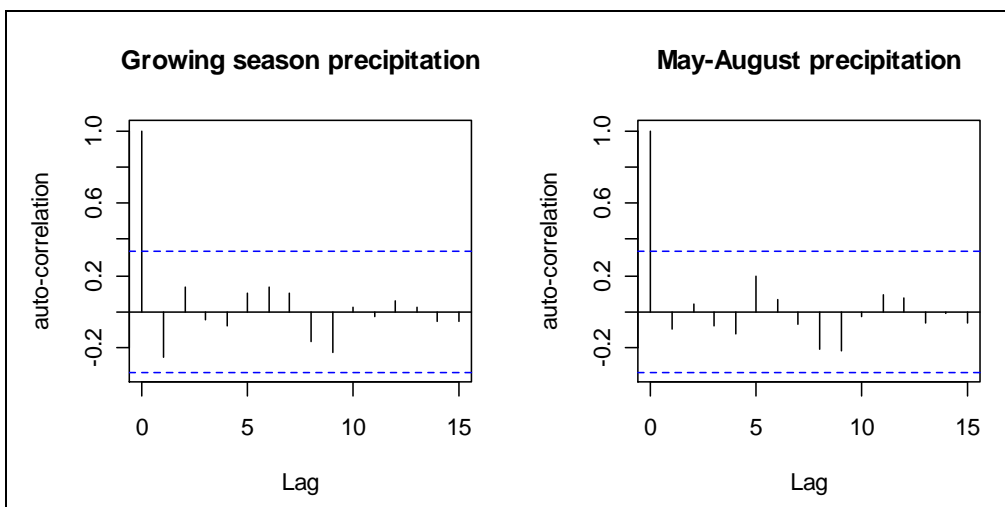


Figure 6-69. Initial autocorrelation in the weather variables that were significant at the Loch Tummel site.

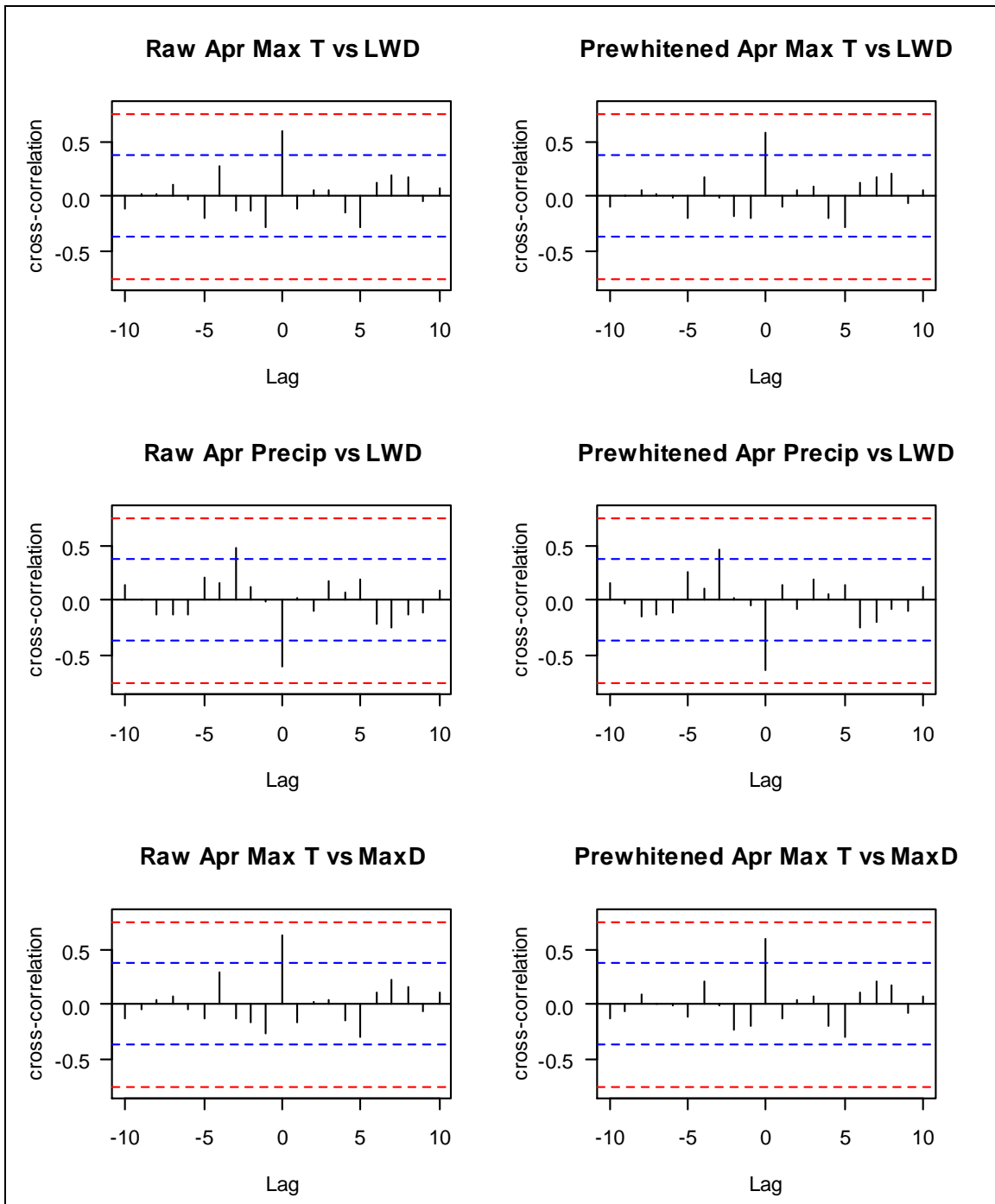


Figure 6-70. Raw (left) and prewhitened (right) March precipitation and maximum temperature variables plotted against latewood density and maximum density from the Coalburn site. Dashed blue lines represent the level of significance for individual comparisons ($\alpha=0.05$). Dashed red line represents multiple comparisons (21) adjusted α' (0.761) that will give an overall α of 0.05.

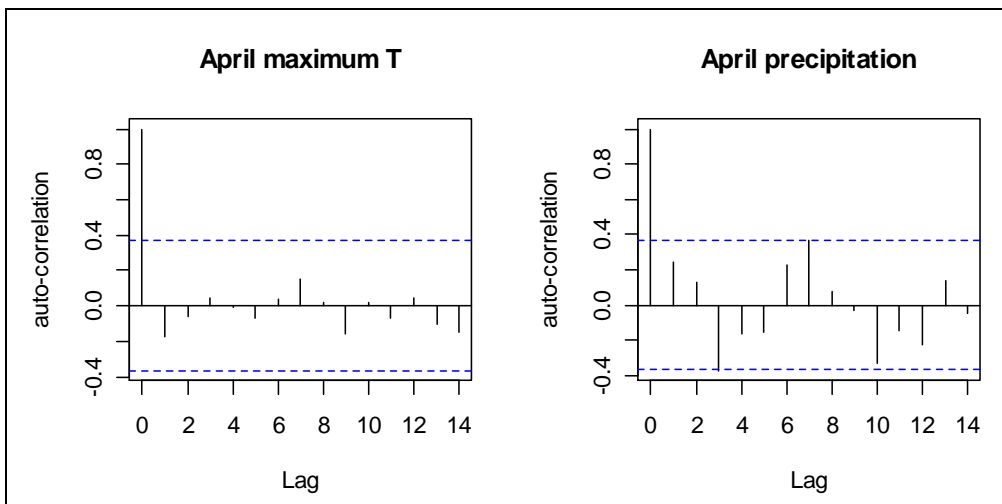


Figure 6-71. Initial autocorrelation in the weather variables that were significant at the Coalburn site.

6.4 Discussion

Disks samples collected from the vicinity of Level II monitoring sites were used to test the average timber density models developed on the wood quality survey data (Benchmarking experiment) and the sub-models to predict model parameters for the radial density model. The results of the model fitting are discussed in section 6.4.1.

The main aim of the Level II experiment was to find a climate signal in plantation grown Sitka spruce. The climatic analysis is complicated by many factors such as short rotation length which restricts the chronology, high level of between-tree competition and in the case of UK also maritime climate. However, to understand the effects of climate change more detailed information on the climatic factors governing growth and timber properties were required. The results of the climatic analysis are discussed below (6.4.2).

6.4.1 Density modelling

It could have been anticipated that the fit of the radial density model using the site average α -values would remain poor since most of the variation in α -values was between the trees. Site specific average α -values could provide accurate predictions in mature wood if the ring density was well controlled by ring number and ring width. In light of these results it seems necessary to use tree specific α -values to make accurate predictions. The sub-models

could be useful in this respect apart from the ones that contain no tree level parameters. Or perhaps some tree parameters could be added to the model equation.

A large proportion of between-tree variation has been commonly found. Zobel and van Buijtenen (1989) wrote that tree to tree variability within a seed source was usually considerably greater than the provenance and stand differences within a provenance. Even differences between related species (eg. southern pines) were small in comparison to tree to tree variation (Zobel and van Buijtenen, 1989). In Sitka spruce across geographical regions of the British Isles, the largest variation in strength and specific gravity was found between-trees within a site (Sunley and Lavers, 1961).

Reparameterising the model on Level II data (for each site separately) improved the fit markedly and adjusted R^2 values for the fixed effects in the range of 0.48-0.56 were obtained, depending on the site. The absolute error in the predictions was 34.5-39.6 kg/m³ and the model was improved by including an ARMA autocorrelation function. However, some trends still remained in the residuals. Furthermore, reparameterising the model requires density data and therefore greatly reduces the usefulness of the model in terms of saving time and obtaining information without time consuming density determinations.

Prediction of area-weighted juvenile wood density from the juvenile DBH was fairly successful for Loch Tummel and Loch Awe sites but less so for Coalburn. In general, the models seemed to predict density variables better for the Loch Tummel site than for the other two as also mature wood density and average density had reasonable fits (ccc 0.562 and 0.571, respectively) for the Loch Tummel site. Mature wood and average density predictions were poor for the Loch Awe and Coalburn sites (ccc-values <0.285). Using separate models based on thinning treatment, geographical location or dominance class did not improve the model predictions.

Tree height effect on cross-section average density was detected at the Loch Tummel site, with the first disk being significantly different from the intermediate ones (2, 3 and 4) but not from disk 5. At the Coalburn site, no height effect was observed. For latewood proportion in Norway spruce Mäkinen et al. (2007) found no effect of tree height. Zobel and van Buijtenen (1989) reported that in earlier studies, a 2% difference in density had been found between the south and north side of a Norway spruce stem, with the south side being higher. In another study on Douglas fir, no azimuthal differences were detected. In this study no effect of direction was observed.

6.4.2 Climatic signal

Maximum density and ring width have been the most widely used variables for climate reconstructions (Vaganov et al., 2008). Maximum density has been found to be most strongly related to climatic data (Schweingruber et al., 1978). In this study, after allowing for multiple comparisons, there were no significant relationships between any tree ring width and climate variables. The only significant correlations ($\alpha'=0.0009$) involved latewood and maximum density and were related to different climatic variables at the two sites. At the Coalburn site, the correlations involved climatic variables (both temperature and rainfall) from April only whereas at Loch Tummel only precipitation variables over longer sections of the growing season were significant.

Commonly current season precipitation is positively related to radial growth, but in Norway spruce in Scandinavia (Mäkinen et al., 2002a) and in Scots pine in Scotland (Grace and Norton, 1990) negative relationships have been detected as well, which were thought to arise due to temperature or waterlogging effects. May temperature was found to be positively related with growth in Norway spruce over a wide latitudinal and altitudinal range (Mäkinen et al., 2003a). Maximum latewood density in white spruce (*Picea glauca* (Moench) Voss) was positively related to growing season temperatures at the tree line in northern Canada (D'Arrigo et al., 1992). Similarly, at the tree line in Northern Quebec, in black spruce (*Picea mariana* (Mill.) BSP), maximum density and latewood density were correlated with growing season temperature sums (Wang et al., 2002). Maximum density in Norway spruce on the southeastern European Alps responded to September temperatures (Levanic et al., 2009). The differences are likely to be due to variation in lignification as the cell division had ceased earlier (Levanic et al., 2009). In Norway spruce in Germany, July and August rainfall were positively correlated with latewood proportion (Wimmer and Grabner, 2000). In addition to these, April precipitation was also positively correlated with latewood proportion. August and September temperature was positively correlated and rainfall of these months negatively correlated with latewood and maximum densities (Wimmer and Grabner, 2000). April and May temperatures were positively correlated with latewood and maximum density (Wimmer and Grabner, 2000). In *Picea glehnii* it was found that cell wall thickness and maximum density were positively related to summer temperature and negatively to August precipitation (Yasue et al., 2000). At the Coalburn site, latewood density and maximum density were positively correlated with April temperature (p-values 0.00061 and 0.00035, respectively) and latewood density was negatively correlated with April precipitation (p-value 0.00046).

In *Abies alba* trees with wider rings ($> 1\text{mm}$), the cell wall deposition and lignification were still ongoing in middle October in Slovenia (Gričar et al., 2005). On Radiata pine in New Zealand it was found that in the late winter, latewood was only partially lignified (Donaldson, 1992). Yasue et al. (2000) concluded that the variation in maximum density was caused by variation in cell wall thickness of the last-formed cells which in turn was influenced by the summer climate. In line with these observations, a negative correlation was observed between May-August precipitation and maximum density at the Loch Tummel site. However, growing season precipitation (April-September) was also found to correlate negatively with maximum density at the Loch Tummel site. At the Coalburn site, maximum density was positively correlated with April maximum temperature which is not in line with the conclusion of Yasue et al. (2000).

In a study of latitudinal and altitudinal gradients in northern and central Europe it was found for Norway spruce that precipitation was a more important factor at southern and low elevation locations, whereas temperature was more significant in the northern and high altitude areas (Mäkinen et al., 2002a). The relationship between growth and climate strengthened towards the extremes of temperature and rainfall ranges studied (Mäkinen et al., 2003a). Similarly, an altitudinal effect in the climatic response of maximum density was found in several conifers in Switzerland and Colorado state (Kienast et al., 1987). At higher altitude, maximum density was more influenced by temperature whereas at lower elevation rainfall became more important. At water stressed sites, maximum density decreased during warm and dry conditions, whereas at subalpine sites, density increased under these conditions (Kienast et al., 1987). A further study in Scotland found in Scots pine that May precipitation was positively related to the growth (Miller et al., 1977).

The UK conditions are not extreme in terms of temperature and moisture limitations therefore it is expected that growth would be controlled by both temperature and rainfall in a more complex manner. In previous studies it has been found that spring rainfall (April) was beneficial for the growth of Scots pine at the altitudinal limit in Scotland (Grace and Norton, 1990). However, summer rainfall was negatively correlated with growth which was thought to arise due to a decrease in temperature during rainy periods. Correlation between growth and temperature was positive and also winter temperatures were important (Grace and Norton, 1990). Dengel et al. (2009) analysed 45 yr long tree ring width chronologies of Sitka spruce from which the juvenile part of the radius had been removed. In addition to temperature and precipitation they analysed vapour pressure deficit, cloud and radiation variables and mainly found weak insignificant correlations except with cosmic ray flux with which the correlations were positive in all months. However, the

authors did not remove the autocorrelation from the cosmic ray data which may have impacted the analysis as visually there appeared to be a trend in the cosmic ray data.

Both at the Coalburn and Loch Tummel sites, in the initial screening of the climatic variables (p -value < 0.05 for individual comparisons), it was found that precipitation from the previous December was negatively correlated with ring density. This relationship might merit further investigation since it was detected at both sites which otherwise had very different climate correlations. In addition to this, negative correlations between annual and growing season precipitation and latewood and maximum densities were observed at both sites but at the Coalburn site these relationships did not remain significant when the α -level was adjusted for multiple comparisons. Also, at both sites, a negative correlation between maximum density and maximum temperature of the previous May was detected. However, for this relationship it is difficult to think of a physiological mechanism to explain it.

In proper dendrochronology, typically centuries-long tree ring chronologies are used to extract climatic signals. There is an obvious statistical benefit in investigating long tree ring series as the sample size is larger and hence the results are more reliable. Furthermore, in long time series the juvenile part of the tree could easily be discarded, whereas in this study the juvenile core (defined as first 10 rings) constituted 1/3 of the segment length and hence could not be excluded. The reasons for excluding this part would be that the growth related trend is particularly strong there and perhaps some competition processes also have a different impact in the stage before canopy closure. So, even if the samples used here were far from ideal in dendrochronological point of view there is still strong interest in relating the growth of these trees to the climate. The Sitka spruce plantation is the commonest woodland type in the UK and these samples represent the typical age at the end of the rotation. Climate change will influence the growth of these forest types in the future and understanding that impact in more detail has significant ecological and financial value.

Faced with the multiple problems of short chronologies, complex maritime climate, plantation forests with high rates of competition and even silvicultural interventions and multiple comparisons, a very conservative approach was adopted in treating the detected correlations. Only the tree ring-climate variable pairs, where significant correlation was detected with $\alpha' = 0.0009$, were investigated further. This was thought as an effective way of not detecting false positives. However, there might be merit in investigating some of the less strong correlations further, in particular the few that were found for both sites, as some genuine relationships have probably been excluded here.

The strongest climatic signal was found for latewood density and maximum density and this effect was consistent between the sites even if the associated climatic variables differed. The prewhitening of the climate series did not change the relationship, probably because there was not much autocorrelation in the climatic variables in question or in general. If the number of comparisons carried out in the cross-correlograms was allowed for, the effects lost their significance. Also, the number of lags used was fairly high and from a physiological point of view, it could be argued that a lag of 5 years would be sufficient to present any effects that could arise due to any real effects. However, investigating a wider range of lags on the cross-correlograms was thought to be interesting as it would allow detection of how often clearly spurious (eg. relating to future weather) correlations would be detected. In any case, setting the maximum lag at 5 would not have changed the conclusions as the α' would only be lifted to (0.0045), resulting in lowering of the red boundaries from 0.761 to 0.726.

In future work it would be interesting to construct separate tree ring chronologies for the dominance classes included in this study as differences in growing season length due to growth vigour have been reported (Gričar, 2007). In trees with wide rings it was observed that cambial activity continues for longer compared to ones with narrow rings (Gričar et al., 2005). Similarly, Denne (1979) found that growth ceased earlier in severely suppressed Sitka spruce in Wales. This would allow investigation of whether the influence of climatic variables in the autumn differs between these groups of trees. If within site differences exist due to social status and the related differences in growth vigour, they would confuse the site signal in the autumn as trees cease to react to climate at different stages. Hence, separating trees of different dominance classes could reduce the potential noise in the common signal.

7 Radial Stiffness

This chapter reports the results of the acoustic velocity measurement on samples from the Loch Awe and Coalburn sites. Initially (7.3), the acoustic velocity and density were investigated separately to understand the radial patterns and interrelationships in different parts of the radius. The velocity data were combined with density measurements to calculate Modulus of Elasticity (MoE) which describes timber stiffness in terms of resistance to deflection under load. The stiffness values were investigated for differences due to azimuth and social status (7.3.1). The variation in stiffness values in the whole cross-section (7.3.2), juvenile wood (7.3.3) and outerwood (7.3.4) were modelled based on site and tree variables. Furthermore, the velocity alone was modelled (7.3.5).

The radial behaviour of stiffness was modelled (7.3.6) and relating the model coefficients to site and tree variables was attempted (7.3.6.1). Lastly, the results of standing tree acoustic measurements were compared to the values derived from the ultrasonic scanning of radial sections (7.3.7).

7.1 Introduction

The main uses of domestic sawn timber are construction, pallets/packaging and fencing (Macdonald and Hubert, 2002). Currently, there is an aim to increase the production of construction grade timber as the market for the lower uses is largely saturated. Main quality criteria for construction use include 1) Dimensions, 2) Stiffness and Strength and 3) Dimensional stability (Macdonald and Hubert, 2002). Modulus of Elasticity (MoE) measures the wood stiffness or resistance to deformation under load (Watt et al., 2006) and is therefore an important indicator of its suitability for construction use. As boards rarely break in normal use, the measure of deformation is considered more important than Modulus of Rupture (MoR) (Watt et al., 2006). EU specifications for C16 classifications require the Modulus of Elasticity (MoE) of timber to exceed a characteristic (fifth percentile) value of 8 kN/mm^2 (Auty and Achim, 2008; Moore et al., 2009a). This corresponds to 8 GPa. Stiffness is mainly influenced by density and microfibril angle which are also linked to dimensional stability. High microfibril angle leads to increased longitudinal shrinkage which causes distortion of timber during drying (Macdonald and Hubert, 2002).

Timber stiffness can be calculated from microfibril angle (MFA) and density data (Cowdrey and Preston, 1966; Evans and Ilic, 2001). Density is an input simply because it describes how much of the wood cross-section is occupied by the walls. Thus, the relationship is approximately linear with density but steep and non-linear with MFA, so that MFA is the dominant influence. The relationship differs slightly between species, which indicates that some additional factors may be involved. Acoustic testing provides a direct means of testing the stiffness of the cell wall, as acoustic velocity integrates the influence of MFA and of any additional cell-wall variables involved. The product of acoustic velocity and density gives dynamic stiffness values, which correlate well with stiffness as measured conventionally ('static' stiffness) although the absolute values differ. Over the recent years there has been increasing interest in acoustic testing of the timber resource in the different stages of the supply chain (Mochan et al., 2009).

At cell wall level, stiffness and shrinkage is influenced by microfibril angle (Figure 7-1) in the S1, S2 and S3 layers (Astley et al., 1997). S2 layer is the thickest and therefore dominates the effects. The microfibril angle decreases from the pith outwards (Hirakawa et al., 1997). In Sitka spruce it reaches a steady value around 6th - 9th ring (Macdonald and Hubert, 2002).

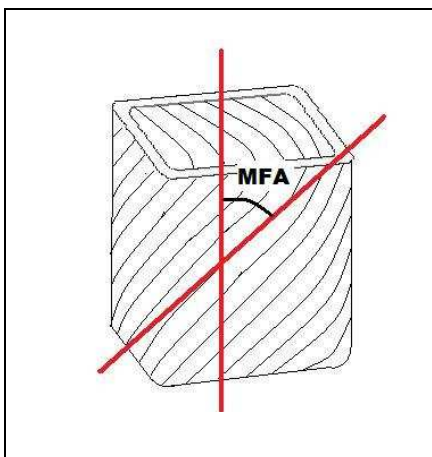


Figure 7-1. Schematic representation of microfibril angle in the S2 layer of a xylem cell.

Stiffness is related to site and tree parameters in a complex manner. DBH (Lasserre et al., 2005) has been found to decrease stiffness in Radiata pine (*Pinus radiata*). High stocking rate (Lasserre et al., 2004; Lasserre et al., 2005), higher level of pruning (Mason, 2006) and stem slenderness (Watt et al., 2006) have been reported to increase stiffness in Radiata pine. In Sitka spruce, increase in yield class, elevation, latitude and spacing have been found to decrease dynamic MoE (Moore et al., 2009c), furthermore, deeper crown was accompanied with lower MoE (Moore et al., 2009b). Watt et al. (2006) also found that higher minimum temperature in the early autumn increased the stiffness, which was thought to be caused by increased latewood growth. They also found in Radiata pine that even though fertilisation had a significant influence on growth, its impact on MoE was small and insignificant. In Norway spruce it was found that fertilisation decreased wood density but caused no change in microfibril angle (Peura

et al., 2008). However, in another experiment Norway spruce clones with the highest growth rate had a poorer MoE than slower growing ones (Koponen et al., 2005; Raiskila et al., 2006). Generally, it is thought that faster growth rate would decrease MoE since wider rings are associated with lower density and higher microfibril angle. However, in an experiment assessing the influence of grass competition on the MoE of Radiata pine, it was found that the trees in grass suppressed treatment that had the lowest growth rate also had lower stiffness than the faster growing grass-free treatments (Mason, 2008). Furthermore, there is a considerable amount of genetic variation. Lasserre et al. (2004) found a clonal stiffness effect of 1.1 – 1.5 GPa between the most extreme clones of Radiata pine. The effect increased with stocking, but there was no significant interaction between stocking and clone. Lasserre et al. (2005) reported that there were 15 % gains in stiffness due to the genetic population used.

Static or dynamic MoE values can be derived for timber (Dinwoodie, 2000). Static MoE is measured in 3 or 4 point bending tests of small clears or battens. For small clears, pieces of timber are cut from the stem with standardised dimensions (20 * 20 * 300 mm) that are analysed under constant conditions (temperature 20 °C and relative humidity 65%) (Saranpää and Repola, 2000). Furthermore, the specimens need to be free of defects such as branches or cracks, so that the bending test assesses the stiffness of the wood material as such and the results are not influenced by weakness caused by these defects. For these tests, seasoned and sawn samples are required. For commercial applications the stiffness information measured on battens arrives too late since the timber has already been transported to a sawmill, dried at high energy cost and sawn. If timber is rejected based on stiffness, all the resources used in the processing have been lost and alternative use or disposal of the material has to be arranged. This naturally leads to loss of material and energy and methods for stiffness assessment at earlier stages of the timber processing chain have been developed. These consist of different acoustic measurements either on standing trees or on logs and battens. These techniques constitute the measurement of dynamic MoE. Standing tree methods are ideal for selection for plant breeding, timber quality prediction from young stand age onwards and screening of current stands, as the individual remains alive and largely undamaged after the measurement. In the case of resonance based measurements on log and battens, the advantage is that no raw material is lost in the testing, and in the case of log measurements, the testing could already be carried out by the road side before transporting any poor quality material to a sawmill. The acoustic measurements also require density values for the calculation of dynamic MoE whereas in the static bending test, the static MoE is derived directly from the strength required to deflect the piece of timber. It is customary to assume constant density of 1000 kg/m³ when

green samples are tested (Lasserre et al., 2004; Mason, 2006; Moore et al., 2009c). The third option is to calculate MoE from microfibril angle measurements and density measurements (Evans and Ilic, 2001), but this can be laborious.

There are some limitations in these methods. In the standing tree methods, access to the log end surface is lacking and the stress waves are introduced from the side of the stem which has consequences for the wave behaviour (Wang et al., 2007). In practice, the sound will travel in the outermost part of the stem (Gorman et al., 2003) and the result will then describe the outerwood stiffness most accurately. However, good correlations have been found between transit time measurements in standing trees and resonance method-based measurements on logs (Auty and Achim, 2008; Carter et al., 2005; Moore et al., 2009b). Chauhan and Walker (2006) showed high R^2 values for the regressions of log velocity and standing tree velocity in Radiata pine but the discrepancy between the measurements increased with age of the trees. Close linear correlation between dynamic and static MoE in Radiata pine has been reported although dynamic moduli were higher in absolute terms (Booker et al., 1997; Lindström et al., 2004). In 3-year old Radiata pine seedlings there was very close agreement of dynamic and static MoE when dynamic MoE was measured with a resonance method (Lindström et al., 2004).

The bending tests on battens and small clears provide fairly coarse resolution data on the radial variation in stiffness within the tree. Whereas, the standing tree acoustic measurement is limited to the outer part of the stem, the acoustic testing of logs integrates the results across the whole cross-section. Bending tests on micro clears can be carried out to obtain high resolution data on radial variation but the sample preparation is extremely laborious (Gabert, 2005). Therefore, in the latter case the number of samples would be very limited. Stiffness can be estimated from MFA and density measurements but the accuracy of the data derived depends on the algorithm used. Therefore, direct calculation of MoE from density and acoustic velocity values could be valuable in order to produce radial stiffness curves for Sitka spruce. A technological innovation developed at the University of Canterbury (Christchurch, New Zealand) allowed acoustic testing of relatively thin radial sections at a high resolution. Using this novel technology this study aimed to provide detailed information on the stiffness variation across the radius in Sitka spruce. The ultrasonic scanner is capable of fast through put of samples and therefore allowed collection of an extensive dataset of acoustic velocity data for stiffness calculations. In addition to detailed stiffness profiles, this experiment aimed to investigate the link between stiffness and tree characteristics as well as compare standing tree measurements (ST300) to the ultrasonic scanning results.

7.2 Materials and Methods

Samples from the Coalburn and Loch Awe Level II sites were used in the ultrasonic scanning experiment. Acoustic velocity data together with the density data allowed the calculation of stiffness. For details on the density analysis, refer to Chapter 2. Acoustic measurements in standing trees were based on the transit-time method (ST300 FiberGen, New Zealand). However, this method is limited to the outerwood of the tree since the stress wave will travel between the probes inserted into the stem (Figure 7-2). In calculating the stiffness from the transit time measurements on standing trees it is customary to use an approximation of 1000 kg/m^3 as the green density of wood (Lasserre et al., 2004; Mason, 2006; Moore et al., 2009c).

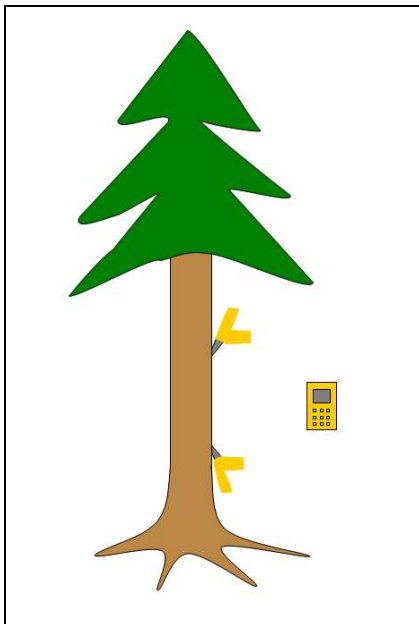


Figure 7-2. Illustration of the use of ST300 time-of-flight tool. The probes inserted into the stem and the wireless datalogger that will record the time required for the sound pulse to travel between the probes as the lower one is tapped with a hammer.

Samples were heat treated at a minimum core temperature of 80°C for several days to meet New Zealand's bio security requirements for imported sawn wood. After shipping, the samples were conditioned at 25°C and 60% relative humidity for approximately 2 weeks in preparation for the ultrasonic scanning. These conditions will result in 12% moisture content in the wood. Samples were sawn to remove the edge caused by extraction of the ITRAX sample strips for density analysis. The surfaces were then sanded to ensure better contact for the scanner probes as well as easier visual inspection of path location and presence of compression wood.

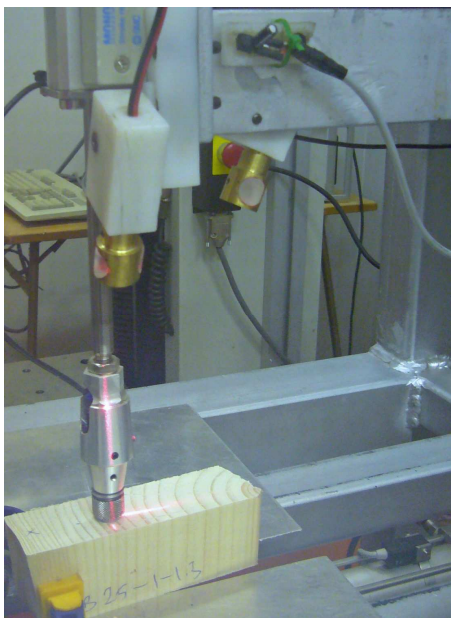


Figure 7-3. Ultrasonic scanner developed at the University of Canterbury, Christchurch, New Zealand analysing a radial sample of Sitka spruce.

The scanner (Figure 7-3) consists of two probes that come together pressing the sample tightly between them. They measure the sample thickness and then send a 1.84 kHz sound wave through. The probes will then move 2.1 mm and repeat the measurements on the next spot and will continue measuring along the sample. The computer programme records the distance travelled, sample thickness and velocity.

The ultrasonic scanner was originally designed for the analysis of disks and a clamping system was developed to hold the radial sections in place. The samples were scanned from bark to pith, carefully marking on the sample the path along which the acoustic data were obtained. Due to the cutting pattern that was used for density samples, the sections had a pointed end on the pith side. To obtain correct results and to protect the probe head from damage, the probe needs an intact surface to land on. Therefore, the scanning needed to be started a few millimetres from the edge and stopped few millimetres before the pointed end on the pith side. The distance from pith values were then corrected for the distance that was left outside the scanning path.

The head of the probe was 9 mm in diameter. The acoustic measurements taken at each point are an average over an area corresponding to a circle with a 4.5 mm radius. The probe then moves 2.1 mm between each measurements producing a kind of moving average as the areas of adjacent measurements overlap. Based on the markings of the acoustic path location, the starting point of ultrasonic scanning was carefully identified in the pixel based density data. To match the acoustic data an average density was calculated including values 4.5 mm in both directions, which corresponds to 180 data points in the 50 μm resolution density data. Averaging was repeated every 2.1 mm step to match the principle of acoustic velocity measurement. As acoustic velocity was measured on samples at 12% moisture content, X-ray density measured at 4% MC was converted to 12% MC according the formula explained in Chapter 3. The acoustic velocity and density values were then used to calculate Modulus of Elasticity (MoE) at each measuring point along the radius, according to the well established relationship expressed in Equation 21 (Auty and Achim, 2008; Carter et al., 2005; Chauhan and Walker, 2006; Lasserre et al., 2005; Lasserre et al., 2007; Lindström et al., 2004; Mason, 2006; Moore et al., 2009a; Wang et al., 2002; Watt et al., 2006)

Equation 21

$$\text{MoE (Pa)} = \rho V^2$$

Where ρ is the density (kg/m^3) and V is the acoustic velocity (m/s). This allowed creation of radial stiffness profiles for Sitka spruce. Using these values, a further three stiffness variables were calculated. These were average stiffness for (a) the whole radius, (b) outer 4 cm and (c) outer 2 cm of the sample. These values were compared to the dynamic MoE values calculated from acoustic velocity measured in standing trees using the ST300 time of flight tool. Stand and tree level variables measured at the sites (for details regarding the fieldwork refer to the Chapter 6) were used in mixed effects model in R to explain variation in average stiffness values.

Furthermore, the radial variation in stiffness was analysed to complement the modelling work done on radial density (Chapters 5 and 6). To study the radial variation in stiffness a non-linear model developed for Sitka spruce static MoE data (McLean, 2007) was employed. This model (Equation 22) had been developed on data derived from bending tests of small clears.

Equation 22

$$\text{MoE} = a / (1 + \exp(b/RN)) + d$$

Where MoE is the modulus of elasticity (GPa), RN is the ring number, a is related to the maximum limit value of the predictions, b sets the point of change in the rate of increase and d is an initial value of MoE in the pith region. How the coefficients govern the behaviour of the radial stiffness curve is illustrated in Figure 7-4.

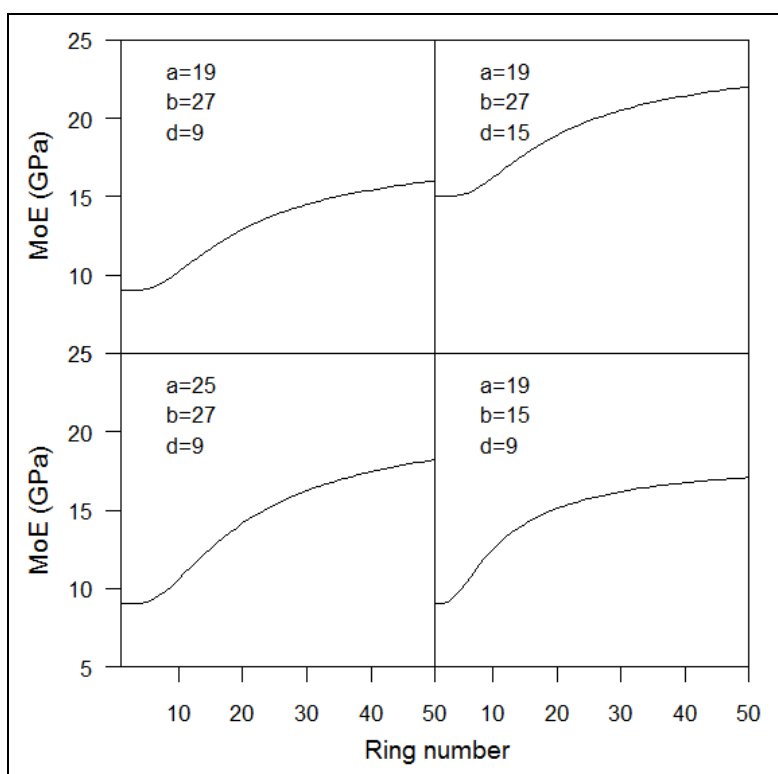


Figure 7-4. The influence of model coefficients a , b and d on the behaviour of the radial stiffness curve.

The ultrasonic data used to calculate stiffness values was measured at 2.1 mm intervals from the pith outwards. The measurements did not respect ring boundaries and in case of a wide ring several measurements could have been made

within the same ring. The model was fitted using non-linear mixed effects, (Pinheiro et al., 2008) in R. Furthermore, the possibility of predicting the model parameters (a, b and d) from the measured tree variables was investigated. For that, the parameters were derived holding either both or one other parameter fixed at their average values.

7.3 Results

When all acoustic velocity data (Figure 7-5) were plotted together, the velocity tended to increase steadily with distance from pith and then level off. As characteristic to Sitka spruce, the density first decreased from the pith outwards. In this case there was only a very slight increase after the minimum. In pooled Benchmarking data (Figure 5-2) there was a clearer increase after the minimum when density was plotted against ring number. However, in the Benchmarking data, the higher ring numbers were based on a limited number of observations and the lowess curve would have been influenced by those few observations for high ring numbers. Also, plotting against ring number aligns the density observations by cambial age whereas plotting against distance from the pith does not. This effect might explain the slight differences. There was a marked amount of variation in the shape of the velocity profiles between the trees (Figure 7-6) and the same was true for density (Figure 7-7) as also discussed previously.

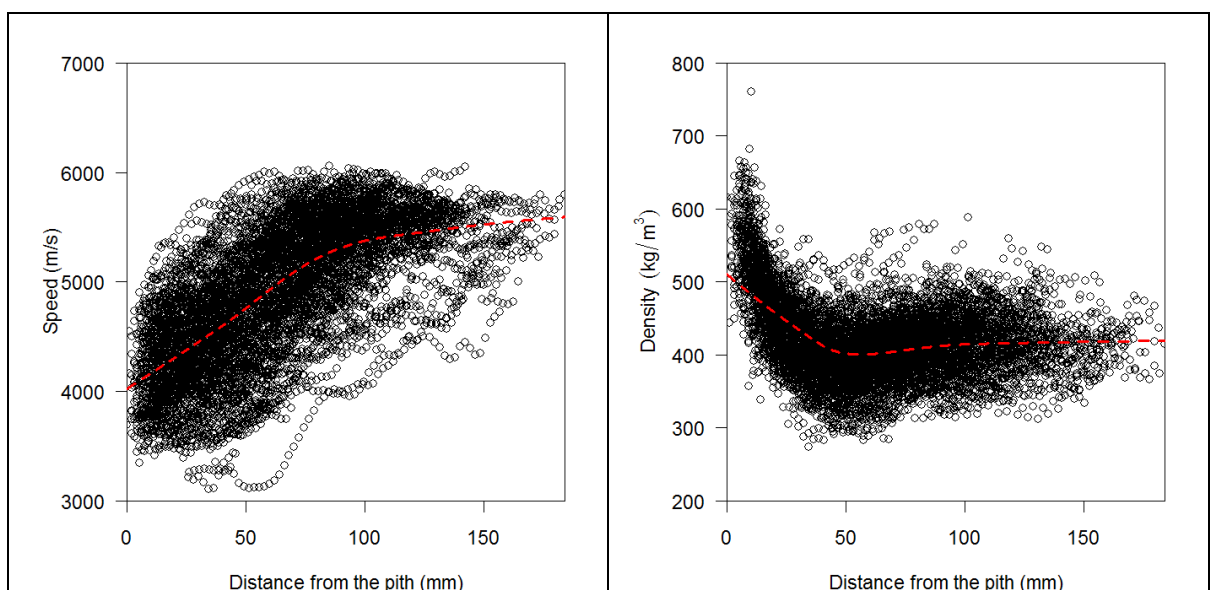


Figure 7-5. Radial acoustic velocity (left) and density (right) data for the studied sites with a smoothing LOWESS curve in red.

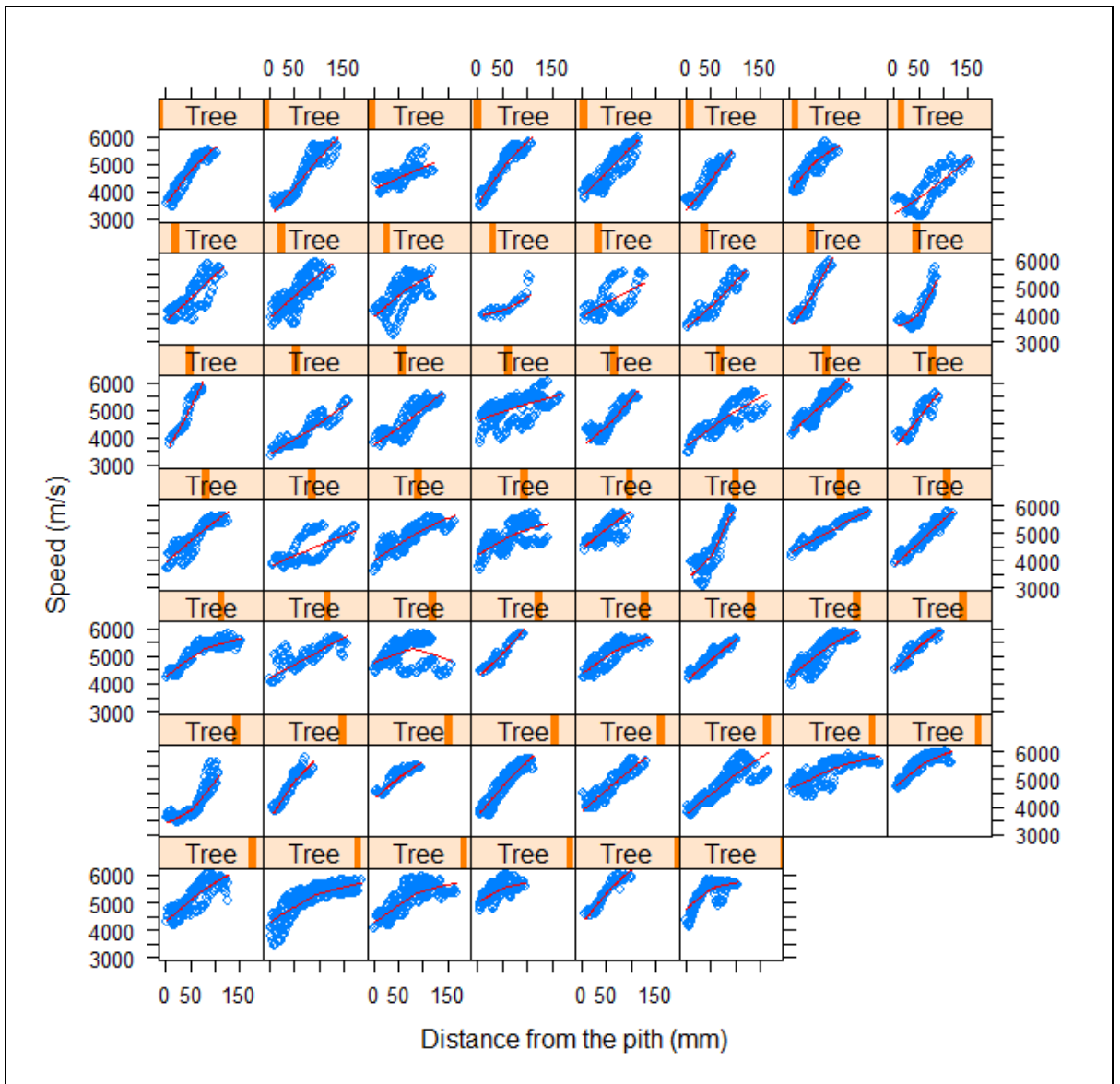


Figure 7-6. Radial trend in acoustic velocity for each of the studied trees at two sites.

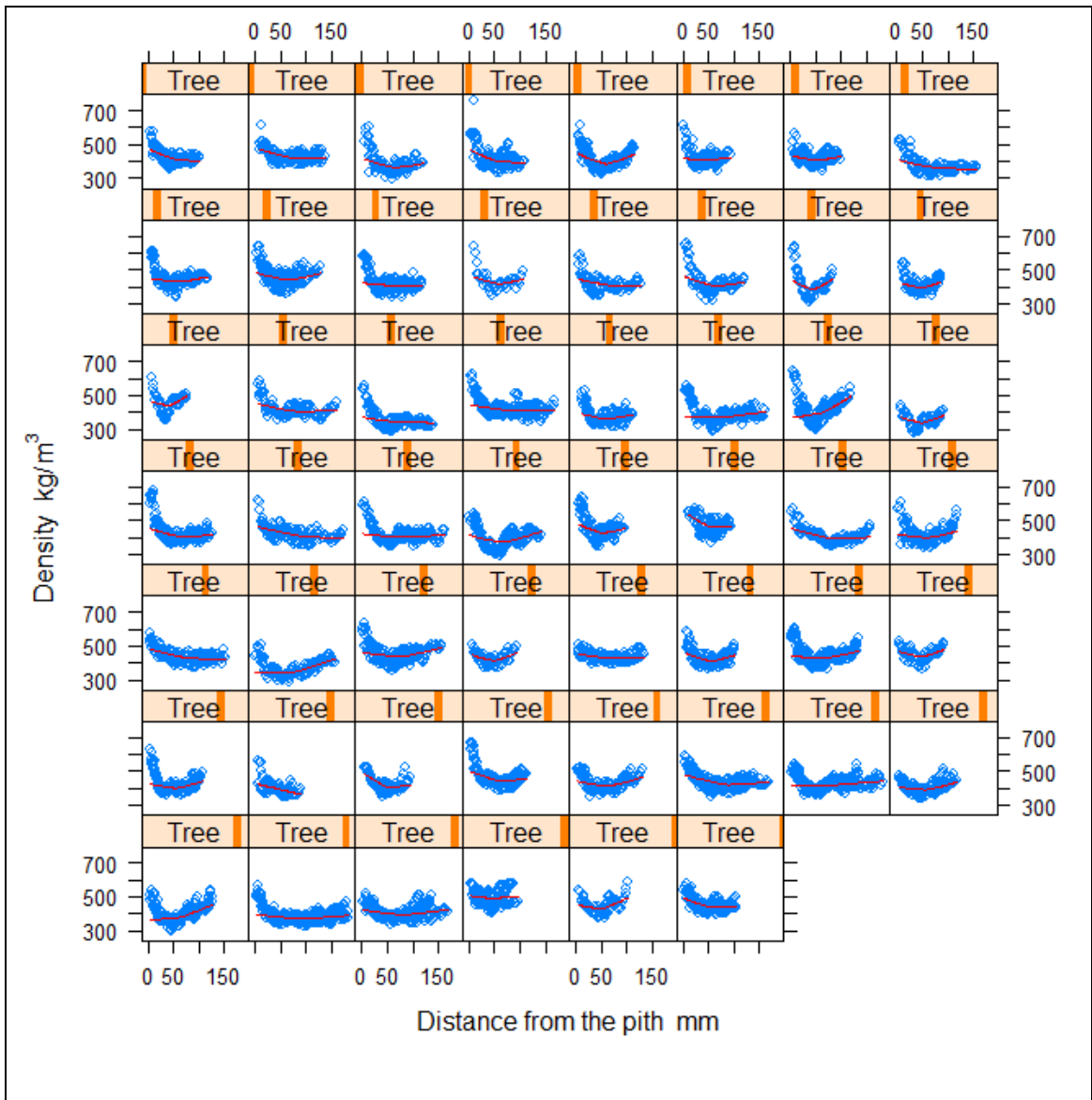


Figure 7-7. Radial trend in density for each of the studied trees at two sites.

When speed and density curves of individual samples, were plotted on the same graphs (Selected graphs presented in Figure 7-8, Figure 7-9, Figure 7-10 and Figure 7-11) it was apparent that the relationship between them varied widely between-trees. Initial decrease in density was consistent. The speed did not seem to be related to density in the juvenile part of the radius. In some cases (Figure 7-9, Figure 7-10, Figure 7-11) the speed increased at a fast rate regardless of the decrease in density. In some trees the increase in speed was less marked (Figure 7-8) and quite variable along the radius. In this tree there was also some clear compression wood in the north sample (approximately 100 mm from the pith) that was characterised by elevated density and low acoustic velocity. It seems that in juvenile wood there was no connection between the trends in acoustic velocity and density. In the mature part of the radius, in general both the density and velocity tended to increase. During the acoustic scanning it was observed that small increases in the acoustic velocity

occurred when the probe landed on latewood. On the graphs these are observed as small humps in the speed curve. The type of wood that the measurements were taken on was not noted down since the interest was in detecting radial trends and not in differences between earlywood and latewood. Furthermore, in practice it might have been difficult to record the type of wood each measurement was taken from due to the fact that the measurement is not a point but integrates information over the probe radius. Therefore, it would be difficult to judge the wood type when the rings are narrow, even if the effect was clearly observed during the analysis for wider rings.

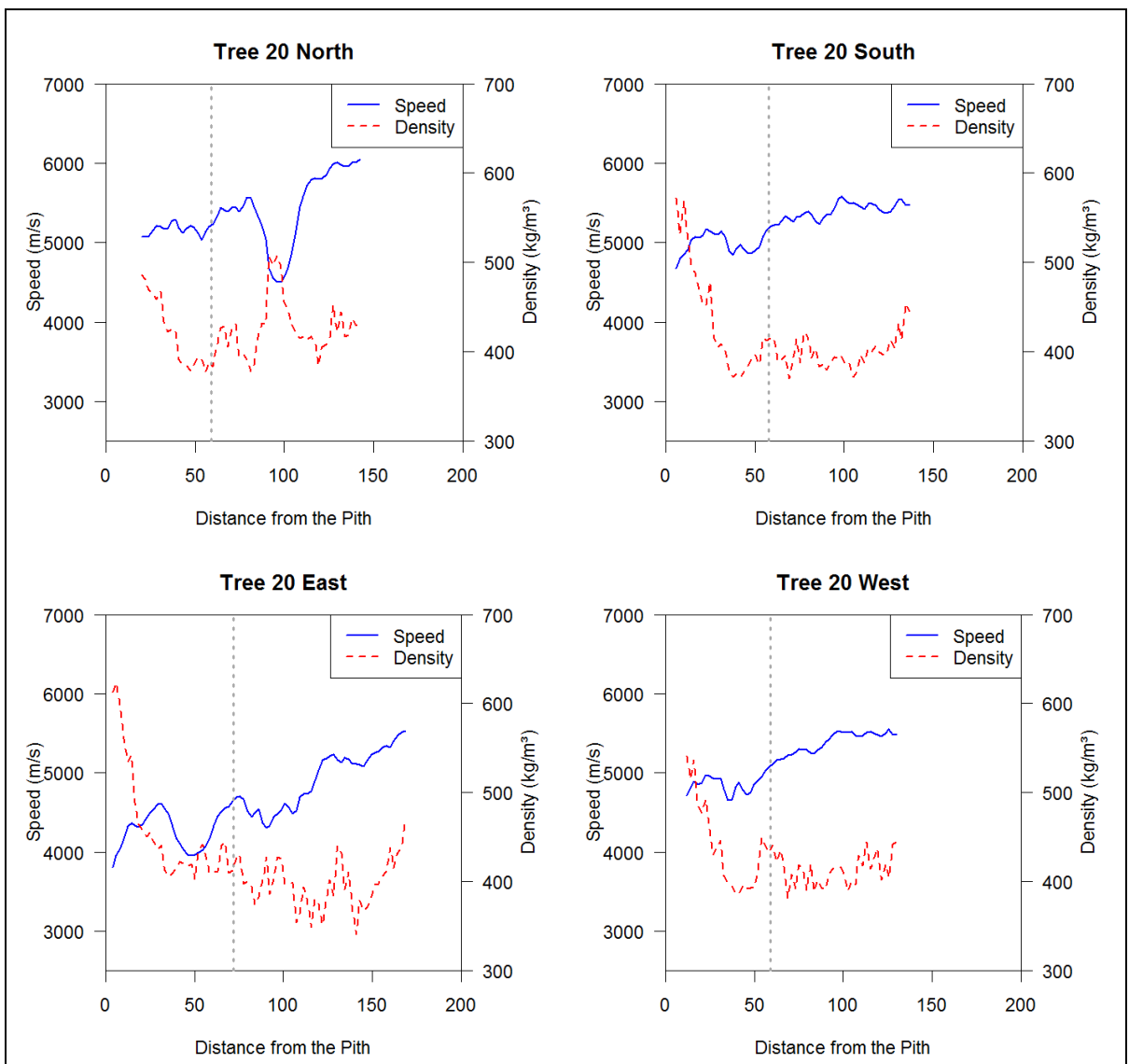


Figure 7-8. Density and acoustic velocity curves for the tree number 20 from the Coalburn site. The dashed vertical line marks the end of juvenile wood (ring 10). A section of compression wood detectable in the North radius where acoustic velocity drops and density increases.

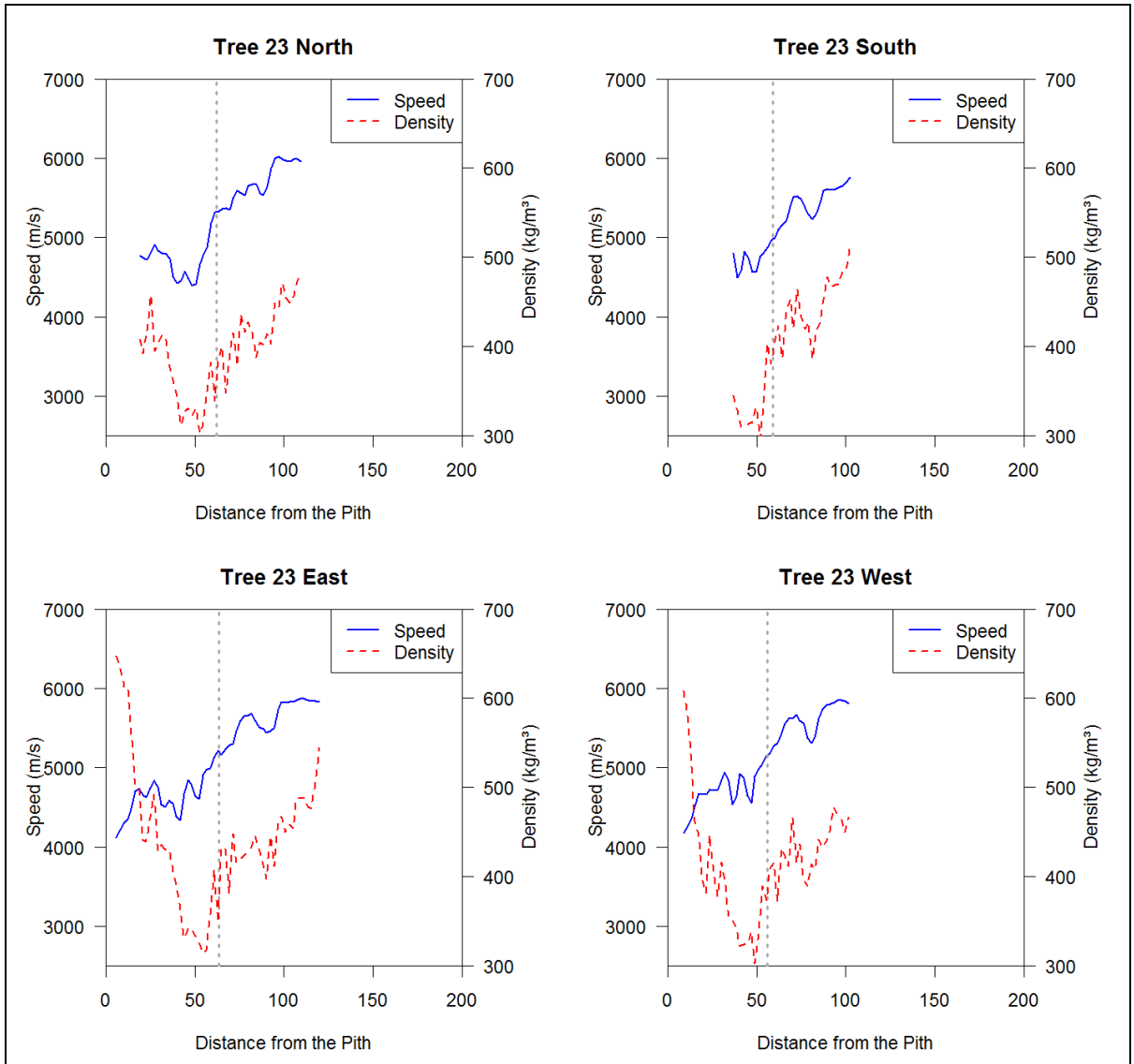


Figure 7-9. Radial profiles of density and acoustic velocity for the tree number 23 from the Coalburn site. The dashed vertical line marks the end of juvenile wood (ring 10).

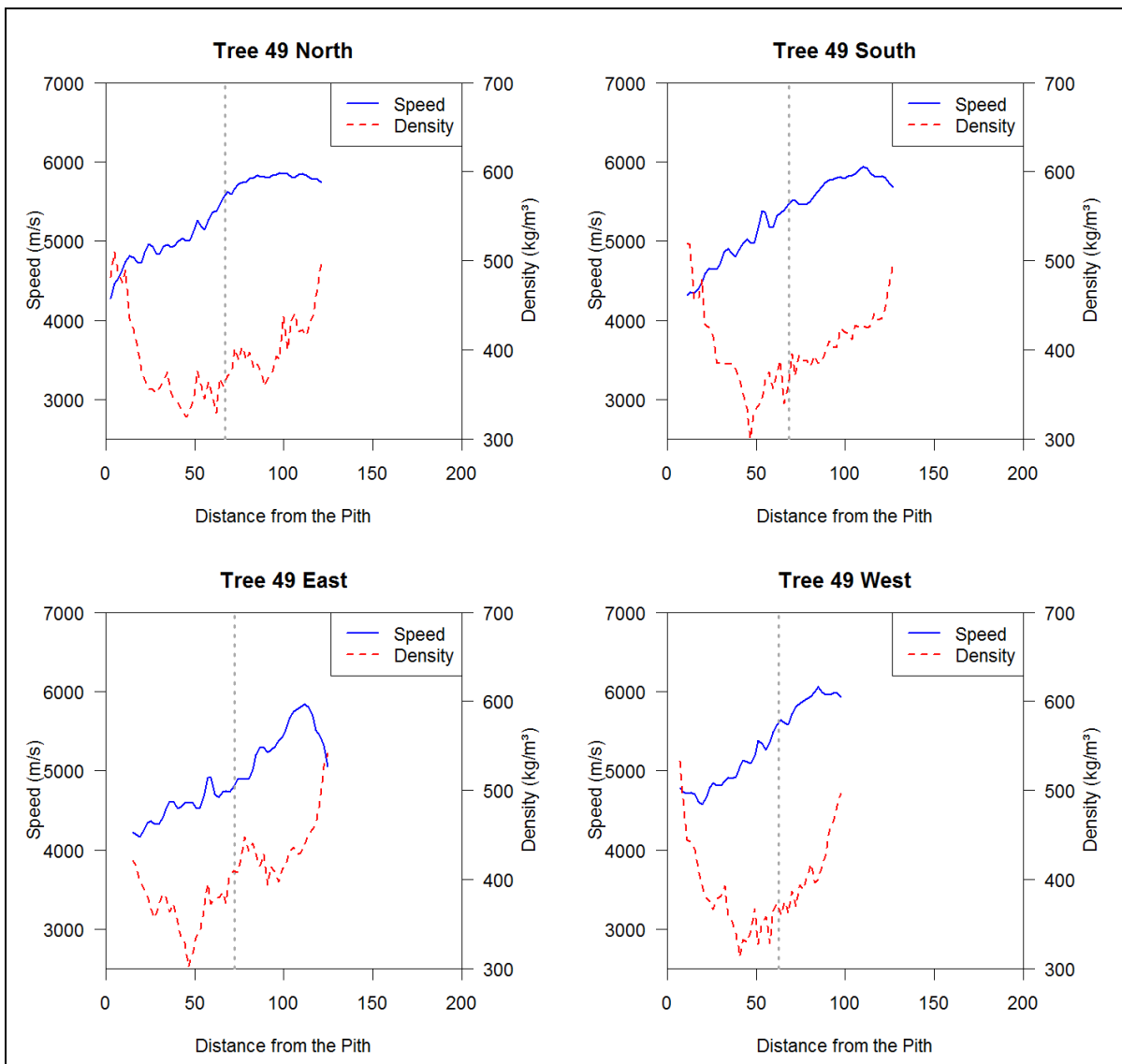


Figure 7-10. Radial profiles of density and acoustic velocity for the tree number 49 from the Loch Awe site. The dashed vertical line marks the end of juvenile wood (ring 10).

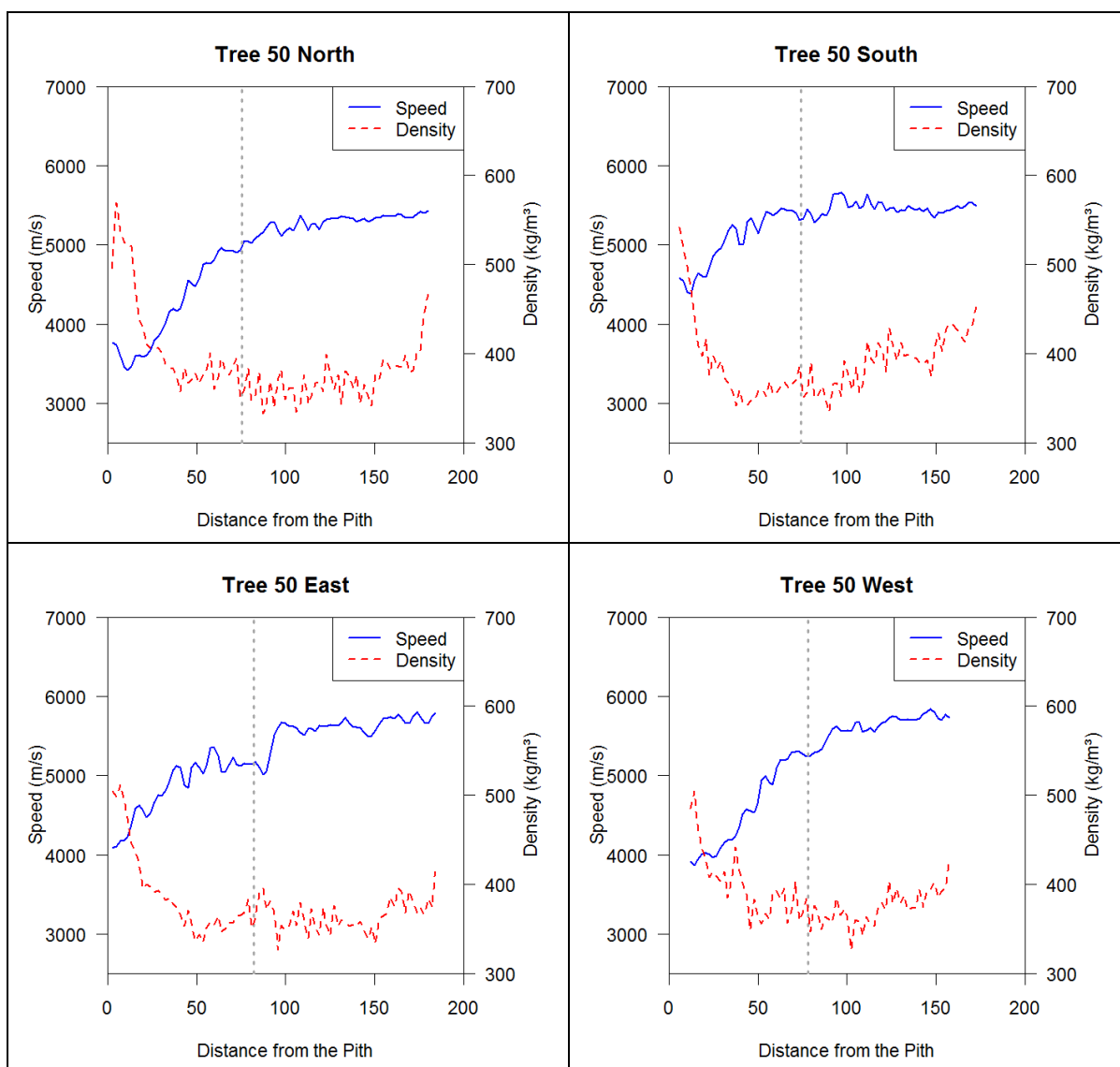


Figure 7-11. Radial profiles of density and acoustic velocity for tree number 50 from the Loch Awe site. The dashed vertical line marks the end of juvenile wood (ring 10).

Coinciding increase in density and acoustic velocity was observed when the smoothed lowess curves fitted to the pooled data were fitted as a function of ring number (Figure 7-12). When these data were plotted against distance from the pith the effect was almost nonexistent. This can be explained by the effect of tree social class. In trees from the second and especially from the third DBH quartile, the outer rings which have higher density and acoustic velocity, are located nearer to the pith than in dominant trees. This lead to the lowess curve presenting values averaged across different ring numbers, which means that the age of the material varied at each point. However, in both cases the changes in the behaviour of density and acoustic velocity took place in different parts of the radius. Change in the rate of increase in acoustic velocity occurred approximately 80 mm or 15 rings from the pith, whereas the dip in density was located 50 mm or 10 rings from the pith. Therefore, the definition that juvenile wood consists of the 10 rings nearest to the pith

seems less suited when acoustic velocity is considered. Also, in previous studies it has been reported that the boundary of the juvenile core varies with the parameter being considered (Alteyrac et al., 2006; Alteyrac et al., 2005), and naturally there is no right answer or a good compromise.

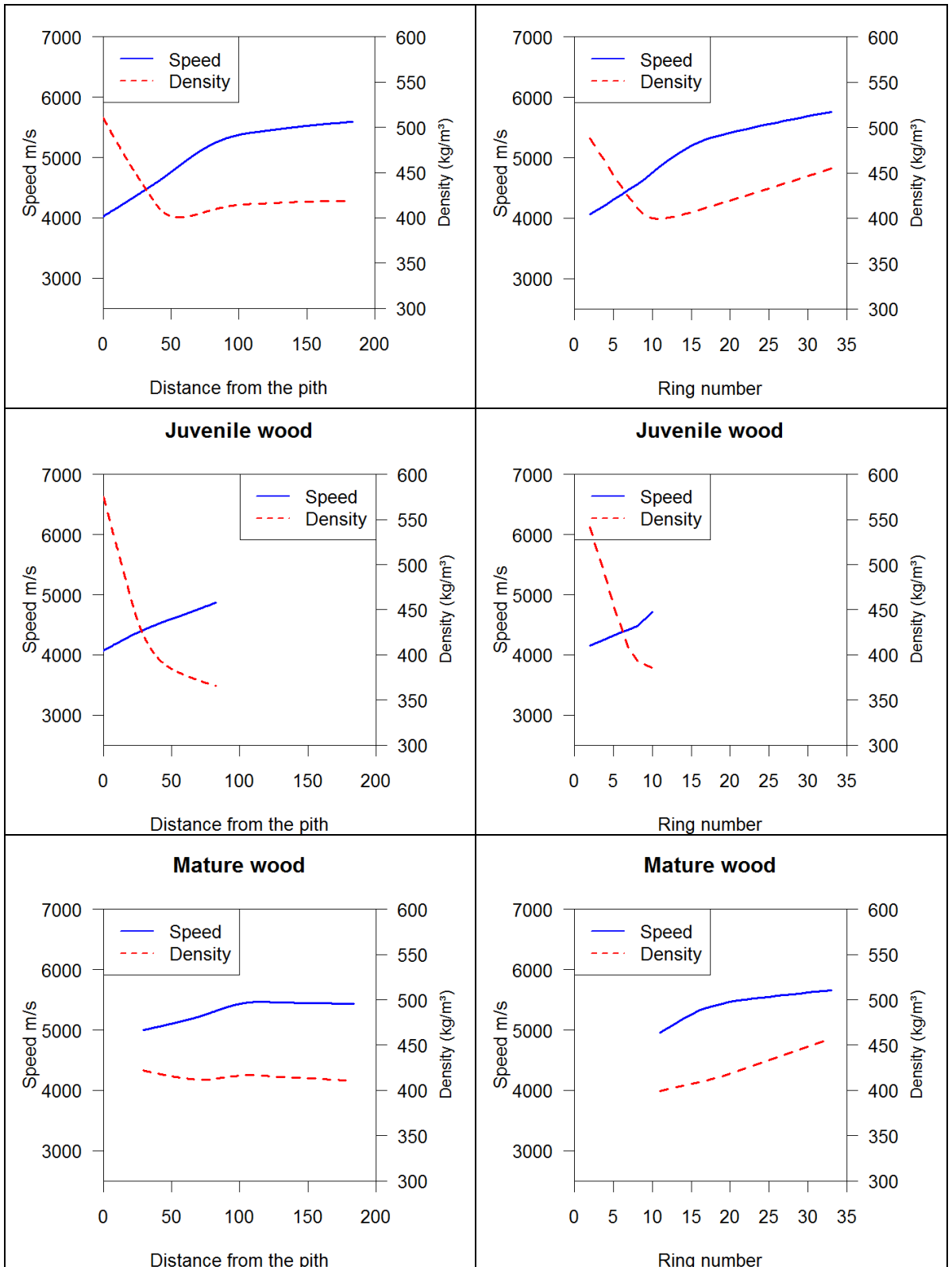


Figure 7-12. LOWESS curves of density and acoustic velocity for all data (top) and for juvenile (middle) and mature wood (bottom) sections of the radius separately plotted as a function of distance from the pith (left) and ring number (ring). 10th ring was considered as the limit between juvenile and mature wood.

The relationship between speed, density and stiffness is illustrated in Figure 7-13. In this graph the colours correspond to different stiffness values (GPa). Stiffness values found for given velocities and densities can be read from the graph. As average stiffness values are influenced by both speed and density, similar stiffness values could be obtained for different combinations of the two variables. For example at density 550 kg/m³ nearly the whole scale of stiffness values can be obtained depending on the acoustic velocity. In the case of a certain velocity value, the range is narrower since velocity has greater influence on stiffness values since it appears squared in the equation. However, at velocity 4500 m/s stiffness values ranging from 6-14 GPa were obtained. At the highest density values, only intermediate stiffness values are obtained. It indicates that where these values are measured the speed is low. This occurred normally in juvenile wood but the same would be true for compression wood. Mild compression wood is common in juvenile wood near the pith as the young stem is easily subjected to environmental stresses (Kennedy, 1995).

Prediction of stiffness from either variable alone would be complicated by this relationship and may not be satisfactory. Problems are caused by the changing relationship between density and acoustic velocity along the radius. The situation is also complicated by the presence of compression wood that will increase density without an accompanying increase in stiffness.

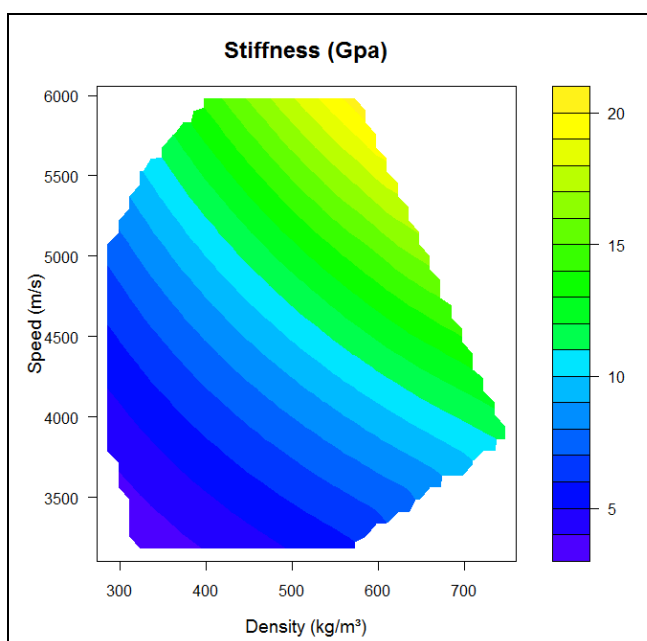


Figure 7-13. Relationship between acoustic velocity, density and stiffness in the studied trees. The coloured area is defined by the values encountered in the data and the colours represent the scale of MoE.

7.3.1 Stiffness

Stiffness values were calculated according to the equation (Equation 21) and average MoE values were derived from these. Significant differences were found in all of the MoE variables (Table 7-1) between the sites. Wood grown at the Loch Awe was stiffer than the wood from the Coalburn site.

Table 7-1. Average MoE values for the studied sites and the p-value for the difference. Standard deviation is reported in the brackets.

	Coalburn	Loch Awe	p-value for the difference
Average MoE	9.4 (\pm 1.42)	11.2 (\pm 1.77)	< 0.001
Outer 4 cm MoE	11.3 (\pm 1.63)	13.1 (\pm 1.75)	< 0.001
Outer 2 cm MoE	12.2 (\pm 1.85)	13.9 (\pm 1.75)	< 0.001
ST300 MoE	12.5 (\pm 2.36)	15.8 (\pm 3.87)	< 0.001
Juvenile MoE	7.7 (\pm 1.43)	9.6 (\pm 1.83)	< 0.001

Visually, there was also variation in the shape of the radial stiffness profiles with the site, tree social status and azimuth. In the case of tree social status and site, there seemed to be some differences in the shape of the radial stiffness curves (Figure 7-14, Figure 7-15).

There was variation in the rate of increase in the mature parts of the radius and sometimes at the Coalburn site there was a slight dip resembling the density curve. However, there were no significant differences in the cross-section average (Table 7-2) or the juvenile (Table 7-3) MoE between the social classes within a site.

Table 7-2. Average MoE for different trees social classes. The standard deviations are reported in the brackets and the letters mark differences between classes within site (alpha 0.05).

	Coalburn	Loch Awe
Dominant	9.1 (\pm 1.47) a	11.1 (\pm 1.12) b
Co-dominant	9.6 (\pm 1.25) a	11.1 (\pm 1.22) b
Non-dominant	9.4 (\pm 1.56) a	11.8 (\pm 3.09) b

Table 7-3. Juvenile wood MoE for different trees social classes. The standard deviations are reported in the brackets and the letters mark differences between classes within site (alpha 0.05) when tested with analysis of variance.

	Coalburn	Loch Awe
Dominant	7.5 (\pm 1.62) a	9.3 (\pm 1.13) b
Co-dominant	7.8 (\pm 0.99) a	9.5 (\pm 1.42) b
Non-dominant	7.8 (\pm 1.68) a	10.4 (\pm 3.07) b

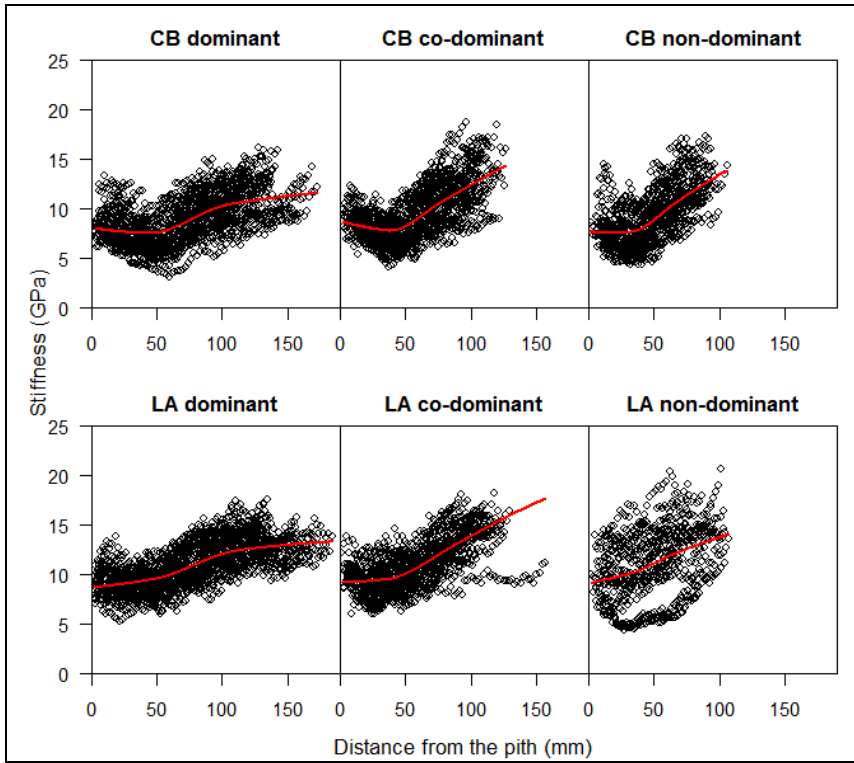


Figure 7-14. Influence of tree social status on the shape of the radial stiffness curves plotted a function of distance from the pith. LOWESS curve fitted to the data drawn on graphs in red.

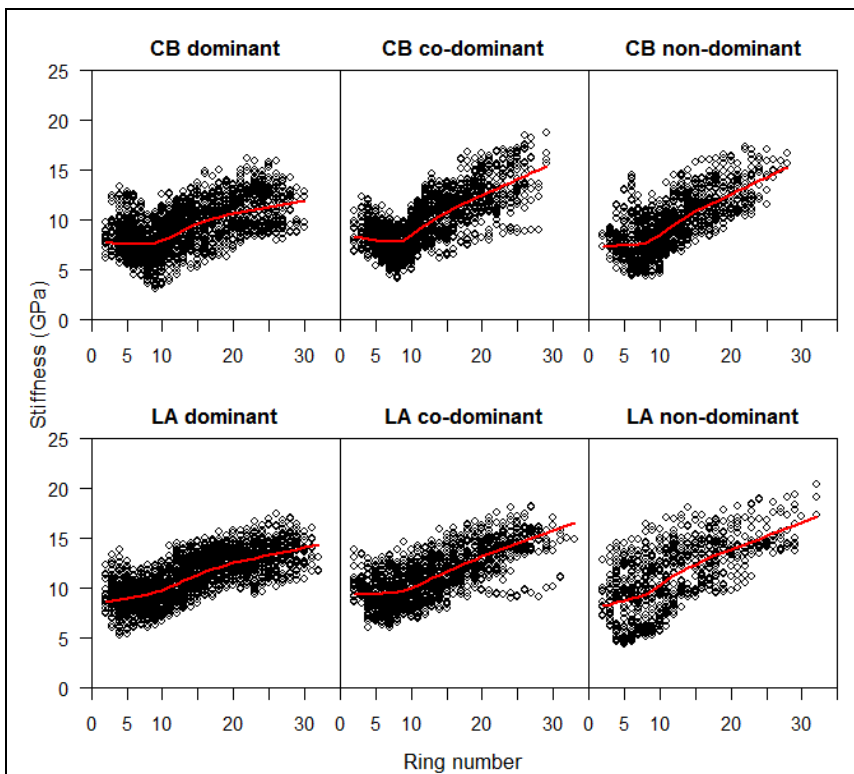


Figure 7-15. Influence of tree social status on the shape of the radial stiffness curves plotted as a function of ring number. LOWESS curve fitted to the data drawn on graphs in red.

With azimuth there was no clear trends at the Loch Awe site (Figure 7-16, Figure 7-17). At the Coalburn site wood on the Eastern side of the stem seemed less stiff than at the other

directions. Furthermore during the sample processing it was noted that the radii tended to be longer at the North and East sides at Coalburn.

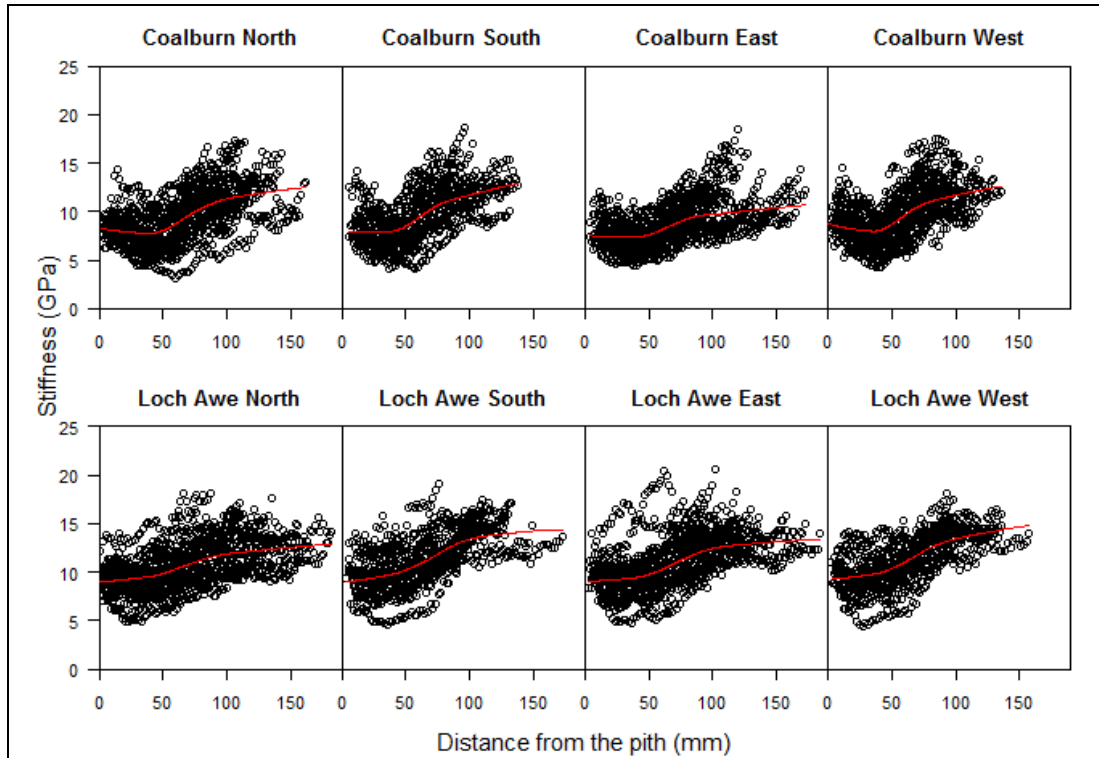


Figure 7-16. Influence of azimuth on the shape of stiffness curves at the Coalburn site. LOWESS drawn in red.

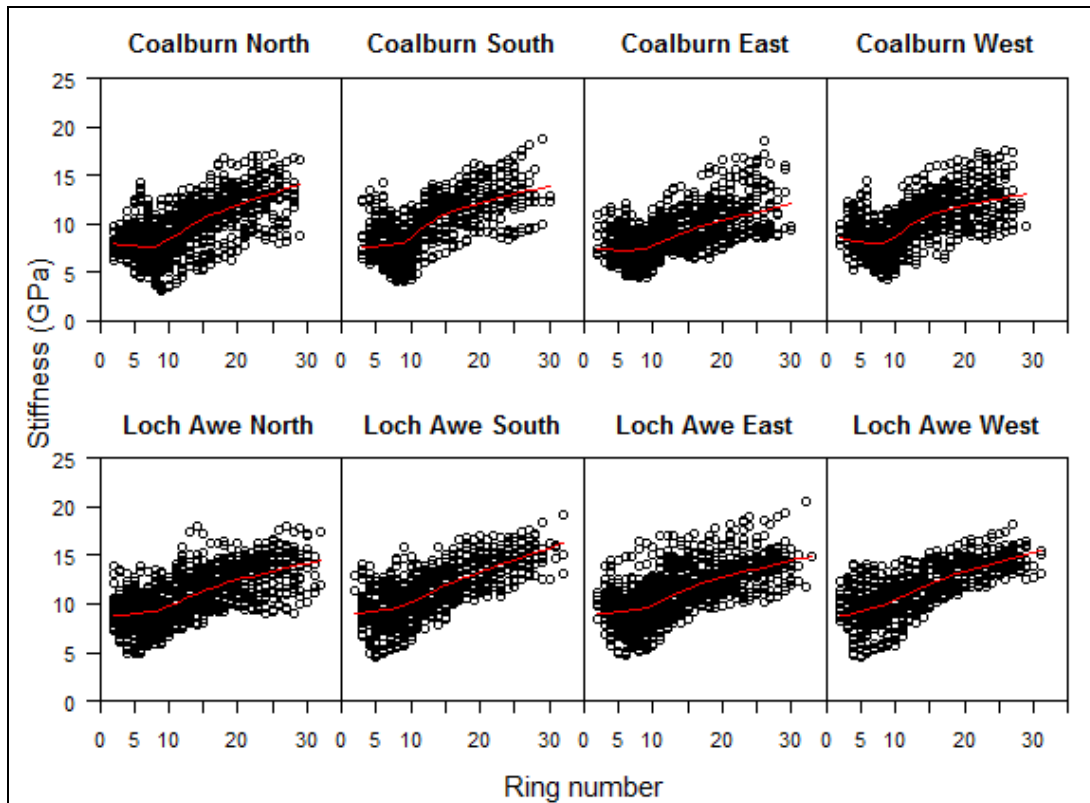


Figure 7-17. Radial variation in the Stiffness with all directions plotted separately for both sites against the ring number.

The possible effect due to direction was investigated further by looking also at average density and speed in addition to the stiffness. It appeared that the direction effect might differ between the sites (Figure 7-18).

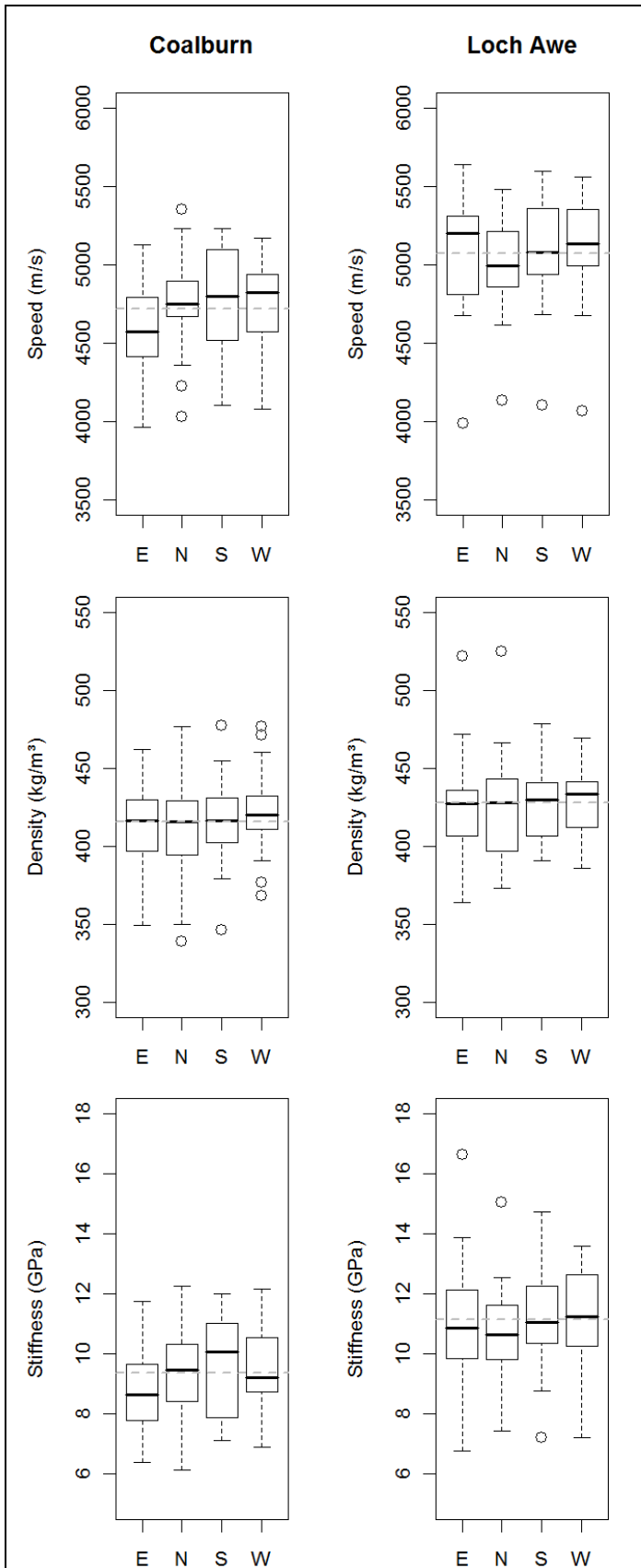


Figure 7-18. Average speed (top), density (middle) and stiffness (bottom) for the each direction at the two sites.

This was observed in speed but it was largely absent in density. Naturally, speed has a larger influence on the resulting stiffness values as it is squared in the equation and therefore the direction effect was also seen in stiffness data. At the Coalburn site, lowest average speeds were measured on the eastern side of the trunk whereas the opposite was true for Loch Awe. At the Loch Awe site, lowest values were measured from the North side. A differing direction effect at the two sites could increase the variation in the data so that no differences between directions were observed when looking at the entire dataset. Therefore, the effect of direction was investigated for each site separately using analysis of variance. No significant differences (alpha 0.05) were detected in sample average speed, density or stiffness between the directions (Figure 7-19).

Since the two sites differed significantly in MoE (Table 7-1 and Figure 7-18) values it was decided that the stiffness is modelled separately for both sites. Both density and velocity contributed to this difference since the sites differed significantly in these properties as well (p-values <0.01). However, the difference was more pronounced in absolute terms for speed.

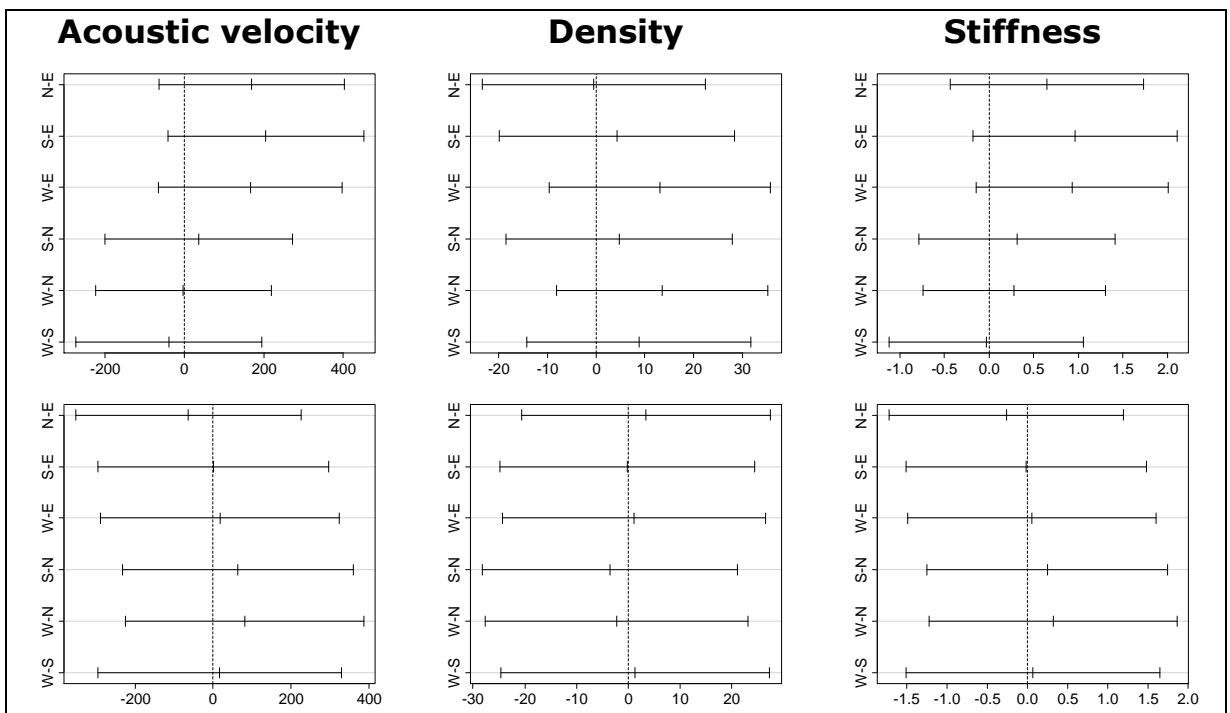


Figure 7-19. 95% confidence intervals for the comparisons between directions in acoustic velocity, density and stiffness using analysis of variance with the Tukey HSD test. Top row presents the results for Coalburn and bottom for Loch Awe site.

Comparing the shape of the stiffness curves that have been plotted against the distance from the pith and ring number (Figure 7-15, Figure 7-17), it seemed that the ring number governs the change in stiffness more accurately than distance from the pith. The variation around the lowest curve was smaller for ring number. In the case of distance from the pith, the changes in the slope of the stiffness curves that characterised the transition from juvenile to mature wood, occurred in different places and the ends of individual curves were visible in places.

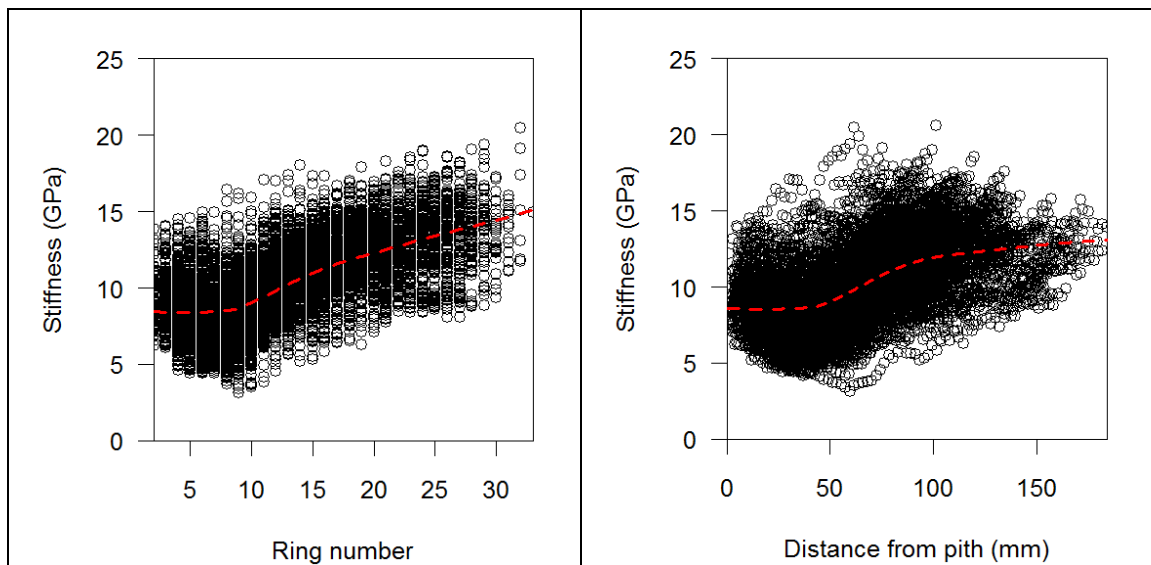


Figure 7-20. The pooled stiffness data plotted against ring number (left) and distance from the pith (right). Dashed red line is the lowest curve fitted to the data.

7.3.2 Average stiffness models

Average stiffness of the radii was modelled with mixed effects models in R (R Development Core Team, 2007) using the Restricted Maximum Likelihood to fit the models. The variables to be included in the initial model were selected by plotting the different variables from each class to see which has the most influence and by using correlation analysis. One variable from each class was selected. This minimised the number of correlated variables in the model as for example for crown dimension several different variables (crown length, crown width, crown volume, crown ratio, lowest living branch and lowest living whorl) were measured in the field or calculated.

After the selection the initial model for pooled data included juvenile radius, slenderness, age, stem straightness score and height of lowest living whorl as explanatory variables. The mixed effects model was fitted with nested random effects consisting of site, tree within site and direction within tree. In the case of site specific models, the random effects

structure naturally only included tree and direction within the tree. The initial model for Coalburn included the following explanatory variables; juvenile radius, average grain angle, stem straightness score and crown width, and the one for Loch Awe juvenile radius, age, slenderness, average grain angle and lowest living whorl.

A final model with the minimum adequate number of significant variables was then derived by model simplification. The final model obtained the forms described in (Table 7-4) which also details the coefficients and the diagnostic values. In all cases, a larger juvenile core leads to lower values of average MoE (Figure 7-23, Figure 7-24 and Figure 7-25) which is to be expected as the lowest values of MoE are measured in the juvenile part of the radius and larger core area influences the average value to a greater extent. At the Loch Awe site the stiffness values seemed to increase with slenderness (Figure 7-25) which was in line with previous studies on Radiata pine (Mason, 2006). In pooled data, stiffness was found to increase with the height of the lowest living whorl (Figure 7-23). This is in line with studies where stiffness has been found to be lower in Sitka spruce trees with deeper crowns (Moore et al., 2009c). Similarly, in juvenile Radiata pine, pruning treatment that restricts the depth of live crown was found to increase MoE (Mason, 2006).

Table 7-4. Coefficients for the explanatory variables in the average MoE models.

All data					
Fixed effects: Average MoE ~ JWRadius + LowestLivingWhorl					
	Value	Std.Error	DF	t-value	p-value
(Intercept)	11.0263	1.402	113	7.87	0.0000
JWRadius	-0.0608	0.011	113	-5.72	0.0000
LowestLivingWhorl	0.2094	0.089	50	2.35	0.0227
Coalburn					
Fixed effects: Average MoE ~ JWRadius + CrownWidth					
	Value	Std.Error	DF	t-value	p-value
(Intercept)	9.6401	1.448	61	6.66	0.0000
JWRadius	-0.0641	0.015	61	-4.29	0.0001
CrownWidth	1.0664	0.411	28	2.60	0.0149
Loch Awe					
Fixed effects: Average MoE ~ JWRadius + Age + Slenderness					
	Value	Std.Error	DF	t-value	p-value
(Intercept)	6.0075	2.841	50	2.12	0.0395
JWRadius	-0.0487	0.014	50	-3.45	0.0012
Age	0.1641	0.065	50	2.52	0.0152
Slenderness	0.0397	0.016	21	2.44	0.0237

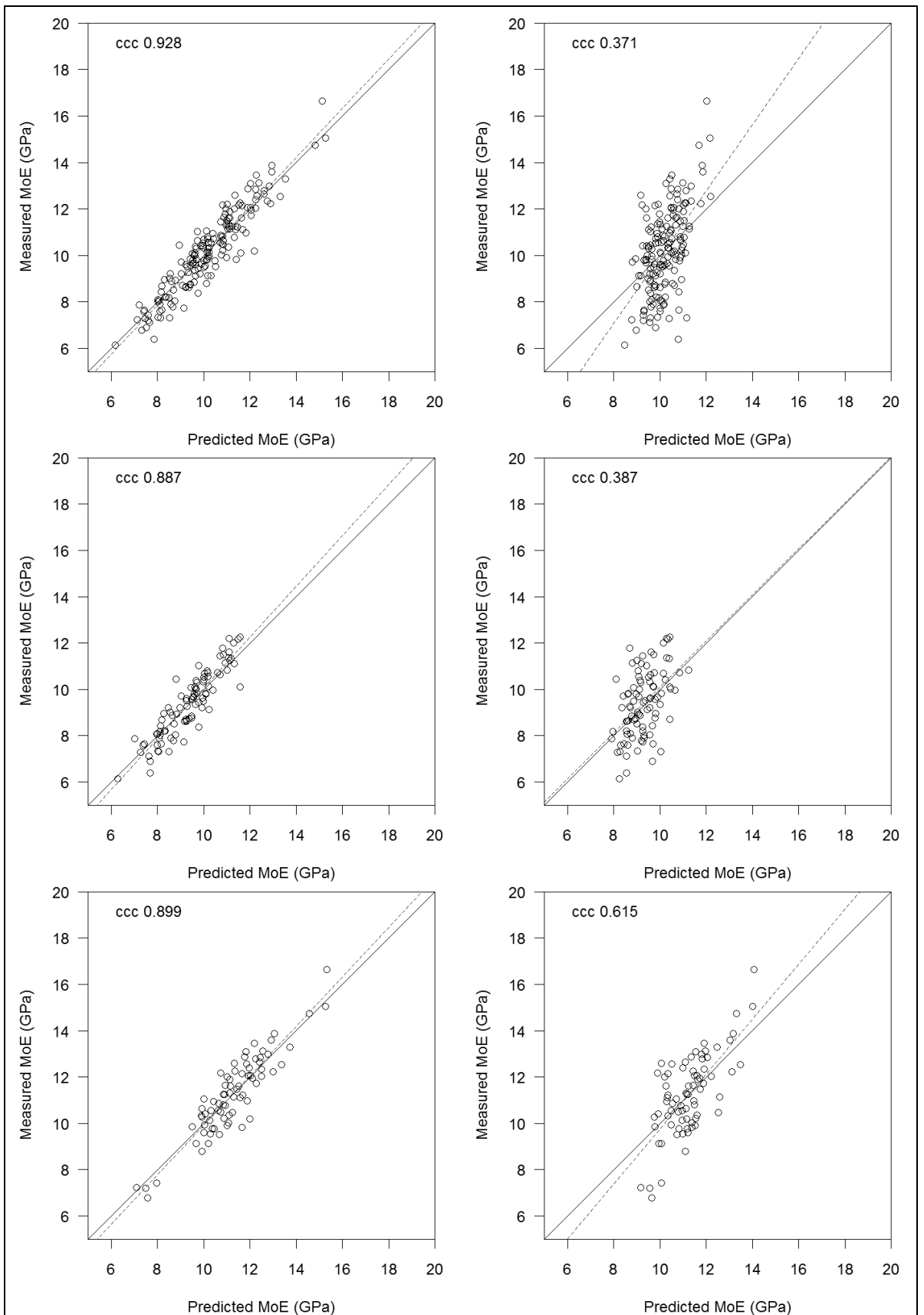


Figure 7-21. Average stiffness model predictions against the measured data for all data (top), Coalburn (middle) and Loch Awe (bottom) including tree effect (left) and using average coefficients only (right). Dashed line is the regression line fitted to the data.

The model predictions (left side, Figure 7-21), including the random tree effects, gave good results. The adjusted R^2 -value for the pooled data was 0.81, for Coalburn 0.71 and Loch Awe 0.73. However, there were quite large random effects (Figure 7-22) and therefore the results were much poorer when only the average coefficients were used to derive the predictions (right side, Figure 7-21). Using the fixed effects only, the adjusted R^2 -values were 0.26, 0.21 and 0.45 for pooled data, Coalburn and Loch Awe, respectively.

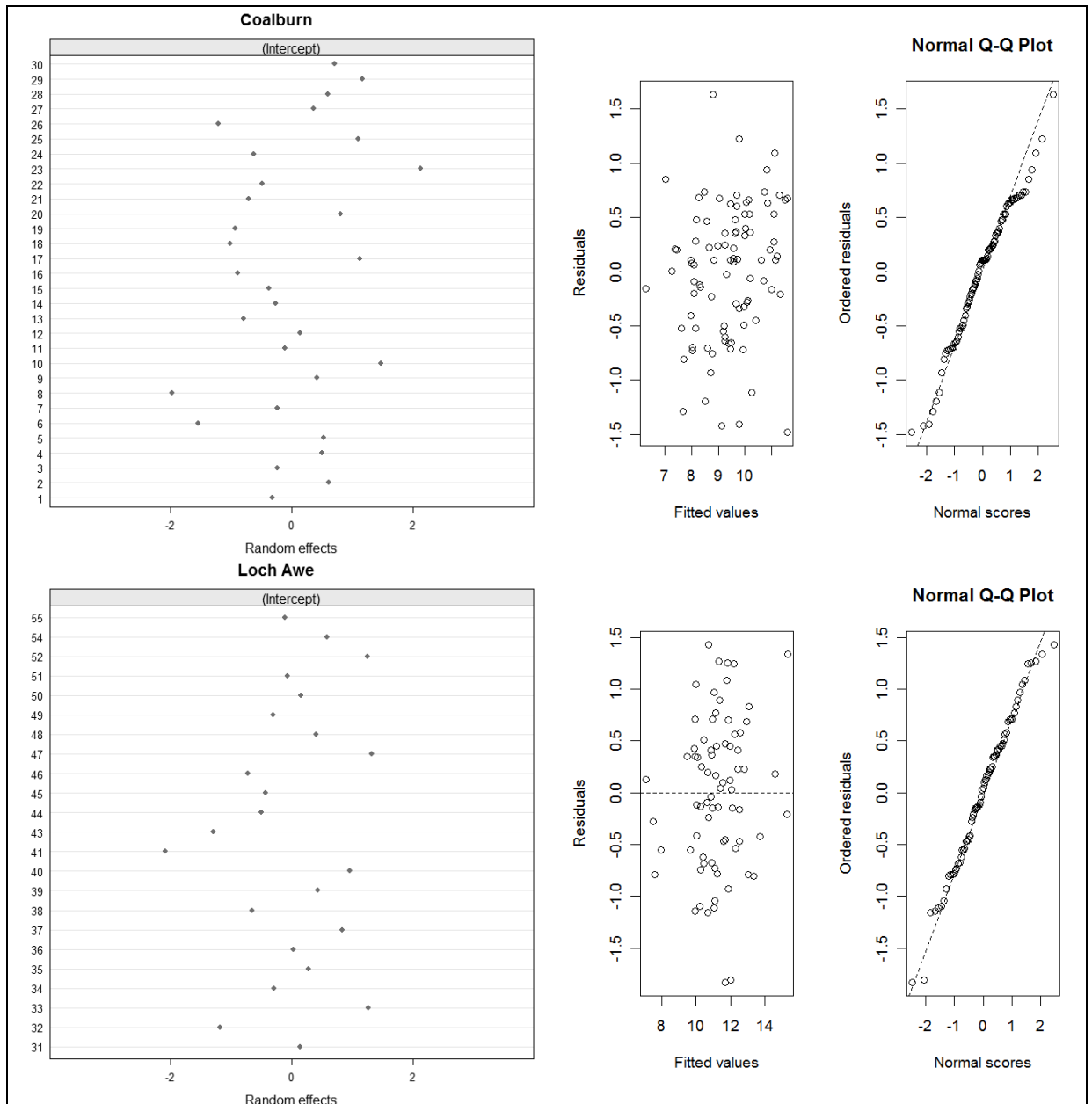


Figure 7-22. Tree specific random effects for the average stiffness model fits and diagnostic plots for Coalburn (top) and Loch Awe data (bottom).

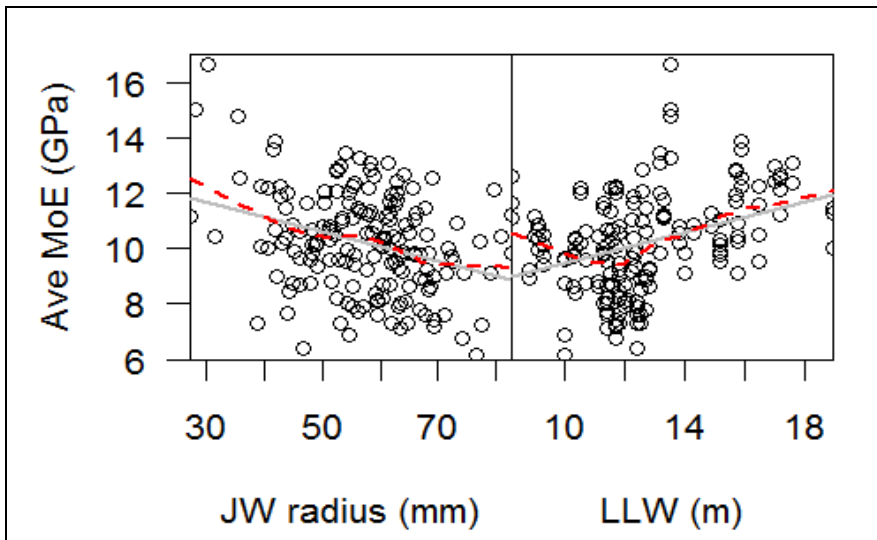


Figure 7-23. MoE (circles) plotted against the explanatory variables included in the final model fitted to all acoustic data. Solid grey line represents the linear regression fitted to the data and dashed red line the LOWESS curve.

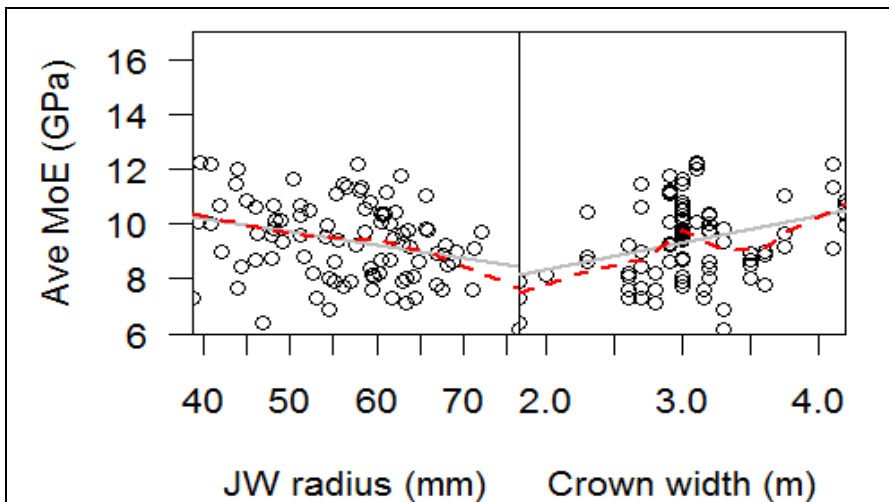


Figure 7-24 MoE (circles) plotted against the explanatory variables included in the final model fitted to the Coalburn data. Solid grey line represents the linear regression fitted to the data and dashed red line the LOWESS curve.

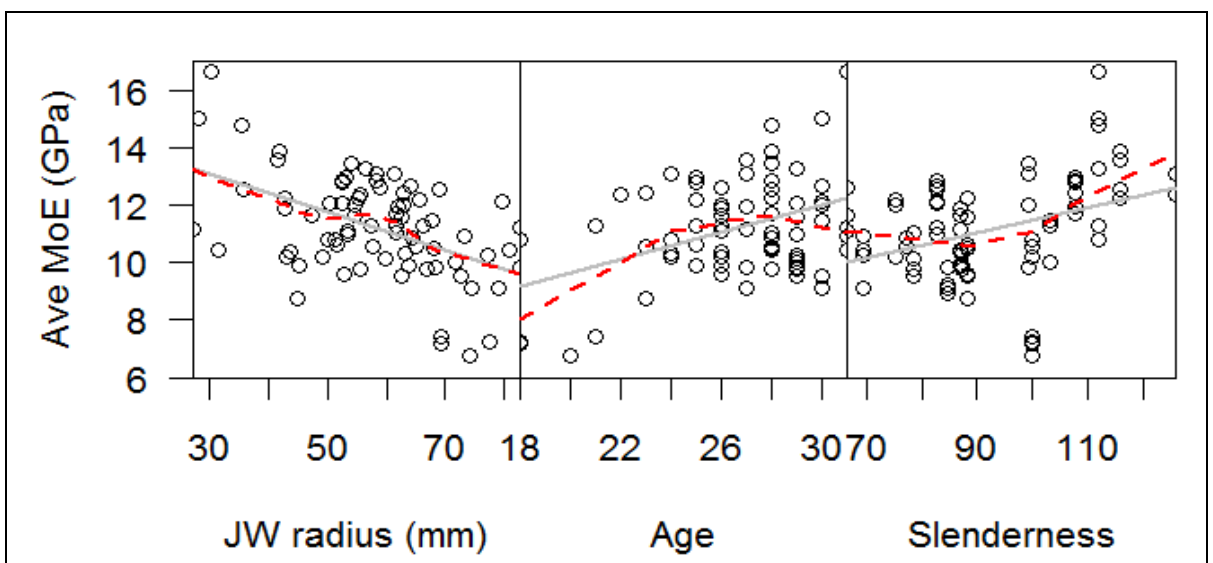


Figure 7-25. MoE (circles) plotted against the explanatory variables included in the final model fitted to the Loch Awe data. Solid grey line represents the linear regression fitted to the data and dashed red line the LOWESS curve.

7.3.3 Juvenile wood MoE

The explanatory variables in the initial juvenile wood MoE model were selected based on scatter plots of juvenile wood MoE against measured tree variables and correlation tests on the significance of observed relationships. The initial model for juvenile wood MoE included juvenile radius, stem straightness score and crown width for Coalburn and juvenile radius and DBH for Loch Awe as the explanatory variables to be tested for significance. After the exclusion step, the final model (Table 7-5) included juvenile radius and crown width as explanatory variables at the Coalburn site and juvenile radius at the Loch Awe site. In both cases there was a negative correlation between juvenile MoE and radius but the effect was more pronounced at the Loch Awe site (Table 7-5, Figure 7-28 and Figure 7-29). As in the case of cross-section average, the higher crown width was related to higher juvenile MoE. Wider crown usually means also deeper crown as well and deeper crown has been found to correlate with lower MoE (Mason, 2006; Moore et al., 2009b). However, the crown was measured in its mature conditions and is not directly related to the juvenile wood as the crown dimensions may have been different at that stage of growth.

Table 7-5. The final models derived for Juvenile wood MoE at Coalburn and Loch Awe sites.

COALBURN					
Fixed effects: Juvenile MoE ~ JWRadius + CrownWidth					
	Value	Std.Error	DF	t-value	p-value
(Intercept)	7.7096	1.368	61	5.64	0.0000
JWRadius	-0.0664	0.015	61	-4.55	0.0000
CrownWidth	1.1866	0.384	28	3.09	0.0045
LOCH AWE					
Fixed effects: Juvenile MoE ~ JWRadius					
	Value	Std.Error	DF	t-value	p-value
(Intercept)	12.0075	0.939	51	12.79	0.0000
JWRadius	-0.0422	0.015	51	-2.76	0.0081

Random trees effects (Figure 7-27) were more pronounced for juvenile wood MoE than for cross-section average MoE (Figure 7-22). This was especially true for Loch Awe and using fixed effects alone to predict MoE (Figure 7-26) values made the R^2 -value drop from 0.78 to 0.17. In the case of the Coalburn site, the R^2 -values were 0.71 for the full model and 0.29 for the fixed effects only.

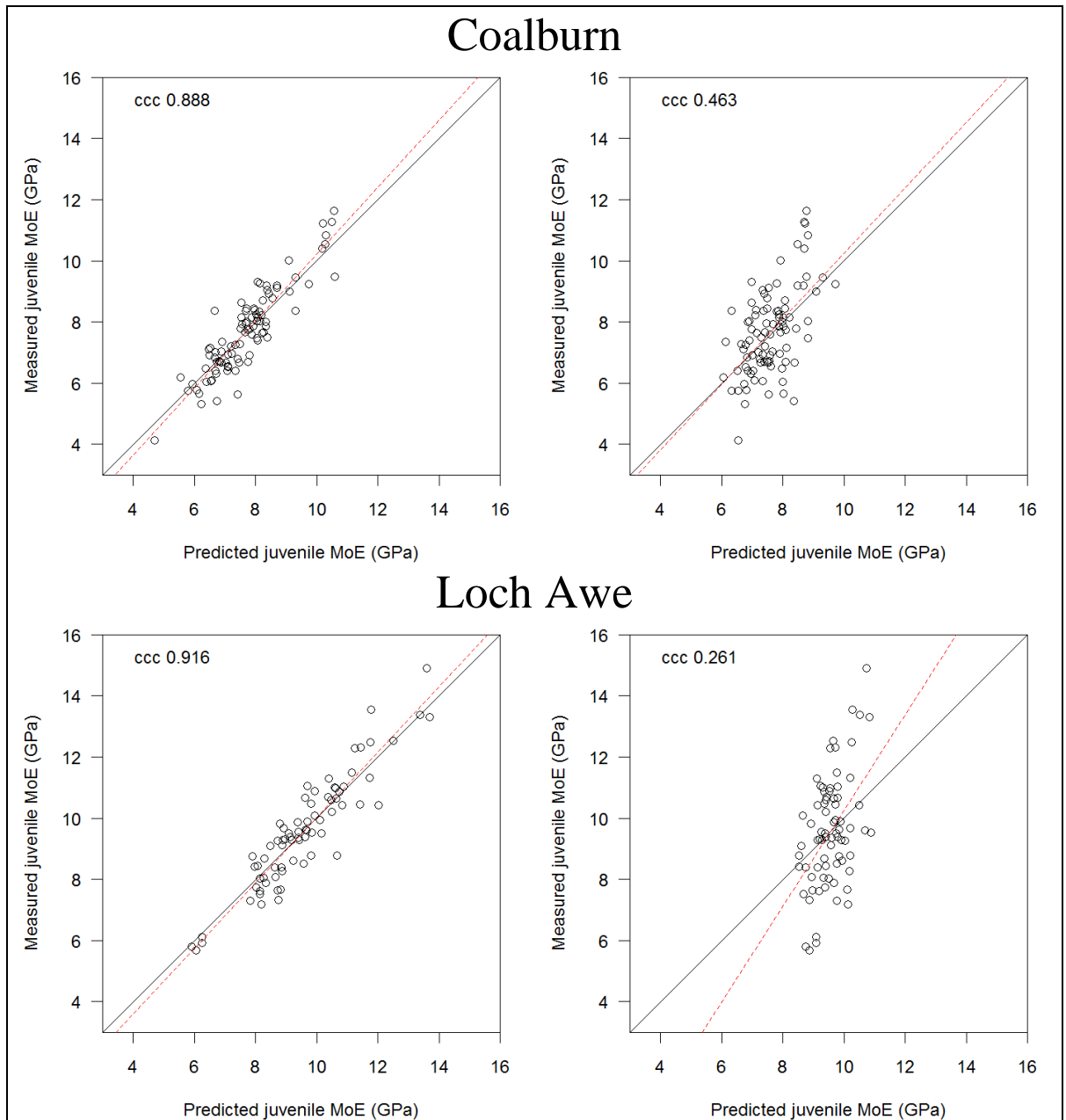


Figure 7-26. Juvenile wood MoE model predictions plotted against the measured data for the 2 sites. In the graphs on the left the random effects were included whereas on the right the predictions were calculated using the fixed effects only. Dashed red line is the linear regression fitted to the data.

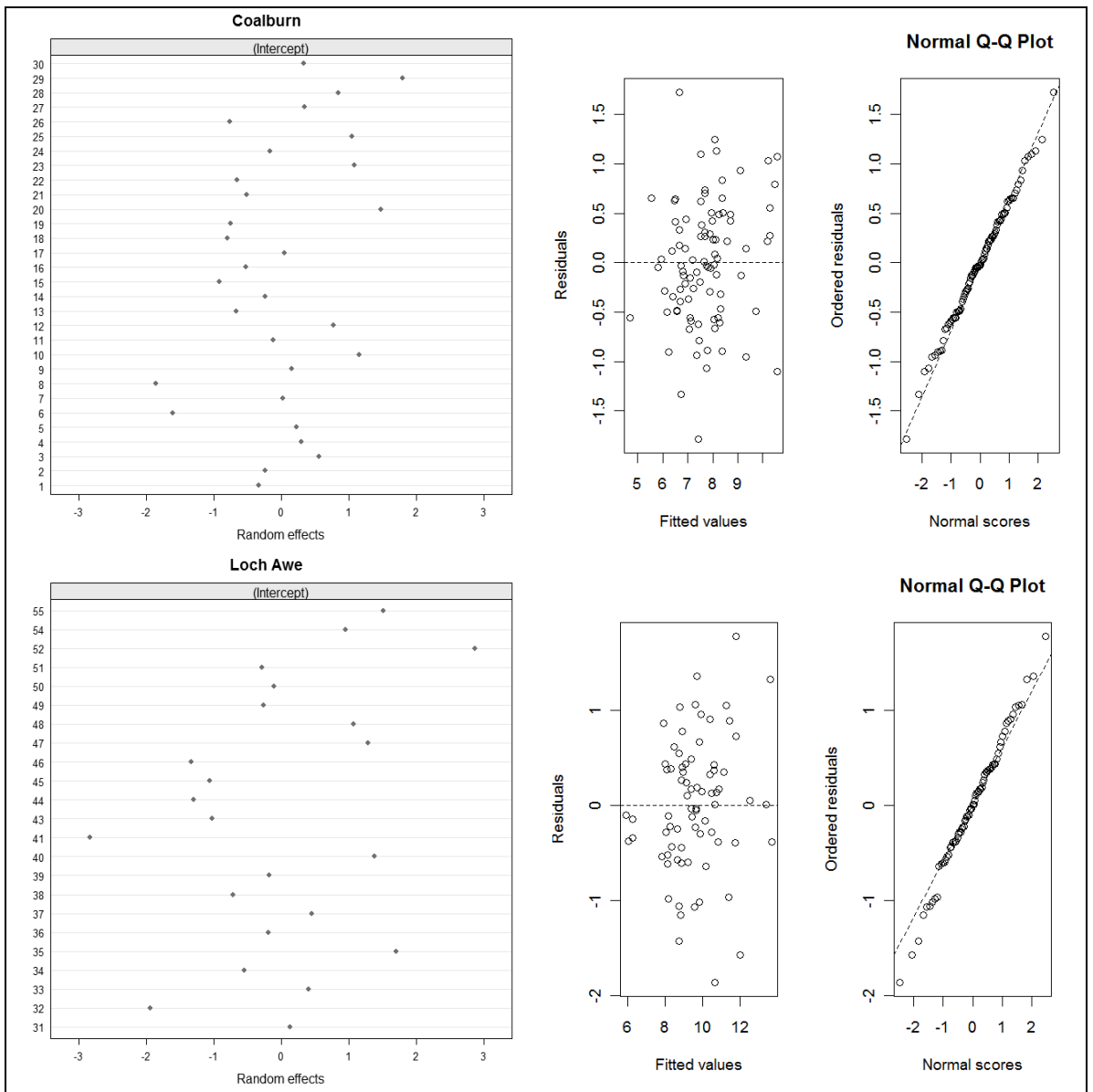


Figure 7-27. Tree specific random effects and juvenile wood MoE model diagnostic plots for Coalburn (top) and Loch Awe (bottom) sites.

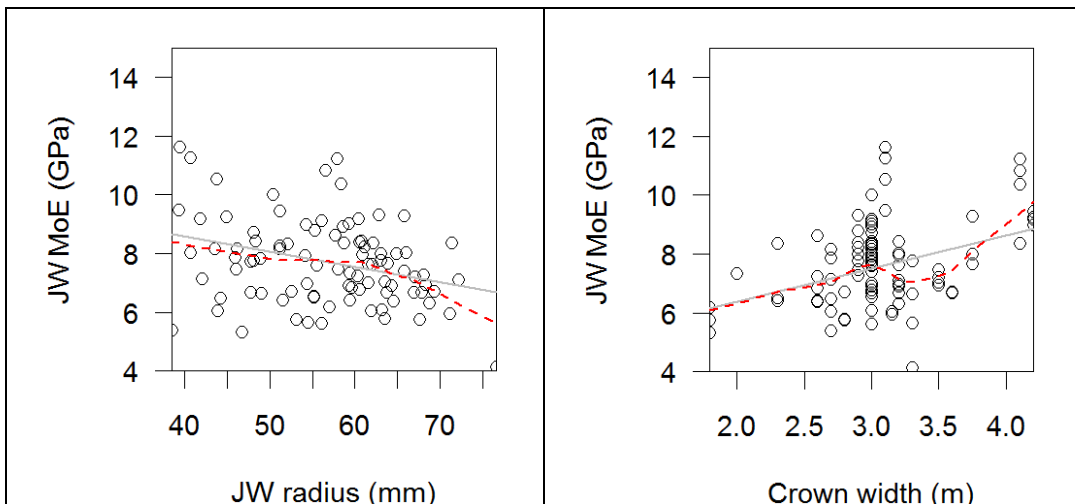


Figure 7-28. Influence of the explanatory variables on juvenile wood stiffness at the Coalburn site

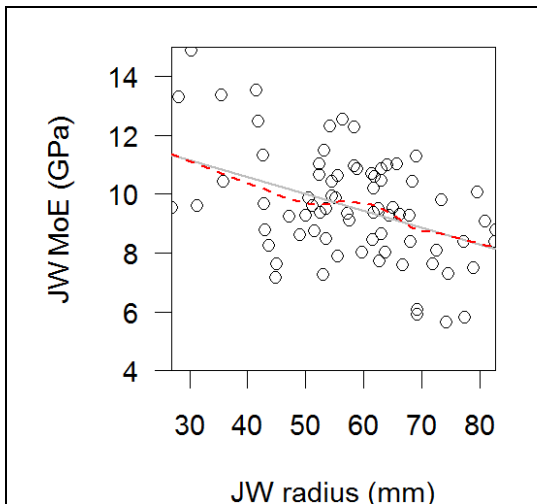


Figure 7-29. Influence of the explanatory variable on the juvenile wood stiffness at the Loch Awe site.

7.3.4 Outerwood MoE

A model was also built to predict the stiffness of the outer 4 cm of the stem. A full model was developed using scatter plots and correlation analysis as described above. The process of model simplification was used to derive the final model (Table 7-6). Again, random tree effects were quite large (Figure 7-30). Therefore, R^2 fell from 0.61-0.66 for the full model to 0.09-0.10 for the fixed effects. The fixed effects have poor explanatory power since the relationship is not very consistent (Figure 7-31). There are several observations that are located relatively far from the regression line. Furthermore, the lowess curve obtained a humped shape.

Table 7-6. The outerwood stiffness models.

COALBURN					
Fixed effects: Outerwood MoE ~ CrownWidth					
	Value	Std.Error	DF	t-value	p-value
(Intercept)	7.7527	1.563	62	4.96	0.000
CrownWidth	1.1055	0.505	28	2.19	0.037
LOCH AWE					
Fixed effects: Outerwood MoE ~ JWRadius					
	Value	Std.Error	DF	t-value	p-value
(Intercept)	15.6301	1.005	51	15.55	0.0000
JWRadius	-0.0429	0.017	51	-2.58	0.0128

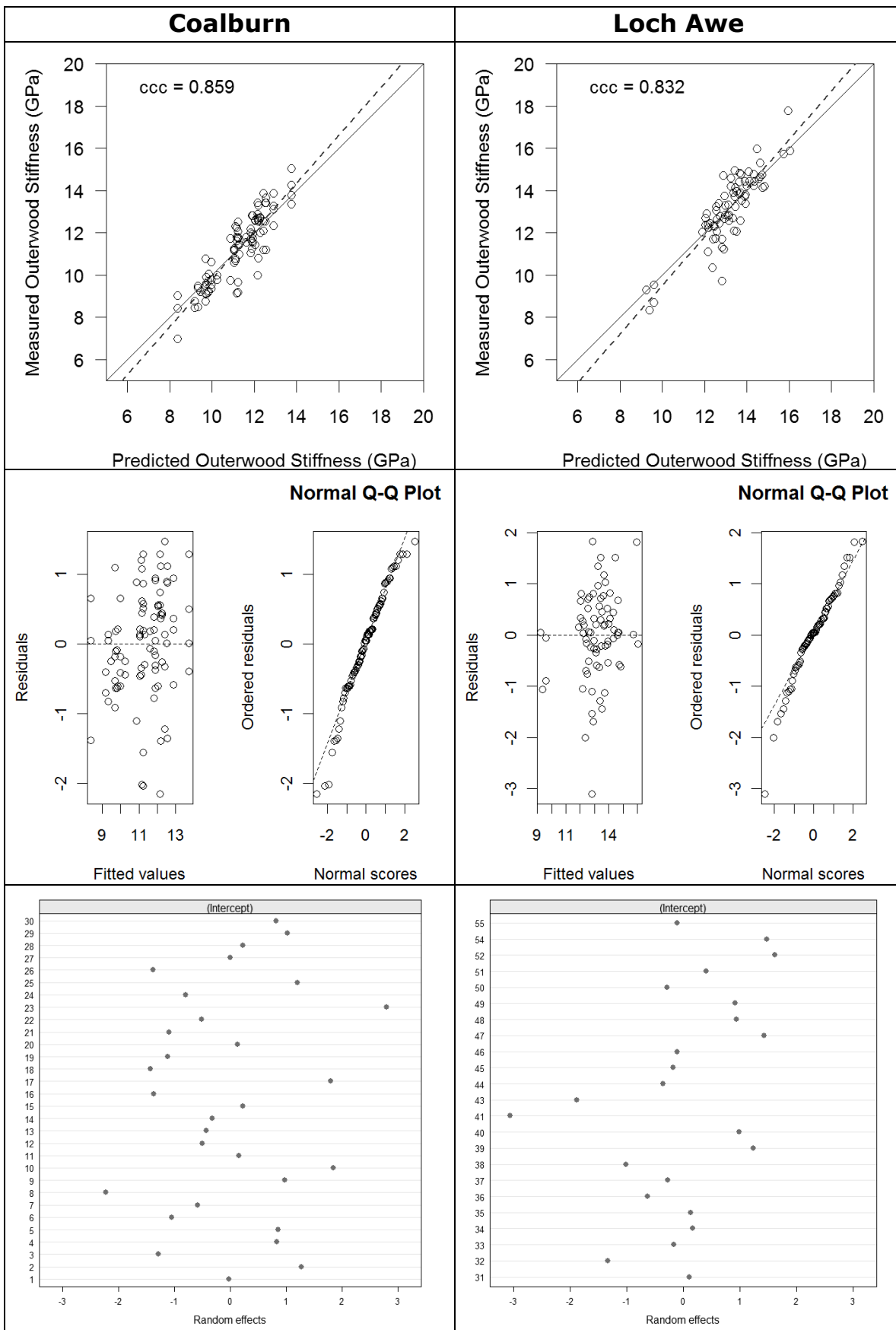


Figure 7-30. Outerwood MoE model predictions against the measured value (top) and diagnostic plots on residuals (middle) and random effects (bottom).

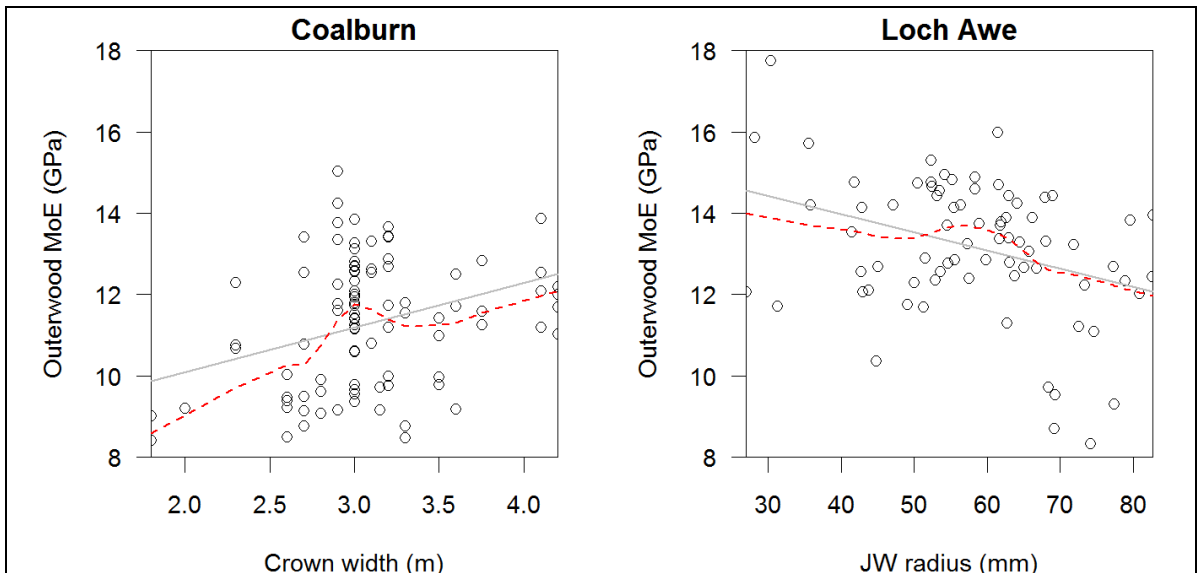


Figure 7-31. Influence of selected explanatory variables in the final outerwood stiffness model developed for the Coalburn site (left) and Loch Awe (right). Regression line is marked in grey and lower curve in red.

7.3.5 Models for acoustic velocity

Average speed models were developed as above, selecting initial variables using scatter plots and correlations analysis, then simplifying the models until they only contained significant variables (Table 7-7). R^2 -values for the models were Coalburn 0.58 and Loch Awe 0.71 and for the fixed effect, they fell to 0.15 and 0.41, respectively. Modelling speed did not solve any problems of stiffness analysis and the relationships between explanatory variables were not improved (Figure 7-33 and Figure 7-34).

Table 7-7. Average speed models.

COALBURN					
Fixed effects: Average Speed ~ CrownWidth					
	Value	Std.Error	DF	t-value	p-value
(Intercept)	3949.999	274.857	62	14.37	0.0000
CrownWidth	239.928	88.718	28	2.70	0.0115
LOCH AWE					
Fixed effects: Average Speed ~ JWRadius + TH					
	Value	Std.Error	DF	t-value	p-value
(Intercept)	3606.701	453.657	51	7.95	0.0000
JWRadius	-10.480	3.053	51	-3.43	0.0012
TH	82.468	19.404	21	4.25	0.0004

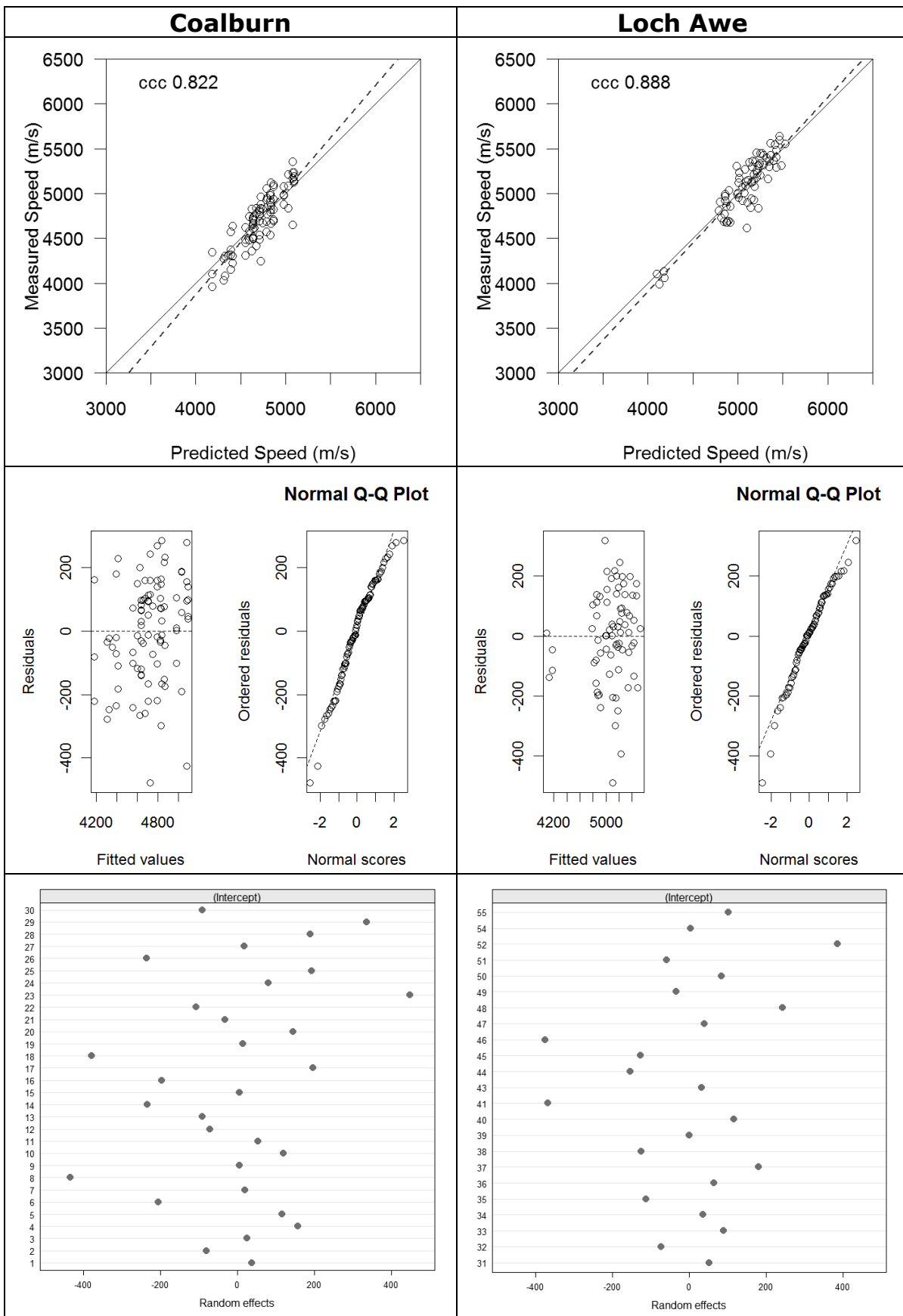


Figure 7-32. Tree average acoustic velocity model predictions against the measured data (top), model diagnostic plots (middle) and random effects (bottom).

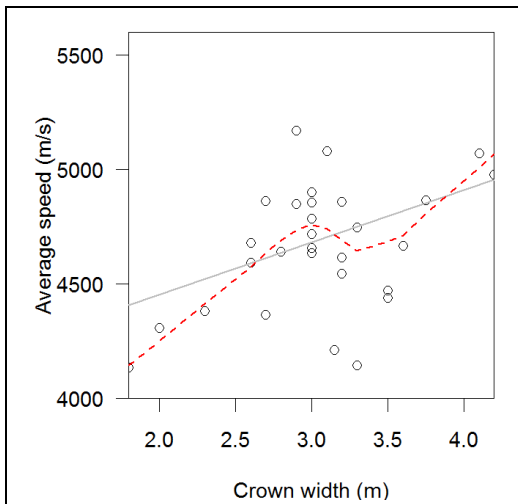


Figure 7-33. Influence of the explanatory variables on the sample average acoustic velocity at Coalburn site.

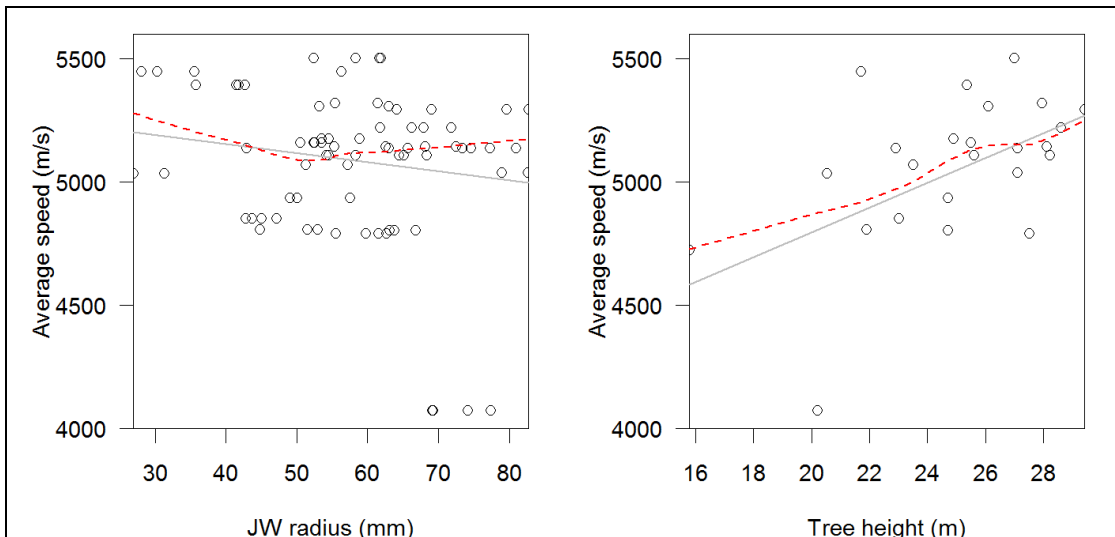


Figure 7-34. Influence of the explanatory variables on the sample average acoustic velocity at the Loch Awe site.

7.3.6 Radial stiffness modelling

The site average MoE values for all parts of the cross-section differed significantly. Even if there was no effect from direction or dominance class, the stiffness curves for the two sites differed in shape (Figure 7-35). The effect was very pronounced when the stiffness values averaged across all the trees within the site for each ring were plotted (Figure 7-36). The parameters a , b and d in the radial stiffness model (Equation 22) aim to match the shape of the curve and fitting will be increasingly difficult if the shape differs largely between-trees. Therefore, it was thought that better results would be obtained if the model was fitted to each site separately.

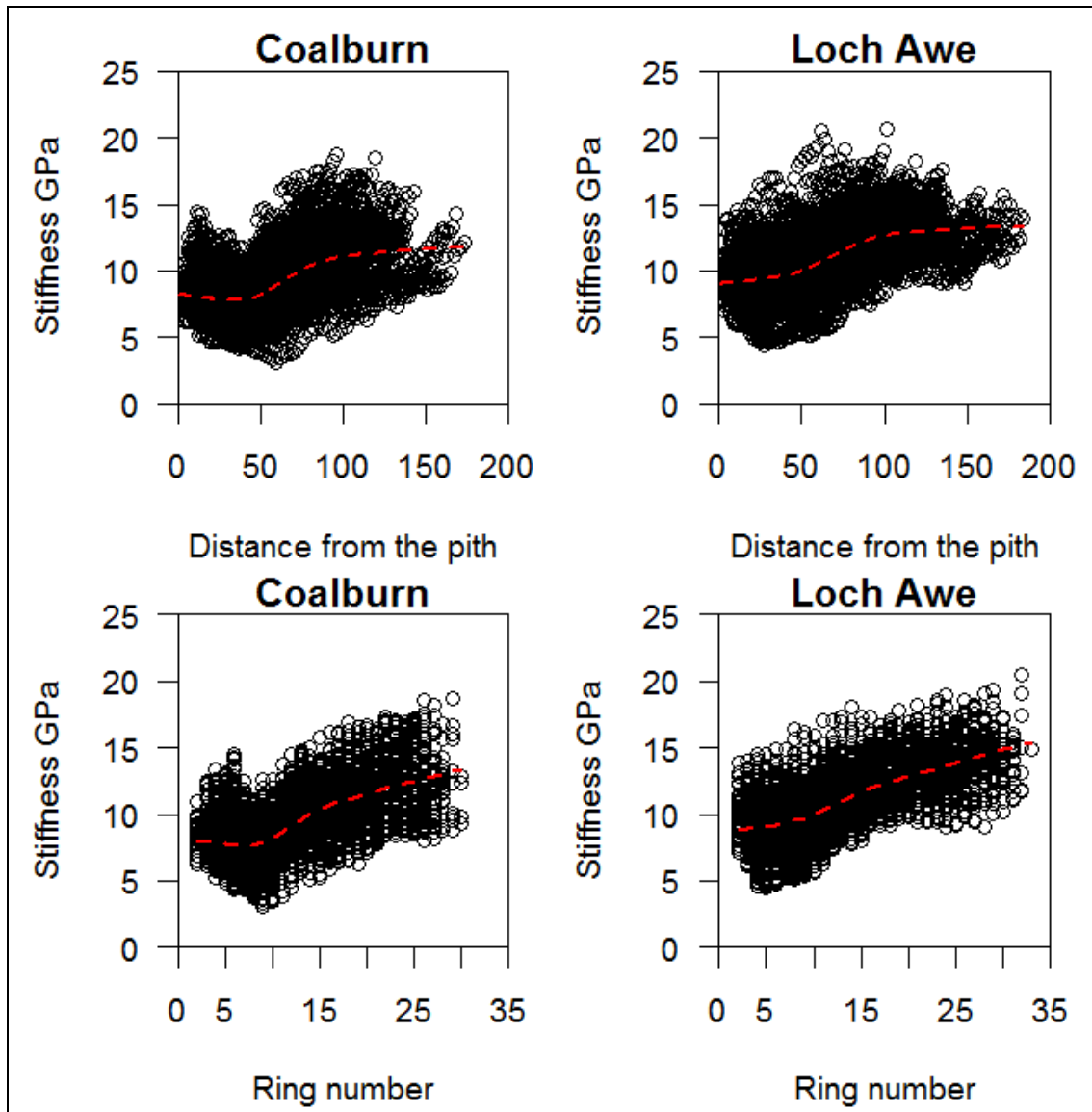


Figure 7-35. Average radial stiffness curves for the Coalburn and Loch Awe sites plotted against the distance from the pith, mm (top) and ring number (bottom).

However, fitting the model to pooled data was tested as well. It turned out that fitting the model to the pooled data yielded good results as well (Figure 7-37). This was probably because during the fitting, tree specific parameters are derived for each sampled tree and therefore the trees are not influenced by the overall shape of the pooled radial data. During the fitting, several samples had to be removed before the model would converge. This seemed to arise when one of the samples differed from the other radii within the tree. From Coalburn 10 and from Loch Awe 1 such problematic samples were removed. At the end, the final dataset for Coalburn included 81 samples from 27 trees and the Loch Awe dataset consisted of 77 samples from 24 trees.

Good fits were obtained when stiffness values were predicted including the random tree effects (left side, Figure 7-37). This means that in practice, tree specific a , b and d

parameters were used in the predictions. The adjusted R^2 -values were 0.77 for Coalburn, 0.80 for Loch Awe and 0.81 for pooled data. When the average parameters (Table 7-8) were used, the fits were considerably poorer (right side, Figure 7-37). The model diagnostic plots (Figure 7-38) reveal that this is at least partially due to the failure to model the stiffness behaviour near the pith. The dip is not modelled adequately when the tree specific random effects are not included. The problem was less pronounced for Loch Awe where the average curve had a much smaller dip. This could also explain why results on pooled data were so good since the dip is also smoother in the pooled data and hence will lead to improved fit.

Ideally, a model that does not need reparameterisation for each tree should be developed since deriving the tree specific parameters requires stiffness measurements as an input. This at least partially defeats the point since ideally, modelling would provide the means of avoiding time consuming density, acoustic velocity or microfibril angle measurements. Therefore, it was investigated if the a, b and d parameters could be predicted using standard forestry measurements as an input.

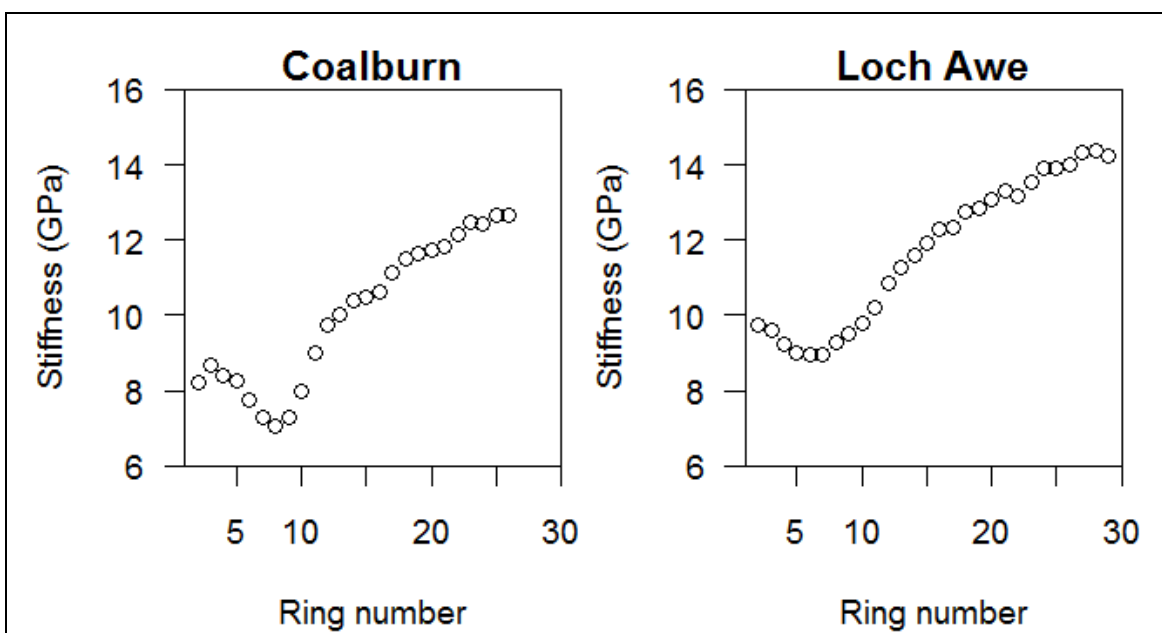


Figure 7-36. Average ring stiffness curves for the Coalburn and Loch Awe sites.

Table 7-8. Average model coefficients of the radial stiffness model for Coalburn, Loch Awe and data pooled from both sites. Standard error in the brackets.

	a	b	d
Coalburn	29.189 (± 2.2128)	33.882 (± 2.0144)	7.318 (± 0.2615)
Loch Awe	25.132 (± 2.4222)	29.607 (± 2.4112)	8.923 (± 0.3197)
Pooled	26.658 (± 1.8475)	31.271 (± 1.7607)	8.351 (± 0.3547)

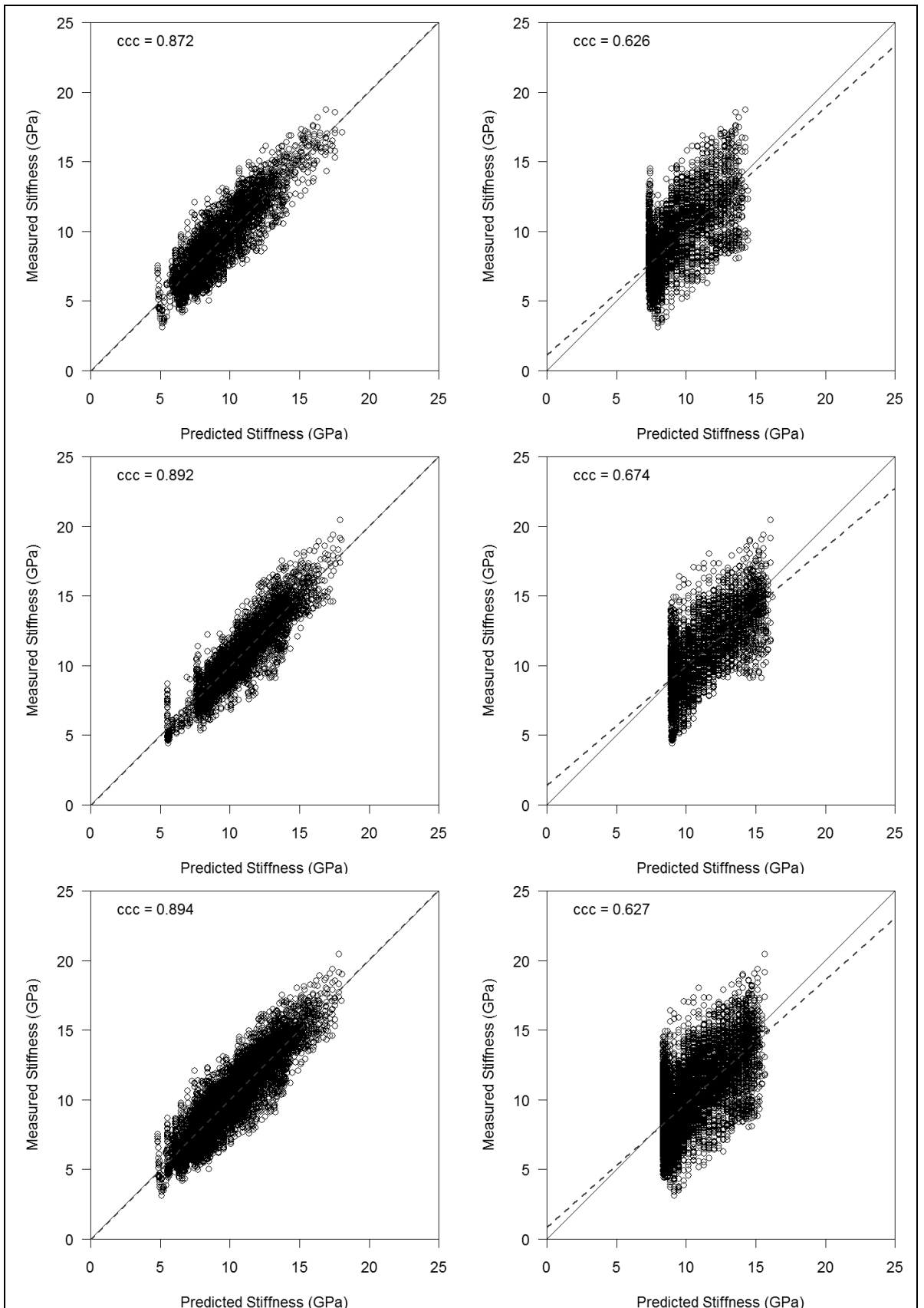


Figure 7-37. Radial Stiffness model predictions including tree effect (left) and using only fixed effects (right) for the Coalburn (top), Loch Awe (middle) and all data combined (bottom). Dashed line is the regression line fitted to the data and ccc is the concordance correlation coefficient.

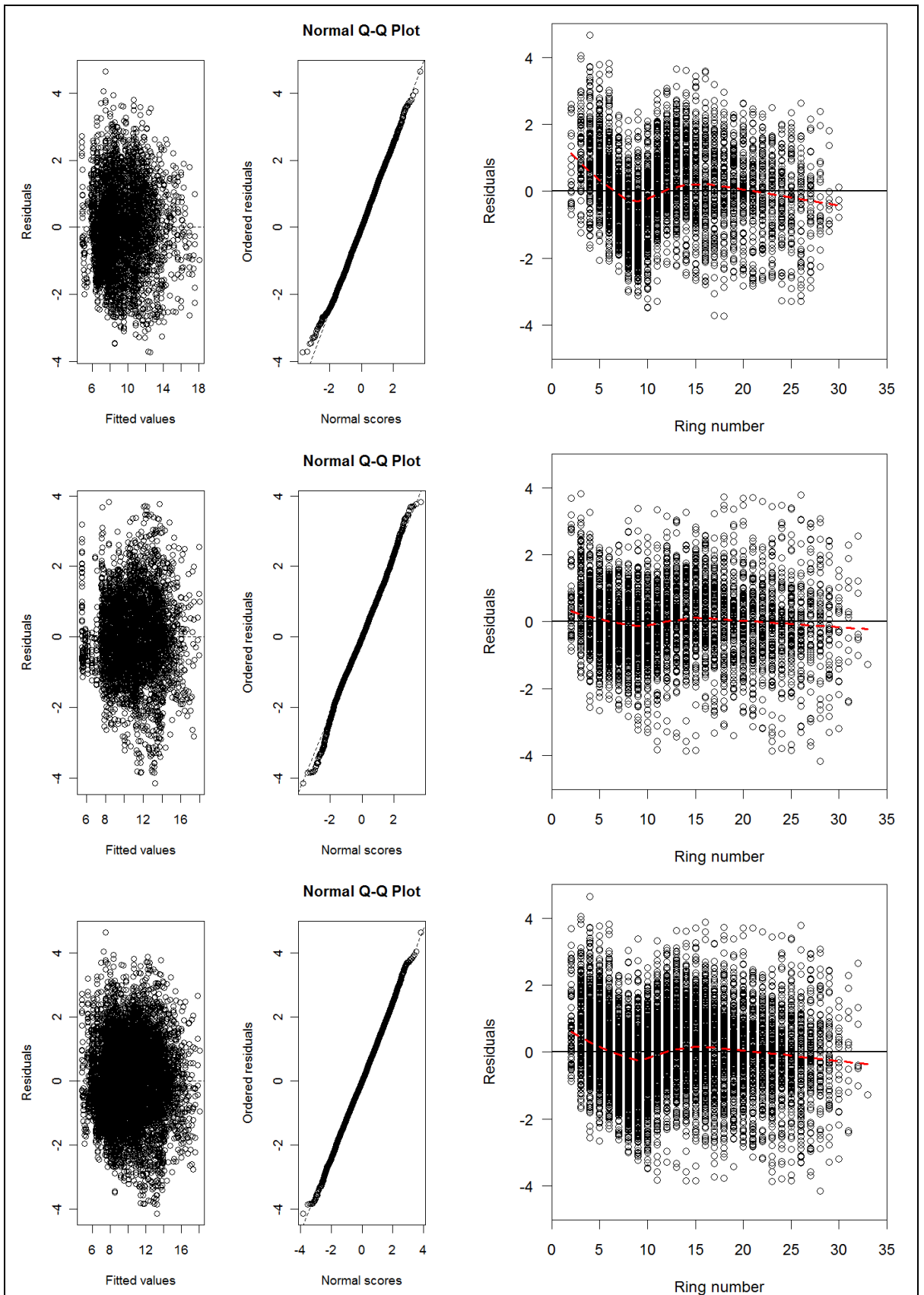


Figure 7-38. Diagnostic plots for the radial stiffness model fitted to Coalburn (top), Loch Awe (middle) and all data combined (bottom).

7.3.6.1 Predicting a, b and d parameters

The a, b and d parameters were derived in turn holding one or both of the remaining parameters fixed at the site average values. It was impossible to derive values for a parameter when both b and d were fixed at their average values since the model would not converge. For b and d it was possible to derive a set of values when both remaining values were held constant. Tree variables were then used to explain variation in these parameter values. The variables in the initial models were selected based on scatter plots and correlation analysis. The linear regression models were fitted since there was no longer a nested error structure in the data since the a, b and d parameters had been defined at tree level and the sites were modelled separately. Also, the relationship between a+d and tree variables was investigated in the regression analysis. The sum a+d describes the maximum range. The models were simplified until only significant parameters remained in the model. As an exception, a borderline variable (p-value 0.0511) was left in one of the models describing the d parameter (Table 7-10) for Loch Awe since it was the last variable in the model. In general the values of R^2 were low 0.13 – 0.35. In the case of the a+d and a parameters for Loch Awe, higher values in the range of 0.46 – 0.58 were obtained (Table 7-9, Table 7-10, Table 7-11, Table 7-12 and Table 7-13). However, more worryingly, the explanatory variables differed between the two sites. The sub-models are not very useful for predicting the parameters at an unknown since the effect of tree variables were not consistent and remained fairly weak. Therefore, the submodel development was deemed inconclusive and the plots for model predictions and residuals are not shown.

Table 7-9. Models for the a parameter for Coalburn and Loch Awe. The values of a were derived keeping b fixed at its average value for each site.

COALBURN				
	Estimate	Std. Error	t value	Pr(> t)
(Intercept)	-17.101	14.472	-1.18	0.2485
Slenderness	0.616	0.189	3.26	0.0032 **

Signif. codes: 0 '***' 0.001 '**' 0.01 '*' 0.05 '.' 0.1 ' ' 1				
Residual standard error: 10.12 on 25 degrees of freedom				
Multiple R-squared: 0.298, Adjusted R-squared: 0.270				
F-statistic: 10.62 on 1 and 25 DF, p-value: 0.0032				
LOCH AWE				
	Estimate	Std. Error	t value	Pr(> t)
(Intercept)	84.567	11.615	7.28	4.84*10 ⁻⁰⁷ ***
Age	-1.720	0.428	-4.02	0.00067 ***
CrownLength	-1.365	0.637	-2.14	0.04463 *

Signif. codes: 0 '***' 0.001 '**' 0.01 '*' 0.05 '.' 0.1 ' ' 1				
Residual standard error: 5.83 on 20 degrees of freedom (1 observation deleted due to missingness)				
Multiple R-squared: 0.588, Adjusted R-squared: 0.547				
F-statistic: 14.29 on 2 and 20 DF, p-value: 0.00014				

Table 7-10. Models for the d parameter for Coalburn and Loch Awe. The values of d were derived keeping b fixed at its average value for each site.

COALBURN				
	Estimate	Std. Error	t value	Pr(> t)
(Intercept)	6.969	0.300	23.23	<2*10 ⁻¹⁶ ***
AveAngle	0.236	0.091	2.60	0.0154 *

Signif. codes: 0 '***' 0.001 '**' 0.01 '*' 0.05 '.' 0.1 ' ' 1				
Residual standard error: 1.22 on 25 degrees of freedom				
Multiple R-squared: 0.213, Adjusted R-squared: 0.182				
F-statistic: 6.769 on 1 and 25 DF, p-value: 0.0154				
LOCH AWE				
	Estimate	Std. Error	t value	Pr(> t)
(Intercept)	12.140	1.465	8.29	4.64*10 ⁻⁰⁸ ***
JWRadius	-0.050	0.024	-2.07	0.0511 .

Signif. codes: 0 '***' 0.001 '**' 0.01 '*' 0.05 '.' 0.1 ' ' 1				
Residual standard error: 1.607 on 21 degrees of freedom (1 observation deleted due to missingness)				
Multiple R-squared: 0.169, Adjusted R-squared: 0.130				
F-statistic: 4.278 on 1 and 21 DF, p-value: 0.0511				

Table 7-11. Models for the d parameter for Coalburn and Loch Awe. The values of d were derived keeping a and b fixed at its average value for each site.

COALBURN				
	Estimate	Std. Error	t value	Pr(> t)
(Intercept)	10.182	1.088	9.36	1.20*10 ⁻⁰⁹ ***
Tot.radius	-0.023	0.009	-2.64	0.0141 *

Signif. codes: 0 '***' 0.001 '**' 0.01 '*' 0.05 '.' 0.1 ' ' 1				
Residual standard error: 1.293 on 25 degrees of freedom				
Multiple R-squared: 0.218, Adjusted R-squared: 0.187				
F-statistic: 6.969 on 1 and 25 DF, p-value: 0.01408				
LOCH AWE				
	Estimate	Std. Error	t value	Pr(> t)
(Intercept)	3.745	1.492	2.51	0.01991 *
Slenderness	0.055	0.016	3.43	0.00238 **

Signif. codes: 0 '***' 0.001 '**' 0.01 '*' 0.05 '.' 0.1 ' ' 1				
Residual standard error: 1.182 on 22 degrees of freedom				
Multiple R-squared: 0.349, Adjusted R-squared: 0.319				
F-statistic: 11.78 on 1 and 22 DF, p-value: 0.00238				

Table 7-12. A model for predicting the sum of a and d parameters (a+d). The a and d parameters were derived holding b fixed at its average value at each site.

COALBURN				
	Estimate	Std. Error	t value	Pr(> t)
(Intercept)	70.692	7.210	9.81	4.76*10 ⁻¹⁰ ***
Tot.radius	-0.277	0.058	-4.79	6.47*10 ⁻⁰⁵ ***

Signif. codes: 0 '***' 0.001 '**' 0.01 '*' 0.05 '.' 0.1 ' ' 1				
Residual standard error: 8.567 on 25 degrees of freedom				
Multiple R-squared: 0.478, Adjusted R-squared: 0.457				
F-statistic: 22.92 on 1 and 25 DF, p-value: 6.47*10 ⁻⁰⁵				
LOCH AWE				
	Estimate	Std. Error	t value	Pr(> t)
(Intercept)	88.760	10.170	8.73	2.96*10 ⁻⁰⁸ ***
Age	-1.511	0.374	-4.04	0.00065 ***
CrownLength	-1.420	0.558	-2.55	0.01923 *

Signif. codes: 0 '***' 0.001 '**' 0.01 '*' 0.05 '.' 0.1 ' ' 1				
Residual standard error: 5.105 on 20 degrees of freedom (1 observation deleted due to missingness)				
Multiple R-squared: 0.614, Adjusted R-squared: 0.576				
F-statistic: 15.94 on 2 and 20 DF, p-value: 7.26*10 ⁻⁰⁵				

Table 7-13. A model for the b parameter for the Coalburn and Loch Awe site. The values of b were derived holding a and d fixed to their average values at each site.

COALBURN				
	Estimate	Std. Error	t value	Pr(> t)
(Intercept)	2.540	9.664	0.26	0.7948
Tot.radius	0.276	0.078	3.56	0.0015 **

Signif. codes: 0 '***' 0.001 '**' 0.01 '*' 0.05 '.' 0.1 ' ' 1				
Residual standard error: 11.48 on 25 degrees of freedom				
Multiple R-squared: 0.336, Adjusted R-squared: 0.310				
F-statistic: 12.66 on 1 and 25 DF, p-value: 0.00153				
LOCH AWE				
	Estimate	Std. Error	t value	Pr(> t)
(Intercept)	48.447	7.244	6.69	1.01*10 ⁻⁰⁶ ***
Slenderness	-0.282	0.077	-3.65	0.00142 **

Signif. codes: 0 '***' 0.001 '**' 0.01 '*' 0.05 '.' 0.1 ' ' 1				
Residual standard error: 5.741 on 22 degrees of freedom				
Multiple R-squared: 0.377, Adjusted R-squared: 0.349				
F-statistic: 13.3 on 1 and 22 DF, p-value: 0.00142				

7.3.7 Comparison to ST300 measurements

ST300 standing tree acoustic measurements were compared to the results of ultrasonic scanning of radial sections (Figure 7-39). The comparisons were done using the results of acoustic scanning of the North section as the ST300 measurements were taken from the North side of the tree. At both sites the highest concordance correlation coefficients were obtained between ST300 measurement and the acoustic MoE calculated for the outer most 2 cm of the acoustic path. In practice this means approximately 2.5 cm into the stem as the acoustic analysis path did not extend to the very edge of the sample to protect the sensor from distortion. The R^2 -values for the regression remained very poor (0.17-0.31).

There was a clear scale shift detectable when the ST300 standing tree measurements were compared to the MoE averaged over the whole North radius. Therefore, ST300 provides most accurate information on the stiffness of the outer part of the stem. The correlation with juvenile MoE was tested as well but it was not significant when only the North radius was used (Figure 7-40). This might in part have been due to the limited number of observations.

However, there was a significant correlation between juvenile wood MoE and outerwood MoE (outerwood defined as the outermost 2 cm on the acoustic scanning path). The Pearson's correlations coefficients were 0.606 and 0.664 ($p < 0.001$), for Coalburn and Loch

Awe, respectively. The regressions fitted explained 36% of the variation in case of the Coalburn site and 43% in the case of Loch Awe site. According to this findings tree screening by measuring MoE in juvenile wood could be used as an indicator of entire stem stiffness.

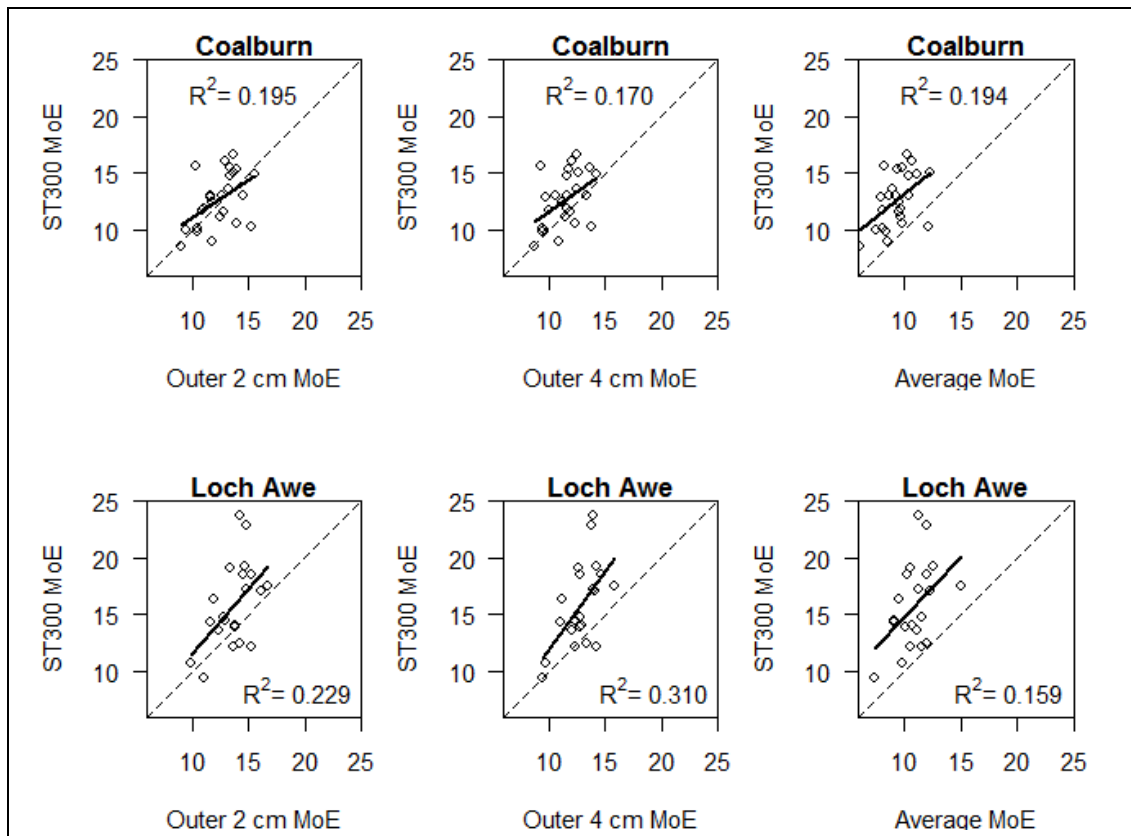


Figure 7-39. Relationship between the dynamic MoE (GPa) measured with the ultrasonic scanner and the ST300 standing tree tool at the two sites. Dashed line is the one to one line and solid black line a regression line fitted to the data.

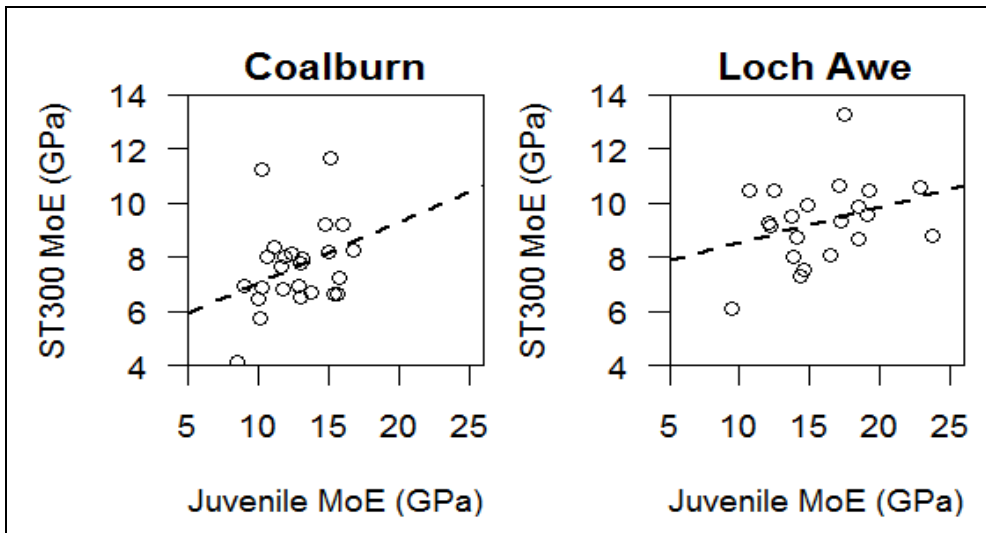


Figure 7-40. Relationship between ST300 standing tree MoE and juvenile wood MoE measured by the ultrasonic scanning method. On the top row juvenile MoE calculated from North sections only was plotted against the ST300 measurements. Dashed line is the linear regression line fitted to the data. R^2 values are not presented since the slope was insignificant.

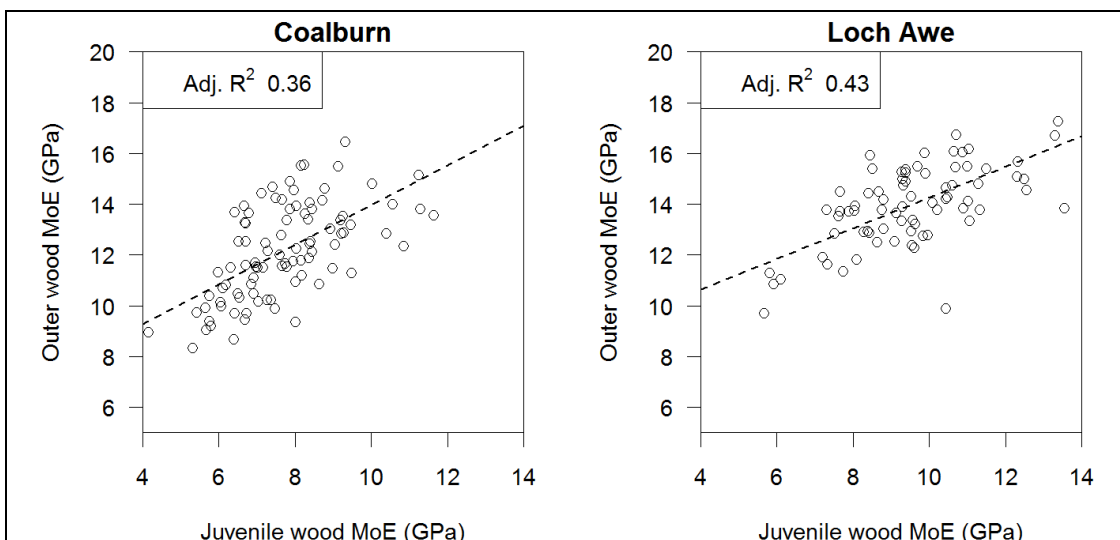


Figure 7-41. Relationship between the juvenile wood stiffness and outerwood stiffness. Outerwood stiffness was calculated for the outermost 2 cm of the stem. A dashed line is the regression line fitted to the data.

It was also tested if the relationship between the acoustic velocities measured with two different methods were clearer than that with MoE values calculated from these data since the density value used for ST300 MoE was estimated as 1000 kg/m^3 , as has been customary (Lasserre et al., 2004; Mason, 2006; Moore et al., 2009c). This estimated value was used for all trees and could therefore potentially mask any variations that might exist. The comparison between velocity values was complicated by the differences in moisture content as ST300 velocity was determined in green conditions and ultrasonic measurement at 12% moisture content. Furthermore, the frequency used influences the measurements

with higher frequency yielding higher MoE (Bucur and Feeney, 1992; Ouis, 2002). Therefore, differences in absolute values were expected. However, also, the relationship between the two measurements was weak and the R^2 -values remained low, particularly in the case of Coalburn (Figure 7-42). The R^2 -values for the outer most sections were higher than when MoE values were compared.

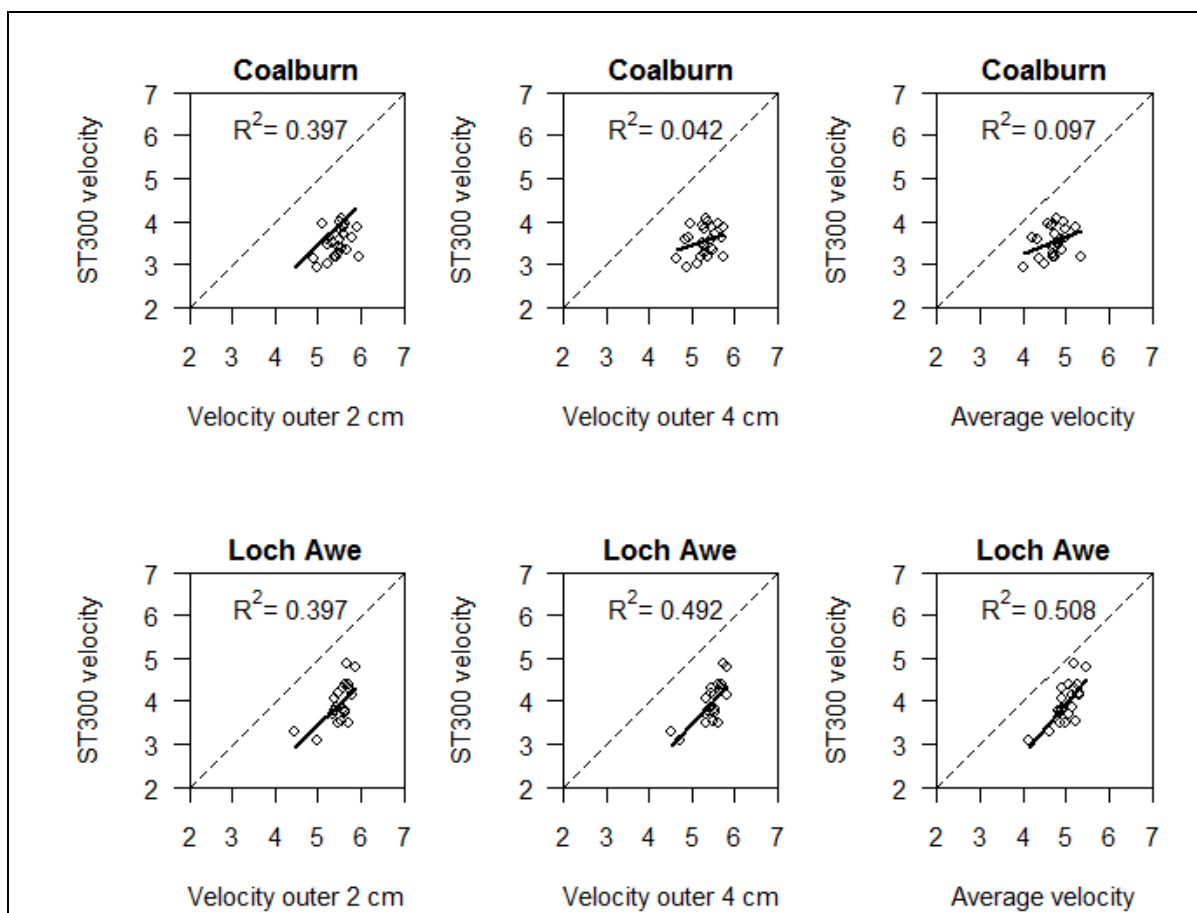


Figure 7-42. Relationship between the acoustic velocity (km/s) measured with the ultrasonic scanner and the ST300 standing tree tool at the two sites. Dashed line is the one to one line and solid black line a regression line fitted to the data.

7.4 Discussion

In addition to density, microfibril angle (MFA) is an important timber quality attribute. They both influence timber stiffness which can be determined as Modulus of Elasticity (MoE). Timber stiffness is a measure of its ability to withstand deformation under load and is therefore an important timber quality indicator for construction use. Both density and microfibril angle have characteristic radial patterns. In juvenile wood, the density and microfibril angle are high. Acoustic velocity can be used as an estimate of the microfibril angle and the stiffness values calculated based on density and acoustic velocity to derive stiffness profiles.

Detailed radial stiffness data did not previously exist for a large number of sample trees. In this study, stiffness profiles were created for Sitka spruce. These results were used to calculate average MoE values in different parts of the radius and relate these values to tree variables in order to understand what influences stiffness in Sitka spruce. In addition to this, radial stiffness model developed on small clear data (McLean, 2007) was fitted to the data to see if it could be used to predict stiffness derived from the higher resolution measurements carried out here.

In a review of timber quality in Sitka spruce, Macdonald and Hubert (2002) reported that microfibril angle had been found to decrease rapidly from the pith outwards, reaching a stable mature value at six to nine rings from the pith. Here, the mean acoustic velocity curve started to level off much later at approximately ring 15. In Sitka spruce samples from the Kershope clonal trial the change in the slope of MFA curve took place at ring 12-13 (McLean, 2007). Perhaps the shapes of the curves may vary between-sites as was found for density in the Benchmarking experiment (Chapter 5).

In this study there was a slight discrepancy observable between the acoustic velocity and density measurements. Due to limitations in sample geometry and possible defects such as remains of small branches that needed to be avoided during both analyses, it was necessary to place the acoustic analysis path in a different location on the radial section than where the ring density analysis had been carried out. This caused some difficulty in aligning the density and velocity data as there were small differences in the path lengths. However, the acoustic measurement was an average over a 9 mm diameter circle and similar averages were derived from the density data in an attempt to smooth the curves. Observed differences in path lengths also had implications for the analysis where ring numbers were used, such as the radial MoE modelling. The ring numbers in the acoustic data were derived from the density dataset. The datasets were combined using distance from the pith as this measurement was common to both analyses. The discrepancies in the path lengths caused the final ring number occasionally to differ from the ring number noted as the final ring in the density analysis. In most cases the difference was one year, occasionally 2 and very rarely, in the case of very narrow outer rings, more than that (maximum 4). As the aim was to describe the radial variation in stiffness, the accuracy of the measurements themselves, as well as the alignment obtained, was concluded sufficient. The tree average values were not influenced by this bias.

One limitation of ring number based data presentation and stiffness modelling was that it only considers the effect of age and ignores the differences in growth rate. Whereas the

distance from the pith would conceal some age dependent trends because the effects are confounded as measurements from different rings are mixed when plotting data from trees that differ in growth rate on a distance axis. However, comparing the stiffness data plotted against distance from the pith and ring number (Figure 7-20) indicated that age had more influence on stiffness than cambial activity. This was concluded as there was less spread about the curves when the data were plotted against ring number.

As noted before, the between-tree variation was large. This is in line with findings that 55 percent of variation in MoE was between-trees within a site (Moore et al., 2009b). Here, the between-tree variation in the average MoE was 44 % of the total variation. The between-tree variation was not well explained by the tree mensuration data and therefore large random tree effects occurred in the models, which compromises the predictive power of the model if applied to new stands. Furthermore, the significant tree variables differed between the sites, which indicated that the relationships were not consistent. However this may also be an artefact caused by the variable selection process since sometimes the differences in the strength of the relationship between similar explanatory variables and the MoE were not great. It would be of interest to look at this on clonal material to eliminate the effect of genetic variation, which can be quite substantial and may have caused much of the random tree effects in this study. It has been found that density is under strong genetic control (Saranpää, 1994). In Radiata pine, the whole-tree clonal heritability of stiffness is high, 0.77 (Lasserre et al., 2004). Lindström et al. (2004) found that the clonal heritabilities of MoE, density and microfibril angle were all high, 80-90%, 78-90 % and 80-90 %, respectively. However, Raiskila et al. (2006) reported that there was fairly large between-tree variation within clones of Norway spruce.

Developing sub-models to predict the radial stiffness model parameters was not successful. Collecting data from more sites might enable determining whether there are some relationships in between-tree variables and a, b and d parameters that exist over a larger number of sites. With just two sites that differ from each other it is impossible to conclude anything on the relationship between the parameters and standard tree variables.

The radial stiffness curves calculated in this study from acoustic velocity and density data tended to have some resemblance to the characteristic Sitka spruce density curve as they had an initial flat section or even a small dip. This was not observed for static MoE data derived using small clears (McLean, 2007). McLean (2007) found in Sitka spruce that MoE increased linearly in juvenile wood and then levelled off. The same shape was also obtained for static MoE in Scots pine (Auty and Achim, 2008). The data collected in this

study were of much finer resolution than was achievable with small clears. In a previous study on Sitka spruce microclears (5 mm * 1 mm * 1 mm) it was found that stiffness increased from the pith outwards (Gabert, 2005). Gabert (2005) investigated two radii and the static MoE appeared to increase almost linearly towards the bark with the variation between samples being higher as well towards the bark. However, one of the radii was only 59 mm long which raises a suspicion that only juvenile wood was investigated. In the longer radii (106.4 mm) the rate of increase in static MoE was greater near the bark. Unfortunately the ages of the trees were not reported.

In the juvenile part of the radius, high density was accompanied with lower speed whereas this trend was reversed in mature wood. This could partially be explained by compression wood that commonly occurs in the juvenile wood of fast grown trees (Saranpää, 1994). Brazier had concluded that the presence of juvenile wood was a more important indicator of strength than density (Macdonald and Hubert, 2002). In Radiata pine it was found that juvenile wood density had no influence on dynamic green MoE measured with a resonance tool (HM-200) on the logs (Lasserre et al., 2009). McLean (2007) concluded that microfibril angle was more important than density in determining the MoE in juvenile wood.

Using path analysis to separate the effects of density and microfibril angle on specific modulus, it has been found that only microfibril angle had a high path coefficient and was significant at the 99% level in Radiata pine (Booker et al., 1997). Booker et al. (1997) considered that the results support a view that velocity is independent of the cell wall thickness, which governs the density, and is influenced by microfibril angle. In this light the observed local humps in the acoustic velocity curves that arose when the probe landed on latewood could actually be caused by the differences in microfibril angle between earlywood and latewood and not by density. Microfibril angle has been found to decrease steadily within the ring (Panshin and de Zeeuw, 1980), therefore, latewood could cause the elevated speed due to a lower microfibril angle than the surrounding earlywood. Evans and Ilic (2001) who studied the relationship between MoE, density and microfibril angle, concluded that microfibril angle had greater influence on MoE. In contrast, Steffenrem et al. (2007) found in more mature Norway spruce that density was strongly correlated with MoE whereas microfibril angle was less important. They proposed that the differences in the findings may be explained by the age of trees studied. Age may have an effect since stiffness increases with ring number until a constant value is reached. Chauhan and Walker (2006) illustrated how an apparent correlation between velocity and density arose in standing tree acoustic testing due to analysis of data from trees of different age. The

relationship disappeared when age groups were looked at individually and therefore they concluded that the effect was caused by the pattern of increasing density and decreasing microfibril angle with increasing ring number. In the present study the entire radius was assessed and hence the age was taken into consideration in ring number. However, it should also be remembered that the findings here are based on only on two sites and those of McLean (2007) on one site.

The Euler buckling formula suggests increases in stem slenderness need to be compensated by increasing stiffness to reduce the risk of buckling (Watt et al., 2006). A strong relationship have been found between slenderness and MoE in Radiata pine (Watt et al., 2006). Here, the correlations between slenderness and average MoE and MoE for the outer 4 cm of the stem were tested; the MoE for the outer 2 cm was ignored here as it represents such a small fraction of the stem. At the Coalburn site there was no relationship between slenderness and MoE. At Loch Awe slenderness was correlated with average MoE (0.361, p-value = 0.0012) and outerwood MoE (0.259, p-value = 0.0220). At Loch Awe the range of slenderness values was also wider (67-126) than at Coalburn (60-95).

Stiffness is also thought to be influenced by spiral grain (Booker et al., 1997). In this study no effect was detected at the Coalburn site. At Loch Awe there was a negative correlation between MoE variables (average and outerwood) and average grain angle expressed in absolute degrees. However, when this relationship was studied in a scatter plot it was revealed that it was caused by a possible outlier and if this tree was excluded the correlation became insignificant as well. Therefore, the trees investigated here do not support the relationship between grain angle and stiffness. However, the grain angle was only measured below bark and therefore does not provide information on possible relationship between these variables in, for example, the juvenile stage of development. In previous studies it had been found that grain angle only had a very slight effect on timber stiffness of Sitka spruce. However, this may have arisen due to low variability in grain angle within the study material (Macdonald and Hubert, 2002).

An exact match between the dynamic MoE calculated from density and ultrasonic scanning results and that measured with ST300 (estimating density as 1000 kg/m^3) was not expected since frequency influences the MoE values obtained. Higher frequency yields higher estimates of MoE (Bucur and Feeney, 1992; Ouis, 2002). However, good agreement should exist between ultrasonic MoE calculated for the outer part of the stem and the ST300 MoE and particularly between the velocities. This was not found here and the R^2 -values remained low for both methods of comparison.

8 Discussion

The signatory nations of the Kyoto protocol have a responsibility to decrease their carbon dioxide emissions. Forests can store significant amounts of carbon and timber constitutes a carbon neutral raw material if harvested areas are replanted or left to regenerate naturally. Therefore, increasing forest areas and the use of timber as a raw material for construction, where carbon will remain stored over long periods, are important means to decrease our carbon footprint.

Currently 692 000 ha of Sitka spruce are grown in the UK, of which 528 000 is in Scotland (Forestry Commission, 2009). In 2008 the total softwood production amounted to 8.4 million tonnes (green weight) (Forestry Commission, 2009) and 63 % was spruce wood (Halsall et al., 2005). Softwood production is forecast to increase by 20% over the next few decades, peaking in the period 2017-2021 (Halsall et al., 2005). The main uses of softwood timber are 1) construction, 2) pallets and packaging and 3) fencing and other outdoor uses. In 2008, the UK imported twice as much softwood timber (5.49 million m³) on a volume basis than is grown domestically (2.57 million m³) (Moore, 2010b). The share of imported material was particularly high for construction use, as only 17% of the construction timber was from home-grown sources (Moore, 2010b). The economic value of all the imported wood products (including softwood and hardwood) was 2.1 billion pounds, of which sawn wood constituted half (Forestry Commission, 2009). Therefore, increasing the share of home-grown timber used for construction purposes has the potential for significant economic gains as well as carbon footprint benefits.

When the large scale afforestation started in the 1920s, Sitka spruce was preferred because of its fast growth in poor soils and climates to provide a strategic reserve of timber. However, in fast growing plantations of Sitka spruce, lower density timber is produced in comparison to slower grown Sitka or other spruce species. If this is accompanied with short rotation lengths as is commonly the case in plantation forestry, the cross section consists mainly of juvenile wood that has poorer properties for use in construction wood than mature wood. This may lead to timber quality concerns and restrictions on possible end uses. Currently, UK grown Sitka spruce typically meets the criteria for C16 grade EN338 (CEN, 2003), which is the minimum requirement for lightly stressed construction uses. However, it could fail to make the C16 grade if timber of lower density (and consequently lower MoE) was grown. This would adversely affect the current aim to increase the share of home-grown construction timber on the UK market, which would

require a higher volume production of at least C16 and potentially C24 grade timber EN338 (CEN, 2003). To achieve this, Sitka spruce trees with better timber properties (plus trees) have been selected for tree breeding in order to develop populations where fast growth is not accompanied by an unacceptable reduction in density (Lee, 1999a; Lee, 1999b).

In the past, density was widely used as a timber quality indicator because it was much easier to determine than other factors involved in the timber stiffness. However, advances in acoustic technology have provided a means for easy and non destructive testing of stiffness in different stages of the timber production chain, ranging from standing tree to batten measurements (Mochan et al., 2009). Therefore, the focus has to some extent shifted away from density as the primary quality indicator as wood density merely quantifies the amount of cell wall present but alone yields no information on the properties (Macdonald and Hubert, 2002). Timber stiffness has been found to be more closely related to the microfibril angle (McLean, 2007) or acoustic velocity (Moore et al., 2009a) than density. However, it still needs to be noted that there are minimum density requirements in the EN338 standard, in addition to the stiffness requirements.

In addition to genetics, environment and silvicultural practices also influence wood density. Therefore, to achieve the goal of improving the growing stock under future conditions that will be modified by climate change, detailed information on the growth response of Sitka spruce and its resulting timber properties are needed. This study aimed to fill some of these gaps in our understanding. The effects of selected site factors and long term average climate were studied in the Benchmarking experiment. The influence of annual variation in climate was investigated in the Level II experiment. Finally, the Dendrometer experiment looked at the short term (intra-annual) variation in tree growth and its relationship to weather.

8.1 Density in UK grown Sitka spruce

Timber density can be analysed at different levels and models developed for different applications. In the Benchmarking study, cross-section area-weighted average density data were modelled, based on site and tree variables. The aim was to produce information on between-site differences caused by site conditions (fertility, climate etc.), altitude or

silvicultural treatments. The tree variables would then allow the prediction of density in more detail within a site.

When the cross section average densities (area-weighted) were investigated, the major part of the variation in wood density was between trees. In previous studies on UK grown Sitka spruce it was reported that there were no significant differences between 6 broad geographic regions in strength and specific gravity, whereas large variations were observed between trees within a site (Sunley and Lavers, 1961). Similarly, in a Sitka spruce respacing trial, a large part of the variation (63%) was between trees within spacings (Savill and Sandels, 1983). In a Sitka spruce progeny trial only approximately 5% of the variation was between the treatments whereas 40% was between trees within the treatment and 50% between samples within a tree (Moore et al., 2009d). The genetics of the trees from the present study are unknown and the seeds were largely from open pollinated sources. Hence, each tree is a unique individual and variation in genotype can be expected to be fairly wide because much of the between tree variation is thought to be genetic (Zobel and van Buijtenen, 1989). Furthermore, in a recent investigation on the influence of genetics in determining density in jack pine, Savva et al. (2010) found that there were no differences in density between seed origins in the 21 populations investigated if the same ring widths and ages were compared. This led the authors to conclude that genetics influenced density indirectly via growth rate. Gerendiain (2009) found considerable differences even within clones of Norway spruce in Finland with maximum standard deviations measured for wood density of 110-120 kg/m³.

In addition to genetics, other factors that were not known for sites in the Benchmarking dataset, and may have contributed to unexplained variation, including soil type and potential fertilizer applications. These factors are more likely to contribute to between site variation. Microsite effects that may contribute to the between tree differences include differences in moisture relations such as if water collects at some parts of the plot on an unevenly surfaced site. Row thinning, commonly used on the thinned Benchmarking sites, opens up the canopy allowing some trees to receive more light and to retain deeper canopies, at least on the side of the thinning track. The importance of these factors in relation to the effect of genotype is not clear and interactions are likely between the factors. These factors are all likely to influence the growth of the trees and should therefore be at least to some extent accounted for in the growth terms of any density models.

Many studies have found negative correlations between density and growth rate in Sitka spruce (Brazier, 1967; Brazier, 1970b; Deans and Milne, 1999; Petty et al., 1990; Savill

and Sandels, 1983; Simpson and Denne, 1997; Sunley and Lavers, 1961) and Norway spruce (Jyske et al., 2008; Mäkinen et al., 2007; Saranpää, 1994) indicating that to a degree density is reduced in fast grown spruce trees. However, findings have been reported for Sitka spruce in a respacing trial at Baronscourt in Northern Ireland where DBH in the highest spacing treatment was 75% higher than the control but no difference in basic or bulk densities existed between the treatments (Moore et al., 2009a). Cameron et al. (2005) reported that the properties of juvenile wood were unaffected by growth rate whereas in mature wood, density and other timber properties were influenced by ring width.

In Sitka spruce, increase in growth rate occurs in the earlywood part of the ring and hence leads to a reduction in ring density as the proportion of denser latewood in the ring is decreased (Brazier, 1970b). In addition to that, vigorous growth was found to decrease both the earlywood and minimum ring density (Brazier, 1970b). These effects were observed in the investigation of detrended tree ring series and average tree ring variables in the Level II site data (Table 6-20 and Table 6-22). Latewood width showed no trends with ring number whereas earlywood width closely followed the pattern of total ring width with a decrease in width towards the bark. In fact, both at the Loch Tummel and Coalburn sites, earlywood width was strongly correlated with ring width ($r=0.810$ and 0.919 , respectively) whereas no significant relationship existed between latewood width and ring width. Ring density was more strongly correlated with earlywood ($r=0.852 - 0.887$) and minimum ($r=0.622 - 0.765$) densities than latewood ($r= 0.533 - 0.591$) and maximum ($r= 0.480 - 0.509$) densities.

In addition to a decrease in latewood proportion, increase in ring width was accompanied by a reduction in earlywood density as observed by Brazier (1970b). Minimum density at the Loch Tummel site was not significantly correlated with ring width ($r= -0.161$) whereas at the Coalburn site, this relationship was significant ($r= -0.617$). The earlywood/latewood boundary definition of 50% of the slope between minimum and maximum density (default WinDENDRO setting) could potentially cause an artefact in these relationships. For example, if maximum density that occurs at the end of the ring was elevated this would not only inflate latewood and maximum density values but would also shift the earlywood/latewood boundary, hence increasing the earlywood density and width. Maximum density was the variable most sensitive to growing season conditions and therefore this effect might occur frequently. However, using minimum density instead of earlywood density should avoid these issues. Furthermore, the correlations involving earlywood and latewood densities were strong which indicates that they are likely to be genuine. The fact that Brazier (1970b) detected the earlywood and minimum density reduction effects while

using a constant threshold value for earlywood/latewood boundary further indicates that also the earlywood density effect is real.

An interesting point to note is that latewood width was also negatively correlated with latewood density (Loch Tummel $r = -0.635$ and Coalburn -0.707) and maximum density (Loch Tummel $r = -0.598$ and Coalburn -0.670). Therefore, some of the potential density increase that could be achieved, if earlier transition to latewood took place but growing period stayed the same, would be compromised by reduction in latewood density. In the light of these results it is concluded that increased growth rate decreases density both by increasing the earlywood proportion and by reducing density in earlywood and latewood. The latter effect was particularly important at the Coalburn site.

Denne (1979) reported that young, severely suppressed Sitka spruce trees ceased to grow earlier in the season than more dominant ones and this limited the production of latewood in the suppressed trees. The author wrote that in these trees increase in crown activity would actually increase ring density further down the stem by allowing latewood production. In the Griffin dendrometer experiment the tree producing the narrowest ring (tree 66) ceased to grow earlier than the other dendrometer measured trees. However, this tree produced the densest timber. The difference in density was more marked in the earlywood with tree 66 being 28% denser than the average of all trees whereas in the latewood it was only 10% above the average. Tree 66 also had a much higher latewood proportion (42%) in comparison to the other trees that ranged from 12% to 25% in the 2008 growth ring. This was not consistent with what was observed by Denne (1979). The trees investigated at Griffin were all selected from the dominant DBH quartile and are therefore not directly comparable to the trees investigated by Denne (1979).

Both density and stiffness were found to be mainly influenced by growth rate. Juvenile wood density in the Benchmarking experiment was largely unaffected by the environmental variables investigated and was explained by the width of the juvenile core (R^2 -value 0.454 for the fixed effects). Temperature sum was a significant explanatory variable in the mature wood density and outerwood density models developed from the Benchmarking data. However, temperature sum, elevation and moisture deficit were heavily intercorrelated, to the extent that they could not be included in the same model due to collinearity problems. However, this indicated that elevation or moisture deficit may also have some direct influence on density (negative and positive, respectively). In fact, a negative effect of elevation on density was observed in the factorial analysis. Negative effects of high altitude and latitude have been reported previously. An altitude effect on

density was found in Radiata pine (Cown and Ball, 2001), whereas latitudinal effects were reported for Radiata pine (Cown and Ball, 2001) and sub alpine fir (Splechtna et al., 2000). In UK grown Sitka spruce, reduction in density was reported with latitude (approximately 10 kg/m^3 for every degree) when age related differences were excluded by comparing 30 year-old samples (Bryan and Pearson, 1955). In a reinvestigation of a dataset on conifer pulpwood material (Jeffers and Dowden, 1964), wood density was found to decrease by 6 kg/m^3 for every degree of increase in latitude in Britain (Moore, 2010a). The analysis by Bryan and Pearson (1955) included samples from six sites extending from southern England to Invernesshire in Scotland which was a wider range than covered in the Benchmarking experiment where the most southern sites were located in northern England. When the site location data (approximate grid reference and altitude) from Bryan and Pearson (1955) were used in Ecological Site Classification (Pyatt et al., 2001) to derive site accumulated temperature sum and moisture deficit data, it was found that the density was closely related to these variables as well (R^2 -values 0.733 and 0.584, respectively). Both variables were positively correlated with density and decreased with latitude. Even if the latitude yielded higher R^2 -values (0.951) when used as an explanatory variable than either moisture deficit or temperature sum, this illustrates how the complex interactions should not be disregarded when variables such as latitude and altitude that integrate several influences are considered. Latitude as such cannot influence tree growth but change in latitude is related to temperature, solar radiation and moisture conditions. Under climate change the significance of altitude and latitude may be altered when temperature and rainfall patterns that are likely to be the causes of current altitudinal and latitudinal differences change.

There have been previous attempts to explain why wood density is reduced at high latitudes and altitudes. Theoretical calculations by Roderick and Berry (2001) showed that to achieve a given growth rate in colder conditions (high altitude and latitude) the area occupied by the cell wall in a tree ring would need to be reduced to accommodate the flow of more viscous water. In Sitka spruce, reduction in fibre wall thickness has been reported with latitude and altitude (Lundqvist et al., 2005). Pipe theory that has been the basis of many structural carbon allocation patterns in mechanistic models assumed a constant ratio between sapwood cross-sectional area and total leaf area (Shinozaki et al., 1964). In more recent work the theory was refined to consider changes in leaf area sapwood area ratio that might be altered by changes in structural properties due to tree aging, climate or stand density (Deckmyn et al., 2006). This model was able to explain higher density in more suppressed conifers as less conductive cross-section (pipe) area was required to support a smaller crown. This model, like the one by Roderick and Berry (2001), was based on the

Poiseuille-Hagen formula of flow in capillary tube which requires increase in pipe radius to achieve a given flow if the viscosity of water was increased due to low temperature.

In addition to, modifying timber density, elevation has also been found to influence growth rate. Elevation was also found to lead to a decrease General Yield Class (GYC) (Allison et al., 1994; Blyth and Macleod, 1981a; Mayhead, 1973) although on better quality sites the reduction was less than on poorer sites (Macmillan, 1991). The reduction in GYC was calculated to be at the rate of 3.2-4.0 m³ ha⁻¹ yr⁻¹ per 100 m increase in elevation and the productivity was closely related to temperature and windiness (Worrell and Malcolm, 1990a). In the western part of the country, higher GYC is found since the climate is warmer and wetter (Allison et al., 1994). GYC was predicted to increase with increasing temperature in the future by 2.4 – 2.8 m³ ha⁻¹ yr⁻¹ for each degree (°C) depending on how the temperature increase would be distributed over the year (Proe et al., 1996). Based on the distribution of Sitka spruce of yield classes across Scotland Allison et al. (1994) concluded that GYC was more sensitive to temperature than rainfall. Increased summer rainfall could increase the growth if it was not linked to reduction in temperature (Allison et al., 1994). In dry areas of northeast Scotland, the growth could be predicted with a moisture availability model (Jarvis et al., 1983). In a process model analysis of the Sitka spruce growth limitations it was reported that variation in solar radiation due to topography had large influence on the differences in growth between plantations (Waring, 2000). In line with this the earlywood production in Sitka spruce was found to be positively correlated with daily solar radiation over a 15 day period of daily sampling of xylem cell development, correlations with temperature and rainfall were non-significant (Ford et al., 1978).

Therefore, compared to low level sites, elevated areas are characterised by lower productivity (Worrell and Malcolm, 1990a) and lower density. In the Benchmarking study no systematic reduction in growth rate was observed with elevation since the sites had deliberately been selected to include both low and high yield class sites at different elevation factor levels. However, negative correlation between ring width and ring density was observed at least in some part of the radius at all Benchmarking sites, which indicated that even if some high elevation sites were of lower productivity and lower density in comparison to low elevation sites, the response to increase in growth rate at an annual level was still the same with more vigorous growth leading to lower density timber. More research is needed to assess if the theories linking the increased viscosity of water at colder temperatures (high altitude and latitude) to a reduction in density as more conductive area is needed to achieve equivalent water transport for a given ring width, are correct.

When mean density was modelled with linear models, the only tree level variable that was included was growth rate. The other explanatory variables were site level terms. This effectively means that a site specific intercept could be predicted from the selected site factors at each site. These density predictions can then be further adjusted according to growth rate which was largely responsible for the between tree variation within each site. Hence density modelling could be achieved in a two stage approach by combining growth rate and site factors such as accumulated temperature sum and altitude. These data are all easily available as input variables since approximate growth rate can be calculated from DBH and age whereas temperature sum can be derived from the Ecological Site Classification and elevation information is readily available from maps.

8.2 Relating ring-based and intra-ring density analysis to weather data

To understand how climate influences growth at an annual level the long term age-related trend needs to be removed from the tree ring series. The detrended indices are then related to the climate data to investigate which factors have caused the growth/density increase or reduction. A requirement for the analysis is that tree growth is limited by climatic conditions. Therefore, samples for dendrochronological analysis are typically collected from temperature- or moisture-limited sites (Fritts, 1976; Schweingruber et al., 1978) such as from the northern tree line or from the vicinity of deserts. In less extreme conditions tree growth may be impacted by several factors and the limiting factor may vary between years, leading to poor correlations (Kienast et al., 1987; Mäkinen et al., 2003a). However, July-August temperatures for Edinburgh from 1721 to 1975 were successfully reconstructed using maximum latewood density and ring width from pine samples collected in the Scottish highlands (Hughes et al., 1984). In recent climatic study on plantation grown Sitka spruce the only very weak and mainly insignificant relationships were found between tree ring width indices and climatic variables (Dengel et al., 2009).

At the two sites investigated in the present study only latewood density and maximum density had significant climatic correlations when correlations with p -value >0.0009 were excluded according to the Bonferroni correction to allow for the multiple comparisons that were tested. Some of the correlations between ring width or density variables and climate with p -value <0.05 for individual comparisons should be investigated further. In this study,

a very large number of climatic variables were screened, which led the p-value for the individual comparisons to be so low (0.0009). Latewood density and maximum density were negatively correlated with the whole growing season (April-September) and May-August rainfall at the Loch Tummel site. At the Coalburn site latewood density and maximum density were positively correlated with April maximum temperature and latewood density was negatively correlated with April precipitation. In addition to that April precipitation and maximum temperature were strongly intercorrelated at the Coalburn site, which indicated that perhaps only precipitation or temperature truly influenced the latewood density and the other relationship arose due to the intercorrelation.

In the future temperature will increase in all seasons and summer rainfall is likely to decrease, whereas, spring and especially winter rainfall are likely to increase (UKCP09, 2009). At the Loch Tummel site, reduction in summer rainfall is likely to increase timber density. In the case of the Coalburn site increase in spring precipitation might have a negative effect on timber density whereas increase in spring temperature would tend to increase density. The overall effect on density will depend on the strength of these factors at that site. As density seemed largely to be negatively correlated with rainfall variables and positively correlated temperature, drier and warmer weather forecast for the growing seasons in the future (UKCP09, 2009) might therefore increase timber density. However, the situation is further complicated by potential modification of growth onset due to decrease in winter chilling (Cannell and Smith, 1983; Cannell and Smith, 1986; Murray et al., 1989), greater potential of pest attacks prior to bud burst (Broadmeadow, 2002) and in the driest areas by adverse effects of moisture deficit, such as drought cracking (Green et al., 2008).

If the wide range of alternative lag periods are considered as a part of the experiment even the correlations between climatic variables and latewood density or maximum density which had p-values <0.0009 did not remain significant after the cross-correlograms were plotted and the significant cross-correlation coefficients adjusted for the multiple lag positions investigated. However, the comparisons with no lag periods may be considered a priori as a free-standing experiment. Perhaps investigation for a less conservative analysis that would be sufficiently rigorous to address these issues would make an interesting statistical project in the future.

According to the dendrometer experiment at Griffin forest near Aberfeldy, radial growth started in late May and terminated by mid September in 2008. The slowing of growth towards the end of the growing season at Griffin coincided with a reduction in soil

moisture, which is in line with the findings of Whitemore and Zahner (1966). Intra-ring bands of higher density observed in three of the trees fitted with a dendrometer, according to the approximate dating, coincided with warmer and drier weather which lends further support to a positive correlation between temperature and density and a negative one between rainfall and density. In another study, it was found that the growth of Sitka spruce was more closely related to moisture deficit and density to accumulated temperature sum (Tene et al., 2010). Furthermore, the dendrometer experiment showed that the trees remained active in water uptake throughout the year as daily radius fluctuations related to the water reserve were also observed in winter. The fact that the trees take up water during the winter renders them less susceptible to physiological drought and also has implications for the relationship of their growth to climatic variables. Previous studies have suggested that, even if radial growth has ceased, latewood cell wall deposition and lignification may extend well into the autumn (Gričar, 2007; Gričar et al., 2005) or winter (Donaldson, 1992). Perhaps Sitka spruce growth is more influenced by weather during the winter than previously thought.

The extraction of climatic signals might be improved by developing separate chronologies for different dominance classes or by focusing on suppressed trees. Findings that the length of the growing season differs for suppressed and dominant trees (Gričar, 2007), suggest that it would be worthwhile to re-examine the tree ring series data, building a separate chronology for each dominance class. Hamilton (1969) reported that Sitka spruce with larger girth in Kincardineshire started growing earlier and stopped later than smaller ones. Shorter growing season has also been reported for severely suppressed Sitka spruce trees in Wales (Denne, 1979). In the present study a shorter growing season was observed in the slowest growing dendrometer tree (tree 66). If growth ceases at different times, the months in which the climate variables govern specific developmental processes (eg. completion of the earlywood part of the ring) might differ between these groups. These effects may have confounded the results when trees from different social classes were pooled in this study, and this could potentially have lowered some of the climatic correlations. A further advantage of this approach is that the climatic signal is better expressed by more suppressed trees than by dominant trees. Travis et al. (1990) found that *Pinus taeda* L. trees damaged by ice produced a stronger climatic signal than their healthy counterparts. At a site with high between-tree competition, such as a plantation, the suppressed trees may be more limited by climate since they have less resources available for them. For example due to less extensive root systems the suppressed trees would be more influenced by drier conditions than the dominant trees. However, in some respects the suppressed

trees might also experience less variation, as to a degree they would be sheltered from strong winds and extremes of temperature by their taller neighbours.

Temperature and rainfall or other water availability variables such as moisture deficit were closely related. In the Benchmarking experiment there was a strong correlation between site moisture deficit and accumulated temperature sum. In addition to that these were both negatively correlated with altitude. In the Level II climate analysis rainfall during the growing season was negatively correlated with many temperature variables (maximum temperature in particular). In the winter positive correlations were observed between rainfall and temperature (in January at Loch Tummel and in January and February at Coalburn site). Weaker negative correlation between rainfall and temperature was also observed in the dendrometer experiment during the summer months. Long term accumulated temperature sum was found to increase density in mature wood and outerwood. At an annual level the summer temperatures were positively correlated with latewood and maximum density at Loch Tummel site albeit they were only significant if individual comparison were considered ($p < 0.05$), whereas precipitation during the growing season had a negative correlation. The formation of intra-ring density bands in three of the dendrometer trees coincided with warmer and drier conditions. Due to high intercorrelations between the temperature and water availability variables it is difficult to pinpoint which would be the limiting factor or whether influence of both variables are required to trigger the changes in density. Furthermore, the impact of these factors is likely to be modified by altitude and latitude but the correlations prevent separation of effects.

8.3 Pith to bark density modelling

A radial density curve (Gardiner et al., 2010) was fitted to the data. This type of model is useful for planning cutting patterns for the sawn timber or estimating pulp yields. Density follows an age dependent radial pattern, which the model parameters need to describe in order to produce good predictions. The density pattern from pith to bark in Sitka spruce is a complex one, with high values of density observed near the pith, with a decrease towards a minimum that is typically observed around the tenth ring and followed by an increase in density, eventually reaching a stable value in the outer mature wood. Furthermore, density is influenced by variation in ring width.

When a model describing the radial density curve (Gardiner et al., 2010) was reparameterised with new data, the model fitted parameters (α_1 , α_2 and α_3) differed widely between and within sites and the original parameters derived from experiments at Kershope and Clocaenog yielded very poor predictions when used to predict the radial density trend for the Benchmarking sites. Reparameterising the model for any particular site requires density data as an input which would be time consuming and expensive to determine. Therefore, attempts were made to derive sub-models for the model parameters that could be used to predict new parameters when the model was applied to new sites. These models were developed on the Benchmarking dataset and then tested on the Level II data. These sub-models used site and tree variables to derive site specific model parameters (α_1 , α_2 and α_3) to fit the radial density model to the Level II site data. The sub-models did not predict the parameters accurately and led to poor fits.

One reason contributing to the failure is that even though there were large differences in the shape of radial density curves and hence in the parameters (α_1 , α_2 and α_3), across the Benchmarking experiment, the parameters (α_1 in particular) were not very strongly influenced by the site variables studied. Perhaps some other factors like the genetic origins of the trees planted at each site influenced the shape of the radial density curve. Additionally, using site specific parameters may not have been an ideal approach and using these models to predict tree specific parameters needs to be tested. The density curves differed markedly between the trees within the Level II sites, which would indicate that tree specific parameters would be required. Predicting tree specific parameters could still be less laborious than reparameterising the model using ring width and density measurements. In addition to this when the model was reparameterised on the Level II data, there were still considerable random tree effects which caused the predictions to be less accurate when the fixed effects alone were used. When the model is applied to new sites the random effects will not be known, so the model should be improved by incorporating further terms that would explain some of this variation. These terms are likely to be tree variables since the radial density curve parameters differed between trees.

A further complication is that the model for the radial density curve in Sitka spruce also includes a ring width parameter. As density is negatively correlated with ring width some kind of growth rate variable is probably required in any radial density model.

Unfortunately ring width measurements are fairly time consuming and hence restrict the utility of the model if ring width is required as an input variable. However, if the density model is coupled with a ring width model these time consuming measurements can be avoided (e.g. see (Macdonald et al., 2010)).

8.4 Stiffness

The use of density to predict timber stiffness (Booker et al., 1997; Cown and Hutchison, 1983; Saranpää and Repola, 2000; Tsehaye et al., 1997) and the relationship between density and microfibril angle (MFA) have been discussed (Chauhan and Walker, 2006). Recent findings on Sitka spruce showed that bulk density divided by MFA or the reciprocal of MFA were better predictors of dynamic and static MoE of small clears than bulk density alone (McLean et al., 2010). Acoustic velocity is considered to be influenced mainly by microfibril angle. Chauhan and Walker (2006) showed that a correlation between density and standing tree acoustic velocity was an artefact resulting from sampling stands of different age. In Sitka spruce, due to the characteristic shape of its radial density curve where high density is found in juvenile wood, the highest density does not yield the highest values of MoE. At intermediate values of density, nearly the full range of stiffness values were observed, presumably depending on MFA for which acoustic velocity is a surrogate. Therefore, using density alone to predict timber properties in Sitka spruce cross-section would be problematic unless its distinctive radial pattern was acknowledged and the juvenile wood effect accounted for. Standing tree acoustic assessment of mature trees is not influenced by these issues since the MoE is measured in the outer few centimetres of the stem. This will allow segregating trees, as there has been shown to be a strong correlation between standing tree and log MoE in Sitka spruce (Mochan et al., 2009). Furthermore, in Sitka spruce, good agreement ($R^2 = 0.84$) has been found between dynamic MoE (derived from log acoustic velocity and bulk density) and global MoE calculated from the results of four point bending tests on the resulting battens (Moore et al., 2009a). In the present study ST300 time-of-flight standing tree acoustic tool results compared poorly with the ultrasonic scanning results when the velocity or calculated MoE results were compared.

Cross-section average MoE (calculated from acoustic velocity and X-ray density data) was influenced by the size of the juvenile core (defined as first 10 rings) with MoE decreasing with increasing juvenile core. The size of the juvenile core is very subjective. In this thesis it was defined as the first 10 rings based on measurements of density but the average acoustic velocity curve started to level off later at around ring 15, which indicates that based on microfibril angle the juvenile core may be larger. When, the stiffness values were averaged per ring the results matched the density observations more closely, which indicates that our juvenile core definition was an acceptable one. In addition to juvenile core some other variables influenced stiffness. At Loch Awe site age and slenderness and

at Coalburn crown width increased MoE. Higher growth rate has been reported to decrease stiffness in Sitka spruce also in previous studies (Brazier and Mobbs, 1993; Moore et al., 2009a; Moore et al., 2009c).

A radial stiffness model developed on small clears data (McLean, 2007) was fitted to the stiffness data calculated from the ultrasonic velocity and X-ray density data. The radial stiffness curves in the present study resembled the density curves particularly when MoE values were averaged for each ring for both sites. Near the pith there was a decreasing trend in MoE, resulting in a minimum value around ring 8 or 9 after which MoE increased steadily. Both the initial MoE value and depth of the dip varied between the sites with the dip being more pronounced at the Coalburn site. Due to these differences in MoE curves the model was fitted separately for each site. The model fits were good ($R^2 = 0.77-0.80$) when the tree effects were included but a trend remained in the residuals because the model did not describe the dip accurately. However, fitting the model to new sites would require the model parameters (a , b and d) to be derived from MoE measurements which would be time consuming. Therefore, the possibility of relating the parameters to tree variables was investigated. There seems to be scope for example for predicting the b parameter from tree radius (Coalburn) or slenderness (Loch Awe). However, since the explanatory variables differed between the sites it is difficult to conclude which variables might be important in case of a new site.

8.5 Conclusions

The largest part of the variation (69-78%) in cross-section average density (juvenile wood, mature wood, outerwood and whole cross-section) was between trees within the site. Both density and stiffness are mainly influenced by the growth rate. Faster growing trees within a site were always characterised by lower density and stiffness than the slower growing ones. Strong correlations were observed between ring width and earlywood width which support the previous results that the growth increase takes place in the earlywood part of the ring and therefore contributes to reduction in ring density. In addition to this the absolute density was reduced in both earlywood and latewood as ring width increased contributing further to the reduction in ring density. Site factors such as accumulated temperature sum and potentially also altitude and moisture deficit, can be used to predict a site specific intercept of density which could then be combined with growth rate to predict between tree differences within a site.

Within tree ring chronologies from a given site earlywood density was positively correlated with latewood density. However, in absolute terms there may be large differences between sites in the range of density observed within the rings. For example, the site that had on average the lowest earlywood density had the highest latewood density, which was sufficiently high to cause the ring density to be higher at this site than other sites measured. This indicates that the within ring density range can also vary between sites.

High resolution stiffness curves were derived for Sitka spruce using X-ray density and ultrasonic scanning data. The methods allowed high throughput of samples and in total samples from 55 trees from two sites were analysed. When stiffness data was averaged for ring number the curves resembled the density curves since a dip was observed around ring 10. This has not been reported in previous studies using small clear wood samples.

Modelling the characteristic Sitka spruce density curve that has a complex shape is difficult. In particular, prediction of the dip in the curve from pith to bark is challenging. The site average radial density curves differed markedly between sites, which will make it difficult to fit these models to new sites without reparameterising the model using density, ring width or stiffness data, unless alternative means of deriving model parameters for new sites are developed. The approach of predicting the parameters from tree and site variables attempted here was largely unsuccessful.

Latewood density and maximum density contained the strongest climatic signals. Temperature and moisture availability variables were strongly intercorrelated across experiments. In the climatic analysis this was illustrated by the latewood density being correlated ($p < 0.0009$) both with precipitation and maximum temperature in April at one site. In experiments on detailed within year growth warmer and drier conditions lead to formation of intra-ring density bands in three of the trees investigated. More research is needed to separate out the relative contributions of temperature and water availability.

In Sitka spruce density was heavily influenced by growth rate. Higher growth rate led to decrease in absolute density of earlywood and latewood as well as to increase in the proportion of earlywood that is of lesser density than latewood. Negative correlation between ring width and density was consistent throughout the extensive dataset therefore based on these findings any silvicultural treatments that increase growth will decrease density. There was evidence that location at high elevation decreases and higher accumulated temperature sum increases timber density in the UK but the influence was

more restricted than that of growth rate. On tree ring level positive correlations were found between temperature variables and latewood and maximum density whereas these density variables had negative correlations with precipitation variables.

8.6 Future work

- In future work separate chronologies should be developed for tree dominance classes to test if the strength of climatic signal could be increased by eliminating the potential differences in growing season length between the classes.
- The relative importance of strongly correlated temperature and moisture variables on growth and density of Sitka spruce timber need more research. An irrigation experiment could be established to decouple the intercorrelation between temperature and rainfall at a given site.
- The reduction of wood density with increasing elevation should be investigated in detail. As a starting point the latewood proportions could be investigated in more detail to see if the transition to latewood occurs later due to ample moisture availability. Furthermore, tracheid diameter and wall thickness should be studied along an altitudinal transects to assess if changes in the conductive “pipe” area predicted by theoretical calculations are occurring.
- The microtome slides cut from the 2008 microcores collected from the dendrometer experiment site need to be analysed further. The cell diameter and cell thickness could be studied under microscope to determine if the intra-ring density bands detected arose due to increase of cell wall thickness or decrease in tracheid diameter as these are under different physiological control (Denne, 1979). In addition to that, the annual phloem growth could also be observed on these samples, to assess its contribution to growth detected by the dendrometers.
- The dendrometer data itself could be used to study the dynamics of water storage in Sitka spruce. And it could be combined with the sap flow data collected from the sampled trees since spring 2009. The dendrometer experiment is continuing beyond this project and the longer time series will allow comparisons between years that differ in meteorological conditions. In particular the growth onset data after the very cold winter

of 2010 will be interesting to assess the impact of a thorough chilling on the growth onset in Sitka spruce.

- Detailed microfibril angle (MFA) analysis on the subset of samples used in the ultrasonic scanning study would provide an interesting point of comparison as this would enable investigation of how closely the ultrasonic velocity and MFA are related and hence quantify to what extent the velocity potentially integrates other properties such as for example grain angle.
- In the longer time the research efforts concerning density in Sitka spruce should be directed at continuing breeding to produce trees that provide a suitable compromise between fast growth rate and acceptable timber density and MFA.
- Due to high variability in density and acoustic velocity between trees within a site, allocating certain areas for producing construction timber does not seem like the optimal way of managing the timber resource. Therefore, further research is essential to develop effective methods for characterising the timber resource at different sites, for example by acoustic testing, and allocating the timber to different end uses according to the required specification.

Appendices

Appendix 1

Correlations between the weather variables at the Griffin site.

	Air T tower	Air T	PPT	humidity	TDR	TDR tower	RG	PPFDg	PPFDd	wind	Soil T1	Soil T2	Soil T3	Soil T4	Bole Int T1	Bole Int T2	Bole Int T3	Bole out T1	Bole out T2	Bole out T3
Air T tower	1	0.995	0.085	-0.225	-0.615	-0.690	0.492	0.500	0.612	-0.001	0.901	0.869	0.799	0.725	0.924	0.908	0.925	0.923	0.925	0.922
Air T	0.995	1	0.052	-0.195	-0.677	-0.675	0.471	0.511	0.604	-0.014	0.809	0.759	0.657	0.555	0.846	0.821	0.847	0.844	0.847	0.843
PPT	0.085	0.052	1	0.319	0.128	0.075	-0.263	-0.239	-0.171	0.155	0.075	0.084	0.098	0.110	0.062	0.066	0.052	0.065	0.060	0.055
humidity	-0.225	-0.195	0.319	1	0.520	0.575	-0.739	-0.728	-0.499	-0.264	-0.089	-0.053	0.006	0.051	-0.144	-0.119	-0.163	-0.133	-0.145	-0.156
TDR	-0.615	-0.677	0.128	0.520	1	0.969	-0.795	-0.780	-0.815	0.002	-0.376	-0.324	-0.228	-0.137	-0.425	-0.409	-0.435	-0.419	-0.426	-0.431
TDR tower	-0.690	-0.675	0.075	0.575	0.969	1	-0.653	-0.666	-0.745	-0.044	-0.571	-0.546	-0.492	-0.438	-0.596	-0.590	-0.604	-0.593	-0.598	-0.602
RG	0.492	0.471	-0.263	-0.739	-0.795	-0.653	1	0.990	0.815	0.054	0.379	0.344	0.277	0.214	0.421	0.400	0.435	0.414	0.423	0.429
PPFDg	0.500	0.511	-0.239	-0.728	-0.780	-0.666	0.990	1	0.830	-0.002	0.361	0.314	0.227	0.149	0.412	0.385	0.428	0.404	0.414	0.420
PPFDd	0.612	0.604	-0.171	-0.499	-0.815	-0.745	0.815	0.830	1	-0.082	0.507	0.467	0.389	0.312	0.540	0.525	0.548	0.537	0.542	0.544
wind	-0.001	-0.014	0.155	-0.264	0.002	-0.044	0.054	-0.002	-0.082	1	0.003	-0.002	-0.012	-0.016	0.022	0.013	0.023	0.021	0.021	0.021
Soil T1	0.901	0.809	0.075	-0.089	-0.376	-0.571	0.379	0.361	0.507	0.003	1	0.995	0.963	0.917	0.994	0.995	0.992	0.996	0.994	0.993
Soil T2	0.869	0.759	0.084	-0.053	-0.324	-0.546	0.344	0.314	0.467	-0.002	0.995	1	0.985	0.952	0.980	0.988	0.977	0.982	0.979	0.979
Soil T3	0.799	0.657	0.098	0.006	-0.228	-0.492	0.277	0.227	0.389	-0.012	0.963	0.985	1	0.990	0.932	0.952	0.928	0.936	0.931	0.932
Soil T4	0.725	0.555	0.110	0.051	-0.137	-0.438	0.214	0.149	0.312	-0.016	0.917	0.952	0.990	1	0.874	0.900	0.868	0.879	0.873	0.873
Bole Int T1	0.924	0.846	0.062	-0.144	-0.425	-0.596	0.421	0.412	0.540	0.022	0.994	0.980	0.932	0.874	1	0.995	1.000	1.000	1.000	0.999
Bole Int T2	0.908	0.821	0.066	-0.119	-0.409	-0.590	0.400	0.385	0.525	0.013	0.995	0.988	0.952	0.900	0.995	1	0.995	0.994	0.994	0.996
Bole Int T3	0.925	0.847	0.052	-0.163	-0.435	-0.604	0.435	0.428	0.548	0.023	0.992	0.977	0.928	0.868	1.000	0.995	1	0.998	0.999	1.000
Bole out T1	0.923	0.844	0.065	-0.133	-0.419	-0.593	0.414	0.404	0.537	0.021	0.996	0.982	0.936	0.879	1.000	0.994	0.998	1	1.000	0.998
Bole out T2	0.925	0.847	0.060	-0.145	-0.426	-0.598	0.423	0.414	0.542	0.021	0.994	0.979	0.931	0.873	1.000	0.994	0.999	1.000	1	0.999
Bole out T3	0.922	0.843	0.055	-0.156	-0.431	-0.602	0.429	0.420	0.544	0.021	0.993	0.979	0.932	0.873	0.999	0.996	1.000	0.998	0.999	1

Appendix 2. Site specific correlation coefficients between ring width and ring density across the whole radius and separately in mature and juvenile wood in the Benchmarking dataset.

Site number	Whole radius		Mature wood		Juvenile wood	
	Corr. Coef	p-value	Corr. Coef	p-value	Corr. Coef	p-value
1	-0.22	**	-0.33	**	0.07	ns
2	-0.48	***	-0.62	***	-0.21	*
3	-0.36	***	-0.64	***	-0.32	***
4	-0.55	***	-0.75	***	-0.36	**
5	-0.37	***	-0.68	***	-0.10	ns
6	-0.52	***	-0.68	***	-0.78	***
7	-0.40	***	-0.64	***	-0.34	**
8	-0.43	***	-0.58	***	-0.56	***
9	-0.58	***	-0.78	***	-0.75	***
10	-0.44	***	-0.61	***	-0.28	*
11	-0.20	***	-0.64	***	-0.20	ns
12	-0.24	***	-0.72	***	0.05	ns
13	-0.32	***	-0.56	***	-0.40	***
14	-0.09	ns	-0.14	*	-0.34	**
15	-0.49	***	-0.67	***	-0.38	**
16	-0.29	***	-0.68	***	-0.52	***
17	-0.38	***	-0.63	***	-0.17	ns
18	-0.25	***	-0.64	***	-0.46	***
19	-0.53	***	-0.62	***	-0.68	***
20	-0.41	***	-0.51	***	-0.40	***
21	-0.53	***	-0.68	***	-0.30	*
22	-0.62	***	-0.78	***	-0.67	***
23	-0.33	***	-0.45	***	-0.67	***
24	-0.48	***	-0.52	***	-0.45	***
25	-0.38	***	-0.62	***	-0.48	***
26	-0.32	***	-0.57	***	-0.46	***
27	-0.37	***	-0.40	***	-0.67	***
28	-0.59	***	-0.53	***	-0.49	***
29	-0.51	***	-0.78	***	-0.72	***
30	-0.54	***	-0.76	***	-0.52	***
31	-0.39	***	-0.63	***	-0.49	***
32	-0.36	***	-0.40	***	-0.69	***
33	-0.58	***	-0.58	***	-0.86	***
34	-0.37	***	-0.59	***	-0.51	***
35	-0.54	***	-0.77	***	-0.35	**
36	-0.61	***	-0.77	***	-0.64	***
37	-0.44	***	-0.53	***	-0.63	***
38	-0.57	***	-0.66	***	-0.56	***
39	-0.50	***	-0.69	***	-0.56	***
40	-0.24	***	-0.68	***	-0.43	***
41	-0.45	***	-0.78	***	-0.66	***
42	-0.39	***	-0.55	***	-0.52	***
43	-0.28	***	-0.76	***	-0.37	**
44	-0.32	***	-0.48	***	-0.52	***
45	-0.43	***	-0.67	***	-0.70	***
46	-0.22	***	-0.55	***	0.11	ns
47	-0.22	**	-0.13	ns	-0.20	ns

48	-0.41	***	-0.62	***	-0.29	*
49	-0.37	***	-0.78	***	-0.26	*
50	-0.44	***	-0.59	***	-0.30	*
51	-0.51	***	-0.75	***	-0.47	***
52	-0.56	***	-0.66	***	-0.66	***
53	-0.31	***	-0.49	***	-0.50	***
54	-0.42	***	-0.65	***	-0.53	***
55	-0.53	***	-0.58	***	-0.68	***
56	-0.10	ns	-0.66	***	-0.22	ns
57	-0.29	***	-0.52	***	-0.77	***
58	-0.53	***	-0.56	***	-0.58	***
59	-0.12	.	-0.53	***	-0.23	*
60	-0.13	*	-0.50	***	-0.42	***
61	-0.62	***	-0.64	***	-0.83	***
62	-0.37	***	-0.43	***	-0.58	***
63	-0.33	***	-0.23	**	-0.66	***
64	-0.39	***	-0.56	***	-0.37	***
65	-0.53	***	-0.68	***	-0.27	*
66	-0.40	***	-0.68	***	-0.54	***
67	-0.45	***	-0.28	***	-0.56	***
68	-0.63	***	-0.62	***	-0.84	***

Levels of significance *** < 0.001, ** < 0,01, * < 0.05, and . < 0.1

Appendix 3 Correlation matrix for the explanatory variables in Benchmarking experiment.

	Thin	East	Elev	Trees /Site	Stems /ha	DBH	Mean DBH	Dom	SS	Slope
Thin	1.00	0.20	-0.01	-0.64	-0.64	0.27	0.40	0.04	0.17	-0.23
East	0.20	1.00	0.26	-0.13	-0.13	0.15	0.17	0.06	-0.03	-0.36
Elev	-0.01	0.26	1.00	0.11	0.11	-0.05	-0.15	0.04	-0.09	0.05
Trees/Site	-0.64	-0.13	0.11	1.00	1.00	-0.30	-0.65	0.09	-0.13	0.18
Stems/ha	-0.64	-0.13	0.11	1.00	1.00	-0.30	-0.65	0.09	-0.13	0.18
DBH	0.27	0.15	-0.05	-0.30	-0.30	1.00	0.47	0.81	0.48	-0.03
Mean DBH	0.40	0.17	-0.15	-0.65	-0.65	0.47	1.00	-0.12	0.14	0.07
Dom	0.04	0.06	0.04	0.09	0.09	0.81	-0.12	1.00	0.46	-0.08
SS	0.17	-0.03	-0.09	-0.13	-0.13	0.48	0.14	0.46	1.00	-0.01
Slope	-0.23	-0.36	0.05	0.18	0.18	-0.03	0.07	-0.08	-0.01	1.00
Ring count	0.08	0.21	0.05	0.10	0.10	0.37	0.18	0.32	0.21	-0.02
DBH ₁₀	0.10	-0.03	-0.08	-0.22	-0.22	0.62	0.29	0.50	0.25	0.08
Growth Rate	0.24	0.04	-0.08	-0.37	-0.37	0.84	0.39	0.67	0.39	-0.02
Growth Rate ₁₀	0.10	-0.03	-0.08	-0.22	-0.22	0.62	0.29	0.50	0.25	0.08
AT	-0.10	-0.29	-0.86	0.04	0.04	-0.01	0.00	-0.01	0.05	-0.05
MD	0.03	0.16	-0.88	-0.10	-0.10	0.09	0.16	-0.00	0.06	-0.21
DAMS	-0.14	-0.15	0.34	-0.00	-0.00	-0.17	-0.29	-0.01	0.01	-0.09
CONT	-0.06	0.62	0.41	0.12	0.12	0.06	-0.03	0.09	-0.13	-0.17
Mean Ht	0.30	-0.01	-0.34	-0.34	-0.34	0.35	0.69	-0.06	0.16	0.24
Ave RC	0.08	0.30	0.08	0.14	0.14	0.15	0.24	0.04	0.02	-0.05

	Ring Count	DBH ₁₀	Growth Rate	Growth Rate ₁₀	AT	MD	DAMS	CONT	Mean Ht	Ave RC
Thin	0.08	0.10	0.24	0.10	-0.10	0.03	-0.14	-0.06	0.30	0.08
East	0.21	-0.03	0.04	-0.03	-0.29	0.16	-0.15	0.62	-0.01	0.30
Elev	0.05	-0.08	-0.08	-0.08	-0.86	-0.88	0.34	0.41	-0.34	0.08
Trees/Site	0.10	-0.22	-0.37	-0.22	0.04	-0.10	-0.00	0.12	-0.34	0.14
Stems/ha	0.10	-0.22	-0.37	-0.22	0.04	-0.10	-0.00	0.12	-0.34	0.14
DBH	0.37	0.62	0.84	0.62	-0.01	0.09	-0.17	0.06	0.35	0.15
Mean DBH	0.18	0.29	0.39	0.30	0.00	0.16	-0.29	-0.03	0.69	0.24
Dom	0.32	0.50	0.67	0.50	-0.01	-0.00	-0.01	0.09	-0.06	0.04
SS	0.21	0.25	0.39	0.25	0.05	0.06	0.01	-0.13	0.16	0.02
Slope	-0.02	0.08	-0.02	0.08	-0.05	-0.21	-0.09	-0.17	0.24	-0.05
Ring Count	1.00	-0.15	-0.18	-0.15	-0.14	-0.00	-0.26	0.06	0.21	0.72
DBH ₁₀	-0.15	1.00	0.75	1.00	0.19	0.12	0.04	0.10	0.25	-0.28
Growth Rate	-0.18	0.75	1.00	0.75	0.06	0.09	-0.03	0.01	0.24	-0.25
Growth Rate ₁₀	-0.15	1.00	0.75	1.00	0.19	0.12	0.04	0.10	0.25	-0.28
AT	-0.14	0.19	0.06	0.19	1.00	0.85	-0.10	-0.06	0.31	-0.21
MD	-0.00	0.12	0.09	0.12	0.85	1.00	-0.31	0.01	0.34	-0.02
DAMS	-0.26	0.04	-0.03	0.04	-0.10	-0.31	1.00	0.10	-0.41	-0.39
CONT	0.06	0.10	0.01	0.10	-0.06	0.01	0.10	1.00	-0.04	0.09
Mean Ht	0.21	0.25	0.24	0.25	0.31	0.34	-0.41	-0.04	1.00	0.28
Ave RC	0.72	-0.28	-0.25	-0.28	-0.21	-0.02	-0.39	0.09	0.28	1.00

Appendix 5. Correlations with p-value <0.1 between the tree ring and climate variables of the previous year at the Loch Tummel site. Significant correlations (alpha 0.05) are highlighted in grey.

LOCH TUMMEL	RW	RD	EWD	EWV	LWD	LW %	LWW	MaxD	MinD
GSdegDayNo									
GDDAnnualTot									
GDDgsTot						0.34			
GDDmayAug	-0.33					0.32			
GDDju.ug	-0.38			-0.33					
JanMaxT	-0.31	0.51	0.33	-0.32	0.42			0.40	
JanMinT		0.52	0.38		0.42			0.40	0.30
JanMeanT		0.53	0.36	-0.32	0.43			0.41	
FebMaxT		0.35				0.32			
FebMinT									
FebMeanT						0.30			
MarMaxT									
MarMinT	-0.30								
MarMeanT									
AprMaxT									
AprMinT									
AprMeanT									
MayMaxT					-0.40		0.37	-0.36	
MayMinT						0.29	0.34		
MayMeanT					-0.42	0.32	0.45	-0.39	
JunMaxT									
JunMinT									
JunMeanT									
JulMaxT									
JulMinT									
JulMeanT									
AugMaxT	-0.44	0.35		-0.36					
AugMinT	-0.33			-0.35		0.30			
AugMeanT	-0.44	0.31		-0.39		0.31			
SepMaxT									
SepMinT									
SepMeanT									
OctMaxT									
OctMinT									
OctMeanT									
NovMaxT									
NovMinT	-0.31								
NovMeanT									
DecMaxT									
DecMinT									
DecMeanT									
GSprecip						0.31	0.40		-0.31
YrPrecip									
MAPrecip			-0.31						-0.29
JAprcip							0.31		-0.30
JanPrecip			-0.31		0.31				
FebPrecip									
MarPrecip	-0.35					-0.30			-0.35
AprPrecip									
MayPrecip									
JunPrecip									
JulPrecip							0.34		
AugPrecip									
SepPrecip						0.38	0.40		
OctPrecip									
NovPrecip									
DecPrecip	0.30	-0.35		0.30		-0.30			

Appendix 6. Autocorrelation within the weather variables at the Loch Tummel site. Level of significance ($r=0.335$)

Lag	0	1	2	3	4	5	6	7	8	9	10	11	12	13	14
GSdegDayNo	1	0.095	0.145	0.088	0.086	-0.092	0.06	-0.187	-0.039	-0.118	-0.033	0.115	-0.007	0.103	-0.017
GDDAnnualTot	1	0.35	0.172	-0.042	-0.124	0.103	0.341	0.337	0.326	0.008	-0.298	-0.087	-0.132	0.002	0.056
GDDgsTot	1	0.208	0.056	0.032	0.038	-0.011	0.138	0.261	0.334	-0.007	-0.364	-0.014	-0.095	-0.034	-0.005
GDD May-Aug	1	0.097	-0.072	-0.101	-0.3	0.005	0.256	0.174	0.401	-0.072	-0.488	0.058	-0.099	0.104	0.206
GDD June-Aug	1	0.17	-0.207	-0.176	-0.276	-0.081	0.158	0.216	0.338	-0.161	-0.43	0.076	0.026	0.185	0.118
JanMaxT	1	0.16	0.073	0.021	-0.244	0.015	0.08	0.054	-0.031	-0.093	-0.158	-0.126	-0.155	-0.056	0.039
JanMinT	1	0.137	0.07	0.032	-0.165	-0.071	0.106	0.14	-0.073	-0.004	-0.107	-0.241	-0.249	0.067	-0.071
JanMeanT	1	0.17	0.083	0.017	-0.197	-0.035	0.11	0.112	-0.059	-0.041	-0.147	-0.21	-0.206	0.002	-0.031
FebMaxT	1	0.218	0.058	0.04	-0.129	0.208	-0.001	0.066	0.379	0.062	-0.034	-0.1	-0.257	-0.051	-0.23
FebMinT	1	0.078	-0.105	-0.179	0.038	0.205	-0.003	-0.059	0.274	0.023	-0.055	-0.191	-0.158	0.068	-0.128
FebMeanT	1	0.16	-0.036	-0.076	-0.054	0.221	-0.014	0.011	0.343	0.041	-0.059	-0.141	-0.219	0.017	-0.196
MarMaxT	1	0.183	-0.057	-0.14	-0.213	0.158	0.007	0.003	0.117	0.032	0.084	0.03	-0.026	-0.041	-0.045
MarMinT	1	0.034	0.098	-0.202	-0.341	-0.032	0.11	0.303	0.165	0.063	-0.092	-0.241	-0.045	-0.002	0.085
MarMeanT	1	0.166	-0.028	-0.157	-0.335	0.106	0.041	0.176	0.181	0.027	-0.031	-0.087	-0.032	-0.019	0.014
AprMaxT	1	-0.037	-0.069	-0.079	-0.144	-0.141	0.227	0.067	0.065	-0.114	-0.024	-0.089	-0.076	0.061	-0.166
AprMinT	1	-0.007	0.048	0.23	-0.049	0.316	0.099	0.002	0.107	0.059	-0.16	0.044	0.173	-0.188	-0.174
AprMeanT	1	-0.067	-0.084	0.025	-0.126	0.082	0.187	-0.015	0.099	-0.038	-0.095	-0.001	0.099	-0.065	-0.213
MayMaxT	1	-0.117	-0.003	0.121	-0.051	-0.378	0.03	-0.041	0.014	0.145	0.197	0.04	0.074	0.014	0
MayMinT	1	0.008	0.228	-0.168	-0.13	0.104	-0.26	-0.022	-0.267	0.018	0.021	0.051	0.207	-0.104	0.166
MayMeanT	1	0.137	0.086	0.073	-0.178	-0.301	-0.052	-0.07	-0.031	0.175	0.083	0.145	0.117	-0.017	0.061
JunMaxT	1	-0.214	0.091	-0.079	0.23	-0.399	-0.043	-0.088	0.048	-0.031	0.013	0.087	-0.097	0.041	0.049
JunMinT	1	-0.1	0.102	-0.16	0.15	-0.123	-0.003	-0.419	0.174	-0.067	0.165	0.028	0.069	0.062	0.044
JunMeanT	1	-0.237	0.129	-0.184	0.288	-0.289	-0.011	-0.259	0.166	-0.069	0.085	0.006	-0.03	0.096	0.067
JulMaxT	1	0.049	-0.148	-0.281	-0.35	0.025	0.238	0.278	0.043	-0.3	-0.117	-0.043	0.128	0.054	0.093
JulMinT	1	-0.3	-0.053	-0.135	0.264	-0.27	0.055	0.003	0.397	-0.258	-0.155	-0.042	0.266	-0.391	0.115
JulMeanT	1	-0.07	-0.138	-0.257	-0.159	-0.112	0.206	0.224	0.179	-0.288	-0.169	-0.064	0.195	-0.101	0.171
AugMaxT	1	0.249	-0.143	-0.23	-0.199	-0.026	0.168	0.271	0.235	-0.248	-0.481	-0.13	0.101	0.109	0.077
AugMinT	1	-0.035	-0.082	-0.071	-0.34	-0.021	0.112	0.208	0.129	-0.007	-0.167	-0.252	-0.014	0.109	0.054
AugMeanT	1	0.184	-0.145	-0.17	-0.286	-0.013	0.202	0.289	0.192	-0.175	-0.445	-0.212	0.098	0.161	0.116
SepMaxT	1	0.453	0.332	0.233	0.145	0.093	0.043	0.297	0.256	0.189	0.126	0.009	-0.229	-0.252	-0.189
SepMinT	1	0.258	0.105	0.029	-0.01	-0.052	-0.143	0.17	0.016	-0.148	-0.042	-0.047	-0.081	-0.275	-0.101
SepMeanT	1	0.453	0.204	0.226	0.114	-0.015	-0.046	0.209	0.177	-0.021	0.072	0.026	-0.212	-0.305	-0.239
OctMaxT	1	0.226	-0.27	-0.486	-0.179	0.139	0.252	0.058	-0.238	-0.183	0.142	0.396	0.192	-0.163	-0.341
OctMinT	1	0.193	-0.208	-0.403	-0.102	0.091	0.13	-0.049	-0.175	-0.106	0.16	0.327	0.079	-0.09	-0.287
OctMeanT	1	0.226	-0.234	-0.491	-0.139	0.126	0.214	0.022	-0.233	-0.152	0.181	0.356	0.131	-0.132	-0.347
NovMaxT	1	-0.324	0.023	0.259	-0.162	0.172	-0.023	-0.165	0.251	-0.037	-0.214	0.169	-0.063	-0.031	-0.04
NovMinT	1	-0.288	-0.081	0.154	-0.096	0.029	0.045	0.098	0.068	-0.166	-0.089	0.019	-0.023	0.153	-0.052
NovMeanT	1	-0.318	-0.035	0.209	-0.131	0.099	0.011	-0.022	0.179	-0.118	-0.172	0.116	-0.033	0.042	-0.025
DecMaxT	1	-0.093	-0.115	0.099	-0.05	0.052	-0.036	-0.371	0.032	-0.102	0.051	-0.039	-0.18	0.12	0.2
DecMinT	1	-0.118	-0.066	0.01	-0.006	-0.028	-0.008	-0.451	0.094	0.028	0.102	-0.005	0.048	0.003	0.271
DecMeanT	1	-0.123	-0.098	0.069	0.004	0.011	-0.028	-0.448	0.066	-0.025	0.086	-0.025	-0.063	0.064	0.267
GSprecip	1	-0.248	0.14	-0.044	-0.075	0.107	0.134	0.103	-0.161	-0.225	0.03	-0.025	0.063	0.03	-0.05
YrPrecip	1	-0.272	0.279	-0.07	0.18	-0.002	0.076	0.07	0.223	-0.035	0.084	-0.122	0.158	-0.234	0.171
MAPrecip	1	-0.096	0.045	-0.074	-0.12	0.2	0.071	-0.067	-0.205	-0.216	-0.029	0.095	0.075	-0.063	-0.008
JAPrecip	1	-0.244	0.038	0.003	-0.172	0.088	0.063	-0.023	-0.13	-0.229	0.112	0.041	0.059	0.121	-0.012
JanPrecip	1	-0.022	-0.095	0.038	-0.204	-0.044	0.021	-0.089	-0.153	0.27	0.032	-0.147	0.085	-0.334	-0.057
FebPrecip	1	0.196	0.113	-0.175	-0.269	0.281	0.18	0.282	-0.028	-0.234	0.027	-0.075	0.233	-0.003	-0.18
MarPrecip	1	0.142	0.089	0.162	-0.022	0.001	-0.058	-0.119	0.049	-0.077	0.026	-0.069	-0.14	0.012	-0.044
AprPrecip	1	0.131	0.186	-0.081	-0.02	0.138	0.394	0.171	0.153	-0.074	-0.239	-0.033	-0.095	0.076	0.025
MayPrecip	1	-0.223	0	0.173	0.023	-0.041	-0.087	0.207	-0.404	0.016	0.181	-0.132	-0.122	-0.084	0.07
JunPrecip	1	-0.209	-0.332	0.223	0.104	-0.107	-0.047	0.118	0.236	-0.242	-0.105	0.297	0.011	-0.178	0.048
JulPrecip	1	-0.038	-0.307	-0.022	-0.116	0.122	-0.003	-0.141	-0.097	-0.133	0.15	0.121	-0.088	0.17	0.041
AugPrecip	1	-0.322	0.02	0.043	0.034	-0.1	-0.044	0.063	0.002	-0.29	0.104	-0.223	0.237	-0.11	-0.018
SepPrecip	1	0.179	-0.136	-0.159	-0.029	-0.105	-0.028	0.113	-0.036	-0.21	-0.117	0.046	-0.055	-0.06	-0.021
OctPrecip	1	0.006	-0.258	-0.05	-0.017	0.151	0.345	-0.028	-0.087	-0.173	0.009	0.095	0.102	0.023	0.087
NovPrecip	1	-0.157	0.075	0.03	-0.012	-0.113	-0.035	-0.001	0.144	-0.323	0.064	-0.134	-0.011	0.023	0.104
DecPrecip	1	-0.026	-0.201	-0.341	0.023	-0.132	0.044	0.189	0.298	-0.129	-0.28	-0.281	0.277	0.077	0.124

Appendix 8. Correlations with p-value <0.1 between the tree ring and climate variables of the previous year at the Coalburn site. Significant correlations (alpha 0.05) are highlighted in grey.

COALBURN	RW	RD	EWD	EWW	LWD	LW %	LWW	MaxD	MinD
GSdegDayNo			0.36						
GDDAnnualTot									
GDDgsTot									
GDDmayAug									
GDDju.ug			0.34						
JanMaxT									
JanMinT									
JanMeanT									
FebMaxT									
FebMinT									
FebMeanT									
MarMaxT									
MarMinT									
MarMeanT									
AprMaxT							0.38		
AprMinT									
AprMeanT							0.34		
MayMaxT					-0.33			-0.42	
MayMinT									
MayMeanT									
JunMaxT									
JunMinT									
JunMeanT									
JulMaxT									
JulMinT					-0.45		0.42	-0.41	-0.34
JulMeanT									
AugMaxT									
AugMinT					-0.40			-0.47	
AugMeanT									
SepMaxT		0.44	0.36						
SepMinT									
SepMeanT		0.42	0.42						0.35
OctMaxT									
OctMinT									
OctMeanT									
NovMaxT									
NovMinT									
NovMeanT									
DecMaxT			-0.40						-0.35
DecMinT			-0.42						-0.35
DecMeanT			-0.40						-0.34
GSprecip									
YrPrecip			-0.32						
MAPrecip			-0.33						
JAprcip									
JanPrecip									
FebPrecip									
MarPrecip									
AprPrecip									
MayPrecip									
JunPrecip									
JulPrecip									
AugPrecip		-0.37	-0.37						
SepPrecip									
OctPrecip								0.35	
NovPrecip					0.34				
DecPrecip		-0.41	-0.37						

Appendix 9. Autocorrelation within the weather variables at the Coalburn site. Level of significance ($r=0.37$).

Lag	0	1	2	3	4	5	6	7	8	9	10	11	12	13	14
GSdegDayNo	1	0.377	0.052	0.096	0.197	0.177	0.086	0.007	-0.029	-0.002	-0.137	-0.21	-0.269	-0.18	-0.036
GDDAnnualTot	1	0.454	0.199	0.158	0.123	0.209	0.28	0.27	0.031	-0.04	-0.192	-0.058	-0.206	-0.326	-0.118
GDDgsTot	1	0.438	0.109	0.057	0.042	0.093	0.229	0.348	0.165	-0.044	-0.21	-0.083	-0.264	-0.312	-0.01
GDD May-Aug	1	0.284	-0.007	-0.044	-0.149	0.057	0.276	0.328	0.189	-0.002	-0.305	-0.03	-0.133	-0.208	0.088
GDD June-Aug	1	0.246	-0.097	-0.142	-0.096	0.032	0.211	0.29	0.223	-0.056	-0.279	-0.023	-0.033	-0.172	0.039
JanMaxT	1	0.24	0.038	0.036	-0.183	0.113	0.223	0.068	-0.027	-0.007	-0.066	-0.121	0.063	-0.114	-0.097
JanMinT	1	0.092	-0.038	0.09	-0.213	0.195	0.232	0.064	0.044	-0.085	-0.077	-0.11	-0.042	0.068	-0.072
JanMeanT	1	0.186	0.021	0.023	-0.254	0.166	0.317	0.101	0.049	-0.035	-0.142	-0.14	0.011	-0.008	0.003
FebMaxT	1	0.172	0.162	0.133	-0.065	0.274	-0.045	0.095	0.196	-0.042	0.086	-0.11	-0.106	-0.077	-0.196
FebMinT	1	-0.053	0.223	-0.073	-0.139	0.087	-0.127	0.096	0.263	0.085	0.032	-0.133	-0.187	-0.045	-0.24
FebMeanT	1	0.145	0.183	0.113	-0.097	0.277	-0.012	0.079	0.268	-0.04	0.061	-0.097	-0.199	-0.02	-0.173
MarMaxT	1	0.215	-0.096	-0.049	-0.171	0.174	0.009	-0.051	0.153	0.037	-0.007	-0.018	-0.024	-0.003	-0.022
MarMinT	1	-0.013	0.009	-0.057	-0.349	0.145	0.139	0.117	0.17	-0.029	-0.08	-0.123	-0.233	0.008	-0.004
MarMeanT	1	0.01	0.026	0.108	-0.268	0.156	0.019	0.045	0.164	0.022	0.04	-0.046	-0.144	-0.063	-0.028
AprMaxT	1	-0.173	-0.057	0.041	-0.006	-0.07	0.04	0.15	0.02	-0.155	0.017	-0.071	0.046	-0.105	-0.153
AprMinT	1	0.233	0.146	0.054	0.03	0.216	0.29	-0.029	-0.024	-0.135	-0.103	0.107	0.058	-0.11	-0.145
AprMeanT	1	-0.014	-0.137	-0.071	-0.086	0.14	0.053	0.144	0.016	-0.157	-0.031	-0.081	0.099	-0.048	-0.081
MayMaxT	1	-0.043	-0.02	0.111	-0.13	-0.189	-0.035	-0.049	0.17	0.216	-0.011	0.032	0.005	-0.13	-0.071
MayMinT	1	0.352	0.082	-0.048	0.278	0.059	-0.088	-0.146	-0.034	-0.052	0.029	0.054	0.129	0.025	-0.04
MayMeanT	1	0.207	0.098	0.223	-0.124	-0.131	-0.122	-0.05	-0.056	0.173	0.02	-0.016	0.025	-0.005	0.162
JunMaxT	1	-0.195	-0.001	0.059	0.193	-0.315	0.042	-0.039	0.03	-0.086	-0.015	0.203	-0.129	-0.055	0.112
JunMinT	1	0.279	0.251	-0.15	0.165	0.208	0.176	-0.164	-0.221	-0.123	0.076	0.109	-0.092	-0.198	-0.273
JunMeanT	1	-0.216	0.301	-0.006	0.164	-0.178	0.225	-0.154	0.207	-0.1	-0.172	-0.024	-0.165	-0.118	-0.017
JulMaxT	1	0.049	-0.121	-0.216	-0.299	0.036	0.196	0.112	-0.027	-0.149	-0.043	0.077	0.171	-0.048	-0.034
JulMinT	1	-0.164	-0.026	-0.294	-0.042	0.03	0.092	-0.074	0.149	-0.025	0.039	0.162	0.189	-0.136	-0.035
JulMeanT	1	0.007	-0.075	-0.169	-0.289	0.008	0.106	0.075	0.184	0.014	-0.246	-0.03	0.064	-0.19	0.141
AugMaxT	1	0.201	-0.073	-0.231	-0.175	0.084	0.308	0.42	0.025	-0.181	-0.356	-0.049	0.117	0.092	0.094
AugMinT	1	0.23	-0.008	-0.293	-0.451	-0.132	0.151	0.452	0.352	0.049	-0.239	-0.312	-0.176	-0.026	0.154
AugMeanT	1	0.262	-0.031	-0.336	-0.211	-0.103	0.411	0.44	0.087	-0.12	-0.239	-0.264	-0.104	0.151	0.085
SepMaxT	1	0.397	0.141	0.206	0.221	0.006	0.195	0.28	0.175	-0.047	0.019	-0.055	-0.273	-0.279	-0.084
SepMinT	1	0.268	0.024	0.166	0.129	-0.076	-0.171	0.143	0.116	-0.196	-0.116	-0.103	-0.364	-0.204	-0.12
SepMeanT	1	0.373	0.062	0.2	0.263	-0.145	0.01	0.282	0.132	-0.173	-0.048	-0.095	-0.404	-0.357	-0.116
OctMaxT	1	0.368	-0.12	-0.265	0.051	0.158	0.163	-0.054	-0.214	-0.028	0.289	0.336	-0.002	-0.206	-0.312
OctMinT	1	0.077	-0.287	-0.165	-0.019	0.135	0.222	-0.128	-0.275	-0.059	0.255	0.164	0.029	-0.006	-0.244
OctMeanT	1	0.298	-0.213	-0.257	0.044	0.168	0.23	-0.069	-0.296	-0.059	0.322	0.28	0.023	-0.166	-0.294
NovMaxT	1	-0.184	-0.018	0.076	-0.094	0.233	-0.03	0.125	0.196	-0.126	-0.359	0.081	0.013	0.041	-0.132
NovMinT	1	-0.385	0.06	0.27	-0.276	0.263	-0.149	0.005	0.175	-0.341	-0.013	0.038	-0.189	0.156	-0.128
NovMeanT	1	-0.251	-0.002	0.175	0.074	0.071	-0.146	0.176	0.081	-0.192	-0.163	0.08	-0.142	0.079	-0.141
DecMaxT	1	0.054	-0.073	0.01	-0.009	-0.129	0.086	-0.332	-0.129	-0.075	-0.066	-0.206	0.045	-0.073	0.291
DecMinT	1	-0.087	-0.141	-0.131	0.076	-0.065	-0.01	-0.361	0.067	0.05	0.168	-0.126	0.043	-0.194	0.314
DecMeanT	1	-0.176	-0.191	0.009	0.062	-0.256	0.117	-0.226	0.116	-0.005	0.129	-0.022	0.034	-0.303	0.247
GSprecip	1	-0.189	-0.188	-0.069	-0.024	0.011	0.048	0.118	-0.055	-0.257	-0.114	0.052	0.14	0.052	-0.055
YrPrecip	1	-0.412	0.224	-0.302	0.112	-0.158	0.102	-0.114	0.243	-0.108	0.018	-0.275	0.243	-0.266	0.208
MAPprecip	1	-0.062	-0.097	0.02	-0.169	0.064	0.041	-0.239	-0.082	-0.212	-0.053	0.147	0.106	-0.014	0.055
JAprcip	1	-0.183	-0.033	0.17	-0.125	-0.11	0.004	-0.141	-0.083	-0.096	-0.002	0.062	0.039	0.139	0.014
JanPrecip	1	-0.035	-0.096	-0.16	-0.089	0.051	0.05	-0.1	-0.132	0.174	-0.01	-0.04	0.049	-0.232	-0.113
FebPrecip	1	0.096	0.117	-0.2	-0.247	0.266	0.053	0.34	-0.115	-0.25	-0.084	-0.104	0.137	-0.014	-0.038
MarPrecip	1	-0.033	0.09	0.09	-0.153	0.232	0.004	0.057	0.053	-0.074	0.187	-0.144	0.075	0.052	-0.261
AprPrecip	1	0.245	0.127	-0.376	-0.165	-0.155	0.224	0.368	0.077	-0.028	-0.328	-0.143	-0.225	0.134	-0.046
MayPrecip	1	-0.115	-0.377	0.055	0.105	-0.06	0.051	0.201	-0.422	-0.021	0.277	-0.015	-0.06	-0.021	-0.091
JunPrecip	1	0.141	-0.179	0.041	0.062	-0.037	-0.05	-0.057	-0.219	-0.157	0.039	0.043	-0.15	0.051	-0.018
JulPrecip	1	0.039	-0.026	0.221	-0.117	-0.036	-0.221	-0.129	-0.123	-0.172	0.103	-0.055	-0.005	0.064	-0.065
AugPrecip	1	-0.422	0.152	-0.043	0.089	-0.167	0.02	-0.079	-0.028	-0.073	-0.019	-0.107	0.066	0.038	-0.025
SepPrecip	1	-0.089	0.002	0.014	0.089	0.023	-0.052	0.156	-0.009	-0.19	-0.049	-0.117	0.095	-0.051	-0.147
OctPrecip	1	-0.225	-0.247	0.139	0.098	-0.114	0.244	-0.07	-0.137	0.091	-0.062	-0.074	0.093	-0.195	0.082
NovPrecip	1	-0.381	0.211	-0.178	-0.028	0.083	-0.045	0.085	0.059	-0.214	0.12	-0.138	0.131	-0.179	0.211
DecPrecip	1	0	-0.427	0.127	0.08	-0.215	-0.051	0.235	0.118	-0.092	-0.093	-0.088	-0.104	0.021	0.233

List of References

- Adam, M., 1999. Nutrient fluctuations in Sitka spruce (*Picea sitchensis*) plantations: the implications for future forest management practice. *Forestry*, 72(3): 249-271.
- Allison, S.M., Proe, M.F. and Matthews, K.B., 1994. The prediction and distribution of general yield classes of Sitka spruce in Scotland by empirical-analysis of site factors using a Geographic Information-System. *Canadian Journal of Forest Research-Revue Canadienne De Recherche Forestiere*, 24(11): 2166-2171.
- Altaner, C., Apperley, D.C. and Jarvis, M.C., 2006. Spatial relationships between polymers in Sitka spruce: Proton spin-diffusion studies. *Holzforschung*, 60(6): 665-673.
- Alteyrac, J., Cloutier, A. and Zhang, S.Y., 2006. Characterization of juvenile wood to mature wood transition age in black spruce (*Picea mariana* (Mill.) BSP) at different stand densities and sampling heights. *Wood Science and Technology*, 40(2): 124-138.
- Alteyrac, J., Zhang, S.Y., Cloutier, A. and Ruel, J.C., 2005. Influence of stand density on ring width and wood density at different sampling heights in black spruce (*Picea mariana* (Mill.) BSP). *Wood and Fiber Science*, 37(1): 83-94.
- Anon., 2001. Wood: Density. *Encyclopedia of Materials: Science and Technology*. Elsevier Science Ltd.
- Anon., 2006. SIRT Workplan – Preliminary study on the effects of environment and management on selected wood properties of Sitka spruce.
- Antonova, G.F. and Stasova, V.V., 2006. Seasonal development of phloem in Scots pine stems. *Russian Journal of Developmental Biology*, 37(5): 306-320.
- Antonova, G.F. and Stasova, V.V., 2008. Seasonal development of phloem in Siberian larch stems. *Russian Journal of Developmental Biology*, 39(4): 207-218.
- Anttonen, S. et al., 2002. Effects of long-term nutrient optimisation on stem wood chemistry in *Picea abies*. *Trees-Structure and Function*, 16(6): 386-394.
- Astley, R.J., Harrington, J.J., Tang, S. and Neumann, J., 1997. Modelling the influence of microfibril angle on stiffness and shrinkage on radiata pine. In: B.G. Butterfield (Editor), *Microfibril angle in wood*. University of Canterbury, Christchurch, New Zealand, pp. 272-295.
- Auty, D. and Achim, A., 2008. The relationship between standing tree acoustic assessment and timber quality in Scots pine and the practical implications for assessing timber quality from naturally regenerated stands. *Forestry*, 81(4): 475-487.
- Bäucker, E., Bues, C.T. and Vogel, M., 1998. Radial growth dynamics of spruce (*Picea abies*) measured by micro-cores. *Iawa Journal*, 19(3): 301-309.
- Beets, P.N., Kimberley, M.O. and McKinley, R.B., 2007. Predicting wood density of *Pinus radiata* annual growth increments. *New Zealand Journal of Forestry Science*, 37(2): 241-266.
- Bergès, L., Nepveu, G. and Franc, A., 2008. Effects of ecological factors on radial growth and wood density components of sessile oak (*Quercus petraea* Liebl.) in Northern France. *Forest Ecology and Management*, 255(3-4): 567-579.
- Blyth, J.F. and Macleod, D.A., 1981a. Sitka Spruce (*Picea sitchensis*) in Northeast Scotland .1. Relationships between Site Factors and Growth. *Forestry*, 54(1): 41-62.
- Blyth, J.F. and Macleod, D.A., 1981b. Sitka Spruce (*Picea sitchensis*) in Northeast Scotland .2. Yield Prediction by Regression-Analysis. *Forestry*, 54(1): 63-73.
- Booker, R.E., Harrington, J.J. and Shiokura, T., 1997. Variation of Young's modulus with microfibril angle, density and spiral grain In: B.G. Butterfield (Editor), *Microfibril angle in wood*. University of Canterbury, Christchurch, New Zealand pp. 296-311.

- Bouriaud, O., Leban, J.M., Bert, D. and Deleuze, C., 2005. Intra-annual variations in climate influence growth and wood density of Norway spruce. *Tree Physiology*, 25(6): 651-660.
- Brazier, J.D., 1967. Timber Improvement .I. A study of variation in wood characteristics in young Sitka spruce. *Forestry*, 40(2): 117-128.
- Brazier, J.D., 1970a. Effect of spacing on wood density and wood yields of Sitka spruce. *Forestry*: 22-28.
- Brazier, J.D., 1970b. Timber Improvement .2. Effect of vigour on young-growth Sitka spruce. *Forestry*, 43(2): 135-150.
- Brazier, J.D. and Mobbs, I.D., 1993. The influence of planting distance on structural wood yields of unthinned Sitka spruce. *Forestry*, 66(4): 333-352.
- Briffa, K.R., 1995. Interpreting High-Resolution Proxy Climate Data - The Example of Dendroclimatology. In: H. von Storch and A. Navarra (Editors), *Analysis of Climate Variability: Applications of Statistical Techniques*. Springer, Berlin, pp. 77-94.
- Broadmeadow, M., 2000. Climate change - implications for forestry in Britain. Forestry Commission Information Note 31, Forestry Commission, Edinburgh.
- Broadmeadow, M.S.J. (Editor), 2002. Climate change: impacts on UK forests, Bulletin 125. Forestry Commission Edinburgh, 198 pp.
- Brockwell, P.J. and Davis, R.A., 1996. *Introduction to Time Series and Forecasting*, Springer Texts in Statistics. Springer, pp. 420.
- Brooks, J.R., Flanagan, L.B. and Ehleringer, J.R., 1998. Responses of boreal conifers to climate fluctuations: indications from tree-ring widths and carbon isotope analyses. *Canadian Journal of Forest Research-Revue Canadienne De Recherche Forestiere*, 28(4): 524-533.
- Bryan, J. and Pearson, F.G.O., 1955. The quality of Sitka spruce grown in Great Britain. *Empire Forest Rev*, 34(2): 144-153.
- Bucur, V. and Feeney, F., 1992. Attenuation of ultrasound in solid wood. *Ultrasonics*, 30(2): 76-81.
- Bunn, A.G., 2008. A dendrochronology program library in R (dplR). *Dendrochronologia*, 26(2): 115-124.
- Burgert, I. and Fratzl, P., 2009. Plants control the properties and actuation of their organs through the orientation of cellulose fibrils in their cell walls. *Integrative and Comparative Biology*, 49(1): 69-79.
- Cahalan, C.M., 1987. Wood properties of Sitka spruce. *Proceedings of the Royal Society of Edinburgh Section B-Biological Sciences*, 93: 205-212.
- Cameron, A.D., Lee, S.J., Livingston, A.K. and Petty, J.A., 2005. Influence of selective breeding on the development of juvenile wood in Sitka spruce. *Canadian Journal of Forest Research-Revue Canadienne De Recherche Forestiere*, 35(12): 2951-2960.
- Cannell, M.G.R., 1984. Sitka spruce. *Biologist*, 31(5): 255-261.
- Cannell, M.G.R., 1987. Photosynthesis, foliage development and productivity of Sitka spruce, pp. 61-73.
- Cannell, M.G.R. and Smith, R.I., 1983. Thermal time, chill days and prediction of bud burst in *Picea sitchensis*. *Journal of Applied Ecology*, 20(3): 951-963.
- Cannell, M.G.R. and Smith, R.I., 1986. Climatic warming, spring budburst and frost damage on trees. *Journal of Applied Ecology*, 23(1): 177-191.
- Cannell, M.G.R., Thornley, J.H.M., Mobbs, D.C. and Friend, A.D., 1998. UK conifer forests may be growing faster in response to increased N deposition, atmospheric CO₂ and temperature. *Forestry*, 71(4): 277-296.
- Caron-Decloquement, A., 2010. *Extractives from Sitka spruce*, University of Glasgow, Glasgow, 171 pp.
- Carter, P., Wang, X., Ross, R.J. and Briggs, D., 2005. NDE of logs and standing trees using new acoustic tools: technical application and results. In: F.-W. Broker

- (Editor), Proceedings of the 14th International Symposium on Nondestructive Testing of Wood Shaker Verlag, Aachen, Germany.
- CEN, 2003. Structural timber - Strength classes. EN338:2003. European Committee for Standardisation, Brussels, 14 pp.
- Chauhan, S.S. and Walker, J.C.F., 2006. Variations in acoustic velocity and density with age, and their interrelationships in radiata pine. *Forest Ecology and Management*, 229(1-3): 388-394.
- Clark, N.A., Wynne, R.H. and Schmoldt, D.L., 2000. A review of past research on dendrometers. *Forest Science*, 46(4): 570-576.
- Conrad, V., 1946. Usual formulas of continentality and their limits of validity. *Trans. Am. Geophys Un.*, 27: 663-664.
- Cook, E.R. and Kairiukstis, L.A. (Editors), 1990. *Methods of Dendrochronology; Applications in the Environmental Sciences*. Kluwer Academic Publishers and International Institute for Applied Systems Analysis, Dordrecht, 394 pp.
- Cook, E.R. and Peters, K., 1981. The smoothing spline: a new approach to standardizing forest interior tree-ring width series for dendroclimatic studies. *Tree-Ring Bulletin*, 41: 45-53.
- Coutts, M.P., 1982. Growth of Sitka spruce seedlings with roots divided between soils of unequal matric potential. *New Phytologist*, 92(1): 49-61.
- Cowdrey, D.R. and Preston, R.D., 1966. Elasticity and microfibrillar angle in wood of Sitka spruce. *Proceedings of the Royal Society Series B-Biological Sciences*, 166(1004): 245-272.
- Cown, D.J. and Ball, R.D., 2001. Wood densitometry of 10 *Pinus radiata* families at seven contrasting sites: influence of tree age, site and genotype. *New Zealand Journal of Forestry Science*, 31(1): 88-100.
- Cown, D.J. and Hutchison, J.D., 1983. Wood Density as an Indicator of the Bending Properties of Pinus-Radiata Poles. *New Zealand Journal of Forestry Science*, 13(1): 87-99.
- Cox Analytical Systems, Itrax density Scanner User and Service manual.
- Curtin, F. and Schulz, P., 1998. Multiple correlations and Bonferroni's correction. *Biological Psychiatry*, 44(8): 775-777.
- D'Arrigo, R.D., Jacoby, G.C. and Free, R.M., 1992. Tree-ring width and maximum latewood density at the North-American tree line - parameters of climatic change. *Canadian Journal of Forest Research-Revue Canadienne De Recherche Forestiere*, 22(9): 1290-1296.
- Deans, J.D. and Milne, R., 1999. Effects of respacing on young Sitka spruce crops. *Forestry*, 72(1): 47-57.
- DeBell, D.S., Singleton, R., Gartner, B.L. and Marshall, D.D., 2004. Wood density of young-growth western hemlock: relation to ring age, radial growth, stand density, and site quality. *Canadian Journal of Forest Research-Revue Canadienne De Recherche Forestiere*, 34(12): 2433-2442.
- Debell, J.D., Tappeiner, J.C. and Krahmer, R.L., 1994. Wood density of Western hemlock - effect of ring width. *Canadian Journal of Forest Research-Revue Canadienne De Recherche Forestiere*, 24(3): 638-641.
- Deckmyn, G., Evans, S.P. and Randle, T.J., 2006. Refined pipe theory for mechanistic modeling of wood development. *Tree Physiology*, 26(6): 703-717.
- Dengel, S., Aeby, D. and Grace, J., 2009. A relationship between galactic cosmic radiation and tree rings. *New Phytologist*, 184(3): 545-551.
- Denne, M.P., 1977. Dating of events from tree growth and wood structure. *Journal of the Forensic Science Society*, 17(4): 257-264.
- Denne, M.P., 1979. Wood structure and production within the trunk and branches of *Picea sitchensis* in relation to canopy formation. *Canadian Journal of Forest Research-Revue Canadienne De Recherche Forestiere*, 9(3): 406-427.

- Denne, M.P. and Smith, C.J., 1971. Daylength effects on growth, tracheid development, and photosynthesis in seedlings of *Picea sitchensis* and *Pinus sylvestris*. *Journal of Experimental Botany*, 22(71): 347-361.
- Deslauriers, A., Anfodillo, T., Rossi, S. and Carraro, V., 2007. Using simple causal modeling to understand how water and temperature affect daily stem radial variation in trees. *Tree Physiology*, 27(8): 1125-1136.
- Deslauriers, A., Morin, H., Urbinati, C. and Carrer, M., 2003. Daily weather response of balsam fir (*Abies balsamea* (L.) Mill.) stem radius increment from dendrometer analysis in the boreal forests of Quebec (Canada). *Trees-Structure and Function*, 17(6): 477-484.
- Diggle, P.J., 1990. *Time Series: A Biostatistical Introduction*. Oxford statistical science series, 5. Clarendon Press, Oxford, 257 pp.
- Dinwoodie, J.M., 2000. *Timber: its nature and behaviour*. E&FN SPON, London, 272 pp.
- Donaldson, L.A., 1992. Lignin distribution during latewood formation in *Pinus radiata* D. Don. *Iawa Bulletin*, 13(4): 381-387.
- Downes, G., Beadle, C. and Worledge, D., 1999. Daily stem growth patterns in irrigated *Eucalyptus globulus* and *E. nitens* in relation to climate. *Trees-Structure and Function*, 14(2): 102-111.
- Downes, G.M., Drew, D., Battaglia, M. and Schulze, D., 2009. Measuring and modelling stem growth and wood formation: an overview. *Dendrochronologia*, 27(2): 147-157.
- Drew, D.M. and Downes, G.M., 2009. The use of precision dendrometers in research on daily stem size and wood property variation: a review. *Dendrochronologia*, 27(2): 159-172.
- Dunham, R.A. and Cameron, A.D., 2000. Crown, stem and wood properties of wind-damaged and undamaged Sitka spruce. *Forest Ecology and Management*, 135(1-3): 73-81.
- Dupouey, J.L., Leavitt, S., Choisnel, E. and Jourdain, S., 1993. Modeling carbon-isotope fractionation in tree-rings based on effective evapotranspiration and soil-water status. *Plant Cell and Environment*, 16(8): 939-947.
- Durrant, D., 2000. *Environmental monitoring in British forests*. Forestry Commission Information Note 37, Forestry Commission, Edinburgh.
- Evans, R., Hughes, N. and Menz, D., 1999. Microfibril angle variation by scanning X-ray diffractometry. *Appita Journal*, 52(5): 363-367.
- Evans, R. and Ilic, J., 2001. Rapid prediction of wood stiffness from microfibril, angle and density. *Forest Products Journal*, 51(3): 53-57.
- Farmer, R.H., 1967. *Chemistry in the Utilisation of Wood*. Furniture and Timber, Volume 9. Pergamon Press Ltd., Oxford, 193 pp.
- Farquhar, G.D., Oleary, M.H. and Berry, J.A., 1982. On the relationship between carbon isotope discrimination and the inter-cellular carbon-dioxide concentration in leaves. *Australian Journal of Plant Physiology*, 9(2): 121-137.
- Ford, E.D., Robards, A.W. and Piney, M.D., 1978. Influence of environmental factors on cell production and differentiation in early wood of *Picea sitchensis*. *Annals of Botany*, 42(179): 683-&.
- Forestry Commission, 2007. *Forests and Climate Change*, Forestry Commission, Edinburgh.
- Forestry Commission, 2009. *Forestry Statistics 2009*, Forestry Commission.
- Forster, T., Schweingruber, F.H. and Denneler, B., 2000. Increment puncher - A tool for extracting small cores of wood and bark from living trees. *Iawa Journal*, 21(2): 169-180.
- Fritts, H.C., 1976. *Tree Rings and Climate*. Academic Press, New York, 567 pp.
- Gabert, F., 2005. *Physics of Wood*, University of Glasgow.
- Gardiner, B., Leban, J.-M., Auty, D. and Simpson, H., 2010. Models for predicting the wood density of British-grown Sitka spruce. *Forestry*, submitted.

- Gardiner, B., Macdonald, E., Hubert, J. and Forbes, J., 2002. Towards a timber quality model for British grown Sitka spruce, Proceedings of 4th IUFRO Workshop on Connection between Forest Resources and Wood Quality, British Columbia, Canada.
- Gaspar, M.J., Louzada, J.L., Silva, M.E., Aguiar, A. and Almeida, M.H., 2008. Age trends in genetic parameters of wood density components in 46 half-sibling families of *Pinus pinaster*. Canadian Journal of Forest Research-Revue Canadienne De Recherche Forestiere, 38(6): 1470-1477.
- Gerendiain, A.Z., 2009. Effects of genetic entry and spacing on growth and wood properties in Norway spruce, University of Joensuu.
- Gorman, T.M., Wagner, F.G. and Wu, S.Y., 2003. Assessment of intensive stress-wave scanning of Douglas-fir trees for predicting lumber modulus of elasticity. Proceedings of the 13th International Symposium on Nondestructive Testing of Wood: 143-147.
- Grace, J., Malcolm, D.C. and Bradbury, I.K., 1975. The effect of wind and humidity on leaf diffusive resistance in Sitka spruce seedlings. Journal of Applied Ecology, 12(3): 931-940.
- Grace, J. and Norton, D.A., 1990. Climate and growth of *Pinus sylvestris* at its upper altitudinal limit in Scotland - evidence from tree growth-rings. Journal of Ecology, 78(3): 601-610.
- Green, S., Hendry, S.J. and Redfern, D.B., 2008. Drought damage to pole-stage Sitka spruce and other conifers in north-east Scotland. Scottish Forestry, 62: 10-18.
- Gričar, J., 2007. Xylo- and phloemogenesis in Silver fir (*Abies alba* Mill.) and Norway spruce (*Picea abies* (L.) Karst.), Slovenian Forestry Institute, 106 pp.
- Gričar, J. and Cufar, K., 2008. Seasonal dynamics of phloem and xylem formation in silver fir and Norway spruce as affected by drought. Russian Journal of Plant Physiology, 55(4): 538-543.
- Gričar, J., Cufar, K., Oven, P. and Schmitt, U., 2005. Differentiation of terminal latewood tracheids in silver fir during autumn. Annals of Botany, 95(6): 959-965.
- Guilley, E., Herve, J.C. and Nepveu, G., 2004. The influence of site quality, silviculture and region on wood density mixed model in *Quercus petraea* Liebl. Forest Ecology and Management, 189(1-3): 111-121.
- Hacke, U.G., Sperry, J.S., Pockman, W.T., Davis, S.D. and McCulloch, K.A., 2001. Trends in wood density and structure are linked to prevention of xylem implosion by negative pressure. Oecologia, 126(4): 457-461.
- Halsall, L., Gilbert, J., Matthews, R. and Fairgrieve, M., 2005. United Kingdom: new forecast of softwood availability Forestry Commission, Available at [www.forestry.gov.uk/pdf/pf2005.pdf/\\$FILE/pf2005.pdf](http://www.forestry.gov.uk/pdf/pf2005.pdf/$FILE/pf2005.pdf).
- Hamilton, G.J., 1969. Dependence of volume increment of individual trees on dominance, crown dimensions, and competition. Forestry, 42(2): 133-144.
- Harris, J.M., 1989. Spiral Grain and Wave Phenomena in Wood Formation. Wood Science. Springer-Verlag, Berlin, 214 pp.
- Hedenberg, Ö., Lundqvist, S.-O. and Wilhelmsson, L., 2004. Fibre dimensions and wood density in Sitka spruce, STFI.
- Herzog, K.M., Hasler, R. and Thum, R., 1995. Diurnal changes in the radius of a sub-Alpine Norway spruce stem - Their relation to the sap flow and their use to estimate transpiration. Trees-Structure and Function, 10(2): 94-101.
- Hirakawa, Y., Yamashita, K., Fujisawa, Y. and Kijidani, Y., 1997. The effects of S2 microfibril angles and density on MOE in sugi. In: B.G. Butterfield (Editor), Microfibril angle in wood. University of Canterbury, Christchurch, New Zealand, pp. 312-322.
- Hoag, M.L. and Krahmer, R.L., 1991. Polychromatic X-ray attenuation characteristics and wood densitometry applications. Wood and Fiber Science, 23(1): 23-31.

- Hoch, G., Richter, A. and Korner, C., 2003. Non-structural carbon compounds in temperate forest trees. *Plant Cell and Environment*, 26(7): 1067-1081.
- Hubert, J. and Lee, S., 2005. A review of the relative roles of silviculture and tree breeding in tree improvement: the example of Sitka spruce in Britain and possible lessons for hardwood breeding. *Forestry*, 78(2): 109-120.
- Hughes, M.K., Schweingruber, F.H., Cartwright, D. and Kelly, P.M., 1984. July-August Temperature at Edinburgh between 1721 and 1975 from Tree-Ring Density and Width Data. *Nature*, 308(5957): 341-344.
- Ikonen, V.P. et al., 2008. Modelling the distribution of wood properties along the stems of Scots pine (*Pinus sylvestris* L.) and Norway spruce (*Picea abies* (L.) Karst.) as affected by silvicultural management. *Forest Ecology and Management*, 256(6): 1356-1371.
- Jaakkola, T., Mäkinen, H. and Saranpää, P., 2005. Wood density in Norway spruce: changes with thinning intensity and tree age. *Canadian Journal of Forest Research- Revue Canadienne De Recherche Forestiere*, 35(7): 1767-1778.
- Jane, F.W., 1970. The structure of wood. Adam&Charles Black, London, 478 pp.
- Jarvis, N.J., Mullins, C.E. and Macleod, D.A., 1983. The prediction of evapotranspiration and growth of Sitka spruce from meteorological records. *Annales Geophysicae*, 1(4-5): 335-343.
- Jeffers, J.N.R. and Dowden, H.G.M., 1964. Moisture content and specific gravity of fresh-felled conifers: [1] weighted tree means; [2] analysis of weighted tree means; [3] analysis of unweighted billet values for specified size classes. *Statistical Section Papers. Forestry Commission, London*(Nos. 67, 70 & 102): 17 + 64 + [4.
- Jyske, T., Mäkinen, H. and Saranpää, P., 2008. Wood density within Norway spruce stems. *Silva Fennica*, 42(3): 439-455.
- Kärkkäinen, M., 1984. Effect of tree social status on basic density of Norway spruce. *Silva Fennica*, 18(2): 155-120.
- Kauppi, P.E., Mielikäinen, K. and Kuusela, K., 1992. Biomass and carbon budget of European forests, 1971 to 1990. *Science*, 256(5053): 70-74.
- Keeland, B.D. and Sharitz, R.R., 1993. Accuracy of tree growth measurements using dendrometer bands. *Canadian Journal of Forest Research- Revue Canadienne De Recherche Forestiere*, 23(11): 2454-2457.
- Kennedy, R.W., 1995. Coniferous wood quality in the future - Concerns and strategies. *Wood Science and Technology*, 29(5): 321-338.
- Kienast, F., Schweingruber, F.H., Braker, O.U. and Schar, E., 1987. Tree ring studies on conifers along ecological gradients and the potential of single-year analyses. *Canadian Journal of Forest Research- Revue Canadienne De Recherche Forestiere*, 17(7): 683-696.
- Kilpeläinen, A., Peltola, H., Ryypö, A. and Kellomäki, S., 2005. Scots pine responses to elevated temperature and carbon dioxide concentration: growth and wood properties. *Tree Physiology*, 25(1): 75-83.
- Koch, G.W., Sillett, S.C., Jennings, G.M. and Davis, S.D., 2004. The limits to tree height. *Nature*, 428(6985): 851-854.
- Koponen, T., Karppinen, T., Hæggström, E., Saranpää, P. and Serimaa, R., 2005. The stiffness modulus in Norway spruce as a function of year ring. *Holzforchung*, 59: 451-455.
- Kostiainen, K. et al., 2004. Effect of elevated [CO²] on stem wood properties of mature Norway spruce grown at different soil nutrient availability. *Global Change Biology*, 10(9): 1526-1538.
- Kostiainen, K. et al., 2009. Stem wood properties of mature Norway spruce after 3 years of continuous exposure to elevated [CO₂] and temperature. *Global Change Biology*, 15(2): 368-379.

- Koubaa, A., Zhang, S.Y., Isabel, N., Beaulieu, J. and Bousquet, J., 2000. Phenotypic correlations between juvenile-mature wood density and growth in black spruce. *Wood and Fiber Science*, 32(1): 61-71.
- Kramer, P.J., 1957. Photosynthesis of Trees as Affected by Their Environment. In: K.V. Thimann (Editor), *International Symposium on Forest Tree Physiology*. The Ronald Press Company, Harvard, pp. 157-186.
- Kramer, P.J. and Kozlowski, T.T., 1960. *Physiology of Trees*. McGraw-Hill Publications in the Botanical Sciences, 642. McGraw-Hill Book Company Inc., London.
- Kubler, H., 1991. Function of Spiral Grain in Trees. *Trees-Structure and Function*, 5(3): 125-135.
- Lasserre, J.-P., Mason, E. and Watt, M., 2004. The influence of initial stocking on corewood stiffness in a clonal experiment of 11-year-old *Pinus radiata* D. Don. *New Zealand Journal of Forestry*, 49(2): 18-23.
- Lasserre, J.-P., Mason, E.G., Watt, M.S. and Moore, J.R., 2009. Influence of initial planting spacing and genotype on microfibril angle, wood density, fibre properties and modulus of elasticity in *Pinus radiata* D. Don corewood. *Forest Ecology and Management*, 258: 1924-1931.
- Lasserre, J.P., Mason, E.G. and Watt, M.S., 2005. The effects of genotype and spacing on *Pinus radiata* [D. Don] corewood stiffness in an 11-year old experiment. *Forest Ecology and Management*, 205(1-3): 375-383.
- Lasserre, J.P., Mason, E.G. and Watt, M.S., 2007. Assessing corewood acoustic velocity and modulus of elasticity with two impact based instruments in 11-year-old trees from a clonal-spacing experiment of *Pinus radiata* D. Don. *Forest Ecology and Management*, 239(1-3): 217-221.
- Laurent, M., Antoine, N. and Joel, G., 2003. Effects of different thinning intensities on drought response in Norway spruce (*Picea abies* (L.) Karst.). *Forest Ecology and Management*, 183(1-3): 47-60.
- Leavitt, S.W. and Long, A., 1982. Stable carbon isotopes as a potential supplemental tool in dendrochronology. *Tree-Ring Bulletin*, 42: 49-56.
- Lee, S., 1999a. Predicted genetic gains from Sitka spruce production populations. *Forestry Commission Information Note 26*, Forestry Commission, Edinburgh.
- Lee, S.J., 1999b. Improving the timber quality of Sitka spruce through selection and breeding. *Forestry*, 72(2): 123-133.
- Leinonen, I., 1996. Dependence of dormancy release on temperature in different origins of *Pinus sylvestris* and *Betula pendula* seedlings. *Scandinavian Journal of Forest Research*, 11(2): 122-128.
- Leonardon, M., Altaner, C.M., Vihermaa, L. and Jarvis, M.C., 2010. Wood shrinkage: influence of anatomy, cell wall architecture, chemical composition and cambial age. *European Journal of Wood and Wood Products*, 68(1): 87-94.
- Levanic, T. et al., 2009. The climate sensitivity of Norway spruce [*Picea abies* (L.) Karst.] in the southeastern European Alps. *Trees-Structure and Function*, 23(1): 169-180.
- Lin, L.I., 1989. A Concordance Correlation Coefficient to Evaluate Reproducibility. *Biometrics*, 45(1): 255-268.
- Lindström, H., 1996a. Basic density in Norway spruce .1. A literature review. *Wood and Fiber Science*, 28(1): 15-27.
- Lindström, H., 1996b. Basic density in Norway spruce .3. Development from pith outwards. *Wood and Fiber Science*, 28(4): 391-405.
- Lindström, H., 1996c. Basic density of Norway spruce .2. Predicted by stem taper, mean growth ring width, and factors related to crown development. *Wood and Fiber Science*, 28(2): 240-251.
- Lindström, H., Harris, P., Sorensson, C.T. and Evans, R., 2004. Stiffness and wood variation of 3-year old *Pinus radiata* clones. *Wood Science and Technology*, 38(8): 579-597.

- Livingston, A.K., Cameron, A.D., Petty, J.A. and Lee, S.L., 2004. Effect of growth rate on wood properties of genetically improved Sitka spruce. *Forestry*, 77(4): 325-334.
- Loader, N.J. et al., 2008. Multiple stable isotopes from oak trees in southwestern Scotland and the potential for stable isotope dendroclimatology in maritime climatic regions. *Chemical Geology*, 252(1-2): 62-71.
- Loader, N.J. and Switsur, V.R., 1996. Reconstructing past environmental change using stable isotopes in tree-rings. *Botanical Journal of Scotland*, 48(1): 65-78.
- Lundqvist, S.-O., Grahn, T. and Hedenberg, Ö., 2005. Models for fibre dimensions in different softwood species : simulation and comparison of within and between tree variations for Norway and Sitka spruce, Scots and Loblolly pine, IUFRO 5th workshop Wood quality modelling, Auckland, NZ.
- Macdonald, E., Gardiner, B. and Mason, W., 2010. The effects of transformation of even-aged stands to continuous cover forestry on conifer log quality and wood properties in the UK. *Forestry*, 83(1): 1-16.
- Macdonald, E. and Hubert, J., 2002. A review of the effects of silviculture on timber quality of Sitka spruce. *Forestry*, 75(2): 107-138.
- Macdonald, E., Mochan, S. and Connolly, T., 2001. Protocol for stem straightness assessment in Sitka spruce. Forestry Commission Information Note 39, Forestry Commission, Edinburgh.
- Mackie-Dawson, L.A., Millard, P. and Proe, M.F., 1995. The effect of nitrogen supply on root-growth and development in Sycamore and Sitka spruce trees. *Forestry*, 68(2): 107-114.
- Macmillan, D.C., 1991. Predicting the general yield class of Sitka spruce on better quality land in Scotland. *Forestry*, 64(4): 359-372.
- Mäkinen, H., Jaakkola, T., Piispanen, R. and Saranpää, P., 2007. Predicting wood and tracheid properties of Norway spruce. *Forest Ecology and Management*, 241(1-3): 175-188.
- Mäkinen, H. et al., 2002a. Radial growth variation of Norway spruce (*Picea abies* (L.) Karst.) across latitudinal and altitudinal gradients in central and northern Europe. *Forest Ecology and Management*, 171(3): 243-259.
- Mäkinen, H. et al., 2003a. Large-scale climatic variability and radial increment variation of *Picea abies* (L.) Karst. in central and northern Europe. *Trees-Structure and Function*, 17(2): 173-184.
- Mäkinen, H., Nöjd, P. and Mielikäinen, K., 2001. Climatic signal in annual growth variation in damaged and healthy stands of Norway spruce [*Picea abies* (L.) Karst.] in southern Finland. *Trees-Structure and Function*, 15(3): 177-185.
- Mäkinen, H., Nöjd, P. and Saranpää, P., 2003b. Seasonal changes in stem radius and production of new tracheids in Norway spruce. *Tree Physiology*, 23(14): 959-968.
- Mäkinen, H., Saranpää, P. and Linder, S., 2002b. Wood-density variation of Norway spruce in relation to nutrient optimization and fibre dimensions. *Canadian Journal of Forest Research-Revue Canadienne De Recherche Forestiere*, 32(2): 185-194.
- Mäkinen, H., Seo, J.W., Nöjd, P., Schmitt, U. and Jalkanen, R., 2008. Seasonal dynamics of wood formation: a comparison between pinning, microcoring and dendrometer measurements. *European Journal of Forest Research*, 127(3): 235-245.
- Malcolm, D.C., 1987. Some ecological aspects of Sitka spruce. *Proceedings of the Royal Society of Edinburgh Section B*, 93: 85-92.
- Mason, E.G., 2006. Interactions between influences of genotype and grass competition on growth and wood stiffness of juvenile radiata pine in a summer-dry environment. *Canadian Journal of Forest Research-Revue Canadienne De Recherche Forestiere*, 36(10): 2454-2463.
- Mason, E.G., 2008. Influences of silviculture, genetics and environment on radiata pine corewood properties: results from recent studies and a future direction. *New Zealand Journal of Forestry*, 53(2): 26-31.

- Mayhead, G.J., 1973. The effect of altitude above sea level on the yield class of Sitka spruce. *Scottish forestry*(23): 231-237.
- Mayr, S. and Cochard, H., 2003. A new method for vulnerability analysis of small xylem areas reveals that compression wood of Norway spruce has lower hydraulic safety than opposite wood. *Plant Cell and Environment*, 26(8): 1365-1371.
- McCarroll, D., and Loader, N. J., 2005. Isotopes in tree rings. In: M.J. Leng (Editor), *Isotopes in Palaeoenvironmental research. Developments in Palaeoenvironmental research* Springer, pp. 67-116.
- McCarroll, D. and Loader, N.J., 2004. Stable isotopes in tree rings. *Quaternary Science Reviews*, 23(7-8): 771-801.
- McLean, J.P., 2007. Wood properties of four genotypes of Sitka spruce, University of Glasgow, Glasgow.
- McLean, J.P., Evans, R. and Moore, J.R., 2010. Predicting the longitudinal modulus of elasticity of Sitka spruce from cellulose orientation and abundance. *Holzforschung*, 64(4): 495-500.
- Miller, H.G., Miller, J.D. and Binns, W.O., 1977. Growth of Scots pine under nutritional and climatic stress. *Plant and Soil*, 48: 103-114.
- Milne, R., 1989. Diurnal water storage in the stems of *Picea sitchensis* (Bong) Carr. *Plant Cell and Environment*, 12(1): 63-72.
- Milne, R., Ford, E.D. and Deans, J.D., 1983. Time lags in the water relations of Sitka spruce. *Forest Ecology and Management*, 5(1): 1-25.
- Mitchell, M.D. and Denne, M.P., 1997. Variation in density of *Picea sitchensis* in relation to within-tree trends in tracheid diameter and wall thickness. *Forestry*, 70(1): 47-60.
- Mochan, S., Lee, S. and Gardiner, B., 2008. Benefits of improved Sitka spruce: volume and quality of timber. *Research Note - Forestry Commission(003)*: 6 pp.
- Mochan, S., Moore, J. and Connolly, T., 2009. Using acoustic tools in forestry and the wood supply chain. *Research Note - Forestry Commission(018)*: 6.
- Moore, J., Achim, A., Lyon, A. and Gardiner, B., 2009a. Effects of early re-spacing on the physical and mechanical properties of Sitka spruce structural timber. *Forest Ecology and Management*, 258(7): 1174-1180.
- Moore, J.R., 2010a. Sitka Spruce in Great Britain: Wood Properties and Uses. In prep.
- Moore, J.R., Lyon, A.J., Searles, G.J. and Ridley-Ellis, D., 2009b. The use of acoustic-based NDT to predict the wood properties of UK-grown Sitka spruce at different stages in the wood supply chain, 16th International Nondestructive Testing and Evaluation of Wood Symposium, Beijing, China.
- Moore, J.R., Lyon, A.J., Searles, G.J. and Vihermaa, L.E., 2009c. The Effects of Site and Stand Factors on the Tree and Wood Quality of Sitka Spruce Growing in the United Kingdom. *Silva Fennica*, 43(3): 383-396.
- Moore, J.R. et al., 2009d. Effects of genetics on the wood properties of Sitka spruce growing in the UK: bending strength and stiffness of structural timber. *Forestry*, 82(5): 491-501.
- Moore, N., 2010b. Improved Timber Utilisation Statistics 2008 & Initial Data 2009 - Consumption of Sawn Softwood in Main End-User Markets in the United Kingdom, for the Forestry Commission, timbertrends.
- Moschler, W.W. and Winistorfer, P.M., 1990. Direct scanning densitometry - an effect of sample heterogeneity and aperture area. *Wood and Fiber Science*, 22(1): 31-38.
- Murray, M.B., Cannell, M.G.R. and Smith, R.I., 1989. Date of budburst of 15 tree species in Britain following climatic warming. *Journal of Applied Ecology*, 26(2): 693-700.
- Nyakuengama, J.G., Downes, G.M. and Ng, J., 2003. Changes caused by mid-rotation fertilizer application to the fibre anatomy of *Pinus radiata*. *Iawa Journal*, 24(4): 397-409.
- Nyakuengama, J.G., Matheson, C., Spencer, D., Evans, R. and Vinden, P., 1998. Correlation among growth, density, fibre diameter and heartwood in radiata pine. *Appita Journal*, 51(1): 35-38.

- O'Leary, M.H., 1981. Carbon isotope fractionation in plants. *Phytochemistry*, 20(4): 553-567.
- O'Leary, M.H., 1988. Carbon isotopes in photosynthesis. *Bioscience*, 38(5): 328-336.
- O'Leary, M.H., Madhavan, S. and Paneth, P., 1992. Physical and chemical basis of carbon isotope fractionation in plants. *Plant Cell and Environment*, 15(9): 1099-1104.
- Offenthaler, I., Hietz, P. and Richter, H., 2001. Wood diameter indicates diurnal and long-term patterns of xylem water potential in Norway spruce. *Trees-Structure and Function*, 15(4): 215-221.
- Ouis, D., 2002. On the frequency dependence of the modulus of elasticity of wood. *Wood Science and Technology*, 36(4): 335-346.
- Panek, J.A. and Waring, R.H., 1997. Stable carbon isotopes as indicators of limitations to forest growth imposed by climate stress. *Ecological Applications*, 7(3): 854-863.
- Panshin, A.J. and de Zeeuw, C., 1980. *Textbook of Wood Technology – Structure, Identification, Properties, and Uses of the Commercial Woods of the United States and Canada*. McGraw-Hill Inc., London, 722 pp.
- Park, Y.-I.D. and Spiecker, H., 2005. Variations in the tree-ring structure of Norway spruce (*Picea abies*) under contrasting climates. *Dendrochronologia*, 23(2): 93-104.
- Penman, H.L., 1948. Natural evaporation from open water, bare soil and grass. *Proceedings of the Royal Society of London Series a-Mathematical and Physical Sciences*, 193(1032): 120-145.
- Petty, J.A., 1970. Permeability and structure of wood of Sitka spruce. *Proceedings of the Royal Society of London Series B-Biological Sciences*, 175(1039): 149-166.
- Petty, J.A., Macmillan, D.C. and Steward, C.M., 1990. Variation of density and growth ring width in stems of Sitka and Norway spruce. *Forestry*, 63(1): 39-49.
- Peura, M. et al., 2008. The elemental composition, the microfibril angle distribution and the shape of the cell cross-section in Norway spruce xylem. *Trees-Structure and Function*, 22(4): 499-510.
- Pinheiro, J., Bates, D., Debroy, S., Sarkar, D. and R Core team, 2008. *nlme: Linear and Nonlinear Mixed Effects Models*. R package version 3.1-89.
- Pinhero, J.C. and Bates, D.M., 2000. *Mixed-Effects Models in S and S-Plus*. Springer-Verlag New York, 528 p. pp.
- Plomion, C., Leprovost, G. and Stokes, A., 2001. Wood formation in trees. *Plant Physiology*, 127(4): 1513-1523.
- Proe, M.F., Allison, S.M. and Matthews, K.B., 1996. Assessment of the impact of climate change on the growth of Sitka spruce in Scotland. *Canadian Journal of Forest Research-Revue Canadienne De Recherche Forestiere*, 26(11): 1914-1921.
- Pyatt, D.G., Ray, D. and Fletcher, J., 2001. *An Ecological Site Classification for Forestry in Great Britain*. Bulletin 124, Forestry Commission, Edinburgh.
- Quine, C.P. and White, I.M.S., 1993. Revised windiness scores for the windthrow hazard classification: the revised scoring method. *Forestry Commission Research Information Note* 230.
- Quine, C.P. and White, I.M.S., 1998. The potential of distance-limited topex in the prediction of site windiness. *Forestry*, 71(4): 325-332.
- R Development Core Team, 2007. *R: A language and environment for statistical computing*. R Foundation for Statistical Computing, Vienna, Austria.
- Raiskila, S. et al., 2006. Growth Rate and Wood Properties of Norway Spruce Cutting Clones on Different Sites. *Silva Fennica*, 40(2): 247-256.
- Rathgeber, C.B.K., 2009.
- Ray, D., 2001. *Ecological Site Classification - User's Guide*, Forestry Commission.
- Ray, D., Wainhouse, D., Webber, J. and Gardiner, B., 2008. *Impacts of climate change on forests and forestry in Scotland*, Forest Research, Forestry Commission.

- Repola, J., 2006. Models for vertical wood density of Scots pine, Norway spruce and birch stems, and their application to determine average wood density. *Silva Fennica*, 40(4): 673-685.
- Robertson, I. et al., 1997. Signal strength and climate relationships in C-13/C-12 ratios of tree ring cellulose from oak in southwest Finland. *Geophysical Research Letters*, 24(12): 1487-1490.
- Roche, L. and Haddock, P.G., 1987. Sitka Spruce (*Picea sitchensis*) in North-America with Special Reference to Its Role in British Forestry, pp. 1-12.
- Roderick, M.L. and Berry, S.L., 2001. Linking wood density with tree growth and environment: a theoretical analysis based on the motion of water. *New Phytologist*, 149(3): 473-485.
- Rossi, S., Anfodillo, T. and Menardi, R., 2006a. Trephor: A new tool for sampling microcores from tree stems. *Iawa Journal*, 27(1): 89-97.
- Rossi, S., Deslauriers, A. and Anfodillo, T., 2006b. Assessment of cambial activity and xylogenesis by microsampling tree species: An example at the alpine timberline. *Iawa Journal*, 27(4): 383-394.
- Rossi, S., Deslauriers, A., Anfodillo, T. and Carraro, V., 2007. Evidence of threshold temperatures for xylogenesis in conifers at high altitudes. *Oecologia*, 152(1): 1-12.
- Rossi, S. et al., 2006c. Conifers in cold environments synchronize maximum growth rate of tree-ring formation with day length. *New Phytologist*, 170(2): 301-310.
- Rossi, S. et al., 2008. Critical temperatures for xylogenesis in conifers of cold climates. *Global Ecology and Biogeography*, 17(6): 696-707.
- Rozenberg, P., Franc, A., Bastien, C. and Cahalan, C., 2001. Improving models of wood density by including genetic effects: A case study in Douglas-fir. *Annals of Forest Science*, 58(4): 385-394.
- Rozenberg, P., Schute, G., Ivkovich, M., Bastien, C. and Bastien, J.C., 2004. Clonal variation of indirect cambium reaction to within-growing season temperature changes in Douglas-fir. *Forestry*, 77(4): 257-268.
- Ryan, M.G. and Yoder, B.J., 1997. Hydraulic limits to tree height and tree growth. *Bioscience*, 47(4): 235-242.
- Saranpää, P., 1994. Wood density and growth. In: J.R. Barnett and G. Jeronimidis (Editors), *Wood quality and its biological basis*. Blackwell Publishing Ltd., Oxford, pp. 87-117.
- Saranpää, P. and Repola, J., 2000. Density of Norway spruce - can it be predicted and related to strength? In: S.E. Stanzl-Tschegg and A. Reiterer (Editors), *Wood Machining - properties of wood and wood composites related to wood machining*, Vienna, Austria, pp. 73-79.
- Satoo, T., 1960. Wind, Transpiration, and Tree Growth. In: T.T. Kozlowski (Editor), *International Conference of Forest Tree Growth*. The Ronald Press Company, Tucson, pp. 299-310.
- Saurer, M. and Siegenthaler, U., 1989. $^{13}\text{C}/^{12}\text{C}$ isotope ratios in trees are sensitive to relative humidity. *Dendrochronologia*, 7: 9-13.
- Savidge, R.A., 1996. Xylogenesis, genetic and environmental regulation - A review. *Iawa Journal*, 17(3): 269-310.
- Savill, P.S. and Sandels, A.J., 1983. The influence of early respacing on the wood density of Sitka spruce. *Forestry*, 56(2): 109-120.
- Savva, Y., Koubaa, A., Tremblay, F. and Bergeron, Y., 2010. Effects of radial growth, tree age, climate, and seed origin on wood density of diverse jack pine populations. *Trees-Structure and Function*, 24(1): 53-65.
- Schweingruber, F.H., 2007. *Wood Structure and Environment*. Springer Series in Wood Science. Springer, 279 pp.
- Schweingruber, F.H., Fritts, H.C., Bräker, O.U., Drew, L.G. and Schär, E., 1978. The X-ray technique as applied to dendro climatology. *Tree-Ring Bulletin*, 38(RECD. 1979): 61-91.

- Seo, J.-W., Eckstein, D. and Schmitt, U., 2007. The pinning method: From pinning to data preparation. *Dendrochronologia*, 25(2): doi:10.1016/j.dendro.2007.04.001.
- Seo, J.W., Eckstein, D., Jalkanen, R., Rickebusch, S. and Schmitt, U., 2008. Estimating the onset of cambial activity in Scots pine in northern Finland by means of the heat-sum approach. *Tree Physiology*, 28(1): 105-112.
- Sevanto, S., Hölttä, T., Hirsikko, A., Vesala, T. and Nikinmaa, E., 2005. Determination of thermal expansion of green wood and the accuracy of tree stem diameter variation measurements. *Boreal Environment Research*, 10(5): 437-445.
- Sevanto, S. et al., 2008. Linking xylem diameter variations with sap flow measurements. *Plant and Soil*, 305(1-2): 77-90.
- Shinozaki, K., Yoda, K., Hozumi, K. and Kira, T., 1964. A quantitative analysis of plant form - the pipe model theory 1. Basic analyses. *Japanese Journal of ecology*, 14(3): 97-105.
- Silim, S.N., Guy, R.D., Patterson, T.B. and Livingston, N.J., 2001. Plasticity in water-use efficiency of *Picea sitchensis*, *P. glauca* and their natural hybrids. *Oecologia*, 128(3): 317-325.
- Simpson, H.L. and Denne, M.P., 1997. Variation of ring width and specific gravity within trees from unthinned Sitka spruce spacing trial in Clocaenog, North Wales. *Forestry*, 70(1): 31-45.
- Simpson, W.T., 1993. Specific Gravity, Moisture Content, and Density Relationship for Wood, US Department of Agriculture, Forest Service, Forest Products Laboratory, Madison WI.
- Splechtna, B.E., Dobry, J. and Klinka, K., 2000. Tree-ring characteristics of subalpine fir (*Abies lasiocarpa* (Hook.) Nutt.) in relation to elevation and climatic fluctuations. *Annals of Forest Science*, 57(2): 89-100.
- St-Germain, J.L. and Krause, C., 2008. Latitudinal variation in tree-ring and wood cell characteristics of *Picea mariana* across the continuous boreal forest in Quebec. *Canadian Journal of Forest Research-Revue Canadienne De Recherche Forestiere*, 38(6): 1397-1405.
- Steffenrem, A., Saranpää, P., Lundqvist, S. and Skroppa, T., 2007. Variation in wood properties among five full-sib families of Norway spruce (*Picea abies*). *Annals of Forest Science*, 64: 799-806.
- Stevenson, M., with contribution from Nunes, T., Sanchez, J. and Thornton, R., 2009. epiR: Functions for analysing epidemiological data. R package version 0.9-18.
- Stirling, G., Gardiner, B., Connolly, T., Mochan, S. and Macdonald, 2000. A survey of Sitka Spruce Stem Straightness In South Scotland, Forest Research, Northern Research Station, Roslin, Midlothian, Scotland.
- Sunley, J.G. and Lavers, G.M., 1961. Variations in the strength and specific gravity of Sitka Spruce grown in Great Britain. *Journal of the Institute of Wood Science*(7): 15-27.
- Switsur, R., Waterhouse, J. S., Field, E. M., and Carter, A. H. C., 1996. Climatic signals from stable isotopes in oak tree rings from East Anglia, Great Britain. In: J.S. Dean, Meko, D. M., and Swetnam, T. W. (Editor), *Tree rings, Environment and Humanity*, pp. 637-645.
- Tene, A. et al., 2010. Tree response to severe climatic stress, IUFRO 7.01.00, Antalya.
- Thomas, P., 2000. *Trees: Their Natural History*. Cambridge University Press, 288 pp.
- Timell, T.E., 1964. Wood and Bark Polysaccharides. In: W.A.J. Côte (Editor), *Ultrastructure of Woody Plants*, Advanced Science Seminar Syracuse University Press, Pinebrook Conference Center Upper Saranac Lake, New York, pp. 127-156.
- Trapletti, A. and Hornik, K., 2009. tseries: Time Series Analysis and Computational Finance. R package version 0.10-22.
- Travis, D., Meentemeyer, V. and Belanger, R.P., 1990. Stressed trees produce a better climatic signal than healthier trees. *Tree-ring bulletin*, 50: 29-32.

- Tsehaye, A., Buchanan, A.H., Meder, R., Newman, R.H. and Walker, J.C.F., 1997. Microfibril angle: determining wood stiffness in radiata pine. In: B.G. Butterfield (Editor), Microfibril angle in wood, University of Canterbury, Christchurch, New Zealand pp. 312-322.
- Turcotte, A., Morin, H., Krause, C., Deslauriers, A. and Thibeault-Martel, M., 2009. The timing of spring rehydration and its relation with the onset of wood formation in black spruce. *Agricultural and Forest Meteorology*, 149(9): 1403-1409.
- UK Meteorological Office, 2009. MIDAS Land Surface Stations data (1853-current), [Internet]. British Atmospheric Data Centre, 2006, Extracted January 2009. Available from <http://badc.nerc.ac.uk/data/ukmo-midas>
- UKCP09, 2009. UK Climate Projections, <http://ukclimateprojections.defra.gov.uk/>.
- Vaganov, E.A., Anchukaitis, K.J. and Evans, M.N., 2008. How well understood are the processes that create dendroclimatic records? A mechanistic model of climatic control on conifer tree-ring growth dynamics. In: M.K. Hughes, T.W. Swetnam and H.F. Diaz (Editors), *Dendroclimatology: Progress and Prospects, Developments in Paleocological Research*. Springer.
- Vaganov, E.A., Hughes, M.K. and Shashkin, A.V., 2006. Growth Dynamics of Conifer Tree Rings - Images of the Past and Future Environments. *Ecological Studies*, 183. Springer, 354 pp.
- Wang, G.G., Chhin, S. and Bauerle, W.L., 2006. Effect of natural atmospheric CO₂ fertilization suggested by open-grown white spruce in a dry environment. *Global Change Biology*, 12(3): 601-610.
- Wang, L., Payette, S. and Begin, Y., 2002. Relationships between anatomical and densitometric characteristics of black spruce and summer temperature at tree line in northern Quebec. *Canadian Journal of Forest Research-Revue Canadienne De Recherche Forestiere*, 32(3): 477-486.
- Wang, X.P., Ross, R.J. and Carter, P., 2007. Acoustic evaluation of wood quality in standing trees. Part I. Acoustic wave behavior. *Wood and Fiber Science*, 39(1): 28-38.
- Waring, R.H., 2000. A process model analysis of environmental limitations on the growth of Sitka spruce plantations in Great Britain. *Forestry*, 73(1): 65-79.
- Watanabe, K., Saito, Y., Avramidis, S. and Shida, S., 2008. Non-destructive measurement of moisture distribution in wood during drying using digital X-ray microscopy. *Drying Technology*, 26(5): 590-595.
- Watt, M.S. et al., 2006. Modelling the influence of stand structural, edaphic and climatic influences on juvenile *Pinus radiata* dynamic modulus of elasticity. *Forest Ecology and Management*, 229(1-3): 136-144.
- Whitmore, F.W. and Zahner, R., 1966. Development of xylem ring in stems of young red pine trees. *Forest Science*, 12(2): 198-210.
- Wigley, T.M.L., Briffa, K.R. and Jones, P.D., 1984. On the average value of correlated timeseries, with applications in dendroclimatology and hydrometeorology. *Journal of Climate and Applied Meteorology*, 23(2): 201-213.
- Wimmer, R., Downes, G.M. and Evans, R., 2002. High-resolution analysis of radial growth and wood density in *Eucalyptus nitens*, grown under different irrigation regimes. *Annals of Forest Science*, 59(5-6): 519-524.
- Wimmer, R. and Grabner, M., 2000. A comparison of tree-ring features in *Picea abies* as correlated with climate. *Iawa Journal*, 21(4): 403-416.
- Wingate, L., 2003. The contribution of photosynthesis and respiration on the net ecosystem exchange and ecosystem ¹³C discrimination of a Sitka spruce plantation, University of Edinburgh.
- Worrell, R. and Malcolm, D.C., 1990a. Productivity of Sitka spruce in Northern Britain .1. the effects of elevation and climate. *Forestry*, 63(2): 105-118.
- Worrell, R. and Malcolm, D.C., 1990b. Productivity of Sitka spruce in Northern Britain .2. Prediction from site factors. *Forestry*, 63(2): 119-128.

- Yamaguchi, D.K., 1991. A simple method for cross-dating increment cores from living trees. *Canadian Journal of Forest Research-Revue Canadienne De Recherche Forestiere*, 21(3): 414-416.
- Yasue, K., Funada, R., Kobayashi, O. and Ohtani, J., 2000. The effects of tracheid dimensions on variations in maximum density of *Picea glehnii* and relationships to climatic factors. *Trees-Structure and Function*, 14(4): 223-229.
- Zobel, B.J. and van Buijtenen, J.P., 1989. *Wood Variation: Its Causes and Control*. Springer-Verlag, Berlin, 363 pp.
- Zweifel, R. and Häsler, R., 2000. Frost-induced reversible shrinkage of bark of mature subalpine conifers. *Agricultural and Forest Meteorology*, 102(4): 213-222.
- Zweifel, R. and Häsler, R., 2001. Dynamics of water storage in mature subalpine *Picea abies*: temporal and spatial patterns of change in stem radius. *Tree Physiology*, 21(9): 561-569.
- Zweifel, R., Item, H. and Häsler, R., 2000. Stem radius changes and their relation to stored water in stems of young Norway spruce trees. *Trees-Structure and Function*, 15(1): 50-57.
- Zweifel, R., Item, H. and Häsler, R., 2001. Link between diurnal stem radius changes and tree water relations. *Tree Physiology*, 21(12-13): 869-877.
- Zweifel, R., Zimmermann, L., Zeugin, F. and Newbery, D.M., 2006. Intra-annual radial growth and water relations of trees: implications towards a growth mechanism. *Journal of Experimental Botany*, 57(6): 1445-1459.